Control of distributed parameter systems

Habilitationsschrift

von Stefan Palis
geb. am 07.08.1981 in Magdeburg

zur Verleihung des akademischen Grades

**Doktor-Ingenieur habilitatus
(Dr.-Ing. habil.)**

genehmigt von der Fakultät für Elektrotechnik und Informationstechnik
der Otto-von-Guericke-Universität Magdeburg am 29.11.2023

Gutachter:
        Prof. Dr.-Ing. habil. Achim Kienle
        Prof. Dr.-Ing. habil. Thomas Meurer
        Prof. Dr.-Ing. habil. Dipl.-Math. Klaus Röbenack

Zusammenfassung

Die vorliegende Arbeit beschäftigt sich mit der Regelung von Systemen mit verteilten Parametern. Im Gegensatz zu Systemen mit konzentrierten Parametern, deren Zustandsvektor nur von der Zeit abhängt, handelt es sich hierbei um Systeme mit einem unendlich-dimensionalen Zustandsraum, d.h. der Systemzustand ist eine Funktion der Zeit und weiterer Variablen, z.B. Orts- oder Eigenschaftskoordinaten. Aus mathematischer Sicht führt die Beschreibung von verteilt-parametrischen Systemen in der Regel auf partielle Differentialgleichungen. Dies erschwert sowohl die Analyse als auch den Reglerentwurf. In der Literatur wurden vor allem Methoden zur Regelung von linearen partiellen Differentialgleichungen untersucht. Für die im Rahmen der vorliegenden Arbeit betrachteten Anwendungen spielen jedoch insbesondere nichtlineare partielle Differentialgleichungen eine große Rolle. Hier konnte die diskrepanzbasierte Regelung vielversprechende Ergebnisse zeigen. Das Grundkonzept wurde in [42] vorgestellt und konnte dort erfolgreich auf die Wirbelschichtsprühgranulation angewendet werden. Ergebnisse zur Kristallisation finden sich in [47]. Während der Habilitation wurden die Konzepte erweitert und auf neue Anwendungsfelder übertragen.

Die Basis für den diskrepanzbasierten Regelungsansatz bildet eine weniger bekannte Stabilitätstheorie, Stabilität bezüglich zweier Diskrepanzen, welche in den 60ern Jahren in der ehemaligen UdSSR entwickelt wurde. Die Hauptidee ist hierbei, das Regelungsproblem als Ein-Ausgangsproblem aufzufassen, wobei der Ausgang problemspezifisch gewählt wird. Zur Illustration wird der Ansatz an drei Anwendungsproblemen verschiedenen Types und variierender Komplexität untersucht. Es handelt sich hierbei um eine nichtlineare Variation der instabilen Wärmeleitungsgleichung, eine Krananlage mit elastischem Verhalten und die Agglomeration. Die Modelle zu den genannten Prozessen werden in Kapitel 2 eingeführt.

Im Anschluss an die Kapitel zur Stabilität bezüglich zweier Diskrepanzen (Kapitel 3) und der diskrepanzbasierten Regelung (Kapitel 4) werden in Kapitel 5 Erweiterungen in Richtung adaptive und Sliding-Mode Regelung beschrieben. Das für die diskrepanzbasierte Regelung zentrale Konzept der internen Dynamik bzw. Nulldynamik ist Gegenstand von Kapitel 6.

Contents

Part I

Summary of the main results

Chapter 1

Introduction

Distributed parameter systems are systems with an infinite-dimensional state space, i.e. the system state is a function of time and additional variables, e.g. spatial or property coordinates. This is in contrast to lumped parameter systems, which have a finite-dimensional state space, i.e. the state is a vector depending on time only. Mathematically, distributed parameter systems often lead to partial differential equations (PDEs), which are challenging from an analysis and control point of view. Especially, the case of linear hyperbolic and parabolic PDEs has received great attention. However, in the fields of applications considered in this thesis often nonlinear PDEs play an essential role. Here, the discrepancy based control approach has been promising. The basic concepts of this approach have been presented in [42]. It has been applied to fluidized bed spray granulation processes [42] and crystallization [47]. During the habilitation the concepts were extended and applied to new fields of application. The foundation of the discrepancy based control approach is a less known stability theory, stability with respect to two discrepancies, which has been developed in the 1960s in the former USSR [21, 22, 23]. The main idea is to study the control problem in an input-output setting, where the output is appropriately chosen to reflect the problem specifics. In the following, the control approach will be examined for different application examples of varying types and complexity. The test problems are:

1. Heat equation with quadratic nonlinearity. This problem is a challenging nonlinear control problem. It is a straightforward extension of the classical heat equation, i.e. a parabolic PDE, and has been proposed in [5, 6].

2. Control of a large crane structure exhibiting elastic behavior.

3. Agglomeration, a particulate process, which can be described using population balance equations [17, 18, 19].

It should be mentioned, that the given test problems are challenging for most infinite-dimensional control approaches, which often require linearity, boundary or full domain actuation or flatness. Among others, popular approaches for infinite-dimensional systems are linear optimal control [35, 36, 37], linear infinite-dimensional port-Hamilton systems [29, 30, 31] and infinite-dimensional backstepping and flatness-based control [32, 33, 34]. In chapter 2 the application examples and their models are introduced. Basic notions of stability with respect to a generalized distance measure, the discrepancy, are summarized in chapter 3.

Chapter 4 covers discrepancy based control, i.e. control based on the stability concept stated in chapter 3. After general considerations, control of the application examples introduced in chapter 2 is presented. In chapter 5 different extensions as adaptive discrepancy based control and sliding mode control are illustrated. In addition, the important problem of zero dynamics stability is studied.

Chapter 2

Selected examples of distributed parameter systems

2.1 Heat-equation

Control design for the heat equation and its variations have been studied for some time, e.g. [1], and still receive considerable attention in the recent literature, e.g. [3, 2, 4, 7, 12]. In the simplest one-dimensional case, it can be assumed that the heat conduction coefficient is equal to one over the whole domain, resulting in the following PDE

$$\frac{\partial w}{\partial t} = \frac{\partial^2 w}{\partial x^2} + f(w),\tag{2.1}$$

where $w(x,t)$ is the system state, $t \geq 0$ is the time and $x \in [0,1]$ is the spatial coordinate. $f(w)$ is a spatially distributed heat source or sink, reflecting for example chemical reactions. The dependence may for example be linear, i.e. $f(w) = \lambda w$. Typical boundary conditions are:

- constant temperature

$$w(0,t) = const.\tag{2.2}$$

- constant heat flux

$$\frac{\partial w(1,t)}{\partial x} = const.\tag{2.3}$$

In [5, 6] a nonlinear variation of the given heat equation has been investigated, where the source term $f(w)$ depends quadratic on the system state w, i.e. $f(w) = w^2$. Therefore, the system is unstable. Furthermore, the state diverges to infinity in finite time and hence the system is not globally stabilizable [5, 6]. Thus, stabilizing control design is a challenging task. In [5, 6] the authors propose an infinite-dimensional backstepping design procedure in combination with an approximation based on Volterra series. An alternative control design procedure will be presented in section 4.1.

2.2   Elastic crane structures

During crane operation elastic oscillations may occur. This is in particular relevant for large crane structures, as for example large gantry cranes or ship-to-shore container bridges. Here, structural dynamic problems are often caused due to hoisting or trolley motion. In the following, only the latter effect is investigated. The influence of trolley motion increases with increasing crane size and reduced stiffness, e.g. due to lightweight construction. As it directly interacts with the load positioning process and may result in sickness of the crane operator, due to its low frequency behavior, different solution approaches have been proposed in the literature:

- increasing structure stiffness by construction optimization [14],

- passive damping via counter weights [15],

- additional active dampers [15],

- extension of the trolley motion system [43, 44].

In general, the last approach is preferable, as no additional changes in the construction nor additional actuators are required.

From a theoretical point of view, an elastic crane structure can be represented as depicted in Fig. 2.1. The supporting crane structure is reflected as an elastic beam, whereas the other parts are assumed to be rigid. In general a crane is supported by two columns. Assuming that both are identical, only one column has to be explicitly included in the model due to symmetry. Further, bending stiffness and mass density are assumed to be constant along the column and rotary inertia, shear deformation and buckling are neglected.
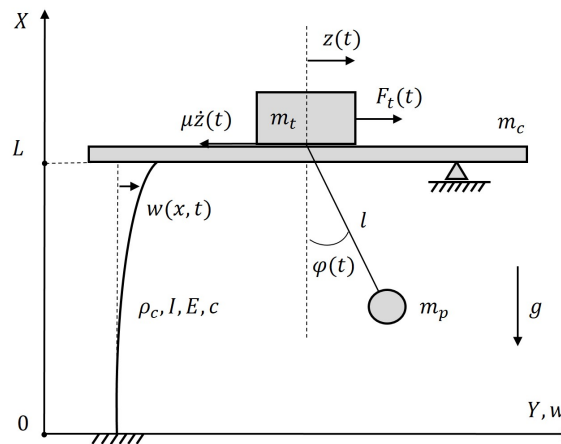

Figure 2.1: Gantry crane [43]

Additional assumptions to simplify the modeling are:

- hoisting and thus variations in the rope length is neglected,

- friction or external forces are neglected.

For modeling the following vector of generalized coordinates is chosen.

$$q = [w(x,t) \; z(t) \; \varphi(t)]^T \tag{2.4}$$

The position of the girder r_c, trolley r_t and payload r_p in terms of the generalized coordinates then are:

$$r_c = \begin{bmatrix} w(L,t) \\ 0 \end{bmatrix}, \tag{2.5}$$

$$r_t = \begin{bmatrix} w(L,t) + z(t) \\ 0 \end{bmatrix}, \tag{2.6}$$

$$r_p = \begin{bmatrix} w(L,t) + z(t) + l \sin \varphi \\ -l \cos \varphi \end{bmatrix}. \tag{2.7}$$

Based on the kinetic and potential energy, T (2.8) and U (2.9):

$$T = \frac{1}{2} \int_0^L \rho_c \dot{w}^2 \, dx + \frac{1}{2} m_c \dot{w}^2(L,t) + \frac{1}{2} m_t (\dot{w}(L,t) + \dot{z})^2 + \ldots$$
$$\ldots + \frac{1}{2} m_p \left[(\dot{w}(L,t) + \dot{z} + \dot{\varphi} l \cos \varphi)^2 + (\dot{\varphi} l \sin \varphi)^2 \right], \tag{2.8}$$

$$U = \frac{1}{2} \int_0^L EI(w'')^2 dx - m_p gl \cos \varphi, \tag{2.9}$$

the equations of motion (2.10)-(2.14) can be derived applying Hamilton's principle.

$$\rho_c \frac{\partial^2 w}{\partial t^2} = -EI \frac{\partial^4 w}{\partial x^4} - c \frac{\partial w}{\partial t} \tag{2.10}$$

$$0 = w(0,t) = \frac{\partial w(0,t)}{\partial t} = \frac{\partial^2 w}{\partial t^2}(L,t) \tag{2.11}$$

$$0 = m_\Sigma \ddot{w}(L,t) + m_s \ddot{z} + m_p l \ddot{\varphi} \cos \varphi - m_p l \dot{\varphi}^2 \sin \varphi - EI \frac{\partial^3 w(L,t)}{\partial x^3} \tag{2.12}$$

$$0 = m_s \ddot{w}(L,t) + m_s \ddot{z} + m_p l \ddot{\varphi} \cos \varphi - m_p l \dot{\varphi}^2 \sin \varphi - F_t + \mu \dot{z} \tag{2.13}$$

$$0 = l \ddot{\varphi} + \ddot{w}(L,t) \cos \varphi + \ddot{z} \cos \varphi + g \sin \varphi \tag{2.14}$$

Here, the dynamics consist of a PDE describing the structural dynamics of the crane support (2.10), its boundary conditions (2.11), two ODEs describing the trolley and load motion (2.13) and (2.14) and a coupling equation (2.12), interconnecting the subsystems.

2.3   Agglomeration

Agglomeration is a particle formation process, where new particles are formed from smaller particles. The particle formation is due to the establishment of solid bridges between particles during collision events. The solid bridges are formed from liquid layers on the particle surfaces, which are created due to added binder solution. The described micro process is depicted in Fig. 2.2. A typical agglomeration process in a fluidized bed configuration is shown in Fig. 2.3. Here, the particles are fluidized through a hot fluidization air stream from below. The binder is added via a spray nozzle. To achieve a continuous process operation, primary particles have to be supplied and agglomerates of a given minimum size have to be removed constantly.
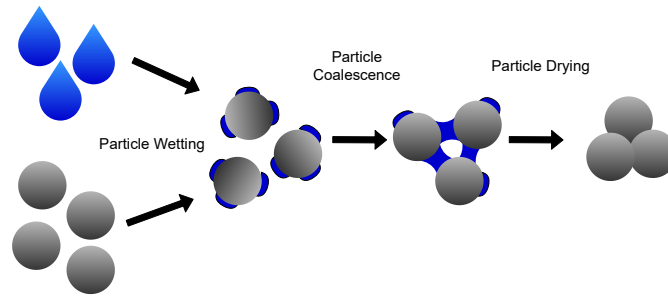
Figure 2.2: Three stages of agglomeration: (a) particle wetting, (b) particle coalescence and (c) particle drying [52]
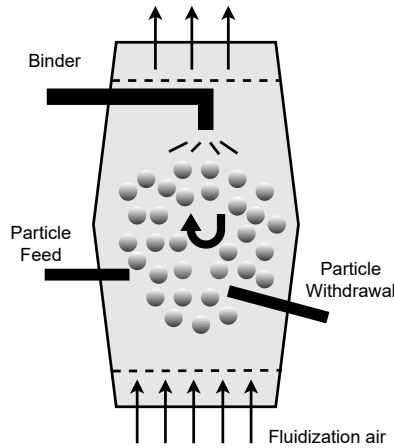
Figure 2.3: Continuous agglomeration process scheme [52]

The agglomeration process can be described applying population balance modeling [17]. Therefore, the particle volume distribution $n(t, v)$ is introduced. A change in the number of particles of a specific volume V is due to agglomeration $\dot{n}_a(t, v)$, external feed $\dot{n}_f(t, v)$ or particle withdrawal $\dot{n}_o(t, v)$.

$$\frac{\partial n(t, v)}{\partial t} = \dot{n}_{\mathrm{a}}(t, v) + \dot{n}_{\mathrm{f}}(t, v) - \dot{n}_{\mathrm{o}}(t, v) \tag{2.15}$$

For simplicity ideal mixing inside the process chamber has been assumed and hence spatial gradients can be neglected. The aggregation term $\dot{n}_a(t,v)$ consists of two terms: a birth and a death term [16]. The birth term accounts for the combination of two or more smaller particles forming a new particle of size v. The death term is a sink term, reflecting events where particles of size v form new particles of greater volume.

$$\dot{n}_\mathrm{a}(t,v) = B(t,v) - D(t,v) \tag{2.16}$$

The birth rate $B(t,v)$ for particles of volume v due to binary aggregation events is represented as follows

$$B(t,v) = \frac{1}{2} \int_0^v \beta(t,u,v-u)n(t,u)n(t,v-u)du, \tag{2.17}$$

where $\beta(t,u,v)$ is the coalescence kernel, describing the likelihood that two particles of size u and v form a new particle of size v. The death rate $D(t,v)$ is defined similarly.

$$D(t,v) = \int_0^\infty \beta(t,v,u)n(t,v)n(t,u)du \tag{2.18}$$

From a modeling point of view, the specific form of the coalescence kernel $\beta(t,u,v)$ is an open question. Although, a number of different options for different processes and operating conditions have been proposed in the literature, uncertainty for a given process is high. Selected coalescence kernels are stated in Tab. 2.1.

Name	$\beta(u,v)$
Size-independent kernel	1
Sum kernel	$u + v$
Product kernel	uv
Brownian kernel	$\left(u^{1/3} + v^{1/3}\right)\left(u^{-1/3} + v^{-1/3}\right)$
EKE kernel	$\left(u^{1/3} + v^{1/3}\right)^2 \sqrt{u^{-1} + v^{-1}}$
Gravitational kernel	$\left(u^{1/3} + v^{1/3}\right)^2 \mid u^{1/6} - v^{1/6} \mid$

Table 2.1: Selected coalescence kernels [52] and references therein

For the particle feed $\dot{n}_f(t,v)$ it is assumed that the particle volume distribution of externally supplied particles is some constant normalized number density distribution $q_{0,\mathrm{f}}(v)$, which is scaled with the total number of added particles $N_\mathrm{f}(t)$.

$$\dot{n}_\mathrm{f}(t,v) = N_\mathrm{f}(t)q_{0,\mathrm{f}}(v) \tag{2.19}$$

To model the particle outlet it is assumed that particles exceeding a specific volume v_prod are removed from the process. This can be achieved by an appropriately chosen separation function $T(v)$, where a cumulative Gaussian function is a typical candidate for a non-ideal withdrawal.

$$T(v) = \int_0^v \frac{1}{\sqrt{2\pi\sigma^2}} \exp \frac{(s - v_\mathrm{prod})^2}{\sigma^2} ds \tag{2.20}$$

Here, σ defines the classification quality and v_prod the separation volume. For a given removal rate $K(t)$ the number density of removed particles thus is

$$\dot{n}_\mathrm{o}(t,v) = K(t)T(v)n(t,v). \tag{2.21}$$

Combining the equations for the particle fluxes (2.17), (2.18) (2.19), (2.21) and the population balance model (2.15) yields

$$\frac{\partial n(t,v)}{\partial t} = \frac{1}{2}\int_0^v \beta(t,u,v-u)n(t,u)n(t,v-u)du - \int_0^\infty \beta(t,v,u)n(t,v)n(t,u)du + \dots$$

$$\dots + N_{\mathrm{f}}(t)q_{0,\mathrm{f}}(v) - K(t)T(v)n(t,v). \tag{2.22}$$

Chapter 3

Stability with respect to two discrepancies

In the following, a general infinite-dimensional system, with a solution $\varphi(.,t)$ and an equilibrium at zero $\varphi_0 = 0$, is considered. Here, the . represents an arbitrary number of spatial or property coordinates. The distance between the process $\varphi(.,t)$ and the equilibrium φ_0 is then measured using the discrepancy or measure $\rho(\varphi(.,t),t)$ defined as follows [21, 22, 23].

Definition 1 *Discrepancy [23]*
A discrepancy is a real valued functional $\rho = \rho(\varphi(.,t),t)$ with the following properties

1. *$\rho(\varphi,t) \geq 0$,*

2. *$\rho(0,t) = 0$,*

3. *for an arbitrary process $\varphi = \varphi(.,t)$ the real valued functional $\rho(\varphi(.,t),t)$ is continuous with respect to t.*

It should be mentioned, that a discrepancy lacks essential properties of a metric, as symmetry, fulfillment of the triangular inequality and in particular definiteness, i.e. a vanishing discrepancy $\rho(\varphi,t) = 0$ does in general not imply $\varphi = 0$. Therefore, the discrepancy is a generalization of the classical distance measures used in infinite-dimensional stability theory, e.g. L_p and L_∞- norms.
To account for deviations of the initial state $\varphi(.,0)$ from the equilibrium φ_0, a second time independent discrepancy ρ_0 can be used. Here, both discrepancies ρ and ρ_0 have to satisfy a continuity condition at time $t = t_0$, i.e. for every $\varepsilon > 0$ and $t_0 > 0$ there exists a $\delta(\varepsilon,t_0) > 0$, such that from $\rho_0 \leqslant \delta(\varepsilon,t_0)$ it follows that $\rho < \varepsilon$.

Definition 2 *Stability with respect to two discrepancies ρ and ρ_0 [23]*
The equilibrium $\varphi_0 = 0$ is stable in the sense of Lyapunov with respect to the two discrepancies ρ and ρ_0 for all $t \geq t_0$ if for every $\varepsilon > 0$ and $t_0 \geq 0$ there exists a $\delta = \delta(\varepsilon,t_0) > 0$ such that for every process $\varphi(.,t)$ with $\rho_0 < \delta(\varepsilon,t_0)$ it follows that $\rho < \varepsilon$ for all $t \geq t_0$. If in addition $\lim_{t\to\infty} \rho = 0$, than the equilibrium φ_0 is called asymptotically stable in the sense of Lyapunov with respect to the two discrepancies ρ and ρ_0.

To introduce according Lyapunov functionals the additional notion of positive definiteness with respect to a discrepancy is required.

Definition 3 *Positive definiteness with respect to a discrepancy ρ [23]*
A functional $V = V(\varphi, t)$ is positive definite with respect to a discrepancy ρ, if $V \geq 0$ and $V(0,t) = 0$ for all φ with $\rho(\varphi, t) < \infty$ and for every $\varepsilon > 0$ there exists a $\delta = \delta(\varepsilon) > 0$, such that $V \geq \delta(\varepsilon)$ for all φ with $\rho(\varphi, t) \geq \varepsilon$.

Based on the above definitions, the following theorem provides the connection between (asymptotic) stability with respect to two discrepancies and the existence of an according Lyapunov functional V.

Theorem 1 *Lyapunov functional [23] The process φ with the equilibrium $\varphi_0 = 0$ is stable with respect to the two discrepancies ρ and ρ_0 if and only if there exists a functional $V = V(\varphi, t)$ positive definite with respect to the discrepancy ρ, continuous at time $t = t_0$ with respect to ρ_0 at $\rho_0 = 0$ and not increasing along the process φ, i.e. $\dot{V} \leq 0$. The process is asymptotically stable if in addition $\lim_{t \to \infty} V = 0$.*

From a stabilization or rather control design point of view, appropriate choices for the second discrepancy ρ_0 and the Lyapunov functional V are often $\rho_0 = \rho(t_0)$ and $V = \rho$. This leaves the discrepancy ρ as the main degree of freedom.
In comparison with the conventional Lyapunov stability theory the main difference of a discrepancy-based stability analysis is that the Lyapunov functional does not have to be connected to any norm of the infinite-dimensional state. To illustrate this point the classical stability problem of the heat equation is revisited.

$$\frac{\partial w}{\partial t} = \frac{\partial^2 w}{\partial x^2} \tag{3.1}$$

$$w(0,t) = 0 \tag{3.2}$$

$$w(1,t) = 0 \tag{3.3}$$

To prove stability with respect to the L_2-norm the following Lyapunov functional can be chosen.

$$V = \frac{1}{2} \int_0^1 w^2(x,t)dx = \|w\|_2^2 \tag{3.4}$$

Calculating the time derivative gives

$$\dot{V} = -\int_0^1 \left(\frac{\partial w}{\partial x}\right)^2 dx. \tag{3.5}$$

The time derivative $\dot{V}$ is bounded and negative. However, since it depends on $\frac{\partial w}{\partial x}$ convergence of V towards zero is not obvious. Therefore, the Poincare inequality and the boundary conditions can be used to derive an estimate of $\dot{V}$.

$$\dot{V} = -\int_0^1 \left(\frac{\partial w}{\partial x}\right)^2 dx \leq -\frac{1}{4} \int_0^1 w^2 dx \leq -\frac{1}{2}V \tag{3.6}$$

This implies

$$V(t) \leq e^{-\frac{t}{2}}V(0), \tag{3.7}$$

and additionally exponential stability with respect to the L_2-norm.

$$\|w(t)\|_2 \leq e^{-\frac{t}{4}}\|w(0)\|_2 \tag{3.8}$$

As can be seen from this example, restriction to norm-based Lyapunov functionals limits Lyapunov stability analysis to a certain class of problems. In contrast, a discrepancy-based stability analysis can chose an arbitrary dependence of the Lyapunov functional on the system state. This additional degree of freedom can be used to significantly simplify the analysis. For example, the nonlinear variation of the heat equation presented in section 2.1 will be stabilized using a weighted mean temperature to construct an appropriate discrepancy-based control-Lyapunov functional.

As has been stated in [49], stability with respect to two discrepancies implies stability in terms of a L_p- or L_∞-norm if and only if the associated internal or zero dynamics are stable. A similar result has been derived in [11] in the context of high-gain stabilization and funnel control. For general problems, as they occur in many practical applications, stability of the infinite-dimensional internal dynamics cannot be shown easily. Here, linear finite-dimensional approximations can often serve as a good approximation. In addition, for some system classes with specific structural properties the stability of the infinite-dimensional zero dynamics can been investigated rigorously, e.g. for port-Hamilton systems [8] and PDEs with a self-adjoint infinitesimal generator of a strongly continuous semigroup [9, 10].

Chapter 4

Discrepancy based control of distributed parameter systems

Despite extensive research on infinite-dimensional control theory, it still does not resemble a unified control theory, but rather a collection of different control approaches. These can roughly be divided into three groups as depicted in Fig. 4.1

- Early lumping, i.e. due to discretization or other model reduction procedures, e.g. method of moments, the infinite-dimensional design model is reduced to a finite-dimensional model, which can then be used for a finite-dimensional control design. The main problem here is guaranteeing stability and performance for the original system.

- Late lumping, i.e. using infinite-dimensional control theory, an infinite-dimensional controller is designed. For implementation reasons, this controller has then to be reduced to a finite-dimensional system, resulting in a possible loss of stability and performance guarantees.

- Direct control design, i.e. designing directly a finite-dimensional controller for the infinite-dimensional plant model.

To face the problems with early lumping control, approaches based on linear finite-dimensional robust control theory can be applied. Here, errors due to varying set-points, discretization and model order reduction can be taken explicitly into account during the control design stage.

Regarding direct or late lumping control, most approaches being developed over the last decades rely on special system properties, e.g. boundary or full-domain actuation, linearity, solvability of the system equations or at least the desired error system. Important representatives are linear optimal control methods [1, 35, 36, 37] and infinite-dimensional backstepping [2, 4, 32, 33, 34], where the first assumes linear system equations and the latter requires in general boundary actuation.

To overcome these structural requirements, a possible approach is to state the control design problem in the aforementioned generalized stability setting, i.e. stability with respect to two discrepancies [21, 23]. Here, the choice of an appropriate discrepancy allows to incorporate engineering expertise on the process or plant into the design procedure to simplify the control design task.
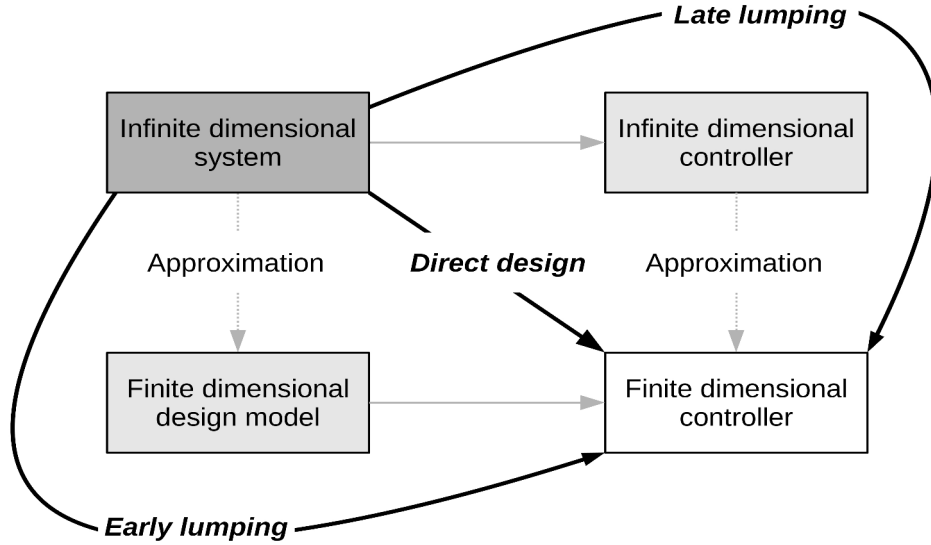
Figure 4.1: Control of distributed parameter systems

As the focus is on control design, rather than on stability analysis, the second discrepancy ρ_0 will be in the following implicitly defined based on $\rho(t)$.

$$\rho_0 = \rho(t = 0) = 0 \tag{4.1}$$

This choice is straightforward and obviously assures continuity at time $t = 0$. The same applies for the Lyapunov functional V, which will be chosen as $V = \rho(t)$. The design procedure will be further illustrated on the basis of the model systems described above.

4.1 Control of the heat equation

In the following, the stabilizing discrepancy based control law for the heat equation with quadratic nonlinearity and boundary actuation as proposed in [46] will be presented. It is assumed that the temperature at the left boundary, i.e. $x = 0$, is equal to zero, and that the heat flux at the right boundary, i.e. $x = 1$, can be controlled. The model presented in section 2.1 thus yields:

$$\frac{\partial w}{\partial t} = \frac{\partial^2 w}{\partial x^2} + w^2, \tag{4.2}$$

$$w(0, t) = 0, \tag{4.3}$$

$$\frac{\partial w(1, t)}{\partial x} = u, \tag{4.4}$$

where u is the control input. The desired steady state temperature distribution is assumed to be zero, i.e. $w_d(x) = 0$. Deviations from the desired steady state will be measured in terms of an integral quantity or weighted average.

$$e = \int_0^1 k(x) \, (w_d - w) \, dx \tag{4.5}$$

From a control point of view, it is clear that errors in a greater distance from the actuated boundary at $x = 1$ are harder to control. Therefore, they should be stronger weighted, which can be achieved by the following exponential function

$$k(x) = \exp(-ax), \tag{4.6}$$

where $a > 0$. Based on the error defined in eq. 4.5 an appropriate discrepancy ρ is given as follows

$$\rho = \frac{1}{2} \left(\int_0^1 k(x)\, (w_d - w)\, dx \right)^2. \tag{4.7}$$

Then, due to Theorem 1, asymptotic stability with respect to the two discrepancies ρ and ρ_0 with $\rho_0 = \rho(t = 0)$ follows from the existence of an appropriate functional V. An obvious choice is the following candidate Lyapunov functional.

$$V = \rho = \frac{1}{2}e^2 = \frac{1}{2} \left(\int_0^1 k(x)\, (w_d - w)\, dx \right)^2 \tag{4.8}$$

Thus, to achieve closed-loop stability in the sense of two discrepancies the control u has to be chosen such that the time derivative of the candidate Lyapunov functional V becomes negative definite along the systems trajectories for all times and vanishes only for $V = 0$.

$$\dot{V} = e\dot{e} \tag{4.9}$$

$$= -e \int_0^1 k \left(\frac{\partial^2 w}{\partial x^2} + w^2 \right) dx \tag{4.10}$$

$$= -e \left[k \frac{\partial w}{\partial x} \Big|_0^1 - \int_0^1 \frac{dk}{dx} \frac{\partial w}{\partial x} - kw^2 dx \right] \tag{4.11}$$

$$= -e \left[k(1)u - k(0)\frac{\partial w(0,t)}{\partial x} - \frac{dk(1)}{dx}w(1,t) + \int_0^1 \frac{d^2k}{dx^2}w + kw^2 dx \right] \tag{4.12}$$

Here, the last equation (4.12) suggests the following control law to guarantee negative definiteness of the time derivative of the candidate Lyapunov functional V.

$$u = \frac{1}{k(1)} \left[k(0)\frac{\partial w(0,t)}{\partial x} + \frac{dk(1)}{dx}w(1,t) + ce - \int_0^1 \left(\frac{d^2k}{dx^2} + kw \right) w dx \right] \tag{4.13}$$

It should be mentioned, that by design the chosen control law (4.13) also guarantees exponential convergence of V, where c defines the convergence speed and can hence be used as a tuning parameter.

$$\dot{V} = -ce^2 = -2cV \tag{4.14}$$

The proposed control scheme is tested in terms of simulations for $a = 2$, $c = 10$. As an initial condition a sinusoidal temperature profile with a peak value of 20, i.e. $w(x,0) = 20\sin(x)$ has been chosen, which is significantly higher than the maximum allowable peak value of 8 in [5]. The closed-loop behavior for the state $w(x,t)$ and the control u is depicted in Fig. 4.2 (left) and (right), respectively.

As can be seen in Fig. 4.2 (left) the proposed control scheme is able to stabilize the process. Here, convergence of w in the sense of the L_2 and L_∞-norm as depicted in Fig.
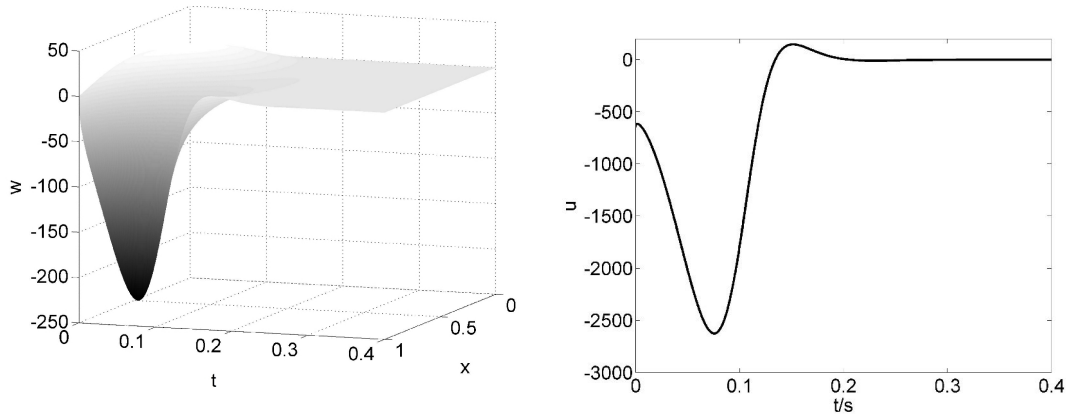
Figure 4.2: Closed loop operation, state $w(x,t)$ (left) and control u (right)
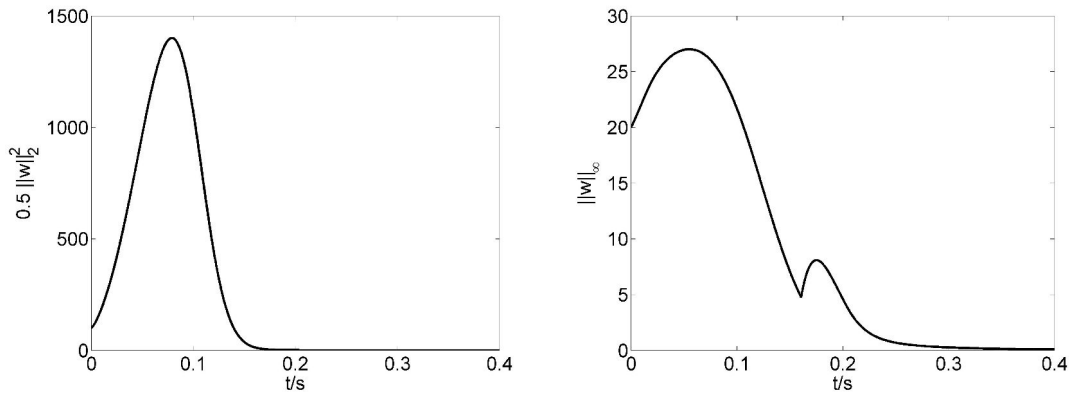
Figure 4.3: Convergence of the L_2-norm in closed loop operation
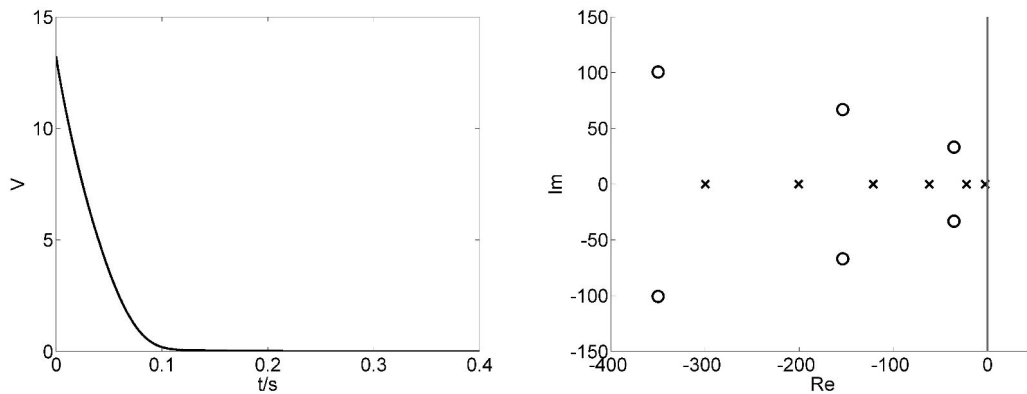
Figure 4.4: Convergence of V in closed loop operation (left), pole/zero map of the linear finite-dimensional approximation (right)

4.3 (left) and (right) respectively is achieved. In addition, the Lyapunov functional V by design converges exponentially as shown in Fig. 4.4 (left).

For a rigorous proof of stability in the L_2 or L_∞-norm, stability of the zero dynamics in the according norm has to be proven. This is challenging due to the nonlinear system

behavior. However, as an approximation a high order finite-dimensional linear approximation can been investigated instead. In the present configuration, as can be seen from the open loop pole/zero map in Fig. 4.4 (right), no zeros are present in the right half plane. Therefore, the zero dynamics of the finite-dimensional linear approximation are stable in the L_2 and L_∞-norm, due to equivalence of norms in finite-dimensions.

4.2 Control of an elastic crane

A typical problem for mechanical systems are weakly-damped oscillations, which need either constructive changes or additional damping. In case of the elastic crane model presented in section 2.2, two types of weakly-damped oscillation are present: load swaying and structural oscillations. As will be shown in the following, both can be sufficiently damped using a single actor, the trolley. The control task can be divided into four parts:

1. damping of oscillations in the crane structure,

2. damping of load oscillations,

3. trolley positioning,

4. load positioning.

In order to reflect all requirements the following discrepancy is chosen, where $k_1, \ldots, k_4$ are weighting coefficients and ε is the trolley position error, i.e. $\varepsilon = z - z_d$.

$$\rho = \frac{1}{2} \left(k_1 \dot{w}(L, t) + k_2 \dot{z} + k_3 \dot{\varphi} l \cos \varphi + k_4 \varepsilon \right)^2 \tag{4.15}$$

From the proposed discrepancy (4.15) the following candidate control Lyapunov functional results.

$$V = \frac{1}{2} \left(k_1 \dot{w}(L, t) + k_2 \dot{z} + k_3 \dot{\varphi} l \cos \varphi + k_4 \varepsilon \right)^2 \tag{4.16}$$

Calculating the time derivative of the candidate Lyapunov functional V along the systems trajectories to design a stabilizing control law results in:

$$\dot{V} = e\dot{e}, \tag{4.17}$$
$$= e \left[k_1 \ddot{w}(L, t) + k_2 \ddot{z} + k_3 \ddot{\varphi} l \cos \varphi - k_3 \dot{\varphi}^2 l \sin \varphi + k_4 \dot{\varepsilon} \right], \tag{4.18}$$
$$= e \left[(k_1 - k_2) \ddot{w}(L, t) + b_1 l \ddot{\varphi} \cos \varphi - b_1 l \dot{\varphi}^2 \sin \varphi + k_4 \dot{\varepsilon} - \frac{k_2 \mu}{m_s} \dot{z} + \frac{k_2}{m_s} F_t \right]. \tag{4.19}$$

Here, the system equations including the boundary conditions have been used. An appropriate choice of the control law for the trolley drive moment $\tau = F_t / k_{tr}$ is given by

$$\tau_t = \frac{m_s}{k_2 k_{tr}} [-(k_1 - k_2) \ddot{w}(L, t) - b_1 l \ddot{\varphi} \cos \varphi + b_1 l \dot{\varphi}^2 \sin \varphi - k_4 \dot{\varepsilon} + \frac{k_2 \mu}{m_s} \dot{z} - ce]. \tag{4.20}$$

where $c > 0$ is a tuning factor to influence convergence speed. This control law results in exponential convergence of the Lyapunov functional.

$$\dot{V} = -ce^2 = -2cV \tag{4.21}$$

As can be seen in Fig. 4.5 and 4.6 the proposed control law is able to stabilize the whole system. It achieves the desired trolley and load positions, and sufficiently damps structural oscillations and load swaying. For reference the results applying a standard motion control system, i.e. pure trolley position control, have been included. Here, undamped structural oscillations and load swaying occur as expected (see Fig. 4.5 and 4.6). Consequential, the L_2-norm of the displacement $w(x, t)$ depicted in Fig. 4.7 converges only for the proposed discrepancy based control law.
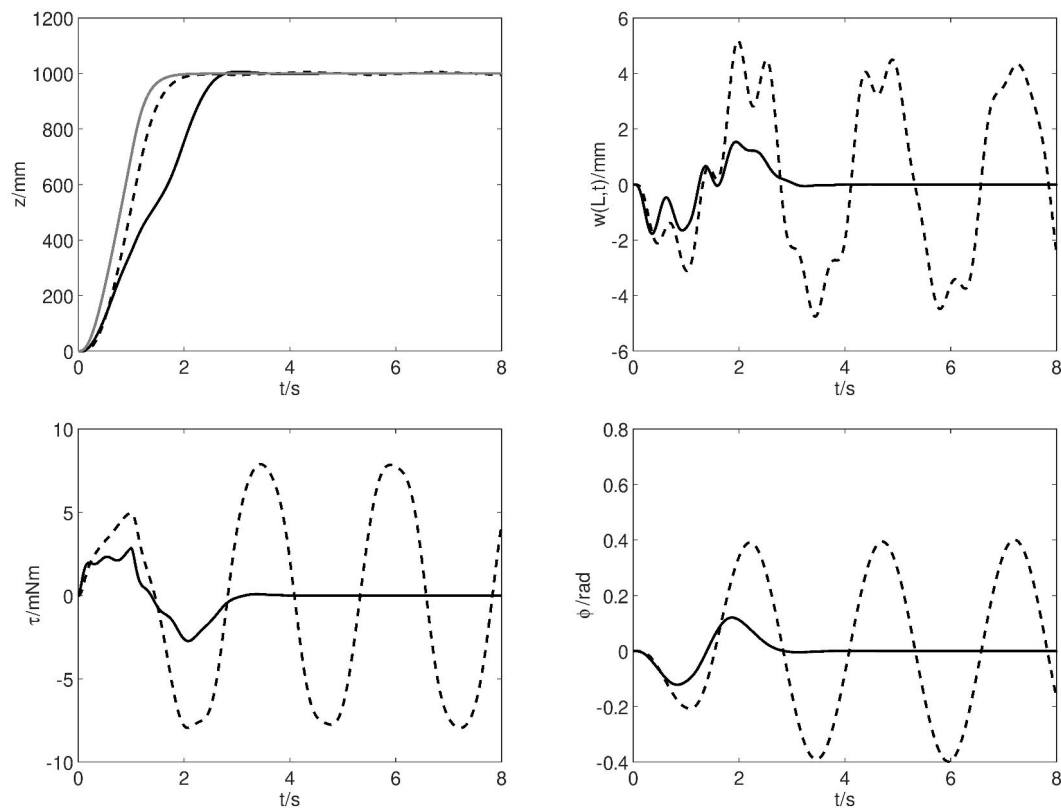

Figure 4.5: Reference tracking for pure trolley position control (dotted black) and discrepancy based control (black), reference position (gray). Trolley position z (top left), displacement at $x = L$, $w(L, t)$ (top right), moment τ (bottom left), load angle ϕ (bottom right) [43].
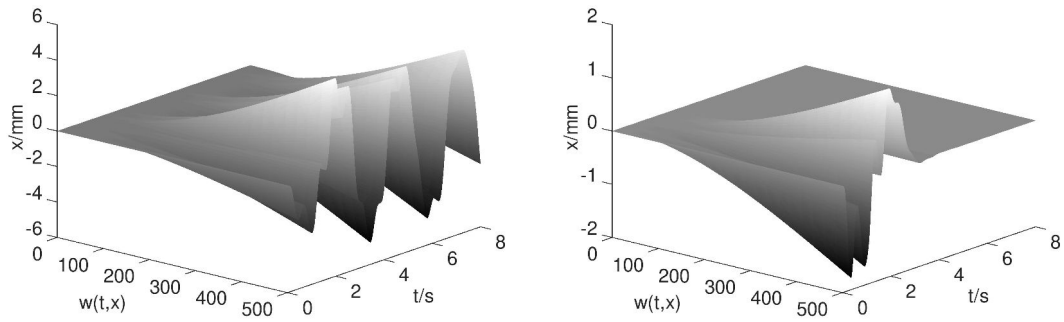
Figure 4.6: Time behavior of the displacement $w(t, x)$ for pure trolley position control (left) and discrepancy based control (right) [43]
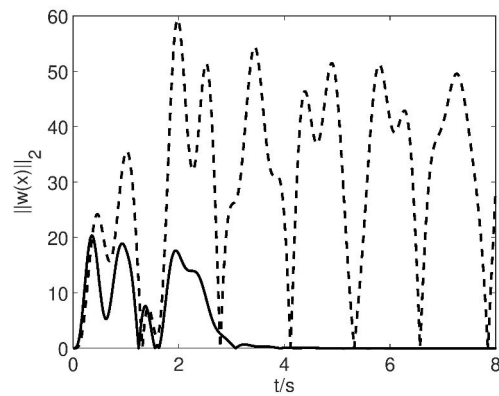

Figure 4.7: L_2-norm of the displacement $w(x, t)$ for pure trolley position control (dotted black) and discrepancy based control (black) [43]

4.3   Control of an agglomeration process

As has been shown in previous contributions [47, 48, 49], discrepancies based on moments of the particle size distributions are often an appropriate choice for particulate processes. Thus, for the agglomeration process presented in section 2.3 the deviation in the total number of particles and thus the difference between the desired and achieved zeroth moment is chosen.

$$e = \Delta\mu_0 = \int_0^\infty (n_d - n)\mathrm{d}v \tag{4.22}$$

Here, n_d is the desired steady state particle volume distribution. The resulting discrepancy and candidate control Lyapunov functional then are

$$V = \rho = \frac{1}{2}e^2. \tag{4.23}$$

To derive the associated discrepancy based control law, the first order time derivative of the Lyapunov functional along the system trajectories is calculated.

$$\dot{V} = e\dot{e} \tag{4.24}$$

$$= -e\int_0^\infty \frac{\partial n}{\partial t}dv \tag{4.25}$$

$$= -e\left(\int_0^\infty \dot{n}_\mathrm{a} + \dot{n}_\mathrm{f}\,dv - K\int_0^\infty Tndv\right) \tag{4.26}$$

From a practical point of view, the withdrawal rate K can be relatively easy adjusted and can hence be used as a control handle for the given configuration. To achieve exponential convergence of the Lyapunov functional the control law for K is chosen as follows

$$K = \frac{1}{\int_0^\infty Tndv}\left(-ce + \int_0^\infty \dot{n}_\mathrm{a} + \dot{n}_\mathrm{f}\,dv\right), \tag{4.27}$$

where $c \geq 0$ is a tuning factor determining the convergence rate. By design the proposed control law achieves exponential convergence of the Lyapunov functional V.

$$\dot{V} = -2cV \tag{4.28}$$

The responses for an initial deviation from a desired steady-state distribution n_d applying the proposed discrepancy based control law are shown in Fig. 4.8 and Fig. 4.9. Here, Fig. 4.8 (left) depicts the convergence of the zeroth moment μ_0 (dotted black) towards its desired steady-state value (gray). The convergence of the first moment μ_1 and the L_2 of the overall deviation between the desired and real particle size distribution $\|n - n_d\|_2$ are shown in Fig. 4.8 (right) and Fig. 4.9 (right), respectively. Although not a priori guaranteed by design, the closed-loop system achieves convergence in terms of the L_2-norm. The associated control action, i.e. the withdrawal rate K, is shown in Fig. 4.9 (left).
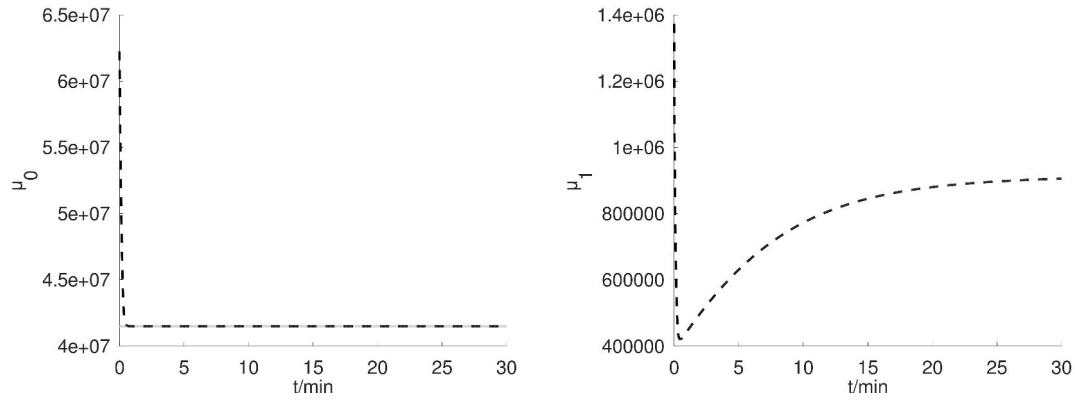
Figure 4.8: Closed-loop response of the zeroth and first moment of the particle size distribution μ_0 (left) and μ_1 (right)
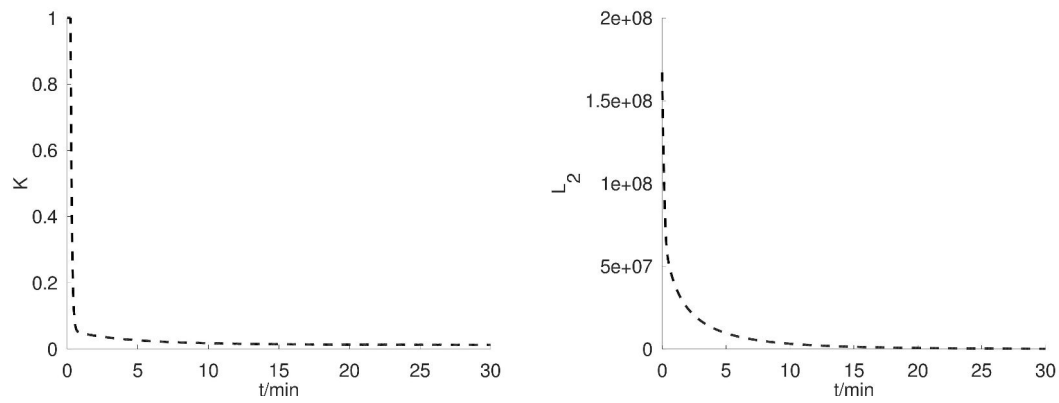

Figure 4.9: Closed-loop withdrawal rate K (left) and L_2-norm of the error in the particle size distribution $\|n - n_d\|_2$

Chapter 5

Extensions

So far the described discrepancy based control approach assumes a known plant model, which perfectly fits the process at hand. For practical applications this is in general not true. Plant parameters may be unknown or vary over time. Also, measurement noise and unstructured uncertainties may have a considerable effect on the closed loop behavior. Therefore, in practical control implementations robustness of stability and performance in the presence of process uncertainties is an important feature.

From a control point of view, two options exist to further improve on the control inherent robustness properties: adaptive and robust control. In adaptive control theory [38, 39] it is assumed that certain process parameters are unknown or slowly varying over time. The adaptive controller then adjusts during its operation to these parameters. Conversely, in robust control theory [40, 41] one fixed controller is designed, which is able to cope with a certain range of structured and unstructured uncertainties.

In the following, two well-known approaches, Lyapunov redesign and sliding mode control, are applied to extend the proposed discrepancy based control schemes. The main steps are illustrated using the agglomeration process described in section 2.3.

5.1   Adaptive discrepancy based agglomeration control

For the given agglomeration process the feed rate N_f is a typical parametric uncertainty, which may vary over time. As can be seen from (4.27) the proposed discrepancy based control law directly depends on the feed rate. Hence, a misfit in N_f will have a direct impact on the control loop.

One option to compensate for this would be to augmented the control loop with a parameter estimator for the feed rate and use its estimate in the control law. This, however, may cause problems regarding overall process stability and has typically implications on the required controller robustness. Here, Lyapunov redesign is an appealing alternative, as it does not impose additional requirements and by design guarantees overall closed-loop stability. Therefore, the original Lyapunov functional (4.23) is augmented with a term reflecting the estimation error $\tilde{N}_\mathrm{f} = \hat{N}_\mathrm{f} - N_\mathrm{f}$, where N_f is the true but unknown feed rate, $\hat{N}_\mathrm{f}$ its estimate and γ a positive constant.

$$V = \frac{1}{2}e^2 + \frac{1}{2\gamma}\tilde{N}_\mathrm{f}^2 \tag{5.1}$$

Calculating the time derivative of the augmented Lyapunov functional under the assumption that the true feed rate N_f is constant, yields

$$\dot{V} = e\dot{e} + \frac{1}{\gamma}\tilde{N}_f\dot{\hat{N}}_f, \tag{5.2}$$

$$= -e\left(\int_0^\infty \dot{n}_a + N_f\, q_{0,f}\, dv - K\int_0^\infty Tn dv\right) + \frac{1}{\gamma}\tilde{N}_f\dot{\hat{N}}_f. \tag{5.3}$$

As the feed rate N_f in the proposed discrepancy based control law (4.27) is unknown it is substituted with its estimate $\hat{N}_f$, resulting in the certainty equivalence control law.

$$K = \frac{1}{\int_0^\infty Tn dv}\left(-ce + \int_0^\infty \dot{n}_a + \hat{N}_f\, q_{0,f}\, dv\right) \tag{5.4}$$

The certainty equivalence control law can then be inserted into the above equation for the time derivative of the Lyapunov functional (5.3) resulting in:

$$\dot{V} = -ce^2 + \tilde{N}_f\left(e + \frac{1}{\gamma}\dot{\hat{N}}_f\right). \tag{5.5}$$

Here, the error in the feed rate estimate results in an additional term of indefinite sign $\tilde{N}_f e$, which may result in a loss of stability. To compensate for this problem the parameter update law $\dot{\hat{N}}_f$ has to be chosen appropriately

$$\dot{\hat{N}}_f = -\gamma e, \tag{5.6}$$

where the constant γ can be seen as a tuning factor to influence rate of change of the parameter estimate. From a practical point of view, a higher value will result in faster adaptations, while increasing sensitivity to disturbances, e.g. measurement noise. As for the non-adaptive discrepancy based control, the proposed certainty equivalence law (5.4) in combination with the parameter update law (5.6), results in exponential convergence of the Lyapunov functional.

$$\dot{V} = -ce^2 \tag{5.7}$$

In the following, an initial parametric uncertainty in the feed rate N_f of 50% will be assumed. As can be seen in Fig. 5.1 (left) after an initial deviation the zeroth moment is controlled to its set-point value. As this different feed rate results in a change of the steady-state particle size distribution, the first moment settles to a new value as shown in Fig. 5.1 (right). The applied withdrawal rate K and estimate for the feed rate $\hat{N}_f$ are shown in Fig. 5.2 (left) and (right), respectively. It should be mentioned, that in general accordingly designed update laws (5.6) do not guarantee convergence of the parameter estimate to the true unknown value. However, for the given configuration convergence can be proven using LaSalle's invariance principle [52].
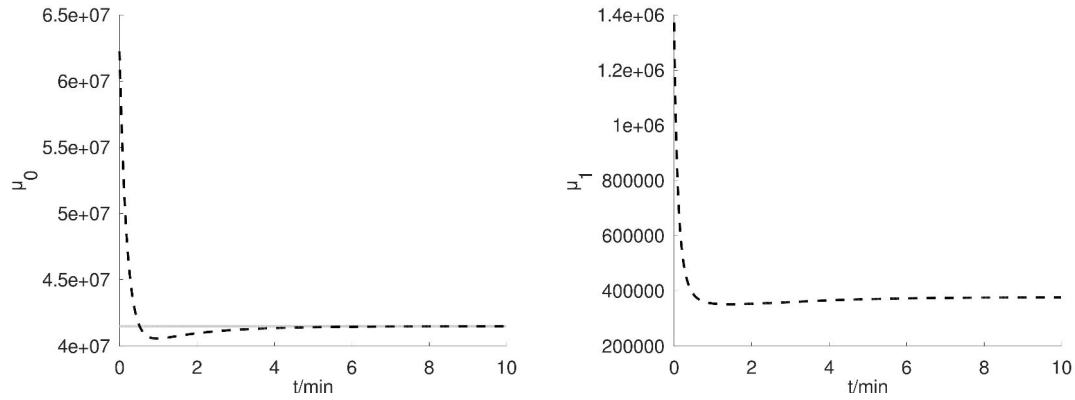
Figure 5.1: Closed-loop response of the zeroth moment μ_0 (left dotted black), its desired value $\mu_{0,d}$ (left gray) and the first moment μ_1 (right) of the particle size distribution
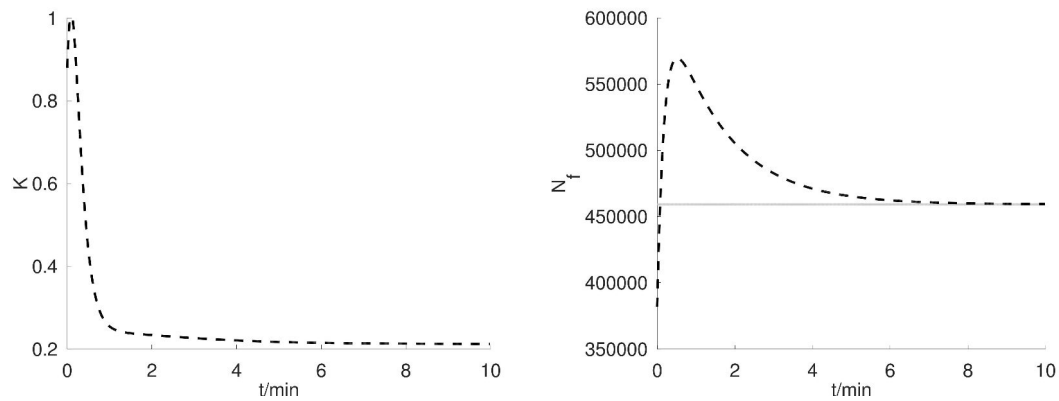

Figure 5.2: Closed-loop withdrawal rate K (left), unknown feed rate N_f (right gray) and its estimate $\hat{N}_\mathrm{f}$ (right dotted black)

5.2   Sliding-mode control

Sliding-mode control is well known for its robustness with respect to matched uncertainties. This is in particular due to its switching control law, which allows to dominate over bounded uncertainties occurring in the design equation. In the following, it will be assumed that the withdrawal rate K is positive and limited from above

$$K \in [0, K_{max}], \tag{5.8}$$

where K_{max} is a certain maximum withdrawal rate. In addition, as agglomeration preserves volume and the feed rate is always positive the following inequality holds.

$$\int_0^\infty \dot{n}_{\mathrm{a}} + \dot{n}_{\mathrm{f}}\, dv \geq 0 \tag{5.9}$$

To design an appropriate discrepancy based sliding mode controller, the same candidate control Lyapunov functional (4.23) as above will be used. Its time derivative along the system trajectory then yields:

$$\dot{V} = -e\left(\int_0^\infty \dot{n}_{\mathrm{a}} + \dot{n}_{\mathrm{f}}\, dv - K\int_0^\infty Tn\, dv\right). \tag{5.10}$$

To achieve $\dot{V} \leq 0$ two cases for the error e have to be studied. If $e > 0$ then due to inequality (5.9) the withdrawal rate K should be equal to zero, resulting in

$$\dot{V} = -e\left(\int_0^\infty \dot{n}_{\mathrm{a}} + \dot{n}_{\mathrm{f}}\, dv\right) \leq 0. \tag{5.11}$$

If $e < 0$ then the withdrawal rate K should be equal to its maximum value K_{max}. Under the assumption that the maximum withdrawal rate and the volume of the product fraction are sufficiently large, such that

$$\int_0^\infty \dot{n}_{\mathrm{a}} + \dot{n}_{\mathrm{f}}\, dv \leq K_{max}\int_0^\infty Tn\, dv, \tag{5.12}$$

holds, this choice yields

$$\dot{V} = -e\left(\int_0^\infty \dot{n}_{\mathrm{a}} + \dot{n}_{\mathrm{f}}\, dv - K_{max}\int_0^\infty Tn\, dv\right) \leq 0. \tag{5.13}$$

The resulting sliding mode control law hence is

$$K = \begin{cases} 0 & \text{if } e \geq 0, \\ K_{\mathrm{max}} & \text{if } e < 0. \end{cases} \tag{5.14}$$

As it achieves the required negative definiteness of the time derivative of the Lyapunov functional, i.e. $\dot{V} \leq 0$, the proposed controller stabilizes the process with respect to the chosen discrepancy. A major advantage of the proposed discrepancy based sliding mode control law, is its robustness to matched uncertainties, i.e. uncertainties occurring in (5.13). Here, negative definiteness is guaranteed for arbitrary uncertainties in the

agglomeration term $\dot{n}_a$, the feed $\dot{n}_f$ or the separation function T as long as inequality (5.12) holds.

To compare the proposed discrepancy based sliding mode controller with the adaptive discrepancy based controller proposed in section 5.1 a 50% disturbance in the feed rate and initial state deviation is assumed. As depicted in Fig. 5.3 (left) both controllers achieve convergences of the zeroth moment μ_0 and the first moment μ_1 (Fig. 5.3 right). The sliding mode controller however has a better performance.
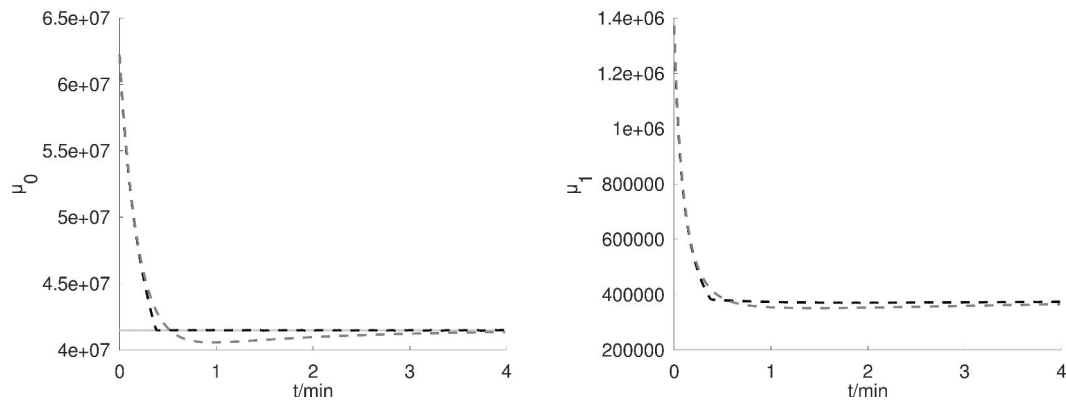

Figure 5.3: Convergence of the zeroth moment μ_0 (left) and first moment μ_1 (right) applying adaptive discrepancy based control (dotted gray) and sliding mode control (dotted black)

Chapter 6

Zero dynamics and control induced instabilities

For linear finite-dimensional systems it is well-known that open-loop zeros in the complex right half-plane pose bounds on the maximum open-loop gain. This is due to the fact, that they serve as attractors for closed-loop poles for increasing gains. In the case of nonlinear systems the situation is comparable although the analysis is less obvious [24]. Here, part of the system dynamics can be rendered unobservable, when applying a nonlinear compensating control law. This can be easily seen for the following affine nonlinear single-input single-output system of order n.

$$\dot{x} = f(x) + g(x)u \tag{6.1}$$
$$y = h(x) \tag{6.2}$$

Based on the output y and its derivatives two new state vectors ξ and η can be introduced

$$\xi = [y, \ldots, y^{(r-1)}]^T, \tag{6.3}$$
$$\eta = [y^{(r)}, \ldots, y^{(n-1)}]^T, \tag{6.4}$$

where r, the relative degree, is the first index for which the Lie derivative $L_g L_f^{r-1} h(x)$ does not vanish, i.e. $L_g L_f^{r-1} h(x) \neq 0$ and $L_g L_f^{k-1} h(x) = 0$ for $k < r$. The system (6.1)-(6.2) can then be represented as follows:

$$\dot{\xi} = \begin{pmatrix} 0 & 1 & 0 & \ldots & 0 \\ 0 & 0 & 1 & \ldots & 0 \\ \vdots & \vdots & \vdots & \ddots & \vdots \\ 0 & 0 & 0 & \ldots & 1 \\ 0 & 0 & 0 & \ldots & 0 \end{pmatrix} \xi + \begin{pmatrix} 0 \\ 0 \\ \vdots \\ 1 \end{pmatrix} (L_f^r h(x) + L_g L_f^{r-1} h(x)u), \tag{6.5}$$
$$\dot{\eta} = l(\xi, \eta). \tag{6.6}$$

In this representation, the first part can be linearized using the following compensating control law

$$u = -(L_g L_f^{r-1} h(x))^{-1}(L_f^r h(x) + v(\xi), \tag{6.7}$$

where an appropriate choice of $v(\xi)$ guarantees stability of (6.5). In contrast, the second subsystem associated with the states η, called the internal dynamics or zero dynamics for

$y = 0$, is rendered unobservable from the output y by the control law (6.7). Furthermore, as stability of the internal dynamics is not guaranteed, it has to be checked to achieve stability of the whole system.

From linear control theory, it is well-known that plant transmission zeros are invariant with respect to feedback. Thus, unstable internal dynamics pose important restrictions on control. To overcome this problem the application of parallel compensation has been proposed in [42, 49, 54, 55, 56].

The described occurrence of the internal dynamics and the associated stability problems, may not be as obvious in practical applications and cause serious and surprising problems. To illustrate this problem, an important configuration of a continuous fluidized bed spray granulation process is studied. Here, applying a particle sieving, only particles in the desired size range are removed from the process. Small particles $\dot{n}_{fine}$ are fed back to the process chamber directly. Large particles $\dot{n}_{oversize}$ are milled to smaller sizes before being fed to the process chamber. To achieve a constant bed mass this configuration is in general operated using a bed mass controller. The process scheme is shown in Fig. 6.1.
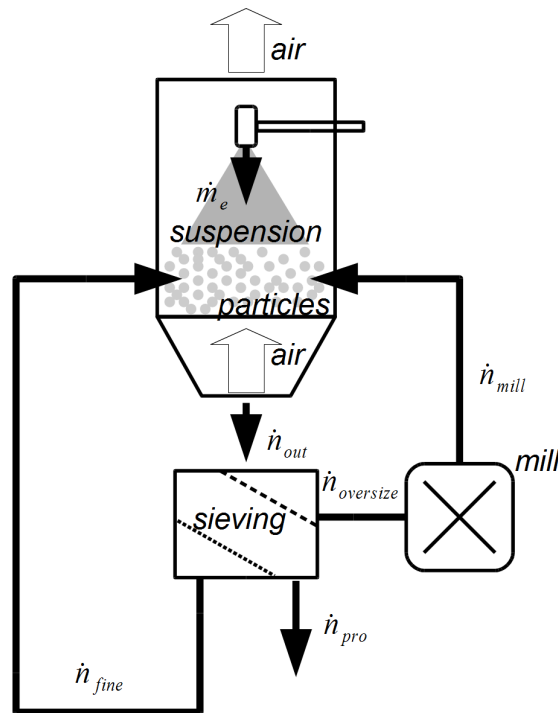

Figure 6.1: Continuous fluidized bed spray granulation process

As has been observed in practice and in the research literature, e.g. [20, 45], this configuration tends to a loss of stability for certain operating conditions. The instability is connected to the occurrence of a stable limit cycle and self-sustained oscillations of the particle size distribution. Results of a one-parameter bifurcation diagram are shown in Fig. 6.2 (right). The instability occurs for a milling diameters less then $0.72mm$.

Interestingly, as has been shown in [50], the open-loop system, i.e. the granulation without a mass controller, is stable over a certain range of operating conditions. This can be seen from the one-parameter bifurcation in Fig. 6.2 (left) and the maximum real part of the open-loop system poles depicted in Fig. 6.3 (left) or the variation of the dominant pole pair shown in Fig. 6.3 (right).

The reason for the observed loss of stability in closed-loop operation lies in the loss of stability of the zero dynamics. This can also be seen from the occurrence of zeros in the complex right half-plane depicted in Fig. 6.3 (right). As shown in Fig. 6.3 (left) the maximum real part of the open-loop zeros crosses zero and remains positive for milling grades smaller than $0.72mm$.
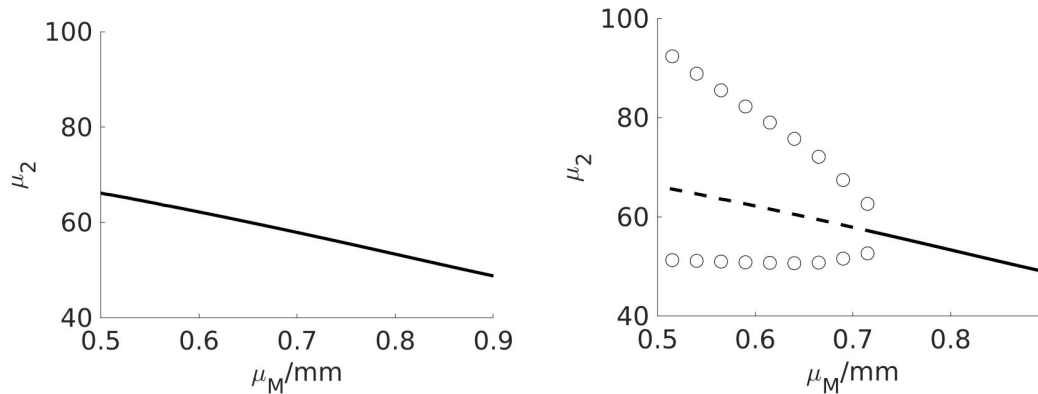

Figure 6.2: One-parameter bifurcation of the granulation process without (left) and with bed mass controller (right). μ_2 of the steady-state particle size distribution - stable (solid black), unstable (dashed black). (o) maximum and minimum value of the occurring limit cycle.
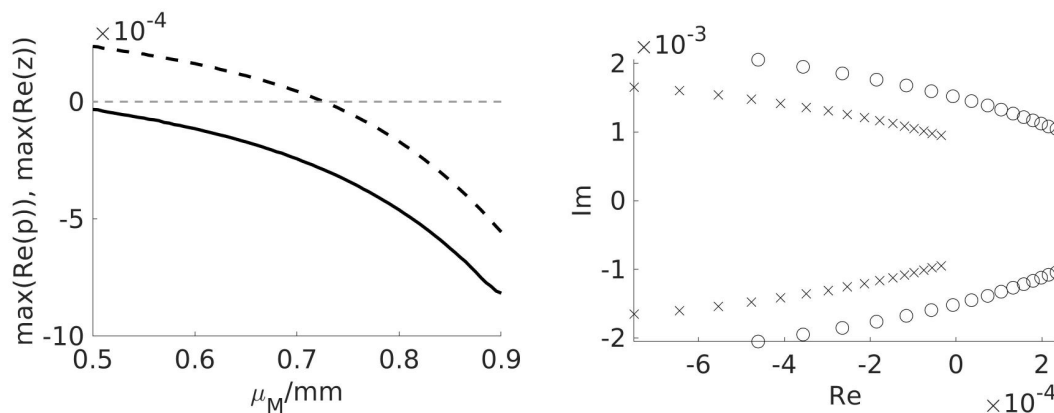

Figure 6.3: Maximum real part of the open-loop poles (solid black) and zeros (dashed black) (left). Location of the dominant pole and zero pair for increasing mill grade (right).

Therefore, for small mill grades and sufficiently high gains in the mass controllers, ignoring the internal dynamics will result in a destabilization of the internal dynamics. Interestingly, these instabilities may be unobservable from the controlled variable (Fig. 6.4 (left)), as the action of the mass controller leads to their compensation. Instead they can be observed in the control actuation itself (Fig. 6.4 (right)).
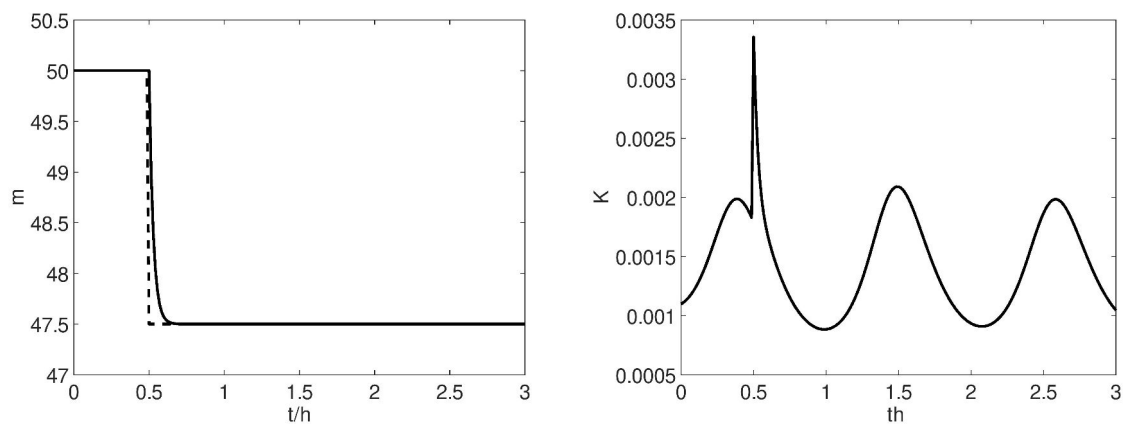
Figure 6.4: Step response for a mass controller at mill grade $\mu_M = 0.7mm$, desired mass m_d (dotted black), mass in the process chamber (solid black) (left) actuated variable, i.e withdrawal rate K (right)

Bibliography

Foreign references

[1] J. L. Lions, Optimal control of systems governed by Partial differential equations, Springer, New York, 1971.

[2] A. Balogh & M. Krstic, Infinite-dimensional backstepping-style feedback transformations for a heat equation with an arbitrary level of instability, European Journal of Control 8, 2002, pp. 165-177.

[3] P. D. Christofides, Nonlinear and robust control of PDE systems: methods and applications to transport-reaction processes, Birkhäuser, 2000.

[4] M. Krstic & A. Smyshlyaev, Adaptive boundary control for unstable parabolic PDEs - Part I: Lyapunov design, IEEE Transactions on Automatic Control 53, 2008, pp. 1575-1591.

[5] R. Vazquez & M. Krstic, Control of 1-D parabolic PDEs with Volterra nonlinearities, Part I: Design, Automatica, 44, 2008, pp. 2778-2790.

[6] R. Vazquez & M. Krstic, Control of 1-D parabolic PDEs with Volterra nonlinearities, Part II: Analysis, Automatica, 44, 2008, pp. 2791-2803.

[7] A. Schaum & T. Meurer, Dissipativity-based output-feedback control for a class of semilinear unstable heat equations, Joint 8th IFAC Symposium on Mechatronic Systems and 11th IFAC Symposium on Nonlinear Control Systems, Vienna (AT), 2019, in IFAC-PapersOnLine 52(16), p. 316-321.

[8] B. Jacob & K. A. Morris & H. Zwart, Zero dynamics for networks of waves, Automatica, 103, 2019, pp. 310-321.

[9] T. Reis & T. Selig, Zero dynamics and root locus for a boundary controlled heat equation, Mathematics of Control, Signals and Systems, 27, 2015, pp. 347-373.

[10] H. Franco-de los Reyes & A. Schaum & T. Meurer & J. Alvarez, Passivity-based output-feedback control for a class of 1-D semilinear PDE models, 16th International Conference on Electrical Engineering, Computing Science and Automatic Control (CCE), 2019.

[11] A. Ilchmann & T. Selig & C. Trunk, The Byrnes-Isidori form for infinite-dimensional systems, SIAM Journal on Control and Optimization, 54, 2016, 1504-1534.

[12] T. Kharkovskaia & D. Efimov & E. Fridman & A. Polyakov & J.-P. Richard, Interval observer design and control of uncertain non-homogeneous heat equations, Automatica, 111, 2020, 108595.

[13] N. Zrnić & Z. Petković & S. Bošnjak, Automation of ship-to-shore container cranes: A review of state-of-the-art, FME Transactions, 33, 2005, pp. 111-121.

[14] N. Zrnić & D. Oguamanam & S. Bošnjak, Dynamics and modelling of mega quayside container cranes, FME Transactions, 34, 2006, pp. 193-198.

[15] A. Recktenwald, Aktiver Schwingungsdämpfer für Krane. In 19. Internationale Kranfachtagung 2011: Der Kran und sein Umfeld in Industrie und Logistik, 2011, pp. 143-146.

[16] H.M. Hulburt & S. Katz, Some problems in particle technology: A statistical mechanical formulation, Chemical Engineering Science 19, pp. 555-574.

[17] M. Peglow & J. Kumar & R. Hampel & E. Tsotsas & S. Heinrich, Towards a complete population balance model for fluidized-bed spray agglomeration, Drying Technology, 25, 2007, pp. 1321-1329.

[18] D. Ramkrishna. The Status of Population Balances. Reviews in Chemical Engineering, 1985, pp. 49-95.

[19] D. Ramkrishna, Population Balances - Theory and Applications to Particulate Systems Engineering, Academic Press, San Diego, CA, 2000.

[20] R. Radichkov, T. Müller, A. Kienle, S. Heinrich, M. Peglow, L. Mörl, A numerical bifurcation analysis of continuous fluidized bed spray granulation with external product classification, Chem. Eng. and Proc., 45, 2006, pp. 826-837.

[21] A.A. Movchan, Stability of processes with respect to two metrics, Journal of Applied Mathematics and Mechanics, 1960, 24, pp. 1506-1524.

[22] A. Martynjuk & R. Gutovski, Integral inequalities and stability of motion, Izdatel'stvo Naukova Dumka, Kiev, 1979.

[23] T. Sirasetdinov, Stability of systems with distributed parameters, Izdatel'stvo Nauka, Novosibirsk, 1987.

[24] A. Isidori, The zero dynamics of a nonlinear system: From the origin to the latest progresses of a long successful story, European Journal of Control, 19, 2013, pp. 369-378.

[25] S. Waldherr & M. Zeitz, Conditions for the existence of a flat input, Internat. J. Control, 81, 2008, pp. 439–443.

[26] S. Waldherr & M. Zeitz, Flat inputs in the MIMO case, 8th IFAC Symposium on Nonlinear Control Systems - NOLCOS 2010 (Bologna), 2010.

[27] F. Nicolau & W. Respondek & J.-P. Barbot, Flat Inputs: Theory and Applications, SIAM Journal on Control and Optimization, 58, 2020, pp. 3293–3321.

[28] H. Schwarz, Changing the unstable zero dynamics of nonlinear systems via parallel compensation, Int. Conf. on Control, 1996.

[29] B. Augner and B. Jacob, Stability and stabilization of infinitedimensional linear port-Hamiltonian systems, Evolution Equations and Control Theory, vol. 3, no. 2, pp. 207–229, 2014.

[30] A. Macchelli, Y. L. Gorrec, H. Ramirez, and H. Zwart, On the synthesis of boundary control laws for distributed parameter port-Hamiltonian systems, IEEE Trans. Automat. Control, vol. 62, no. 4, pp. 1700–1713, 2017.

[31] J. Humaloja & L. Paunonen, Robust Regulation of Infinite-Dimensional Port-Hamiltonian Systems, IEEE Transactions on Automatic Control, 63, 2018, pp. 1480-1486.

[32] S. Koga & M. Krstic & J. Beaman, Laser sintering control for metal additive manufacturing by PDE backstepping, IEEE Transactions on control systems technology, vol. 28, no. 5, pp. 1928-1939, 2020.

[33] G. Freudenthaler & T. Meurer, PDE-based multi-agent formation control using flatness and backstepping: analysis, design and robot experiments, Automatica, 115, 108897, 2020.

[34] T. Meurer, Motion planning for PDEs, in: Encyclopedia of Systems and Control, Baillieul J., Samad T. (eds), Springer, London, 2. edition, 2020.

[35] J. Ng & S.Dubljevic, Optimal boundary control of a diffusion–convection-reaction PDE model with time-dependent spatial domain: Czochralski crystal growth process, Chemical Engineering Science, 67, pp. 111-119, 2012.

[36] X. Xu & S. Dubljevic, Optimal tracking control for a class of boundary controlled linear coupled hyperbolic PDE systems: Application to plug flow reactor with temperature output feedback, European Journal of Control, 39, pp. 21–34, 2018.

[37] I. Aksikas, Duality-based optimal compensator for boundary control hyperbolic PDEs system: Application to a tubular cracking reactor, Journal of the Franklin Institute, 357, pp. 9692-9708, 2020.

[38] K. S. Narendra & A. M. Annaswamy, Stable adaptive systems, Prentice Hall, 1989.

[39] M. Krstic & I. Kanellakopoulos & P. Kokotovic, Nonlinear and adaptive control design, John Wiley and Sons, 1995.

[40] K. Zhou & J. C. Doyle, Essentials of robust control, Prentice Hall, 1999.

[41] G. E. Dullerud & F. Paganini, A course in robust control theory: a convex approach, Springer, 2000.

Own references

[42] S. Palis, Control of fluidized bed spray granulation processes, Doctoral thesis, 2012.

[43] I. Golovin & S. Palis, Modeling and discrepancy based control of underactuated large gantry cranes, IFAC 2020 World Congress - IFAC 2020 (Berlin), 2020.

[44] I. Golovin & S. Palis, Robust control for active damping of elastic gantry crane vibrations, Mechanical Systems and Signal Processing, 121, 2019, pp. 264-278.

[45] C. Neugebauer & E. Diez & A. Bück & S.Palis & S. Heinrich & A. Kienle, On the dynamics and control of continuous fluidized bed layering granulation with screen-mill-cycle, Powder Technology, 354, 2019, pp. 765-778.

[46] S. Palis & A. Kienle, Discrepancy-based control of a heat equation with quadratic nonlinearity, American Control Conference - ACC (Portland), 2014.

[47] S. Palis & A. Kienle, Stabilization of continuous fluidized bed spray granulation - a Lyapunov approach, 8th IFAC Symposium on Nonlinear Control Systems - NOLCOS (Bologna), 2010.

[48] S. Palis & A. Kienle, Discrepancy based control of continuous fluidized bed spray granulation with internal product classification, 8th IFAC International Symposium on Advanced Control of Chemical Processes - ADCHEM (Singapore), 2012, pp. 756-761.

[49] S. Palis & A. Kienle, Discrepancy based control of particulate processes, Journal of Process Control 24, 2014, pp. 33-46.

[50] S. Palis, Control induced instabilities in fluidized bed spray granulation, Journal of Process Control, 93, 2020, pp. 97-104.

[51] I. Golovin & E. Otto & R. Dürr & S. Palis & A. Kienle, Lyapunov-based online parameter estimation in continuous fluidized bed spray agglomeration processes, 12th IFAC Symposium on Dynamics and Control of Process Systems - DYCOPS 2019 (Florianopolis), 2019.

[52] E. Otto & S. Palis & A. Kienle, Nonlinear Control of Continuous Fluidized Bed Spray Agglomeration Processes, in: Stabilization of Distributed Parameter Systems: Design Methods and Applications, G. Sklyar & A. Zuyev (eds), Springer, 2021.

[53] C. Neugebauer & E. Diez & L. Mielke & S. Palis & A. Bück & E. Tsotsas & A. Kienle & S. Heinrich, Dynamics of Spray Granulation in Continuously Operated Horizontal Fluidized Beds, Dynamic Flowsheet Simulation of Solids Processes, Springer, 2020, pp. 67-107, 2020.

[54] I. Golovin & S. Palis & A. Timoschenko & V. Klepikov, Damping of friction-induced vibrations applying parallel compensator, Advanced Problems of Mechanics - APM (St. Petersburg), 2016.

[55] I. Golovin & S. Palis, Design of parallel feed-forward compensator and its application to electromechanical system with friction load, IFAC 2017 World Congress - IFAC2017 (Toulouse), 2017.

[56] K. Röbenack & S. Palis, On the control of non-minimum phase systems using a parallel compensator, 23rd International Conference on System Theory, Control and Computing - ICSTCC (Sinaia), 2019.

Own publications from 2013-2021

Journal contributions

[1] S. Palis, Control induced instabilities in fluidized bed spray granulation, Journal of Process Control, 93, 2020, pp. 97-104.

[2] M. Kutia & N. Mukhin & H. Petrova & A. Oseev & L. Bakhchova & M.-P. Schmidt & A. Aman & S. Palis & S. Tarasov & S. Hirsch, Sensor for the evaluation of dielectric properties of sulphurcontaining heteroatomic hydrocarbon compounds in petroleum based liquids at a microfluidic scale, AIP Advances, 10(2), 2020.

[3] A. Fomin & V. Koshuro & A. Shumilin & A. Voyko & P. Palkanov & A. Aman & N. Mukhin & S. Palis, Induction heat treatment of steel punches with Zr-containing coatings and preliminary results of FLD characteristics when drawing C45 carbon steel, Journal of Physics: Conference Series, 1410, 2019.

[4] M. Silaev & D. Dvorkin & V. Tulskii & S. Palis & I. Kartashev, Intermittent Current Unsymmetry in an Electric Grid and Its Assessment for Busbars of Traction Substations, Russian Electrical Engineering, 90, 2019, pp. 66-72.

[5] N. Mukhin & M. Kutia & A. Oseev & U. Steinmann & S. Palis & R. Lucklum, Narrow Band Solid-Liquid Composite Arrangements: Alternative Solutions for Phononic Crystal-Based Liquid Sensors, Sensors 2019, 19(17), 3743.

[6] C. Neugebauer & E. Diez & A. Bück & S.Palis & S. Heinrich & A. Kienle, On the dynamics and control of continuous fluidized bed layering granulation with screen-mill-cycle, Powder Technology, 354, 2019, pp. 765-778.

[7] I. Golovin & S. Palis, Robust control for active damping of elastic gantry crane vibrations, Mechanical Systems and Signal Processing 121, 2019, pp. 264-278.

[8] I. Golovin & G. Strenzke & R. Dürr & S. Palis & A. Bück & E. Tsotsas & A. Kienle, Parameter identification for continuous fluidized bed spray agglomeration, Processes, 2018, pp. 1-14.

[9] C. Neugebauer & A. Bück & S. Palis & L. Mielke & E. Tsotsas & A. Kienle, Influence of thermal conditions on particle properties in fluidized bed layering granulation, Processes, 2018, pp. 1-17.

[10] M. Silaev & D. Dvorkin & V. Tulsky & S. Palis & I. Kartashev, Investigation of intermittent current unbalance occurrence in electrical grid and its calculation on the railway substation buses, Russian Electrical Engineering 10, 2018, pp. 66-17.

[11] S. Palis, Non-identifier-based adaptive control of continuous fluidized bed spray granulation, Journal of Process Control 71, 2018, pp. 46-51.

[12] D. Dvorkin & V. Tulsky & S. Palis, The Consumer Scoring Based on Their Impacts on the Voltage Imbalance, Elektrichestvo 8, 2018, pp. 18-23.

[13] B. Oleksyuk & V. Tulsky & S. Palis, Magnetically Controlled Shunt Reactors as Sources of Current and Voltage Harmonics, IEEE Transactions on Power Delivery 33, 2018, pp. 1818-1824.

[14] R. Geyyer & R. Dürr & E. Temmel & T. Li & H. Lorenz & S. Palis & A. Seidel-Morgenstern & A. Kienle, Control of Continuous Mixed-Solution Mixed-Product Removal Crystallization Processes, Chemical Engineering & Technology 40, 2017, pp. 1362-1369.

[15] D. Dvorkin & M. Silaev & V. Tulsky & S. Palis, Problems of the Estimation of the Consumer's Contribution to the Power Quality Distortion in the Point of Common Coupling, Elektrichestvo 7, 2017, pp. 12-19.

[16] A. Kienle & S. Palis & M. Mangold & R. Dürr, Modeling and simulation of particulate processes, Electronic Modeling 38, 2016, pp. 23-33.

[17] C. Neugebauer & S. Palis & A. Bück & E. Tsotsas & S. Heinrich & A. Kienle, A dynamic two-zone model of continuous fluidized bed layering granulation with internal product classification, Particuology 31, 2017, pp. 8-14.

[18] A. Bück & C. Neugebauer & K. Meyer & S. Palis & E. Diez & A. Kienle & S. Heinrich & E. Tsotsas, Influence of operation parameters on process stability in continuous fluidised bed layering with external product classification, Powder Technology 300, 2016, pp. 37-45.

[19] M. Kutia & M. Fyk & O. Kravchenko & S. Palis & I. Fyk, Improvement of technological-mathematical model for the medium-term prediction of the work of a gas condensate field, Eastern-European Journal of Enterprise Technologies 83, 2016, pp. 40-48.

[20] C. Dreyschultze & C. Neugebauer & S. Palis & A. Bück & E. Tsotsas & S. Heinrich & A. Kienle, Influence of zone formation on stability of continuous fluidized bed layering granulation with external product classification, Particuology 23, 2015, pp. 1-7.

[21] M. Mangold & L. Feng & D. Khlopov & S. Palis & P. Benner & D. Binev & A. Seidel-Morgenstern, Nonlinear model reduction of a continuous fluidized bed crystallizer, Journal of Computational and Applied Mathematics 289, 2015, pp. 253-266.

[22] A. Bück & S. Palis & E. Tsotsas, Model-based control of particle properties in fluidised bed spray granulation, Powder Technology 270, 2015, pp. 575-583.

[23] M. Mangold & D. Khlopov & G. Danker & S. Palis & V. Svjatnyj & A. Kienle, Development and nonlinear analysis of dynamic plant models in ProMoT/Diana, Chemie Ingenieur Technik 86, 2014, pp. 1107-1116.

[24] S. Palis & A. Kienle, Discrepancy based control of particulate processes, Journal of Process Control 24, 2014, pp. 33-46.

Book contributions

[25] E. Otto & S. Palis & A. Kienle, Nonlinear Control of Continuous Fluidized Bed Spray Agglomeration Processes, in: Stabilization of Distributed Parameter Systems: Design Methods and Applications, G. Sklyar & A. Zuyev (eds), Springer, 2021.

[26] C. Neugebauer & E. Diez & L. Mielke & S. Palis & A. Bück & E. Tsotsas & A. Kienle & S. Heinrich, Dynamics of Spray Granulation in Continuously Operated Horizontal Fluidized Beds, Dynamic Flowsheet Simulation of Solids Processes, Springer, ISBN 978-3-030-45167-7, 2020, pp. 67-107.

[27] S. Palis, Genetic algorithms for modeling and control of drying processes, Intelligent Control in Drying, CRC Press, ISBN 978-1-4987-3275-8, 2018, pp. 173-187.

Conference contributions

[28] A. Maksakov & S. Palis, Koopman-based optimal control of boost DC-DC converter, 25th IEEE International Conference on Problems of automated electric drive - PAEP 2020 (Kremenchuk), 2020.

[29] I. Golovin & A. Maksakov & S. Palis, Gantry crane position control via parallel feedforward compensator, 28th Mediterranean Conference on Control and Automation - MED 2020 (Saint-Raphael), 2020.

[30] C. Neugebauer & C. Seidel & S. Palis & A. Kienle, Robust control of fluidized bed layering granulation, IFAC 2020 World Congress - IFAC 2020 (Berlin), 2020.

[31] R. Dürr & C. Neugebauer & S. Palis & A. Bück & A. Kienle, Inferential control of product properties for fluidized bed spray granulation layering, IFAC 2020 World Congress - IFAC 2020 (Berlin), 2020.

[32] E. Otto & C. Neugebauer & S. Palis & A. Kienle, Lyapunov-based online parameter estimation for continuous fluidized bed layering granulation, IFAC 2020 World Congress - IFAC 2020 (Berlin), 2020.

[33] I. Golovin & S. Palis, Modeling and discrepancy based control of underactuated large gantry cranes, IFAC 2020 World Congress - IFAC 2020 (Berlin), 2020.

[34] K. Röbenack & S. Palis, On the control of non-minimum phase systems using a parallel compensator, 23rd International Conference on System Theory, Control and Computing - ICSTCC (Sinaia), 2019.

[35] S. Palis, Adaptive discrepancy based control of continuous fluidized bed spray granulation with external sieve-mill cycle, 3rd IFAC Workshop on Control of Systems Governed by Partial Differential Equation, XI Workshop Control of Distributed Parameter Systems - CPDE-CDPS 2019 (Oaxaca), 2019.

[36] I. Golovin & E. Otto & R. Dürr & S. Palis & A. Kienle, Lyapunov-based online parameter estimation in continuous fluidized bed spray agglomeration processes, 12th IFAC Symposium on Dynamics and Control of Process Systems - DYCOPS 2019 (Florianopolis), 2019.

[37] S. Palis, Control of Multi-Chamber Continuous Fluidized Bed Spray Granulation, 12th IFAC Symposium on Dynamics and Control of Process Systems - DYCOPS 2019 (Florianopolis), 2019.

[38] S. Palis & D. Palis, Optimierungsbasierte Steuerung für Krananlagen mit zusätzlichen Anschlagmittel, Internationale Kranfachtagung (Bochum), 2019.

[39] A. Fomin & V. Koshuro & A. Shumilin & A. Voyko & P. Palkanov & A. Aman & N. Mukhin & S. Palis, Induction heat treatment of steel punches with Zr-containing coatings and preliminary results of FLD characteristics when drawing C45 carbon steel, Journal of Physics: Conference Series (1410), 2019.

[40] D. Dvorkin & S. Palis & V. Tulsky & N. Novikov, On Problems of Balanced Load Identification at a Real Substation, 1st IEEE 2019 International Youth Conference on Radio Electronics, Electrical and Power Engineering - REEPE, 2019.

[41] K. Röbenack & S. Palis, Nonlinear control of flat systems using a non-flat output with dynamic extension, 22nd International Conference on System Theory, Control and Computing - ICSTCC (Sinaia), 2018.

[42] G. Strenzke & I. Golovin & M. Wegner & S. Palis & A. Bück & A. Kienle & E. Tsotsas, Influence of drying conditions on process properties and parameter identification for continuous

fluidized bed spray agglomeration, 21st International Drying Symposium - IDS (Valencia), 2018.

[43] C. Neugebauer & A. Bück & S. Palis & L. Mielke & E. Tsotsas & A. Kienle, Influence of thermal conditions on particle properties in fluidized bed layering granulation, 6th International Conference on Population Balance Modelling - PBM (Ghent), 2018.

[44] I. Golovin & G. Strenzke & M. Wegner & S. Palis & A. Bück & A. Kienle & E. Tsotsas, Parameter identification for continuous fluidized bed spray agglomeration, 6th International Conference on Population Balance Modelling - PBM (Ghent), 2018.

[45] M. Franke & K. Röbenack & R. Weiß & S. Palis, Control of a tower crane by means of algorithmic differentiation, 59th Ilmenau Scientific Colloquium - IWK (Ilmenau), 2017.

[46] S. Palis & A. Kienle, Online parameter identification for continuous fluidized bed spray granulation with external sieve-mill cycle, 22nd International Conference on Methods and Models in Automation and Robotics - MMAR (Miedzyzdroje), 2017.

[47] I. Golovin & S. Palis, Control-based damping of elastic gantry crane vibrations, 22nd International Conference on Methods and Models in Automation and Robotics - MMAR (Miedzyzdroje), 2017.

[48] I. Golovin & S. Palis, Design of parallel feed-forward compensator and its application to electromechanical system with friction load, IFAC 2017 World Congress - IFAC2017 (Toulouse), 2017.

[49] A. Bück & M. Schmidt & C. Neugebauer & S. Palis & A. Kienle & S. Heinrich & E. Tsotsas, Process dynamics of continuous fluidised bed layering granulation, Proc. 8th International Granulation Workshop (Sheffield), 2017.

[50] D. Dvorkin & S. Palis & M. Silaev & V. Tulsky, Balanced load identification based on the correlation of the phase currents, 58th International Scientific Conference on Power and Electrical Engineering of Riga Technical University - RTUCON (Riga), 2017.

[51] M. Franke & K. Röbenack & A. Wobar & R. Weiß & S. Palis, Simulation und Regelung eines Drehkrans mit Hilfe des algorithmischen Differenzierens, Mechatronik 2017 (Dresden), 2017.

[52] N. Förster & R. Leidhold & S. Palis, Maximisation of back EMF in a high performance PMSM machine with concentrated windings, 2016 IEEE International Power Electronics and Motion Control Conference - PEMC (Varna), 2016.

[53] D. Palis & S. Palis, Efficient Unit Commitment - A Modified Branch-and-Bound Approach, Technologies for Smart Nation - TENCON (Singapore), 2016.

[54] R. Geyyer & R. Dürr & E. Temmel & T. Li & H. Lorenz & S. Palis & A. Seidel-Morgenstern & A. Kienle, Control of MSMPR crystallization processes, 23th International Workshop on Industrial Crystallization - BIWIC (Magdeburg), 2016.

[55] I. Golovin & S. Palis & A. Timoschenko & V. Klepikov , Damping of friction-induced vibrations applying parallel compensator, Advanced Problems of Mechanics - APM (St. Petersburg), 2016.

[56] S. Palis & C. Neugebauer & A. Bück & S. Heinrich & E. Tsotsas & A. Kienle, Control of multichamber continuous fluidized bed spray granulation, PARTEC (Nürnberg), 2016.

[57] C. Neugebauer & S. Palis & A. Bück & S. Heinrich & E. Tsotsas & A. Kienle, Nonlinear dynamics of continuous fluidized bed layering granulation with internal product classification, PARTEC (Nürnberg), 2016.

[58] M. Wegner & C. Neugebauer & S. Palis & A. Bück, Analysis of the process behaviour of continuous fluidized bed agglomeration with external product classification, PARTEC (Nürnberg), 2016.

[59] E. Diez & S. Heinrich & K. Meyer & A. Bück & E. Tsotsas & C. Neugebauer & S. Palis & A. Kienle, Influence of drying conditions on particle properties in a multi-staged continuous fluidized bed spray granulation process, PARTEC (Nürnberg), 2016.

[60] A. Bück & M. Wegner & C. Neugebauer & S. Palis & E. Tsotsas: Bifurcation analysis of process stability of continuous fluidized bed agglomeration with external product classification, 26th European Symposium on Computer Aided Process Engineering (Portoroz), 2016.

[61] C. Neugebauer & S. Palis & A. Bück & E. Diez & S. Heinrich & E. Tsotsas & A. Kienle, Influence of mill configuration on stability of continuous fluidised bed layering granulation with external product classification, 26th European Symposium on Computer Aided Process Engineering (Portoroz), 2016.

[62] S. Palis, Adaptive discrepancy based control of particulate processes, 1st IFAC Conference on Modelling, Identification and Control of Nonlinear Systems - MICNON 2015 (Saint Petersburg), 2015.

[63] R. Geyyer & A. Kienle & S. Palis, Robust control of continuous crystallization processes, 1st IFAC Conference on Modelling, Identification and Control of Nonlinear Systems - MICNON 2015 (Saint Petersburg), 2015.

[64] S. Palis & A. Bück: Entropy-based control of continuous fluidized bed spray granulation processes, 5th IFAC Workshop on Lagrangian and Hamiltonian Methods for Non Linear Control (Lyon), 2015.

[65] A. Bück & C. Neugebauer & K. Meyer & S. Palis & E. Diez & A. Kienle & S. Heinrich & E. Tsotsas, Influence of process parameters on process stability in continuous fluidised bed layering with external classification, Proc. 7th International Granulation Workshop (Sheffield), 2015.

[66] K. Meyer & A. Bück & E. Tsotsas & S. Palis & A. Kienle & C. Neugebauer & S. Heinrich & E. Diez, Discrete estimation of particle dispersion at weirs in horizontal fluidised beds, 10th European Congress of Chemical Engineering (Nice), 2015.

[67] E. Diez & S. Heinrich & K. Meyer & A. Bück & E. Tsotsas & S. Palis & A. Kienle & C. Neugebauer, Investigation of the particle transport in a continuously operated horizontal fluidized bed by means of Discrete Particle Modelling, 10th European Congress of Chemical Engineering (Nice), 2015.

[68] S. Palis & C. Dreyschultze & A. Kienle, A methodology for experimental determination of stability boundaries with application to fluidized bed spray granulation, 24th European Symposium on Computer Aided Process Engineering - ESCAPE (Budapest), 2014.

[69] S. Palis & A. Kienle, Discrepancy-based control of a heat equation with quadratic nonlinearity, American Control Conference - ACC (Portland), 2014.

[70] S. Palis & C. Dreyschultze & C. Neugebauer & A. Kienle, Auto-tuning control systems for improved operation of continuous fluidized bed spray granulation processes with external product classification, Procedia Engineering 102, 2014, pp. 131-141.

[71] R. Dürr & S. Palis & A. Kienle, Online parameter identification of facet growth kinetics in crystal morphology population balance models, Procedia Engineering 102, 2014, pp. 1336-1345.

[72] S. Höme & S. Palis & C. Diedrich, Design of communication systems for networked control system running on PROFINET, 10th IEEE Workshop on Factory Communication Systems - WFCS (Toulouse), 2014.

[73] S. Palis & A. Bück & Achim Kienle, Discrepancy based control of systems of population balances, 1th IFAC Workshop on Control of Systems Modeled by Partial Differential Equations - CPDE (Paris), 2013.

[74] S. Palis & A. Kienle, Online parameter identification for continuous fluidized bed spray granulation, 5th International Conference on Population Balance Modelling - PBM (Bangalore), 2013.

[75] S. Palis & A. Bück & Achim Kienle, Adaptive discrepancy based control of continuous fluidized bed spray granulation with internal classification, 9th IFAC Symposium on Nonlinear Control Systems - NOLCOS (Toulouse), 2013.

[76] S. Palis & D. Binev & H. Lorenz & A. Seidel-Morgenstern & A. Kienle, Population balance modeling of crystallization in fluidized beds, 20th International Workshop on Industrial Crystallization - BIWIC (Odense), 2013.

[77] A. Bück & S. Palis & E. Tsotsas, Model-based control of particle properties in fluidised bed spray granulation, 6th International Granulation Workshop (Sheffield), 2013.

[78] S. Palis & O. Kopp & S. Höme & D. Palis, Development of control strategies for low voltage networks with high penetration level of distributed generation, Powertech (Grenoble), 2013.

[79] F. Palis & O. Tyshakin & S. Palis & D. Bazhutin, Strategie zur suboptimalen Steuerung von Drehkranen, Internationale Kranfachtagung (Bochum), 2013.

[80] S. Palis & S. Antonyuk & M. Dosta & S. Heinrich, Optimization-based estimation of agglomerate properties for microscale simulations from experiments, International Congress on Particle Technology - Partec (Nürnberg), 2013.

[81] S. Palis & S. Antonyuk & M. Dosta & S. Heinrich, Identification of micro parameters for discrete element simulation of agglomerates, 7th International Conference on Micromechanics of Granular Media - Powders and Grains (Sydney), 2013.

Part II

Selected publications

Control approaches of infinite-dimensional systems can be roughly divided into early and late lumping and direct design approaches. Here, early lumping approaches are based on a finite-dimensional system approximation in combination with a finite-dimensional control design. In own contributions early lumping has been investigated to control elastic crane structures [4, 15] and particulate processes, granulation [8] and crystallization [17]. The focus has been however on late lumping and direct control design approaches. Here, with except for the entropy-based control of a particular configuration of a granulation process [18], discrepancy-based control and its extensions have been investigated for various applications:

- unstable heat equation with quadratic nonlinearity [19],

- elastic crane structures [9],

- pellet coating [21],

- agglomeration [1],

- granulation [6, 3, 10, 12],

- crystallization [7, 16].

The proposed adaptive discrepancy-based control is especially promising for particulate processes, where the determination of process parameters and kinetics is challenging. As here parameter convergence cannot be assumed in general, additional estimation schemes based on optimization [5] and Lyapunov stability theory [11, 14, 20, 22] have been proposed.

Stability of the internal dynamics is a crucial property for discrepancy-based control approaches and should be ideally taken into account with an appropriate choice of the discrepancy. Otherwise, they can result in control induced stability problems [2], which are often hard to detect and analyze. A complementary approach to the choice of the discrepancy is the design of a parallel compensator, which stabilizes the internal dynamics. In the past, design methods have been limited to linear systems. The first promising results on a nonlinear parallel compensator design for a finite-dimensional system has been proposed in [13].

[1] E. Otto & S. Palis & A. Kienle, Nonlinear Control of Continuous Fluidized Bed Spray Agglomeration Processes, in: Stabilization of Distributed Parameter Systems: Design Methods and Applications, G. Sklyar & A. Zuyev (eds), Springer, 2021.

[2] S. Palis, Control induced instabilities in fluidized bed spray granulation, Journal of Process Control, 93, 2020, pp. 97-104.

[3] C. Neugebauer & E. Diez & A. Bück & S.Palis & S. Heinrich & A. Kienle, On the dynamics and control of continuous fluidized bed layering granulation with screen-mill-cycle, Powder Technology, 354, 2019, pp. 765-778.

[4] I. Golovin & S. Palis, Robust control for active damping of elastic gantry crane vibrations, Mechanical Systems and Signal Processing 121, 2019, pp. 264-278.

[5] I. Golovin & G. Strenzke & R. Dürr & S. Palis & A. Bück & E. Tsotsas & A. Kienle, Parameter identification for continuous fluidized bed spray agglomeration, Processes, 2018, pp. 1-14.

[6] S. Palis, Non-identifier-based adaptive control of continuous fluidized bed spray granulation, Journal of Process Control 71, 2018, pp. 46-51.

[7] R. Geyyer & R. Dürr & E. Temmel & T. Li & H. Lorenz & S. Palis & A. Seidel-Morgenstern & A. Kienle, Control of Continuous Mixed-Solution Mixed-Product Removal Crystallization Processes, Chemical Engineering & Technology 40, 2017, pp. 1362-1369.

[8] A. Bück & S. Palis & E. Tsotsas, Model-based control of particle properties in fluidised bed spray granulation, Powder Technology 270, 2015, pp. 575-583.

[9] I. Golovin & S. Palis, Modeling and discrepancy based control of underactuated large gantry cranes, IFAC 2020 World Congress - IFAC 2020 (Berlin), 2020.

[10] S. Palis, Adaptive discrepancy based control of continuous fluidized bed spray granulation with external sieve-mill cycle, 3rd IFAC Workshop on Control of Systems Governed by Partial Differential Equation, XI Workshop Control of Distributed Parameter Systems - CPDE-CDPS 2019 (Oaxaca), 2019.

[11] I. Golovin & E. Otto & R. Dürr & S. Palis & A. Kienle, Lyapunov-based online parameter estimation in continuous fluidized bed spray agglomeration processes, 12th IFAC Symposium on Dynamics and Control of Process Systems - DYCOPS 2019 (Florianopolis), 2019.

[12] S. Palis, Control of Multi-Chamber Continuous Fluidized Bed Spray Granulation, 12th IFAC Symposium on Dynamics and Control of Process Systems - DYCOPS 2019 (Florianopolis), 2019.

[13] K. Röbenack & S. Palis, On the control of non-minimum phase systems using a parallel compensator, 23rd International Conference on System Theory, Control and Computing - ICSTCC (Sinaia), 2019.

[14] S. Palis & A. Kienle, Online parameter identification for continuous fluidized bed spray granulation with external sieve-mill cycle, 22nd International Conference on Methods and Models in Automation and Robotics - MMAR (Miedzyzdroje), 2017.

50

[15] I. Golovin & S. Palis, Control-based damping of elastic gantry crane vibrations, 22nd International Conference on Methods and Models in Automation and Robotics - MMAR (Miedzyzdroje), 2017.

[16] S. Palis, Adaptive discrepancy based control of particulate processes, 1st IFAC Conference on Modelling, Identification and Control of Nonlinear Systems - MICNON 2015 (Saint Petersburg), 2015.

[17] R. Geyyer & A. Kienle & S. Palis, Robust control of continuous crystallization processes, 1st IFAC Conference on Modelling, Identification and Control of Nonlinear Systems - MICNON 2015 (Saint Petersburg), 2015.

[18] S. Palis & A. Bück: Entropy-based control of continuous fluidized bed spray granulation processes, 5th IFAC Workshop on Lagrangian and Hamiltonian Methods for Non Linear Control (Lyon), 2015.

[19] S. Palis & A. Kienle, Discrepancy-based control of a heat equation with quadratic nonlinearity, American Control Conference - ACC (Portland), 2014.

[20] R. Dürr & S. Palis & A. Kienle, Online parameter identification of facet growth kinetics in crystal morphology population balance models, Procedia Engineering 102, 2014, pp. 1336-1345.

[21] S. Palis & A. Bück & Achim Kienle, Discrepancy based control of systems of population balances, 1th IFAC Workshop on Control of Systems Modeled by Partial Differential Equations - CPDE (Paris), 2013.

[22] S. Palis & A. Kienle, Online parameter identification for continuous fluidized bed spray granulation, 5th International Conference on Population Balance Modelling - PBM (Bangalore), 2013.

Nonlinear Control of Continuous Fluidized Bed Spray Agglomeration Processes

Eric Otto, Stefan Palis, and Achim Kienle

Abstract Fluidized bed spray agglomeration is a complex particle formation process widely used in the agricultural, food, and pharmaceutical industry. It can described mathematically by population balance equations. This chapter deals with controlling the nonlinear partial integro-differential equation. Therefore, discrepancy based control, which guarantees exponential stability with respect to some generalized distance measure, is introduced. Conditions for convergence in a norm are discussed. Furthermore, robustness with respect to model uncertainties is shown.

1 Introduction

Fluidized bed spray agglomeration (FBSA) is an industrial particle formation process with the goal of producing particles with predefined properties. Hereby, two or more so-called primary particles are combined to form a new particle with different properties. For this purpose, a particle bed is fluidized within an upward air stream while a binder solution is sprayed into the process chamber wetting the particles. Due to particle collision and drying of the liquid layer, solid bridges between particles are formed. This process is depicted schematically in Fig. 1.

Important examples of products in particulate form are fertilizers in the agricultural industry, milk powder in the food industry, or medicals in the pharmaceutical

E. Otto
Otto von Guericke University Magdeburg, Magdeburg, Germany
e-mail: eric.otto@ovgu.de

S. Palis (✉)
Otto von Guericke University Magdeburg, Magdeburg, Germany

National Research University "Moscow Power Engineering Institute", Moscow, Russia
e-mail: stefan.palis@ovgu.de

A. Kienle
Otto von Guericke University Magdeburg, Max Planck Institute for Dynamics of Complex Technical Systems Magdeburg, Magdeburg, Germany
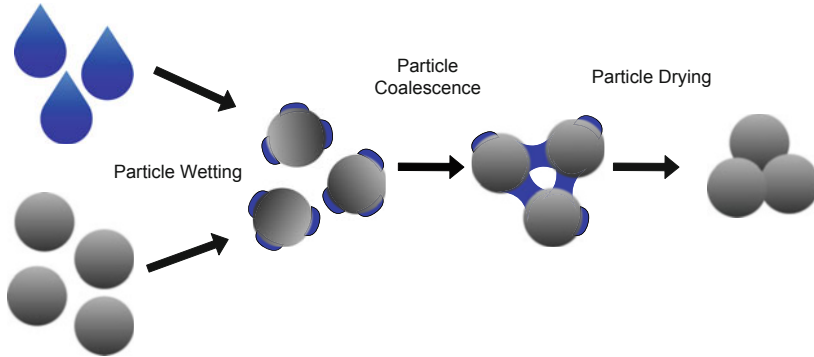
Fig. 1 Three stages of agglomeration: (a) particle wetting, (b) particle coalescence, and (c) particle drying

industry [1]. Particle properties such as size and shape, porosity, and flowability determine the quality of the product and its suitability in the subsequent processing. Model-based process control is one way to achieve a constant production rate on the one hand and the desired product quality on the other hand. Two factors are currently limiting the effective use of process control. Firstly appropriate process models capturing the important dynamics are hardly available and secondly deriving stabilizing controllers is a major challenge due to the complexity of the nonlinear infinite dimensional system description. In this contribution discrepancy based control [9, 10, 12] is used to design a stable closed-loop system for a simple process model. Here, stability with respect to a generalized distance measure is considered. Furthermore, conditions for stability with respect to a norm are discussed.

2   Process Modeling

The technical realization of the FBSA process is depicted schematically in Fig. 2. In continuous operation mode, new primary particles as well as binder solution are fed constantly while particles exceeding a predefined size are withdrawn. Advantages of this mode of operation are higher throughputs compared to batch agglomeration.

The standard approach for mathematical modeling of FBSA is using a population balance equation (PBE) balancing the number density distribution (NDD) $n(t, \mathbf{x})$ depending on time $t \in \mathscr{R}_{\geq 0}$ and some internal or external coordinates $\mathbf{x} \in \mathscr{R}^n$. The external coordinates are usually the spatial coordinates describing the position in three-dimensional space. However, under the assumption of ideal mixing of the particle population in the fluidized bed, the spatial distribution of particles can be lumped. Typical candidates for internal coordinates are particle properties such as particle size, porosity, or shape. A standard simplifying assumption for the modeling of agglomeration processes [5] is that particles are spherical, therefore

Fig. 2 Process scheme
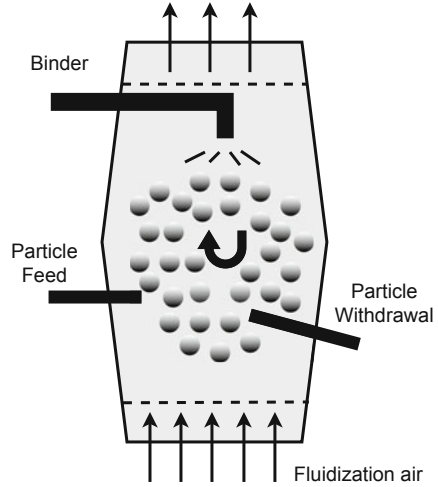
their shape can be neglected. Additionally, further particle properties except for the characteristic volume $v \in \mathscr{R}_{\geq 0}$ are neglected, i.e. $\mathbf{x} = v$. The population balance equation is thus given as

$$\frac{\partial n(t, v)}{\partial t} = \dot{n}_a(t, v) + \dot{n}_f(t, v) - \dot{n}_o(t, v) \tag{1}$$

with the aggregation term $\dot{n}_a$ describing the formation of new particles, the feed term $\dot{n}_f$ describing the particles added to the process, and the output term $\dot{n}_o$ describing the withdrawn particles. In the following the terms are described in detail.

The aggregation term was originally derived by Hulburt and Katz [5] and consists of a birth and a death term

$$\dot{n}_a(t, v) = B(t, v) - D(t, v). \tag{2}$$

The agglomeration rate

$$r = \beta(t, u, v - u)n(t, u)n(t, v - u) \tag{3}$$

with the agglomeration kernel $\beta(t, u, v)$ describes the number of agglomeration events per unit of time. Usually $\beta(t, u, v)$ is divided into a size-independent part $\beta_0(t)$ called the agglomeration efficiency and a size-dependent part $\beta(u, v)$ called the coalescence kernel. An agglomeration event is defined as collision and coalescence of two particles with volume u and $v - u$, forming a new particle of volume v. The agglomeration kernel can be interpreted as the frequency of particles aggregating per unit of time depending on the coordinate v. In the literature a variety of both empirical and analytical coalescence kernels have been proposed. A selection can be found in Table 1. As has been investigated in Bück et. al. [2],

Table 1 Selected
coalescence kernels

Name	$\beta(u, v)$
Size-independent kernel	1
Sum kernel	$u + v$
Product kernel	uv
Brownian kernel	$\left(u^{1/3} + v^{1/3}\right)\left(u^{-1/3} + v^{-1/3}\right)$
EKE kernel	$\left(u^{1/3} + v^{1/3}\right)^2 \sqrt{u^{-1} + v^{-1}}$
Gravitational kernel	$\left(u^{1/3} + v^{1/3}\right)^2 \mid u^{1/6} - v^{1/6} \mid$

the agglomeration kernel can have a significant influence on the qualitative process
behavior. A selection of suitable kernels has been evaluated and identified for a
laboratory scale continuous fluidized bed spray agglomeration in Golovin et. al.
[3, 4].

In order to obtain the birth rate of particles with volume v, Eq. (3) is integrated
over the interval $[0, v]$:

$$B(t, v) = \frac{1}{2} \int_0^v \beta(t, u, v - u) n(t, u) n(t, v - u)\, du \, . \tag{4}$$

The death rate is defined analogously as

$$D(t, v) = \int_0^\infty \beta(t, v, u) n(t, v) n(t, u)\, du \, . \tag{5}$$

Finally, the agglomeration term is given as

$$\dot{n}_a(t, v) = \frac{1}{2} \int_0^v \beta(t, u, v - u) n(t, u) n(t, v - u)\, du - \int_0^\infty \beta(t, v, u) n(t, v) n(t, u)\, du \, . \tag{6}$$

The particle feed is modeled as the product of the normalized number density
distribution $q_{0,f}(v)$ and the total number $N_f(t)$ of added particles:

$$\dot{n}_f(t, v) = N_f(t) q_{0,f}(v). \tag{7}$$

For the particle outlet it is assumed that particles exceeding a specific volume v_{prod}
are removed from the process. Therefore, the separation function $T(v)$ is introduced.
Since the separation is not ideal, $T(v)$ is modeled as a cumulative Gaussian function

$$T(v) = \int_0^v \frac{1}{\sqrt{2\pi\sigma^2}} \exp\left\{ \frac{(s - v_{prod})^2)}{\sigma^2} \right\} ds \, , \tag{8}$$

where σ is a measure of the classification quality. The number density of removed
particles is then defined as follows:

$$\dot{n}_o(t, v) = K(t) T(v) n(t, v) \tag{9}$$

with removal rate $K(t)$. Inserting Eqs. (6), (7), and (9) in Eq. (1) yields the final process model:

$$\frac{\partial n(t, v)}{\partial t} = \frac{1}{2} \int_0^v \beta(t, u, v - u)n(t, u)n(t, v - u) \, \mathrm{d}u - \int_0^\infty \beta(t, v, u)n(t, v)n(t, u) \, \mathrm{d}u$$
$$+ N_\mathrm{f}(t)q_{0,\mathrm{f}}(v) - K(t)T(v)n(t, v).$$

$$(10)$$

For general kernels $\beta(t, u, v)$ this PDE cannot be solved analytically. Thus, numerical solution techniques have to be used. In this contribution the cell-average method developed by Kumar et al. [6] is utilized for process simulation.

3 Control of Fluidized Bed Spray Agglomeration

This section is concerned with the derivation of stabilizing controllers for the FBSA. Therefore, the method of discrepancy based control is introduced in the first subsection and applied to the process in the following subsection. Furthermore, simulation studies are given and practical problems such as robustness with respect to parametric uncertainties are discussed.

3.1 Introduction to Discrepancy Based Control

A discrepancy $\rho(\varphi(., t), t)$ is a generalized distance measure. It measures the distance between the process state $\varphi(., t)$, i.e. a solution of the distributed parameter system, and the equilibrium φ_0. Here, it is of great importance that not all properties of a metric or norm have to be fulfilled. In the following, the main properties and facts on stability with respect to two discrepancies are stated in accordance to [7, 8, 13, 14].

Definition 1 Discrepancy A discrepancy is a real valued functional $\rho = \rho$ $[\varphi(., t), t]$ with the following properties

1. $\rho(\varphi, t) \geq 0$.
2. $\rho(0, t) = 0$.
3. for an arbitrary process $\varphi = \varphi(., t)$ the real valued functional $\rho(\varphi(., t), t)$ is continuous with respect to t.

In the context of stability with respect to two discrepancies besides the discrepancy $\rho(\varphi(., t, t))$, measuring the distance between $\varphi(., t)$ and the equilibrium φ_0, a second time independent discrepancy ρ_0 is used. It describes the distance between the initial state $\varphi(., 0)$ and the equilibrium φ_0. The two discrepancies ρ and ρ_0 have to satisfy, that $\rho(\varphi(., t), t)$ is continuous at time $t = t_0$ with respect to ρ_0

at $\rho_0 = 0$, i.e. for every $\varepsilon > 0$ and $t_0 > 0$ there exists a $\delta(\varepsilon, t_0) > 0$, such that from $\rho_0 \leqslant \delta(\varepsilon, t_0)$ it follows that $\rho < \varepsilon$.

Definition 2 Stability with respect to two discrepancies ρ and ρ_0

The equilibrium $\varphi_0 = 0$ is stable in the sense of Lyapunov with respect to the two discrepancies ρ and ρ_0 for all $t \geq t_0$ if for every $\varepsilon > 0$ and $t_0 \geq 0$ there exists a $\delta = \delta(\varepsilon, t_0) > 0$ such that for every process $\varphi(., t)$ with $\rho_0 < \delta(\varepsilon, t_0)$ it follows that $\rho < \varepsilon$ for all $t \geq t_0$. If in addition $\lim_{t \to \infty} \rho = 0$, then the equilibrium φ_0 is called asymptotically stable in the sense of Lyapunov with respect to the two discrepancies ρ and ρ_0.

Based on the stated stability concept, i.e. stability with respect to two discrepancies, an according Lyapunov functional V can be introduced.

Definition 3 Positivity with respect to a discrepancy ρ.

The functional $V = V[\varphi, t]$ is called positive with respect to the discrepancy ρ, if $V \geq 0$ and $V[0, t] = 0$ for all φ with $\rho(\varphi, t) < \infty$.

Definition 4 Positive definiteness with respect to a discrepancy ρ.

The functional $V = V[\varphi, t]$ is positive definite with respect to a discrepancy ρ, if $V \geq 0$ and $V[0, t] = 0$ for all φ with $\rho(\varphi, t) < \infty$ and for every $\varepsilon > 0$ there exists a $\delta = \delta(\varepsilon) > 0$, such that $V \geq \delta(\varepsilon)$ for all φ with $\rho[\varphi, t] \geq \varepsilon$.

The following two theorems state the conditions for a function V guaranteeing (asymptotic) stability with respect to two discrepancies.

Theorem 1 ([14]) *The process φ with the equilibrium $\varphi_0 = 0$ is stable with respect to the two discrepancies ρ and ρ_0 if and only if there exists a functional $V = V[\varphi, t]$ positive definite with respect to the discrepancy ρ, continuous at time $t = t_0$ with respect to ρ_0 at $\rho_0 = 0$ and not increasing along the process φ, i.e. $\dot{V} \leq 0$.*

Theorem 2 ([14]) *The process φ with the equilibrium $\varphi_0 = 0$ is asymptotically stable with respect to the two discrepancies ρ and ρ_0 if and only if there exists a functional $V = V[\varphi, t]$ positive definite with respect to the discrepancy ρ, continuous at time $t = t_0$ with respect to ρ_0 at $\rho_0 = 0$ and not increasing along the process φ, i.e. $\dot{V} \leq 0$, with $\lim_{t \to \infty} V = 0$.*

As has been discussed in Palis and Kienle [12], stability with respect to two discrepancies can be interpreted as special output stability, where the discrepancy defines a virtual system output. Therefore, given a system, which is stable with respect to two discrepancies, stability of the full system state in terms of a norm is guaranteed if the zero dynamics are stable.

3.2 Application to Fluidized Bed Spray Agglomeration

In this section the discrepancy based control introduced above is applied to FBSA. Therefore, appropriate discrepancies have to be found. For a continuous granulation process, Palis and Kienle [10–12] showed, that the differences between desired and actual moments of the size distribution

$$\Delta \mu_i(t) = \int_0^\infty v^i \left(n_{\mathrm{d}}(v) - n(t, v) \right) \mathrm{d}v , \tag{11}$$

where $N_{\mathrm{d}}(v)$ is the desired NDD, are a suitable choice. Here, the zeroth and the first moment represent the total particle number and the total particle volume, respectively. In this contribution the zeroth moment is chosen as control variable since it can be interpreted physically and its impact on the agglomeration term $\dot{n}_{\mathrm{a}}$ is of greater significance. In the following, two discrepancy based controllers are derived and evaluated. The first controller is a continuous controller guaranteeing exponential convergence of the control error. The second controller is a discrepancy based sliding mode controller. Both approaches are then compared.

3.2.1 Discrepancy Based Control

For the control of the zeroth moment, the control error is given as

$$e = \Delta \mu_0 = \int_0^\infty (n_d - n) \mathrm{d}v, \tag{12}$$

where n_d is the desired steady state. The according discrepancy and Lyapunov functional can hence be chosen as

$$\rho = \frac{1}{2} e^2, \tag{13}$$

$$V = \frac{1}{2} e^2. \tag{14}$$

Obviously, the error, the discrepancy, and the Lyapunov functional vanish not only at the desired steady state distribution but for all distributions with an equal zeroth moment. In order to derive a discrepancy based control law, the first order time derivative of the Lyapunov functional along the system trajectories is calculated

$$\dot{V} = e\dot{e} = -e \int_0^\infty \frac{\partial n}{\partial t} \mathrm{d}v = -e \left(\int_0^\infty \dot{n}_{\mathrm{a}} + n_{\mathrm{f}} \, \mathrm{d}v - K \int_0^\infty T n \, \mathrm{d}v \right). \tag{15}$$

Here, the withdrawal rate K is the control handle. In order to achieve exponential convergence of the Lyapunof functional, K is chosen as

$$K = \frac{1}{\int_0^\infty Tn \, \mathrm{d}v} \left(-ce + \int_0^\infty \dot{n}_a + n_f \, \mathrm{d}v \right), \tag{16}$$

where c is a positive constant determining the convergence rate. This gives

$$\dot{V} = -2cV. \tag{17}$$

Applying the control law therefore exponentially stabilizes the agglomeration process with respect to the introduced discrepancy, i.e. the zeroth moment converges exponentially to the desired value. If the zero dynamics of the system are asymptotically stable in terms of a norm, stability of the distribution in terms of the same norm follows. Since a full analysis of the zero dynamics is usually not feasible for this type of PDE, a local stability analysis, i.e. using the linearization around the desired steady state of the discretized system, has been conducted showing that the associated transfer function does not possess zeros in the right half-plane. Thus, the zero dynamics are at least locally stable.

Furthermore, it should be mentioned that the denominator in Eq. (16) can vanish for some distributions leading to an undefined control law or take values close to zero leading to high controller gains. Due to the latter, K has to be bounded in practical applications.

To verify the designed control laws, the system was simulated numerically using the process parameters from Table 2. As agglomeration kernel the Brownian kernel was used. In Figs. 3 and 4 simulation results comparing open-loop and closed-loop operation are presented. It is shown that the moments as well as the L_2-norm of $(n_d - n)$ converge in both cases. While the zeroth moment and the L_2-norm converge faster in closed-loop operation the total particle volume μ_1 does not. To achieve better performance with respect to this measure, a two-dimensional controller using the feed rate as another manipulated variable could be derived.

Table 2 Process parameters

Parameter	Value
N_f	380,000
β_0	1×10^{-10}
v_{prod}	0.9 mm
σ	0.3 mm
K_{nom}	$0.0125 \, \mathrm{s}^{-1}$
K_{max}	$1 \, \mathrm{s}^{-1}$
γ	1×10^{-3}
c	0.2

(a) Zeroth moment μ_0 (b) First moment μ_1

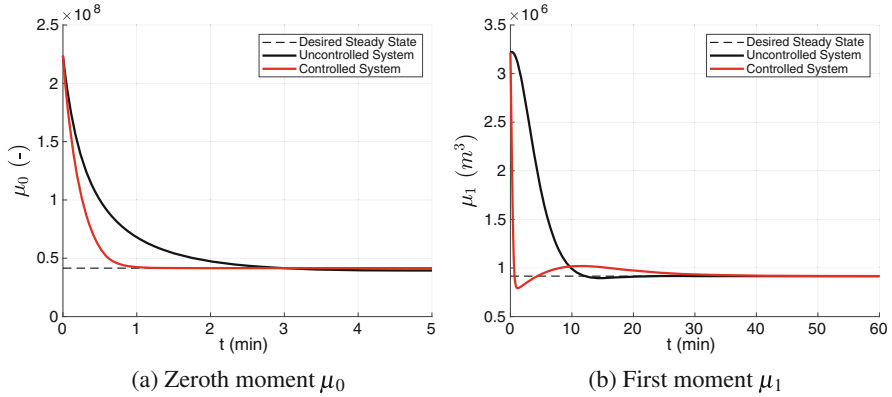**Fig. 3** Convergence of the zeroth (**a**) and the first moment (**b**) in closed-loop (red) and open-loop (black) operation

(a)   (b)
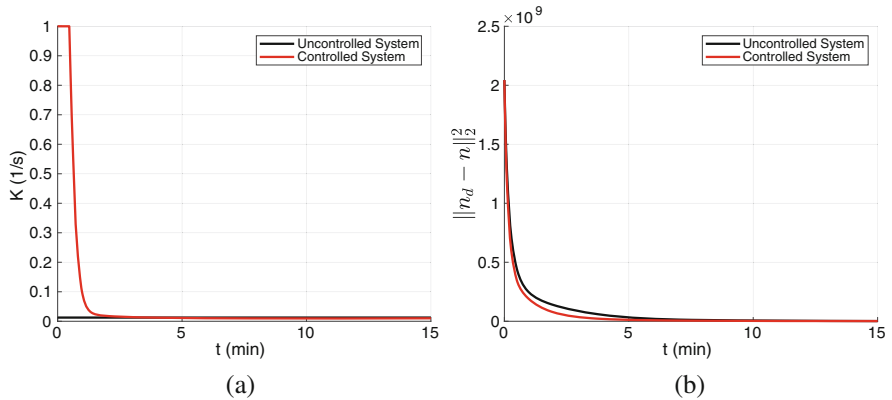
Fig. 4 Manipulated variable K (left) and convergence in L_2-norm (right) in closed-loop (red) and open-loop (black) operation. (**a**) Withdrawal rate K. (**b**) L_2-norm

3.2.2 Discrepancy Based Sliding Mode Control

In this section a discrepancy based sliding mode controller is derived and tested using simulations. For the sake of simplicity and in order to improve comparability, the same discrepancy and Lyapunov functional as in the previous section are chosen. The time derivative of the Lyapunov functional along the system trajectory thus is

$$\dot{V} = -e \left(\int_0^\infty \dot{n}_\mathrm{a} + n_\mathrm{f} \, \mathrm{d}v - K \int_{v_\mathrm{prod}}^\infty n \, \mathrm{d}v \right). \tag{18}$$

Assuming there exists a maximum withdrawal rate $K_{max} > 0$ with

$$\int_0^\infty \dot{n}_a + n_f \, dv < K_{max} \int_{v_{prod}}^\infty n \, dv \tag{19}$$

the following sliding mode control law

$$K = \begin{cases} 0 & \text{if } e \geq 0 \\ K_{max} & \text{if } e < 0 \end{cases} \tag{20}$$

can be chosen, resulting in the required negative definiteness of the time derivative of the Lyapunov functional

$$\dot{V} \leq 0. \tag{21}$$

Therefore, the controller stabilizes the control variable.

Applying the derived sliding mode controller in the simulation setting results in the closed-loop behavior shown in Fig. 5. As can be seen on the left-hand side, by applying the discrepancy based sliding mode control law the zeroth moment converges. In contrast to the discrepancy based controller from the previous section, this happens in finite time. Shown on the right-hand side, the difference in the closed-loop convergence behavior of the first moment shown is however less significant. In Fig. 6 the phase portrait of the two moments (left) and the convergence in the L_2-norm (right) are depicted.

Besides the simple implementation of the discrepancy based sliding mode control law, a major advantage compared to the continuous control law is the robustness
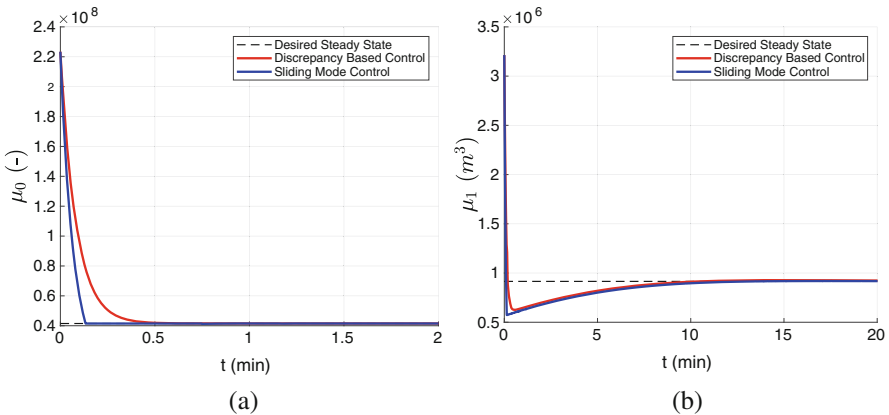
Fig. 5 Convergence of the zeroth (left) and the first moment (right) with discrepancy based (red) and sliding mode(blue) control. (**a**) Zeroth moment μ_0. (**b**) First moment μ_1
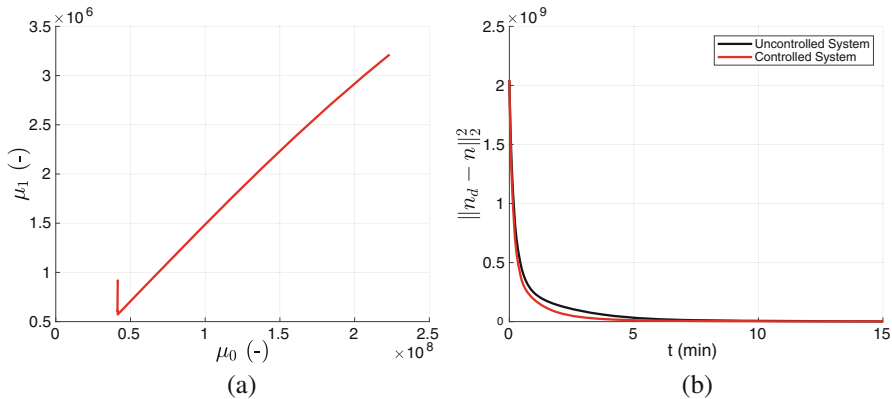
Fig. 6 Phase portrait (left) and convergence in L_2-norm (right) in closed-loop (red) and open-loop (black) operation. (**a**) Phase portrait in the μ_0–μ_1 plane. (**b**) L_2-norm

with respect to uncertainties in the model equations. This behavior is examined in the following section.

3.3 Robustness with Respect to Parametric Uncertainties

For practical implementation robustness of the control laws with respect to model uncertainties is an important feature. A typical parametric uncertainty for the given agglomeration process is the feed rate. While the proposed discrepancy based sliding mode control law does not depend on the feed and therefore possesses a natural robustness, the control law from Sect. 3.2.1 depends explicitly on the parameter N_f. Thus, stability is not guaranteed if the feed rate is disturbed. In order to compensate for this, the closed-loop control system can be augmented by a parameter estimator for the feed rate. Then the estimated feed rate is used to compute the according withdrawal rate. It has to be mentioned that the given parametric disturbance in the PDE changes the steady state distributions $n_s(v)$. Therefore, it is generally not possible to stabilize the desired distribution $n_d(v)$ under occurrence of disturbances even if the moments converge.

In order to derive a parameter estimation law the estimation error is defined using the unknown feed rate N_f and its estimate $\hat{N}_f$ as follows:

$$\tilde{N}_f = \hat{N}_f - N_f. \tag{22}$$

The certainty equivalence discrepancy based control law using the estimated feed rate $\hat{N}_f$ is given as

$$K = \frac{1}{\int_0^\infty Tn \, dv} \left(-ce + \int_0^\infty \dot{n}_a + \hat{N}_f q_{0,f} \, dv \right). \tag{23}$$

Following the well-known Lyapunov redesign approach, the Lyapunov functional is augmented with a term reflecting the estimation error

$$V = \frac{1}{2}e^2 + \frac{1}{2\gamma}\tilde{N}_f^2, \tag{24}$$

where γ is a positive constant. Deriving the time derivative of the augmented Lyapunov functional along the closed-loop system trajectories, i.e. the controlled agglomeration process, yields

$$\dot{V} = e\dot{e} + \frac{1}{\gamma}\tilde{N}_f\dot{\hat{N}}_f = -ce^2 + \tilde{N}_f\left(e + \frac{1}{\gamma}\dot{\hat{N}}_f\right). \tag{25}$$

Here, the first term is as before negative definite in e. Due to the unknown sign of the estimation error $\tilde{N}_f$ the second term is indefinite. Therefore, an appropriate choice of the parameter update law $\dot{\hat{N}}_f$ is

$$\dot{\hat{N}}_f = -\gamma e, \tag{26}$$

resulting in

$$\dot{V} = -ce^2. \tag{27}$$

Therefore, the error system is stable. To show asymptotic stability and thus convergence of the parameter estimate, LaSalles invariance principle can be used. Converging to and remaining at $\dot{V} = 0$ the error e has to vanish, i.e. $e = 0$. Here, the dynamics of e at $e = 0$ are given by

$$\dot{e} = -\int_0^\infty \dot{n}_a + N_f q_{0,f} - KTn \, dv. \tag{28}$$

After introducing the control law (23) and some simplifications this results in

$$\dot{e} = \tilde{N}_f. \tag{29}$$

Therefore, the derivative of the control error vanishes only if the estimation error is also equal to zero. Thus, the estimated parameter converges asymptotically to the unknown parameter value.

In the following, simulation results for the system with a 50% disturbance in the feed rate, starting in the desired steady state, are presented. In Fig. 7 it can be seen that the zeroth moment μ_0 converges for both controllers, while the first moment is significantly smaller than desired. The sliding mode controller however has a better performance. The convergence of the parameter estimator and the (non-converging) L_2-norm are shown in Fig. 8.

Although it is, for the given configuration, generally not possible to achieve convergence of the L_2-norm in the presence of a non-vanishing disturbance due to the change of steady states, performance could be improved by using a different discrepancy, e.g. the average particle volume, which is the ratio between μ_1 and μ_0.
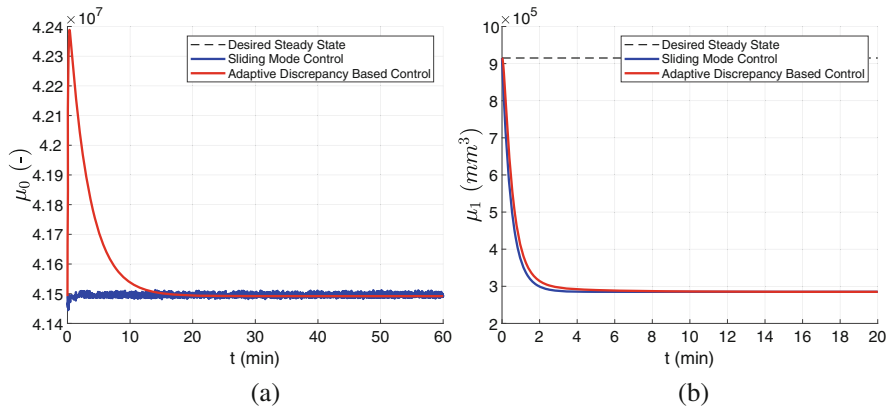
Fig. 7 Convergence of the zeroth and first moment. (**a**) Zeroth moment μ_0. (**b**) First moment μ_1

(a) Unknown parameter N_f (dotted red) and the parameter estimate $\hat{N}_f$ (black)
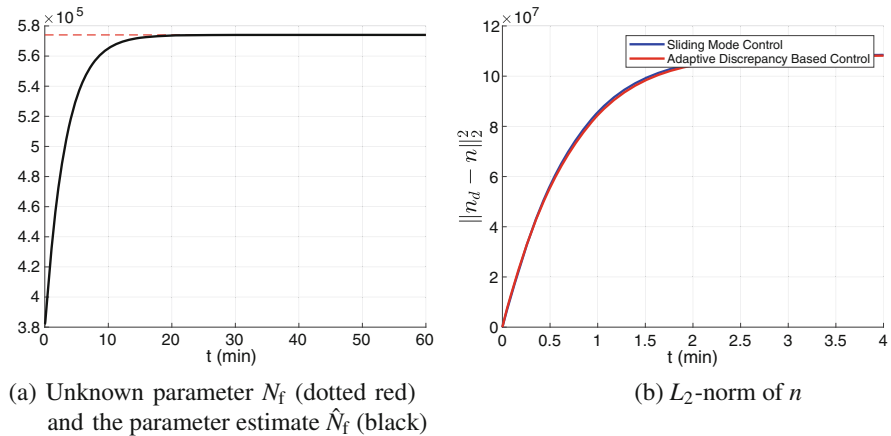
(b) L_2-norm of n

Fig. 8 Convergence of the parameter estimator (**a**) and L_2-norm of n (**b**)

4   Conclusion

In this contribution discrepancy based control for continuous fluidized bed spray agglomeration processes has been proposed. Here, two controller types, continuous and discontinuous, have been derived and analyzed. By design, both control laws guarantee stability with respect to the chosen discrepancy. For the given process configuration the zeroth moment of the number density distribution has been an appropriate choice. Furthermore, from a local stability analysis of the discretized zero dynamics and the simulation results it has been shown that the distributed state is also stabilized asymptotically in terms of a norm. General conditions for the stability of the zero dynamics could not be stated yet. Additionally, robustness with respect to parametric uncertainties was examined. Therefore, in order to guarantee asymptotic stability the continuous control law was augmented by a parameter estimator. Both the adaptive continuous controller and the sliding mode controller stabilize the chosen moment at the desired value.

References

1. Bück, A., Tsotsas, E.: Agglomeration. In: Caballero, B., Finglas, P.M., Toldrá, F. (eds.) Encyclopedia of Food and Health, pp. 73–81. Academic Press (2016). ISBN 9780123849533
2. Bück, A., Wegner, M., Neugebauer, C., Palis, S., Tsotsas, E.: Bifurcation analysis of process stability of continuous fluidized bed agglomeration with external product classification. In: 26th European Symposium on Computer Aided Process Engineering (Portoroz) (2016)
3. Golovin, I., Strenzke, G., Dürr, R., Palis, S., Bück, A., Tsotsas, E., Kienle, A.: Parameter identification for continuous fluidized bed spray agglomeration. Processes **6**, 246 (2018)
4. Golovin, I., Otto, E., Dürr, R., Palis, S., Kienle, A.: Lyapunov-based online parameter estimation in continuous fluidized bed spray agglomeration processes. In: 12th IFAC Symposium on Dynamics and Control of Process Systems - DYCOPS 2019 (Florianopolis) (2019)
5. Hulburt, H.M., Katz, S.: Some problems in particle technology: a statistical mechanical formulation. Chem. Eng. Sci. **19**, 555–574 (1964)
6. Kumar, J., Peglow, M., Warnecke, G., Heinrich, S.: The cell average technique for solving multi-dimensional aggregation population balance equations. Comput. Chem. Eng. **32**, 1810–1830 (2008)
7. Martynjuk, A., Gutovski, R.: Integral inequalities and stability of motion [in Russian]. Naukowa, Dumka (1979)
8. Movtschan, A.: Stability of processes with respect to two metrics [in Russian]. J. Appl. Math. Mech. **24**, 988–1001 (1960)
9. Palis, S.: Non-identifier-based adaptive control of continuous fluidized bed spray granulation. J. Process. Control **71**, 46–51 (2018)
10. Palis, S., Kienle, A.: Discrepancy based control of continuous crystallization. At-Automatisierungstechnik **60**, 145–154 (2012)
11. Palis, S., Kienle, A.: Stabilization of continuous fluidized bed spray granulation with external product classification. Chem. Eng. Sci. **70**, 200–209 (2012)
12. Palis, S., Kienle, A.: Discrepancy based control of particulate processes. J. Process. Control **24**, 33–46 (2014)

13. Sirasetdinov, T.: On the theory of stability of processes with distributed parameters [in Russian]. J. Appl. Math. Mech. **31**, 37–48 (1967)
14. Sirazetdinov, T.K.: Stability of Systems with Distributed Parameters [in Russian]. Nauka, Novosibirsk (1987)

Control induced instabilities in fluidized bed spray granulation

Stefan Palis [*]

Otto-von-Guericke-University, Universitätsplatz 2, D-39106 Magdeburg, Germany
National Research University "Moscow Power Engineering Institute", Krasnokazarmennaya 14, 111250 Moscow, Russia

ARTICLE INFO

ABSTRACT

This contribution is concerned with the stability problems occurring during the operation of continuous fluidized bed spray granulation processes with external sieve mill cycle. These processes are in general operated by a mass controller, which guarantees that the overall mass of particles in the granulation chamber stays in well-defined bounds. It is well-known that, depending on the milling diameter, instabilities may occur, which result in a nonlinear limit cycle of the particle size distribution. To overcome this problem two approaches have been proposed in the literature, constrain the admissible parameter space to exclude regions of instability and design additional stabilizing control loops. In the present contribution, the cause of this instability phenomenon will be studied. It will be shown that the instability is not inherent to the process, which turns out to be open-loop stable over the studied parameter range, but due to the mass controller. More specifically, it will be demonstrated that the zero dynamics of the granulation process become unstable for certain parameter ranges resulting in closed-loop unstable process behavior. To point out, that this behavior does not depend on the specific mass controller design procedure, three prototypical mass controllers of practical relevance are designed and analyzed.

1. Introduction

A large number of products from chemical, pharmaceutical, and food industries are converted into a solid particulate state. Here, the particle properties have an important influence on the product properties, e.g. flowability and dust formation. Depending on the material at hand, different production processes can be used. One important process is granulation [1]. It can be combined with fluidized bed technology, where a particle bed is fluidized by a temperature-controlled air stream. This fluidization results in an increased surface of the particle bed and thus an improved heat and mass transfer. Starting with an initial set of particles, a solution or suspension is applied through a nozzle. The additional liquid settles on the particle surface and forms a new solid layer due to drying. This layer formation results in particle growth. In this contribution, a specific configuration of continuous fluidized bed spray granulation processes is investigated. Here, only particles in the desired size range are removed from the process. This is achieved by particle sieving. Particles being too small are directly fed back to the process chamber, whereas large particles are milled to smaller sizes. Due to the milling, a

continuous stream of nuclei particles is generated, which is required for a continuous process operation. The schematic process scheme is depicted in Fig. 1.

In principle, the described granulation process can be operated with [2] and without [3,4] a bed mass controller. However, as the bed mass has an influence on important process and particle properties, as e.g. fluidization behavior, residence time, it is often desired to keep it constant applying a bed mass controller. Here, the pressure drop across the fluidized bed is often used as a measure for the bed mass. Examples for the actuated variable are the rotation velocity of a rotary valve [2] or the countercurrent flow rate of the withdrawal. The dynamic behavior of different configurations of continuous fluidized bed spray granulation processes has been thoroughly investigated on the basis of mathematical models and in experiments. There, it has been shown that the qualitative dynamics may vary significantly with process conditions [5,6]. One common situation is a loss of stability due to the change of a system parameter. This loss of stability is often connected to the occurrence of a stable limit cycle and results in self-sustained oscillations of the particle size distribution [5,6]. As this loss of stability is in general undesired different control approaches have been proposed to stabilize the granulation process. From a practical point of view, these additional control loops increase system complexity and are connected to additional costs. Therefore, in this contribution, the stability problem is revisited. It is shown, that the main cause for the aforementioned stability

---
 * Correspondence to: Otto-von-Guericke-University, Universitätsplatz 2, D-39106 Magdeburg, Germany.
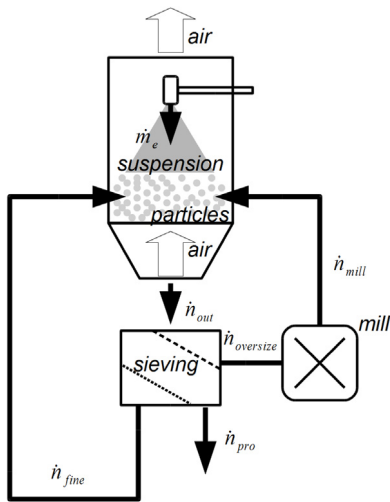   *E-mail address:* stefan.palis@ovgu.de.

Fig. 1. Scheme of a continuous fluidized bed spray granulation process.

problem is the mass controller itself. From a practical point of view, this finding is crucial and should hence be considered in the control system design for continuous fluidized bed spray granulation processes. The paper is organized as follows: in Section 2 the population balance model for a continuous fluidized bed spray granulation with external product classification, is introduced. In Section 3 different bed mass controller are designed for the given configuration. Simulation studies show the described loss of stability. This is further investigated in Section 4 by means of bifurcation analysis. Here, also a system theoretic explanation for the observed loss of stability is provided. Some final remarks conclude the paper.

2. Fluidized bed spray granulation

To describe the dynamical process behavior a population balance model for the particle size distribution according to [7] will be stated. As has been shown in [5] the model does reflect the process behavior well. Regarding the particle size distribution the main assumptions are that granulation chamber is well-mixed and that the particles are spherical. Therefore, the dynamics can be described using one property coordinate, the particle diameter L, and no spatial coordinates, resulting in an one-dimensional population balance model for the number distribution $n(t, L)$. As can be seen in Fig. 1 the change in the number of particles is a result of the in- and outfluxes:

- $\dot{n}_{growth}$ growth of particles,
- $\dot{n}_{prod}$ particle flux due to product removal,
- $\dot{n}_{fines}$ particle flux of fine particles,
- $\dot{n}_{oversize}$ particle flux due to oversize removal,
- $\dot{n}_{mill}$ particle flux due to particles fed back from mill.

The flux of fines particles $\dot{n}_{fines}$ can be neglected, as sink and sources terms cancel. This can be justified by the assumption that the delay introduced by the sieving is neglectable compared to the dynamics of particle growth. The resulting population balance equation therefore is:

$$\frac{\partial n}{\partial t} = -\dot{n}_{growth} - \dot{n}_{prod} - \dot{n}_{oversize} + \dot{n}_{mill}. \tag{1}$$

The particle growth is due to injected fluid and its settling and drying on the particles. Due to the intensive particle mixing inside the fluidized bed, it can be assumed that particles are uniformly coated. The effective mass flow rate of solid material to the

particle population is $\dot{m}_e$ and depends on the feed composition and injection rate. The growth rate G is thus a function of the effective mass flow rate and the overall particle surface. Here, the latter can be calculated from the second moment μ_2 of the particle size distribution $n(t, L)$ [8].

$$G = \frac{2\dot{m}_e}{\varrho A} = \frac{2\dot{m}_e}{\varrho \pi \mu_2}. \tag{2}$$

The according flux $\dot{n}_{growth}$ is given by

$$\dot{n}_{growth} = G\frac{\partial n}{\partial L}. \tag{3}$$

As described above, in the continuous configuration of the fluidized bed spray granulation particles are continuously removed and fed to a sieving box. The particle flux being removed from the granulator $\dot{n}_{out}$ is

$$\dot{n}_{out} = Kn. \tag{4}$$

where K is the drain, which in general serves as the actuated variable for the bed mass controller. The removed particles are sieved in two sieves, where each sieve can be described by an according size-dependent sieving function $T_1(L)$ and $T_2(L)$.

$$T_{1/2} = \frac{\int_0^L e^{-\frac{(L'-\mu_{1/2})^2}{2\sigma_{1/2}^2}} dL'}{\int_0^\infty e^{-\frac{(L-\mu_{1/2})^2}{2\sigma_{1/2}^2}} dL}. \tag{5}$$

Due to the sieving, the withdrawn particles are separated into three classes:

1. small or fine particles passing both screens, which are fed directly back to the granulator,

$$\dot{n}_{fines} = (1 - T_2)(1 - T_1)\dot{n}_{out}, \tag{6}$$

2. particles passing only one screen, product particles, which are removed from the whole process

$$\dot{n}_{prod} = T_2(1 - T_1)\dot{n}_{out}, \tag{7}$$

3. big particles passing no screen, oversized particles, which are grinded in a mill and fed back to the ganulator

$$\dot{n}_{oversize} = T_1\dot{n}_{out}. \tag{8}$$

Milling of particles is a complex process, resulting in general in multi-modal particle size distributions of milled particles [9]. For convenience it is assumed that the particle distribution fed back from the mill is a normal distribution with mean diameter μ_M. This is in accordance with [7,10] and does not influence the qualitative process behavior. To assure that no mass is lost nor generated during grinding, the particle size distribution of the milled particles is scaled with the third moment of the flux oversized particles.

$$\dot{n}_{mill} = 6\frac{e^{-\frac{(L-\mu_M)^2}{2\sigma_M^2}}}{\sqrt{2\pi}\pi\varrho\sigma_M}\int_0^\infty L^3\dot{n}_{oversize}dL. \tag{9}$$

The population balance model Eq. (1) together with the defining equations for the fluxes Eqs. (3)–(9) fully describe the dynamics of the particle size distribution. From an operational point of view, however, a mass balance model, seems to be often more appropriate due to its simplicity. This applies also to controller design.
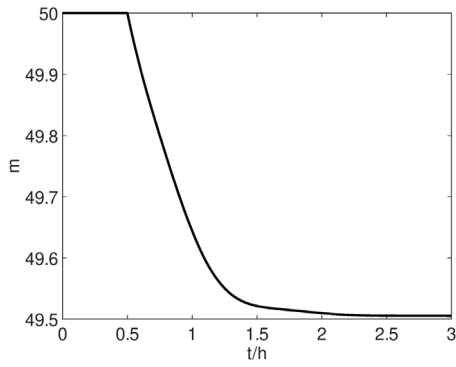
Fig. 2. Open-loop response for a 1% step-wise increase of the steady-state withdraw rate K_0 at $t = 0.5h$.

Fig. 3. Open-loop Bode diagram without (solid black) and with (dotted black) PI-controller.

2.1. Mass balance

The mass balance model can be directly derived from the population balance equation (1). For this purpose, the mass of the particle size distribution $n(t, L)$ inside the granulation chamber at a given moment in time t is calculated using its third moment $\mu_3(t)$.

$$m = \frac{\pi}{6} \varrho \int_0^\infty L^3 n(t, L) dL = \frac{\pi}{6} \varrho \mu_3(t) \tag{10}$$

The change in mass is given by the time derivative of Eq. (10).

$$\dot{m} = \frac{\pi}{6} \varrho \int_0^\infty L^3 \frac{\partial n}{\partial t} dL \tag{11}$$

$$= \frac{\pi}{6} \varrho \int_0^\infty L^3 \left(-G \frac{\partial n}{\partial L} - \dot{n}_{prod} - \dot{n}_{oversize} + \dot{n}_{mill} \right) dL \tag{12}$$

Taking into account that the mill is mass conserving, the terms for the flux of oversized particles and from the mill cancel resulting in the mass balance equation.

$$\dot{m} = \dot{m}_e - \frac{\pi}{6} \varrho \int_0^\infty L^3 K T_2 (1 - T_1) n dL \tag{13}$$

Here, the first term is the effective mass injected with the liquid into the granulation chamber and the second term reflects the mass removed with the product.

3. Mass controller

From an operational point of view, it is desired to keep the mass inside the granulation chamber at a certain set-point to guarantee a certain fluidization behavior. It is common practice to achieve this by designing a mass controller based on the derived mass balance equation, i.e. Eq. (13). In the following, three different control strategies will be presented. These can be seen as prototypes for other possible control design methods. All will use the drain K as the actuated variable.

3.1. PI control

As can be seen for example from the open-loop step response in Fig. 2 the open-loop granulation process is stable. Therefore, a simple loop-shaping procedure can be applied to design a PI-controller.

The open-loop Bode diagram of the granulation process with K as control input and the mass m as output is depicted in Fig. 3. To achieve a zero steady-state error for constant reference changes
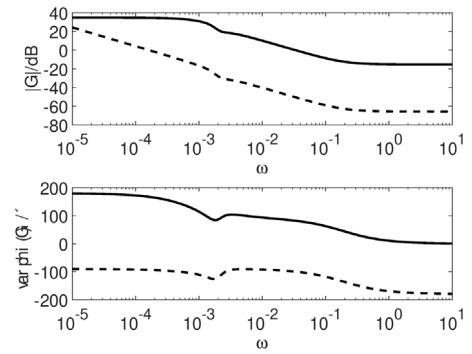
and increase the dynamics of the mass control, the following PI controller has been chosen:

$$C(s) = K_p \left(1 + \frac{1}{T_N s} \right) \tag{14}$$

where $K_p = -0.001$ and $T_N = 1000$. The open-loop Bode diagram of the granulation in series with the PI controller is depicted in Fig. 3. As can be seen the designed controller achieves a phase margin of 90° and an amplitude margin of 60 dB.

Testing the designed PI controller on the nonlinear granulation process for a coarse mill grade, i.e. $\mu_M = 0.9$ mm results in the behavior depicted in Fig. 4.

3.2. Compensation based control design

The next control design is closely related to nonlinear design, feedback linearization or backstepping, where undesired terms, e.g. nonlinearities or time-variant behavior, can be compensated either in a normal form or at each integrator. However, due to the fact, that the mass balance equation is a first-order differential equation and hence possesses a relative degree of one no further transformations are needed. Therefore, in a first step the error dynamics are derived by calculating the difference between the desired mass m_d and the actual mass m.

$$e = m_d - m \tag{15}$$

Taking the time derivative and assuming that the task is set-point tracking, i.e. $m_d = const.$, yields:

$$\dot{e} = -\dot{m}_e + \frac{\pi}{6} \varrho \int_0^\infty L^3 K T_2 (1 - T_1) n dL. \tag{16}$$

From a control point of view, the effective mass injected and the third moment of $T_2(1 - T_1)n$ can be viewed as some known time-varying functions. Therefore, the following compensating control law can be chosen:

$$K = \frac{6}{\pi \varrho} \frac{\dot{m}_e - ce}{\int_0^\infty L^3 T_2 (1 - T_1) n dL} \tag{17}$$

to achieve exponential convergence of the control error e:

$$\dot{e} = -ce \tag{18}$$

where c is the tuning factor to adjust the desired convergence rate. Here, it is required that the product fraction is always greater than zero in order to prevent division by zero.

It should be mentioned, that setting the constant c to zero will result in a vanishing time-derivative of the error e in (18) and hence constant mass. Therefore, starting with a desired mass inside the granulation chamber, the reduced control law (17) will
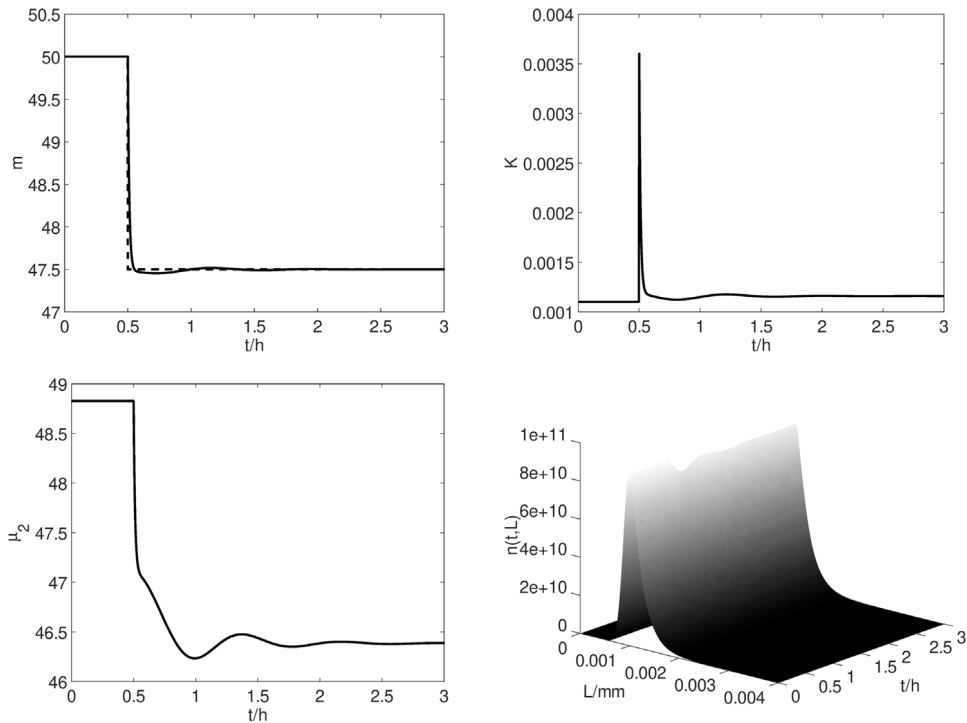
Fig. 4. Closed-loop response of the designed PI controller for a set-point change of 5%, (top left) mass $m(t)$ (solid black) and desired mass m_d (dotted black), (top right) withdraw rate K, (bottom left) second moment μ_2, (bottom right) particle size distribution $n(t, L)$.
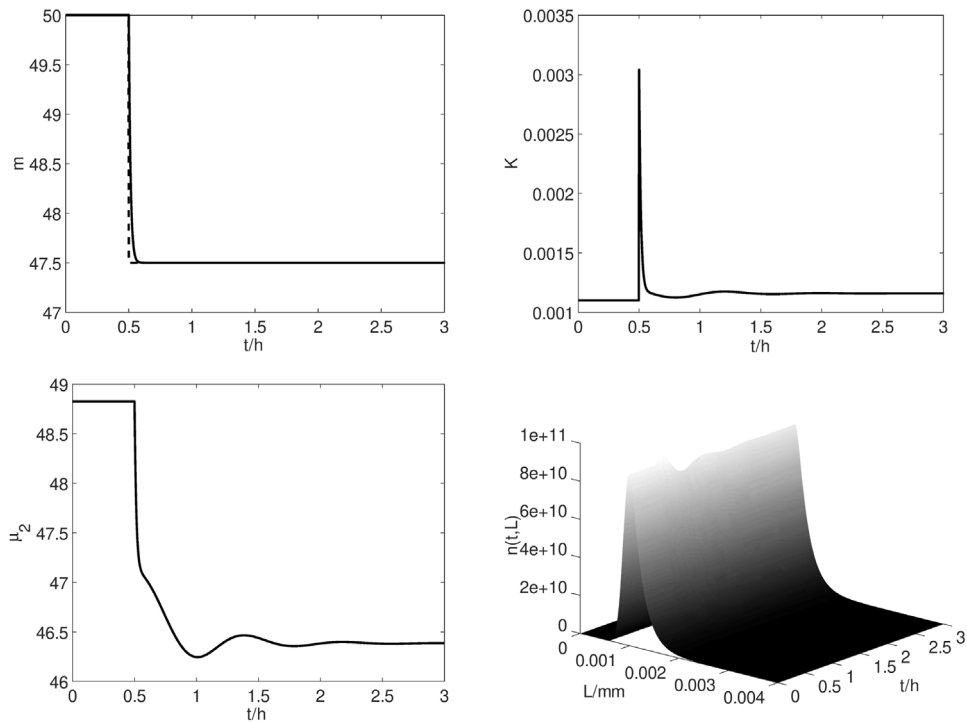

Fig. 5. Closed-loop response of the designed compensation based controller for a set-point change of 5%, (top left) mass $m(t)$ (solid black) and desired mass m_d (dotted black), (top right) withdraw rate K, (bottom left) second moment μ_2, (bottom right) particle size distribution $n(t, L)$.

result in a constant mass. This approach has been applied for example in [10,11]. There, the drain K has been calculated from an algebraic equation to achieve the desired mass.

Testing the designed compensation based controller on the nonlinear granulation process for a coarse mill grade, i.e. $\mu_M = 0.9$ mm results in the behavior depicted in Fig. 5.

3.3. Sliding mode control design

From a practical point of view, the compensating control approach has one drawback. It assumes the knowledge of the effective mass injected and the particle size distribution, which is in general difficult to achieve. To overcome this sliding mode control provides a robust alternative. Based on the error dynamics
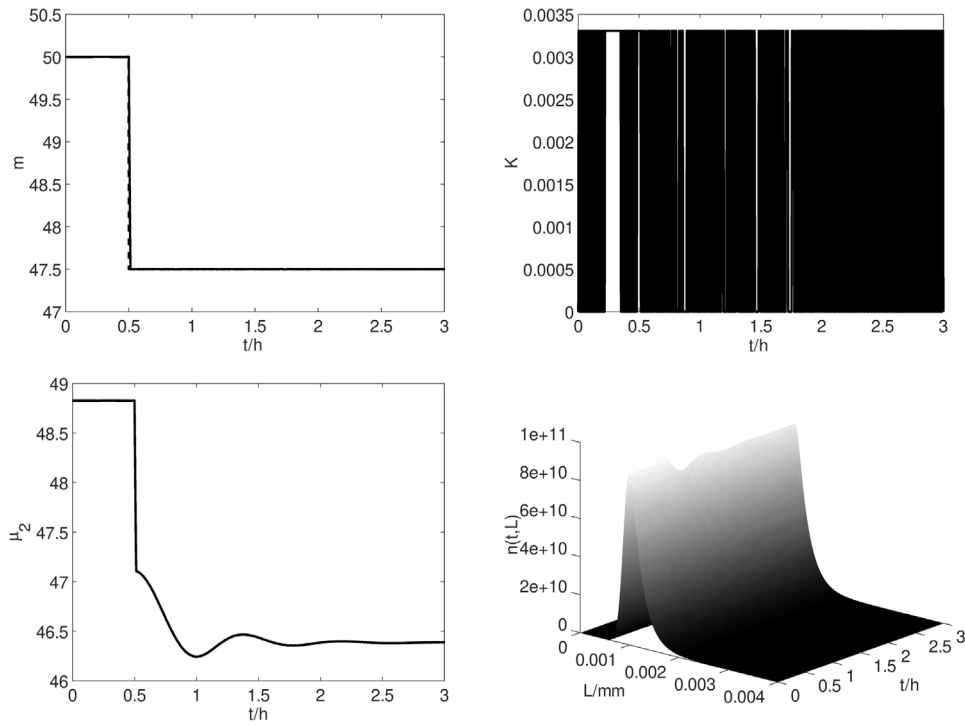
Fig. 6. Closed-loop response of the designed sliding mode controller for a set-point change of 5%, (top left) mass $m(t)$ (solid black) and desired mass m_d (dotted black), (top right) withdraw rate K, (bottom left) second moment μ_2, (bottom right) particle size distribution $n(t, L)$.
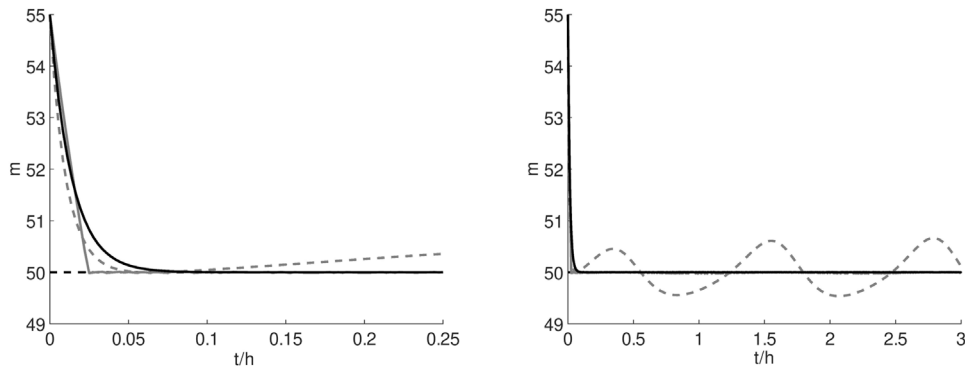

Fig. 7. Closed-loop response of the designed mass controllers for a reduced mill grade $\mu_M = 0.7$ mm, desired mass m_d (dotted black), PI controller (dotted gray), compensation based controller (solid black), sliding-mode controller (solid gray) for a shorter (left) and longer time-scale (right).

Eq. (16) and assuming that the third moment of the product fraction is greater than zero and the effective mass injected bounded, the following sliding mode control law is chosen

$$K = \begin{cases} 0 & \text{if } e \geq 0 \\ K_{max} & \text{if } e < 0 \end{cases} \tag{19}$$

where K_{max} is the maximum drain. Assuming the maximum drain K_{max} is chosen such that the following inequality holds:

$$K_{max} > \frac{6}{\pi \varrho} \frac{\dot{m}_e}{\int_0^\infty L^3 T_2 (1 - T_1) n dL} \tag{20}$$

this control results in the following stable closed-loop error dynamics:

$$e = \begin{cases} -\dot{m}_e & \text{if } e \geq 0 \\ -\dot{m}_e + K_{max} \frac{\pi}{6} \varrho \int_0^\infty L^3 K T_2 (1 - T_1) n dL > 0 & \text{if } e < 0 \end{cases} \tag{21}$$

It should be mentioned, that the sliding mode control law uses only the error signal and does not require any additional measurement information. In addition, it is robust with respect to

parameter variations or unforeseen disturbances, e.g. feed variations, for sufficiently high values of K_{max}.

Testing the designed sliding mode controller on the nonlinear granulation process for a coarse mill grade, i.e. $\mu_M = 0.9$ mm results in the behavior depicted in Fig. 6.

The simulation results for all three designed mass controllers seem promising. The proposed PI controller possesses a considerable stability margin and the sliding mode controller is known for its robustness against matched uncertainties. Therefore, a considerable degree of robustness with respect to process uncertainties can be expected. This will be further studied for a variation of the mill grade, i.e. for changes in the parameter μ_M.

3.4. Closed-loop simulations for fine mill grade

In the following, the behavior of the same granulation process, i.e. including a mass controller, will be investigated for a reduced mill grade reduced, i.e. $\mu_M = 0.7$ mm, with an initial mass excess of 10%. As can be seen from Fig. 7 (left) the compensation
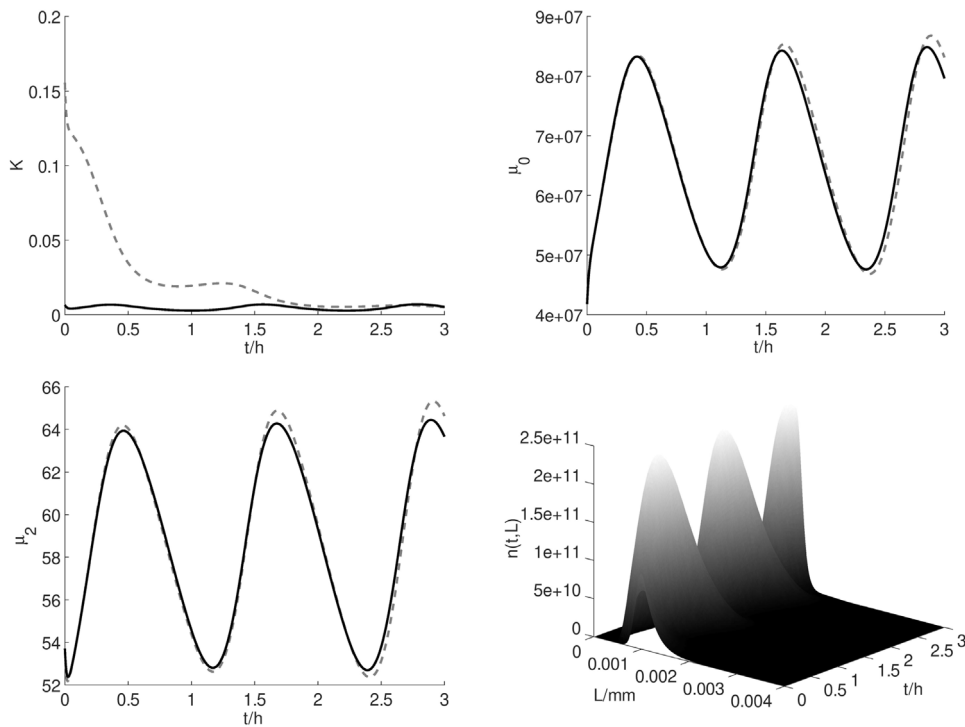
Fig. 8. Closed-loop response of the designed mass controllers for a reduced mill grade $\mu_M = 0.7$ mm, (top left) drain K, (top right) zeroth moment, (bottom left) second moment for PI controller (dotted gray), compensation based controller (solid black), (bottom right) particle size distribution $n(t, L)$ for compensation based controller.
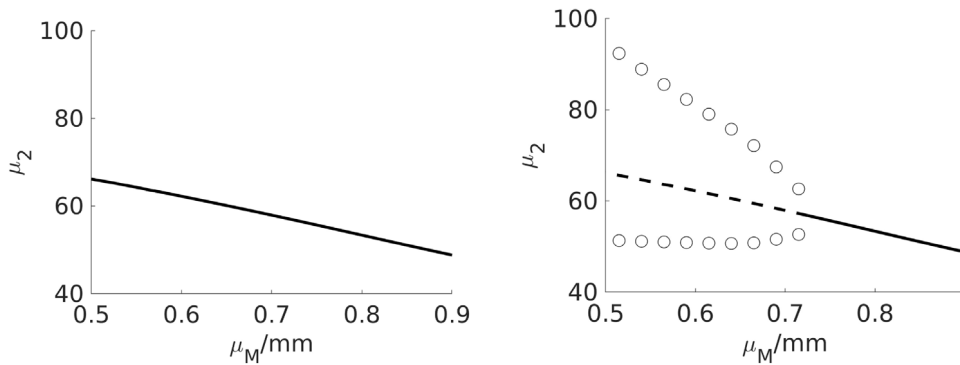

Fig. 9. One-parameter continuation of the open-loop granulation process (left) and applying the compensation based mass controller (right). Second moment of the steady-state particle size distribution — stable (solid black), unstable (dashed black). (o) maximum and minimum value of the occurring limit cycle.

based and sliding mode controller are able to keep the mass at the desired set-point. The PI controller after a convergence phase starts to diverge again. However, as can be seen from Fig. 7 (right) this deviation ends up in small oscillations around the desired set-point. It should be mentioned, that the amplitude of the oscillations can be reduced by further increasing the open-loop gain K_p of the PI controller. Interestingly, do all controller show oscillations in the control variable, i.e. the drain K, the zeroth and second moment μ_0 and μ_2 and the particle size distribution $n(t, L)$ itself (Fig. 8).

From an operational point of view, this behavior is highly undesired. It has been studied in a number of contributions [5, 6,10,12]. Solution approaches, which have been proposed are of two kinds:

1. avoidance of critical parameter areas by the use of stability maps derived from a bifurcation analysis [13,14],
2. design of additional stabilizing control loops [9,13,15–18].

Although both approaches circumvent the stability problem, none of them gives an explanation of the root cause of the observed instabilities. This will be the scope of the following investigations.

4. Zero dynamics of continuous fluidized bed spray granulation

4.1. Bifurcation analysis of the open-loop process

In order to understand the mechanisms, which lead to the observed loss of stability, a bifurcation analysis for the open-loop system, i.e. the continuous fluidized bed spray granulation without mass control is conducted. As can be seen in Fig. 9 (left) the uncontrolled system with the second moment μ_2 as output is stable over a large range of mill grades, i.e. for $\mu_M \in$ [0.9 mm, 0.5 mm]. This is in contrast to the closed-loop system, i.e. applying the proposed compensating mass controller (Fig. 9 (right)). The results for the PI and the sliding mode controller
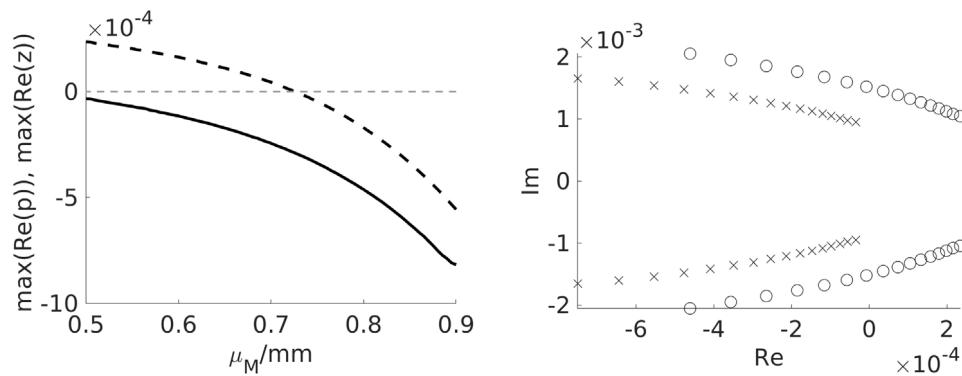
Fig. 10. Maximum real part of the open-loop poles (solid black) and zeros (dashed black) (left). Location of the dominant pole and zero pair for increasing mill grade (right).

are similar. Independent of the chosen mass controller a loss of stability and the occurrence of nonlinear oscillations are observed at around $\mu_M = 0.7$ mm.

4.2. Analysis of the zero dynamics

From a linear control theory point of view, it is well-known that open-loop zeros in the complex right half-plane, result in bounds on the maximum open-loop gain, as they act as attractors for closed-loop poles during gain increase. For nonlinear systems [19] the situation is comparable. Here, applying a nonlinear compensating control law may render part of the system dynamics unobservable from the chosen output. As will be shown in the following, the reason for the decreased stability region when applying mass control lies in the occurrence of zeros in the complex right half-plane and thus the loss of stability in the zero dynamics.

As have been discussed already based on the bifurcation analysis of the open-loop system (Fig. 9 (left)) the uncontrolled granulation process is stable in the investigated parameter range. This can also be seen from Fig. 10 (left), where the maximum real part of the open-loop system poles for variations in the mill grade μ_M are depicted. Here, the maximum real part of the open-loop poles remains negative and thus all poles remain in the left half-plane. In contrast, the maximum real part of the open-loop system zeros changes sign at $\mu_M \approx 0.72$ mm (Fig. 10 (left)). Thus, the zero dynamics of the continuous fluidized bed spray granulation with external sieve mill cycle change their stability behavior and become unstable for sufficiently fine milling. As depicted in Fig. 10 (right) the two dominant pairs of poles and zeros move towards the imaginary axis for decreasing mill grade. The dominant zero pair, which can be seen as a linear two-dimensional approximation of the zero dynamics of the infinite-dimensional process model, crosses the imaginary axis and thus becomes unstable. Therefore, mass controllers with sufficiently high-gains will, in this parameter region, result in a destabilization of the subsystem associated with the zero dynamics. As has been observed in the closed-loop simulations for $\mu_M = 0.7$ mm these instabilities may be not observable from the controlled variable (Fig. 7), as they are compensated by the action of the mass controller. However, they can be observed in the control actuation (Fig. 8 (top left)).

5. Conclusion

It is well-known that continuous fluidized bed spray granulation with external sieve mill cycle may become unstable for certain parameter ranges, in particular fine grinding. These instabilities led to nonlinear oscillations in the particle size distribution, which are in general undesired. In this contribution, the mass controller has been identified as the root cause of the observed instabilities. It has been shown that the open-loop system is stable and the instability is induced by the mass controller. Therefore, control system design for continuous fluidized bed spray granulation processes should be reconsidered. In the literature two principal approaches have been proposed to overcome the aforementioned stability problem. This contribution forms the basis for a third possibility. Future work will be thus concerned with a mass controller redesign, taking into account the unstable zero dynamics, and the application parallel compensator for zero dynamics stabilization.

CRediT authorship contribution statement

Stefan Palis: Conceptualization, Methodology.

Declaration of competing interest

The authors declare that they have no known competing financial interests or personal relationships that could have appeared to influence the work reported in this paper.

References

[1] J. Litster, B. Ennis, The Science and Engineering of Granulation Processes, Springer, 2004.
[2] L. Mörl, S. Heinrich, M. Peglow, Handbook of Powder Technology, in: Fluidized Bed Spray Granulation, Elsevier, 2007, pp. 21–188 (Chapter 2).
[3] D.E. Bertin, I.M. Cotabarren, V. Bucalá, J. Piña, Analysis of the product granulometry, temperature and mass flow of an industrial multichamber fluidized bed urea granulator, Powder Technol. 206 (2011) 122–131.
[4] I. Cotabarren, D. Bertín, J. Piña, V. Bucalá, Analysis of optimal control problems and plant debottlenecking for urea granulation circuits, Ind. Eng. Chem. Res. 50 (2011) 11996–12010.
[5] C. Neugebauer, S. Palis, A. Bück, E. Tsotsas, S. Heinrich, A. Kienle, A dynamic two-zone model of continuous fluidized bed layering granulation with internal product classification, Particuology 31 (2017) 8–14.
[6] M. Schmidt, A. Bück, E. Tsotsas, Experimental investigation of process stability of continuous spray fluidized bed layering with internal separation, Chem. Eng. Sci. 126 (2015) 55–66.
[7] S. Heinrich, M. Peglow, M. Ihlow, M. Henneberg, L. Mörl, Analysis of the start-up process in continuous fluidized bed spray granulation by population balance modeling, Chem. Eng. Sci. 57 (2002) 4369–4390.
[8] L. Mörl, M. Mittelstrass, J. Sachse, Zum kugelwachstum bei der Wirbelschichttrocknung von Lösungen oder Suspensionen, Chem. Tech. 29 (1977) 540–542.
[9] C. Neugebauer, E. Diez, A. Bück, S. Palis, S. Heinrich, A. Kienle, On the dynamics and control of continuous fluidized bed layering granulation with screen-mill-cycle, Powder Technol. 354 (2019) 765–778.
[10] R. Radichkov, T. Müller, A. Kienle, S. Heinrich, M. Peglow, L. Mörl, A numerical bifurcation analysis of continuous fluidized bed spray granulation with external product classification, Chem. Eng. Proc. 45 (2006) 826–837.
[11] N. Hampel, A. Bück, M. Peglow, E. Tsotsas, Continuous pellet coating in a wurster fluidized bed process, Chem. Eng. Sci. 86 (2013) 87–98.

[12] A. Bück, C. Neugebauer, K. Meyer, S. Palis, E. Diez, A. Kienle, S. Heinrich, E. Tsotsas, Influence of operation parameters on process stability in continuous fluidised bed layering with external product classification, Powder Technol. 300 (2016) 37–45.

[13] S. Palis, A. Kienle, Stabilization of continuous fluidized bed spray granulation with external product classification, Chem. Eng. Sci. 70 (2012) 200–209.

[14] C. Neugebauer, A. Bück, S. Palis, L. Mielke, E. Tsotsas, A. Kienle, Influence of thermal conditions on particle properties in fluidized bed layering granulation, Processes (2018) 1–17.

[15] A. Bück, S. Palis, E. Tsotsas, Model-based control of particle properties in fluidised bed spray granulation, Powder Technol. 270 (2015) 575–583.

[16] A. Bück, R. Dürr, M. Schmidt, E. Tsotsas, Model predictive control of continuous layering granulation in fluidised beds with internal product classification, J. Process Control 45 (2016) 65–75.

[17] S. Palis, A. Kienle, Discrepancy based control of particulate processes, J. Process Control 24 (2014) 33–46.

[18] S. Palis, Non-identifier-based adaptive control of continuous fluidized bed spray granulation, J. Process Control 71 (2018) 46–51.

[19] A. Isidori, The zero dynamics of a nonlinear system: From the origin to the latest progresses of a long successful story, Eur. J. Control 19 (2013) 369–378.

On the dynamics and control of continuous fluidized bed layering granulation with screen-mill-cycle

C. Neugebauer [a], E. Diez [b], A. Bück [c], S. Palis [a], S. Heinrich [b], A. Kienle [a,d,*]

[a] *Automation / Modeling, Otto von Guericke University, Magdeburg, Germany*
[b] *Institute of Solids Process Engineering and Particle Technology, Hamburg University of Technology, Hamburg, Germany*
[c] *Institute of Particle Technology, Friedrich-Alexander University Erlangen-Nürnberg, Erlangen, Germany*
[d] *Max Planck Institute for Dynamics of Complex Technical Systems, Magdeburg, Germany*

ABSTRACT

This paper is concerned with an experimental and theoretical study of dynamics and control of fluidized bed layering granulation with external screen mill cycle. To achieve quantitative agreement between model calculations and experiments an extended dynamic process model is proposed. In contrast to previous work by Dreyschultze et al. [1] specific plant characteristics are taken explicitly into account including a more detailed model of the milling process and a classifying particle withdrawal from the granulation chamber. The model is then used to develop new control strategies. First, a novel bed mass controller is designed and validated. Afterward, a second control loop is introduced to dampen the oscillatory behavior of the particle size distribution. It is shown that the new control concepts achieve stable steady-state operation within a short time and thereby improve the process dynamics significantly. Theoretical predictions and experimental results are shown to be in good agreement.

1. Introduction

In fluidized bed layering granulation (FBLG), product granules of high quality are formulated by spraying a solid-containing liquid, e.g. a solution or suspension, onto a bed of particles fluidized with a heated gas [2]. While the liquid fraction of the injection evaporates, the solid fraction remains on the surface of the particles inducing a layer-wise growth [3]. For high production rates, FBLG is operated as a continuous process. Since product particles are continuously removed, this in turn requires a continuous supply of new nuclei. This can be achieved either by internal nucleation due to thermal overspray [4] or grinding of oversized particles [5].

As was shown by means of experiments, presented by Schütte et al. [6] and Schmidt et al. [7–9], continuous FBLG tends to instabilities in the form of self-sustained non-linear oscillations of the particle size distribution (PSD). These oscillations lead to variations in the product properties or, in the worst case, may even lead to a breakdown of the granulation process. They are therefore highly undesired. To clarify the potential reasons for these instabilities, different processes configurations were studied by means of model-based analysis. While the authors Vreman et al. [10] and Neugebauer et al. [11] studied the dynamics of FBLG with internal nucleation, Radichkov et al. [12] and

Dreyschultze et al. [1] put the focus on FBLG with formation of seed particles by milling of oversized particles. All contributions revealed a significant impact of the operating conditions on the dynamic stability. However, besides stability, the operating parameters also affect the particle properties: The contributions of Hoffmann et al. [13], Rieck et al. [14], and Diez et al. [15] proved the dependency of selected particle characteristics, for instance, particle porosity, on the thermal conditions inside the granulation chamber. Therefore, a careful selection of operating parameters is essential for the formation of particles with tailor-made properties under stable conditions. In addition, it has been shown theoretically that the application of feedback control strategies is promising to enhance the dynamic stability and the transient behavior of continuous FBLG. Palis & Kienle [16] showed that a linear PI-controller is capable to stabilize continuous FBLG processes in the neighborhood of some given reference point. The robustness can be increased by H∞ loop shaping as presented by Palis & Kienle [16,17]. Further suitable approaches to enhance process stability and the dynamics are adaptive control strategies [18,19], model predictive control [20,21], and non-linear control strategies as discrepancy based control [22,23]. In multi-stage operation the process chamber is subdivided into compartments with different functionalities leading to additional measurements and actuating values. Therefore, Cotabarren et al. [24] and Palis [25] introduced multiple input multiple output control strategies for this type of processes. Even though the simulation results of the

* Corresponding author.
E-mail address: kienle@mpi-magdeburg.mpg.de (A. Kienle).

different control approaches are quite promising, an experimental implementation and validation is still missing.

This gap is closed in the present paper. Focus is on continuous FBLG with screen-mill-cycle as presented in Fig. 1: Particles are withdrawn from the granulation chamber via a rotary valve and classified by screening into fine, product and oversized fraction. After milling, the oversized fraction is, together with the fines, re-fed to the granulation chamber while product particles are removed from the process. The experiments are carried out in a pilot plant located at TU Hamburg. Besides control of PSD, special attention is also given to the control of the bed mass, which turned out to be non-trivial and is a necessary prerequisite for stable long term operation of the plant. Furthermore, an extended mathematical model of the plant is presented and compared to the experimental findings.

The remainder of the present paper is structured as followed: In the upcoming Section 1.1 a detailed process description is given. The dynamic model of the investigated FBLG is introduced in Section 2. The results of the experiments are presented and compared to simulation results in the subsequent Section 3. First, focus is on bed mass control. Afterward, control of PSD is addressed. Using the developed mathematical model a corresponding controller is designed to dampen the particle size distribution. Finally, the results of this contribution are summarized and an outlook on future directions is presented in Section 4.

1.1. Process description

The experimental examination has been carried out in a horizontal fluidized bed plant of type *Procell 25* of the manufacturer *Glatt GmbH*, Weimar, Germany. The process chamber, presented in Fig. 2, has a width of 1.00 m, a depth of 0.25 m and a height of 0.40 m and can be divided into four different compartments by introducing weirs. However, throughout this contribution, no weirs were used and the granulator was operated as a single process chamber with uniform conditions due to intensive mixing. All presented experiments were performed under similar conditions. At the start of each experiment, sodium benzoate particles of the overall mass of 27.5 kg were fed to the process chamber. The particles were fluidized by fluidization medium. For this

purpose, ambient air was heated up to 85 °C and blown into the granulation chamber. A proper choice of the fluidization conditions is crucial for the FBLG. Too little fluidization air induces a too small fluidization velocity u_{fluid} resulting in an insufficient fluidization of the particles. Otherwise, too much fluidization air leads to the blow out of the bed since u_{fluid} is too high. An overview of the fluidization conditions, based on [2], is presented in Fig. 3. There, the minimum fluidization velocity is denoted as u_{mf} while u_{elu} describes the permissible maximum value of u_{fluid}. Throughout the experimental investigations, the fluidization velocity u_{fluid} is 2.3 m/s.

The injected solution consists of 35 wt% sodium benzoate dissolved in demineralized water. Per hour of process time 40 kg solution were atomized by three two-fluid nozzles located at the bottom of the granulation chamber. As atomizing gas compressed air was used. The injected droplets sprinkled the particles surface. Due to the enhanced heat exchange between particles and fluidization medium, the liquid phase of the droplets evaporated. The vapor was carried out by the fluidization medium. Because of the evaporation, the temperature of the fluidization medium within the process chamber decreased to 50 °C. Meanwhile, the remaining sodium benzoate solidified on the particles surface inducing the layering-growth. Under the examined process conditions, layering was the dominant granulation mechanism. In accordance with Ennis et al. [26], the influence of agglomeration, attrition, and internal nucleation, was limited by an appropriate choice of the operating parameters.

Particles were withdrawn from the granulation chamber by a rotary valve. The utilized valve is shown in Fig. 2. The discharged particles were transported to a two-deck tumbler screen by pneumatic conveyance. According to the mesh width of the screens, the particles were classified into three fractions: The fines fraction consists of particles smaller than 0.8 mm, the product fraction comprises particles in the range of 0.8 mm to 1.2 mm, and the oversized fraction contains particles larger than 1.2 mm. While the product fraction was removed from the process, the oversized fraction was milled and, together with the fines fraction, re-fed to the granulation chamber. For grinding of the oversized particles an impact mill of type *Rekord A* of *Gebr. Jehmlich GmbH, Nossen, Germany* was utilized. As illustrated in Fig. 2, the mill was equipped with pin-mill grinding elements.
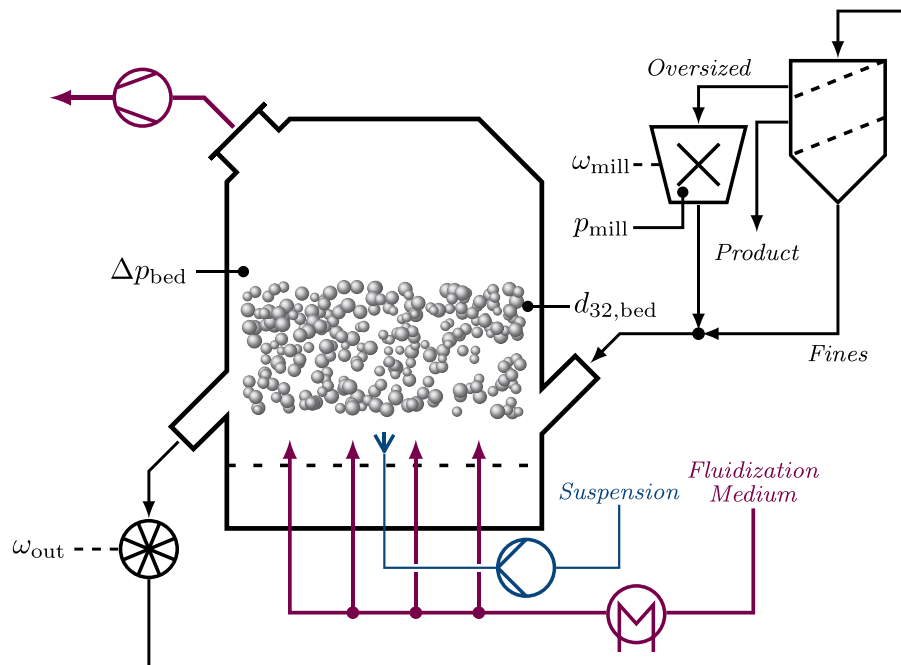

Fig. 1. Process scheme of fluidized bed layering granulation (FBLG) with external screen-mill-cycle.
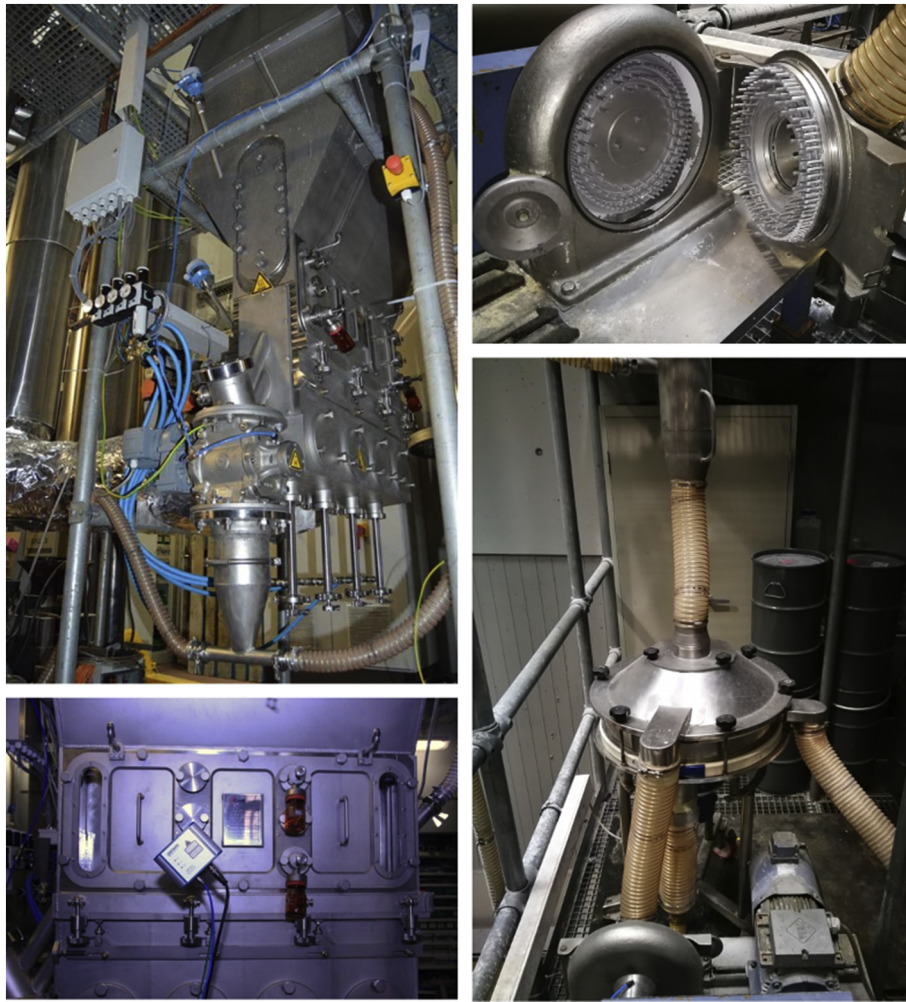
Fig. 2. Pictures of the utilized equipment: **Upper Left:** Granulation chamber *Procell 25* of Glatt GmbH. **Lower Left:** Granulation chamber equipped with Parsum Probe and sampling device. **Upper Right:** Impact mill equipped with pin-mill grinding elements. **Lower Right:** Two-deck-tumbler screen and impact mill.

To obtain online information about the particle sizes, the process chamber was equipped with the inline probe *IPP 70-S (Parsum GmbH, Chemnitz, Germany)*. Based on spatial filter velocimetry (Petrak [27]), the probe determines the chord length distribution of the measured particles, which was used for control purposes. In addition, particle samples of the bed and the outlet were taken every 20 minutes. By means of digital imaging processing, the particle size distributions of those samples were determined with a CamSizer XT (Retsch Technology GmbH, Haan, Germany) in the post-processing.

Fig. 3. Left: Velocity of the fluidization medium within the process chamber as well as elutriation u_{elu} and minimum fluidization u_{mf} velocity with respect to particles size **L.** **Right:** Cross section of the process chamber Procell 25 of Glatt GmbH with corresponding width l_i and temperatures of the fluidization medium θ_i: At bottom $l_0 = 0.25$ m and $\theta_0 = 85\,^\circ$C, in the process chamber $l_1 = 0.25$ m and $\theta_1 \approx 50\,^\circ$C, and at top $l_2 = 1.0$ m and $\theta_2 \approx 45\,^\circ$C.

2. Dynamic model

The following is based on the population balance model (PBM) presented in Dreyschultze et al. [1]. In this model, it is assumed that the granulation chamber is divided into two functional zones. In the first zone, the *spraying zone* (index '1'), the surface of the particles is wetted by the injected solution. In the second zone, the *drying zone* (index '2'), the liquid fraction of the injected solution evaporates from the surface of the particles while the solid fraction remains. Each of the functional zones is considered as well mixed. Particles are assumed to be spherical with diameter L. Agglomeration and breakage are neglected as discussed above.

With these assumptions, the population balance equations of the spraying and the drying zones are

$$\frac{\partial n_1(t,L)}{\partial t} = G\frac{\partial n_1}{\partial L} - \dot{n}_{12} + \dot{n}_{21} + \dot{n}_{1,\mathrm{in}} - \dot{n}_{1,\mathrm{out}} \tag{1}$$

$$\frac{\partial n_2(t,L)}{\partial t} = \dot{n}_{12} - \dot{n}_{21} + \dot{n}_{2,\mathrm{in}} - \dot{n}_{2,\mathrm{out}} \tag{2}$$

Therein, G describes the growth rate, n_i the number density of particles in zone 'i', and $\dot{n}_i$ the particles flows according to Fig. 4:

- $\dot{n}_{12}$ and $\dot{n}_{21}$ describe the particle exchange between the spraying and the drying zone,
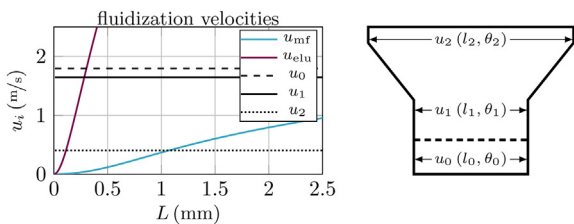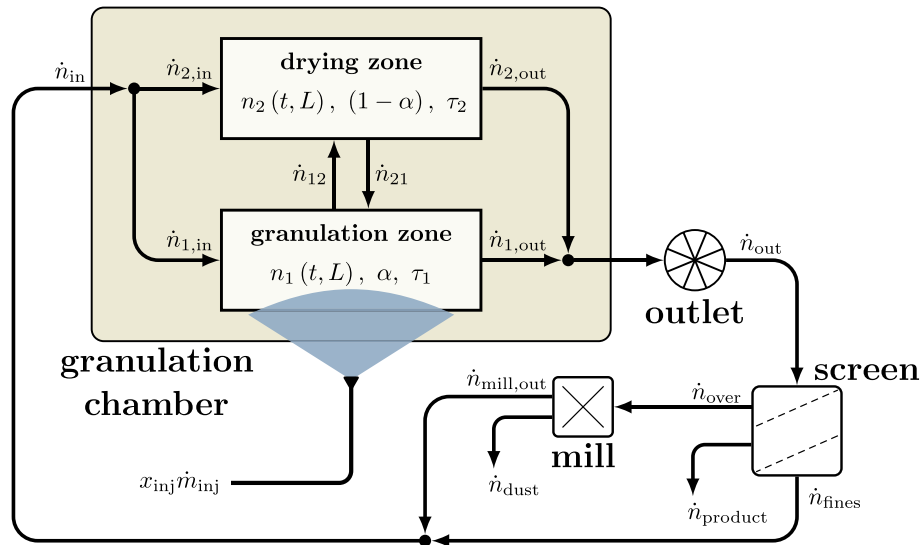
Fig. 4. Flow sheet of the fluidized bed layering granulation with external screen-mill-cycle.

- $\dot{n}_{i,in}$ the particle inlet to the spraying and the drying zone, and
- $\dot{n}_{i,out}$ the particle removal from the spraying and the drying zone.

Following Mörl et al. [2], the particle growth rate G is based on a uniform particle growth depending on the total surface of particles in the spraying zone $A_1(t) = \pi \int_0^\infty (L^2 n_1(t,L))dL$, by

$$G = \frac{2x_{inj}\dot{m}_{inj}}{\rho_s A_1(t)} \tag{3}$$

with the injection rate $\dot{m}_{inj}$ and the corresponding mass fraction x_{inj} and mass density ρ_s of the solid fraction within the injected suspension.

The relative volume of particles within the spraying zone

$$\alpha = \frac{\mu_3(n_1)}{\mu_3(n_1) + \mu_3(n_2)} \quad \text{with} \quad \mu_j(n_i) = \int_0^\infty L^j n_i(t,L)dL \tag{4}$$

and the drying zone $(1 - \alpha)$ are assumed to be constant.

Thus, the condition $\mu_3(\dot{n}_{12}) = \mu_3(\dot{n}_{21})$ with the particle exchange rates between the spraying and the drying zones

$$\dot{n}_{12}(t,L) = n_1/\tau_1 \quad \text{and} \quad \dot{n}_{21}(t,L) = n_2/\tau_2 \tag{5}$$

are expressed in terms of residence times τ_1 and τ_2. Assuming $\mu_3(\dot{n}_{12}) = \mu_3(\dot{n}_{21})$, yields the following relation between the residence times and α [28]

$$1/\tau_1 = (1-\alpha)/(\alpha\tau_2) . \tag{6}$$

Characteristic values for α and τ_2 for different process configurations were given in the literature (see Bück et al. [29] and references therein).

Main differences to the model presented in [1] are related to the calculation of $\dot{n}_{1,in}, \dot{n}_{1,out}, \dot{n}_{2,out}$ in Eqs. (1) and (2), which depend on the product withdrawal, the bed mass control and the model of the mill. These aspects have been modified as follows to gain a better quantitative description of the plant dynamics:

a) The model used in this paper admits a variable total bed mass to simulate the behavior of the bed mass control strategy. In contrast to this, a constant bed mass was assumed in [1] corresponding to an ideal controller.
b) In the experiments to be discussed subsequently, it was observed that larger particles are preferably withdrawn from the bed compared to smaller particles. Therefore, the assumption of a representative product removal from the bed in [1] was replaced by a classified product removal.
c) The model of the mill is crucial for a quantitative prediction of the process dynamics. Therefore, a more detailed model of the mill was identified from stand-alone milling experiments and added to the plant model.

Details of these modifications are given in the following step by step.

2.1. Particle withdrawal from the bed and external product screening

Particles are withdrawn from the process chamber by a rotary valve. It is assumed that the rotary speed of the valve ω_{out} determines the

Table 1
Nomenclature according to the presented fluidized bed layering granulation.

| Nomenclature		
A	(mm^2)	particle surface
d_{32}	(mm)	Sauter mean diameter
e	$(-)$	control error
G	(mm/s)	growth rate
k	$(-)$	gain
K	$(-)$	gain of the withdrawal
L	(mm)	diameter of particle
L_i	(mm)	separation diameter
$\dot{m}$	(kg/s)	mass flow rate
n	$(1/mm)$	number density of particles
$\dot{n}$	$(1/mm)$	number density of particle flow
p	(W)	electrical power
q_0	$(1/mm)$	normalized number density of particle
q_3	$(1/mm)$	normalized volume density of particle
Q_i	$(1/mm)$	cumulative normalized particle size distribution
t	(s)	time
T	$(-)$	separation function
u	(m/s)	velocity of fluidization medium
x	(s)	mass fraction
Greek letters		
α	$(-)$	relative size of granulation zone
Δp	$(mBar)$	pressure drop
θ	$(°C)$	temperature
$\mu_i(\cdot)$	$(mm^{(i-1)})$	i^{th} order moment of argument
Π_i	$(-)$	parameter set of power of mill
ρ	(kg/mm^3)	mass density
σ	(mm)	variance of separation
τ	(s)	time constant
ω	$(\%)$	relative rotational velocity
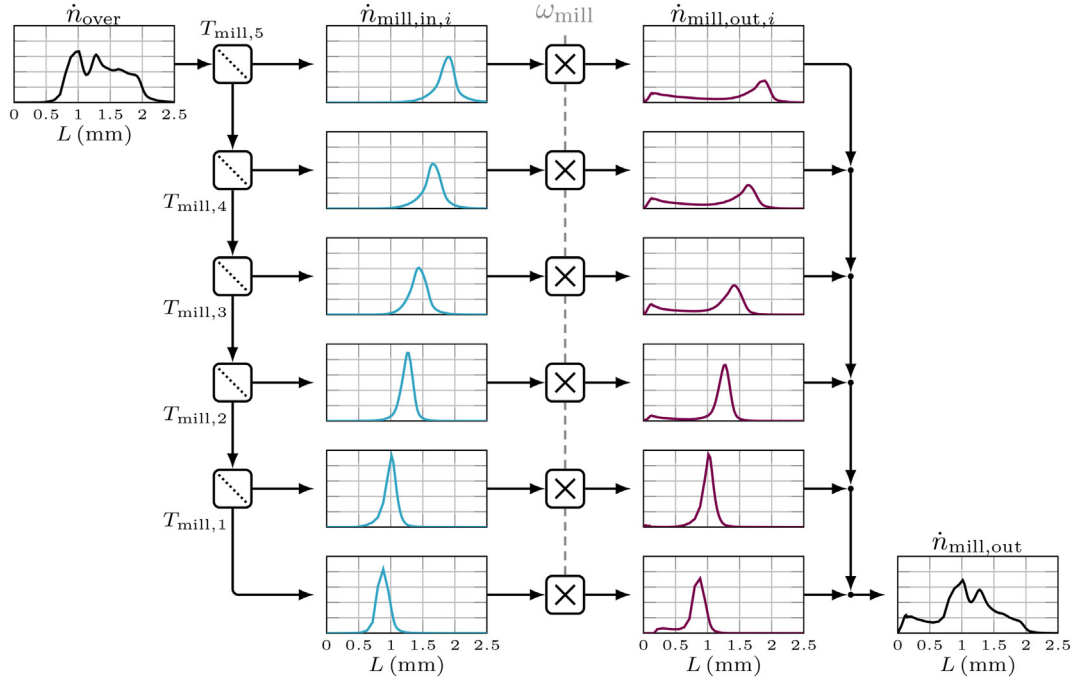
Fig. 5. Scheme of the size-dependent mill model: Oversized particles $\dot{n}_{over}$ are classified into the six fractions $\dot{n}_{mill,in,i}$ by separation functions $T_{mill,i}$. Each fraction i is milled with ω_{mill} to the corresponding $\dot{n}_{mill,out,i}$. Finally, the milled fractions are merged to $\dot{n}_{mill,out}$.

mass flow of the discharged particles by

$$\dot{m}_{out}(t) = k_{out} \cdot \omega_{out} \quad 0 \leq \dot{m}_{out} \leq \dot{m}_{out,max} \tag{7}$$

Thus, in a first step, ω_{out} is used as manipulated variable to control the bed mass m_{bed}. Bed mass is measured by means of pressure drop across the bed Δp_{bed}, which is in good approximation proportional to the bed mass for constant fluidization conditions applied in the experiments. Control is done with a PI controller according to

$$\omega_{out}(t) = k_{p,out} \left(e_{\Delta p_{bed}} + 1/\tau_{i,out} \int_0^t e_{\Delta p_{bed}} dt \right) \tag{8}$$

with $0 \leq \omega_{out} \leq \omega_{out,max}$ and $e_{\Delta p_{bed}}(t) = (\Delta p_{bed,ref} - \Delta p_{bed})$ where $\Delta p_{bed,ref}$ denotes the reference value of the pressure drop.

Based on $\dot{m}_{out}$ the number density flow of the withdrawn particles is calculated with

$$\dot{n}_{out}(t, L) = \dot{n}_{1,out} + \dot{n}_{2,out} \tag{9}$$

$$= KT_{out}(n_1 + n_2) \tag{10}$$

where the drain gain K is determined by

$$K = \frac{\dot{\mu}_{3,out}}{\mu_3(T_{out}(n_1 + n_2))} \tag{11}$$

with $\dot{\mu}_{3,out} = 6\dot{m}_{out}/\pi\rho_s$. The term T_{out} accounts for the classified product removal from the bed which was observed in the experiments. This is modeled with the separation function

$$T_i(L_i, \sigma_i) = \frac{\int_0^L \exp\left(-(L-L_i)^2/(2\sigma_i^2)\right)}{\int_0^\infty \exp\left(-(L-L_i)^2/(2\sigma_i^2)\right)} \tag{12}$$

with separation diameter $L_i = L_{out}$ and variance $\sigma_i = \sigma_{out}$. As will be shown in Section 3, the separation diameter depends on the current particle size distribution of the bed. In particular, it is assumed that L_{out} equals the characteristic value $x_{3,60}$, i.e. the particle size were the

cumulative volume based particle size distribution $Q_3(n_1 + n_2)$ equals 0.6:

$$L_{out} = x_{3,60} \quad \text{with} \quad Q_3(L = x_{3,60}) = 0.6 . \tag{13}$$

Table 2
Parameter set according to the simulation study.

| Granulation chamber and injection		
m_{bed}	27.50	(kg)
α	0.05	(−)
τ_2	100.00	(s)
x_{inj}	0.35	(−)
$\dot{m}_{inj}$	40.00	(kg/h)
ρ_s	1440.00	(kg/m³)
Particle withdrawal		
$k_{p,out}$	−60.00	(%/mm)
k_{out}	2.00	(kg/%·h)
σ_{out}	0.75	(mm)
$\tau_{i,out}$	120.00	(s)
$\omega_{out,max}$	40.00	(%)
Particle screening		
$L_{screen,I}$	1.20	(mm)
$\sigma_{screen,I}$	0.125	(mm)
$L_{screen,II}$	0.80	(mm)
$\sigma_{screen,II}$	0.05	(mm)
Milling process		
k_{bypass}	0.75	(−)
$L_{cutsize}$	0.375	(mm)
$\sigma_{cutsize}$	0.105	(mm)
$L_{mill,i}$	[1.01, 1.14, 1.37, 1.58, 1.80]	(mm)
$\sigma_{mill,i}$	[4.05, 13.44, 8.64, 8.58, 9.41]	(mm)
Power of the mill		
$\Pi_{mill,i}$	[−3.09, −286.04, 25.85, 0.04, −0.0008]	(−)
τ_{mill}	0.10	(1/s)
Parameter of controllers		
$k_{p,p_{mill}}$	0.005	(%/w)
$\tau_{i,p_{mill}}$	12.00	(s)
$k_{p,d_{32}}$	250.00	(W/mm)
$p_{mill,0}$	120.00	(W)
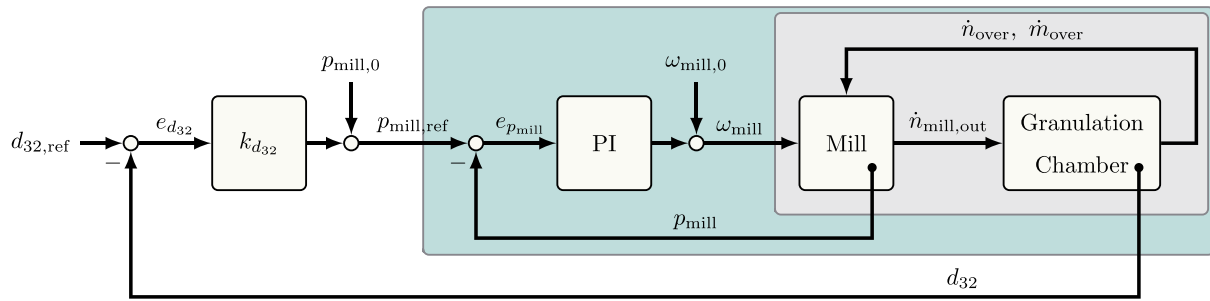
Fig. 6. Control schemes of the experiments: gray configuration was used in experiment 1, green configuration in experiments 2–4, and overall configuration in experiment 5.

By screening, the withdrawn particles are further classified into three fractions: Fines $\dot{n}_{\text{fines}}$, product $\dot{n}_{\text{product}}$, and oversized $\dot{n}_{\text{over}}$. The screening process is described by

$$\dot{n}_{\text{over}}(t,L) = T_{\text{screen,I}} \ \dot{n}_{\text{out}} \ , \tag{14}$$

$$\dot{n}_{\text{product}}(t,L) = (1 - T_{\text{screen,I}}) T_{\text{screen,II}} \ \dot{n}_{\text{out}} \ , \ \text{and} \tag{15}$$

$$\dot{n}_{\text{fines}}(t,L) = (1 - T_{\text{screen,I}})(1 - T_{\text{screen,II}}) \ \dot{n}_{\text{out}} \ . \tag{16}$$

Again, the separation functions $T_{\text{screen,I}}$ and $T_{\text{screen,II}}$ are given by Eq. (12) with the parameters $\{L_{\text{screen,I}}, \sigma_{\text{screen,I}}\}$ and $\{L_{\text{screen,II}}, \sigma_{\text{screen,II}}\}$ respectively. While the product fraction is removed from the process, the oversized fraction is milled, and together with the fine fraction, recycled to the granulation chamber serving as new nuclei (Table 1).

2.2. Particle milling

The milling of oversized particles has a significant influence on the dynamics of the investigated FBLG process [1,8,12]. Thus, a detailed model of the milling is essential for the quantitative prediction of the plant dynamics. In general, milling of granules is complex. For instance, the type and configuration of the mill as well as particle properties, e.g. porosity and size, have a major influence on the breakage of particles during milling [30,31,32]. Following the ideas in Neugebauer et al. [33], an empirical PBM of the grinding process was established. However, compared to [33] a more detailed model of the mill was developed in the present work taking into account the influence of particle size distribution of the feed to the mill on the grinding processes. Since the PSD of milled particles cannot be measured inline, the following preliminary experimental study was performed: Particles of different sizes were classified into six fractions by screening. Samples of 0.5 kg were milled with the relative rotational velocities $\omega_{\text{mill}} = \{10,15,20,25\}\%$, i.e. 24 experiments were performed in total. The PSDs of the samples were determined before and after milling with the CamSizer XT. Based on the measurements, the separation functions of the five screens

$$T_{\text{mill,i}}(L_{\text{mill,i}}, \sigma_{\text{mill,i}}) = \left(1 + (L_{\text{mill,i}}/L)^2\right) \exp\left(\frac{\sigma_{\text{mill,i}}}{1 - (L/L_{\text{mill,i}})^2}\right) \tag{17}$$

with $i \in \{1,2,3,4,5\}$ were parameterized. Further, the normalized
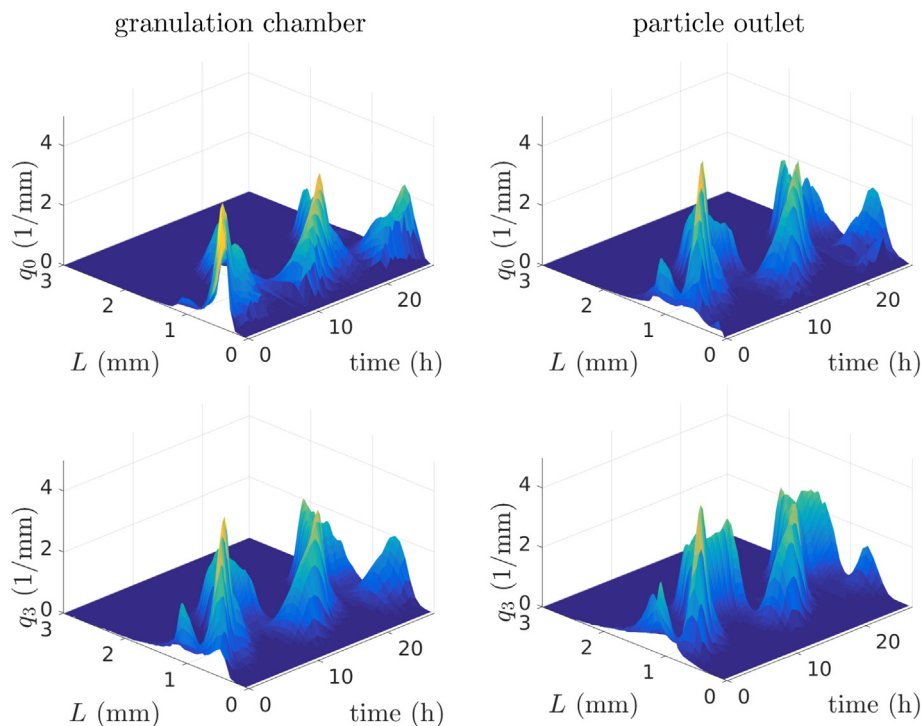

Fig. 7. Experiment 1: Number and volume based, normalized size distributions $q_0(t,L)$ and $q_3(T,L)$ of particles in granulation chamber and particle outlet. The distributions were determined by measuring the taken samples with a CamSizer XT.
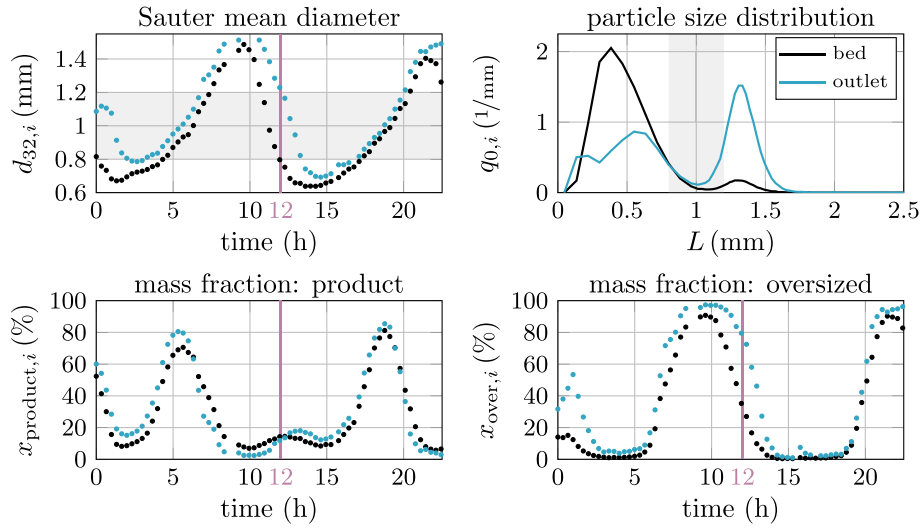
Fig. 8. Experiment 1: **Upper Left:** Sauter mean diameter of particles in granulation chamber and outlet over time. Product range is high-lighted in gray. **Upper Right:** normalized particle size distribution $q_0(t,L)$ of bed and outlet at $t = 12\,$h. Product range is high-lighted in gray. **Lower left and right:** *mass* fractions of product and oversized particles in bed and outlet.

number densities of the particle size distributions of the milled particle fractions $q_{0,\text{mill,out},i}$ were determined for the different values of ω_{mill}.

These quantities are used for modeling the mill as follows (see also Fig. 5). First $\dot{n}_{\text{over}}$ is separated into six fractions with the according screen functions $T_{\text{mill,i}}$

$$\dot{n}_{\text{mill,in},i}(t,L) = T_{\text{mill},i-1} \prod_{j=i}^{5}(1-T_{\text{mill},j})\dot{n}_{\text{over}} \ , \quad i \in \{6,5,...,2\} \qquad (18)$$

and

$$\dot{n}_{\text{mill,in},1}(t,L) = \prod_{j=1}^{5}(1-T_{\text{mill},j})\dot{n}_{\text{over}} \ . \qquad (19)$$

The relative mass of each fraction i is conserved and determined by $k_{\text{mill},i}(t) = \mu_3(\dot{n}_{\text{mill,in},i})/\mu_3(\dot{n}_{\text{over}})$. Based on $k_{\text{mill},i}$, the milled particle

flow rate of each fraction i is determined:

$$\dot{n}_{\text{mill,out},i}(t,L) = k_{\text{mill,i}} \frac{q_{0,\text{mill,out},i}(\omega_{\text{mill}},L)}{\mu_3\big(q_{0,\text{mill,out},i}(\omega_{\text{mill}},L)\big)} \ . \qquad (20)$$

Subsequently, the fractions $\dot{n}_{\text{mill,out},i}$ are merged again. The particle size distribution ω_{mill} of the milled particles were obtained by linear interpolation between available measurements for the specific values of ω_{mill} given above. Further, it is taken into account, that, due to the increased throughput during the continuous FBLG, the efficiency of the milling decreases. For that purpose, a by-pass of particles with gain k_{bypass} is introduced, representing the uncomminuted particles of $\dot{n}_{\text{over}}$:

$$\dot{n}_{\text{mill,out}}(t,L) = k_{\text{bypass}}\dot{n}_{\text{over}} + (1 - k_{\text{bypass}}) \sum_{i=1}^{6} \dot{n}_{\text{mill,out},i} \ . \qquad (21)$$
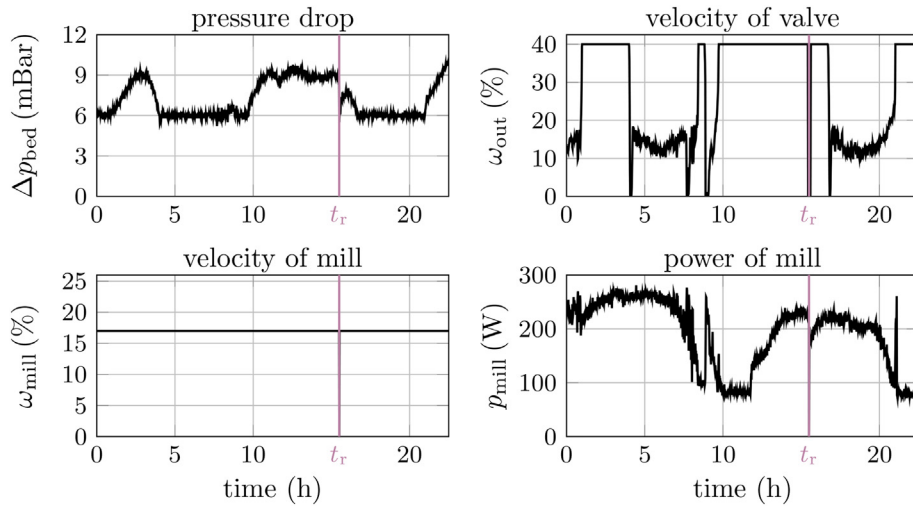

Fig. 9. Experiment 1: measured pressure drop over bed Δp_{bed}, relative rotational speed of the rotary valve at the outlet ω_{out}, relative rotational speed of the mill ω_{mill}, and electrical power of the mill p_{mill}. In the experiment, the mill was operated with a constant $\omega_{\text{mill}} = 17\%$. Alternations of p_{mill} indicate an uneven particle comminution resulting in variations of the Δp_{bed} (reference value: $\Delta p_{\text{bed,ref}} = 6\,$mBar). The experiment was interrupted at $t_r = 15.5\,$h.
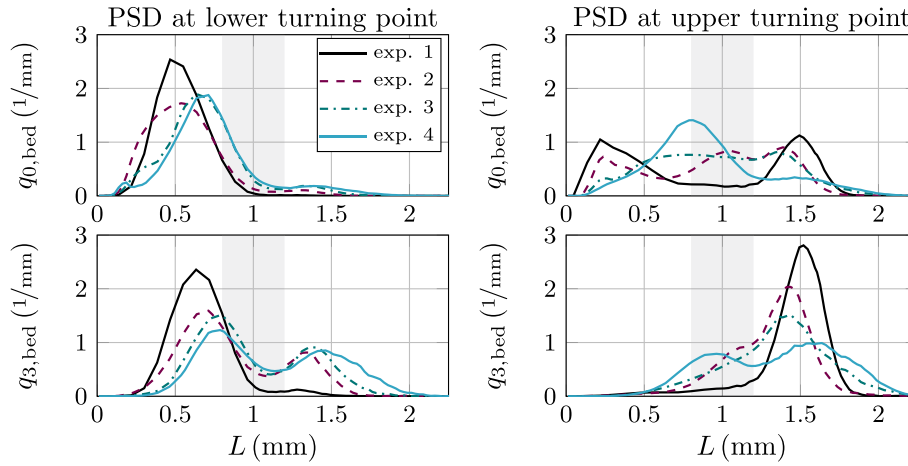
Fig. 10. Particle size distributions of samples at lower and upper turning point of $d_{32,\text{bed}}$ for open-loop experiments 1–4. Corresponding sampling times: experiment 1–13.6 h (lower turning point) and 21.4 h (upper turning point), experiment 2–13.0 h and 10.6 h, experiment 3–33.4 h and 37.7 h, experiment 4–31.3 h and 35.3 h. Product range is highlighted in gray.

Finally, it is assumed, that, because of the fluidization conditions presented in Fig. 3, dust particles are blown out according to

$$\dot{n}_{\text{dust}}(t,L) = (1 - T(L_{\text{cutsize}}, \sigma_{\text{cutsize}}))\dot{n}_{\text{mill,out}} \ . \tag{22}$$

Again, the separation function $T(L_{\text{cutsize}}, \sigma_{\text{cutsize}})$ is described by Eq. (12). The remaining particles are, together with $\dot{n}_{\text{fines}}$, re-fed to the granulation chamber:

$$\dot{n}_{\text{in}}(t,L) = \dot{n}_{\text{fines}} + T(\mu_{\text{cutsize}}, \sigma_{\text{cutsize}}) \ \dot{n}_{\text{mill,out}} \ . \tag{23}$$

The recycled particles are distributed to the spraying and drying zone with respect to the respective relative volume:

$$\dot{n}_{1,\text{in}}(t,L) = \alpha \ \dot{n}_{\text{in}} \quad \text{and} \quad \dot{n}_{2,\text{in}}(t,L) = (1-\alpha)\dot{n}_{\text{in}} \ . \tag{24}$$

2.3. Numerical solution

The dynamic model was implemented in MATLAB (2018a, MathWorks, Natick, MA, USA, 2018) applying a method of lines approach. Based on a finite volume method approach, the partial
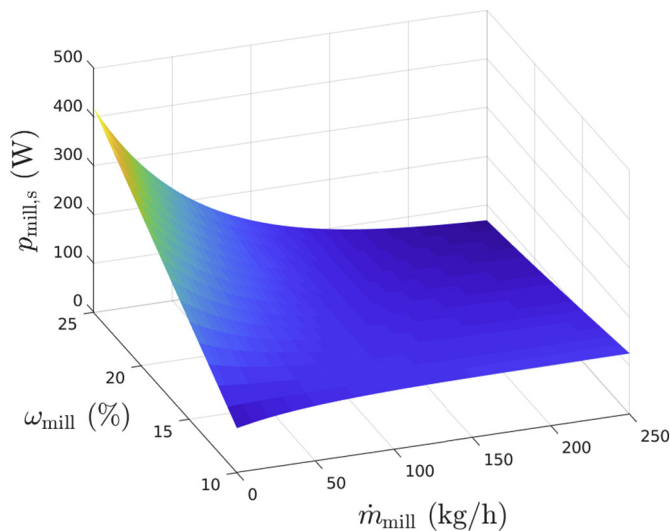
differential Eqs. (1) and (2) were discretized using a first order upwind scheme with 200 equidistant grid points in the domain $L = [0,5]$ mm. To solve the resulting system of ordinary equations the MATLAB built-in solver *ode15s* was utilized. The model parameters used for all simulations are shown in Table 2. The initial particle size distributions $n_1(t = 0,L)$ and $n_2(t = 0,L)$ are based on the CamSizer measurement of the first sample of the particle bed of the related experiment.

3. Experiments and simulation study

3.1. Operation with constant rotational speed of the mill

In the first experiment, the pin mill was operated with a constant relative rotational speed as introduced in the previous section and illustrated in Fig. 6 with the gray box. This operation mode is the standard configuration of the investigated FBLG and was, for instance, also used by Schmidt et al. [8,9,34].

The corresponding temporal evolution of the number and volume based normalized particle size distribution $q_{0,i}(t,L)$ and $q_{3,i}(t,L)$ of bed and outlet are presented in Fig. 7. The size distributions are characterized by oscillations with long periods. As depicted in Fig. 8, the oscillations can also be observed by monitoring the Sauter mean diameter of bed $d_{32,\text{bed}}$ and outlet $d_{32,\text{out}}$. The Sauter mean diameter, defined as the area-weighted mean size of a particle population and determined by $d_{32,i} = \mu_3(q_{0,i})/\mu_2(q_{0,i})$, is a representative of the PSD. Throughout the experiment, $d_{32,\text{out}}$ was larger than $d_{32,\text{bed}}$. The deviation indicates the classifying impact of the particle withdrawal. As illustrated by the particle size distribution $q_{0,i}$ of bed and outlet, as an example the samples at $t = 12h$ are presented in Fig. 8, primarily large particles were discharged from the process chamber.

Because of the oscillations of the PSD, the related mass fractions of fines x_{fines}, product x_{product}, and oversized particles x_{over} varied. As the bed mass is controlled via Δp_{bed} and ω_{out}, see Eqs. (7) and (8), the

Fig. 11. Black box model of the stationary electrical power of mill: $p_{\text{mill,s}}$ with respect to mill throughput $\dot{m}_{\text{mill}}$ and relative rotational speed of the mill ω_{mill}.

Table 3
Overview of the experiments.

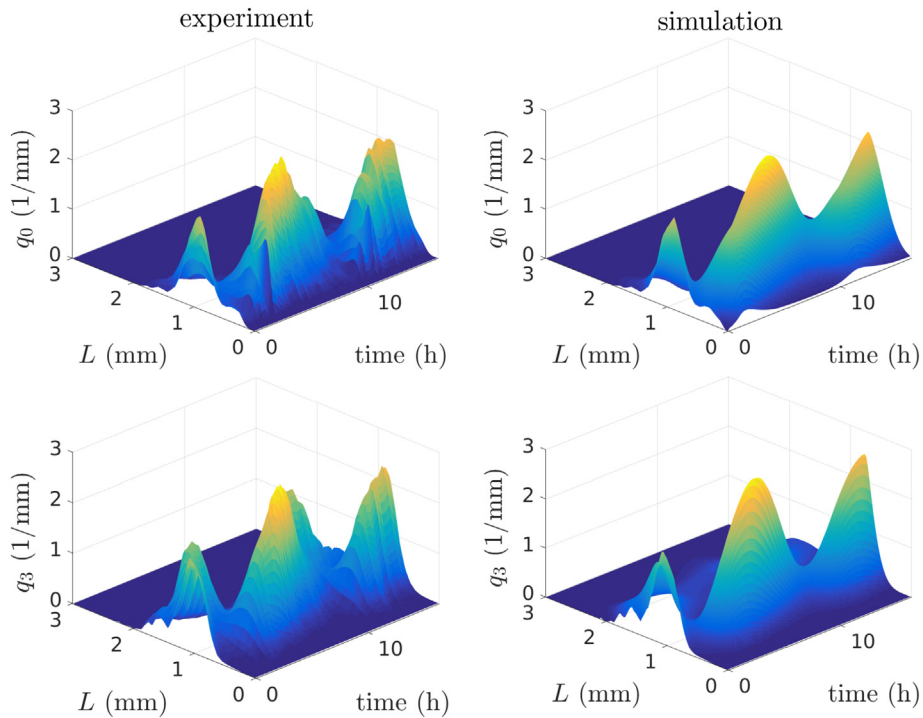| ID	Product	ω_{mill}	$p_{\text{mill,ref}}$	$d_{32,\text{ref}}$
1	0.8–1.2 mm	17%	–	–
2	0.8–1.2 mm	–	170 W	–
3	0.8–1.2 mm	–	140 W	–
4	0.8–1.2 mm	–	120 W	–
5	0.8–1.2 mm	–	–	1.2 mm

Fig. 12. Left Column: normalized number and volume based particle size distributions $q_{0,bed}$ and $q_{3,bed}$ of experiment 2. PSDs were determined with CamSizer XT. **Right Column:** PSDs of the corresponding simulation.

oscillations led to variations of the mass flow of withdrawn particles $\dot{m}_{out}$. Since $\dot{m}_{out}$ cannot be measured online, the variations of $\dot{m}_{out}$ can only be observed by monitoring the rotational speed of the rotary valve at the particle outlet ω_{out}. As shown in Fig. 9, ω_{out} varied in the range of $[0,\omega_{out,max}]$ throughout the experiment. Based on previous experiments, the upper limit $\omega_{out,max}$ was found to be 40% as a further increase of ω_{out} did not raise $\dot{m}_{out}$. It is due to this restriction that not enough product particles were discharged from the FBLG. This was exacerbated by the classifying particle withdrawal: in the outlet, product particles were displaced by oversized particles (see Fig. 8). The insufficient product removal induced a rise of m_{bed} and, as illustrated in Fig. 9, an increase of the pressure drop Δp_{bed}. Similar patterns of behavior were observed by Schmidt [34]. In the present case, the continuously increasing bed mass finally led to the shutdown of the process.

In addition, the classifying outlet induced an overgrowing of particles in the further course of the experiment. Particles of product fraction were not withdrawn from the process chamber in a sufficient quantity. In consequence, particle growth proceeded such that the particles entered the oversized fraction. This is illustrated in Fig. 10. There, $q_{0,bed}$ and $q_{3,bed}$ at a local minimum and maximum, in the following denoted as turning points, of $d_{32,bed}$ are shown for the experiments 1–4. Of special interest are the modes, viz. the peaks, of the PSDs. At the lower turning point, $t = 13.6$ h, the modes of the PSDs are in the fines fractions. In the progress of the experiment, the particles have grown, leading to a shift of the modes to higher particles sizes. At $t = 21.4$ h, the upper turning point of $d_{32,bed}$, the modes are in the oversized fraction. In consequence, the mass portion x_{over} in bed and outlet increased resulting in a higher mill throughput $\dot{m}_{mill}$.
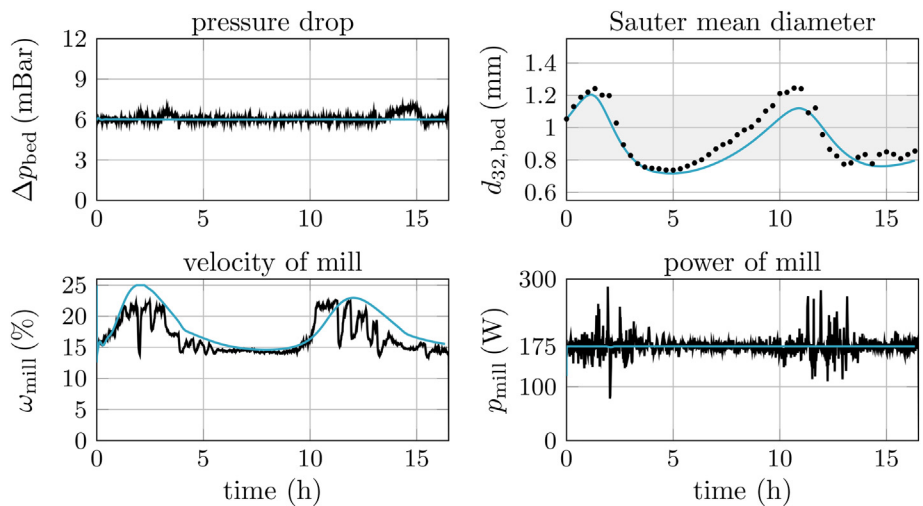

Fig. 13. Comparison of selected data of experiment 2 (black line) and the corresponding simulation results (blue line). By adjusting ω_{mill}, the mill was operated with constant $p_{mill} = 175$ W. While Δp_{bed} is at a constant level, the Sauter mean diameter $d_{32,bed}$ is characterized by non-linear oscillations. The measured Sauter mean diameter is based on the measurements of the CamSizer XT.
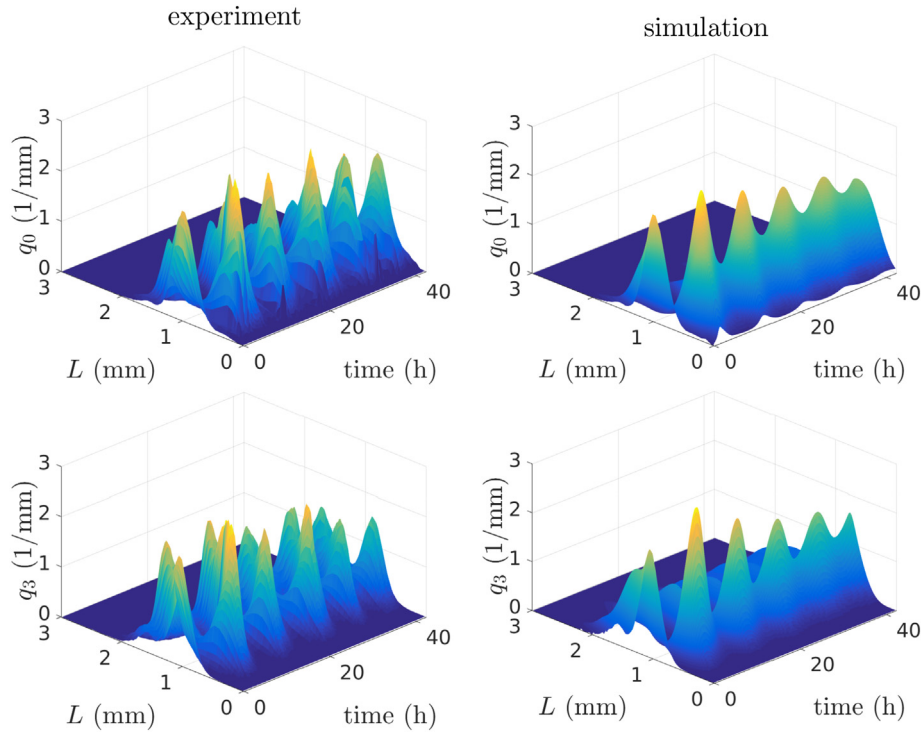
experiment

simulation

Fig. 14. **Left Column:** normalized number and volume based particle size distributions $q_{0,\text{bed}}$ and $q_{3,\text{bed}}$ of experiment 3. PSDs were determined with CamSizer XT. **Right Column:** PSDs of the corresponding simulation.

As illustrated in Fig. 9, the milling process is influenced by $\dot{m}_{\text{mill}}$. An increase of the mill throughput, characterized by high values of ω_{out} and x_{over}, led to a decrease of the electrical power consumption of the mill p_{mill}. This indicates, in combination with the large maxima of $d_{32,\text{bed}}$ and $d_{32,\text{out}}$, the inadequate comminution of oversized particles. The uneven milling supported the overgrowing of the particles and therefore the occurrence of the observed oscillations.

3.2. Closed loop control of the mill power

To enable an even milling of oversized particles feedback control was applied to keep the mill power constant at a given reference value by readjusting the rotational speed of the mill. For this purpose

again a PI controller was used. The block diagram of the control loop is illustrated in green in Fig. 6. The dynamic model was extended accordingly. In particular, it was assumed, that the dynamic behavior of p_{mill} can be described by a first order lag element (PT$_1$):

$$\dot{p}_{\text{mill}}(t) = (p_{\text{mill,s}} - p_{\text{mill}})/\tau_{mill} \tag{25}$$

As indicated by experimental findings, the stationary value of the electrical power $p_{\text{mill,s}}$ depends on ω_{mill} and the mass throughput $\dot{m}_{\text{mill}} = (\pi\rho_s/6)\mu_3(\dot{n}_{\text{over}})$. Based on previous measurements, the correlation

$$p_{\text{mill,s}}(\omega_{\text{mill}}, \dot{m}_{\text{mill}}) = \\ \Pi_1 + \Pi_2\omega_{\text{mill}} + (\Pi_3 + \Pi_4\omega_{\text{mill}}) \exp(-(\Pi_5 + \Pi_6\omega_{\text{mill}})\dot{m}_{\text{mill}}) \tag{26}$$
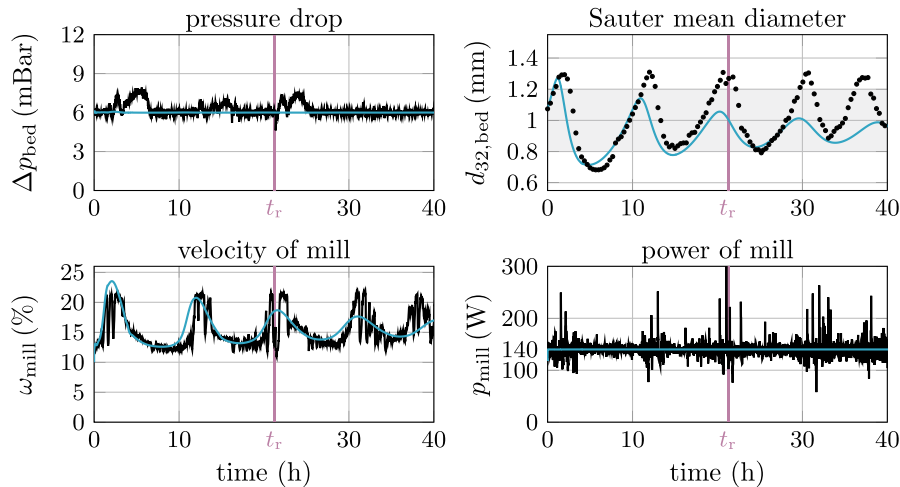

Fig. 15. Comparison of selected data of experiment 3 (black line) and the corresponding simulation (blue line). The mill was operated with constant $p_{\text{mill}} = 140$W. While Δp_{bed} is at a constant level, the Sauter mean diameter $d_{32,\text{bed}}$ is characterized by slow decaying, non-linear oscillations. The measured Sauter mean diameter is based on the measurements of the CamSizer XT, the experiment was interrupted at $t_r = 21.25$ h.
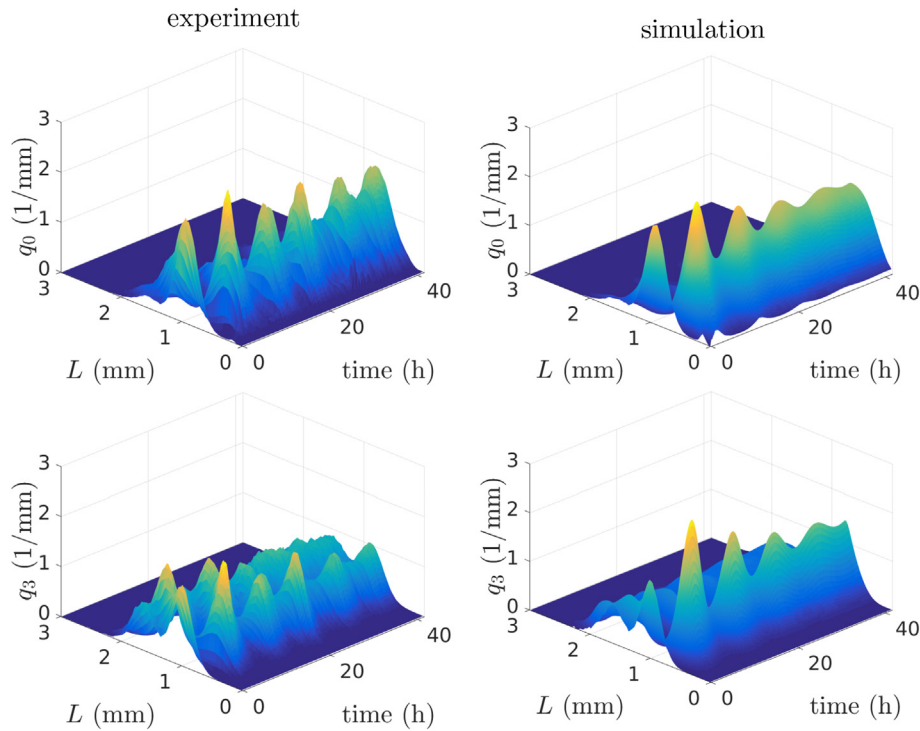
Fig. 16. Left Column: normalized number and volume based particle size distributions $q_{0,\text{bed}}$ and $q_{3,\text{bed}}$ of experiment 4. PSDs were determined with CamSizer XT. **Right Column:** PSDs of the corresponding simulation.

was established by a least square fit. The functional correlation of $p_{\text{mill,s}}$ and its arguments is presented in Fig. 11.

To study the influence of the milling on the process stability, experiments 2–4 were performed with different reference values of the mill power $p_{\text{mill,ref}}$. The set-points of the different experiments are presented in Table 3. Following Dreyschultze et al. [1] and Radichkow et al. [12], it is expected that a reduction of $p_{\text{mill,ref}}$ leads to an enhanced process stability. Throughout the experiments 2–4, the classifying effect of the particle withdrawal described in the previous section is observed again.

In experiment 2, the mill was operated with $p_{\text{mill,ref}} = 175$ W. The results are presented in Figs. 12 and 13. Again, $q_{0,\text{bed}}$ and $q_{3,\text{bed}}$ are characterized by oscillations. As shown in Fig. 10 the measured PSDs are now more compact than in the first experiment: Firstly, the distance between the modes of $q_{0,\text{bed}}$ and $q_{3,\text{bed}}$ at lower ($t = 13.0$ h) and upper

turning point of $d_{32,\text{bed}}$ ($t = 10.6$ h) narrowed. Secondly, the amplitudes of the corresponding modes decreased. This leads, as depicted in Fig. 13, to a decrease in the amplitudes of $d_{32,\text{bed}}$. In consequence, the mass portion of the product fraction is of sufficient size throughout the experiment. Thus, the adequate removal of product particles from the FBLG is guaranteed such that, as monitored by the pressure drop Δp_{bed}, the bed mass m_{bed} is constant over time. Although the operating conditions of the FBLG are constant, the intense milling of oversized particles induced the formation of a large number of small nuclei. In accordance with [1], this leads to the formation of self-sustained oscillation of the PSDs. Therefore, it was not expected that the process settles down to a stable steady state so that the experiment was terminated at $t = 17$ h.

In experiment 3, the reference value of the electrical power of the mill $p_{\text{mill,ref}}$ was reduced to 140 W. Due to the large run-time of 40 h,
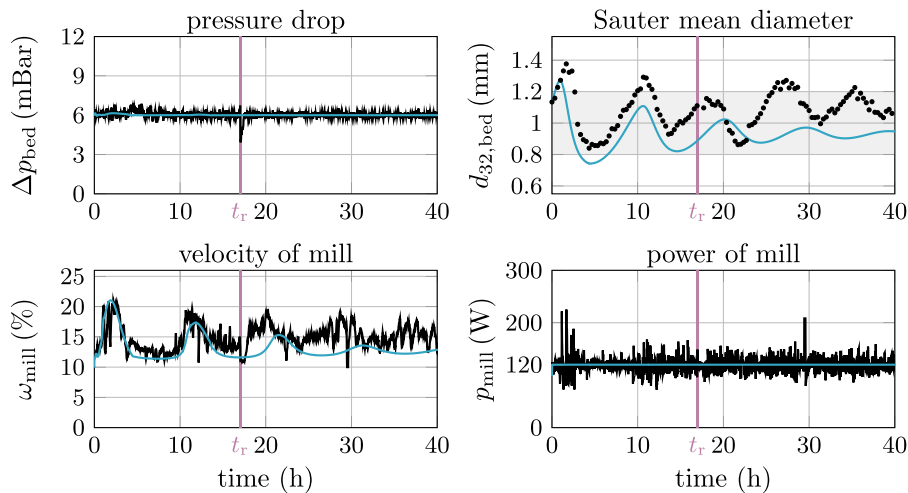

Fig. 17. Comparison of selected data of experiment 4 (black line) and the corresponding simulation results (blue line). The mill was operated with constant $p_{\text{mill}} = 120$ W. While Δp_{bed} is at a constant level, the Sauter mean diameter $d_{32,\text{bed}}$ is characterized by decaying, non-linear oscillations. The measured Sauter mean diameter is based on the measurements of the CamSizer XT, the experiment was interrupted at $t_{\text{r}} = 17.0$ h.
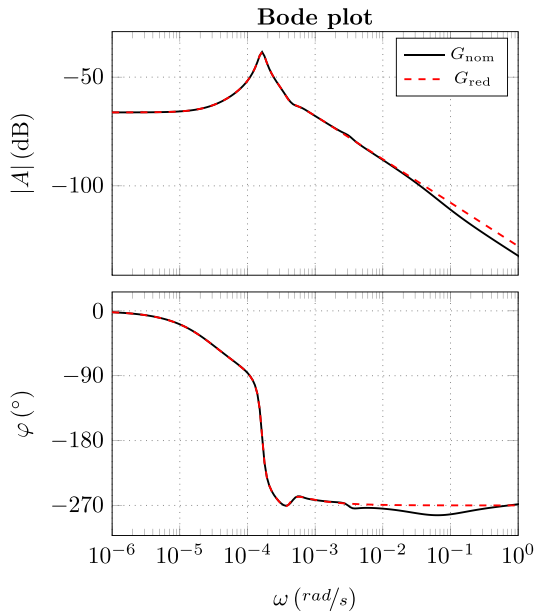
Fig. 18. Bode plots of the full order system $G_{\mathrm{nom}}(j\omega)$ and the reduced system $G_{\mathrm{red}}(j\omega)$ of order 5.

the experiment was interrupted after 21.25 h of process time and restarted again. Figs. 14 and 15 present the related particle size distributions of the bed and further measurement information. Once again, Δp_{bed} and p_{mill} are at a constant level throughout the experiment. Due to the decreased p_{mill}, the particle grinding was reduced. As shown in Fig. 10, the modes of $q_{0,\mathrm{bed}}$ and $q_{3,\mathrm{bed}}$ shifted to a larger particle size L at the lower turning point of $d_{32,\mathrm{bed}}$ at $t = 33.4$ h. This leads to a more even particle growth resulting in a slow decay of the oscillations of the particle size distributions and, in consequence, of the oscillations of $d_{32,\mathrm{bed}}$.

Afterwards, $p_{\mathrm{mill,ref}}$ was further reduced to 120 W in experiment 4. Related PSDs and measurements are presented in Figs. 16 and 17. In experiment 4, a faster decay of the oscillatory behavior is observed compared to experiment 3. As illustrated in Fig. 10, the deviations between the PSDs at the lower and upper turning point of $d_{32,\mathrm{bed}}$, sampling times are $t = 31.3$ h and $t = 35.3$ h, are, compared to the

previous experiments 1–3, quite small. It is expected, that in the further course of the process these deviations would vanish such that the process would reach stable steady-state conditions. However, the decay to steady state is very slow due to the oscillatory behavior. In addition, the settling is aggravated by disturbances, such as the restart of the FBLG at $t_r = 17$ h. Therefore, the experiment was terminated at $t = 40$ h.

Comparison between experiments and model predictions are also shown in Figs. 12–17 for experiments 2–4. In general, simulation results and experimental findings are in good agreement. The maximum values of $q_{0,\mathrm{bed}}$ and $q_{3,\mathrm{bed}}$, as well as the period of the oscillations in Figs. 12, 14, and 16, are at the same level resulting in a similar shape of measured and simulated PSDs. Furthermore, Figs. 13, 15, and 17 show the good agreement of p_{mill} and ω_{mill} between experiments and simulations. With respect to $p_{\mathrm{mill,ref}}$, the model is capable to reproduce the different forms of dynamic behavior. As illustrated in Fig. 12, $p_{\mathrm{mill,ref}} = 170$ W induced oscillations of $q_{0,\mathrm{bed}}$ and $q_{3,\mathrm{bed}}$ with large amplitudes. In contrast to this, the PSDs are characterized by slowly decaying oscillations for $p_{\mathrm{mill,ref}} = 140$ W and $p_{\mathrm{mill,ref}} = 120$ W (see Figs. 14 and 16).

3.3. Additional closed loop control of the Sauter mean diameter

To enhance the dynamics of the process and establish operation with constant PSD as fast as possible, a cascade controller was designed: As illustrated in Fig. 6, the PI-controller for the bed mass is extended by an outer loop to control the Sauter mean diameter $d_{32,\mathrm{bed}}$ by readjusting the reference value of the mill power $p_{\mathrm{mill,ref}}$. The plant model presented in this paper was used for controller design. As a first step, the dynamic model is numerically linearized at the stationary state according to the default parameter set with $p_{\mathrm{mill,ref}} = 120$ W. The resulting linear time-invariant (LTI) transfer function $G_{\mathrm{nom}}(j\omega)$ of order 403 describes the dynamic behavior of the output signal $d_{32,\mathrm{bed}}$ with respect to the input signal $p_{\mathrm{mill,ref}}$ in the neighborhood of the steady state. By means of a balanced truncation, the full-order system is reduced to a system of order 5 [35]. The reduced model $G_{\mathrm{red}}(j\omega)$ shows good agreement with the nominal system $G_{\mathrm{nom}}(j\omega)$ as illustrated with the Bode plots in Fig. 18.

Based on the transfer function $G_{\mathrm{red}}(j\omega)$, a feedback controller is designed by means of the root locus method [36]. Root loci represent the location of the closed loop poles in the complex plane depending on the controller gain. They are illustrated in Fig. 19 for a P controller (left figure) compared to a PI controller (right figure). They start in
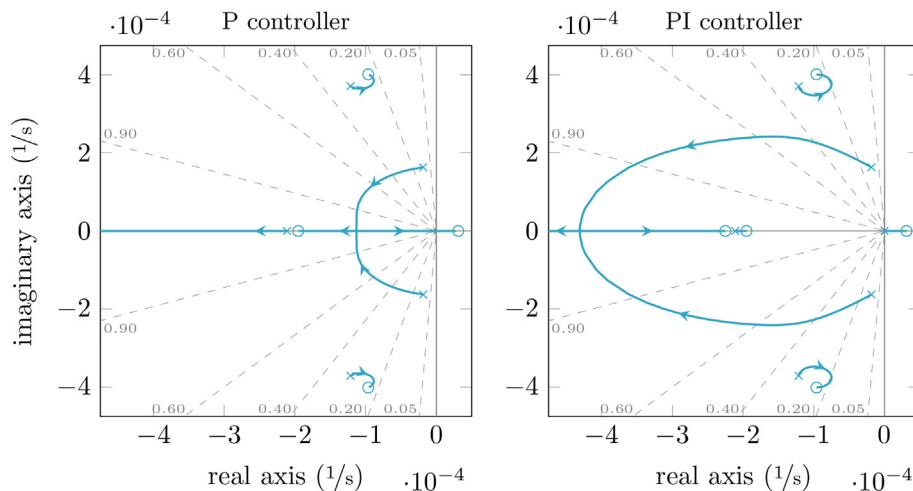

Fig. 19. The root-locus of the closed-loop system $G_{\mathrm{cl}}(j\omega)$ with respect to controller gain $k_{d_{32}}$. Poles of $G_{\mathrm{ol}}(j\omega)$ are indicated by x, the according zero by o. The damping ratios of $G_{\mathrm{cl}}(j\omega)$ are specified in gray. Left: A suitable tuned P controller $k_{d_{32}}$ increases the damping ratio of $G_{\mathrm{cl}}(j\omega)$ and guarantees a stable steady-state operation. Right: Due to the pole introduced at the origin, one pole of the PI controlled closed-loop system is in the right half-plane hence $G_{\mathrm{cl}}(j\omega)$ is unstable for all $k_{d_{32}}$.
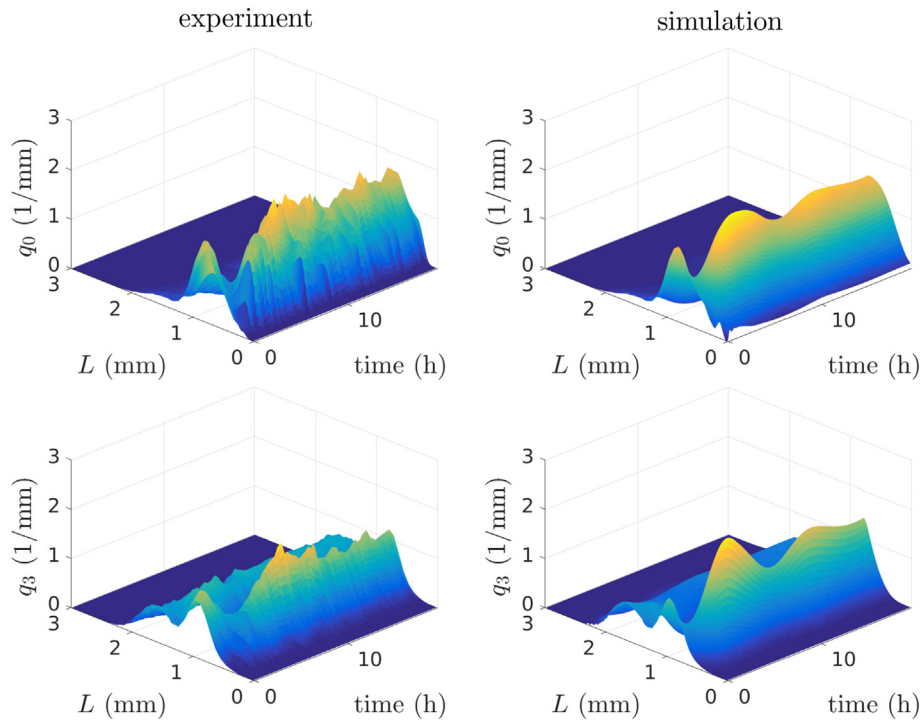
Fig. 20. **Left Column:** normalized number and volume based particle size distributions $q_{0,\text{bed}}$ and $q_{3,\text{bed}}$ of experiment 5. PSDs were determined with CamSizer XT. **Right Column:** PSDs of the corresponding simulation.

the open loop poles of the controller and the system to be controlled indicated by the crosses in Fig. 19 and end in the open loop zeros indicated by the circles in Fig. 19. In both diagrams one branch is tending to $-\infty$. The controlled LTI system is stable if and only if all closed loop poles lie in the left half plane. Usually, controllers with integral action are preferred in view of steady state accuracy [36]. However, from Fig. 19 it is readily concluded, that the system is not stabilizable if the controller includes integral action like the PI controller in the right diagram. This is due to the fact, that any integral action introduces an open loop pole in the origin and that the branch starting from the origin lies entirely in the right half plane. Therefore, a P controller was selected, which allows stabilization with good damping for some suitable controller gain

as illustrated in the left diagram. From this diagram, we further conclude that this will even work for higher mill powers when the open loop system becomes unstable and the pair of conjugate complex poles of the plant close to the imaginary axis is shifted from the left to the right half plane.

In the next step, the designed P controller was validated with a simulation study. For this purpose, the nonlinear dynamic plant model presented in Section 2 was extended by the controller according to

$$p_{\text{mill,ref}}(t) = k_{d_{32}} e_{d_{32,\text{bed}}} + p_{\text{mill,0}} \qquad (27)$$

with the control error $e_{d_{32,\text{bed}}} = d_{32,\text{ref}} - d_{32,\text{bed}}$.
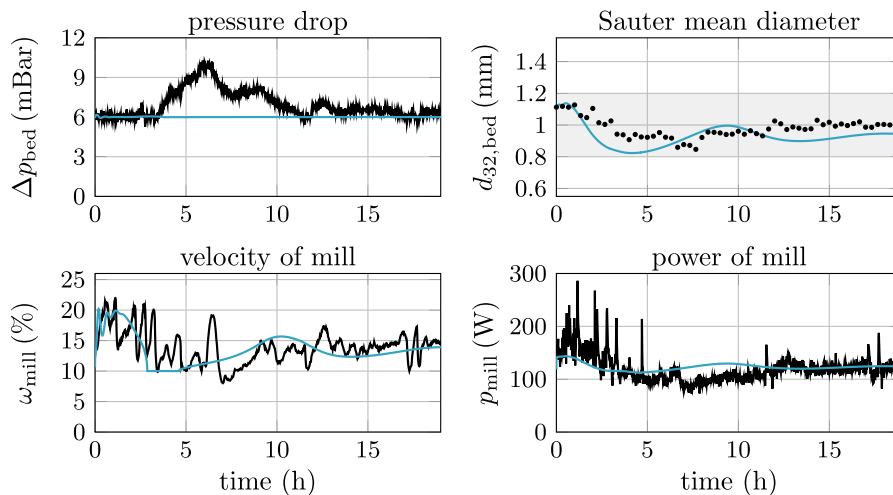

Fig. 21. Comparison of selected data of experiment 5 (black line) and the corresponding simulation results (blue line). Based on the inline measured particles size distribution the process is controlled. The related control scheme is presented in Fig. 6. After a sufficient time the process settles at steady state characterized by constant Δp_{bed} and $d_{32,\text{bed}}$.

As the simulation results were promising, the designed P controller was implemented at the plant and tested in experiment 5. The Sauter mean diameter was measured inline with the equipped Parsum probe.

Simulation and experimental results are illustrated in Figs. 20 and 21. It is shown that the overall control strategy dampens the oscillations of $d_{32,bed}$ and thus also the oscillations of the PSD within relatively short time and achieves a stable steady state with constant bed mass m_{bed}. Compared to the corresponding scenario without control of the Sauter mean diameter which was shown in Fig. 17, the process dynamics were improved significantly. In Fig. 17 a stable steady state could not be achieved within the first 40 hours, whereas in Figs. 20 and 21 a stable steady state is reached within 5 hours. Again, there is a good agreement between simulation and experiments.

4. Conclusion

In this article, control strategies for stabilizing the bed mass and the particle size distribution of a continuous fluidized bed layering granulation process with sieve-mill-cycle were developed step by step and validated experimentally. For the first time, it was shown experimentally, that the process dynamics can be improved considerably by using even relatively simple control strategies. The theoretical development was based on an extended plant model, accounting for a more realistic description of the product removal, the grinding of the oversized particles and the bed mass control compared to our previous work [1,12,33]. The model showed good agreement with the experimental findings and can be used for further studies on dynamics and control of continuous FBLG processes.

Future work will focus on a rigorous evaluation of more advanced control strategies as described for example in [16,23]. Furthermore, the dynamic model can be extended to account for other important particle properties, like particle porosity, for example [37]. Such a model could be used to develop and test more advanced process configurations in silico. A typical example are multi chamber processes, which admit different operating conditions in different process chambers and can therefore be used for the formulation of more advanced particles. To enhance the performance of those processes and guarantee the formation of particles with desired properties, suitable control strategies for multi chamber processes can also be developed using such an extended dynamic model.

Acknowledgments

References

[1] C. Dreyschultze, C. Neugebauer, S. Palis, A. Bück, E. Tsotsas, S. Heinrich, A. Kienle, Influence of zone formation on stability of continuous fluidized bed layering granulation with external product classification, Particuology 23 (2015) 1–7.

[2] L. Mörl, S. Heinrich, M. Peglow, Fluidized bed spray granulation, in: M.H.A.D. Salman, J. Seville (Eds.), Granulation, Vol. 11 of Handbook of Powder Technology, Elsevier Science B.V 2007, pp. 21–188.

[3] E. Tsotsas, Influence of drying kinetics on particle formation: A personal perspective, Dry. Technol. 30 (11−12) (2012) 1167–1175.

[4] G. Grünewald, B. Westhoff, M. Kind, Fluidized bed spray granulation: Nucleation studies with steady-state experiments, Dry. Technol. 28 (3) (2010) 349–360.

[5] I. Cotabarren, P.G. Schulz, V. Bucalá, J. Piña, Modeling of an industrial double-roll crusher of a urea granulation circuit, Powder Technol. 183 (2) (2008) 224–230.

[6] R. Schütte, A. Ruhs, I. Pelgrim, C.-J. Klasen, L. Kaiser, Fluidised Bed Spray Granulation Process Producing Two or more Different Size Distributions, 1998.

[7] M. Schmidt, A. Bück, E. Tsotsas, Experimental investigation of process stability of continuous spray fluidized bed layering with internal separation, Chem. Eng. Sci. 126 (2015) 55–66.

[8] M. Schmidt, C. Rieck, A. Bück, E. Tsotsas, Experimental investigation of process stability of continuous spray fluidized bed layering with external product separation, Chem. Eng. Sci. 137 (2015) 466–475.

[9] M. Schmidt, A. Bück, E. Tsotsas, Experimental investigation of the influence of drying conditions on process stability of continuous spray fluidized bed layering granulation with external product separation, Powder Technol. 320 (2017) 474–482 Supplement C.

[10] A. Vreman, C. van Lare, M. Hounslow, A basic population balance model for fluid bed spray granulation, Chem. Eng. Sci. 64 (21) (2009) 4389–4398 390.

[11] C. Neugebauer, S. Palis, A. Bück, E. Tsotsas, S. Heinrich, A. Kienle, A dynamic two-zone model of continuous fluidized bed layering granulation with internal product classification, Particuology 31 (2017) 8–14.

[12] R. Radichkov, T. Müller, A. Kienle, S. Heinrich, M. Peglow, L. Mörl, A numerical bifurcation analysis of continuous fluidized bed spray granulation with external product classification, Chem. Eng. Process. Process Intensif. 45 (10) (2006) 826–837.

[13] T. Hoffmann, C. Rieck, M. Schmidt, A. Bück, M. Peglow, E. Tsotsas, Prediction of shell porosities in continuous fluidized bed spray layering, Dry. Technol. 33 (13) (2015) 1662–1670.

[14] C. Rieck, T. Hoffmann, A. Bück, M. Peglow, E. Tsotsas, Influence of drying conditions on layer porosity in fluidized bed spray granulation, Powder Technol. 272 (2015) 120–131.

[15] E. Diez, K. Meyer, A. Bück, E. Tsotsas, S. Heinrich, Influence of process conditions on the product properties in a continuous fluidized bed spray granulation process, Chem. Eng. Res. Des. 139 (2018) 104–115.

[16] S. Palis, A. Kienle, Stabilization of continuous fluidized bed spray granulation with external product classification, Chem. Eng. Sci. 70 (2012) 200–209 4th International Conference on Population Balance Modeling.

[17] S. Palis, A. Kienle, H∞ loop shaping control for continuous fluidized bed spray granulation with internal product classification, Ind. Eng. Chem. Res. 52 (1) (2013) 408–420.

[18] S. Palis, C. Dreyschultze, C. Neugebauer, A. Kienle, Auto-tuning control systems for improved operation of continuous fluidized bed spray granulation processes with external product classification, Proc. Eng. 102 (2015) 133–141 new Paradigm of Particle Science and Technology Proceedings of The 7th World Congress on Particle Technology.

[19] S. Palis, Non-identifier-based adaptive control of continuous fluidized bed spray granulation, J. Process Control 71 (2018) 46–51.

[20] A. Bück, S. Palis, E. Tsotsas, et al., Powder Technology 270 (Part B) (2015) 575–583 (6th International Workshop on Granulation: Granulation across the length scales).

[21] A. Bück, R. Dürr, M. Schmidt, E. Tsotsas, Model predictive control of continuous layering granulation in fluidis ed beds with internal product classification, J. Process Control 45 (2016) 65–75.

[22] S. Palis, A. Kienle, Discrepancy based control of continuous fluidized bed spray granulation with internal product classification, IFAC Proc. Vol. 45 (15) (2012) 756–761 8th IFAC Symposium on Advanced Control of Chemical Processes.

[23] S. Palis, A. Kienle, Discrepancy based control of particulate processes, J. Process Control 24 (3) (2014) 33–46.

[24] I.M. Cotabarren, D.E. Bertn, V. Bucal, J. Pia, Feedback control strategies for a continuous industrial fluidized-bed granulation process, Powder Technol. 283 (2015) 415–432.

[25] S. Palis, C. Neugebauer, A. Bück, S. Heinrich, E. Tsotsas, A. Kienle, Control of multi-chamber continuous fluidized bed spray granulation, Proceedings of PARTEC 2016 2016, pp. 1–4.

[26] B.J. Ennis, G. Tardos, R. Pfeffer, A microlevel-based characterization of granulation phenomena, Powder Technol. 65 (1) (1991) 257–272 a Special Volume Devoted to the Second Symposium on Advances in Particulate Technology.

[27] D. Petrak, Simultaneous measurement of particle size and particle velocity by the spatial filtering technique, Part. Part. Syst. Charact. 19 (6) (2002) 391–400.

[28] N. Hampel, A. Bück, M. Peglow, E. Tsotsas, Continuous pellet coating in a wurster fluidized bed process, Chem. Eng. Sci. 86 (0) (2013) (450 87 – 98, 5th International Granulation Workshop).

[29] A. Bück, C. Neugebauer, K. Meyer, S. Palis, E. Diez, A. Kienle, S. Heinrich, E. Tsotsas, Influence of operation parameters on process stability in continuous fluidised bed layering with external product classification, Powder Technol. 300 (2016) 37–45.

[30] S. Antonyuk, J. Tomas, S. Heinrich, L. Mörl, Breakage behaviour of spherical granulates by compression, Chem. Eng. Sci. 60 (14) (2005) 4031–4044.

[31] S. Antonyuk, M. Khanal, J. Tomas, S. Heinrich, L. Mörl, Impact breakage of spherical granules: experimental study and dem simulation, Chem. Eng. Process. Process Intensif. 45 (10) (2006) 838–856 (particulate Processes A Special Issue of Chemical Engineering and Processing).

[32] L. Vogel, W. Peukert, Breakage behaviour of different materials-construction of a mastercurve for the breakage probability, Powder Technol. 129 (1) (2003) 101–110.

[33] C. Neugebauer, S. Palis, A. Bück, E. Diez, S. Heinrich, E. Tsotsas, A. Kienle, Influence of mill characteristics on stability of continuous layering granulation with external product classification, in: Z. Kravanja, M. Bogataj (Eds.), 26th European Symposium on Computer Aided Process Engineering, Vol. 38 of Computer Aided Chemical Engineering, Elsevier 2016, pp. 1275–1280.

[34] M. Schmidt, Process Dynamics and Structure Formation in Continuous Spary Fluidized Bed Processes, Ph.D. thesis Otto-von-Guericke-Universität, April 2018.

[35] S. Skogestad, I. Postlethwaite, Multivariable Feedback Control: Analysis and Design, 2nd edition John Wiley & Sons Ltd, 2007.

[36] R.C. Dorf, R.H. Bishop, Modern Control Systems, 13th edition Pearson, 2017.

[37] C. Neugebauer, A. Bück, S. Palis, L. Mielke, E. Tsotsas, A. Kienle, Influence of thermal conditions on particle properties in fluidized bed layering granulation, Processes 6 (12) (2019).

Robust control for active damping of elastic gantry crane vibrations

Ievgen Golovin [a,*], Stefan Palis [a,b]

[a] Otto-von-Guericke-Universität, Universitätsplatz 2, D-39106 Magdeburg, Germany
[b] National Research University "Moscow Power Engineering Institute", Krasnokazarmennaya 14, 111250 Moscow, Russia

ABSTRACT

One of the most significant structural dynamics problems of large gantry cranes are elastic vibrations in trolley travel direction. They put additional mechanical stresses on a crane construction and reduce crane operation performance. As these vibrations are mostly excited by trolley acceleration forces, they can be taken into account in the trolley motion control system. This article presents a robust control-based approach for active damping of the gantry crane elastic structural vibrations. The crane model with additional uncertainty models are derived using the finite element method (FEM). In order to achieve low order models that can be directly used for the control system design modal truncation as a model reduction technique is performed. The robust controller is then designed by the H_∞-loopshaping design procedure evaluating the associated robustness margins. The proposed feedback strategy has been successfully verified on a laboratory gantry crane.

© 2018 Elsevier Ltd. All rights reserved.

1. Introduction

Currently, well-thought-out logistics and faster cargo transportation play an important role in the enhancement of trade and industry. In order to consume less time for these operations, application of automated equipment, including cranes, is needed. Gantry cranes are commonly used for loading and unloading of containers at port terminals (Fig. 1). To increase efficiency, a lot of the gantry cranes are operated at high velocities of the crane trolley, which causes larger swing angles of the crane cargo [2].

Over the last five decades there has been a vast research in the field of the modelling and control of cranes. Here, a variety of models and control approaches for different types of cranes has been covered [3,4]. One of the most important topics in this field is the reduction of load swaying due to the positioning process applying different control strategies: sliding mode control [5–8], error tracking control [9], adaptive tracking control [10,11], energy-based control design [12,13], and output-based input shaping techniques [14,15] etc. In the majority of the contributions it is assumed that the crane structure is of infinite stiffness and therefore structural dynamics can be neglected. Verification is predominantly provided using mathematical crane models or small scaled laboratory cranes with ideal stiff structure. However, with the continuous increase of crane dimensions and utilizing lightweight construction structures the assumption of ideal stiffness becomes more and more less valid and the coupling between elastic structural vibrations and the trolley movements has to be taken into account.

---

* Corresponding author.
  E-mail address: ievgen.golovin@ovgu.de (I. Golovin).

Fig. 1. The gantry crane from a container port [1].

In the last two decades the problem of the structural flexibility has been stated for different types of cranes ranging from gantry, overhead and ship-to-shore (STS) container cranes [16–25] to slewing cranes [26–28]. This contribution is concerned with large gantry cranes. Here, two main structural dynamical problems are of interest: vertical girder vibrations due to the trolley travel and low frequency vibrations in the trolley travel direction. The first problem is called the moving load problem and has been well covered with the modelling and analysis in [16,18,19,29,30].

In this paper the low frequency vibrations of the crane structure in the trolley movement direction are studied. Being particularly negative because of the large amplitudes and only weakly damped behaviour, these vibrations reduce the crane operation performance of load positioning and produce additional mechanical stresses which leads to faster construction wear. Moreover, these vibrations may have a disturbing influence on the crane operator, deteriorating his working conditions and comfort [24]. In Fig. 2 the vibration measurements from real gantry crane by normal operation and its fast Fourier transform are depicted. It can be seen that the first eigenfrequency $f_1 = 0.5$ Hz is the important significant in the system dynamics during normal cargo transportation operations.

Currently, several approaches can be found for vibrations reduction in the gantry crane structures. In [22] the authors offer to optimize the crane structure by increasing supporting legs thickness or by stiffening the gantry. A passive and an active damper via additional passive and actuated weight as counter-mass have been proposed in [31]. In the first case, the obtained system damping was relative small (up to 10%) comparing to the implementation and material costs (30 t counterweight). In the second case, the resulting system damping was more notable (up to 60−70%). However, an additional linear drive system (with 5 t counterweight) for its application is needed resulting in additional costs.

For a different crane type it has been shown that the structural dynamics can be taken into account as an additional control task for the motion control system. In [29] authors offer an active damping approach for vertical container crane vibrations using the modal coupling. Here, the classical crane model is extended with the a FEM based crane structure model. The vertical vibrations are then taken into account designing an appropriate anti-sway damping strategy using pole placement. As a control handle the hoist drive system is used. In [27,28] active damping approaches for flexible tower cranes are proposed. Here, control of the slewing motion provides the damping of the elastic jib and tower vibrations. In [27] the authors propose an early lumping control approach to control the rotating Euler-Bernoulli beam. After spatial discretization and modal order reduction pole placement and LQR control are suggested for the crane damping control. In [28] the optimal control problem for a rotating elastic crane coupled with a trolley-load system is introduced. In [32] it has been shown that including the elastic crane model in anti-sway control for simultaneous damping of the load swinging and crane structural vibrations is possible. The proposed approaches have shown promising results in simulations.

Motivated by aforementioned studies, a robust control-based approach for active damping of the gantry crane vibrations is presented in this article. For this purpose, the trolley position control system has been extended by the elastic crane model. In order to design the robust controller for the extended plant, the H_∞-loopshaping design procedure has been applied and
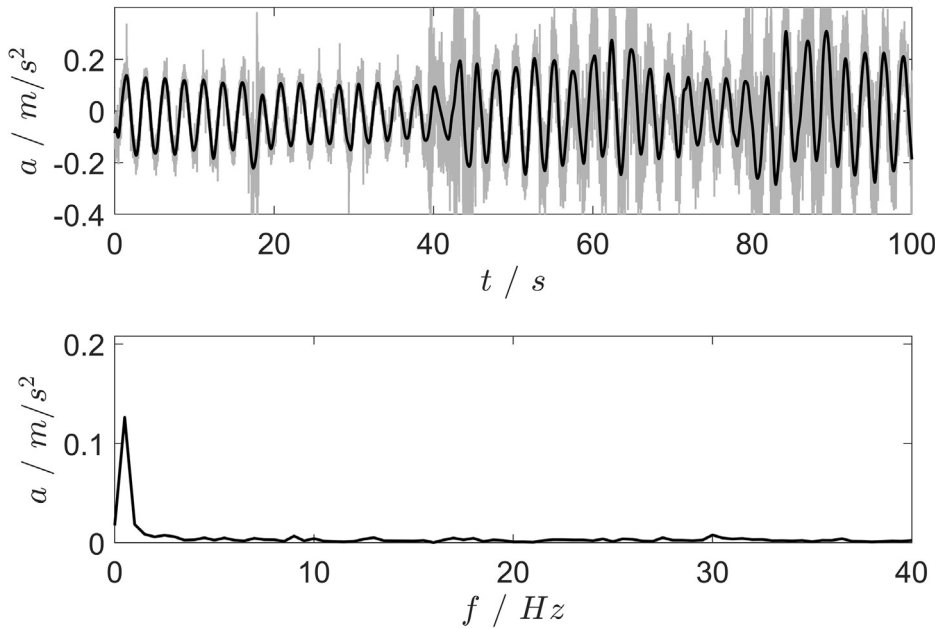
Fig. 2. Crane vibrations acceleration (above, grey), its filtered values (above, black) and its fast Fourier transform (below, black).

robustness margins have been evaluated in the terms of the gap metric. The resulting controller has been verified on a laboratory gantry crane.

Section 2 presents the modelling of the elastic gantry crane and model order reduction. Model uncertainties and errors are described in Section 3. The robust controller design is introduced in Section 4. Section 5 concludes the article with experimental results from a laboratory gantry crane.

2. Gantry crane modelling

In this section the dynamic model of the gantry crane plant is derived. As depicted in Fig. 3 this model includes a controlled electric drive as it is used in most crane applications for tracking the reference position and elastic structural dynamics. The classical cascade control structure performs the trolley positioning using the motor voltage as a control input u_d. This implies that in the considered robust control design the actuated variable is the reference position r_r. In this contribution the following assumptions for modelling are made:

1. the position controlled drive eliminates the feedback action of load movement and elastic crane oscillations on the trolley, and compensates the friction forces;
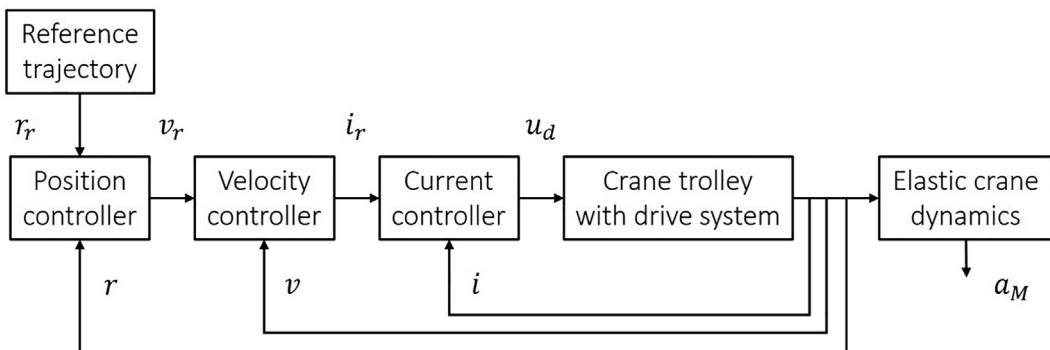
Fig. 3. Crane plant model.

2. coupling between the load swinging and the crane vibrations can be neglected as from the practical point of view they are in a different frequencies range, e.g. load swinging range of frequencies – $f_l = 0.08 - 0.2$ Hz for rope length variations between $l_r = 30 - 5$ m respectively, first natural frequency of real gantry cranes – $f_1 = 0.5 - 0.8$ Hz;
3. external disturbances on the crane and load are neglected, e.g. wind, waves etc.;
4. the load swinging is neglected, assuming that it can be stabilized by a competent operator or optimized reference trajectory.

2.1. Model of laboratory gantry crane

It has been introduced that weakly damped low-frequency crane vibrations is a serious structural dynamics problem, which can be taken into account by the crane trolley motion control. In order to reflect the dynamic behaviour of large gantry cranes and to verify the robust controller, a laboratory model has been designed (Fig. 4). Here, the legs have been built of thin plate material, resulting in a limit stiffness and oscillating dynamic behaviour in trolley direction. This laboratory crane is considered for the further mathematical modelling and control design.

The structural scheme of the model is represented in Fig. 5. Here, the model consists of a trolley travelling over a girder (jib) and elastic supporting legs, which are fixed in the lower part. The trolley is moved via a tooth-belt drive by a DC-motor with reduction gear, mounted on the girder. According to the aforementioned assumptions no hoist system nor load are taken into account in this contribution. The trolley loading is performed by a rigid fixing of the crane trolley and an additional load on the top of the trolley.
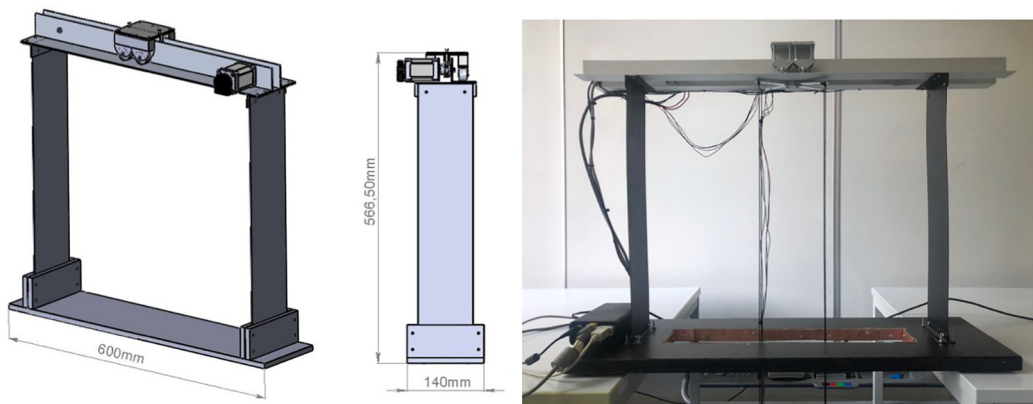

Fig. 4. CAD Model and photo of the laboratory gantry crane model.
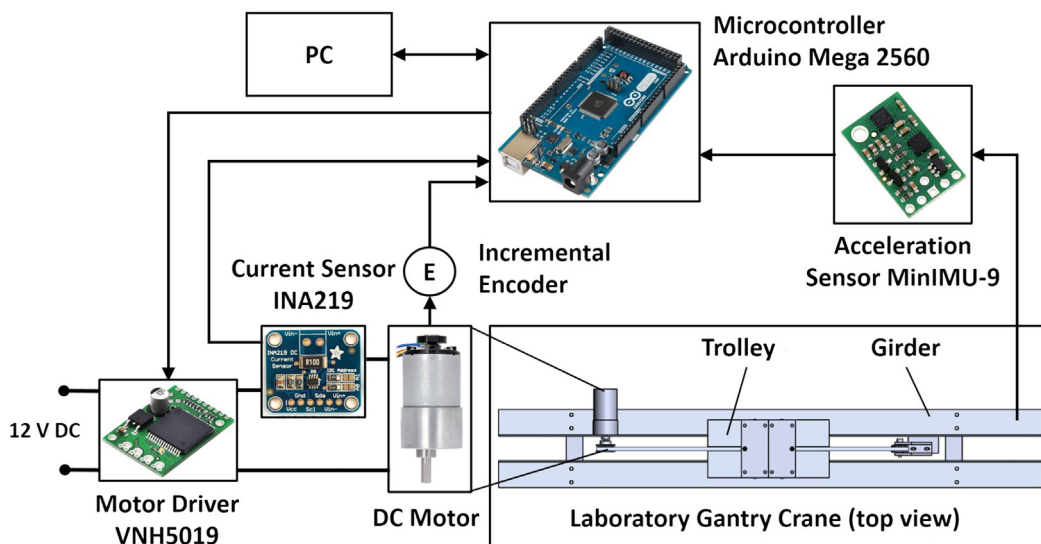

Fig. 5. Laboratory gantry crane.

The position controlled DC drive accomplishes the trolley movement along the linear girder axis. This drive is equipped with a current sensor and an incremental encoder providing digital measurements of current, rotation velocity and angle of the trolley motor. In addition, inertial motion unit (MinIMU-9) is mounted on the girder, which measures girder acceleration of the laboratory model. The trolley drive control system, damping control and bandpass filter for acceleration signal are implemented on a micro-controller (Arduino Mega 2560). The trolley cascade position control is described in next section.

2.2. Model of trolley drive system

Currently, most crane systems are equipped with electric drives that typically provide velocity or position control of trolley travel via classical cascade control with P and PI controllers (Fig. 6) [2]. Here, the control system consists of an outer position control loop $G_r(s)$ and inner velocity $G_v(s)$ and current (torque) control loops $G_i(s)$. For the following cascade structure the control design is usually performed step by step. The inner PI controller $C_i(s)$ for the motor current plant $P_i(s)$ is designed first, after which the PI controller $C_v(s)$ for the augmented velocity plant $G_i(s)P_v(s)$ is designed. At the last step, the position P controller $C_r(s)$ for the $G_v(s)P_r(s)$ is tuned [33,34]. The electrical and mechanical subsystems and the corresponding controllers can be represented as follows:

$$P_i(s) = \frac{i(s)}{u(s)} = \frac{1}{T_\mu s + 1} \cdot \frac{1/R_a}{T_a s + 1}, \tag{1}$$

$$C_i(s) = k_i \cdot \frac{T_i s + 1}{T_i s}, \tag{2}$$

$$P_v(s) = \frac{v(s)}{i(s)} = \frac{1}{k_m s}, \tag{3}$$

$$C_v(s) = k_v \cdot \frac{T_v s + 1}{T_v s}, \tag{4}$$

$$P_r(s) = \frac{r(s)}{v(s)} = \frac{1}{s}, \tag{5}$$

$$C_r(s) = k_r, \tag{6}$$

where T_μ is the time constant of the rectifier, T_a is the electrical time constant of the DC drive, R_a is the resistance of the electrical part of the DC drive, k_i and T_i are the proportional gain and time constant of current PI controller, k_m is the mechanical parameter which resembles the inertial mass of the drive system and conversion of the angular motor velocity coordinate into linear velocity, k_v and T_v are the proportional gain and time constant of the velocity PI controller and k_r is the proportional gain of the position P controller. In this work all controllers coefficients are adjusted according to the magnitude (modulus) optimum procedure that is explained in details in [33,35]. Application of this procedure for the electric drive systems results in a good reference performance with small overshoot values. The trolley drive system simulation parameters are represented in Table 1.

In order to verify the crane model with laboratory crane the positioning reference tracking of the crane trolley has been studied with a step change of the desired position to $r_r = 200$ mm. Simulation and experimental results are depicted in Fig. 7. As can be seen, the linear simulation model of controlled trolley drive reflects the dynamics of the laboratory gantry crane and the positioning behaviour resembles the linear first order system dynamics. The current mismatches are a result of the neglected friction forces and the peak of the current value during the positioning is about $1.5A$ which is 50% of the maximum limitation value $i_{max} = 3A$. Therefore, it can be assumed that the laboratory crane operates in its linear region. Hence, for convenience, in the further gantry crane plant modelling and damping control design, we consider that the position control loop $G_r(s)$ can be approximated as a simple first order system:

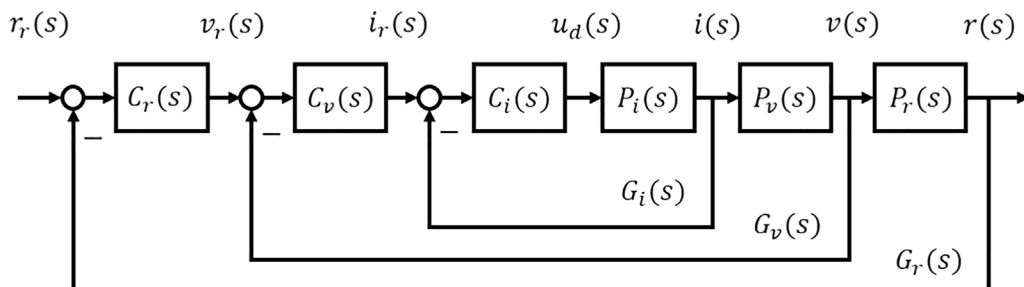$$G_r(s) = \frac{r(s)}{r_r(s)} = \frac{1}{T_r s + 1}, \tag{7}$$

Fig. 6. Gantry crane position control scheme.

Table 1
Trolley drive system parameters.

Parameter	Value	Unit	Parameter	Value	Unit
T_a	$5.6 \cdot 10^{-4}$	[s]	T_μ	$5 \cdot 10^{-5}$	[s]
R_a	2.5	[Ω]	k_i	3.7	[–]
T_i	$6 \cdot 10^{-3}$	[s]	k_m	$6.6 \cdot 10^3$	[–]
k_v	6	[–]	T_v	$5.8 \cdot 10^{-2}$	[s]
k_r	4.1	[–]	T_r	0.1	[s]
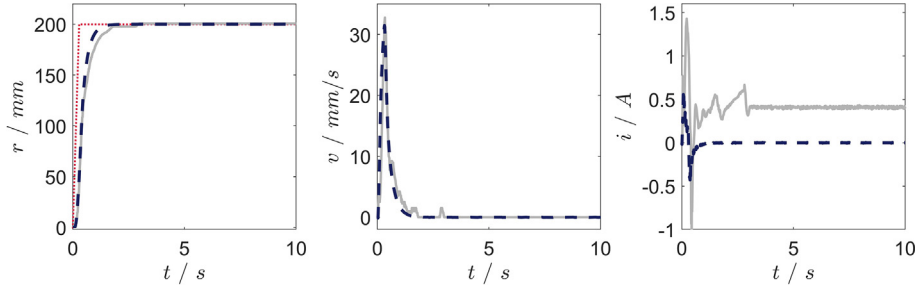
Fig. 7. Simulation (dashed, blue) and experiment (solid, grey) time responses for trolley positioning with reference trajectory (dotted, red). (For interpretation of the references to colour in this figure legend, the reader is referred to the web version of this article.)

where T_r is the time constant which can be identified using the experimental data.

2.3. Model of elastic crane

Modelling and control of mechanical elastic structures is a non-trivial task due to its infinite-dimensional nature. Application of analytical approaches is restricted in most cases to simple geometries and boundary conditions. For more complex structural geometries, e.g. geometry of gantry cranes, utilizing numerical methods for model lumping are usually preferred [23,27,29].

Currently, there are a lot of commercial finite element packages that are suitable for modelling and analysis of a wide range of infinite-dimensional physical problems. Most of them provide options for importing CAD model geometries and exporting dynamic models. Having reliable models available allows to design and to test the control system at the stage of crane production and to accomplish virtual commissioning.

In order to derive the dynamic model of the elastic crane, including the displacements and its derivatives, the Solid Mechanics interface of the commercial software COMSOL Multiphysics is used. The gantry crane geometry is imported from the CAD model of the laboratory crane, where small dimensional parts of the model have been simplified to reduce computational time. In Fig. 8 the model of the gantry crane is depicted in two dimensions. It consists of the aluminium solid girder and the aluminium alloy solid legs. All masses of the simplified geometry correspond to the masses of the real elements of the laboratory crane. The physical parameters of the FEM model are summarized in the Table 2. For the lower cranes legs fixed constraint boundary conditions are applied. An external point force F_t resembles the excitation due to the trolley travel. The damping coefficient $\xi = 0.1$ has been obtained from practical measurements. The crane structure is discretized applying a distributed mesh with quadrilateral elements resulting in $n_d = 1124$ degrees of freedom (DOF).

Here, the spatial discretization of the partial differential equations yields the equations of motion with n_d DOF:

$$M\ddot{U} + D\dot{U} + KU = F, \tag{8}$$

where K, D and M are assembled the global stiffness, damping and mass matrices; $U, \dot{U}$ and $\ddot{U}$ are displacement, velocity and acceleration vectors at all structure domain nodes and F is the nodal forces vector.

Material induced damping can be performed by the Rayleigh damping where the damping matrix D is a linear combination of the stiffness K and mass M matrices:

$$D = \alpha M + \beta K, \tag{9}$$

where β is the stiffness-proportional and α is the mass-proportional factors.

Assuming the external force is an input to the crane plant $u(t) = F_t$ and the point at the girder M is the displacement output $y(t) = q_M$, the model can be expressed for small variations as a linear state-space model of high order
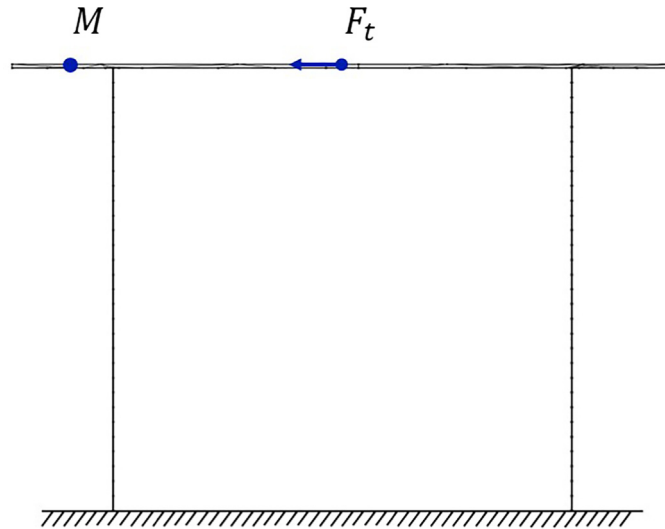
Fig. 8. Gantry crane FEM model.

Table 2
FEM elastic crane model parameters.

Parameter	Value	Name	Parameter	Value	Name
g_l	0.82 [m]	Girder length	g_h	0.005 [m]	Girder height
l_w	0.001 [m]	Legs width	l_h	0.548 [m]	Legs height
m_t	0.3 [kg]	Trolley mass	m_l	0–0.6 [kg]	Load mass
E_g	$2 \cdot 10^{12}$ [Pa]	Elastic modulus (girder)	$\bar{E}_l$	$34 \cdot 10^9$ [Pa]	Elastic modulus (crane legs)
v_g	0.3	Poisson's ratio (girder)	v_l	0.28	Poisson's ratio (crane legs)
ρ_g	2363 [kg/m³]	Density (girder)	ρ_l	6124 [kg/m³]	Density (crane legs)

$$\dot{x}(t) = Ax(t) + Bu(t), \tag{10}$$
$$y(t) = Cx(t) + Du(t), \tag{11}$$

where A, B, C and D are the system matrices.

2.4. Model order reduction

The order of the derived state-space model is 2248. For the further control design an additional model order reduction should be introduced. In this contribution modal truncation is used. One of the advantages of this technique is that the poles of the low order model are a subset of the poles of the high order model and, hence, all of the eigenfrequencies preserved retain a physical interpretation [36,37].

The modal truncation technique is based on a special modal representation form of the state-space model. If the system matrix A of state space model Eq. (10), (11) has complex conjugate eigenvalues, it is possible to transform this matrix into a block diagonal form using the similarity transformation

$$\widehat{A} = \widehat{T}^{-1} A \widehat{T} = \begin{bmatrix} \lambda_1 & 0 & \cdots & 0 \\ 0 & \lambda_2 & \cdots & 0 \\ \vdots & \vdots & \ddots & \vdots \\ 0 & 0 & 0 & \lambda_n \end{bmatrix}, \quad \lambda_i = \begin{bmatrix} \sigma_i & -\omega_i \\ \omega_i & \sigma_i \end{bmatrix}, \quad |\omega_1| < |\omega_2| < \cdots < |\omega_n|, \tag{12}$$

where the matrix $\widehat{T}$ is composed of the eigenvectors of matrix A and $\lambda_i = \sigma_i \pm j\omega_i$ are the eigenvalues of matrix A. From a physical point of view, these values represents the main properties of mechanical system modes. Namely, $Re(\lambda_i) = \sigma_i$ characterizes the mode damping, and $Im(\lambda_i) = \omega_i$ represents the natural frequency of the eigenmode.

Transforming the state-space model Eq. (10), (11) into its modal form

$$\dot{\widehat{x}}(t) = \widehat{A}\widehat{x}(t) + \widehat{B}u(t), \tag{13}$$
$$y(t) = \widehat{C}\widehat{x}(t) + \widehat{D}u(t), \tag{14}$$

where

$$\widehat{A} = \widehat{T}^{-1}A\widehat{T}, \quad \widehat{B} = \widehat{T}^{-1}B, \quad \widehat{C} = C\widehat{T}, \quad \widehat{D} = D,$$

the state vector $\widehat{x}$ can be partitioned into two parts $[\widehat{x}_1 \ \widehat{x}_2]^T$. Here, the vector $\widehat{x}_1$ represents the slow eigenmodes and $\widehat{x}_2$ represents the fast modes. Hence, model Eq. (13), (14) can be rewritten as follows:

$$\begin{bmatrix} \dot{\widehat{x}}_1 \\ \dot{\widehat{x}}_2 \end{bmatrix} = \begin{bmatrix} \Lambda_1 & 0 \\ 0 & \Lambda_2 \end{bmatrix} \begin{bmatrix} \widehat{x}_1 \\ \widehat{x}_2 \end{bmatrix} + \begin{bmatrix} \widehat{B}_1 \\ \widehat{B}_2 \end{bmatrix} u, \tag{15}$$

$$y = \begin{bmatrix} \widehat{C}_1 & \widehat{C}_2 \end{bmatrix} \begin{bmatrix} \widehat{x}_1 \\ \widehat{x}_2 \end{bmatrix} + Du. \tag{16}$$

Removing the system part corresponding to $\widehat{x}_2$, will result in an approximation of (10), (11) as

$$\dot{\widehat{x}}_1 = \Lambda_1\widehat{x}_1 + \widehat{B}_1 u, \tag{17}$$

$$y = \widehat{C}_1\widehat{x}_1 + \widehat{D} u \tag{18}$$

with the following equivalent transfer function

$$G_1(s) = \widehat{C}_1(sI - \Lambda_1)^{-1}\widehat{B}_1 + \widehat{D}. \tag{19}$$

The number of eigenmodes that should be included in $G_1(s)$ after the truncation always depends on an individual application case. From a practical point of view, in order to decide on the appropriate order, the elastic crane dynamics and the trolley drive system dynamics should be analysed in frequency domain. In general, the faster the drive system dynamics is, the more system eigenmodes can be excited and therefore should be conserved. In Fig. 9 the Bode magnitude plots of the system are depicted. As can be seen, the trolley drive system in this case is relatively slow and we assume that only the first system eigenmode with angular eigenfrequency $\omega_1 = 5.84$ rad/s can be influenced. Therefore, the second order approximated model $G_1(s)$ is considered for the damping control design.

2.5. Model of overall gantry plant

The overall plant model $G_o(s)$ which reflects the influence of the loaded or unloaded trolley movement on the crane structure is represented in Fig. 10. Here, the elastic vibrations are excited due to the trolley acceleration forces F_t that can be derived from the second derivative of the trolley position $r(s)$ and the trolley mass m_t. The output of interest of the overall gantry plant model $G_o(s)$ for the further control design is the girder acceleration a_M. Simulation and experimental results of trolley positioning and elastic vibrations excitation are depicted in Fig. 11. Reduced order simulation model of elastic gantry crane reflects the dynamics of the laboratory model with only small mismatches due to non-linearities of real elastic structure.

3. Uncertainty models

The idea of this paper is to propose and verify the robust control law that satisfies a robust stability and a certain performance criteria for a gantry crane with varying and uncertain parameters. Assuming that although the equations of motion are the same, parameters of the system structural dynamics for loaded and unloaded cranes are different and the stiffness of the crane legs is not exactly known. In this case, additional performing of uncertainty models is needed. Moreover, using model order reduction techniques yields additional errors, which should be taken into account.
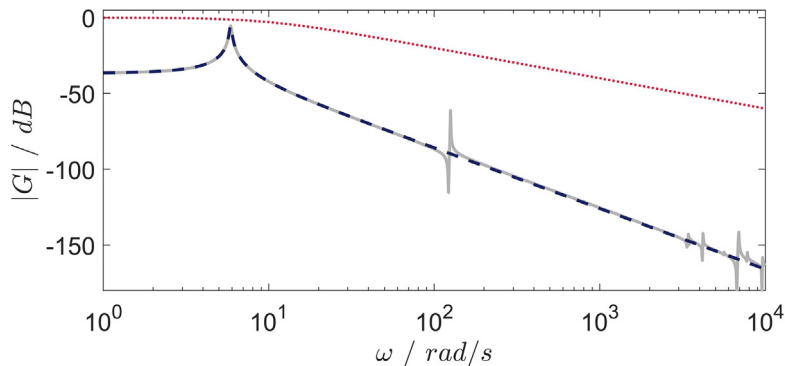

Fig. 9. The Bode magnitude plots of the high order (solid, grey), low order (dashed, blue) and trolley drive system (dotted, red) models. (For interpretation of the references to colour in this figure legend, the reader is referred to the web version of this article.)
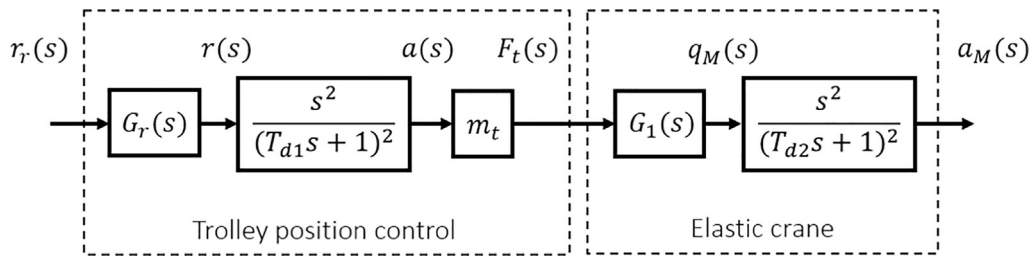
Fig. 10. Crane plant augmented by the trolley position control.

3.1. Coprime factor description and gap metric

From a robust control design perspective, the considered set of models for different parameters can be encapsulated in a nominal plant $G_o(s)$ and a set of bounded uncertainties [36,38]. The uncertainties must be stable and have a finite H_∞-norm. In order to include the model uncertainties for weakly damped or undamped elastic structure models, application of the coprime factor description should be preferred. The nominal system normalized coprime factorization can be formulated as follows:

$$G_o(s) = \frac{N_n(s)}{M_n(s)},$$
(20)

where $M_n(s), N_n(s) \in H_\infty$ are coprime transfer functions that satisfy the Bezout identity

$$M_n(s)M_n(-s) + N_n(s)N_n(-s) = 1.$$
(21)

The family of uncertain system models $G_\Delta(s)$ can be described by the nominal system $G_o(s)$ and coprime factor uncertainties $\Delta_M(s)$ and $\Delta_N(s)$ as illustrated in Fig. 12.

$$G_\Delta(s) = \frac{N_n(s) + \Delta_N(s)}{M_n(s) + \Delta_M(s)}.$$
(22)

In general, application of the coprime factor description for the uncertain models yields an additional degree of freedom for selection of $\Delta_M(s)$ and $\Delta_N(s)$. To reduce conservatism, a coprime factor description with a minimal H_∞ – norm for $\Delta_M(s)$ and $\Delta_N(s)$ should be selected, which leads to the introduction of the gap metric.

As stated in [39,40] the gap metric δ_g between the nominal system model $G_o(s)$ and the uncertainty model $G_\Delta(s)$ can be estimated as a maximum of the directed gaps between these systems

$$\delta_g(G_o, G_\Delta) = max\left\{\overrightarrow{\delta_g}(G_o, G_\Delta), \overrightarrow{\delta_g}(G_\Delta, G_o)\right\},$$
(23)

where

$$\overrightarrow{\delta_g}(G_o, G_\Delta) := \inf_{[\Delta_M \Delta_N] \in H_\infty} \left\{\|[\Delta_M \Delta_N]\|_\infty : G_\Delta\right\}.$$
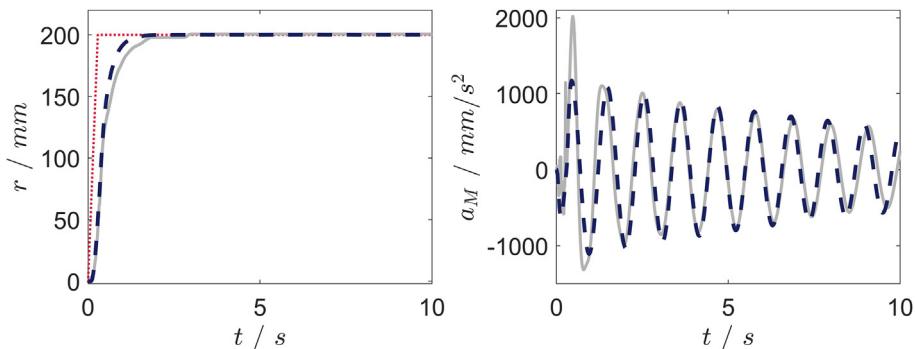(24)

Fig. 11. Simulation (dashed, blue) and experiment (solid, grey) time responses of the gantry crane with trolley position control. (For interpretation of the references to colour in this figure legend, the reader is referred to the web version of this article.)
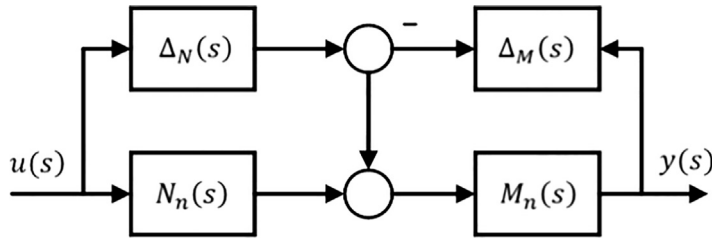
Fig. 12. Coprime factor uncertainty.

The gap metric possesses values between zero and one. The systems are close in terms of the gap metric if the value is close to zero. From the control point of view, it means that the two systems can be stabilized by the same control law. For a robust controller design the maximum value of the gap metric between the nominal model and set of uncertain models can be used as a measure for the required robustness margin.

Being a metric, the gap metric satisfies the triangular inequality

$$\delta(G_1, G_3) \leqslant \delta(G_1, G_2) + \delta(G_2, G_3), \tag{25}$$

which can be used for calculations of corresponding estimates by multiple error sources. For instance, the triangular inequality can be utilized to calculate an estimate for the distance between the low order uncertain model G_Δ and the original nominal model G in the terms of the gap metric $\delta(G_n, G)$ taking into account a low order approximation of the uncertain system $G_1 = G_\Delta$, a low order approximation of the original nominal system $G_2 = G_o$ and a high order representation of the original nominal system $G_3 = G$. Hence, the model order reduction errors or numerical lumping errors can be considered in a unified manner.

3.2. Gantry crane model uncertainties

In this work, we consider that the system structural dynamics for a loaded and unloaded gantry crane varies and the crane legs stiffness is not exactly known. Therefore, a set of gantry crane models can be obtained using the steps proposed in *Section 2.3 - 2.5*. This set of models Π_c, including 169 models, is generated from the nominal FEM-model by variations of additional mass on the girder m_Σ consisting of constant trolley m_t and varying load masses m_l, and elastic modulus of gantry legs material E_l. It is considered that these parameters for model variations are within certain intervals:

$$m_\Sigma = \bar{m}_\Sigma(1 + k_m \Delta_m), \ E_l = \bar{E}_l(1 + k_E \Delta_E), \tag{26}$$

where $\bar{m}_\Sigma$ and $\bar{E}_l$ are the values of the nominal model, k_m, k_E and Δ_m, Δ_E define possible variations.

In this contribution, the following parameter values are chosen $k_m = 0.5, k_E = 0.3$ and $-1 \leqslant \Delta_m, \Delta_E \leqslant 1$ representing up to 50% uncertainty in the crane loading and up to 30% in crane legs stiffness (Fig. 13). The nominal model $G_o(s) \in \Pi_c$ corresponds to half of the crane loading capacity and can be achieved for $\Delta_m = \Delta_E = 0$. The transfer function of the nominal model for the given in the Table 2 parameters yields:

$$G_o(s) = -3 \cdot 10^7 \cdot \frac{s^4}{(s + 10)(s + 50)^4(s^2 + 0.16s + 34.62)}. \tag{27}$$

The Bode magnitude plots and the gap metrics for a set of crane models are depicted in Fig. 14 and 15.
As can be seen from Fig. 15 the maximum of the gap metric is
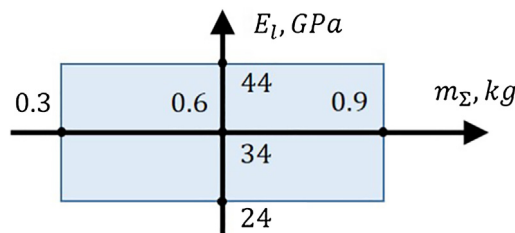
$$\delta_g(G_\Delta, G_o) = 0.29 \tag{28}$$

Fig. 13. Domain of parameter variations.

and the error due to the order reduction in terms of the gap metric is

$$\delta_g(G_o, G) = 0.02. \tag{29}$$

Therefore, the required robustness margin for the robust controller can be calculated from the triangular inequality Eq. (25) [40]

$$\delta(G_\Delta, G) \leqslant \delta(G_\Delta, G_o) + \delta(G_o, G) = 0.31. \tag{30}$$

4. Control design

In this section the robust control design for active crane vibrations is performed. In order to reduce the elastic swinging in the trolley travel direction for the described set of varying gantry cranes the control law is obtained using H_∞ – loopshaping procedure.

4.1. H_∞ – loopshaping control

The idea of the H_∞ – loopshaping design procedure is based on the combination of classical loopshaping ideas and H_∞ – robust stabilization [36,38,41]. Here, the control design consists of two steps. In the first step the open-loop system eigenvalues are adjusted using a compensator in such a manner, that certain requirements for the closed loop system are fulfilled. In a second step a robust, with respect to normalized coprime factor uncertainty, stabilizing controller for the shaped plant is obtained.

To reflect closed-loop performance requirements the open-loop singular values can be adjusted using a weighting function $W(s)$ as depicted in Fig. 16

$$G_s(s) = G(s)W(s). \tag{31}$$

For a given shaped open-loop plant in its normalized coprime factor representation $G_s(s) = N(s)/M(s)$ the controller K_∞, which guarantees a maximum robustness margin with respect to the normalized coprime factor uncertainties, can be obtained from the following H_∞ – control problem

$$\left\| \begin{bmatrix} K_\infty \\ 1 \end{bmatrix} \frac{1}{(1 + G_s K_\infty)M} \right\|_\infty \leqslant \epsilon^{-1}. \tag{32}$$

The maximum robustness margin ϵ_{max} can be calculated as follows:

$$\epsilon_{max} = (1 + \rho(XZ))^{-1/2}, \tag{33}$$

where X and Z are the positive definite solutions of the following algebraic Riccati equations

$$\left(A - BR^{-1}DC\right)^T X + X\left(A - BR^{-1}DC\right) - XB^T R^{-1}BX + CR^{-1}C^T = 0, \tag{34}$$

$$\left(A - BR^{-1}DC\right)Z + Z\left(A - BR^{-1}DC\right)^T - ZC^T R^{-1}CZ + BR^{-1}B^T = 0, \tag{35}$$

with $R = 1 + D^2$. Based on the stabilizing controller K_∞ for the augmented plant $G_s(s)$ the overall controller K can be derived as

$$K(s) = K_\infty(s)W(s). \tag{36}$$

Application of the H_∞ – loopshaping for the plant $G_s(s)$ with robust stability margin ϵ, results in a controller K, which stabilizes all plants $G_\Delta(s)$ with gap metric $\delta_g(G_s, G_\Delta) < \epsilon$.

4.2. Simulation results

For the controller design the nominal plant transfer function $G(s)$ is considered (Fig. 14, blue line). Here, the transfer function has a slope $n_l = +80$ dB/decade at the low frequency range, a slope $n_h = -60$ dB/decade at the high frequency range, a peak at the eigenfrequency $\omega_1 = 5.84$ rad/s with magnitude $|G_s(j\omega_1)| = 47$ dB and a gain crossover frequency $\omega_c = 191$ rad/s. It can be seen, that the transfer function has an unbiased output state and a high value of gain crossover frequency ω_c, which can boost the influence of the measurement noise or neglected high frequency modes dynamics. Hence, the main objective for the loop shaping is to reduce the frequency ω_c. The compensator $W(s)$ providing the open loop shape for the robust control design is therefore chosen as follows:
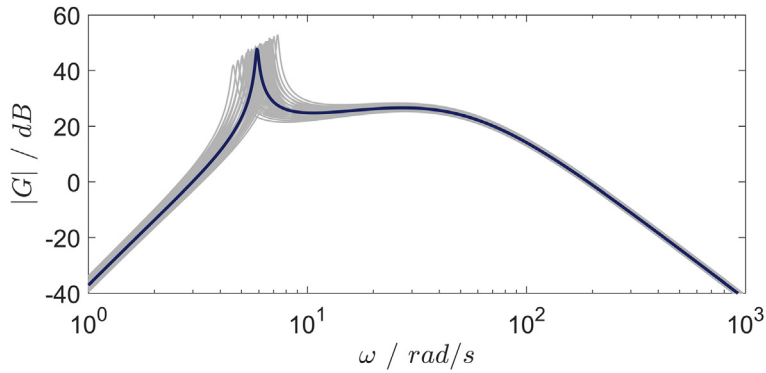
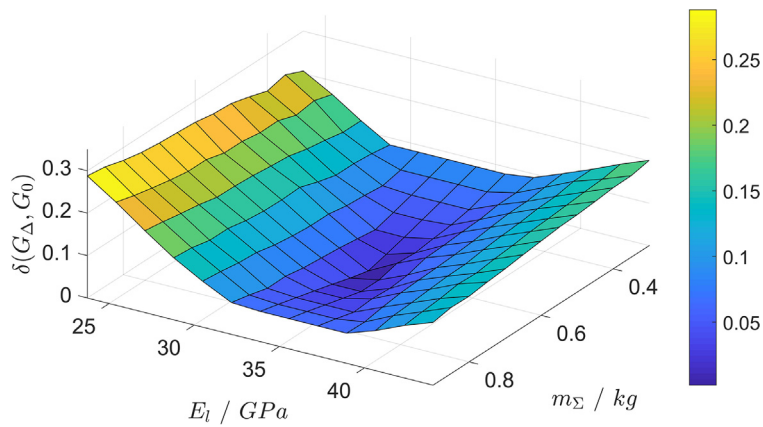**Fig. 14.** The Bode magnitude plots for two sets of uncertain systems.
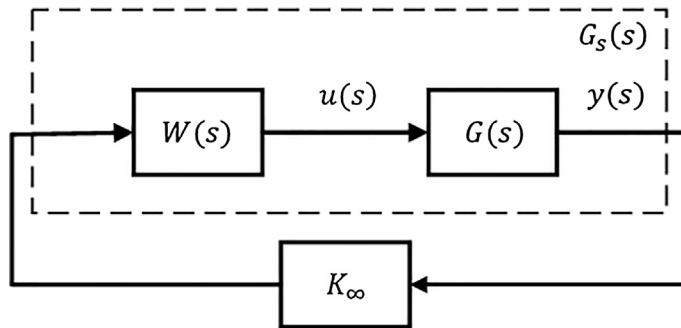

Fig. 15. Gap metric sequence.

Fig. 16. H_∞-loopshaping.

$$W(s) = k_W \cdot \frac{1}{T_W s + 1}, \tag{37}$$

where $k_W = 0.1$ and $T_W = 0.05$ are gain and time constant of the weighting function $W(s)$ respectively. The Bode magnitude plots of the nominal system plant and the shaped plant are depicted in Fig. 17. In order to adjust these parameters the trade-off between fast transients and robustness requirements has been taken into account.

For the shaped crane plant model $G_s(s) = G(s)W(s)$ the robust controller K_∞ is derived with stability margin $\epsilon = 0.48$. As the margin is greater than the maximum of the gap metric $\delta_{g,max} = 0.32$, the achieved controller guarantees robust stability for the set of the uncertain gantry crane models.
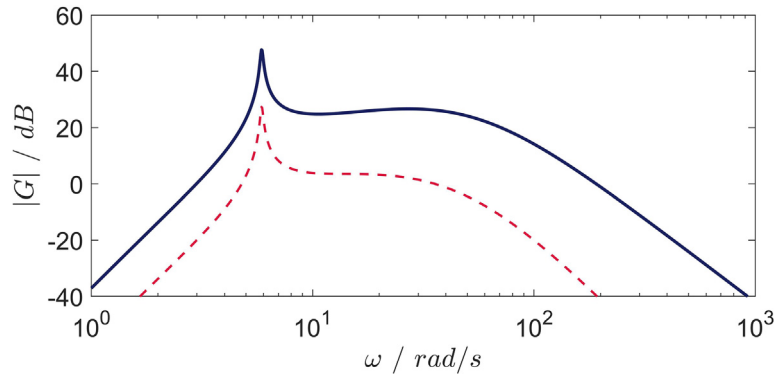
Fig. 17. Bode magnitude plots for the nominal system plant (solid, blue) and the shaped system plant (dashed, red). (For interpretation of the references to colour in this figure legend, the reader is referred to the web version of this article.)
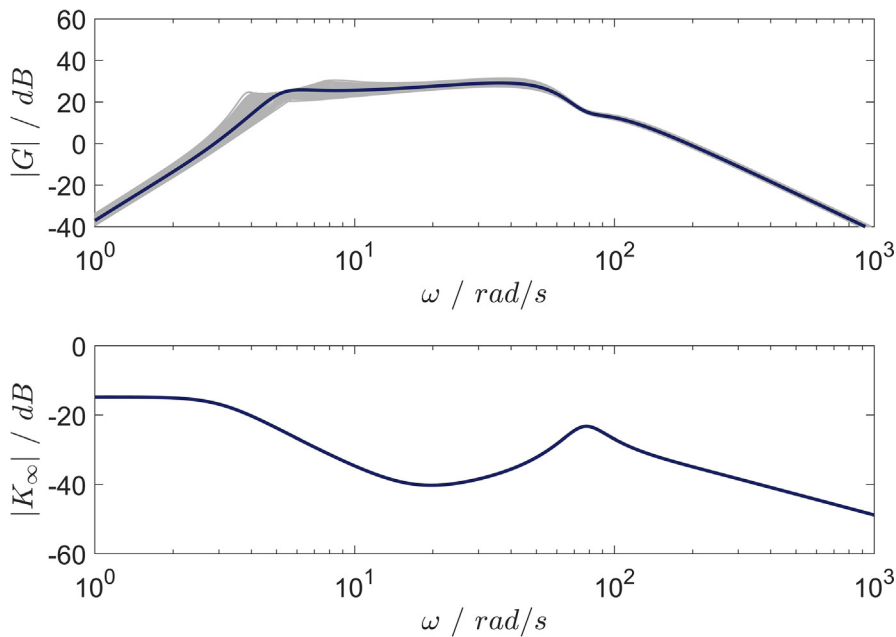

Fig. 18. The Bode magnitude plots for two sets of uncertain closed loop systems.

In Fig. 18 the Bode magnitude plots for the set of uncertain closed loop systems and obtained controller are illustrated.

5. Practical application

The presented active damping method using the crane trolley has been implemented on a laboratory gantry crane. For verifications the same scenario of trolley positioning as in *Section 2.2* is used. In Fig. 19 the comparison of simulation and experimental results are presented. Here, position mismatches are a result of the neglected friction forces and non-linearities of the reduction gear. It is observable that using the proposed active damping approach as an additional task for the trolley motion control system yields a notable system damping. Moreover, this redesign of the trolley control system can be also extended for a simultaneous anti-sway load damping and active damping of the crane structural vibrations [32].

In order to verify the robustness properties of the achieved controller, additional experiments for a varying mass m_Σ are shown in Fig. 20. Here, $m_\Sigma = 0.6$ kg corresponds to the nominal case with half loading of the crane capacity, $m_\Sigma = 0.9$ kg corresponds to the maximum loading and $m_\Sigma = 0.3$ kg contains only the mass of trolley. It can be seen that the designed control law completely fulfils the robustness requirements and a notable system damping for different crane loading conditions can be achieved.
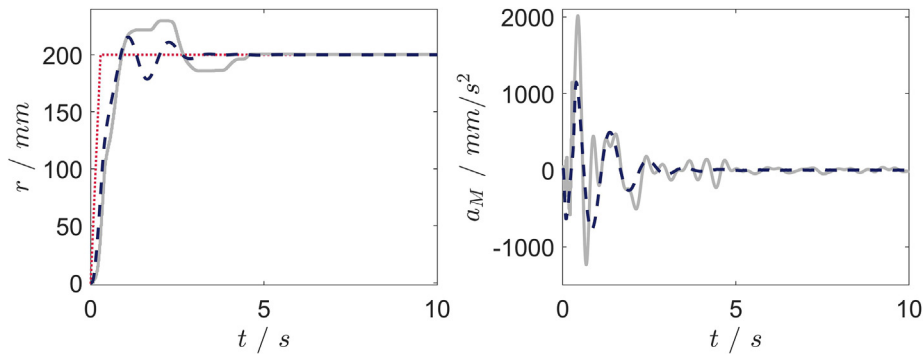
Fig. 19. Simulation (dashed, blue) and experiment (solid, grey) time responses of elastic gantry crane with damping control. (For interpretation of the references to colour in this figure legend, the reader is referred to the web version of this article.)
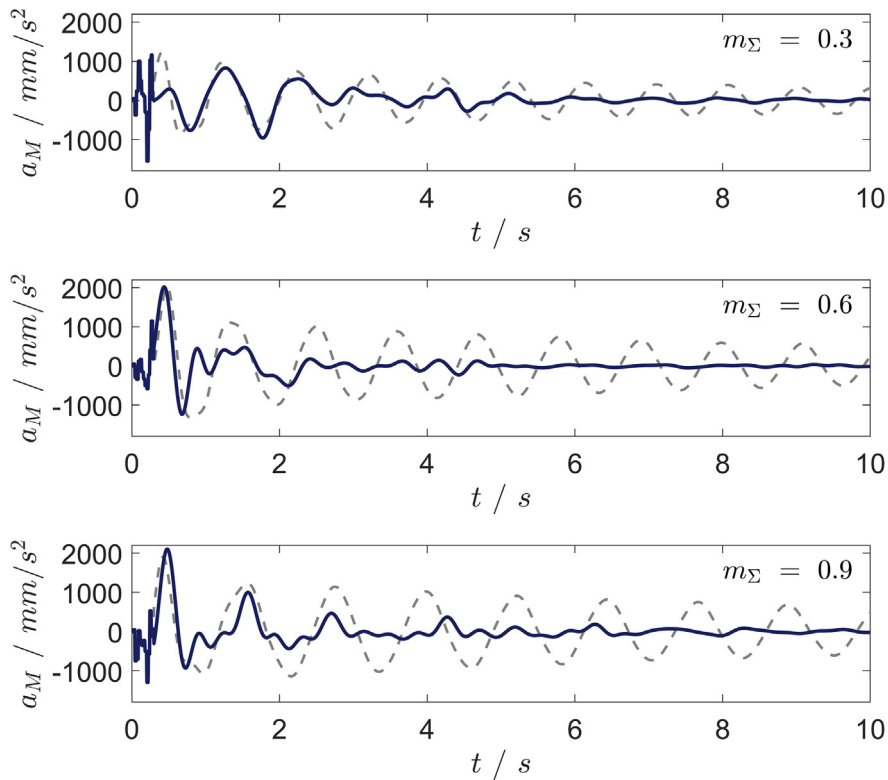

Fig. 20. Experiment time responses of elastic gantry crane with (solid, blue) and without (dashed, grey) damping control for varying loads. (For interpretation of the references to colour in this figure legend, the reader is referred to the web version of this article.)

6. Conclusion

A new damping approach for gantry crane vibrations, using only trolley acceleration forces, has been presented and successfully verified on a laboratory gantry crane. For designing a robust control law, that guarantees the robust stability and the performance specifications for gantry cranes with different loading and unknown stiffness parameters, H_∞ – loopshaping synthesis has been applied. In order to derive a mathematical description of the elastic gantry crane dynamics, FEM has been used. The derived high order models have been reduced using modal truncation approximation. In order to represent a set of gantry cranes, a normalized coprime factor description has been used for the parametric uncertainties. The robust controller

has been designed and successfully applied to the laboratory gantry crane. For further verifications the presented robust damping approach has to be verified on a full-scale real crane in combination with an anti-sway control system.

In human operated gantry cranes undamped elastic crane vibrations of high amplitudes are unacceptable for the crane operator. However, an excessive additional actuation on the trolley motion due to the additional damping strategy can also disturb the crane operator. Therefore, future work should explicitly take into account the comfort of the crane operator introducing an additional performance criteria.

References

[1] M. Lehnert, Dämpfung von elastischen Kranschwingungen Bachelor thesis, Otto-von-Guericke Universität Magdeburg, 2014.
[2] J. Verschoof, Cranes – Design, Practice and Maintenance, Professional Engineering Publishing, 2002.
[3] E.M. Abdel-Rahman, A.H. Nayfeh, Z.N. Masoud, Dynamics and control of cranes: a review, J. Vib. Control 9 (2003) 863–908.
[4] L. Ramli, Z. Mohamed, A.M. Abdullahi, H.I. Jaafar, I.M. Lazim, Control strategies for crane systems: a comprehensive review, Mech. Syst. Signal Process. 95 (2017) 1–23.
[5] M. Zhou, N. Sun, H. Chen, Y. Fang, A novel sliding mode control method for underactuated overhead cranes, IEEE Proc. Chin. Autom. Congr. (2017) 4548–4552.
[6] R. Xiao, Z. Wang, Z. Chen, J. Shen, Anti-swing design for overhead crane based on dual sliding mode control, Proc. IEEE Int. Conf. Ind. Technol. (2018) 81–86.
[7] T. Wang, N. Tan, C. Zhou, C. Zhang, Y. Zhi, A novel anti-swing positioning controller for two dimensional bridge crane via dynamic sliding mode variable structure, Procedia Comput. Sci. 131 (2018) 626–632.
[8] B. Lu, Y. Fang, N. Sun, Sliding mode control for underactuated overhead cranes suffering from both matched and unmatched disturbances, Mechatronics 47 (2017) 116–125.
[9] M. Zhang, X. Ma, X. Rong, X. Tian, Y. Li, Error tracking control for underactuated overhead cranes against arbitrary initial payload swing angles, Mech. Syst. Signal Process. 84 (2017) 268–285.
[10] M. Zhang, X. Ma, X. Rong, X. Tian, Y. Li, Adaptive tracking control for double-pendulum overhead cranes subject to tracking error limitation, parametric uncertainties and external disturbances, Mech. Syst. Signal Process. 76–77 (2016) 15–32.
[11] S. Das, K. Maroo, P. Dhalmahapatra, J. Maiti, A self-tuning neuromorphic controller to minimize swing angle for overhead cranes, in: 2018 4th Int. Conf. Recent Adv. Inf. Technol., IEEE, 2018, pp. 1–6.
[12] I. Won, N.Q. Hoang, Comparative study of energy-based control design for overhead cranes, Int. Robot. Autom. J. Res. 4 (2018) 197–203.
[13] N. Sun, Y. Wu, H. Chen, Y. Fang, An energy-optimal solution for transportation control of cranes with double pendulum dynamics: Design and experiments, Mech. Syst. Signal Process. 102 (2018) 87–101.
[14] A.M. Abdullahi, Z. Mohamed, H. Selamat, H.R. Pota, M.S. Zainal Abidin, F.S. Ismail, A. Haruna, Adaptive output-based command shaping for sway control of a 3D overhead crane with payload hoisting and wind disturbance, Mech. Syst. Signal Process. 98 (2018) 157–172.
[15] L. Ramli, Z. Mohamed, H.I. Jaafar, A neural network-based input shaping for swing suppression of an overhead crane under payload hoisting and mass variations, Mech. Syst. Signal Process. 107 (2018) 484–501.
[16] V. Gašić, N. Zrnić, M. Milovančević, Considerations of various moving load models in structural dynamics of large gantry cranes, FME Trans. 41 (2013) 311–316.
[17] J.-J. Wu, An Analysis of the Structural Dynamics of a Mobil Gantry Crane with Application to Automation of Container Management, University of Glasgow, 2000.
[18] E. Yazid, S. Parman, K. Fuad, Vibration analysis of flexible gantry crane system subjected swinging motion of payload, J. Appl. Sci. 11 (2011) 1707–1715.
[19] D. Younesian, E. Ghafoori, M. Sadeghpour, Nonlinear vibration of a three-dimensional moving gantry crane subjected to a travelling trolley hoisting a swinging object, Trans. Can. Soc. Mech. Eng. 34 (2010) 333–350.
[20] L. Sowa, W. Piekarska, T. Skrzypczak, P. Kwiatoń, The effect of the gantry crane beam cross section on the level of generated stresses, MATEC Web Conf. 157 (2018) 1–9.
[21] N. Miloradović, R. Vujanac, Analysis of overhead travelling crane's motion in horizontal plane, Ann. Fac. Eng. Hunedoara Int. J. Eng. XIV (2016) 21–24.
[22] N. Zrnić, Z. Petković, S. Bošnjak, Automation of ship-to-shore container cranes: a review of state-of-the-art, FME Trans. 33 (2005) 111–121.
[23] N. Zrnić, D. Oguamanam, S. Bošnjak, Dynamics and modelling of mega quayside container cranes, FME Trans. 34 (2006) 193–198.
[24] U. Pietryga, Aktuelle trends in der entwicklung von ship-to-shore (STS) containerkrane, in: 19. Int. Kranfachtagung 2011 Der Kran Und Sein Umfeld Ind. Und Logistik, 2011, pp. 129–140.
[25] L.S. Khalid, W. Singhose, S. Dickerson, A controller enabling precise positioning and sway reduction in bridge and gantry cranes, Control Eng. Pract. 15 (2007) 825–837.
[26] P. Schlott, F. Rauscher, O. Sawodny, in: Proceedings of the IEEE International Conference in Advanced Intelligent Mechatronics (AIM), 2016, pp. 763–768.
[27] F. Rauscher, O. Sawodny, An elastic jib model for the slewing control of tower cranes, IFAC Papers Online 50-1 (2017) 9796–9801.
[28] S.J. Kimmerle, M. Gerdts, R. Herzog, An optimal control problem for a rotating elastic crane-trolley-load system, IFAC Papers Online 51-2 (2018) 272–277.
[29] E. Kreuzer, C. Rapp, Modal coupling for active damping of load swing of container cranes, Proc. Appl. Math. Mech. (2010) 625–626.
[30] B.-J. Ryu, Y.-S. Kong, Dynamic responses and active vibration control of beam structures under a travelling mass, in: Adv. Anal. Control Vib. – Theory Appl., 2012, pp. 231–252.
[31] A. Recktenwald, Aktiver Schwingungsdämpfer für Krane, in: 19. Internationale Kranfachtagung Der Kran und sein Umfeld in Industrie und Logistik, Otto-von-Guericke University Magdeburg, 2011, pp. 143–146.
[32] I. Golovin, S. Palis, in: Proceedings of the IEEE International Conference on Methods and Models in Automation and Robotics (MMAR), 2017, pp. 599–604.
[33] C. Bajracharya, M. Molinas, J.A. Suul, T.M. Undeland, Understanding of tuning techniques of converter controllers for VSC-HVDC, Nordic Workshop Power Indus. Electron. (2008).
[34] D. Schröder, Elektrische Antriebe – Grundlagen, Springer, 2013.
[35] I. Golovin, S. Palis, Design of parallel feed-forward compensator and its application to electromechanical system with friction load, IFAC Papers OnLine 50-1 (2017) 15524–15529.
[36] S. Skogestad, I. Postlethwaite, Multivariable Feedback Control: Analysis and Design, John Willey and Sons, 2001.
[37] C. Ceton, Model reduction for robust controller design, Philips Electron. (1992).
[38] K. Zhou, J.C. Doyle, Essentials of Robust Control, Prentice-Hall, 1998.
[39] T.T. Georgiou, M.C. Smith, Optimal robustness in the gap metric, IEEE Trans. Automatic Control. 35 (1990) 673–685.
[40] G. Vinnicombe, Measuring Robustness of A Feedback Systems, University of Cambridge, 1993.
[41] D. McFarlane, K. Glover, A loop-shaping design procedure using H-infinity synthesis, IEEE Trans. Automat. Contr. 37 (1992) 759–769.

Parameter Identification For Continuous Fluidized Bed Spray Agglomeration

Ievgen Golovin [1], **Gerd Strenzke** [2], **Robert Dürr** [3,*], **Stefan Palis** [1,4], **Andreas Bück** [5], **Evangelos Tsotsas** [2] **and Achim Kienle** [1,3]

[1] Institute for Automation Engineering; Otto-von-Guericke University, D-39106 Magdeburg, Germany; ievgen.golovin@ovgu.de (I.G.); stefan.palis@ovgu.de (S.P.); achim.kienle@ovgu.de (A.K.)

[2] Institute of Process Engineering; Otto-von-Guericke University, D-39106 Magdeburg, Germany; gerd.strenzke@ovgu.de (G.S.); evangelos.tsotsas@ovgu.de (E.T.)

[3] Process Synthesis and Process Dynamics; Max-Planck-Institute for Complex Technical Dynamics, D-39106 Magdeburg, Germany

[4] Moscow Power Engineering Institute, National Research University, 111250-Moscow, Russia

[5] Institute of Particle Technology, Friedrich-Alexander University Erlangen-Nürnberg, D-91058 Erlangen, Germany; andreas.bueck@fau.de

* Correspondence: duerr@mpi-magdeburg.mpg.de; Tel.: +49-391-67-57195

Abstract: Agglomeration represents an important particle formation process used in many industries. One particularly attractive process setup is continuous fluidized bed spray agglomeration, which features good mixing as well as high heat and mass transfer on the one hand and constant product throughput with constant quality as well as high flow rates compared to batch mode on the other hand. Particle properties such as agglomerate size or porosity significantly affect overall product properties such as re-hydration behavior and dissolubility. These can be influenced by different operating parameters. In this manuscript, a population balance model for a continuous fluidized bed spray agglomeration is presented and adapted to experimental data. Focus is on the description of the dynamic behavior in continuous operation mode in a certain neighborhood around steady-state. Different kernel candidates are evaluated and it is shown that none of the kernels are able to match the first six minutes with time independent parameters. Afterwards, a good fit can be obtained, where the Brownian and the volume independent kernel models match best with the experimental data. Model fit is improved for identification on a shifted time domain neglecting the initial start-up phase. Here, model identifiability is shown and parameter confidence intervals are computed via parametric bootstrap.

1. Introduction

Agglomeration is a particle formation process in which at least two primary particles are combined to form a new one. This principle is often used in many industries, e.g., pharmaceutical manufacturing and food processing. The properties of the formed agglomerates, e.g., size, shape and porosity, significantly affect its end-use properties, e.g., dissolubility of food powders, processability and storeability [1]. In industrial practice, agglomerates are often formed in drums, pans or fluidized beds. The advantages of the latter include good mixing as well as high heat and mass transfer between particles, liquid and gas phase [2]. Compared to widely applied batch processes, an additional benefit of operating in continuous mode is a constant throughput with constant quality due to the steady-state

operation. Therefore, in this contribution the focus is on continuous fluidized bed spray agglomeration, which was not in the focus of research efforts so far.

The process scheme is shown in Figure 1. The particles in the chamber are fluidized by a flow of hot gas from the bottom, liquid binder is sprayed on the particles in the form of small droplets to make them wet. Due to random collisions liquid bridges between particles are formed. These can become solid by drying and thereby agglomerates consisting of different numbers of individuals are formed. Microscopic pictures of primary particles and agglomerates are depicted in Figure 2.
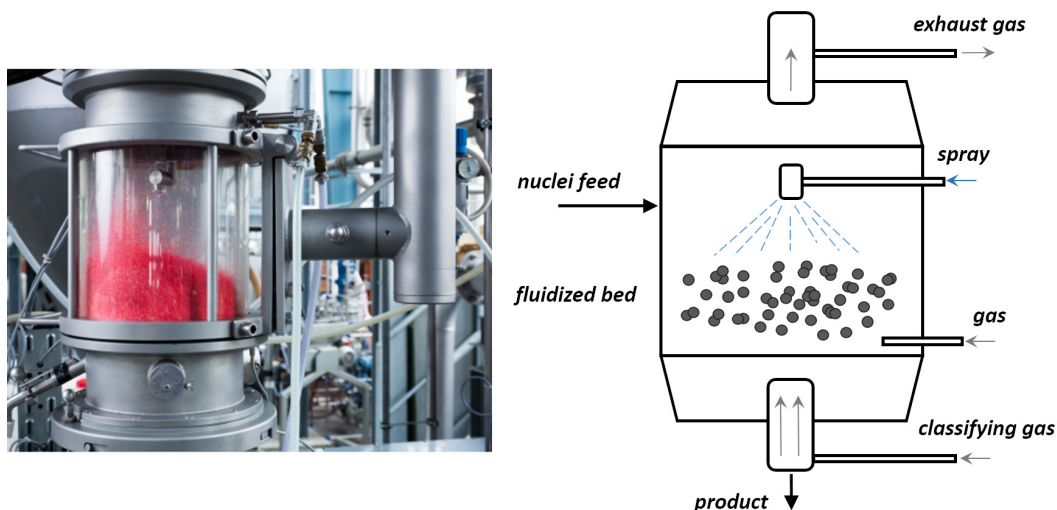
Figure 1. (**Left**) Real pilot scale fluidized bed used for experiments (**Right**) Schematic representation of fluidized bed spray agglomeration process.
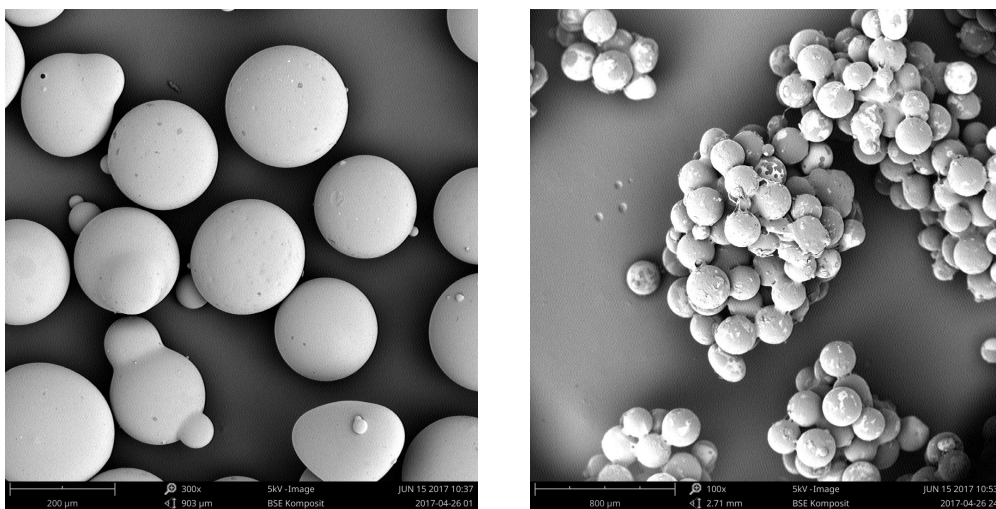

Figure 2. (**Left**) Scanning electron microscope (SEM) picture of primary particles; (**Right**) SEM picture of agglomerates at steady state.

The formation of the agglomerates and thereby the product properties can be influenced by variation of different operating parameters and process configurations, such as feed rate, binder concentration and temperature of the fluidization gas [3,4].

It is well-known that the individual particle properties, such as characteristic volume and porosity, differ from particle to particle. The emerging heterogeneity significantly affects the process and thereby the overall product properties. As an alternative to Monte-Carlo modeling approaches [5–7] the framework of population balance modeling (PBM) [8] can be used to account for the aforementioned heterogeneity in particle formation processes such as granulation (see [9–11] and the references therein)

or agglomeration. Detailed modeling of all involved mechanisms would results in multi-dimensional population balance equations, which are in general multi-dimensional partial integro-differential equations and thus challenging to solve numerically (see [12,13] for an example). For this reason, studies usually account for a single particle property, mostly characteristic size or volume. The resulting model represents a one-dimensional nonlinear partial integro-differential equation, which can be solved numerically, e.g., applying the cell average [14] or spectral method [15]. In contrast to the more complex modeling approaches [16,17], in this contribution the kinetics are described in a more mechanistic fashion [18] on the basis of the agglomeration kernel characterizing the formation of new particles by binary agglomeration. This is favorable, as the resulting model will be used to design a model based controller, which allows to keep the process close to a desired steady state in case of unforeseen disturbances. In this contribution, a number of physically motivated or heuristically derived kernel candidates ([19] and references therein) will be used. This results in a set of model candidates, which can be fitted individually to experimental data [20–23] by minimization of an objective function. To ensure that the obtained estimates are unique, i.e., there is a unique set of parameters achieving a minimum value of the objective function for the given measurements, identifiability of the parameters for the different models has to be checked [24,25]. As an alternative to analytical methods [26], the framework of profile likelihoods provides an easy accessible algorithm to investigate structural identifiability [27]. If this necessary premise is fulfilled, parameter confidence intervals have to be computed to infer how errors in the available measurements affect the estimates. Ideally, these could be determined by re-estimation of the model parameters for a large number of experimental replicates. However, if only a low number or even no replicates are available, parametric bootstrap can be applied [28,29], which is less restrictive than classical methods based on the Fisher-Information Matrix [30]. Those methods use artificially reproduced ("bootstrapped") measurement sets. For each set, a parameter estimate is computed yielding a bootstrapped set of parameter estimates, which can subsequently be used to derive parameter confidence intervals.

The manuscript is structured as follows. In Section 2, the experimental setup, mathematical modeling and parameter identification procedure are explained in detail. The results of the parameter estimation are shown in Section 3. Furthermore, identifiability of the best model candidates is investigated and results for the parametric bootstrap are shown. Section 4 concludes this work and gives an outlook to possible future research directions.

2. Materials and Methods

2.1. Experimental Setup

The experiment was realized in a pilot scale plant depicted in Figure 1. The cylindrical fluidized bed has a inner diameter of 300 mm, schematically shown in Figure 1. Particles were fluidized by a heated gas stream, which enters the fluidized bed chamber from the bottom through a distributor plate. The primary particles were sprayed by a two-fluid nozzle (Model 940, liquid orifice diameter 0.8 mm, Düsen-Schlick GmbH, Untersiemau/Coburg, Germany) which was installed in a top-spray configuration at a distance of 420 mm above the distributor plate of the fluidized bed. To reduce clogging, the shape of the air cap was modified to hemispherical. An external pump supplied the feeding of the sprayed binder solution. Particles having the target size are continuously discharged by a classification tube, which is centrally installed at the bottom of the fluidized bed.

The starting materials of the fluidized bed and continuous feeding during the process were glass beads with a Sauter mean diameter (SMD) of 0.2 mm and mean sphericity of 0.92 (see Figure 2). The used binder solution contained 6 wt% hydroxylpropylmethylcellulose (HPMC) and 94 wt% of water. HPMC is a white, sweet smelling powder, also known as Pharmacoat. It is typically used in food and pharmaceutical industries.

The duration of the experiment was approximately 120 min process time with a total mass of 38 kg used primary particles and 6.56 kg mass of sprayed liquid with a binder content of 6 wt%. The initial

bed mass for the experiment was 8 kg. The inlet air was heated up to 100 °C before starting the process. An overview of the process parameters is shown in Table 1. The mass of discharged product was 29 kg. The produced agglomerates are shown in Figure 2.

For offline analysis, 32 bed samples and 16 product samples were taken. The sample time starts with 2 min sample intervals for bed and 4 min sample intervals for product samples and reached up to 10 min for bed and 20 min for product samples. The particle size distribution (PSD) of each sample was measured offline with a Camsizer (Retsch Technologies GmbH, Haan, Germany), which infers particle size via dynamic image analysis. The output data from the Camsizer is the PSDs, normalized with respect to the total number resulting in q_0 and the volume resulting in q_3 of the particle collective for each sample and thereby over the process time. The shape was investigated at randomly selected bed and product samples with a scanning electron microscope (SEM). The samples were pretreated by a SEM sputter coater with a thin gold layer to amplify the measurement signal and investigated with the Phenom G2 Pro (Phenom-World BV, Eindhoven, The Netherlands). The bed mass was measured and calculated from the pressure drop of distributor plate and the fluidized bed.

Table 1. Overview of experimental parameters.

Parameter	Unit	Value
Initial bed mass	kg	8
Sauter mean diameter of primary particles	mm	0.2
Inlet temperature	°C	100
Inlet mass flow	kg/h	275
Feed rate	kg/h	15
Spray rate	kg/h	3.3
Binder content	wt%	6
Density of particle material	kg/m^3	2500

2.2. Mathematical Modeling

In particle production processes, significant heterogeneities with respect to the individual particle properties such as size or shape emerge. Population balance modeling represents an established concept to describe such property distributed parameter systems [8]. Instead of describing a large number of particles and their interactions, PBM characterizes the dynamics of the particles via the number density distribution function (NDF) $n(t, \mathbf{z})$ representing information of the number of particles within an infinitesimal section of the particle property state space $\mathbf{z} \in \mathbb{R}^{N_z}$. In the following, it is assumed that individual particles do only differ with respect to their characteristic volume v such that $\mathbf{z} = v$ and $N_z = 1$. Furthermore, it is assumed that other effects than agglomeration, i.e., nucleation, particle growth and breakage can be neglected by an appropriate choice of the operating conditions. Under these assumptions, the dynamics of the particle distribution during the agglomeration process can be described by the following population balance equation (PBE)

$$\frac{\partial n(t,v)}{\partial t} = \dot{n}_{\text{feed}}(t,v) - \dot{n}_{\text{prod}}(t,v) + \dot{n}_{\text{agg}}(t,v) \tag{1}$$

The corresponding initial NDF $n(0, v)$ can be determined from the experimental data. The left hand side of Equation (1) accounts for temporal evolution while the first two elements of the right hand side describe feed of new seed particles to and removal of the desired product particles from the fluidized bed. The feed is given as

$$\dot{n}_{\text{feed}}(t,v) = \dot{N}_{in} \frac{\exp\left(\frac{-(v-\mu_1)^2}{2\sigma_1^2}\right)}{\int_0^\infty \exp\left(\frac{-(v-\mu_1)^2}{2\sigma_1^2}\right) \mathrm{d}v} \tag{2}$$

with $\dot{N}_{in}$ denoting the constant feed rate. The parameters μ_1 and σ_1 characterize mean and variance of feed particle volumes. Product particle removal can be modeled as

$$\dot{n}_{\text{prod}}(t,v) = \dot{N}_{out}K(v)n(t,v) \qquad (3)$$

where $\dot{N}_{out}$ is the constant removal rate of particles and $K(v)$ represents the separation function given by

$$K(v) = \frac{\int_0^v \exp(\frac{-(\xi-\mu_2)^2}{2\sigma_2^2})\,\mathrm{d}\xi}{\int_0^\infty \exp(\frac{-(\xi-\mu_2)^2}{2\sigma_2^2})\,\mathrm{d}\xi} \qquad (4)$$

The last element of the right hand side of Equation (1) denotes the formation of new particles of volume v by agglomeration of two particles with volumes u and $v - u$

$$
\begin{aligned}
\dot{n}_{agg}(t,v) &= \dot{n}_{agg}^+(t,v) - \dot{n}_{agg}^-(t,v) \\
&= \frac{1}{2}\int_0^v \beta(t,u,v-u)n(t,u)n(t,v-u)\mathrm{d}u \\
&\quad - \int_0^\infty \beta(t,u,v)n(t,v)n(t,u)\mathrm{d}u
\end{aligned} \qquad (5)
$$

Here, the agglomeration kernel $\beta(t,u,v)$ contains information about the probability of forming a new agglomerate and is often separated into a volume and time-dependent part

$$\beta(t,v,u) = \beta_0(t)\beta_v(v,u). \qquad (6)$$

In general, the volume-dependent part $\beta_v(v,u)$, also called coalescence kernel, is a non-negative symmetric function of two variables. As motivated in the introduction, focus in this publication is on rather simple agglomeration kernels (e.g., [19,31]). These are either physically motivated, e.g., the Brownian motion coalescence kernel and kernel based on equipartition of kinetic energy (EKE kernel), or rather empirical, e.g., Kapur kernel and volume-independent (constant) kernel. Additionally, abstract parametric approaches, e.g., Laurent-polynomials [23], can be used. The kernel candidates studied in this contribution are summarized in Table 2.

In contrast, the time dependent part $\beta_0(t)$, also called the agglomeration efficiency, mirrors the effects of the process conditions and operating parameters. In this work, as a first step, it is assumed that the time dependency of the agglomeration efficiency can be neglected, such that $\beta_0(t) = const$.

2.3. Parameter Identification

The estimation of the agglomeration process is especially challenging due to the highly nonlinear process dynamics. In order to describe the formation of the agglomerates and to parametrize the model, five different agglomeration kernels are considered (see Table 2). The first four kernels represent rather simple approaches, which do not have any free parameters. Thus, only the agglomeration efficiency $p_{est} = \beta_0$ has to be estimated from experimental data. Besides these simple kernel candidates, the fifth formulation in the table represents a more complex parametric model candidate based on Laurent polynomials of rank $K = 2$ [23]:

$$
\begin{aligned}
\beta_v(u,v) =\ & k_1 + k_2\,(u+v) + k_3\,(u^{-1}+v^{-1}) + k_4\,uv + k_5\,(u^{-1}v+v^{-1}u) + k_6\,(u^{-1}v^{-1}) + k_7\,(u^2+v^2) \\
& + k_8\,(u^{-2}+v^{-2}) + k_9\,(u^2v+v^2u) + k_{10}\,(u^{-2}v+v^{-2}u) + k_{11}\,(u^{-1}v^2+v^{-1}u^2) \\
& + k_{12}\,(u^{-2}v^{-1}+v^{-2}u^{-1}) + k_{13}\,(u^2v^2) + k_{14}\,(u^{-2}v^2+v^{-2}u^2) + k_{15}\,(u^{-2}v^{-2})
\end{aligned} \qquad (7)
$$

Here, the parameter vector to be estimated $\mathbf{p_{est}} = [k_1,\ k_2,\ \dots,\ k_{15}]$ contains the of unknown polynomial coefficients.

Substituting one of the kernels given in Table 2 into the PBE (1) the unknown parameters can be estimated from the experimental data by minimizing the following objective function

$$J(\mathbf{p}_{est}) = \sum_{i=1}^{N_t} w_1 \|e_{u,rel}(t_i, x, \mathbf{p}_{est})\|_2 + w_2 \|e_{m,rel}(t_i, \mathbf{p}_{est})\|_2 \tag{8}$$

where w_1 and w_2 are weighting coefficients and N_t is the number of samples. Weighting coefficients are chosen such that the first and the second term of the right hand side are in the same order of magnitude. Here, the first part represents the errors between simulated and measured bed mass scaled by the maximum bed mass

$$e_{m,rel}(t_i, \mathbf{p}_{est}) = \frac{m_{b,act}(t_i) - m_{b,est}(t_i, \mathbf{p}_{est})}{max(m_{b,act}(t_i))} \tag{9}$$

Furthermore, J contains the L_2-norm of the error in the weighted particle size distribution $u(t, x)$

$$e_{u,rel}(t_i, x, p_{est}) = \frac{u_{act}(t_i, x) - u_{est}(t_i, x, p_{est})}{max(u_{act}(t_i, x))} \tag{10}$$

where $u(t, x)$ is defined as

$$u(t, x) = \frac{\pi}{6} x^3 n(t, x) \tag{11}$$

and x represents the characteristic size of the particles. Using local conservation of the particle number

$$n(t, v) dv = n(t, x) dx$$
$$n(t, x) = n(t, v) \frac{dv}{dx} \tag{12}$$

$u_{est}(t_i, x, p_{est})$ is computed from the simulated particle volume distribution as

$$u_{est}(t_i, x) = \frac{\pi}{6} x^3 n_{est}(t_i, v) \frac{dv}{dx} \tag{13}$$

Its experimental counterpart $u_{act}(t_i, x)$ is computed from the normalized particle size distribution $q_{3,act}(t_i, x)$ provided by the Camsizer measurements and the measured bed mass $m_{b,act}(t_i)$ under the assumption of spherical particle shape and particle material density ρ.

Table 2. Kernel model candidates used for parameter identification.

Expression	Kernel Name
$\beta_v(u, v) = (u + v)^1 \times (u\,v)^{-1}$	Kapur kernel
$\beta_v(u, v) = (u^{1/3} + v^{1/3}) \times (u^{-1/3} + v^{-1/3})$	Brownian motion kernel
$\beta_v(u, v) = (u^{1/3} + v^{1/3})^2 \times \sqrt{u^{-1} + v^{-1}}$	EKE kernel
$\beta_v(u, v) = 1$	Volume-independent kernel
$\beta_v(u, v) = \sum\limits_{m=-K}^{K} \sum\limits_{n=-K}^{K} k_{m,n}\, v^m\, u^n$	Laurent polynomials kernel

2.4. Parameter Identifiability

Identifiability is a necessary premise to ensure meaningful parameter estimates. In the following the profile likelihood will be used to infer model identifiability. Here, the core idea is to explore the cost functional *J* around the optimal parameter vector

$$\mathbf{p}^* = \left[p_1^*, \ldots, p_{N_p}^* \right]^T \tag{14}$$

A parameter p_i is said to be (locally) structural identifiable if the corresponding profile likelihood

$$J_{PL}(p_i) = \min_{p_{j \neq i}} J \tag{15}$$

has a unique minimum in the neighborhood of $\mathbf{p}^*$. Therefore, for fixed values of p_i the other parameters are re-estimated resulting in a one-dimensional functional curve. If each curve features a distinct minimum, the model is said to be (locally) structural identifiable. In contrast, flat or semi-flat profile likelihoods without a unique minimum indicate structural non-identifiability. In this case, parameters can not be uniquely determined even under ideal measurement conditions.

2.5. Confidence Intervals

Besides estimation of the unknown kernel parameters it is also highly desirable to evaluate their confidence intervals. These give a measure of the estimates sensitivity to stochastic fluctuations in the experimental data. Classical methods, e.g., approaches based on evaluation of the Fisher-Information-Matrix [30], are only able to give an approximate centered and symmetric measure of the true confidence region as they rely on rather strong assumptions on the underlying model dynamics. Alternatively, the bootstrap approach has been established as a valuable method to infer model parameter confidence [28]. The core idea will be described in the following: all measurements underlie stochastic variations, which would result in a certain variance within a large set of replicate experimental data vectors

$$\mathbb{Y} = \left\{ \mathbf{y}_1, \ldots, \mathbf{y}_{N_{rep}} \right\} \tag{16}$$

For each element of $\mathbb{Y}$, model parameters can be (re-)estimated resulting in a corresponding set of adapted parameter vectors

$$\mathbb{P} = \left\{ \mathbf{p}_1^*, \ldots, \mathbf{p}_{N_{rep}}^* \right\} \tag{17}$$

containing information of the model parameters sensitivity to variations in the measurements. Statistical measures as mean and variance can be easily calculated from $\mathbb{P}$. Commonly, the percentile method is applied to compute the confidence intervals. Let p^α denote the $100(1 - \alpha)$-percentile of a parameter p_i extracted from $\mathbb{P}$, then the corresponding parameter confidence interval is given by

$$\left[p_i^{lo}, p_i^{up} \right]_\alpha = \left[p_i^{0.5\alpha}, p_i^{1-0.5\alpha} \right] \tag{18}$$

In general, the number of experimental replicates is limited. This is in particular true for the given agglomeration process, where time and costs connected with each experiment are considerable. Therefore, the resulting set of (re-)estimated parameter vectors $\mathbb{P}$ does not give a reliable measure of the true confidence intervals. To improve the situation, the parametric bootstrap method [28,30] can be applied. Here, $\mathbb{Y}$ is replaced by a set of artificial replicates

$$\mathbb{Y}^{BS} = \left\{ \mathbf{y}_1^{BS}, \ldots, \mathbf{y}_{N_{BS}}^{BS} \right\} \tag{19}$$

which are generated with a Monte-Carlo method. The corresponding set of parameters is given by

$$\mathbb{P}^{BS} = \left\{ \mathbf{p}_1^{BS}, \dots, \mathbf{p}_{N_{BS}}^{BS} \right\} \tag{20}$$

and is further used to determine the parameter confidence intervals.

3. Results

The proposed parameter identification procedure has been implemented in MATLAB 2018a (The MathWorks, Inc., Natick, MA, USA). For the solution of the PBM, the method of lines has been applied, where the spatial coordinate is lumped using the cell-average method on a logarithmic grid with $N_v = 55$ grid points [14]. The model parameters utilized for simulations are derived from the experimental conditions and are presented in Table 3. The stated unconstrained optimization problem does not guarantee that the estimated parameters are positive, which they are for physical reasons. In order to exclude non-physical solutions corresponding constraints should be added, resulting in a constrained optimization problem. For its solution, the active-set algorithm as part of the MATLAB optimization toolbox was applied.

Table 3. Model parameters used for simulation.

Parameter	Value	Parameter	Value
μ_1	4.2×10^{-3}	σ_1	6.4×10^{-6}
μ_2	3.8×10^{-1}	σ_2	1.4×10^{-2}
$\dot{N}_{in}$	4×10^5	$\dot{N}_{out}$	5.5×10^{-4}
w_1	1	w_2	50

3.1. Kernel Estimation

3.1.1. Identification on the Whole Time Domain

Applying the proposed approach for all five kernels and using the first experimental sample as initial condition yields in estimates for the agglomeration efficiency β_0 and the Laurent polynomials coefficients, respectively. The obtained results are depicted in Figure 3. As can be seen from the L_2-norm of the errors between measured and simulated PSD (Figure 3 (left)) and the simulated and measured bed mass (Figure 3 (right)), the mismatch for all fitted models is considerable in the first ten minutes of the process and decreases rapidly for larger process times. Here, the models with the Brownian motion kernel, the volume-independent kernel and the Laurent polynomials perform better, in terms of the L_2-norm, than the models with EKE and Kapur kernel.

Figure 4 shows the comparison of the fitted models based on the Brownian motion and volume-independent kernels and the measured PSD in terms of normalized PSD $q_3(t, x)$

$$q_3(t, x) = \frac{x^3 n(t, x)}{\int_0^\infty x^3 n(t, x) \mathrm{d}x} \tag{21}$$

For $t > 80$ min no significant change in the normalized particle size distributions was obtained in the experiment, indicating steady-state operation.
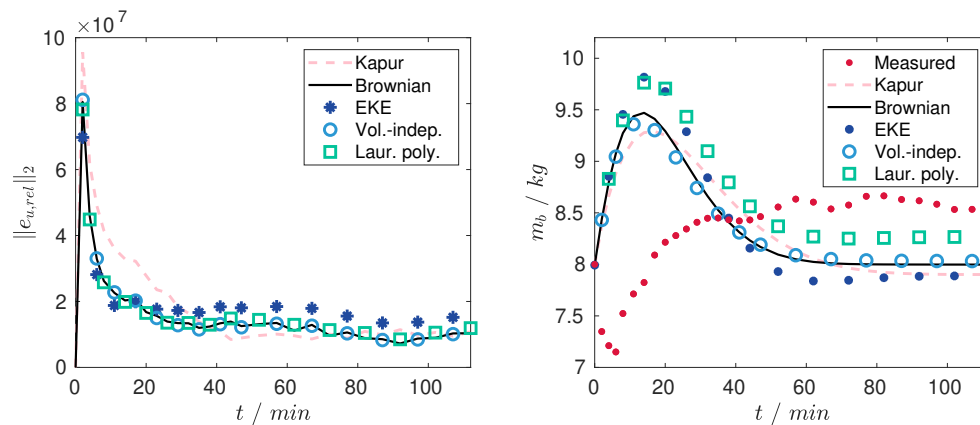
Figure 3. (**Left**) Comparison of the L_2 norms of the particle size distribution (PSD) error for different kernel candidates (**Right**) Comparison of the actual bed mass and bed masses of the identified models.
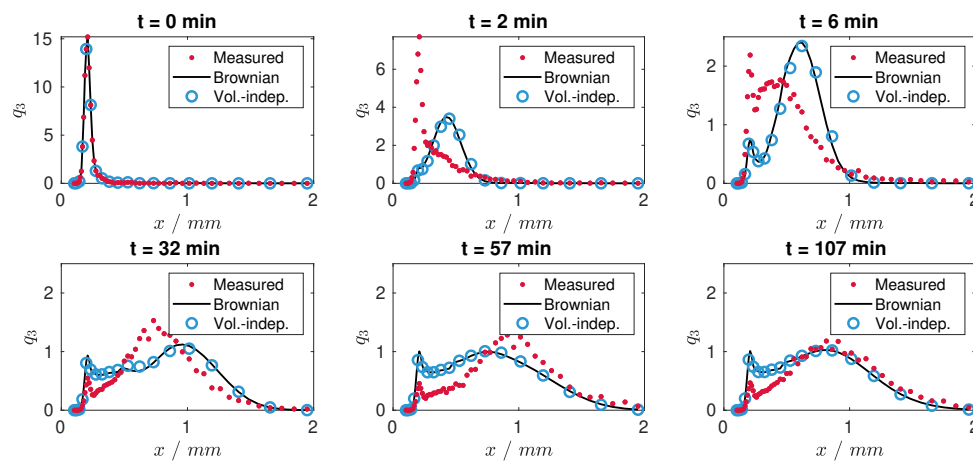

Figure 4. Snapshots of particle size distributions q_3 of the actual plant and identified models.

Generally, it can be seen that the results improve for larger time values, i.e., closer to the steady-state operation. The big misfit in the initial phase demonstrates that the model structure does not reflect the start-up dynamics of the agglomeration process. Possible reasons may be additional internal transients, e.g., a temperature decrease due to spraying, which would result in a time-varying kernel. In addition, the decrease in the actual bed mass, which can be observed in the first couple of minutes, indicates that during start-up even particles being smaller than the product fraction are withdrawn from the process. This is however not reflected by the model, where a constant separation function for the product removal has been assumed. However, as the focus in this contribution and future research is on continuous agglomeration, only the dynamic behavior close to the steady-state is of importance. Therefore, in the following the initial start-up, i.e., the first six minutes, will be neglected resulting in a shifted time-domain.

3.1.2. Identification for the Shifted Time Domain

In the following, the described parameter estimation will be repeated for all kernels for the experimental data shifted by 6 min. Here, the experimental data sample at $t = 6$ min will be used as the initial condition. Results of the nonlinear optimization are depicted in Figures 5 and 6. As can be seen the matching between the parametrized model and the measurements has been improved considerably. The misfit in the region of the first mode (Figure 6) is presumable due to the measurement uncertainties. As before, the best results, in terms of the L_2-norm, are achieved for the model with the Brownian motion kernel, the volume-independent kernel and the Laurent polynomials. Yet, the

latter does not show significant improvement despite its higher number of model parameters and will therefore be excluded from subsequent analysis.
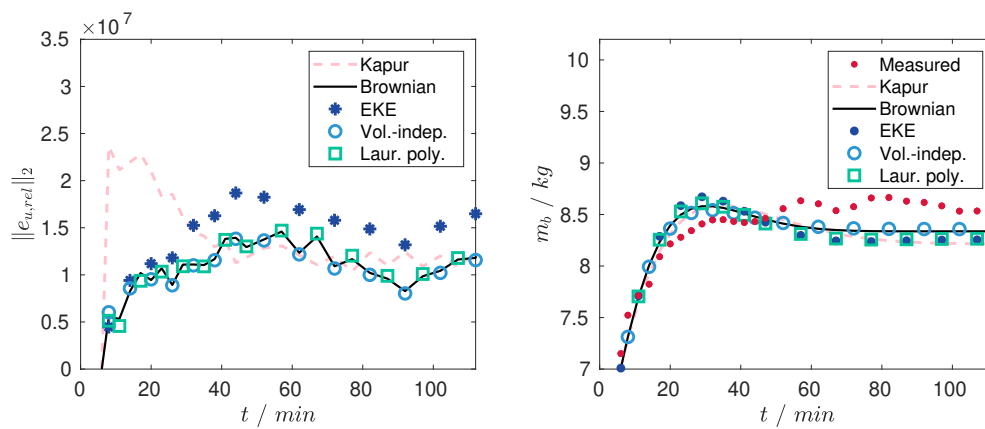

Figure 5. Comparison of the L_2 norms of the PSD error (**Left**) and the actual bed mass and bed masses of the identified models (**Right**) for the shifted time domain.
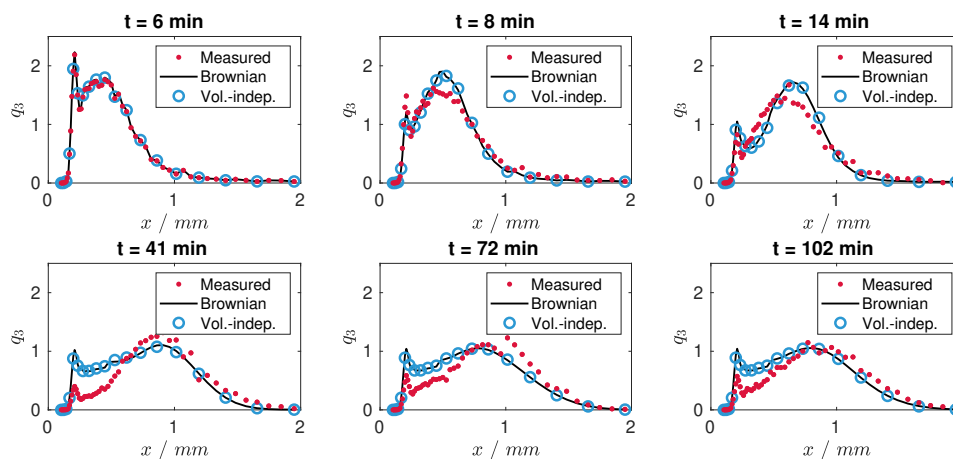

Figure 6. Particle size distributions q_3 of the actual plant and the identified models for the shifted time domain.

3.2. Model Identifiability

For the Brownian and volume-independent kernel, the agglomeration efficiency β_0 is the only unknown model parameter. Hence, the corresponding profile likelihood computation reduces to a parameter study, i.e., evaluation of the cost functional J for different values of β_0. The resulting curves, depicted in Figure 7, possess a distinct minimum, which indicates that the unknown β_0 is structurally identifiable in both cases.
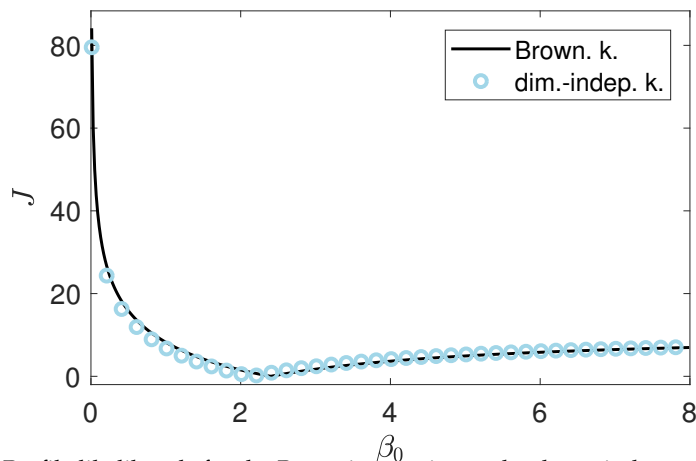
Figure 7. Profile likelihoods for the Brownian motion and volume-independent kernel.

3.3. Confidence Intervals

To compute parameter confidence intervals, a set of 1000 parametric bootstrap measurements was generated from the fitted model. Here, it was assumed that the measurements of $q_3(t, x)$ were corrupted by a relative error

$$q_3(t,x)_k^{BS} = q_3(t,x)^* + q_3^{res}(t,x)_k^{BS}, \quad q_3^{res}(t,x)_k^{BS} \sim \mathcal{N}(0, \Sigma_{q_3}) \cdot q_3(t,x)^*, \quad k = 1, \dots, N_{BS} \quad (22)$$

and thus the corresponding residual $q_3^{res}(t,x)_k^{BS}$ is proportional to the magnitude of $q_3(t,x)^*$. For the total bed mass measurement, bootstrap measurements were generated assuming an relative error

$$m_{bed}(t)_k^{BS} = m_{bed}(t)^* + m_{bed}^{res}(t)_k^{BS}, \quad m_{bed}^{res}(t)_k^{BS} \sim \mathcal{N}(0, \Sigma_{m_{bed}}), \quad k = 1, \dots, N_{BS} \quad (23)$$

The model was refitted to the bootstrapped measurement set for the Brownian motion and the volume-independent kernel. Results by means of histograms of the obtained bootstrapped parameter sets and percentile plots over the number of bootstrap runs are shown in Figures 8 and 9.

It can be seen that for both cases approximately symmetric Gaussian-like distributions are obtained. Furthermore, it is shown that the values for the percentiles and the mean do not significantly change for $k > 400$ thereby indicating convergence of the bootstrapped parameter distribution. The overall confidence intervals and means are given in Table 4.
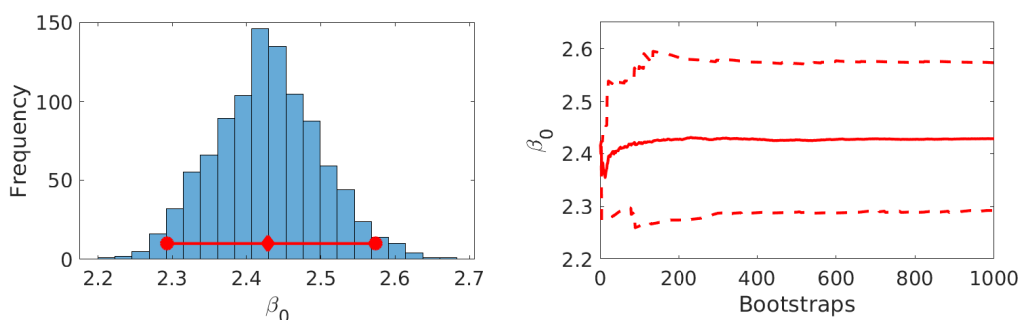

Figure 8. Results for parameter estimation for Brownian motion kernel with parametric bootstrap data: Histogram of bootstrapped parameter set, confidence interval $\left[\beta_0^{0.025}, \beta_0^{0.975}\right]$ (red circles) and mean $\bar{\beta}_0$ (red rectangle) (**Left**) Change of $\left[\beta_0^{0.025}, \beta_0^{0.975}\right]$ (dashed) and $\bar{\beta}_0$ (solid) over number of bootstrap runs (**Right**).
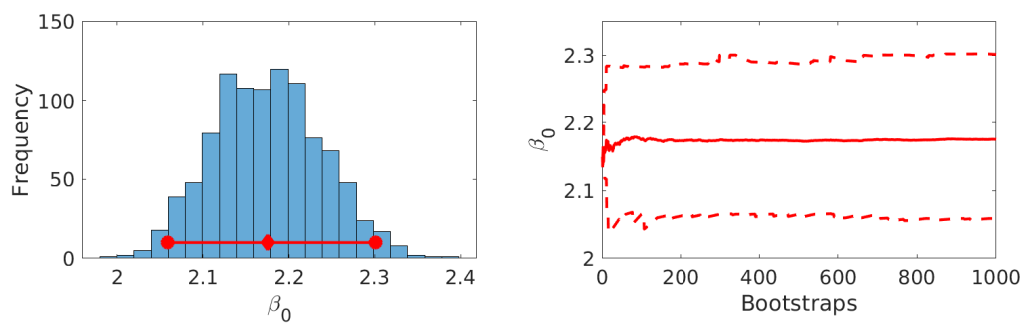
Figure 9. Results for parameter estimation for volume-independent agglomeration kernel with parametric bootstrap data: Histogram of bootstrapped parameter set, confidence interval $\left[\beta_0^{0.025},\ \beta_0^{0.975}\right]$ (red circles) and mean $\bar{\beta}_0$ (red rectangle) (**Left**) Change of $\left[\beta_0^{0.025},\ \beta_0^{0.975}\right]$ (dashed) and $\bar{\beta}_0$ (solid) over number of bootstrap runs (**Right**).

Table 4. Mean parameter values and confidence intervals from parametric bootstrap.

Agglomeration Kernel	$\bar{\beta}_0$	$\left[\beta_0^{lo},\ \beta_0^{up}\right] = \left[\beta_0^{0.025},\ \beta_0^{0.975}\right]$
Brownian motion	2.4284×10^{-11}	$\left[2.2926 \times 10^{-11},\ 2.5736 \times 10^{-11}\right]$
Volume-independent	$2.1754 \times 5 \times 10^{-12}$	$\left[2.0588 \times 5 \times 10^{-12},\ 2.3011 \times 5 \times 10^{-12}\right]$

4. Conclusions

In this paper the parameter identification for continuous fluidized bed spray agglomeration was presented. For the estimation of the agglomeration kernel from the experimental data a set of five different kernel model candidates has been fitted to experimental data applying nonlinear optimization. Applying the estimation procedure on the whole time domain showed that the initial start-up phase could not be reflected well by the given model structure. Possible reasons may be additional internal transients in this phase, e.g., temperature decrease due to spraying. Those would result in a time-varying kernel. However, the focus of future work is on the continuously operating agglomeration, process this initial phase is of minor importance. Therefore, the estimation procedure has been repeated for a shifted time domain, i.e., neglecting the first six minutes, resulting in significant better results. It has been shown that models based on the Brownian motion, the volume-independent and the Laurent polynomial kernel provide the best results in terms of the L_2-norm of the error based on the PSD. Despite its higher complexity and higher number of free model parameters, the latter approach is not superior to the two simpler kernel models. Thus, following good modelers practice, the Brownian and the volume-independent approaches were preferred. For both kernel models identifiability in terms of the corresponding profile likelihoods was shown and confidence intervals for the model parameters were determined using a parametric bootstrap method.

Future work will be concerned with qualitative process behavior for varying process conditions. As has been shown in earlier contributions, stability of continuously operated particulate processes strongly depends on the chosen process conditions (e.g., [32,33]). In order to increase robustness with respect to unforeseen disturbances and stabilize the process for varying operating conditions, feedback control will be studied. Here, a number of finite-dimensional [34,35] and infinite-dimensional [36] approaches have been investigated and developed for related continuous granulation processes in fluidized beds.

Author Contributions: S.P., A.B., A.K. and E.T. designed and conceived the study; G.S. performed the experiments; G.S., I.G. and R.D. analyzed the data; I.G. and R.D. performed the numerical studies; G.S., I.G., R.D., S.P., A.B., E.T. and A.K. wrote the paper.

Conflicts of Interest: The authors declare no conflict of interest.

References

1.　Bück, A.; Tsotsas, E. Agglomeration. In *Encyclopedia of Food and Health*; Caballero, B., Finglas, P.M., Toldrá, F., Eds.; Academic Press: Oxford, UK, 2016; pp. 73–81. [CrossRef]

2.　Groenewold, H.; Tsotsas, E. Drying in fluidized beds with immersed heating elements. *Chem. Eng. Sci.* **2007**, *62*, 481–502. [CrossRef]

3.　Dadkhah, M.; Tsotsas, E. Influence of process variables on internal particle structure in spray fluidized bed agglomeration. *Powder Technol.* **2014**, *258*, 165–173. [CrossRef]

4.　Esmailpour, A.A.; Mostoufi, N.; Zarghami, R. Effect of temperature on fluidization of hydrophilic and hydrophobic nanoparticle agglomerates. *Exp. Therm. Fluid Sci.* **2018**, *96*, 63–74. [CrossRef]

5.　Zhao, H.; Maisels, A.; Matsoukas, T.; Zheng, C. Analysis of four Monte Carlo methods for the solution of population balances in dispersed systems. *Powder Technol.* **2007**, *173*, 38–50. [CrossRef]

6.　Terrazas-Velarde, K.; Peglow, M.; Tsotsas, E. Kinetics of fluidized bed spray agglomeration for compact and porous particles. *Chem. Eng. Sci.* **2011**, *66*, 1866–1878. [CrossRef]

7.　Rieck, C.; Schmidt, M.; Bück, A.; Tsotsas, E. Monte Carlo modeling of binder-Less spray agglomeration in fluidized beds. *AIChE J.* **2018**, *64*, 3582–3594. [CrossRef]

8.　Ramkrishna, D. *Population Balances: Theory and Applications to Particulate Systems in Engineering*; Academic Press: San Diego, CA, USA, 2000. [CrossRef]

9.　Cotabarren, I.; Schulz, P.G.; Bucalá, V.; Piña, J. Modeling of an industrial double-roll crusher of a urea granulation circuit. *Powder Technol.* **2008**, *183*, 224–230. [CrossRef]

10.　Cotabarren, I.M.; Bertín, D.E.; Bucalá, V.; Piña, J. Feedback control strategies for a continuous industrial fluidized-bed granulation process. *Powder Technol.* **2015**, *283*, 415–432. [CrossRef]

11.　Vreman, A.; van Lare, C.; Hounslow, M. A basic population balance model for fluid bed spray granulation. *Chem. Eng. Sci.* **2009**, *64*, 4389–4398. [CrossRef]

12.　Immanuel, C.D.; Doyle, F.J. Solution technique for a multi-dimensional population balance model describing granulation processes. *Powder Technol.* **2005**, *156*, 213–225. [CrossRef]

13.　Poon, J.M.H.; Immanuel, C.D.; Francis, J.; Doyle, I.; Litster, J.D. A three-dimensional population balance model of granulation with a mechanistic representation of the nucleation and aggregation phenomena. *Chem. Eng. Sci.* **2008**, *63*, 1315–1329. [CrossRef]

14.　Kumar, J.; Peglow, M.; Warnecke, G.; Heinrich, S.; Mörl, L. Improved accuracy and convergence of discretized population balance for aggregation: The cell average technique. *Chem. Eng. Sci.* **2006**, *61*, 3327–3342. [CrossRef]

15.　Bück, A.; Klaunick, G.; Kumar, J.; Peglow, M.; Tsotsas, E. Numerical Simulation of Particulate Processes for Control and Estimation by Spectral Methods. *AIChE J.* **2012**, *58*, 2309–2319. [CrossRef]

16.　Hussain, M.; Kumar, J.; Peglow, M.; Tsotsas, E. Modeling spray fluidized bed aggregation kinetics on the basis of Monte-Carlo simulation results. *Chem. Eng. Sci.* **2013**, *101*, 35–45. [CrossRef]

17.　Hussain, M.; Peglow, M.; Tsotsas, E.; Kumar, J. Modeling of aggregation kernel using Monte Carlo simulations of spray fluidized bed agglomeration. *AIChE J.* **2014**, *60*, 855–868. [CrossRef]

18.　Peglow, M.; Kumar, J.; Heinrich, S.; Warnecke, G.; Tsotsas, E.; Mörl, L.; Wolf, B. A generic population balance model for simultaneous agglomeration and drying in fluidized beds. *Chem. Eng. Sci.* **2007**, *62*, 513–532. [CrossRef]

19.　Aldous, D.J. Deterministic and Stochastic Models for Coalescence (Aggregation and Coagulation): A Review of the Mean-Field Theory for Probabilists. *Bernoulli* **1999**, *5*, 3–48. [CrossRef]

20.　Bramley, A.S.; Hounslow, M.J.; Ryall, R.L. Aggregation during Precipitation from Solution: A Method for Extracting Rates from Experimental Data. *J. Colloid Interface Sci.* **1996**, *183*, 155–165. [CrossRef]

21.　Mahoney, A.W. Inverse Problem Modeling of Particulate Systems. Ph.D. Thesis, Purdue University Graduate School, West Lafayette, IN, USA, 2001.

22.　Chakraborty, J.; Kumar, J.; Singh, M.; Mahoney, A.; Ramkrishna, D. Inverse Problems in Population Balances. Determination of Aggregation Kernel by Weighted Residuals. *Ind. Eng. Chem. Res.* **2015**, *54*, 10530–10538. [CrossRef]

23.　Eisenschmidt, H.; Soumaya, M.; Bajcinca, N.; Le Borne, S.; Sundmacher, K. Estimation of aggregation kernels based on Laurent polynomial approximation. *Comput. Chem. Eng.* **2017**, *103*, 210–217. [CrossRef]

24. Vilas, C.; Arias-Méndez, A.; García, M.R.; Alonso, A.A.; Balsa-Canto, E. Toward predictive food process models: A protocol for parameter estimation. *Criti. Rev. Food Sci. Nutr.* **2018**, *58*, 436–449. [CrossRef] [PubMed]

25. Van Hauwwermeiren, D.; De Beer, T.; Nopens, I. On the identifiability of kernels for population balance modelling. In Proceedings of the 6th International Conference on Population Balance Modelling, Gent, Belgium, 7–9 May 2018.

26. Chis, O.T.; Banga, J.R.; Balsa-Canto, E. Structural Identifiability of Systems Biology Models: A Critical Comparison of Methods. *PLoS ONE* **2011**, *6*, e27755. [CrossRef] [PubMed]

27. Raue, A.; Becker, V.; Klingmüller, U.; Timmer, J. Identifiability and observability analysis for experimental design in nonlinear dynamical models. *Chaos* **2010**, *20*, 045105. [CrossRef] [PubMed]

28. Joshi, M.; Seidel-Morgenstern, A.; Kremling, A. Exploiting the bootstrap method for quantifying parameter confidence intervals in dynamical systems. *Metab. Eng.* **2006**, *8*, 447–455. [CrossRef] [PubMed]

29. Joshi, M.; Kremling, A.; Seidel-Morgenstern, A. Model based statistical analysis of adsorption equilibrium data. *Chem. Eng. Sci.* **2006**, *61*, 7805–7818. [CrossRef]

30. Schenkendorf, R.; Kremling, A.; Mangold, M. Optimal experimental design with the sigma point method. *IET Syst. Biol.* **2009**, *3*, 10–23. [CrossRef] [PubMed]

31. Le Borne, S.; Shahmuradyan, L.; Sundmacher, K. Fast evaluation of univariate aggregation integrals on equidistant grids. *Comput. Chem. Eng.* **2015**, *74*, 115–127. [CrossRef]

32. Dreyschultze, C.; Neugebauer, C.; Palis, S.; Bück, A.; Tsotsas, E.; Stefan, H.; Kienle, A. Influence of zone formation on stability of continuous fluidized bed layering granulation with external product classification. *Particuology* **2015**, *23*, 1–7. [CrossRef]

33. Neugebauer, C.; Palis, S.; Bück, A.; Tsotsas, E.; Stefan, H.; Kienle, A. A dynamic two-zone model of continuous fluidized bed layering granulation with internal product classification. *Particuology* **2017**, *31*, 8–14. [CrossRef]

34. Palis, S.; Kienle, A. Stabilization of continuous fluidized bed spray granulation with external product classification. *Chem. Eng. Sci.* **2012**, *70*, 200–209. [CrossRef]

35. Palis, S.; Kienle, A. H_∞ loop shaping control for continuous fluidized bed spray granulation with internal product classification. *Ind. Eng. Chem. Res.* **2013**, *52*, 408–420. [CrossRef]

36. Palis, S.; Kienle, A. Discrepancy based control of particulate processes. *J. Process Control* **2014**, *24*, 33–46. [CrossRef]

Non-identifier-based adaptive control of continuous fluidized bed spray granulation

Stefan Palis [a,b,]*

[a] *Otto-von-Guericke-University, Universitätsplatz 2, D-39106 Magdeburg, Germany*
[b] *National Research University "Moscow Power Engineering Institute", Krasnokazarmennaya 14, 111250 Moscow, Russia*

ABSTRACT

This paper is concerned with stabilizing control for continuously operated fluidized bed spray granulation with internal product classification. It is well-known that these processes may become unstable for certain operating conditions giving rise to nonlinear oscillations in the particle size distribution. In contrast to previous works, in this contribution a model-free adaptive control is proposed. It is shown that the given fluidized bed spray granulation process fulfills the required structural assumptions. The designed control schemes, universal adaptive and λ-tracking control, are tested in a noise-free scenario and including measurement noise.

© 2018 Elsevier Ltd. All rights reserved.

1. Introduction

Granulation is an important production process resulting in larger particles and improved product properties, e.g. decreased dust during material handling and increased flowability. Fluidized bed spray granulation involves the injection of an additional liquid, which settles on the particles, dries and thus forms a new solid layer on the particle surface. An important configuration is the continuous fluidized bed spray granulation with internal classification. Here, only particles with a minimum diameter are redrawn from the process by applying a counter-current flow in the outflow. The critical separation diameter can be influenced by the counter-current flow velocity. In order to permanently generate new particles a relative high nozzle height is chosen, such that part of the liquid drops dry before hitting the particle surface. The schematic process scheme is depicted in Fig. 1. As shown in [1–3] qualitative dynamics of continuous fluidized bed spray granulation processes may vary significantly with process conditions. In [1] a detailed bifurcation analysis has been conducted, which, from a practical point of view, gives valuable information in which parameter region to operate the plant at hand. In addition, the derived models can be used for a model-based control design, e.g. robust PI

or model predictive control [4,5], H_∞-control [6,7] or nonlinear discrepancy based control [9], to compensate for the undesired losses of stability, i.e. the occurrence of nonlinear oscillations. However, model validation, being the basis of the presented analysis and control design, based on experiments may be often difficult to perform in a production setting due to significant additional costs and undesired set-point changes. Therefore, in this contribution model-free adaptive control approaches [10–12] will be investigated on their feasibility for fluidized bed spray granulation control. The paper is organized as follows: in Section 2 the model of continuous fluidized bed spray granulation with internal product classification as proposed by [3] is stated. In addition, a numerical bifurcation analysis of the process is used to motivate the need for stabilizing control. In Section 3 the universal adaptive and λ-tracking control schemes are introduced together with the main structural assumptions on the process. It is further studied whether these requirements are fulfilled by the given type of process. Some final remarks conclude the paper.

2. Fluidized bed spray granulation

Particles produced during fluidized bed spray granulation processes are of high sphericity and can thus be described by their diameter. Due to the very high number of particles, this leads to the particle size distribution and its dynamical behavior. Applying

* Correspondence to: Otto-von-Guericke-University, Universitätsplatz 2, D-39106 Magdeburg, Germany.
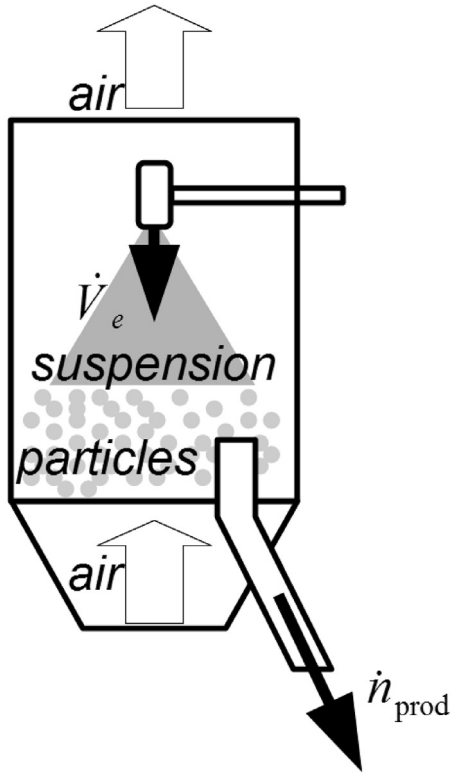*E-mail address:* stefan.palis@ovgu.de

Fig. 1. Process scheme.

Table 1
Simulation parameters.

$\dot{V}_e$	$1.68 \cdot 10^{-4} \, \mathrm{m^3/s}$	injection rate
ε	0.5	fluidized bed porosity
A	$5 \, \mathrm{m^2}$	granulator cross-sectional area
h_{noz}	$0.44 \, \mathrm{m}$	nozzle height
b_∞	0.028	minimum nucleation rate
L_0	$0.3 \, \mathrm{mm}$	medium diameter of nuclei
σ_0	$0.05 \, \mathrm{mm}$	standard deviation of nuclei diameter
L_1	$0.7 \, \mathrm{mm}$	medium classification diameter
σ_1	$0.05 \, \mathrm{mm}$	classification selectivity
K	$1.92 \cdot 10^{-4} \, \mathrm{1/s}$	Product removable rate
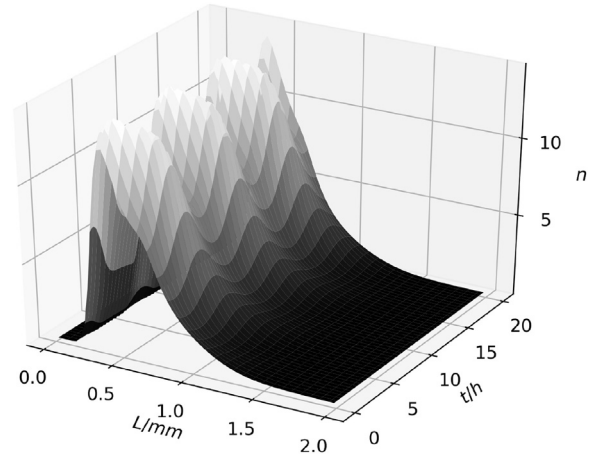
Fig. 2. Time behavior of the particle size distribution $n(t, L)$ for small $\dot{V}_e$.

population balance modeling [13] for the number density of the particle size distribution leads to the following equation

$$\frac{\partial n}{\partial t} = -G \frac{\partial n}{\partial L} + \dot{n}_{nuc} - \dot{n}_{prod} \tag{1}$$

where the first term is related to the particle growth, the second term accounts for the generation of new nuclei and the third for product withdrawal [3]. Depending on the distance between the particle bed and the nozzle, part of the injected liquid contributes to nucleation and the rest to growth. In [3] it is assumed that the part contributing to nucleation $b(n)$ varies linearly with the bed height between its minimum value b_∞ and maximum value $b = 1$.

$$b(n) = b_\infty + \max\left(0, (1 - b_\infty) \frac{h_{noz} - h(n)}{h_{noz}}\right) \tag{2}$$

The bed height $h(n)$ depends on the overall particle volume $V = \pi \mu_3$, which is proportional to the third moment, and the bed porosity ε, which is assumed to be constant.

$$h(n) = \frac{V}{(1 - \varepsilon)A} = \frac{\pi \mu_3}{(1 - \varepsilon)A} \tag{3}$$

For the nucleation it is assumed that new particles are uniformly distributed with a medium diameter L_0.

$$\delta(L) = \frac{n_u(L; L_0, \sigma_0)}{\mu_3(n_u(L; L_0, \sigma_0))} \tag{4}$$

where

$$n_u(L; \mu, \sigma) = \exp\left(\frac{-(L - \mu)^2}{2\sigma^2}\right). \tag{5}$$

The classification function of the product removal is given by

$$T(L) = \frac{\int_0^L n_u(L; L_1, \sigma_1) dL}{\int_0^\infty n_u(L; L_1, \sigma_1) dL}. \tag{6}$$

Therefore, the overall population balance model is given by

$$\frac{\partial n}{\partial t} = -\frac{2(1 - b(n))\dot{V}_e}{\pi \mu_2(n)} \frac{\partial n}{\partial L} + \frac{b(n)\dot{V}_e \delta(L)}{1/6\pi} - KT(L)n. \tag{7}$$

For simulation the population balance model has been discretized along the property coordinate L using a finite volume method with an upwind scheme. For the uniform grid of the property coordinate 150 grid points have been used. The parameters are given in Table 1 and are in accordance with [3,7].

It is well-known [3,2,1] that the given process configuration may become unstable depending on the given operation conditions, e.g. the injection rate. The loss of stability results in the occurrence of nonlinear oscillations in the particle size distribution as depicted in Fig. 2. A systematic study of this behavior, in terms of a one-parameter bifurcation analysis, shows that below a certain injection rate $\dot{V}_e$ the steady-state solution becomes unstable and a limit cycle occurs (Fig. 3). This periodic behavior in product quality and availability is in general undesired. It has also been observed in real granulation processes, e.g. [2]. In order to overcome this problem feedback control should be applied. From a practical point of view, one would be interested to control the third moment, as it correlates with the overall bed mass and can thus be derived from simple pressure measurements.

$$y = \mu_3 \tag{8}$$

As the actuated variable the effective volume flow rate $\dot{V}_e$ is chosen, which can be manipulated using the injection pumps.

$$u = \dot{V}_e \tag{9}$$

However, the main difficulties connected with the presented model as a basis for model-based control approaches are:
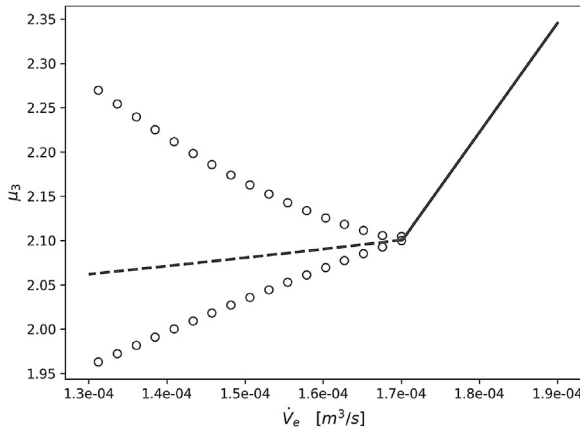
Fig. 3. One-parameter bifurcation diagram for varying $\dot{V}_e$.

- model validation and parameter identification are very time-consuming due to the slow time constants as can be seen from Fig. 2,
- the assumption that the nucleation rate depends linearly on the bed height and saturates for a given bed volume, is a strong simplification and thus connected with considerable uncertainties,
- the drying kinetics strongly depend on the process conditions, e.g. solid concentration in the injected suspension, fluidization air flow rate, humidity and temperature, and are thus typically time-varying and unknown.

3. Model-free adaptive control

To provide an alternative to model-based control of the described fluidized bed spray granulation with internal product classification [7] the focus will be on model-free controller design approaches with stability guarantees. Here, the class of non-identifier based high-gain adaptive controllers [10,11] will be investigated, as these do rely on specific structural properties only and have been successfully implemented for other chemical processes, e.g. [14,15]. The main idea can be easily illustrated on a linear time-invariant first order system:

$$\dot{y}(t) = ay(t) + bu(t) \tag{10}$$

It is well-known that the uncontrolled plant, i.e. $u(t) = 0$, is unstable for any $a > 0$. In order to stabilize the given system the following feedback law:

$$u(t) = -ky(t) \tag{11}$$

can be applied, where the controller gain k has to be chosen sufficiently large or small, depending on the sign of b, such that the closed loop system (12) is stable.

$$\dot{y}(t) = (a - kb)y(t) \tag{12}$$

In the following it will be assumed that b is positive, which is without loss of generality. In this case a possible time-varying choice for the controller gain k is given by the nonlinear adaptation law

$$\dot{k}(t) = y(t)^2. \tag{13}$$

Obviously, the defined adaptation law results in a continuously increasing controller gain $k(t)$ until $y(t)$ reaches steady state, i.e. $y(t) = 0$. Both, negative output feedback for $b > 0$ and a continuously increasing controller gain guarantee closed loop stability as has been proven for example in [10]. Starting from the presented idea, i.e. high-gain output feedback in combination with an adaptation law, a number of different adaptive control approaches have been developed. In this contribution, the application of universal

adaptive control and the closely related λ-tracking control will be investigated. For both approaches a number of assumptions have to be fulfilled by the process to be controlled:

- the sign of the combined input-output operator $\mathcal{CB}$ has to be known. In the introductory example the output operator $\mathcal{C}$ is the identity operator, i.e. c is equal to 1. Therefore, only the input operator $\mathcal{B}$, i.e. b, has been investigated.
- the relative degree, i.e. the minimum order of output time derivative directly depending on the control input, has to be equal to one,
- stable zero dynamics, i.e. the system achieved for constraining the controlled output $y(t)$ to zero has to be stable.

In case of a nonlinear process, it has to be assumed that the according nonlinear perturbations can be dominated by the linear feedback law for appropriate gain values.

3.1. Known sign of the input–output operator $\mathcal{CB}$

Using the population balance model (7) together with the output equation (8) yields

$$\dot{\mu}_3 = -\int_0^\infty L^3 \left(\frac{2(1 - b(n))\dot{V}_e}{\pi \mu_2(n)} \frac{\partial n}{\partial L} + \frac{b(n)\dot{V}_e}{1/6\pi} \delta(L) - KT(L)n \right) dL \tag{14}$$

$$= -\frac{2(1 - b(n))\dot{V}_e}{\pi \mu_2(n)} \left(\lim_{L \to \infty} n(L) - n(0) \right) + \cdots \tag{15}$$

$$\cdots + \frac{b(n)\dot{V}_e}{1/6\pi} \int_0^\infty L^3 \delta(L) dL - \int_0^\infty L^3 KT(L)n dL \tag{16}$$

Due to the fact that there are no particles of infinite or zero size, i.e. $\lim_{L \to \infty} n(L) = 0$ and $n(0) = 0$, the first term vanishes, resulting in

$$\dot{\mu}_3 = \mathcal{A}(n) + \mathcal{CB}(n)\dot{V}_e \tag{17}$$

where $\mathcal{A}(n) = -\int_0^\infty L^3 KT(L)n dL$ and $\mathcal{CB}(n) = \frac{b(n)}{1/6\pi} \int_0^\infty L^3 \delta(L) dL$. As both $b(n)$ and $\int_0^\infty L^3 \delta(L) dL$ are positive, the input-output operator $\mathcal{CB}(n)$ is always positive. This is obviously true as an increase in injection rate leads to an increase of overall particle volume.

3.2. Relative degree one

Calculating the relative degree for a given system is typically an iterative procedure, starting with the zeroth time derivative of the output $y(t)$, i.e. with the output itself. Obviously, the third moment at time instant t does not directly depend on the injection rate $\dot{V}_e$. Therefore, the relative degree has to be greater than zero. Taking the first time derivative results in:

$$\dot{y} = \dot{\mu}_3 = \int_0^\infty L^3 \frac{\partial n}{\partial t} dL \tag{18}$$

$$= \int_0^\infty L^3 \left(-\frac{2(1 - b(n))\dot{V}_e}{\pi \mu_2(n)} \frac{\partial n}{\partial L} + \frac{b(n)\dot{V}_e \delta(L)}{1/6\pi} - KT(L)n \right) dL \tag{19}$$

Due to the direct dependence on the controlled variable $u = \dot{V}_e$, the relative degree is equal to one. Thus, the second assumption is fulfilled.

3.3. Stable zero dynamics

In order to show stability of the zero dynamics, one has to prove stability of (7) under the additional constraint that $y = 0$. As the given granulation process is described by a nonlinear integro-partial differential equation, this is an at least very difficult task. Therefore, here only a set of finite-dimensional linear approximations, i.e.
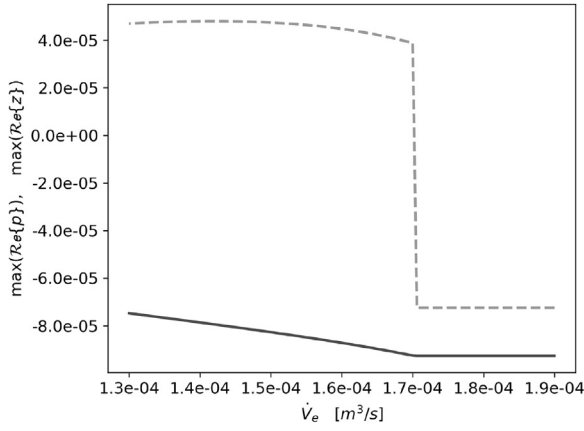
Fig. 4. Maximum real part of system zeros (black solid) and poles (dotted gray) for varying $\dot{V}_e$.

transfer functions, will be investigated. These approximations have been derived in parallel with the bifurcation analysis and reflect the system behavior in a neighborhood around the path of steady states. From a system theoretic point of view, they form a parametric family of transfer functions $G_{\dot{V}_e}(s)$ depending on the bifurcation variable $\dot{V}_e$. It is well-known, e.g. [16,17], that instability of the zero dynamics is directly connected to the presence of right-half plane zeros for the according transfer function. Thus, it is sufficient to check that the maximum real part of system zeros remains smaller than zero to prove stability of the zero dynamics. In Fig. 4 the maximum real part of all system zeros and poles is depicted for varying $\dot{V}_e$. As can be seen, no right-half plane zeros occur in the studied region of injection rates $\dot{V}_e$ and hence the zero dynamics remain stable. In addition, it can be seen that the open-loop system becomes unstable, i.e. right-half plane poles occur, for injection rates smaller than $1.7 \cdot 10^{-4} \frac{m^3}{s}$.

As has been shown, the continuous fluidized bed spray granulation process fulfills the required structural properties for high-gain adaptive control approaches.

3.4. Universal adaptive and λ-tracking control

Universal adaptive control is a proportional output feedback control with time-varying controller gain.

$$u(t) = k(t)e(t) \tag{20}$$

Here, $e(t)$ is the control error, i.e. the difference between desired output y_d and measured output $y(t)$. For convenience and numerical reasons an additional scaling factor $k_e = 2 \cdot 10^{-7}$ has been introduced.

$$e(t) = k_e(y_d - y(t)) \tag{21}$$

The nonlinear adaptation law for the controller gain is chosen as follows

$$\dot{k}(t) = e(t)^2. \tag{22}$$

It is clear from (22) that the controller gain is non-decreasing and increases when ever a control error is present. This behavior results in a continuously increasing controller sensitivity and may result in problems in the presence of controller saturations. It is of particular importance for practical implementations, where the control error $e(t)$ is typically not vanishing due to process disturbances and measurement noises. In order to overcome the aforementioned problem the λ-tracking control approach [11] has been developed. The main idea here, is the introduction of an additional dead-zone,
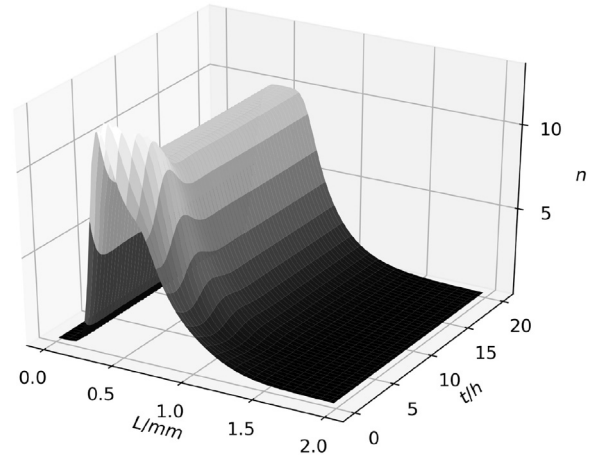

Fig. 5. Time behavior of the particle size distribution $n(t, L)$ for universal adaptive control.
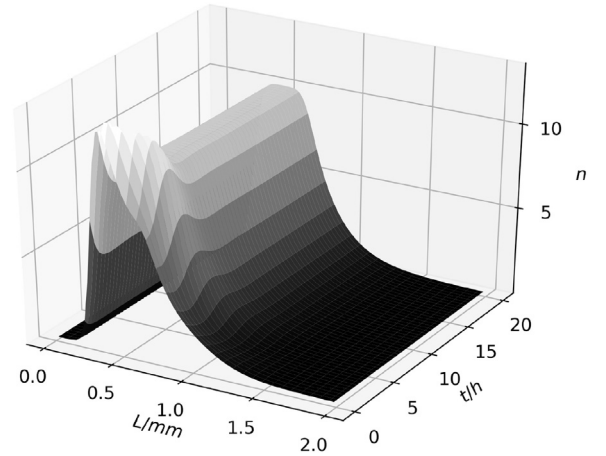

Fig. 6. Time behavior of the particle size distribution $n(t, L)$ applying λ-tracking control.

i.e. a neighborhood around the desired set-point, where the controller gain stops increasing and remains constant.

$$\dot{k}(t) = \begin{cases} e(t)^2 & \text{if } \|e(t)\| > \lambda \\ 0 & \text{else} \end{cases} \tag{23}$$

Here, the parameter λ defines the described width of the dead-zone. Typically, λ should be chosen such that measurement noise and uncritical disturbances do not result in a newly controller gain increase.

3.5. Results

In order to verify the designed universal adaptive controller it is connected to the plant in the region of instability, i.e. in the regime of nonlinear oscillations, at $t = 12$ h. As depicted in Figs. 5–11 the proposed universal adaptive control scheme allows for stabilization of the continuous granulation starting in the region of instability on the limit cycle. The required control actuation stays within reasonable limits (here plus/minus 50% of the nominal value, i.e. $\dot{V}_e \in [0.75 \cdot 10^{-4}, 2.25 \cdot 10^{-4}]$). Applying the λ-tracking control to the same scenario shows (Figs. 6–11), that similar behavior in terms of control performance can be achieved. However, the controller gain does not further increase when reaching the λ-region as depicted in Fig. 7. Due to the assumptions, stable zero dynam-
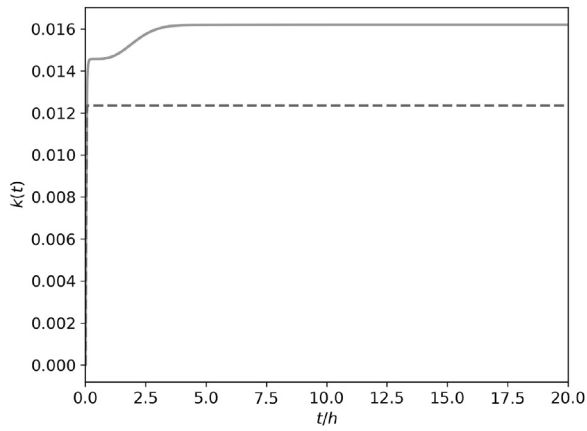
Fig. 7. Adaptive controller gain $k(t)$ for universal adaptive control (solid gray), λ-tracking control (dashed black).
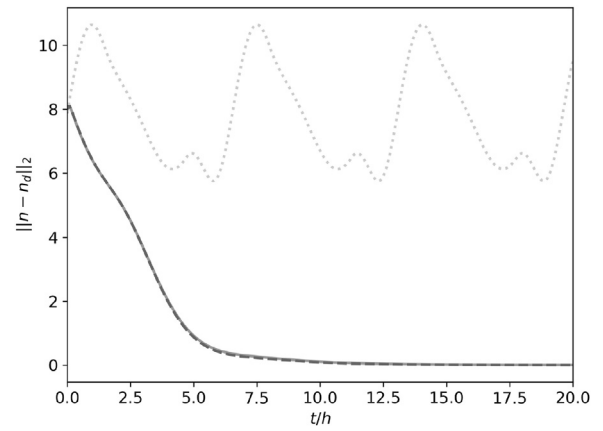

Fig. 10. L_2-norm of error in the particle size distribution for universal adaptive control (solid gray), λ-tracking control (dashed black) and without control (dotted gray).
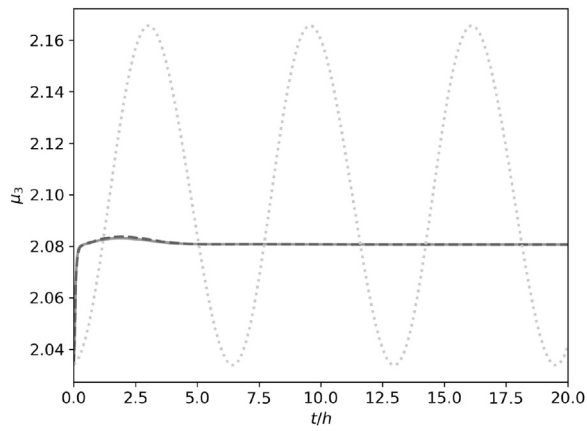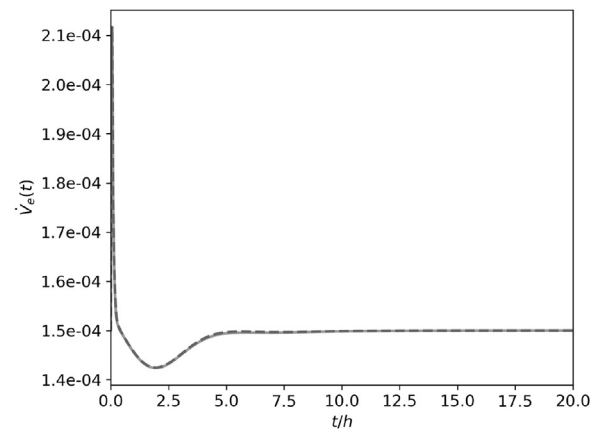

Fig. 8. Third moment of the particle size distribution for universal adaptive control (solid gray), λ-tracking control (dashed black) and without control (dotted gray).

Fig. 11. Injection rate $\dot{V}_e$ for universal adaptive control (solid gray), λ-tracking control (dashed black).
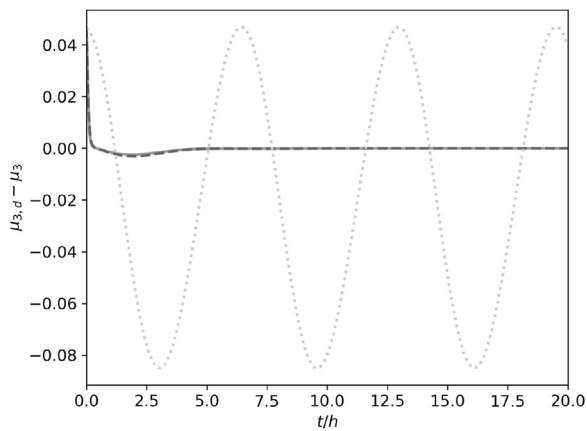

Fig. 9. Control error $e(t)$ for universal adaptive control (solid gray), λ-tracking control (dashed black) and without control (dotted gray).
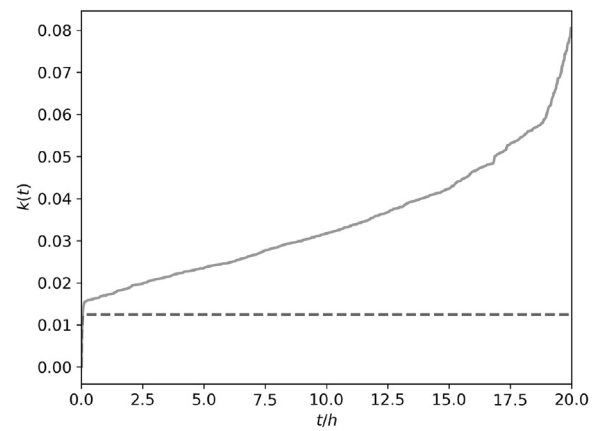

Fig. 12. Adaptive controller gain $k(t)$ for universal adaptive control (solid gray), λ-tracking control (dashed black) in the presence of measurement noise.

ics and relative degree one, closed-loop stability is guaranteed for a controller gain K being larger or smaller than a critical gain K_{crit} depending on the known sign of the combined input-output operator $\mathcal{CB}$. Thus, if the controller gain is sufficiently large when the control error enters the defined λ-neighborhood process stability is guaranteed.

Adding uniformly distributed measurement noise in the range of plus/minus 0.45% of the steady-state third moment to the simulation, already leads to significant deterioration of the closed-loop

performace in case of the universal adaptive control. As can been seen in Figs. 12–16, the controller gain of the universal adaptive control scheme is continuously increasing, destabilizing the process. On the other hand, the λ-tracking control scheme is hardly effected.

It should be mentioned, that both control laws show only a very low convergence rate in terms of the L_2-norm as depicted in Fig. 10, which is however of limited relevance for the given application.
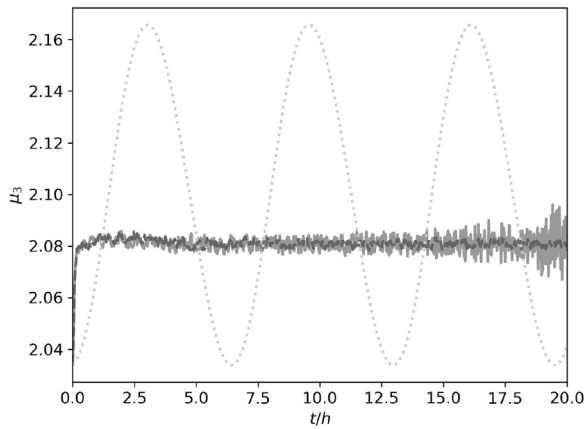
Fig. 13. Third moment of the particle size distribution for universal adaptive control (solid gray), λ-tracking control (dashed black) and without control (dotted gray) in the presence of measurement noise.

Fig. 14. Control error $e(t)$ for universal adaptive control (solid gray), λ-tracking control (dashed black) and without control (dotted gray) in the presence of measurement noise.
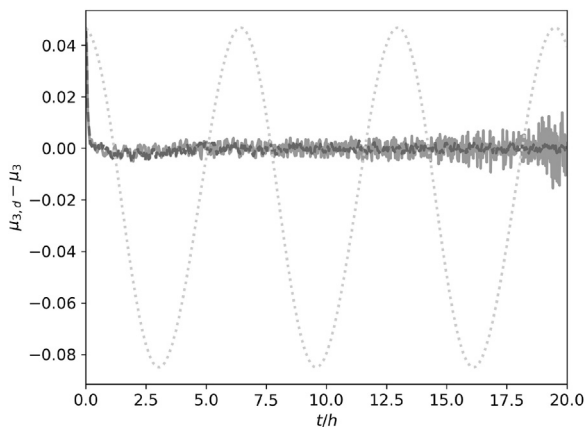

Fig. 15. L_2-norm of error in the particle size distribution for universal adaptive control (solid gray), λ-tracking control (dashed black) and without control (dotted gray) in the presence of measurement noise.
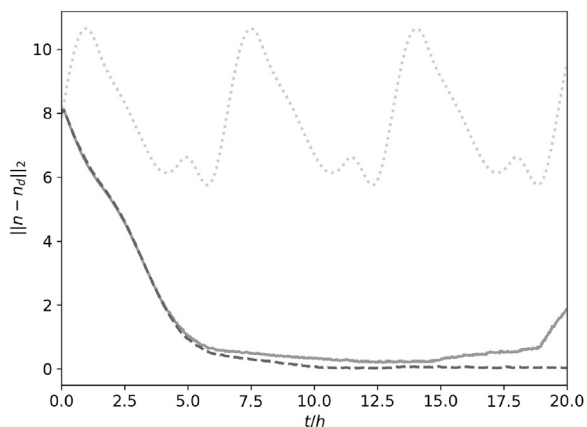
4. Conclusion

In this contribution two model-free adaptive control schemes, universal adaptive control and the closely related λ-tracking, and their application to continuous fluidized bed spray granulation pro-
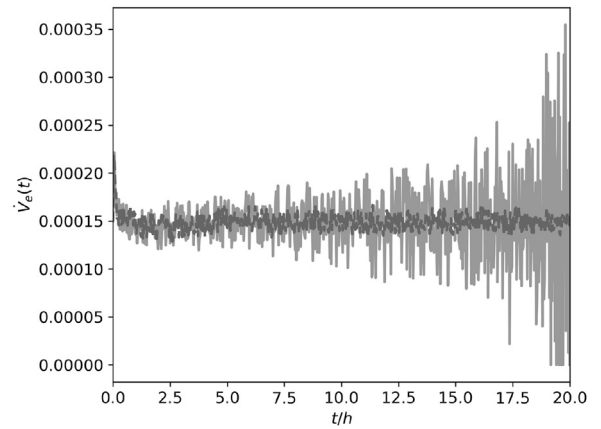

Fig. 16. Injection rate $\dot{V}_e$ for universal adaptive control (solid gray), λ-tracking control (dashed black) in the presence of measurement noise.

cesses with internal product classification have been investigated. It has been shown that the given process configuration fulfills all structural requirements. Applying the proposed control laws stabilizes the particle size distribution with reasonable performance and control actuation. Including measurement noise into the simulation, showed the advantage of including a λ-neighborhood in the λ-tracking control. Future work will be concerned with practical verification of the proposed control approach on a pilot plant and the investigation of other particulate processes, e.g. granulation with mill cycle [6] or continuous crystallization [8].

References

[1] C. Neugebauer, S. Palis, A. Bück, E. Tsotsas, S. Heinrich, A. Kienle, A dynamic two-zone model of continuous fluidized bed layering granulation with internal product classification, Particuology 31 (2017) 8–14.
[2] M. Schmidt, A. Bück, E. Tsotsas, Experimental investigation of process stability of continuous spray fluidized bed layering with internal separation, Chem. Eng. Sci. 126 (2015) 55–66.
[3] A.W. Vreman, C.E. van Lare, M.J. Hounslow, A basic population balance model for fluid bed spray granulation, Chem. Eng. Sci. 64 (2009) 4389–4398.
[4] A. Bück, S. Palis, E. Tsotsas, Model-based control of particle properties in fluidised bed spray granulation, Powder Technol. 270 (2015) 575–583.
[5] A. Bück, R. Dürr, M. Schmidt, E. Tsotsas, Model predictive control of continuous layering granulation in fluidised beds with internal product classification, J. Process Control 45 (2016) 65–75.
[6] S. Palis, A. Kienle, Stabilization of continuous fluidized bed spray granulation with external product classification, Chem. Eng. Sci. 70 (2012) 200–209.
[7] S. Palis, A. Kienle, H_∞ loop shaping control for continuous fluidized bed spray granulation with internal product classification, Ind. Eng. Chem. Res. 52 (2013) 408–420.
[8] R. Geyyer, R. Dürr, E. Temmel, T. Li, H. Lorenz, S. Palis, A. Seidel-Morgenstern, A. Kienle, Control of continuous mixed-solution mixed-product removal crystallization processes, Chem. Eng. Technol. 40 (2017) 1362–1369.
[9] S. Palis, A. Kienle, Discrepancy based control of particulate processes, J. Process Control 24 (2014) 33–46.
[10] A. Ilchmann, Non-identifier-based high-gain adaptive control, in: Springer, Lecture Notes in Control and Information Sciences, 1993, pp. 189.
[11] A. Ilchmann, E.P. Ryan, Universal λ-tracking for nonlinearly-perturbed systems in the presence of noise, Automatica 30 (1994) 337–346.
[12] A. Ilchmann, E.P. Ryan, High-gain control without identification: a survey, GAMM-Mitteilungen 31 (2008) 115–125.
[13] A.D. Randolph, M.A. Larson, Theory of Particulate Processes, Academic Press Inc., 1988.
[14] N. Beniich, A. El Bouhtouri, D. Dochain, Adaptive local tracking of a temperature profile in tubular reactor with partial measurements, J. Process Control 50 (2017) 29–39.
[15] A. Ilchmann, S. Trenn, Input constrained funnel control with applications to chemical reactor models, Syst. Control Lett. 53 (2004) 361–375.
[16] A. Isidori, The zero dynamics of a nonlinear system: from the origin to the latest progresses of a long successful story, Eur. J. Control 19 (2013) 369–378.
[17] F. Svaricek, Nulldynamik linearer und nichtlinearer Systeme, Definitionen, Eigenschaften und Anwendungen, at – Automatisierungstechnik 54 (2006) 311–322.

Rostyslav Geyyer[1,2,*]

Robert Dürr[3]

Erik Temmel[2]

Tao Li[2]

Heike Lorenz[2]

Stefan Palis[1]

Andreas Seidel-
Morgenstern[1,2]

Achim Kienle[1,2]

Control of Continuous Mixed-Solution Mixed-Product Removal Crystallization Processes

Continuous mixed-solution mixed-product removal (MSMPR) crystallization is considered. This process has been studied well, however, different aspects, in particular, process modeling, monitoring, and control remain challenging. An innovative approach for online measurement of the crystal size distribution is presented. Furthermore, unscented Kalman filtering is applied to overcome biased concentration measurement. Finally, a discrepancy-based control is applied to continuous MSMPR crystallization and its closed-loop performance is evaluated.

1 Introduction

Crystallization is an important separation and purification process to produce different solid materials from liquids in chemical, food, and pharmaceutical industries. It allows adjusting such properties as crystal size, shape, polymorphic form, and purity [1]. Control of the product quality as a whole, in most cases expressed in terms of its crystal size distribution (CSD), is difficult but worthwhile and requires both an online monitoring of this product quality and detailed knowledge of the considered process [2]. CSD affects product dissolution behavior, bioavailability, and can facilitate downstream processing, so its adjustment has a strong influence on product quality and production performance.

In recent years, the interest in continuous manufacturing grew dramatically. Within this field, continuous mixed-solution mixed-product removal (MSMPR) crystallization is a powerful approach. The main features of the continuous MSMPR crystallization are a constant solution feed and a constant vessel content withdraw, which contribute to the improvement of product quality and production rates, compared to a similar batch operation.

In this paper, continuous MSMPR crystallization modeling, online monitoring, and control problems are considered. Image processing techniques are tested for their application to crystallization processes: Canny edge detector [3], model-based recognition [4], genetic algorithm-based restoration from axis-length distribution (ALD) [5]; a sufficient image processing rate was reached for online operation using a multiprocessing system [6]. In [7], it is claimed that realization in Matlab by Mathworks shows good quality, but remains sluggish.

Image processing is a promising approach for online CSD measurement, but the mentioned imaging systems require sophisticated hardware and high computational power, so a new embedded approach will be discussed. During experiments

an issue with concentration measurement was observed: measurement bias caused by crystal growth on the probe. One straightforward approach to reduce or even overcome this undesired phenomenon may be to alter the probe location within the tank or to change process conditions. Alternatively, model-based state estimation techniques, e.g., unscented Kalman filtering (UKF) can be applied to reconstruct the solute concentration from the biased measurement [8]. Acquired and reconstructed measurements of the CSD and the concentration can now be applied to design controls and operate the process in a desired way.

In order to control the CSD, different strategies have been proposed including robust control [9–11], C-control [12], decentralized proportional-integral-differential (PID) and nonlinear model predictive control (NMPC) [13], and direct nucleation control [14]. A Lyapunov-function-based approach called discrepancy-based control (DBC) was presented in [15], which was later generalized for particle systems [16]. In contrast to linearization-based control techniques, DBC considered in this contribution is applied to a nonlinear model taking system nonlinearities into account. The general structure of the system

[1]Rostyslav Geyyer, Prof. Stefan Palis, Prof. Andreas Seidel-Morgenstern, Prof. Achim Kienle
Otto-von-Guericke University, Universitaetsplatz 2, 39106 Magdeburg, Germany.

[2]Rostyslav Geyyer, Dr. Erik Temmel, Tao Li, Prof. Heike Lorenz, Prof. Andreas Seidel-Morgenstern, Prof. Achim Kienle
geyyer@mpi-magdeburg.mpg.de
Max Planck Institute for Dynamics of Complex Technical Systems, Sandtorstrasse 1, 39106 Magdeburg, Germany.

[3]Dr. Robert Dürr
KU Leuven, Bio- & Chemical Systems Technology, Reactor Engineering and Safety Section, Celestijnenlaan 200f – Box 2424, 3001 Leuven, Belgium.

including plant measurement, state estimation, and control subsystems is illustrated in Fig. 1.

2 Mathematical Modeling

Besides sophisticated experimental work, mathematical modeling of the process is necessary to obtain a thorough understanding of crystallization processes [17]. Here, the population balance modeling (PBM) approach [18] is used. Contents of the crystallizer to be well-mixed are considered. Crystallization is governed by growth and secondary nucleation phenomena. The growth rate is assumed to be size-independent. Nucleating crystals have the size L_{min}[1] [19]. Dynamics of the CSD is described by the following population balance equation (PBE):

$$\frac{\partial n(L,t)}{\partial t} + G(t)\frac{\partial n(L,t)}{\partial L} = -\frac{n(L,t)}{\tau_v} \tag{1}$$

where $n(L,t)$ is the crystal size distribution, t is the time, L is the characteristic length of a crystal, $G(t)$ is the growth rate, and τ_v is the residence time. The initial condition is:

$$n(L, t_0 = 0) = n_0(L) \tag{2}$$

and the boundary condition is:

$$n(L_0 = L_{min}, t) = \frac{B(t)}{G(t)} \tag{3}$$

where nucleation is governed by:

$$B(t) = K_b(S(t) - 1)^b \mu_3(t) \tag{4}$$

with nucleation kinetics parameters K_b and b. Crystal growth is characterized by the following growth rate:

$$G(t) = K_g \exp\left(\frac{-E_{A,g}}{R_{gas} T_v(t)}\right)(S(t) - 1)^g \tag{5}$$

with growth kinetics parameters K_g and g, activation energy $E_{A,g}$, gas constant R_{gas}, vessel temperature $T_v(t)$, and supersaturation $S(t)$:

$$S(t) = \frac{c_v(t)}{c_{sat}(t)} \tag{6}$$

where the equilibrium concentration $c_{sat}(t)$ is approximated as a polynomial:

$$c_{sat}(t) = \sum_{i=0}^{4} K_i(T_v(t))^i \tag{7}$$

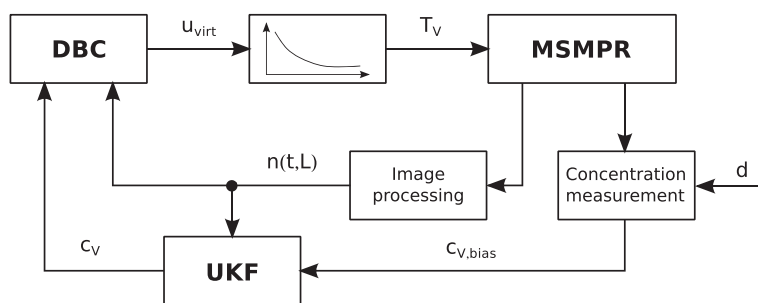1) List of symbols at the end of the paper.

Figure 1. General structure of image processing, unscented Kalman filter (UKF), and discrepancy-based control (DBC).

Properties of the modeled substance KDP (monopotassium phosphate): growth and nucleation kinetics as well as solubility parameters listed in Tab. 1 were evaluated experimentally using the methodology described in [20, 21].

Table 1. KDP kinetics and solubility.

Variable	Value
K_g [−]	5112597.405
g [−]	1.2586921036
$E_{A,g}$ [J mol^{-1}]	69859.933026
K_b [−]	26856478430.55499
b [−]	4.235315794045159
K_0 [−]	15.2361
K_1 [−]	0.2058
K_2 [−]	0.0101
K_3 [−]	-1.4506×10^{-4}
K_4 [−]	1.2292×10^{-6}

The liquid-phase concentration dynamics is governed by:

$$\frac{dc_v(t)}{dt} = \frac{1}{\tau_v}\left(c_{v,f} - c_v(t)\right) - \frac{3k_V \rho_s G(t)}{V_v \rho_v}\mu_2(t) \tag{8}$$

where $c_{v,f}$ is the feed concentration, k_V is the volumetric shape factor, ρ_s is the solid phase density, V_v is the total vessel contents volume, ρ_v is the liquid-phase density and $\mu_2(t)$ is the second moment of the CSD. Arbitrary moments can be described by the moment transform:

$$\mu_i(t) = \int_{L_{min}}^{\infty} L^i n(L,t)\,dL \tag{9}$$

with the corresponding dynamics:

$$\frac{d\mu_i(t)}{dt} = B(t)L_{min}^i + iG(t)\mu_{i-1}(t) - \frac{1}{\tau_v}\mu_i(t) \tag{10}$$

3 Online CSD Measurement

Feedback control is based on process monitoring, so acquisition of representative data is crucial for efficient control. The proposed hardware design is a pragmatic combination of an online microscope and a low-cost single-board computer (Raspberry Pi by the Raspberry Pi foundation). Such system can be mounted on the flow-through cell and form a noninvasive online embedded video microscopy tool. Particle flow orients particles with bigger facet toward the microscope; therefore, analyzed shots represent characteristic lengths of crystals. In this contribution, the algorithm suggested in [22] is coded in Python programming language using the OpenCV library.

Let $f(x,y)$ represent a 2D image, with coordinates x and y. The first step for edge detection is smoothing and noise removal with the Gaussian function:

$$G_{\text{filt}}(\sigma) = \exp\left(\frac{-x^2 + y^2}{2\sigma^2}\right) \tag{11}$$

where σ is the standard deviation of the Gauss kernel:

$$f_{\text{filt}}(x, y) = G_{\text{filt}}(\sigma)f(x, y) \tag{12}$$

In the next step of the Canny edge detection algorithm, the gradient $\nabla f(x,y)$ is calculated over the filtered image $f_{\text{filt}}(x,y)$:

$$\nabla f(x, y) = \begin{pmatrix} \frac{\partial f_{\text{filt}}(x,y)}{\partial y} \\ \frac{\partial f_{\text{filt}}(x,y)}{\partial x} \end{pmatrix} \tag{13}$$

Therefore, the edge gradient $F(x,y)$ and direction $\Theta(x,y)$ can be determined:

$$F(x, y) = \sqrt{\left(\frac{\partial f_{\text{filt}}(x, y)}{\partial x}\right)^2 + \left(\frac{\partial f_{\text{filt}}(x, y)}{\partial y}\right)^2} \tag{14}$$

$$\Theta(x, y) = \operatorname{atan}\left(\left(\frac{\partial f_{\text{filt}}(x, y)}{\partial x}\right)^{-1} \frac{\partial f_{\text{filt}}(x, y)}{\partial y}\right) \tag{15}$$

Further analysis is called non-maximum suppression. The gradient value is analyzed for local maxima in gradient and antigradient directions and marked as an edge, otherwise pixels are marked as background and thus set to zero. To obtain more robust results, double threshold filtration should be applied. The idea is to ignore low gradient values and keep high values, so F_{low} and F_{high} should be defined. The pixel $f_p(x_p, y_p)$ is treated as a strong edge if $F(x_p, y_p) > F_{\text{high}}$, as a weak edge if $F_{\text{low}} < F(x_p, y_p) < F_{\text{high}}$, otherwise suppressed. Weak edge pixels are then tested for neighborhood of strong edge pixels. In the positive case, they are kept as an edge, otherwise it is suppressed.

It is reasonable to normalize threshold parameters as median f_{median} over the whole image and variance v. Therefore, $F_{\text{low}} = f_{\text{median}}(1-v)$, $F_{\text{high}} = f_{\text{median}}(1+v)$. Consequently, the CSD is an array of

circle diameters corresponding to detected edges. Useful information about crystal/solution ratio can be acquired by calculation of the area ratio $\frac{V_{\text{solid}}}{V_{\text{v}}} = \frac{A_{\text{solid}}}{A_{\text{v}}}$, where A_{solid} is the area of crystals in the image, A_{v} is the crystal-free area, V_{solid} is the volume of crystals in the vessel, and V_{v} is the volume of solution in the vessel. This relation can be used for exact calculation of the third moment such that $\mu_3 = \frac{A_{\text{solid}}}{A_{\text{v}}} V_{\text{v}}$.

The described image analysis software operates on Raspberry Pi hardware with the Raspbian operating system with an approximate rate of ten frames per second (fps). For flow-through cell design, such rate represents data well and makes online operation possible. An analyzed image example is given in Fig. 2. The first image depicts an instance of taken images, the second image shows results of Canny edge detection, and the third image represents the resulting CSD, similar to the theoretically derived exponential distribution. The edge detection algorithm robustness is an important problem to discuss, especially if the crystal/solution ratio is high. As seen in Fig. 2 ii, crystal agglomerations, overlapping crystals, and optical artifacts can influence the quality of the measurements, so the detection sensitivity should be thoroughly tuned for each setup.

4 State Estimation

During the experiments, crystal formation on the surface of the concentration sensor was observed resulting in a biased measurement of the solute concentration:

$$c_{\text{v,bias}} = c_{\text{v}} + d \tag{16}$$

Nevertheless, the unbiased concentration can be reconstructed using a model-based state estimator. Therefore, an unscented Kalman filter (UKF) [8] was implemented, which is also used to estimate the bias d. Here, it is sufficient to include the dynamic equations of the first four moments of the CSD according to Eq. (10) instead of the full PBM (1). The overall UKF algorithm implements the discrete time and the corresponding dynamics for the estimation of the states and the bias is given by:

$$x(t_{k+1}) = \begin{pmatrix} \mu_0(t_{k+1}) \\ \mu_1(t_{k+1}) \\ \mu_2(t_{k+1}) \\ \mu_3(t_{k+1}) \\ c_v(t_{k+1}) \\ d(t_{k+1}) \end{pmatrix} = x(t_k) + f(x(t_k), w(t_k))\Delta t, \tag{17}$$
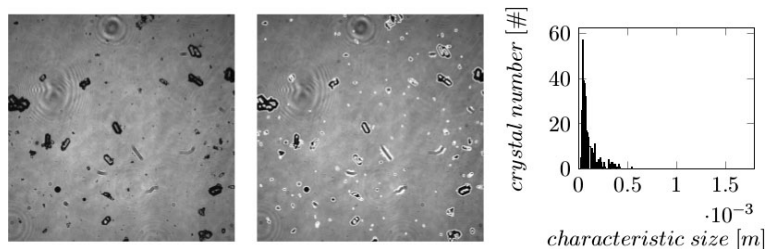

Figure 2. Crystal size measurement procedure: (i) acquired image, (ii) edge detection results, (iii) crystal size histogram.

$$
f(x(t_k), w(t_k)) = \begin{pmatrix} B(t_k) - \frac{\mu_0(t_k)}{\tau_v} \\ B(t_k)L_{\min} + G(t_k)\mu_0(t_k) - \frac{\mu_1(t_k)}{\tau_v} \\ B(t_k)L_{\min}^2 + 2G(t_k)\mu_1(t_k) - \frac{\mu_2(t_k)}{\tau_v} \\ B(t_k)L_{\min}^3 + 3G(t_k)\mu_2(t_k) - \frac{\mu_3(t_k)}{\tau_v} \\ \frac{1}{\tau_v}\left(c_{v,f} - c_v(t_k)\right) - \frac{3k_v\rho_s G(t_k)}{V_v\rho_v}\mu_2(t_k) \\ 0 \end{pmatrix} + w(t_k)
$$

(18)

$$
y(t_k) = (\mu_0(t_k), \mu_1(t_k), \mu_2(t_k), \mu_3(t_k), c_v(t_k) + d(t_k))^T + v(t_k)
$$

(19)

Here, w and v denote the zero mean process and measurement noises with covariance matrices Q and R. To evaluate the performance, artificial measurements were generated using the simulation of the idealized model Eqs. (1)–(6) and the theoretical bias was implemented as:

$$
d(t) = -0.15c_v(t_0)\left(1 - \exp\left(-3 \times 10^{-4}t\right)\right)
$$

(20)

Thereby, it is assumed that the crystal layer on the probe is increasing up to a certain maximum thickness. The performance of the UKF is displayed in Fig. 3. It can be seen that both, a good reconstruction of the unbiased solute concentration and estimation of the disturbance, is obtained for different assumptions on the measurement noise. Even for a relatively large noise, the estimation is reasonably accurate.

5 Discrepancy-Based Control

The shift from batch to continuous operation has high potential, but this task is not trivial, especially in pharmaceutical industry, where uniformity of properties is extremely important. The continuous MSMPR crystallization is a nonlinear distributed-parameter system, therefore, control design is a challenging task. Different strategies have been proposed including robust control [9–11], C-control [12], decentralized PID, nonlinear model predictive control (NMPC) [13], and direct nucleation control [14]. A Lyapunov-function-based approach called discrepancy-based control was presented in [15] and generalized to particle systems in [16]. This approach uses a generalized distance measure, discrepancy, and Lyapunov stability theory in order to design a stabilizing control law for the nonlinear infinite-dimensional model. The choice of the appropriate discrepancy is motivated by the physical insight. In contrast to conventional linearization-based approaches, the full nonlinear behavior and complexity of the plant can be taken into account.

Consider a dynamical system which satisfies Eqs. (1)–(6). Control is designed for the third moment μ_3 as controlled variable and the temperature in the vessel T_v as manipulated variable. Defining a discrepancy ρ based on the third moment as:

$$
\rho = \mu_{3,\text{set}} - \mu_3 = \int_0^\infty L^3(n_\text{set} - n)\mathrm{d}L
$$

(21)

with initial condition $\rho(t_0=0):=\rho_0$, the associate control Lyapunov candidate functional is given by:

$$
V = \frac{1}{2}\rho^2 = \frac{1}{2}\left(\int_0^\infty L^3(n_\text{set} - n)\mathrm{d}L\right)^2
$$

(22)

which is continuously differentiable and positive definite. In order to guarantee closed-loop stability, its time derivative should be negative definite for a non-zero discrepancy ρ. Calculating the time derivative results in:

$$
\dot{V} = \rho\dot{\rho} = \int_0^\infty L^3(n_\text{set} - n)\mathrm{d}L\left(-\int_0^\infty L^3\frac{\partial n}{\partial t}\mathrm{d}L\right)
$$

(23)

Inserting the population balance Eq. (1) with the nucleation term yields:

$$
\dot{V} = -\int_0^\infty L^3(n_\text{set} - n)\mathrm{d}L
$$
$$
\left(-\int_0^\infty L^3 G\frac{\partial n}{\partial L}\mathrm{d}L - \frac{1}{\tau_v}\int_0^\infty L^3 n\mathrm{d}L + \int_0^\infty L^3 B\delta(L - L_{\min})\mathrm{d}L\right)
$$

(24)

The condition of closed-loop exponential stability with respect to the discrepancy ρ is given by:

$$
\dot{V} = -2cV
$$

(25)

where c is the convergence rate, the only parameter to be tuned. As the manipulated variable T_v enters growth kinetics dependency in a complicated way, the crystal growth rate G will be used as a virtual control input u_virt. This is possible as only the growth rate is affected by the vessel temperature. Substitution of Eqs. (22) and (23) into Eq. (24) and rearrangement with respect to the growth rate yields the virtual control law:

$$
u_\text{virt} = \frac{c\rho + \frac{1}{\tau_v}\int_0^\infty L^3 n\mathrm{d}L - \int_0^\infty L^3 B\delta(L - L_{\min})\mathrm{d}L}{\int_0^\infty L^3\frac{\partial n}{\partial L}\mathrm{d}L}
$$

(26)

The temperature T_v can be derived from the virtual control input by solving the following nonlinear algebraic equation at each instance of time:

$$
u_\text{virt} = K_g\exp\left(\frac{-E_{A,g}}{R_\text{gas}T_v}\right)\left(\frac{c_v}{c_\text{sat}(T_v)} - 1\right)^g
$$

(27)

Closed-loop performance is displayed in Fig. 4 and the simulation parameters are presented in Tab. 2. Simulation of the feedback loop with the derived discrepancy-based control shows the expected exponential convergence with reasonable control effort.

The presented control technique is compared with the PI-controller tuned according to the module optimum for a
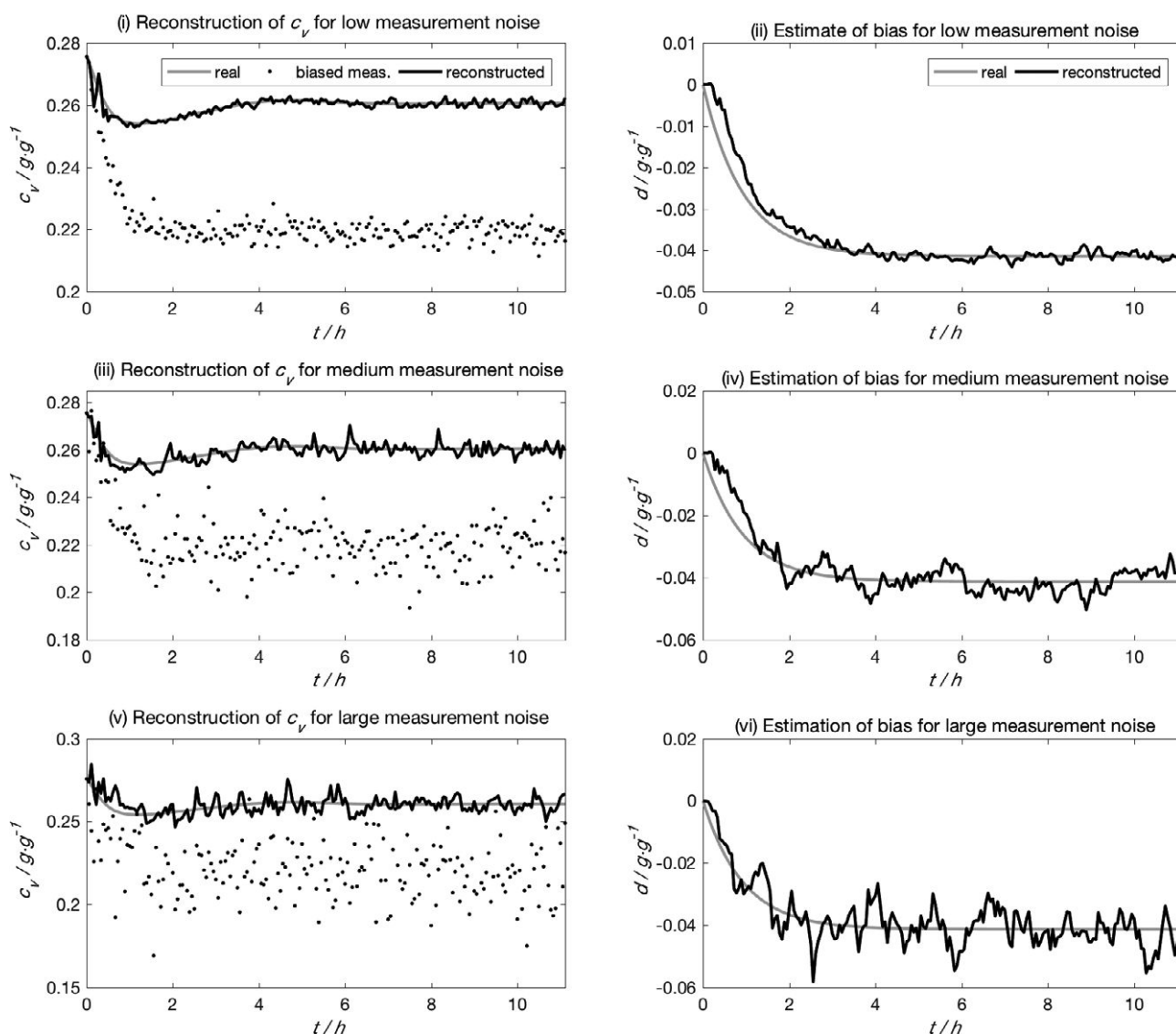
Figure 3. State estimation results for three scenarios. Low noise: (i) ideal, biased, and reconstructed measurement, (ii) estimation of bias compared to "real" bias; medium noise: (iii) ideal, biased, and reconstructed measurement, (iv) estimation of bias compared to "real" bias; large noise: (v) ideal, biased, and reconstructed measurement, (vi) estimation of bias compared to "real" bias.

specific set point [23]. The tuning parameters of the controllers are listed in Tab. 3.

The integral square error (ISE) is used as a performance indicator and the comparison is given in Tab. 4. In Fig. 4 three scenarios with different setpoints are depicted: the first setpoint is $\mu_{3,set} = 2.6 \times 10^{-4} \mathrm{m}^3$, the second is $\mu_{3,set} = 2.8 \times 10^{-4} \mathrm{m}^3$, and the third is $\mu_{3,set} = 3 \times 10^{-4} \mathrm{m}^3$. It is noticeable that linear control performance worsens as the set point drifts away from the linearization point, whereas DBC keeps a decent performance in different regimes. In [24], it is claimed that the robustness of the controller towards substance properties uncertainty, in other words plant-model mismatch, should be assured. To overcome such issue, the adaptive form of the DBC [25] should be considered.

6   Conclusions

Important issues of continuous MSMPR crystallization were tackled: CSD online monitoring, state estimation and control, forming a general process control structure as in Fig. 1. Noninvasive online embedded video microscopy is an efficient, affordable, and flexible tool to enhance crystallization monitoring. Suggested online monitoring reaches a performance of approximately 10 fps, which allows applying sophisticated control schemes based on solid-state measurements.

Noninvasive online embedded video microscopy can be used not only for CSD measurements, but for metastable zone detection or morphology analysis as well. Although the Canny edge detector allows tackling some drawbacks of video microscopy, the application of different schemes such as Otsu's binarization
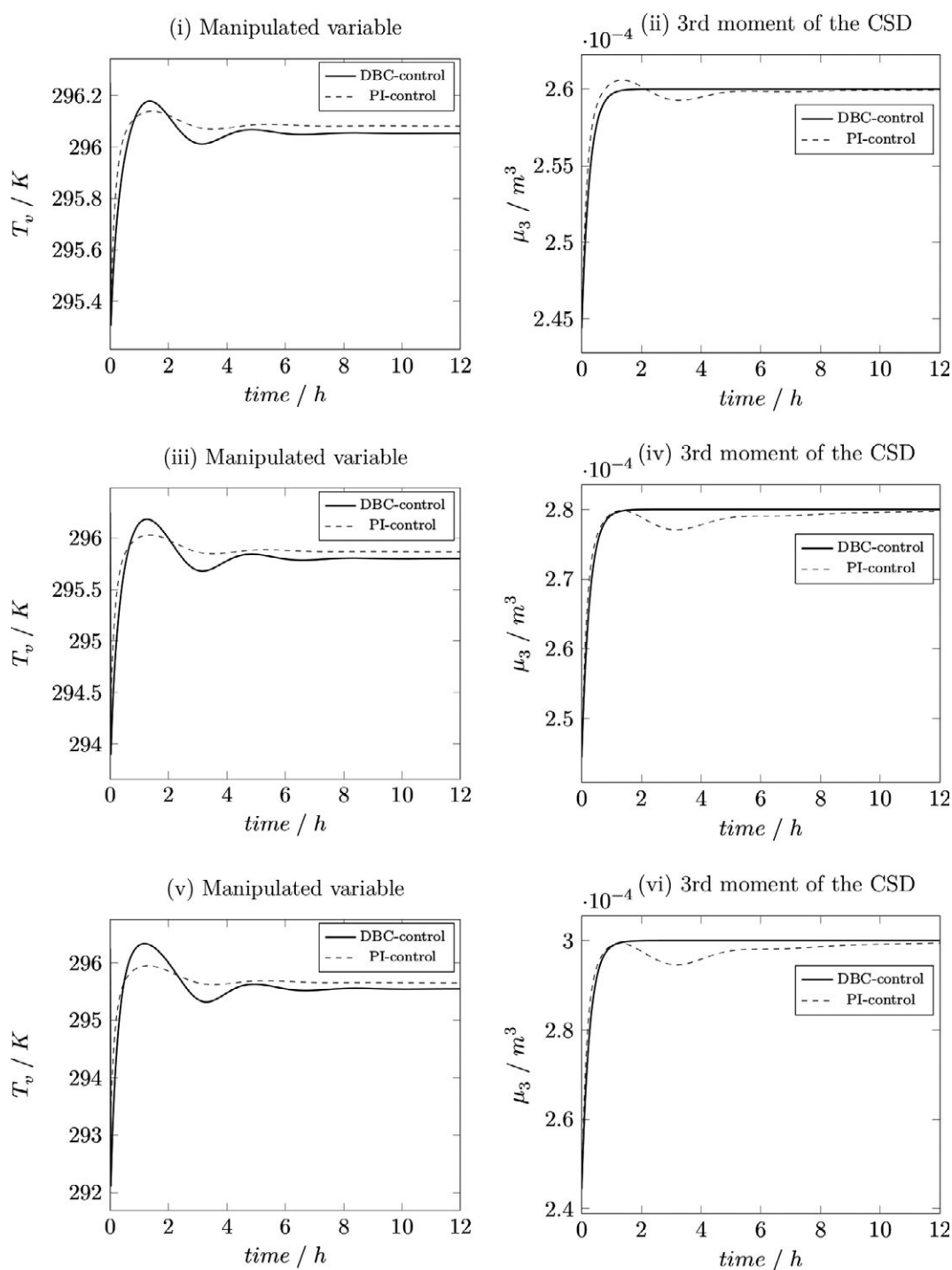
Figure 4. MSMPR control simulation for three scenarios. $\mu_{3,set} = 2.6 \times 10^{-4}\,m^3$: (i) manipulated variable T_v, (ii) controlled variable μ_3; $\mu_{3,set} = 2.8 \times 10^{-4}\,m^3$: (iii) manipulated variable T_v, (iv) controlled variable μ_3; $\mu_{3,set} = 3.0 \times 10^{-4}\,m^3$: (v) manipulated variable T_v, (vi) controlled variable μ_3.

or watershed transform should improve the overall performance, i.e., reduce computational costs, expand the possible crystal density range, alleviate the detection of overlapping crystals, and avoid false-positive detections.

During experiments, the concentration measurement issue was retrieved and solved by unscented Kalman filtering which allowed reconstruction of solute concentration from biased measurement. It shows good performance and overcomes emerging measurement noise. The control design for continu-

Table 2. Process parameters and initial conditions.

Parameter	Value
V_v [m^3]	0.026
ρ_v [kg m^{-3}]	1140
k_V [–]	0.7498
ρ_s [kg m^{-3}]	2340
τ_v [s]	3120
$c_{v,f}$ [g g^{-1}]	0.2757
$T_v(0)$ [K]	296.25
$c_{sat}(0)$ [g g^{-1}]	0.2396
$c_v(0)$ [g g^{-1}]	0.2613
$B(0)$ [#s^{-1}]	250.4878
$G(0)$ [m s^{-1}]	1.1973×10^{-7}
$n(L,0)$ [#m^{-1}]	$\dfrac{B(0)}{G(0)} \exp\left(-\dfrac{L}{G(0)\tau_v}\right)$

Table 3. Control parameters.

Control parameter	Value
DBC: convergence rate c	0.001
PI-control: proportional factor	–48 000
PI-control: integral factor	–3.86

Table 4. Control performance, set points, and initials.

Controller	$\mu_{3,set}$ [m^3]	ISE
DBC	2.6×10^{-4}	0.0162
PI-control	2.6×10^{-4}	0.0175
DBC	2.8×10^{-4}	0.0370
PI-control	2.8×10^{-4}	0.0707
DBC	3.0×10^{-4}	0.0578
PI-control	3.0×10^{-4}	0.1237

ous MSMPR crystallization is a challenging task due to nonlinear and distributed-parameter behavior. This motivated the application of discrepancy-based control design. System simulation exhibits exponential convergence according to the Lyapunov stability theory. Measurements based on different algorithms, their verification and validation is the next iteration of research as well as the implementation of the designed state estimator and controller.

The authors have declared no conflict of interest.

Symbols used

A_{solid}	[m^2]	solid-phase area
A_v	[m^3]	solution volume
$B(t)$	[#s^{-1}]	nucleation rate
c	[–]	tuning parameter
$c_{sat}(t)$	[g g^{-1}]	equilibrium concentration
$c_{v,f}$	[g g^{-1}]	feed concentration
$c_{v,bias}$	[g g^{-1}]	biased concentration
$c_v(t)$	[g g^{-1}]	liquid-phase concentration
d	[g g^{-1}]	bias
$E_{A,g}$	[J mol^{-1}]	growth activation energy
$\nabla f(x,y)$	[–]	image gradient
$f_{filt}(x,y)$	[–]	filtered function
F_{low}, F_{high}	[–]	threshold values
f_{median}	[–]	median threshold value
$f_p(x_p,y_p)$	[–]	pixel intensity
$f(x,y)$	[–]	image
$F(x,y)$	[–]	gradient magnitude
$G_{filt}(\sigma)$	[–]	Gaussian function
$G(t)$	[m s^{-1}]	growth rate
K_b, b, K_g, g	[–]	kinetic parameters
K_i	[–]	interpolation factors
k_V	[–]	volumetric shape factor
L	[m]	characteristic crystal length
L_{min}	[m]	nucleus size
$n_0(L)$	[#m^{-1}]	initial seeding
$n(L,t)$	[#m^{-1}]	crystal size distribution
n_{set}	[#m^{-1}]	size distribution set point
R_{gas}	[J K^{-1}mol^{-1}]	gas constant
$S(t)$	[–]	supersaturation
t	[s]	time
$T_v(t)$	[K]	solution temperature
u_{virt}	[m s^{-1}]	virtual manipulated variable
V	[m^6]	candidate Lyapunov functional
V_{solid}	[m^3]	solid-phase volume
V_v	[m^3]	solution volume
x, y	[–]	Cartesian coordinates
$\mathbf{Q}, \mathbf{R}$	6-by-6 matrices	covariance matrices
$\mathbf{w}$	6-by-1 vector	process noise
$\mathbf{v}$	5-by-1 vector	measurement noise
$\mathbf{x}$	6-by-1 vector	state vector
$\mathbf{y}$	5-by-1 vector	output vector

Greek letters

τ_v	[s]	residence time
σ	[–]	standard deviation
ν	[–]	threshold variance
ρ_s	[kg m^{-3}]	solid-phase density
ρ_v	[kg m^{-3}]	liquid-phase density
μ_i	[m^i]	i-th moment
$\mu_{3,set}$	[m^3]	third moment set point
ρ	[m^3]	discrepancy
$\Theta(x,y)$	[–]	gradient argument

Sub- and superscripts

0	at initial time moment
b	nucleation/birth
filt	filtered
g	growth
k	on the k-th step
min	minimal
s	related to the solid phase
set	set point
v	related to the solution in the vessel

Abbreviations

ALD	axis-length distribution
CSD	crystal size distribution
DBC	discrepancy-based control
MSMPR	mixed solution mixed product removal
NMPC	nonlinear model predictive control
PBM	population balance modeling
PID	proportional-integral-differential
PI	proportional-integral
UKF	unscented Kalman filter

References

[1] Z. K. Nagy, G. Fevotte, H. J. M. Kramer, L. L. Simon, *Chem. Eng. Res. Des.* **2013**, *91*, 1903–1922. DOI: 10.1016/j.cherd.2013.07.018

[2] A. Chianese, H. J. M. Kramer, *Industrial Crystallization Process Monitoring and Control*, Wiley-VCH Verlag, Weinheim **2012**.

[3] J. Calderon De Anda, X. Z. Wang, K. J. Roberts, *Chem. Eng. Sci.* **2005**, *60*, 1053–1065. DOI: 10.1016/j.ces.2004.09.068

[4] P. A. Larsen, J. B. Rawlings, N. J. Ferrier, *Chem. Eng. Sci.* **2007**, *62*, 1430–1441. DOI: 10.1016/j.ces.2006.11

[5] M. Kempkes, J. Eggers, M. Mazzotti, *Chem. Eng. Sci.* **2008**, *63*, 4656–4675. DOI: 10.1016/j.ces.2007.10.030

[6] S. Schorsch, T. Vetter, M. Mazzotti, *Chem. Eng. Sci.* **2012**, *77*, 130–142. DOI: 10.1016/j.ces.2011.11.029

[7] B. Presles, J. Debayle, G. Févotte, J.-C. Pinoli, *J. Electron. Imaging* **2010**, *19*, 031207. DOI: 10.1117/1.3462800

[8] A. Mesbah, A. E. M. Huesman, H. J. M. Kramer, P. M. J. Van Den Hof, *J. Process Control* **2011**, *21*, 652–666. DOI: 10.1016/j.jprocont.2010.11.013

[9] T. Chiu, P. D. Christofides, *AIChE J.* **1999**, *45*, 1279–1297. DOI: 10.1002/aic.690450613

[10] U. Vollmer, J. Raisch, *Chem. Eng. Sci.* **2002**, *57*, 4401–4414. DOI: 10.1016/S0009-2509(02)00354-8

[11] R. Geyyer, A. Kienle, S. Palis, *IFAC-PapersOnLine* **2015**, *48*, 598–603. DOI: 10.1016/j.ifacol.2015.09.252

[12] Q. Su, Z. K. Nagy, C. D. Rielly, *Chem. Eng. Process.* **2015**, *89*, 41–53. DOI: 10.1016/j.cep.2015.01.001

[13] Y. Yang, Z. K. Nagy, *Chem. Eng. Sci.* **2015**, *127*, 362–373. DOI: 10.1016/j.ces.2015.01.060

[14] Y. Yang, L. Song, Y. Zhang, Z. K. Nagy, *Ind. Eng. Chem. Res.* **2016**, *55 (17)*, 4987–4996. DOI: 10.1021/acs.iecr.5b04956

[15] S. Palis, A. Kienle, *Automatisierungstechnik* **2012**, *60*, 145–154. DOI: 10.1524/auto.2012.0981

[16] S. Palis, A. Kienle, *J. Process Control* **2014**, *24*, 33–46. DOI: 10.1016/j.jprocont.2013.12.003

[17] T. Togkalidou, H. Tung, Y. Sun, A. T. Andrews, R. D. Braatz, *Ind. Eng. Chem. Res.* **2004**, *43*, 6168–6181. DOI: 10.1021/ie0340847

[18] H. M. Hulburt, S. Katz, *Chem. Eng. Sci.* **1964**, *19*, 555–574. DOI: 10.1016/0009-2509(64)85047-8

[19] A. D. Randolph, M. A. Larson, *Theory of Particulate Processes: Analysis and Techniques of Continuous Crystallization*, Academic Press, New York **1988**.

[20] E. Temmel, *Ph.D. Thesis*, Max Planck Institute for Dynamics of Complex Technical Systems, Magdeburg **2016**.

[21] E. Temmel, M. Eicke, H. Lorenz, A. Seidel-Morgenstern, *Cryst. Growth Des.* **2016**, *16 (12)*, 6756–6768. DOI: 10.1021/acs.cgd.6b00789

[22] J. Canny, *IEEE Trans. Pattern Anal. Mach. Intell.* **1986**, 679–698.

[23] H. Lutz, W. Wendt, *Taschenbuch der Regelungstechnik: mit MATLAB und Simulink*, Verlag Harri Deutsch, Frankfurt **2012**.

[24] A. Saengchan, P. Kittisupakorn, W. Paengjuntuek, A. Arpornwichanop, *J. Ind. Eng. Chem.* **2011**, *17 (3)*, 430–438. DOI: 10.1016/j.jiec.2010.09.025

[25] S. Palis, A. Bück, A. Kienle, *IFAC-PapersOnLine* **2013**, *9*, 400–405. DOI: 10.3182/20130904-3-FR-2041.00168

Model-based control of particle properties in fluidised bed spray granulation

Andreas Bück [a,*], Stefan Palis [b], Evangelos Tsotsas [a]

[a] *Thermal Process Engineering, Otto von Guericke University Magdeburg, Universitätsplatz 2, 39106 Magdeburg, Germany*
[b] *Automation and Modelling, Otto von Guericke University Magdeburg, Universitätsplatz 2, 39106 Magdeburg, Germany*

ARTICLE INFO

ABSTRACT

In this contribution different control approaches, ranging from standard linear control to non-linear model predictive control, are applied to fluidised bed spray granulation processes with internal and external product classification. These processes exhibit sustained non-linear oscillations in the particle property distribution, i.e. size distribution, that have negative influence on steady-state operation, for example a constant product mass flow with constant properties. The controllers are applied to stabilise these open-loop unstable steady-states.

© 2014 Elsevier B.V. All rights reserved.

1. Introduction

Particulates processes play an important role in various fields of application: There are many examples of particulate products in everyday-life, for instance milk powder, milled and roasted coffee, instant cacao powder, and sugar, to name just a few. Additionally, particulate products play an important role in other fields: health-care (e.g. in the form of an active pharmaceutical ingredient pressed into a tablet), in agriculture in the form of fertilisers, or in the chemical industry as catalyst powders. It is reported that approximately three quarters of all industrially processed goods are in solid state — either in their final state or in intermediate production stages [1].

The product properties can often be characterised by the particle properties, or rather the particle properties affect the properties of the product. Important particle properties are for instance the particle size and form, the porosity of the particle, the moisture content, and the enthalpy (temperature).

The particle size and form determine for instance the flow-ability of a powder: If the particles in the powder are too small, then cohesive forces between the particles prevent a free flow. This can be observed by comparison of sugar powder and crystal sugar: Although both products consist of the same material, sugar powder flows less freely because of the increased cohesive forces between smaller sized particles.

For the production of particulate substances from liquid starting material (solutions, emulsions, or suspensions) various processes exist: e.g. crystallisation, granulation, and spray drying. These can be further specialised depending on the characteristic effect that is used for the transformation, for example cooling crystallisation or spray granulation.

Crystallisation and granulation are complex dynamic processes, involving multiple phases (fluid and solid), heat and mass transfer between these phases, as well as particle formation processes, e.g. layer formation.

One process that is often used in industries, e.g. in pharmaceuticals, foods, and fertilisers, is fluidised bed spray layering granulation. It allows for the production of dustless, free-flowing particles from liquid raw materials: The suspension (or solution) is sprayed onto particles in the process chamber and due to drying – the bed is fluidised by hot air – the liquid evaporates. The remaining solid builds up a new layer of solid material on the particles.

Fluidised bed spray granulation can be run in batch as well as continuous mode (Fig. 1), and drying and particle formation processes can be coupled and run simultaneously in one apparatus. The structure of the apparatuses is simple, and due to the high heat and mass transfer between the phases induced by the fluidisation, compact plants – compared to other technologies – can be designed. In both modes, a suspension or solution is sprayed leading to particle growth by layering as explained before (centre of Fig. 1). Additionally, in continuous operation, several ways exist to remove the product from the fluidised bed, for example by an external classification circuit which is depicted in Fig. 1 or by an internal classification. Both cases will be described in detail in later sections.

In the practical realisation of particle formation processes the following problem arises: The particles are not uniform, i.e. they differ in their properties, for instance in size, form or colour. This means that the particles in the powder do possess a distribution with respect to their properties, and therefore the product also possesses a property distribution. Given a product specification requires that the distribution lies within the limits posed by the specifications to be accepted by a customer.

The product specifications can be very strict, for instance in processes with expensive raw materials or where the product is a hazardous good,
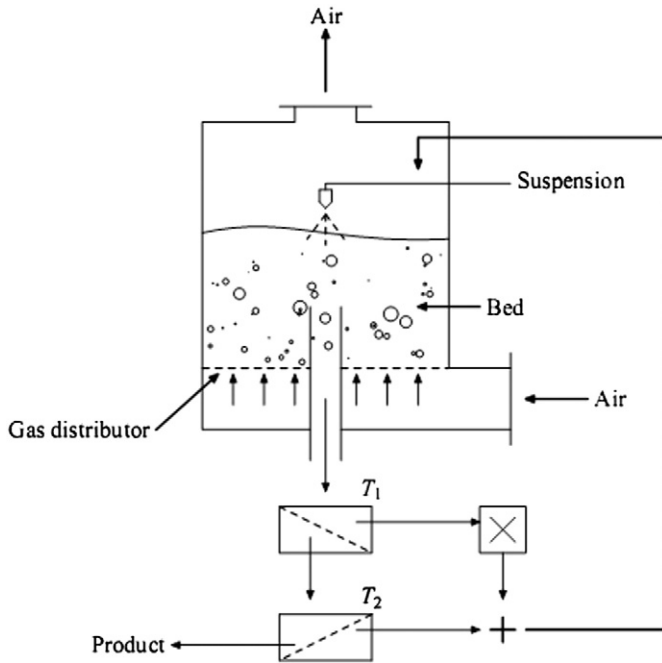
Fig. 1. Schematics of a continuous spray granulation process with external classification and particle recycle.

and the requirements are further increasing. The need to guarantee that the product complies to the specification motivates the use of process control systems in particle processes. This becomes especially important if the process designed according to the product specifications turns out to be unstable [2,3], i.e. even small process disturbances yield an undesired drift in the product properties. The necessary compliance of the product to specifications motivates the use of model-based feedback controllers.

One well-established framework for the macroscopic modelling of particulate processes, which are from a systems-theoretic point of view infinite-dimensional processes, that is well-suited for the modelling of industrial-scale processes, is the population balance approach, introduced for problems in statistical mechanics by Hulburt and Katz in the 1960s [4]. To the field of particulate processes it was transported by the work of Randolph and Larson [5] (with a focus on crystallisation); it was advertised and established in the field by D. Ramkrishna and co-workers [6].

In the literature, many successful applications of population balance modelling to particulate processes can be found, for instance in crystallisation [7–9], granulation [2,3,10–12], drying [13–15], or aerosol processes [16,17].

The main obstacle in the analysis and development of general control design methods for distributed parameter systems is the complex mathematical theory due to the infinite-dimensional character of the processes.

In the case of nonlinear distributed systems the treatment is restricted in most cases to practically important process structures, see for instance [18–20]. Nonetheless, control schemes are successfully designed for distributed parameter systems, for applications to spatially-distributed systems, see for instance [20–22].

There are also contributions in the field of property-distributed processes available, for instance Kalani and Christofides [17] who proposed nonlinear controller design for an aerosol process on the basis of a reduced model, and Chiu and Christofides [23] who applied a nonlinear controller to a crystallisation process on the basis of a reduced model. Pottmann et al. [24] designed a model-predictive controller for a drum granulation system; Vollmer and Raisch [25] and Palis and Kienle [26]

designed a stabilising controller for an unstable crystallisation process using H_∞-theory and discrepancy-based control; Shi et al. [27] designed a model-predictive controller for a batch crystallisation process; Dueñas Díez et al. [28] controlled inventories of a property-distributed process by passivity-based control. Villegas et al. [13] presented a distributed control scheme in a batch fluidised bed dryer and Glaser et al. [29] presented the design of a model-predictive controller for continuous drum granulation.

Recently, Palis and Kienle [30–32] presented results on stabilisation of unstable steady-states in continuous fluidised bed spray granulation using H_∞-theory and discrepancy-based control in continuous granulation with internal product classification, assuming that the size distribution of particles can be measured. Apart from these publications, the control of particle size distributions in fluidised bed spray granulation has not received much attention, so that today, practically implemented control systems mainly concentrate on the regulation of heat and mass transfer (e.g. temperature), integral values (e.g. total mass of product) or mean values (e.g. mean particle size) of the particles in the stable process regime. Although the control schemes are for most part sufficient for their tasks, they cannot guarantee that the property distribution as a whole complies to the specifications. This means that in light of the increasing strictness of product specifications the control schemes have to be improved.

In this contribution two industrially appealing process control schemes for the important cases of continuous fluidised bed spray granulation with internal product classification and external classification and particle reflux are presented that allow for the stabilisation of unstable operating points and particle size distributions in these processes.

2. Process modelling

Limiting the scope to a purely macroscopic modelling, which is well-suited for the description of large-scale processes, population balance modelling is often applied [5,6].

The state of a particle is characterised by its properties. In general, two types of coordinates are distinguished: external coordinates **x** (the spatial position in the system), and internal coordinates e (particle properties, e.g. the size ξ). In total, these properties span a property state-space (denoted by $\Omega \times E$): Usually, during the process the properties of a particle will change; this corresponds to a movement
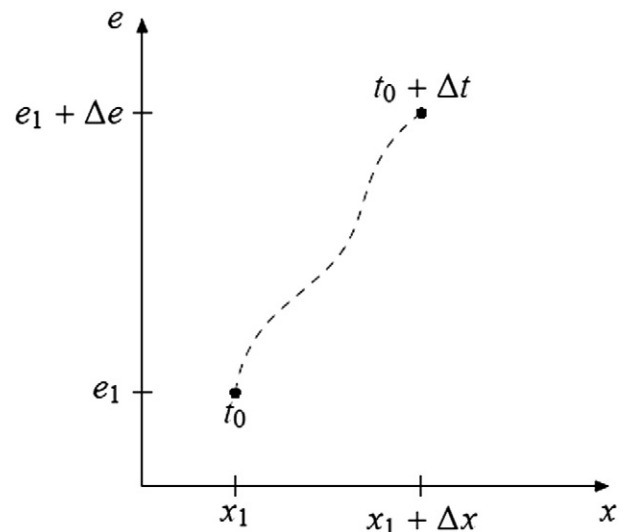

Fig. 2. Movement of a particle in property state-space.

in state-space as shown in Fig. 2 for one external and one internal property.

Population balance modelling is the description of the temporal evolution of a number density function n (or other functions derived from it, for example the mass density function):

$$N(t) = \int_\Omega \int_E n(t, \mathbf{x}, e) \, \mathrm{d}e \, \mathrm{d}\mathbf{x} \,, \quad \mathbf{x} \in \Omega, \ e \in E. \tag{1}$$

It describes how many of the particles in the process under consideration possess a certain property, e.g. how many particles are at position $\mathbf{x}$ having the property ξ. For this, all sub-processes have to be modelled in terms of the number density function.

In the special case of no external coordinates, $\dim(\mathbf{x}) = 0$, corresponding to a well-mixed system, the differential or local formulation of the population balance equation can be derived:

$$\frac{\partial n}{\partial t} + \mathrm{div}_\xi[\varphi(n, \xi)] - p(n, \xi) = 0. \tag{2}$$

This is a formal balance law for the temporal change of the number density function n. Open are the expressions for the transport flux φ and the local production rate p. They depend on the process to be modelled and therefore no general expression can be given. Further required are initial and boundary conditions, depending on the modelled process. These details will be given in the following sub-sections.

From the number density distribution a set of integral values, called the moments of the distribution, can be derived which are often easier to interpret than the density distribution itself. For the case of one property coordinate only, the jth moment can be calculated by:

$$\mu_j(t) = \int_{\xi_0}^{\xi_{\max}} \xi^j \, n(t, \xi) \, \mathrm{d}\xi \,. \tag{3}$$

For certain j a physical interpretation is possible, for instance $j = 0$ gives the total number of particles, i.e. $\mu_0(t) = N(t)$. For higher moments the meaning of ξ has to be taken into account. If, for example, ξ denotes the particle size, then $\mu_1(t)$ is equal to the total length of particles (laid out and measured in a row), $\mu_2(t)$ is proportional to the surface area of all particles in the population, and $\mu_3(t)$ is proportional to the total volume of particles. The proportionality factors depend on the geometric shape of the particles.

2.1. Continuous granulation with internal product classification

Vreman et al. [3] derived a model for the continuous granulation with internal product classification which is summarised in the following: A suspension or solution is sprayed by a nozzle onto the particles in the fluidised bed. Assuming that the particles are almost spherical, the characteristic size can be described by the diameter of the particles. Assuming that the sprayed droplets can spread over the total particle surface the buildup of new solid layers can be described by a surface-proportional law [11]:

$$G = \frac{2\dot{M}_{solid}}{\rho_{solid} \, \pi \, \mu_2} \,, \tag{4}$$

where $\dot{M}_{solid}$ denotes the solid mass sprayed onto the particles. Vreman et al. use a slightly modified version of this growth law by splitting up the sprayed mass flow: They consider not only the growth of particles already present but also the formation of new particles, nuclei, due to pre-drying of the sprayed droplets:

$$G = \frac{2(1-b)\dot{M}_{solid}}{\rho_{solid} \, \pi \, \mu_2} \,. \tag{5}$$

Here, b denotes the fraction of the sprayed solid that is used to form new nuclei and is related to the distance between the nozzle and the particle bed. The number flow of nuclei, B_n, can be calculated – assuming that they have a normalised size distribution $q_{0,nuclei}(\xi)$ –:

$$B_n(\xi) = \frac{6 \, b\dot{M}_{solid}}{\rho_{solid} \, \pi \displaystyle\int_{\xi_0}^{\infty} \xi^3 \, q_{0,nuclei}(\xi) \, \mathrm{d}\xi} \,. \tag{6}$$

The particle flow at the outlet of the apparatus is regulated by a classifying gas flow in the outlet tube: Depending on the gas velocity certain particle sizes leave the apparatus whereas other sizes are transported back into the process chamber, that is, in order to obtain a product with a certain (mean) size a fixed gas flow is set. The classifying effect is modelled by a separation function T which depends on the particle size and the gas velocity in the outlet tube. The product mass flow can then be described by:

$$\dot{n}_{prod} = KT(\xi) \, n \,, \tag{7}$$

where K is a drain factor. The population balance equation for this process then reads:

$$\frac{\partial n}{\partial t} + \frac{\partial(Gn)}{\partial \xi} = -\dot{n}_{prod} + B_n(\xi) \,. \tag{8}$$

As was shown by Vreman et al., depending on the spraying rate $\dot{M}_{solid}$ either a stable steady-state operation or a sustained oscillation in the number density function and the product mass flow rate is obtained. The control task is here to dampen out these oscillations in order to obtain a constant product mass flow with constant properties.

2.2. Continuous granulation with external classification and particle reflux

A similar process configuration is continuous spray granulation with external classification as depicted in Fig. 1. The core of this configuration is again a process chamber with a nozzle in either a top-spray or bottom-spray configuration, and an outlet tube is installed in the centre of the gas distributor plate. During granulation particles will leave the chamber by this tube. This mass flow is then screened twice: The over-sized particles from the first screen are sent to a mill where they are milled and then re-fed into the process chamber. The under-sized particles are screened once more. Here, the over-sized particles are accepted as product, whereas the undersized particles are also re-fed into the process chamber for further growth.

For population balance modelling of the number density function of particles in the bed, the same assumptions as in the case of the internal classification are used. This means that the population balance equation can be used as a basis for this process — it only has to be augmented by terms accounting for the particle outlet and the re-cycle of particles. This requires to model the screens and the mill using the population balance framework. It is assumed that no hold-up of particles occurs, that particles do not break during screening and that the performance of screens and mill does not vary with age or particle loading. Then the screens can be described by well-known separation functions $T(\xi)$ individually for the upper and the lower screen. In modelling the mill, it is assumed that the particles having passed the mill possess a normalised size distribution $q_{0,mill}(\xi)$ depending on the characteristics of the mill:

$$\dot{n}_{mill}(t, \xi) = B_m(t) \, q_{0,mill}(\xi) \,, \tag{9}$$

where B_m denotes the number flow of milled particles which can be obtained from the knowledge of the mass flow entering the mill and the milling function. Usually, $q_{0,mill}$ cannot be obtained exactly and has to be approximated.

The number density flux of particles re-fed into the process chamber consists of the under-sized particles of the second screen and the milled particles, i.e.

$$\dot{n}_{recycle} = (1-T_1)(1-T_2)\dot{n}_{out} + \dot{n}_{mill} \ . \tag{10}$$

If it is assumed that no particle size is preferred, then the particle outlet can be expressed as being proportional to the number of particles that possess a certain size:

$$\dot{n}_{out} = Kn \ , \tag{11}$$

where K can be designed, for instance, to achieve a pre-set bed mass [2]:

$$K = 1 - \min\left(1, \ m_{bed,set}/m_{bed}\right) \ . \tag{12}$$

The population balance equation for this process can then be written as

$$\frac{\partial n}{\partial t} + \frac{\partial (Gn)}{\partial \xi} = -\dot{n}_{out} + \dot{n}_{recycle} \tag{13}$$

with appropriate initial and boundary conditions.

This process configuration was extensively investigated by Heinrich et al. [2] and Radichkov et al. [33] concerning the dynamic behaviour. As was shown in Radichkov et al. by bifurcation analysis, the process exhibits different dynamic behaviours depending, amongst others, on the value of the average size of milled particles: For a certain range a stable steady-state distribution is attained which would yield a constant mass flow of product with constant particle properties, but for a large parameter range the system exhibits sustained oscillations in the number density function resulting in an unwanted time-varying mass flow of product (Fig. 3). As this poses several difficulties in the post-processing of the product process control is required to stabilise these unstable operating points.

3. Feedback control design

3.1. Continuous granulation with internal product classification

As was motivated in the process description, this granulation process can exhibit nonlinear oscillations in the number density distribution and thereby in important product characteristics. An analysis shows that the solid spraying rate has huge influence on the process
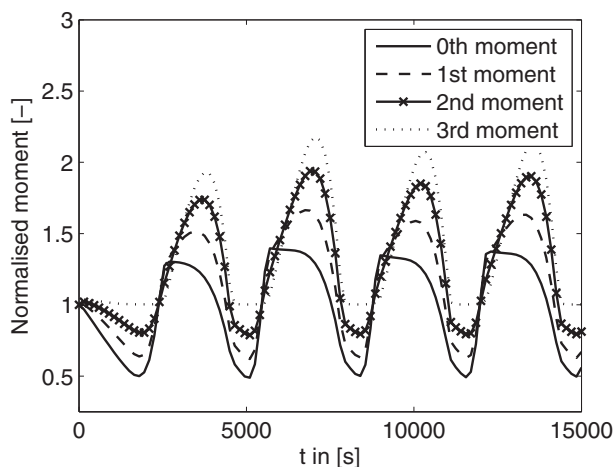

Fig. 3. Exemplary behaviour of the first four moments, normalised with respect to the initial value $\mu_j(0)$, in the case of a unstable steady-state in continuous spray granulation with external classification.

stability and by this qualifies as a manipulated variable to attenuate the oscillations. It is further found that the third moment μ_3, which is proportional to the total mass of particles in the bed, is a suitable measurement to detect the oscillating behaviour as very fine particles are blown back into to the process chamber and accumulate there.

In order to control this process a feedback controller with a simple, industrially accepted proportional-integral structure is to be designed. To that purpose a linear transfer function model $P_0(s)$ linking the manipulated (the spraying rate) and the controlled variable (the third moment) is derived based on the linearisation of the nonlinear process model.

It has to be noted that the derived plant model is uncertain due to uncertainties in the process parameters, e.g. the amount of nuclei formation, unmodelled dynamics in the initial nonlinear process model due to the use of assumptions in the derivation, and approximation errors, amongst them uncertainties in the linearisation which is only valid in a region around one steady-state and errors due to the transition of the initially infinite-dimensional process model to a finite-dimensional model that can be implemented and solved numerically, i.e. the discretisation of the population balance equation. However, for these uncertainties individual bounds are often available.

The presence of the uncertainties yields that not only the derived transfer function, the nominal model P_0, but a set of transfer functions incorporating the uncertainty bounds has to be considered in a controller design. A controller which is able to perform the required control task for all transfer functions in this set, which may have a quite different dynamic behaviour, for instance due to a transition from a stable to an unstable process regime, is called a robust controller.

The design requires the expression of the uncertainties in a suitable way, the normalised left coprime factorisation being one of them. Here, the nominal, possibly unstable, transfer function $P_0(s)$ is split up into the product of two stable transfer functions:

$$P_0(s) = M_0^{-1}(s) \ N_0(s) \ . \tag{14}$$

The uncertainties are then formulated as additive errors Δ_M and Δ_N in both factors individually, resulting in:

$$P(s) = [M_0(s) + \Delta_M(s)]^{-1}[N_0(s) + \Delta_N(s)] \ . \tag{15}$$

The uncertainty models Δ_M and Δ_N are stable transfer function matrices, with a known bound ε expressed in the H_∞-norm:

$$\|[\Delta_M \ , \Delta_N]\|_\infty < \varepsilon. \tag{16}$$

In order to derive the minimum value of ε various sophisticated methods from systems-theory have to be applied. The details for the derivation of the bound for this process can be found in Palis [34].

The controller with transfer function C which is of PI-structure in the present case is then designed for the nominal model P_0 by standard methods, e.g. the root-locus method [35]. The controller is robust if the H_∞-norm of a special closed-loop transfer function satisfies:

$$\left\| \begin{bmatrix} C \\ I \end{bmatrix} (I + P_0 C)^{-1} M_0^{-1} \right\|_\infty < \varepsilon^{-1}. \tag{17}$$

If this condition is fulfilled, the controller stabilises not only the nominal plant model, but also the set of uncertain models. As the infinite-dimensional system, i.e. the granulation process, is included in this set, it is also stabilised. If the condition is not fulfilled then the controller C has to be re-parameterised in an interative way.

3.2. Continuous granulation with external classification and particle recycle

The continuous spray granulation with external classification and a particle recycle utilising screens and a mill is known to possess unstable

steady-states, i.e. a stable limit cycle in the number density distribution of the particles in the bed can occur (Fig. 3). Although this oscillation does not influence the quality of the obtained product – this is determined by the choice of the screens – the quantity of product is strongly influenced: At some time instants a large amount of product is generated whereas at other times the product mass flow nearly vanishes. As this is a generally unwanted effect, feedback control is applied to damp out these oscillations.

A bifurcation analysis of the population balance model shows that the dynamic behaviour is strongly dependent on the size of the milled particles that are re-cycled into the bed [33]: If they are too small then oscillations occur otherwise a stable steady-state operation takes place. From a control engineering point of view the size of the milled particles is a manipulated variable. It can be regulated, for instance by manipulation of the speed of the mill. In order to detect the oscillations, it is found that the second moment of the number density distribution μ_2 is a suitable measurement. Although it is not directly measurable it can be obtained by other means, for instance a model-based measurement system [36].

For stabilisation of these unstable steady-states, model predictive control is applied [37]. Its main idea is to calculate the manipulated variable as the solution of a dynamic optimisation programme. The main ingredients are: (a) A dynamic process model that allows for the prediction of the process state given the information about the current state of the process. (b) A cost functional that measures the deviation of the current and predicted states from the desired process states. (c) An optimisation algorithm that calculates the input trajectory by minimising the difference between the predicted and desired states. Due to the iterative re-calculation of the input trajectory, i.e. at each time instant the future process states are predicted and the optimisation programme is solved again, a closed-loop feedback control law is obtained which is able to cope with process disturbances and changes in the reference signal (Fig. 4).

The main advantages of model predictive control are that it is conceptually simple, which is of great importance if the controller is to be applied industrially, and it is able to incorporate constraints explicitly into the problem formulation, e.g. known limits of the manipulated variables can be stated directly and are met in the resulting input trajectory. The main problem of model predictive control is the need to solve an optimisation programme: If constraints are present then the programme is nonlinear and a closed analytic solution is for almost all cases impossible. This requires the use of iterative numerical algorithms which introduce various difficulties, for instance in the real-time availability of the computed input trajectory. However, focussing on linear model predictive control, it is possible to derive an analytic solution in the unconstrained case which closely resembles a state-feedback controller with a pre-filter for reference tracking.
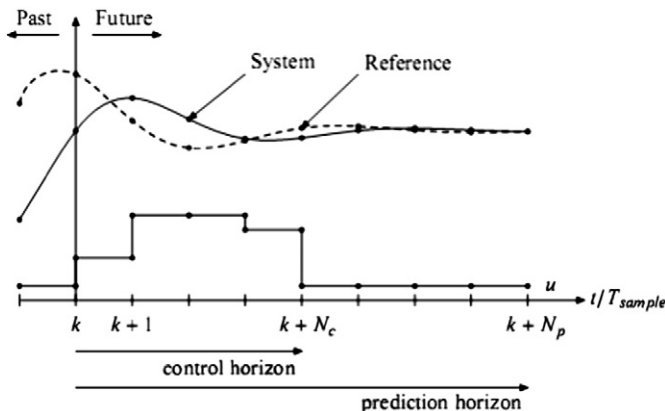

Fig. 4. General principle of model-predictive control.

Given an augmented state-space model in incremental form

$$z(k+1) = \mathbf{A}z(k) + \mathbf{B}\Delta u(k), \quad y(k) = \mathbf{C}z(k), \tag{18}$$

the predicted output can be expressed as

$$Y = \mathbf{F}z(k|k) + \Phi\Delta U, \tag{19}$$

where the vectors Y and ΔU as well as the matrices $\mathbf{F}$ and Φ are created by stacking the equations for all sampling times, i.e.

$$Y = \begin{bmatrix} y(k+1|k) \\ \vdots \\ y\big(k+N_p|k\big) \end{bmatrix}, \tag{20}$$

$$\Delta U = \begin{bmatrix} \Delta u(k) \\ \vdots \\ \Delta u(k+N_c-1) \end{bmatrix}, \mathbf{F} = \begin{bmatrix} \mathbf{CA} \\ \mathbf{CA}^2 \\ \vdots \\ \mathbf{CA}^{N_p} \end{bmatrix}, \tag{21}$$

$$\Phi = \begin{bmatrix} \mathbf{CB} & 0 & 0 \\ \mathbf{CAB} & \mathbf{CB} & 0 \\ \vdots & \vdots & \vdots \\ \mathbf{CA}^{N_p-1}\mathbf{B} & \mathbf{CA}^{N_p-2}\mathbf{B} & \mathbf{CA}^{N_p-N_c}\mathbf{B} \end{bmatrix}. \tag{22}$$

With these results a quadratic cost functional can be formulated

$$J(\Delta U) = (R-Y)^{\mathrm{T}}(R-Y)^{\mathrm{T}} + (\Delta U)\mathbf{W}(\Delta U), \tag{23}$$

where R is the stacked reference signal over the prediction horizon. The matrix $\mathbf{W}$ is used to scale the influence of the input on the cost. The optimum input sequence $(\Delta U)_{opt}$ then minimises the cost functional, i.e.

$$(\Delta U)_{opt} = \arg \min_{\Delta U} J(\Delta U). \tag{24}$$

In the unconstrained case this optimisation problem can be solved analytically, yielding

$$(\Delta U)_{opt} = \left(\Phi^{\mathrm{T}}\Phi + \mathbf{W}\right)^{-1}\Phi^{\mathrm{T}}R - \left(\Phi^{\mathrm{T}}\Phi + \mathbf{W}\right)^{-1}\Phi^{\mathrm{T}}\mathbf{F}z(k|k). \tag{25}$$

The second part of the right-hand side of the equation can be interpreted as state feedback, the first part is a pre-filter that will guarantee a zero steady-state control error.

In the case of linear constraints, e.g. bounds on the manipulated variables, Eq. (24) is a quadratic optimisation programme, the solution can be obtained efficiently, for instance by active-set or SQP methods (cf. [38]).

4. Results and discussion

4.1. Continuous granulation with internal product classification

In order to stabilise the oscillations in this process, for a given required steady-state given by the parameters in Table. 1, the linear

Table 1
Process parameters for the continuous spray granulation process with internal classification after [3].

Nozzle height [m]	h_{nozzle}	0.44
Bed porosity [−]	ψ	0.5
Drain factor [s^{-1}]	K	1.92×10^{-4}
Solid volume spray rate [mm^3 s^{-1}]	$\dot{V}_{solid}$	1.313×10^5
Minimum nucleation fraction [−]	b_∞	0.028
Controller proportional gain	K_p	0.0144
Integrator gain	K_I	8×10^{-6}

transfer function model is derived and reduced in the model order yielding a third-order SISO transfer function. This is done to simplify the controller design. Afterward, the uncertainties Δ_M and Δ_N are derived, including the model reduction error, and incorporated into the controller design as shown before (cf. [34]). For this particular process, a simple PI-controller is designed using the root-locus method, i.e. after setting the general structure of the controller it is parameterised by this method such that the closed loop is stable and shows a desirable dynamic behaviour (Fig. 5). The robustness of the closed-loop system with respect to the model uncertainties is checked by application of Eq. (16). The corresponding gains of the controller are also listed in Table. 1.

Simulation results for the application of the designed PI-controller to the nonlinear process, i.e. the discretised population balance equation, are shown in Fig. 6–Fig. 8. Here, after approximately 60 h the controller is applied to the process and stabilises the number density distribution by manipulating the spraying rate. Note that the change in spraying rate is only temporarily, i.e. the steady-state spraying rate is the same (illustrated by the dashed line in Fig. 8). However, now a constant product mass flow with the desired (mean) particle size is obtained, a huge improvement over the oscillating amount achieved without feedback control (Fig. 7). Another virtue of the designed controller is that although highly sophisticated methods had to be used to derive it and to show that it stabilises the system, it can be implemented easily using a standard PI-controller component.

4.2. Continuous granulation with external classification and particle recycle

In order to calculate and parameterise the model predictive controller for the number density distribution, at first the unstable steady-state solution belonging to the process parameters given in Table. 2 is obtained by analytically solving the steady-state population balance equation (cf. [38]). A finite-dimensional linear state-space model was then obtained by linearising the nonlinear population balance equation, which is discretised with respect to the particle size by a higher-order finite volume method, in the vicinity of the steady-state solution. This linear model, a system of linear ordinary differential equation, is then discretised in time resulting in a set of linear difference equations which are used to predict the future process states.

Given the steady-state solution, the cost functional is set up, measuring the quadratic difference between the current second moment of the
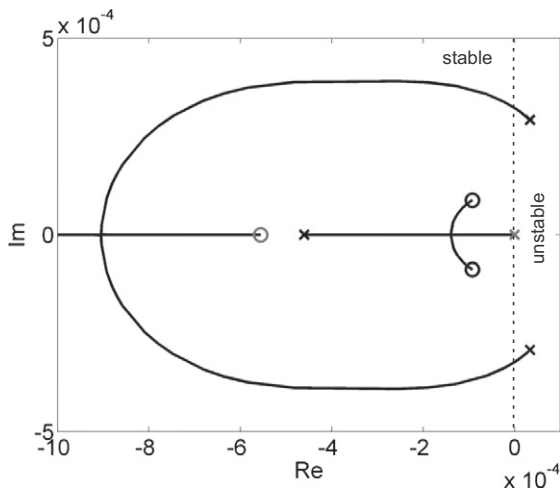

Fig. 6. Plot of the number density distributions in the fluidised bed chamber with and without feedback control. The controller is activated after 60 h and the sustained open-loop oscillation is eliminated and the number density distribution in the bed attains a steady-state.

number density distribution and the value of the second moment in the steady state and a weighting of the applied input is added:

$$J(u) = \sum_{k=1}^{N_p} \left\{ v_k \left(\mu_2[k] - \mu_{2,ref}[k] \right)^2 + w_k (u[k])^2 \right\} . \tag{26}$$

Additionally, constraints are imposed on the range of the manipulated variable, representing the fact that particles cannot be milled to arbitrary sizes:

$$u_{min}[k] \leq u[k] \leq u_{max}[k] . \tag{27}$$

The corresponding values for the prediction and control horizons as well as the constraints can also be found in Table. 2.

This then leads to a quadratic optimisation programme that has to be solved online at each time instant k. However, the computational time needed to re-calculate the input trajectory is – compared to the time constant of the process in the order of minutes – negligible. In Fig. 9 the results obtained by the application of the linear model predictive controller to the nonlinear process after 160 min are shown. Compared

Fig. 5. Plot of the root locus of the nominal plant P_0 with PI-controller. The poles and zeros of P_0 are shown as black crosses and bullets, the poles of the controller are shown in grey. It can be seen that the initially unstable poles (to the right of the dashed line) are pulled into the stable region, i.e. the closed loop is stable.
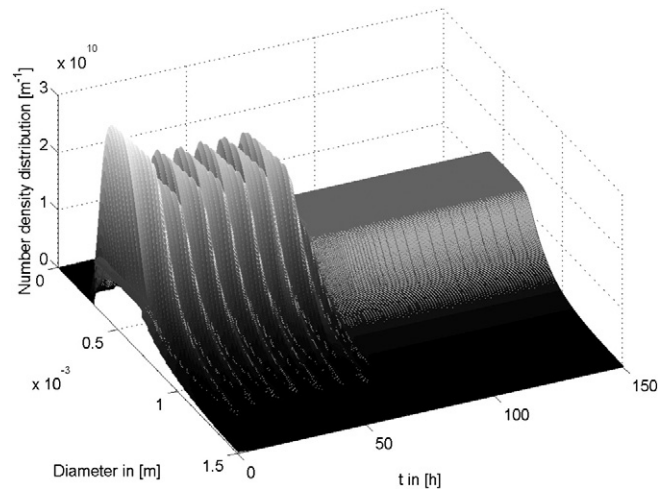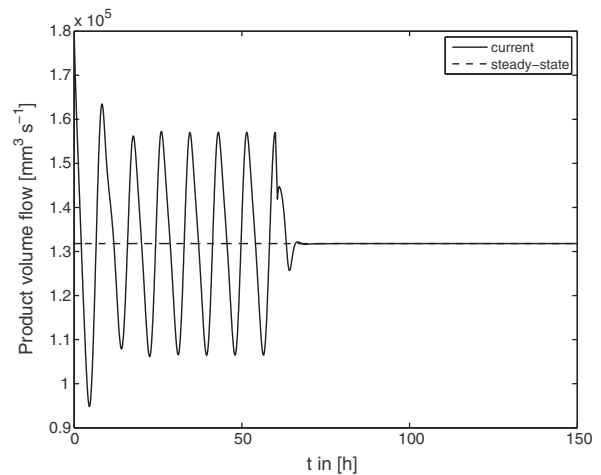

Fig. 7. Plot of the product volume flows for the case of internal classification with and without feedback control (control is activated after 60 h). The solid line (up to 60 h) denotes open-loop operation, afterwards the results correspond to closed-loop operation.
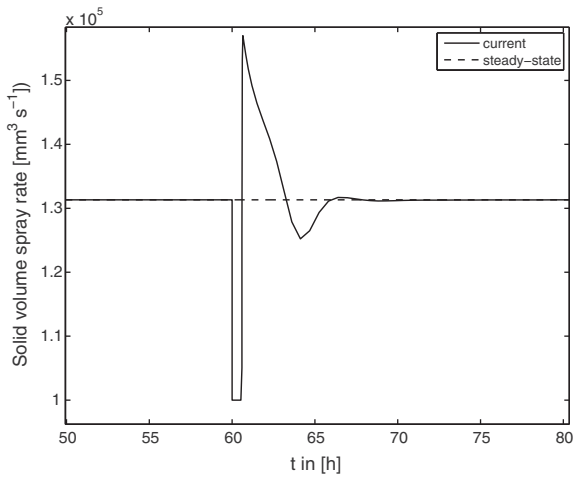
Fig. 8. Plot of the profile of the manipulated variable (solid volume spray rate). The value is constant until the controller is activated after 60 h. It then changes the manipulated variable as indicated. Afterwards the value remains constant for the rest of the process duration.
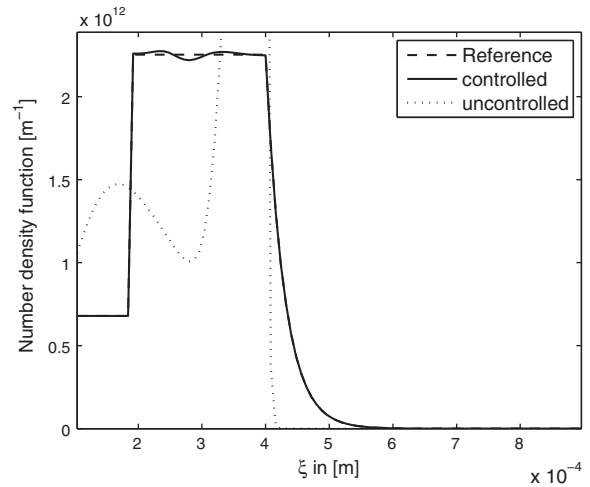

Fig. 9. Plot of the number density distributions in the fluidised bed chamber with and without feedback control after 160 min, as well as the desired steady-state reference.

to the uncontrolled process where a sustained oscillation develops the controller is able to stabilise the steady-state, resulting in a constant mass flow of product with a constant particle size distribution (Fig. 10). The profile of the manipulated variable, the mean diameter of the milled and re-cycled particles, is shown in Fig. 11. It can be seen that the value is at all times in the bounds specified by u_{min} and u_{max}. The non-smooth appearance of the profile is due to the time discrete implementation of the control law and the unstable dynamics of the process. It can be smoothed by decreasing the sample time T_{sample} at the cost of an increased computational load.

5. Summary and outlook

In this work the stabilisation of unstable, oscillatory steady-states in continuous fluidised bed spray layering granulation was investigated. Two practically important process configuration – with internal product classification and with external product classification – which can exhibit unstable process behaviour under a wide set of operating conditions were considered. These unstable process states, which in both cases are due to nuclei formulation, limit the current range of achievable product properties.

Based on practical as well as model-based considerations, manipulated variables were chosen which allow influencing the stability of the processes. Two linear feedback controllers with industrially

accepted structures were designed to determine a-priori determined unstable steady-state: A robust PI controller for the continuous process with internal product classification, which takes explicitly into account process uncertainties, and a model-predictive controller for the continuous process with external classification which takes into account constraints on the manipulated variables. It was shown in simulations that the designed controllers are able to achieve the stabilisation; however, – being linear feedback controllers – the underlying linearised process dynamics must be sufficiently close to the nonlinear process dynamics.

This current restriction has to be overcome if in addition to stabilisation also the start-up and shutdown of the continuous processes are to be realised. These processes are inherently nonlinear and feedback controller design has to incorporate this. A possible way to do this in future work is for instance the use of gain-scheduling controllers: There, a set of linear process models is derived where each model is a able to represent the nonlinear dynamics over a certain range. The complete nonlinear dynamics are recovered by suitably switching between the linear models. Simultaneously, a set of linear feedback controllers for each of the linear process models is designed as well as a switching mechanism between the controllers.

Another restriction that has to be handled in future work is the influence of the continuous (gas) phase on the particle growth. Based on the

Table 2
Process parameters for the continuous spray granulation process with external classification.

|		
Initial bed mass [kg]	m_{bed}	10.0
Reference bed mass [kg]	$m_{bed,set}$	10.0
Mass flow of nuclei [kg s^{-1}]	M_{nuc}	5.55×10^{-5}
Mass flow of solid [kg s^{-1}]	ϱ_{solid}	1.38×10^{-2}
Solid density [kg m^{-3}]	ϱ_{solid}	1440.0
Size of nuclei [m]	ξ_0	0.1×10^{-3}
Screen size upper screen [m]	ξ_u	0.5×10^{-3}
Screen size lower screen [m]	ξ_l	0.4×10^{-3}
Milling diameter (osc.) [m]	ξ_M	0.2×10^{-3}
Number of discretised states		100
Simulation time interval [s]	t_{end}	12,000
Sampling time [s]	T_{sample}	60
Prediction horizon	N_p	30
Control horizon	N_c	10
Minimum input [m]	u_{min}	0.18×10^{-3}
Maximum input [m]	u_{max}	0.22×10^{-3}
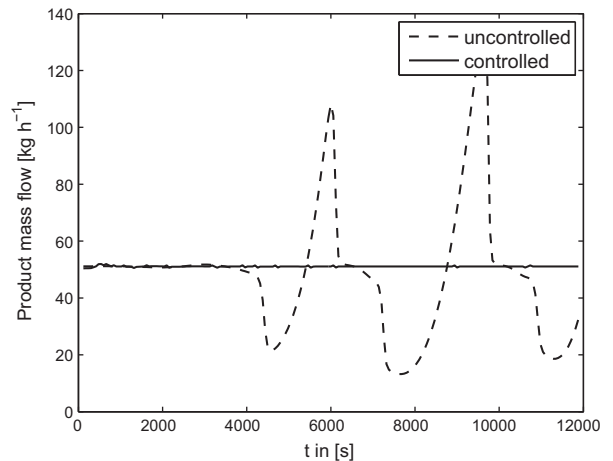
Fig. 10. Plot of the product mass flows for the case of external classification with and without feedback control.
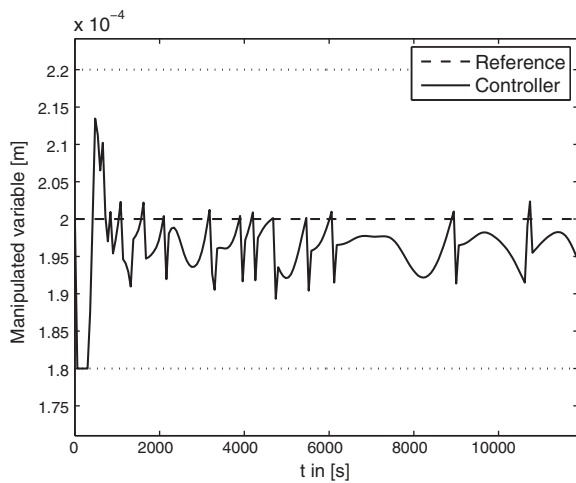
Fig. 11. Plot of the profile of the manipulated variable obtained by constrained model-predictive control. The dashed lines correspond to the minimum and maximum value for the manipulated variable (see Table. 2).

drying conditions, the morphology of the layers can differ from fairly compact to highly porous. This results in different size growth rates due to the added void in the layers although the same of amount of solid was sprayed, i.e. additional changes in the particle size distribution, which have to be considered in feedback control design and plant operation.

Notation

b	mass fraction of solid spray that creates nuclei
e	internal property coordinate
h	height [m]
m	mass [kg]
n	number density function $[m^{-1}]$
q_0	normalised number density function $[m^{-1}]$
u	manipulated variable
$\mathbf{x}$	external/spatial coordinates
$\mathbf{A}, \mathbf{B}, \mathbf{C}, \mathbf{F}$	state space matrices
B_n	number flow of nuclei $[s^{-1}]$
B_m	number flow of milled particles $[s^{-1}]$
C	state space matrices
E	property space
G	particle growth rate $[m\ s^{-1}]$
K	drain factor $[s^{-1}]$
K_I	integrator gain
K_p	proportional gain
M_0, N_0	transfer function
$\dot{M}$	mass flow rate $[kg\ s^{-1}]$
N	total number of particles
N_c	number of control steps
N_p	number of prediction steps
P, P_0	transfer function
R	reference over prediction horizon $[m^2]$
T_{sample}	MPC sampling time [s]
T	separation function
$\dot{V}$	volume spray rate $[m^3\ s^{-1}]$
$\mathbf{W}$	controller design matrices
Y	measurements over prediction horizon $[m^2]$
ε	robustness measure
μ_j	j-th total moment of number density function $[m^j]$
ξ	particle diameter [m]
ρ	mass density $[kg\ m^{-3}]$
ψ	bed porosity
Δ_M, Δ_N	transfer function
ΔU	change in u over control horizon [m]
Φ	state space matrix
Ω	physical space

References

[1] H.G. Merkus, Particle Size Measurements — Fundamentals, Practice, Quality, Springer Science + Business Media B.V., Dordrecht, 2009.
[2] S. Heinrich, M. Peglow, M. Ihlow, L. Mörl, Particle population modeling in fluidized bed spray granulation — analysis of the steady state and unsteady behavior, Powder Technol. 130 (2003) 154–161.
[3] A.W. Vreman, C.E. van Lare, M.J. Hounslow, A basic population balance model for fluid bed spray granulation, Chem. Eng. Sci. 64 (2009) 4389–4398.
[4] H.M. Hulburt, S. Katz, Some problems in particle technology: a statistical mechanical formulation, Chem. Eng. Sci. 19 (1964) 555–574.
[5] A.D. Randolph, M.A. Larson, Theory of Particulate Processes: Analysis and Techniques of Continuous Crystallization, Academic Press, 1972.
[6] D. Ramkrishna, Population Balances: Theory and Application to Particulate Systems in Engineering, Academic Press, New York, 2000.
[7] G.R. Jerauld, Y. Vasatis, M.F. Doherty, Simple conditions for the appearance of sustained oscillations in continuous crystallizers, Chem. Eng. Sci. 38 (10) (1983) 1675–1681.
[8] D.L. Ma, D.K. Tafti, R.D. Braatz, High-resolution simulation of multidimensional crystal growth, Ind. Eng. Chem. Res. 41 (2002) 6217–6223.
[9] Q. Hu, S. Rohani, A. Jutan, Modelling and optimization of seeded batch crystallizers, Comput. Chem. Eng. 29 (4) (2005) 911–918.
[10] F.Y. Wang, I.T. Cameron, Review and future directions in the modelling and control of continuous drum granulation, Powder Technol. 124 (2002) 238–253.
[11] L. Mörl, S. Heinrich, M. Peglow, Granulation, Chapter Fluidized Bed Spray Granulation, Pages 21–188, Elsevier B. V., Amsterdam, 2007.
[12] [12] J. Li, B. Freireich, C. Wassgren, and J.D. Litster. A general compartment-based population balance model for particle coating and layering granulation. *AIChE Journal*, 10.1002/aic.12678.
[13] J.A. Villegas, S.R. Duncan, H.G. Wang, W.Q. Yang, R.S. Raghavan, Distributed parameter control of a batch fluidised bed dryer, Control. Eng. Pract. 17 (2009) 1096–1106.
[14] M. Peglow, J. Kumar, S. Heinrich, G. Warnecke, E. Tsotsas, L. Mörl, B. Wolf, A generic population balance model for simultaneous agglomeration and drying in fluidized beds, Chem. Eng. Sci. 62 (2007) 513–532.
[15] M. Peglow, U. Cunäus, E. Tsotsas, An analytical solution of population balance equations for continuous fluidized bed drying, Chem. Eng. Sci. 66 (2011) 1916–1922.
[16] J.C. Barrett, N.A. Webb, A comparison of some approximate methods for solving the aerosol general dynamic equation, J. Aerosol Sci. 29 (1998) 31–39.
[17] A. Kalani, P.D. Christofides, Nonlinear control of spatially inhomogeneous aerosol processes, Chem. Eng. Sci. 54 (1999) 2669–2678.
[18] P.D. Christofides, Control of nonlinear distributed process systems: recent developments and challenges, AIChE J 47 (2001).
[19] H. Shang, J. Fraser Forbes, M. Guay, Feedback control of hyperbolic distributed parameter systems, Chem. Eng. Sci. 60 (2005) 969–980.
[20] P.D. Christofides, P. Daoutidis, Feedback control of hyperbolic PDE systems, AIChE J 42 (11) (1996) 3063–3086.
[21] I. Aksikas, A. Fuxman, J. Fraser Forbes, J.J. Winkin, LQ control design of a class of hyperbolic PDE systems: applications to fixed-bed reactor, Automatica 45 (2009) 1542–1548.
[22] M. Mangold, A. Bück, R. Hanke-Rauschenbach, Passivity based control of a distributed PEM fuel cell model, J. Process Control 20 (2010) 292–313.
[23] T. Chiu, P.D. Christofides, Nonlinear control of particulate processes, AIChE J 45 (6) (1999) 1279–1297.
[24] M. Pottmann, B.A. Ogunnaike, A.A. Adetayo, B.J. Ennis, Model-based control of a granulation system, Powder Technol. 108 (2000) 192–201.
[25] U. Vollmer, J. Raisch, Population balance modelling and H∞-controller design for a crystallization process, Chem. Eng. Sci. 57 (2002) 4401–4414.
[26] S. Palis, A. Kienle, Diskrepanzbasierte Regelung der kontinuierlichen Flüssigkristallisation, at – Automatisierungstechnik 60 (2012) 145–154.
[27] D. Shi, N.H. El-Farra, M. Li, P. Mhaskar, P.D. Christofides, Predictive control of particle size distributions in particulate processes, Chem. Eng. Sci. 61 (2006) 268–281.
[28] M. Duenas Diez, B.E. Ydstie, M. Fjeld, B. Lie, Inventory control of particulate processes, Comput. Chem. Eng. 32 (2008) 46–67.
[29] T. Glaser, C.F.W. Sanders, F.Y. Wang, I.T. Cameron, J.D. Litster, J.M.-H. Poon, R. Ramachandran, C.D. Immanuel, F.J. Doyle III, Model predictive control of continuous drum granulation, J. Process Control 19 (2009) 615–622.
[30] S. Palis, A. Kienle, Stabilization of continuous fluidized bed spray granulation — a Lyapunov approach, Proceedings of the 8th IFAC Symposium on Nonlinear Control Systems, 2010.
[31] S. Palis, A. Kienle, Stabilization of continuous fluidized bed spray granulation with external product classification, Chem. Eng. Sci. 70 (5) (2012) 200–209.

[32] S. Palis, A. Kienle, Discrepancy based control of continuous fluidized bed spray granulation with internal product classification, Proceedings of the IFAC Conference on Advanced Control of Chemical Processes — ADCHEM, Singapore, 2012, pp. 756–761.

[33] R. Radichkov, T. Müller, A. Kienle, S. Heinrich, M. Peglow, L. Mörl, A numerical bifurcation analysis of continuous fluidized bed spray granulation with external product classification, Chem. Eng. Process. 45 (2006) 826–837.

[34] S. Palis, Control of Fluidized Bed Spray Granulation Processes, PhD thesis Otto von Guericke University, Magdeburg, Germany, 2012. 1–2614 (urn:nbn:de:gbv:ma9).

[35] W.R. Evans, Control system synthesis by root locus method, Trans. AIEE 69 (1) (1950) 66–69.

[36] A. Bück, M. Peglow, E. Tsotsas, M. Mangold, A. Kienle, Model-based measurement of particle size distributions in layering granulation processes, AIChE J 57 (4) (2011) 929–941.

[37] D.Q. Mayne, J.B. Rawlings, C.V. Rao, P.O.M. Scokaert, Constrained model predictive control: stability and optimality, Automatica 36 (2000) 789–814.

[38] A. Bück, Model-based Measurement and Control of Fluidised Bed Spray Granulation Processes, PhD thesis Otto von Guericke University Magdeburg, Germany, 2012. 1–2707 (urn:nbn:de:gbv:ma9).

Modeling and discrepancy based control of underactuated large gantry cranes

Ievgen Golovin [*,*] Stefan Palis [*,**]

Otto-von-Guericke University, D-39106 Magdeburg, Germany
**National Research University "Moscow Power Engineering Institute", Moscow, Russia*

Abstract: An important structural dynamics problem of the large gantry cranes are horizontal elastic oscillations mainly excited by the trolley motion. They reduce the crane operation performance and lead to faster material wear of the crane construction. In this article a distributed parameter model of large gantry cranes applying Hamilton's principle is presented. In order to stabilize the system dynamics the use of a generalized error measure, called discrepancy, is proposed. Applying the associated stability theory, i.e. stability with respect to two discrepancies, a nonlinear stabilizing control for the underactuated gantry crane is derived. The proposed control strategy has been verified by simulations.

Keywords: Distributed parameter system; discrepancy based control; gantry crane; payload oscillations; position control; structural dynamics.

1. INTRODUCTION

Currently, the control of underactuated crane systems is an active field of research. In Abdel-rahman et al. (2003) and Ramli et al. (2017) authors overviewed a variety of models and control techniques for different types of cranes. Most of the contributions focus on the damping of load swaying due to the crane positioning applying different feedback and feedforward control approaches, e.g. energy-based control Sun and Fang (2012), Sun et al. (2018), Won and Hoang (2018), sliding mode control Zhou et al. (2017), Xiao et al. (2018), Wang et al. (2018), Lu et al. (2017) and input shaping techniques Abdullahi et al. (2018), Ramli et al. (2018). In the majority of contributions the structural system dynamics has been neglected. However, continuous increase of crane dimensions and utilizing lightweight profiles led to limited stiffness of the structure. Thus, this assumption is not valid for large cranes and a coupling between elastic structural vibrations and the trolley movements has to be taken into account.

In the last years, the structural dynamics problem has been stated for different types of cranes (Zrnić et al. (2006); Rauscher and Sawodny (2017); Schlott et al. (2016); Kimmerle et al. (2018); Miloradovic and Vujanac (2016); Sowa et al. (2018)) including large gantry cranes (Golovin and Palis (2019); Gašić et al. (2013); Yazid et al. (2011); Kreuzer et al. (2012); Ryu and Kong (2012)). Here, two main structural dynamical problems can be stated: vertical girder vibrations due to the trolley travel and load hoisting, and horizontal low frequency oscillations in the trolley motion direction. In this contribution, the focus is on the horizontal oscillations as they are particularly unfavorable due to the large amplitudes and their weakly damped behaviour. They provide additional mechanical stresses leading to faster construction wear and decrease

crane operation performance. In addition, applying feedback control, neglecting the structural dynamics, may result in the excitation of resonance frequencies and even unstable closed loop dynamics.

In the literature different approaches to solve the structural dynamics problem for large gantry cranes have been proposed, e.g. structure stiffening by construction optimization Zrnić et al. (2005), passive and active dampers via additional weight as counter-mass Recktenwald (2011) and linear robust active damping approach as an extension for the trolley motion control system Golovin and Palis (2019). The later has been verified on a laboratory gantry crane.

This contribution is concerned with the modeling and nonlinear control of underactuated large gantry cranes with limited stiffness. In order to derive the distributed parameter crane model Hamilton's principle has been utilized. The main control objectives for underactuated large gantry cranes are payload positioning without swaying and a simultaneous reduction of structural oscillations in the trolley travel direction. Here, in order to stabilize the system dynamics the use of a generalized error measure, called discrepancy, is proposed (Palis and Kienle (2012, 2014)). Applying the associated Lyapunov stability theory a nonlinear stabilizing control has been derived. The resulting control law has been verified in a simulation study, where the distributed dynamics have been discretized using finite differences.

Section 2 presents the derivation of the coupled model of the gantry crane including its structural dynamics. The concept of stability with respect to two discrepancies as well as the corresponding discrepancy based control design are introduced in section 3. Section 4 concludes the article with results from a simulation study.

---

[*] Correponding author: ievgen.golovin@ovgu.de

2. GANTRY CRANE MODELING

In this contribution, a nonlinear model-based control approach for the gantry crane is proposed. It requires the establishment of the corresponding dynamic plant model. Essentially, an operational cycle of the gantry crane consists of the hoisting of the load, its horizontal movement and deposition. From a control point of view, the horizontal movement phase is the most challenging tasks. The payload should be delivered as fast as possible to the desired position without swaying. However, for large cranes such movements may excite the natural frequencies of the crane structure. These important effects should be reflected in the dynamic model. For convenience, the following assumptions for model derivations are made:

(1) as the scope of the contribution is on the horizontal vibrations the considered frame structure of the crane consists of the upper horizontal beam which is rigid in flexure and two supported columns that have limited lateral stiffness;
(2) the structure is assumed to be symmetrical such that the problem can be reduced and only one half of the structure has to be taken into account;
(3) the mass density and the bending stiffness of the crane columns are distributed along the spatial coordinate, and they are assumed to be constant along the spatial coordinate;
(4) rotary inertia, shear deformation and buckling effects can be neglected;
(5) the hoisting process is neglected, such that the rope length can be assumed to be constant;
(6) the trolley and the payload are connected by a massless rigid rope and the elongation of the rope is neglected;
(7) the moment of inertia of the load can be neglected;
(8) nonlinear friction effects can be neglected;
(9) external disturbances on the crane and load can be neglected, e.g. wind;
(10) the trolley is actuated via a current controlled DC-motor with gear, therefore the force $F_t(t)$ depends linearly on the motor torque $\tau(t)$, i.e. $F_t(t) = k_{tr}\tau(t)$ where k_{tr} is the transformation coefficient.

In Fig. 1 the schematic diagram of the motion of the gantry crane is depicted. Here, m_t is the mass of the crane trolley, m_p is the mass of the payload, m_c is the mass of the crane girder, F_t is the external force being applied to the trolley, $\varphi(t)$ is the sway angle, $z(t)$ is the trolley displacement, l is the rope length, $w(x,t)$ is the displacement of the crane structure in horizontal direction depending on both position x and time t, L is the length of the crane legs, ρ_c is the mass density, E is Young's modulus and I is the moment of inertia of a cross-sectional area.

In order to derive a suitable gantry crane model Hamilton's principle based on the kinetic energy $T(t)$, potential energy $U(t)$ and virtual work done by non-conservative forces $W(t)$ can be written as follows

$$\int_{t_1}^{t_2} (\delta T - \delta U + \delta W)\, \mathrm{d}t = 0\,, \tag{1}$$

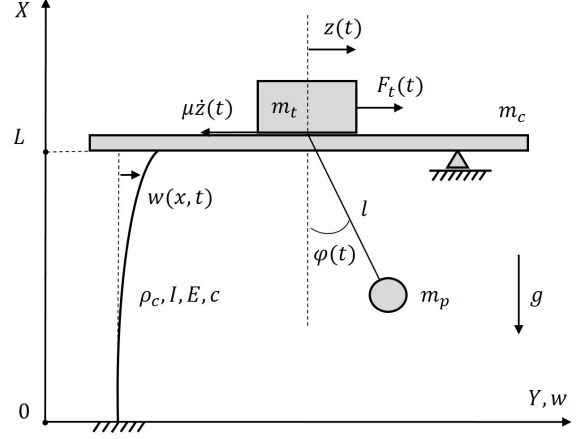where δ represents the variational operator, t_1 and t_2 are initial and final moments in time.

Fig. 1. *Gantry crane*

The vector of generalized coordinates is chosen as follows

$$q = [w(x,t)\ z(t)\ \varphi(t)]\,. \tag{2}$$

Then the position vectors of girder r_c, trolley r_t and payload r_p can be written as follows

$$r_c = \begin{bmatrix} w(L,t) \\ 0 \end{bmatrix}\,, \tag{3}$$

$$r_t = \begin{bmatrix} w(L,t) + z(t) \\ 0 \end{bmatrix}\,, \tag{4}$$

$$r_p = \begin{bmatrix} w(L,t) + z(t) + l\sin\varphi \\ -l\cos\varphi \end{bmatrix}\,. \tag{5}$$

The corresponding kinetic energy of the gantry crane can be represented as follows

$$T = \frac{1}{2}\int_0^L \rho_c \dot{w}^2\, \mathrm{d}x + \frac{1}{2}m_c\dot{w}^2(L,t) + \frac{1}{2}m_t(\dot{w}(L,t) + \dot{z})^2$$
$$+ \frac{1}{2}m_p\left[(\dot{w}(L,t) + \dot{z} + \dot{\varphi}l\cos\varphi)^2 + (\dot{\varphi}l\sin\varphi)^2\right]\,, \tag{6}$$

and the potential energy can be formulated as follows

$$U = \frac{1}{2}\int_0^L EI(w'')^2\, \mathrm{d}x - m_p gl\cos\varphi\,, \tag{7}$$

where the *dot symbol* denotes the derivative along the time and the *prime symbol* along the spatial coordinate.

According to Fig. 1 the work done by non-conservative forces, namely actuating force, trolley viscous friction force and structural linear damping force, can be written as

$$\delta W = (F_t - \mu\dot{z})\,\delta z - \int_0^L c\dot{w}\,\delta w\, \mathrm{d}x\,, \tag{8}$$

where μ is the viscous friction coefficient and c is the linear structural damping.

Substituting energies (6), (7) and (8) into Hamilton's principle (1), taking corresponding variations and applying integration by parts with respect to t and x, the following equation is obtained:

$$0 = -\int_{t_1}^{t_2}\int_0^L [\rho_c \ddot{w} + EIw'''' + c\dot{w}]\,\delta w\,\mathrm{d}x\,\mathrm{d}t$$
$$-\int_{t_1}^{t_2} [EIw'''(0,t)]\,\delta w(0,t)\,\mathrm{d}t$$
$$+\int_{t_1}^{t_2} [EIw''(0,t)]\,\delta w'(0,t)\,\mathrm{d}t$$
$$-\int_{t_1}^{t_2} [EIw''(L,t)]\,\delta w'(L,t)\,\mathrm{d}t$$
$$-\int_{t_1}^{t_2} [m_\Sigma \ddot{w}(L,t) + m_s \ddot{z} + m_p l\ddot{\varphi}\cos\varphi$$
$$- m_p l\dot{\varphi}^2 \sin\varphi - EIw'''(L,t)]\,\delta w(L,t)\,\mathrm{d}t$$
$$-\int_{t_1}^{t_2} [m_s \ddot{w}(L,t) + m_s \ddot{z} + m_p l\ddot{\varphi}\cos\varphi$$
$$- m_p l\dot{\varphi}^2 \sin\varphi - F_t + \mu\dot{z}]\delta z\,\mathrm{d}t$$
$$- m_p l\int_{t_1}^{t_2} [l\ddot{\varphi} + \ddot{w}(L,t)\cos\varphi + \ddot{z}\cos\varphi$$
$$+ g\sin\varphi]\delta\varphi\,\mathrm{d}t\,, \tag{9}$$

where $m_\Sigma = m_p + m_t + m_c$ and $m_s = m_p + m_t$.

Here, as variations are arbitrary, eq. (9) holds only if the integrands vanish. Thus, taking into account the geometrical boundary conditions $w(0,t) = w_x(0,t) = 0$ the equations of motion follow:

$$0 = \rho_c \ddot{w} + EIw'''' + c\dot{w}\,, \tag{10}$$
$$0 = w(0,t) = w'(0,t) = w''(L,t)\,, \tag{11}$$
$$0 = m_\Sigma \ddot{w}(L,t) + m_s \ddot{z} + m_p l\ddot{\varphi}\cos\varphi$$
$$- m_p l\dot{\varphi}^2 \sin\varphi - EIw'''(L,t)\,, \tag{12}$$
$$0 = m_s \ddot{w}(L,t) + m_s \ddot{z} + m_p l\ddot{\varphi}\cos\varphi$$
$$- m_p l\dot{\varphi}^2 \sin\varphi - F_t + \mu\dot{z}\,, \tag{13}$$
$$0 = l\ddot{\varphi} + \ddot{w}(L,t)\cos\varphi + \ddot{z}\cos\varphi + g\sin\varphi\,. \tag{14}$$

3. CONTROL DESIGN

This section focuses on stability with respect to two discrepancies and the associate control design. The derived equations of motion consist of a partial differential equation (PDE) (10) with corresponding boundary conditions (b.c.) (11) representing the structural dynamics of the crane and a system of nonlinear ordinary differential equations (ODE) (12-14), which act on the boundary of the PDE and represent the coupled motion of the girder, trolley and payload.

In this contribution it is assumed, that all system states related to the trolley motion, payload motion and crane oscillations at the boundary $x = L$ can be measured. The actuation is represented by a DC motor operating in current control mode, where the desired current is proportional to the control applied torque $\tau(t)$.

3.1 Stability with respect to two discrepancies

According to the works (Movchan (1960); Sirazetdinov (1967, 1987)) the most important properties and definitions about stability with respect to two discrepancies are presented in the following. Here, the process $\phi(.,t)$ is a solution of a distributed parameter system and $\phi_0 = 0$ is an equilibrium of the system.

Definition 1. Discrepancy
A discrepancy is a real valued functional $\rho = \rho[\phi(.,t),t]$ with the following properties

- $\rho(\phi,t) \geq 0$
- $\rho(0,t) = 0$
- for an arbitrary process $\phi(.,t)$ the real valued functional $\rho[\phi(.,t),t]$ is continuous with respect to t
- presenting the second discrepancy $\rho_0(\phi)$ with $\rho_0(\phi) \geq 0$ and $\rho_0(0) = 0$. Than the discrepancy $\rho[\phi(.,t),t]$ is continuous at time $t = t_0$ with respect to ρ_0 at $\rho_0 = 0$, if for every $\epsilon > 0$ and $t_0 > 0$ there exists a $\beta(\epsilon, t_0) > 0$, such that from $\rho_0 \leq \beta(\epsilon, t_0)$ follows $\rho < \epsilon$

From this definition one can state that a discrepancy does not satisfy all properties of a metric, e.g. symmetry $d(x,y) = d(y,x)$ or triangular inequality $d(x,y) = d(y,z) + d(z,y)$. And more importantly, it has not to satisfy the property of definiteness, i.e. a vanishing discrepancy $\rho(\phi,t) = 0$ does not automatically mean $\phi = 0$. Thus, the discrepancy is an extension of the distance measures normally used in stability theory of DPS like L_p and L_∞-norms.

Definition 2. Stability with respect to two discrepancies ρ and ρ_0
The equilibrium $\phi_0 = 0$ is stable in terms of Lyapunov with respect to the two discrepancies ρ and ρ_0 for all $t \geq t_0$ if for every $\epsilon > 0$ and $t_0 \geq 0$ there exists a $\beta = \beta(\epsilon, t_0)$ such that for every process $\phi(.,t)$ with $\rho_0 < \beta(\epsilon, t_0)$ it follows that $\rho < \epsilon$ for all $t \geq t_0$. If in addition $\lim_{t\to\infty}\rho = 0$, than the equilibrium ϕ_0 is called asymptotically stable in terms of Lyapunov with respect to the two discrepancies ρ and ρ_0.

A lot of nonlinear control approaches are based on the Lyapunov stability theory. In order to define a relationship between the existence of a Lyapunov functional V and stability with respect to two discrepancies the notions of positivity and positive definiteness of a functional with respect to a discrepancy should be presented.

Definition 3. Positivity with respect to a discrepancy ρ
The functional $V = V[\phi,t]$ is called positive with respect to the discrepancy ρ, if $V \geq 0$ and $V[0,t] = 0$ for all ϕ with $\rho(\phi,t) < \infty$.

Definition 4. Positive definiteness with respect to a discrepancy ρ
The functional $V = V[\phi,t]$ is positive definite with respect to the discrepancy ρ, if $V \geq 0$ and $V[0,t] = 0$ for all ϕ with $\rho(\phi,t) < \infty$, and for every $\epsilon > 0$ exists a $\beta = \beta(\epsilon) > 0$, such that $V \geq \beta(\epsilon)$ for all ϕ with $\rho[\phi,t] \geq \epsilon$.

The next two theorems state the conditions for a function V to guarantee (asymptotic) stability with respect to two discrepancies (Sirazetdinov (1987)).

Theorem 1. The process ϕ with equilibrium $\phi_0 = 0$ is stable with respect to the two discrepancies ρ and ρ_0 if and only if there exists a functional $V = V[\phi,t]$ positive definite with respect to the discrepancy ρ, continuous at time $t = t_0$ with respect to ρ_0 at $\rho_0 = 0$ and not increasing along the process ϕ, i.e. $\dot{V} \leq 0$.

Theorem 2. The process ϕ with equilibrium $\phi_0 = 0$ is asymptotically stable with respect to the two discrepancies ρ and ρ_0 if and only if there exists a functional $V =$

$V[\phi,t]$ positive definite with respect to the discrepancy ρ, continuous at time $t = t_0$ with respect to ρ_0 at $\rho_0 = 0$ and not increasing along the process ϕ, i.e. $\dot{V} \leq 0$, with $\lim_{t \to \infty} V = 0$.

In addition, it should be mentioned that stability with respect to two discrepancies is necessary but in general not sufficient for stability with respect to a L_p norm or L_∞ norm.

3.2 Discrepancy based control

The objective of the control system is to move the trolley according to the desired position reference signal $z_{ref}(t)$ and a simultaneous reduction of the payload swaying and crane structural oscillations. One of the options to derive a nonlinear control law for a damping strategy could be to take the overall mechanical energy $E_o = T + U$ as a candidate Lyapunov functional. However, calculating its time derivative along the system trajectory results in:

$$\dot{E}_o = \dot{z} F_t . \tag{15}$$

Here, choosing $F_t = -k\dot{z}$ as the input and $\dot{z}$ as the output yields in the well-known energy dissipation. However, due to the underactuated nature of the system, the control law contains neither terms related to the crane structural motion nor the payload. One way to overcome this problem is to couple eq. (15) with a term depending on the payload velocity and to find reversely an appropriatly shaped energy functional (Sun and Fang (2012)).

In this contribution another approach based on the discrepancy is proposed. The generalized system error can be chosen as follows

$$e = k_1 \dot{w}(L,t) + k_2 \dot{z} + k_3 \dot{\varphi} l \cos\varphi + k_4 \varepsilon , \tag{16}$$

where $\varepsilon(t) = z(t) - z_{ref}(t)$ is the deviation from the reference position signal and k_1 to k_4 are the corresponding weights.

Here, the generalized error e is established in such way, that it includes the position error ε, velocity of the trolley $\dot{z}$ and for increasing the system coupling the corresponding velocities of the girder $\dot{w}(L,t)$ and horizontal velocity of the payload $\dot{\varphi} l \cos\varphi$. In order to shape the error the additional weights are introduced. Using the given generalized error results in the following discrepancy ρ

$$\rho = \frac{1}{2}\left(k_1 \dot{w}(L,t) + k_2 \dot{z} + k_3 \dot{\varphi} l \cos\varphi + k_4 \varepsilon \right)^2 . \tag{17}$$

The second discrepancy ρ_0 is selected to be equal to ρ at time $t = t_0 = 0$:

$$\rho_0 = \rho(t = 0) = 0 . \tag{18}$$

As stated in *Theorem 2* existence of a suitable functional V is sufficient to guarantee asymptotic stability with respect to the two discrepancies ρ and ρ_0. For this aim the corresponding Lyapunov functional can be easily represented as follows

$$V = \frac{1}{2}\left(k_1 \dot{w}(L,t) + k_2 \dot{z} + k_3 \dot{\varphi} l \cos\varphi + k_4 \varepsilon \right)^2 . \tag{19}$$

According to stability in terms of two discrepancies the control input should be chosen such that the time derivative $\dot{V}$ is negative definite along the state trajectories and vanishes only for $V = 0$. Calculating the time derivative yields

$$\dot{V} = e\dot{e} = e[k_1 \ddot{w}(L,t) + k_2 \ddot{z} + k_3 \ddot{\varphi} l \cos\varphi$$
$$- k_3 \dot{\varphi}^2 l \sin\varphi + k_4 \dot{\varepsilon}] . \tag{20}$$

Substituting eq. (13) in (20) yields in

$$\dot{V} = e[(k_1 - k_2)\ddot{w}(L,t) + b_1 l \ddot{\varphi} \cos\varphi$$
$$- b_1 l \dot{\varphi}^2 \sin\varphi + k_4 \dot{\varepsilon} - \frac{k_2 \mu}{m_s} \dot{z} + \frac{k_2}{m_s} F_t] , \tag{21}$$

where

$$b_1 = \frac{k_3 m_s - k_2 m_p}{m_s} .$$

In order to achieve the required negative definiteness of $\dot{V}$ the control law is chosen as follows

$$\tau = \frac{m_s}{k_2 k_{tr}}[-(k_1 - k_2)\ddot{w}(L,t) - b_1 l \ddot{\varphi} \cos\varphi$$
$$+ b_1 l \dot{\varphi}^2 \sin\varphi - k_4 \dot{\varepsilon} + \frac{k_2 \mu}{m_s} \dot{z} - ae] , \tag{22}$$

where $a > 0$ is a design parameter influencing the control performance.

The proposed control law guarantees not only stability, in the aforementioned sense, but also exponential convergence of V

$$\dot{V} = -ae^2 = -2aV . \tag{23}$$

The overall control scheme is depicted in Fig. 2.
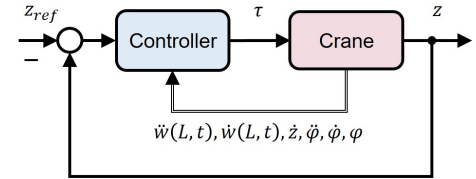

Fig. 2. *Control scheme*

4. RESULTS

The simulation model, including the proposed control law, has been implemented in MATLAB. For the solution of the PDE (10) the method of lines have been applied. Here, the spatial coordinate is lumped applying the finite difference method (via central difference scheme) with $N = 50$ points. For the solution of the resulting system of ODEs the *ode15s* solver has been used. All simulation parameters are summarized in Table 1.

For contrast, the results of the proposed control law can be compared with additional classical cascade scheme for drive position control where no additional damping purposes are provided. This simple control law can be written as follows

$$\tau = [k_{p,pos}(z_{ref} - z) - \dot{z}]\left(k_{p,vel} + k_{i,vel}\frac{1}{s}\right) , \tag{24}$$

where $k_{p,pos}$ is position controller gain, $k_{p,vel}$ and $k_{i,vel}$ are parameters of the velocity PI controller that can be adjusted according to the modulus optimum.

In order to verify both control laws (22) and (24) time responses of the positioning reference tracking have been studied. The results are depicted in Fig. 3, 4, 5 and 6. In Fig. 3 the convergence of the Lyapunov functional V is shown. From Fig. 4, it can be seen, that applying the classical cascade motion control (24) without additional

system information results in oscillatory closed loop system dynamics with large amplitudes of payload and crane swinging. Applying the designed discrepancy based control (22) yields a good damping of payload and structural motion. As can be seen from Fig. 5 and 6 not only the motion of the girder point $w(L,t)$ but also the distributed state $w(x,t)$ itself and its L_2-norm are stabilized. This is noteworthy, as this has not been part of the design. However, it can be shown that stability in the sense of Lyapunov with respect to two discrepancies results in stability with respect to the L_p- or the L_∞-norm if the zero dynamics associated with the discrepancy ρ is stable in the sense of the L_p- or L_∞-norm.
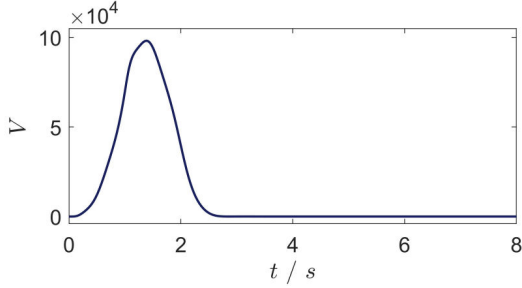
Fig. 3. *Time response of the Lyapunov functional V*
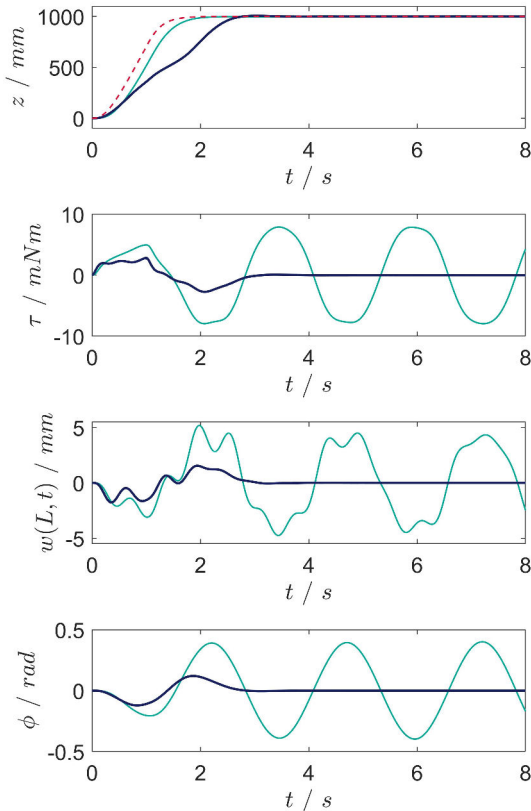
Fig. 4. *Reference tracking applying cascade position control (green) and discrepancy based control (dark blue), reference position (red)*
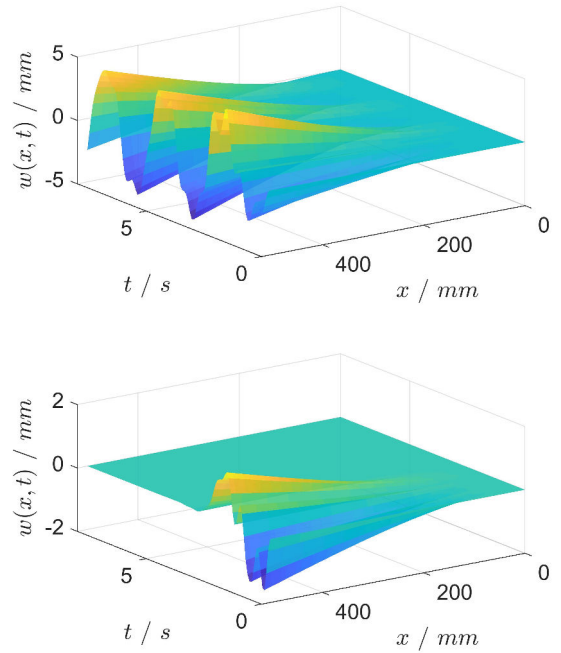
Fig. 5. *Time responses of the distributed state applying cascade position control (upper) and discrepancy based control (lower)*
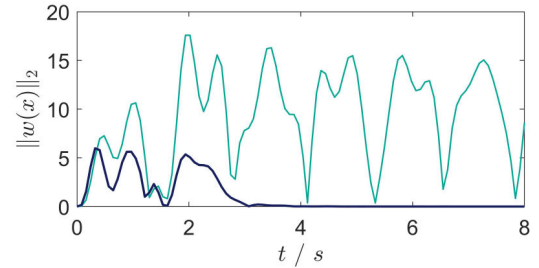
Fig. 6. *L_2-norm with respect to x of the displacement $w(x,t)$ applying cascade position control (green) and discrepancy based control (dark blue)*

Table 1. *Model parameters used for simulation*

Parameter	Value	Parameter	Value
m_t	0.1	m_p	0.18
m_c	0.97	l	$1.5 \cdot 10^3$
μ	0.01	EI	6.9
ρ_c	3	c	5
$k_{p,pos}$	5	$k_{p,vel}$	1.4
$k_{i,vel}$	26	k_{tr}	83.33
k_1	1.3	k_2	1
k_3	0.7	k_4	0.6
a	0.035		

5. CONCLUSION

In this contribution a discrepancy based control approach for underactuated large gantry cranes is proposed. In order to derive a mathematical description of elastic gantry crane dynamics Hamilton's principle has been utilized. From a control point of view, the main objective is to achieve good load positioning and simultaneously to damp load sway and structural oscillation induced by trolley

movements. Due to the distributed nature, strong coupling and only one control handle this is a challenging task. In order to solve this problem a generalized stability theory, stability with respect to two discrepancies and the associated control approach, discrepancy based control, have been successfully applied and verified in simulations.

Future work will be concerned with the robustness analysis of the proposed approach and its practical implementation for further verifications on a laboratory flexible gantry crane.

REFERENCES

Abdel-rahman, E.M., Nayfeh, A.H., and Masoud, Z.N. (2003). Dynamics and Control of Cranes: A Review. *Journal of Vibration and Control*, 9, 863–908.

Abdullahi, A.M., Mohamed, Z., Selamat, H., Pota, H.R., Zainal Abidin, M.S., Ismail, F.S., and Haruna, A. (2018). Adaptive output-based command shaping for sway control of a 3D overhead crane with payload hoisting and wind disturbance. *Mechanical Systems and Signal Processing*, 98, 157–172.

Gašić, V., Zrnić, N., and Milovancevic, M. (2013). Considerations of Various Moving Load Models in Structural Dynamics of Large Gantry Cranes. *FME Transactions*, 41, 311 – 316.

Golovin, I. and Palis, S. (2019). Robust control for active damping of elastic gantry crane vibrations. *Mechanical Systems and Signal Processing*, 121(September 2019), 264–278.

Kimmerle, S.J., Gerdts, M., and Herzog, R. (2018). An Optimal Control Problem for a Rotating Elastic Crane-Trolley-Load System. *IFAC-PapersOnLine*, 51(2), 272 – 277.

Kreuzer, E., Sri Namachchivaya, N., Pick, M.A., and Rapp, C. (2012). Reduced normal form approach to swing control of crane systems: theory and experiments. *Cybernetics and Physics*, 1(1), 42 – 50.

Lu, B., Fang, Y., and Sun, N. (2017). Sliding mode control for underactuated overhead cranes suffering from both matched and unmatched disturbances. *Mechatronics*, 47(September), 116–125.

Miloradovic, N. and Vujanac, R. (2016). Analysis of overhead travelling crane's motion in horizontal plane. *ANNALS of Faculty Engineering Hunedoara - International Journal of Engineering*, XIV, 21 – 24.

Movchan, A.A. (1960). Stability of processes with respect to two metrics. *Journal of Applied Mathematics and Mechanics*, 24(6), 1506–1524.

Palis, S. and Kienle, A. (2012). Discrepancy based control of continuous crystallization. *At - Automatisierungstechnik*, 60(3), 145–154.

Palis, S. and Kienle, A. (2014). Discrepancy based control of particulate processes. *Journal of Process Control*, 24(3), 33–46.

Ramli, L., Mohamed, Z., Abdullahi, A.M., Jaafar, H.I., and Lazim, I.M. (2017). Control strategies for crane systems: A comprehensive review. *Mechanical Systems and Signal Processing*, 95, 1–23.

Ramli, L., Mohamed, Z., and Jaafar, H.I. (2018). A neural network-based input shaping for swing suppression of an overhead crane under payload hoisting and mass variations. *Mechanical Systems and Signal Processing*, 107, 484–501.

Rauscher, F. and Sawodny, O. (2017). An Elastic Jib Model for the Slewing Control of Tower Cranes. *IFAC-PapersOnLine*, 50(1), 9796 – 9801.

Recktenwald, A. (2011). Aktiver Schwingungsdämpfer für Krane. In *19. Internationale Kranfachtagung 2011: Der Kran und sein Umfeld in Industrie und Logistik*, 143 – 146.

Ryu, B.J. and Kong, Y.S. (2012). Dynamic Responses and Active Vibration Control of Beam Structures Under a Travelling Mass. In *Advances on Analysis and Control of Vibrations – Theory and Applications*, 231 – 252.

Schlott, P., Rauscher, F., and Sawodny, O. (2016). Modelling the structural dynamics of a tower crane. *IEEE/ASME International Conference on Advanced Intelligent Mechatronics, AIM*, 763–768.

Sirazetdinov, T.K. (1967). On the theory of stability of processes with distributed parameters. *Journal of Applied Mathematics and Mechanics*, 31(1), 36–47.

Sirazetdinov, T.K. (1987). Stability of Systems with Distributed Parameters (in Russian).

Sowa, L., Piekarska, W., Skrzypczak, T., and Kwiatoń, P. (2018). The effect of the gantry crane beam cross section on the level of generated stresses. *MATEC Web of Conferences*, 157, 1–9.

Sun, N. and Fang, Y. (2012). New energy analytical results for the regulation of underactuated overhead cranes: An end-effector motion-based approach. *IEEE Transactions on Industrial Electronics*, 59(12), 4723–4734.

Sun, N., Wu, Y., Chen, H., and Fang, Y. (2018). An energy-optimal solution for transportation control of cranes with double pendulum dynamics: Design and experiments. *Mechanical Systems and Signal Processing*, 102, 87–101.

Wang, T., Tan, N., Zhou, C., Zhang, C., and Zhi, Y. (2018). A Novel Anti-Swing Positioning Controller for Two Dimensional Bridge Crane via Dynamic Sliding Mode Variable Structure. *Procedia Computer Science*, 131, 626 – 632.

Won, I.s. and Hoang, N.Q. (2018). Comparative study of energy-based control design for overhead cranes. *International Robotics & Automation Journal Research*, 4(3), 197–203.

Xiao, R., Wang, Z., Chen, Z., and Shen, J. (2018). Anti-swing design for overhead crane based on dual sliding mode control. In *Proceedings of the IEEE International Conference on Industrial Technology*, 81–86.

Yazid, E., Parman, S., and Fuad, K. (2011). Vibration analysis of flexible gantry crane system subjected swinging motion of payload. *Journal of Applied Sciences*, 11, 1707 – 1715.

Zhou, M., Sun, N., Chen, H., and Fang, Y. (2017). A Novel Sliding Mode Control Method for Underactuated Overhead Cranes. In *IEEE Proceedings of the Chinese Automation Congress (CAC)*, 4548 – 4552.

Zrnić, N., Petković, Z., and Bošnjak, S. (2005). Automation of ship-to-shore container cranes: A review of state-of-the-art. *FME Transactions*, 33, 111–121.

Zrnić, N., Oguamanam, D., and Bošnjak, S. (2006). Dynamics and modelling of mega quayside container cranes. *FME Transactions*, 34, 193–198.

Adaptive discrepancy based control of continuous fluidized bed spray granulation with external sieve-mill cycle

Stefan Palis

Otto-von-Guericke-Universität,
Universitätsplatz 2, D-39106 Magdeburg, Germany

National Research University "Moscow Power Engineering Institute"
Krasnokazarmennaya 14, 111250 Moscow, Russia

stefan.palis@ovgu.de

Abstract:
In this contribution control design for continuous fluidized bed spray granulation with external sieve-mill cycle in the presence of uncertain mill behavior is presented. It is well-known that this specific particulate process becomes unstable in certain parameter regions. Being described by a population balance model, a nonlinear partial integro-differential equation, control design is challenging. To overcome this problem control design is studied in terms of a generalized stability theory, i.e. stability with respect to two discrepancies. The resulting discrepancy based control can be extended by additional parameter adaptation to cope with the present uncertainties.

1. INTRODUCTION

Granulation is an important process class for transforming a liquid product into its final solid form. It is often applied in food production or chemical and pharamaceutical industries. From a production point of view, granulation in fluidized beds is, due to the increased active surface and particle mixing, often attractive. Therefore, an initially solid particle bed is fluidized by a gas or liquid stream.
From an operational point of view, it is however well known that different continuous fluidized bed spray granulation configurations may become unstable [2, 3, 13, 14, 15]. Here, instability often results in the occurrence of non-linear limit cycles in dependence of the chosen operation conditions and the specific process configuration. Therefore, stabilizing control is needed and has been studied to some extend [4, 5, 6, 7, 8]. As all controllers depend on a parametrized plant model, parameter uncertainty or variation may result in performance deterioration or even loss of stability. In order to cope with these uncertainties in this contribution adaptive discrepancy based control will be studied for a continuous fluidized bed spray granulation with external sieve-mill cycle, where the particle size distribution generated from the mill is assumed to be unknown.

2. CONTINUOUS FLUIDIZED BED SPRAY GRANULATION

Applying an air stream with predefined properties, e.g. flow rate, temperature and humidity, to particles inside the granulation chamber a fluidized bed is formed. Particles in this fluidized bed are then coated by a liquid, which is injected from a nozzle and settles on these particles. Due to the increased temperature and low humidity of the supplied air the liquid fraction is evaporated and the remaining solid fraction forms a new solid layer on the particle surface. This continuous process results thus in a particle size increase, which can be described for the particle ensemble by

$$G = \frac{2\dot{m}_e}{\pi \mu_2}. \tag{1}$$

Here, $\dot{m}_e$ is the effective solid mass injected into the process chamber and μ_2 is the second moment of the particle size distribution $\mu_2 = \int_0^\infty L^2 n dL$, which correlates with the overall surface of the particle bed [1].
In a continuous fluidized bed spray granulation, particles are continuously removed with a drain K.

$$\dot{n}_{out} = Kn \tag{2}$$

This particle flux is then fed to two sieves and results in three particle fractions: product $\dot{n}_p$, fines $\dot{n}_f$ and oversized $\dot{n}_o$. The fines and oversize fraction consist of particles being smaller or bigger than the product specification.

$$\dot{n}_p = T_2(L)(1 - T_1(L))\dot{n}_{out} \tag{3}$$

$$\dot{n}_f = (1 - T_2(L))(1 - T_1(L))\dot{n}_{out} \tag{4}$$

$$\dot{n}_o = T_1(L)\dot{n}_{out} \tag{5}$$

Here, $T_1(L)$ and $T_2(L)$ are the associated screening functions depicted in Fig. 1.

$$T_{1,2}(L; \mu, \sigma) = \frac{\int_0^L \exp\left(\frac{-(\hat{L}-\mu)^2}{4\sigma^2}\right) d\hat{L}}{\int_0^\infty \exp\left(\frac{-(\hat{L}-\mu)^2}{4\sigma^2}\right) d\hat{L}} \tag{6}$$

Whereas the product fraction is removed from the process, the fines and the oversize fraction remain in the process. The fines fraction is directly fed back. The oversize fraction is first fed to a mill, where it is grinded, and then the milled particles are fed back into the process chamber, where they serve as new nuclei for the particle population. The overall
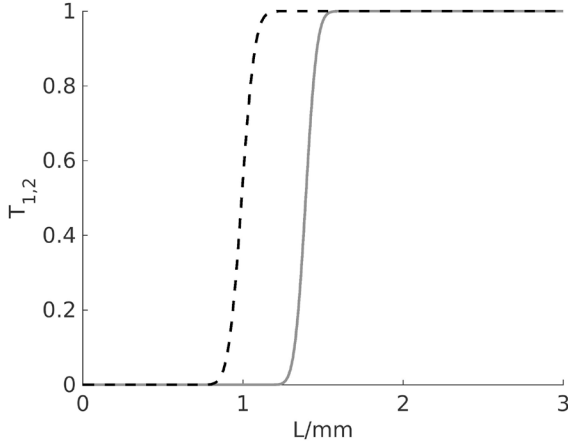
Fig. 1. Screening functions T_1 (gray) and T_2 (black dotted)

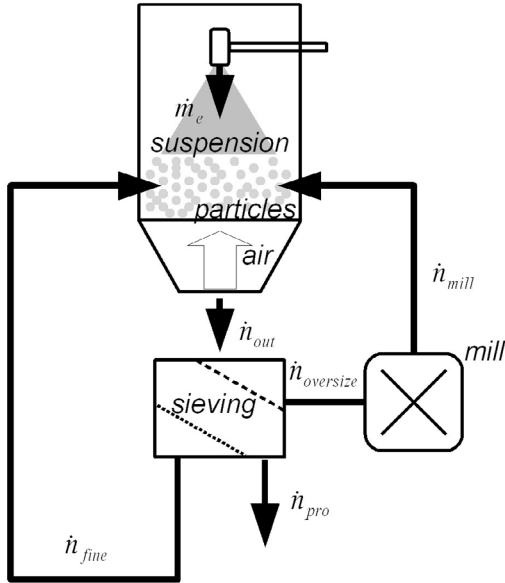process scheme is depicted in Fig. 2.

Fig. 2. Process scheme

From practical investigations it is known, that the particle size distribution generated by the mill is typically tri-modal (Fig. 3) [12], where the proportion of each distribution depends on the particle properties and the specific mill power P_{mill}.

It can be assumed that the mill is mass conserving, i.e. the third moment of the oversize fraction is equal to the third moment of the particle distribution generated by the mill. The mill model is hence given by

$$\dot{n}_m = \sum_{i=1}^{3} a_i \varphi_i(L) \int_0^\infty L^3 \dot{n}_o dL \qquad (7)$$

where a_i are the weights of the distributions $\varphi_i(L)$ and $\int_0^\infty L^3 \dot{n}_o dL$ is the third moment of the oversize fraction [13]. In order to ensure the aforementioned mass conserva-
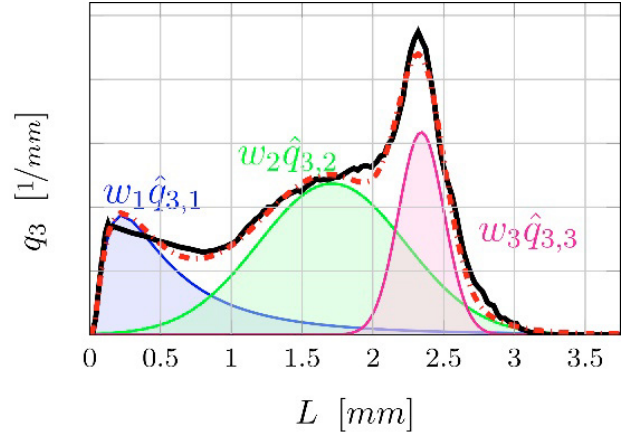
Fig. 3. Particle size distribution of milled particles [12]

tion an additional constraint on the distribution weights has to hold.

$$\int_0^\infty L^3 \sum_{i=1}^{3} a_i \varphi_i(L) dL = 1 \qquad (8)$$

Therefore, only two of the three parameters are independent of each other. The third coefficient a_3 can thus be calculated from a_1 and a_2.

$$a_3 = \frac{1 - \int_0^\infty L^3 \sum_{i=1}^{2} a_i \varphi_i(L) dL}{\int_0^\infty L^3 \varphi_3(L) dL} \qquad (9)$$

This yields an unconstrained mill model with two independent parameters a_1 and a_2.

$$\dot{n}_m = \left[\sum_{i=1}^{2} a_i \left(\varphi_i(L) - \frac{\int_0^\infty L^3 \varphi_i(L) dL}{\int_0^\infty L^3 \varphi_3(L) dL} \varphi_3(L) \right) + \dots \right.$$
$$\left. \dots + \frac{\varphi_3(L)}{\int_0^\infty L^3 \varphi_3(L) dL} \right] \int_0^\infty L^3 \dot{n}_o dL \qquad (10)$$

$$= \left(\sum_{i=1}^{2} a_i \phi_i(L) + \bar{\varphi}_3(L) \right) \int_0^\infty L^3 \dot{n}_o dL \qquad (11)$$

where

$$\phi_i(L) = \varphi_i(L) - \frac{\int_0^\infty L^3 \varphi_i(L) dL}{\int_0^\infty L^3 \varphi_3(L) dL} \varphi_3(L), \qquad (12)$$

$$\bar{\varphi}_3(L) = \frac{\varphi_3(L)}{\int_0^\infty L^3 \varphi_3(L) dL}. \qquad (13)$$

From a practical point of view, the knowledge of the weights a_i of each distribution is of utmost importance for control. However, offline identification using individual experiments is very expensive and raises many uncertainties. In addition, the mill behavior changes during the process with the particle properties at hand. Therefore, in this contribution it will be assumed that the weights a_i of each distribution are unknown. To describe the process, the following population balance model, consisting of the particle fluxes due to product particle withdrawal $KT_1(1 - T_2)n$, particle growth and the reflux from the mill, can be used.

$$\frac{\partial n}{\partial t} = -G\frac{\partial n}{\partial L} - KT_1(1-T_2)n - KT_1T_2n + \dots$$

$$\dots + \left(\sum_{i=1}^{2} a_i\phi_i + \bar{\varphi}_3\right)\int_0^\infty L^3\dot{n}_o dL \qquad (14)$$

It is well known [2, 3, 14] that the given process configuration becomes unstable for sufficiently high mill power and a resulting reduced mill grade. This loss of stability is connected with the occurrence of a stable limit cycle depicted in Fig. 4. In order to stabilize the particle size
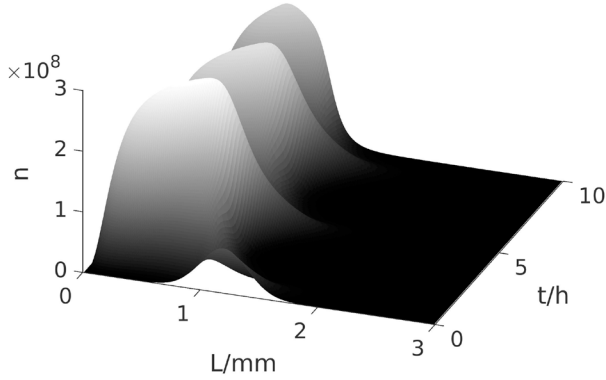

Fig. 4. Limit cycle of the particle size distribution

distribution in this contribution discrepancy based control, i.e. control based on a generalized stability theory, will be applied using the drain K as a manipulated variable. It should be mentioned, that this choice differs from earlier investigations, where the drain K has be used to implement a bed mass controller and the mill grade μ_M has been used to stabilize the particle size distribution. In addition, the mill behavior in this contribution is described by a tri-modal distribution instead of a uni-modal normal distribution with known parameters. As has been stated earlier the weights of the fractions generated by the mill are often unknown or connected with great uncertainty. Therefore, the discrepancy based control law will be extended by appropriate adaptation mechanisms.

3. ADAPTIVE DISCREPANCY BASED CONTROL

From a mathematical point of view, the presented population balance model is an unstable nonlinear partial-integro differential equation with in-domain actuation. Therefore, stabilizing control design is a challenging problem. However, as has been shown in previous contributions [4, 5, 7] this type of problems can be handled by introducing a generalized stability notion, i.e. stability with respect to two distance measures, the discrepancies [9, 10, 11]. In the following it is assumed, that the process $\varphi(.,t)$ is a solution of the distributed parameter system and $\varphi_0 = 0$ an equilibrium of the system.

Definition 1. Discrepancy

A discrepancy is a real valued functional $\rho = \rho[\varphi(.,t),t]$ with the following properties

(1) $\rho(\varphi,t) \geq 0$

(2) $\rho(0,t) = 0$
(3) for an arbitrary process $\varphi = \varphi(.,t)$ the discrepancy $\rho(\varphi(.,t),t)$ is continuous with respect to t.
(4) introducing a second discrepancy $\rho_0(\varphi)$ with $\rho_0(\varphi) \geq 0$ and $\rho_0(0) = 0$. Than the discrepancy $\rho(\varphi(.,t),t)$ is continuous at time $t = t_0$ with respect to ρ_0 at $\rho_0 = 0$, if for every $\varepsilon > 0$ and $t_0 > 0$ there exists a $\delta(\varepsilon,t_0) > 0$, such that from $\rho_0 \leq \delta(\varepsilon,t_0)$ follows $\rho < \varepsilon$.

Definition 2. Stability with respect to two discrepancies ρ and ρ_0

The equilibrium $\varphi_0 = 0$ is stable in the sense of Lyapunov with respect to the two discrepancies ρ and ρ_0 for all $t \geq t_0$ if for every $\varepsilon > 0$ and $t_0 \geq 0$ there exists a $\delta = \delta(\varepsilon,t_0) > 0$, such that for every process $\varphi(.,t)$ with $\rho_0 < \delta(\varepsilon,t_0)$ follows $\rho < \varepsilon$ for all $t \geq t_0$. If in addition $\lim_{t\to\infty}\rho = 0$, than the equilibrium φ_0 is called asymptotically stable in the sense of Lyapunov with respect to the two discrepancies ρ and ρ_0.

Theorem 3. The process φ with the equilibrium $\varphi_0 = 0$ is asymptotically stable with respect to the two discrepancies ρ and ρ_0 if and only if there exists a functional $V = V[\varphi,t]$ positive definite with respect to the discrepancy ρ, continuous at time $t = t_0$ with respect to ρ_0 at $\rho_0 = 0$ and not increasing along the process φ, i.e. $\dot{V} \leq 0$, with $\lim_{t\to\infty} V = 0$.

In order to derive a stabilizing controller the above presented stability concept is applied. Here, we choose the error e and the discrepancy ρ as follows

$$e = \int_0^\infty L^2(n_d - n)dL, \qquad (15)$$

$$\rho = \frac{1}{2}\left(\int_0^\infty L^2(n_d - n)dL\right)^2. \qquad (16)$$

Obviously, the above requirements on a discrepancy are met. In order to guarantee continuity at time $t = t_0$ at $t_0 = 0$ the second discrepancy ρ_0 is simply chosen as $\rho_0 = \rho(t = 0)$.

In order to derive a control law, guaranteeing stability with respect to the discrepancies ρ and ρ_0, the following candidate Lyapunov functional is introduced

$$V = \frac{1}{2}\left(\int_0^\infty L^2(n_d - n)dL\right)^2. \qquad (17)$$

To account for the aforementioned uncertainty in the unknown parameters a_1 and a_2 this candidate Lyapunov functional is extended by a term, which takes the estimation errors $\tilde{a}_{1,2} = \hat{a}_{1,2} - a_{1,2}$ into account.

$$V = \frac{1}{2}\left(\int_0^\infty L^2(n_d - n)dL\right)^2 + \sum_{i=1}^{2}\frac{1}{2\gamma}\tilde{a}_i^2 \qquad (18)$$

This approach, i.e. Lyapunov redesign, is well known for finite dimensional systems. In order to achieve stability in the sense described above the control variable has to be chosen such that the time derivative of V along the system trajectories (14) is negative definite for all times and vanishs only for $V = 0$.

$$\dot{V} = e \int_0^\infty L^2 G \frac{\partial n}{\partial L} + K(T_{prod} + T_1)ndL$$

$$\dots + eK \int_0^\infty L^2 \left(\sum_{i=1}^2 a_i \phi_i + \bar{\varphi}_3 \right) dL \int_0^\infty L^3 T_1 ndL$$

$$\dots + \sum_{i=1}^2 \tilde{a}_i \frac{\dot{\hat{a}}_i}{\gamma} \qquad (19)$$

In the absence of any parameter uncertainty, i.e. $\hat{a} = a$, the following certainty equivalence law for the withdraw rate could be chosen in order to achieve exponential convergence of the proposed Lyapunov functional, i.e. $\dot{V} = -2cV$ with $c > 0$.

$$K = - \left[\int_0^\infty L^2 G \frac{\partial n}{\partial L} dL + ce \right] \left[\int_0^\infty L^2 (T_{prod} + T_1)ndL \right.$$

$$\left. \dots + \int_0^\infty L^2 \left(\sum_{i=1}^2 \hat{a}_i \phi_i + \bar{\varphi}_3 \right) dL \int_0^\infty L^3 T_1 ndL \right]^{-1} (20)$$

Inserting the certainty equivalence law (20) into (19) and using the definition of the parameter estimation error $\tilde{a}_i$, i.e. $a_i = \hat{a}_i - \tilde{a}_i$, results after some calculation in

$$\dot{V} = -2cV - \sum_{i=1}^2 \tilde{a}_i \left(eK \int_0^\infty L^2 \phi_i dL \int_0^\infty L^3 T_1 ndL - \frac{\dot{\hat{a}}_i}{\gamma} \right). \qquad (21)$$

Here, the second term can be rendered zero by chosing the following parameter adaptation laws

$$\dot{\hat{a}}_i = \gamma eK \int_0^\infty L^2 \phi_i dL \int_0^\infty L^3 T_1 ndL \qquad (22)$$

Therefore, the designed certainty equivalence control law in combination with the adaption law guarantees stability with respect to the two discrepancies ρ and ρ_0. As has been shown in [7] this generalized stability results in pointwise stability, i.e. stability of the particle size distribution with respect to the L_∞-norm, if the zero dynamics associated with the discrepancy ρ are stable.

4. RESULTS

For numerical simulation the population balance model has been discretized along the property coordinate. Here, a 1st order finite volume scheme with 150 grid points has been applied. In order to verify the proposed control scheme the process is started in the region of instability. Therefore, the uncontrolled process would exhibit self-sustained oscillations in the particle size distribution. For the unknown mill parameters a_1 and a_2 an initial misfit of 10% has been assumed.

As can be seen in Fig. 5 the proposed discrepancy based controller stabilizes the particle size distribution. The parameter estimates $\hat{a}_1$ and $\hat{a}_2$ slowly converge towards values, which are close to the unknown parameter values. As can be seen from Fig. 7 and Fig. 9 the second moment of the particle size distribution converges exponentially towards its desired value. The third moment shown in Fig. 8, being correlated with the overall bed mass, is also stable and stays within a reasonable range. As can be seen from
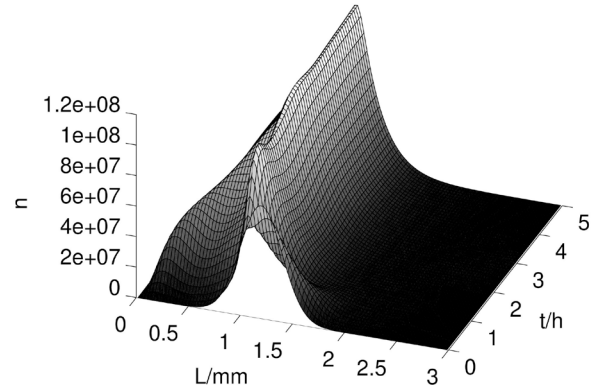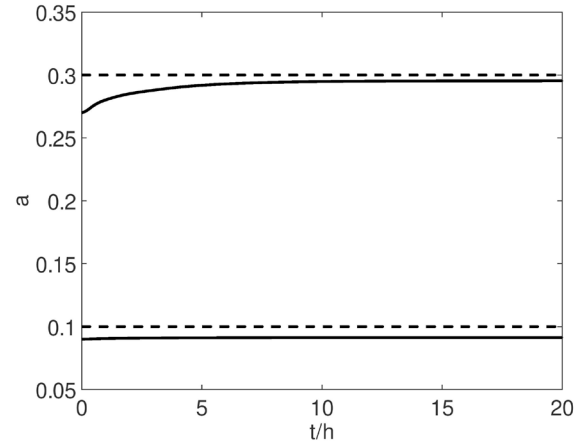

Fig. 5. Particle size distribution n

Fig. 6. Mill parameters a_1 and a_2 (black dotted) and their estimates $\hat{a}_1$ and $\hat{a}_2$
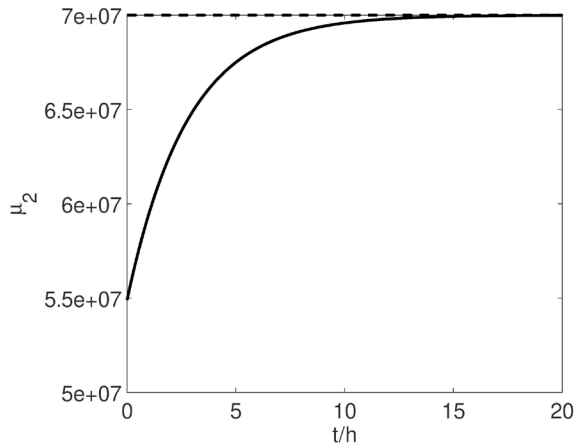

Fig. 7. Second moment of the particle size distribution and desired second moment (dotted black)

the particle size distribution depicted in Fig. 5 and the L_2-norm of the deviation between desired particle size distribution and the real particle size distribution (Fig. 10), the proposed adaptive discrepancy based control law achieves asymptotic stability in the desired classical sense.
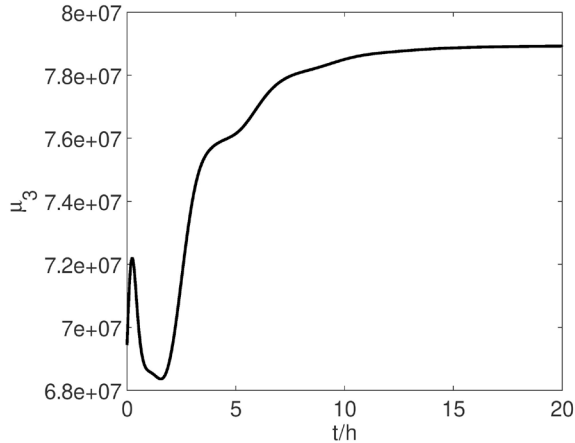
Stefan Palis / IFAC PapersOnLine 52-2 (2019) 218–222

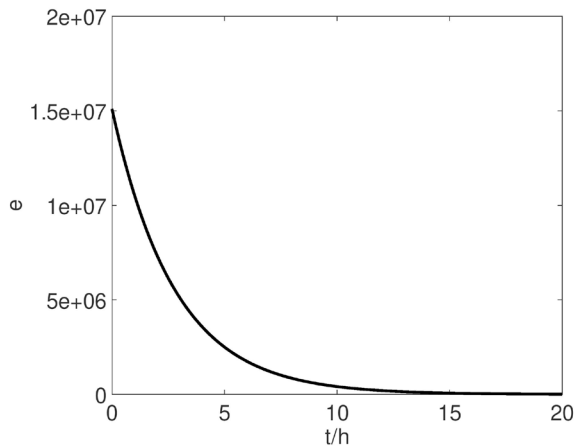Fig. 8. Third moment of the particle size distribution

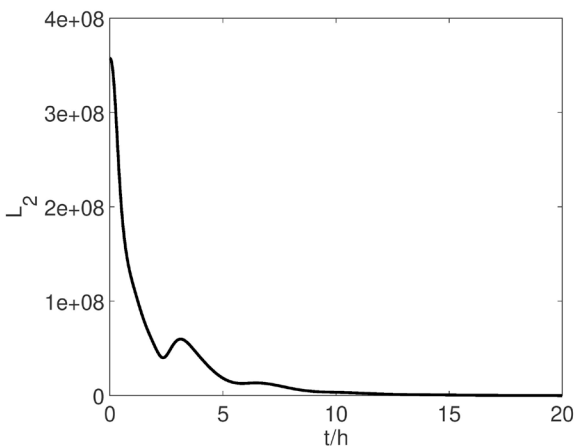Fig. 9. Error e of the particle size distribution

Fig. 10. L_2-norm of the error between desired and actual particle size distribution

5. CONCLUSION

In this contribution adaptive discrepancy based control of fluidized bed spray granulation with external sieve-mill cycle has been studied. It has been shown that the proposed control law consisting of a certainty equivalence law and two adaption laws allows a stabilization of the

unstable particulate process even in the presence of unknown parameters. Future work will be concerned with robustness with respect to measurement noise and real plant experiments.

REFERENCES

[1] L. Mörl, M. Mittelstrass, J. Sachse, Zum Kugelwachstum bei der Wirbelschichttrocknung von Lösungen oder Suspensionen, Chem. Techn. 29, 1977, Heft 10, pp. 540-542.

[2] M. Schmidt, C. Rieck, A. Bück and E. Tsotsas, Experimental investigation of process stability of continuous spray fluidized bed layering with external product separation, Chemical Engineering Science, 2015, pp. 466-475.

[3] C. Dreyschultze, C. Neugebauer, S. Palis, A. Bück, E. Tsotsas, S. Heinrich and A. Kienle, Influence of zone formation on stability of continuous fluidized bed layering granulation with external product classification, Particuology, 2015, pp. 1-7.

[4] S. Palis & A. Kienle, Stabilization of continuous fluidized bed spray granulation - a Lyapunov approach, 8th IFAC Symposium on Nonlinear Control Systems - NOLCOS, 2010.

[5] S. Palis & A. Kienle, Stabilization of continuous fluidized bed spray granulation with external product classification, Chem. Eng. Sci. 70, 2012, pp. 200-209.

[6] S. Palis & A. Kienle, H_∞ loop shaping control for continuous fluidized bed spray granulation with internal product classification, Industrial & Engineering Chemistry Research, 2013, pp. 408-420.

[7] S. Palis and A. Kienle, Discrepancy based control of particulate processes, Journal of Process Control, 2014, pp. 33-46.

[8] S. Palis, Non-identifier-based adaptive control of continuous fluidized bed spray granulation, Journal of Process Control 71, 2018, pp. 46-51.

[9] A.A. Movchan, Stability of processes with respect to two metrics, Journal of Applied Mathematics and Mechanics, 1960, 24, pp. 1506-1524.

[10] T. Sirasetdinov, Stability of systems with distributed parameters, 1987.

[11] A. Martynjuk & R. Gutovski, Integral inequalities and stability of motion, Naukowa Dumka, 1979.

[12] S. Palis & C. Neugebauer & A. Bück & S. Heinrich & E. Tsotsas & A. Kienle, Control of multi-chamber continuous fluidized bed spray granulation, International Congress on Particle Technology - PARTEC, 2016.

[13] C. Neugebauer & S. Palis & A. Bück & E. Tsotsas & S. Heinrich & A. Kienle, A dynamic two-zone model of continuous fluidized bed layering granulation with internal product classification, Particuology 31, 2017, pp. 8-14.

[14] A. Bück & C. Neugebauer & K. Meyer & S. Palis & E. Diez & A. Kienle & S. Heinrich & E. Tsotsas, Influence of operation parameters on process stability in continuous fluidised bed layering with external product classification, Powder Technology 300, 2016, pp. 37-45.

[15] C. Neugebauer & A. Bück & S. Palis & L. Mielke & E. Tsotsas & A. Kienle, Influence of thermal conditions on particle properties in fluidized bed layering granulation, 2018, pp. 1-17.

Lyapunov-based online parameter estimation in continuous fluidized bed spray agglomeration processes

Ievgen Golovin [*,★] **Eric Otto** [*] **Robert Dürr** [**] **Stefan Palis** [*,***]
Achim Kienle [*,**]

* *Otto-von-Guericke University, D-39106 Magdeburg, Germany*
** *Max-Planck-Institute for Dynamics of Complex Technical Systems,
D-39106 Magdeburg, Germany*
*** *National Research University "Moscow Power Engineering
Institute", Moscow, Russia*

Abstract: Fluidized bed spray agglomeration is a particle formation process in many industrial applications, e.g. pharmaceutical and food processing. The properties of the formed agglomerates, like characteristic volume, significantly affect the product quality and can be affected by variation of certain operating parameters. Mathematical modeling not only provides an abstract characterization of the effects of those on the product properties but also supports thorough understanding of the underlying physical and chemical mechanisms. Moreover, it enables application of advanced process analysis, control and intensification schemes. As characteristic properties underlie variations within the ensemble of agglomerates the process can be described as a distributed parameter system, where the resulting model equations are partial differential equations. Adaption to experimental data requires the solution of inverse problems, which tend to be ill-conditioned. As an alternative approach, in this contribution an adaptive identification procedure is presented. Therefore, a modified plant model is run in parallel to the process and adaption rates are chosen based on a Lyapunov-function. The approach is validated in a parametric study for two scenarios: In the first, it is assumed that the structure of the dynamics is fully known, while in the second, this assumption does not hold. It is shown that the proposed approach allows to reconstruct unknown kinetic information of the process dynamics.

Keywords: Adaptive identification, distributed parameter systems, population balance equations, partial differential equations

1. INTRODUCTION

Agglomeration is a particle formation process in which at least two primary particles are combined to form a new one. This principle is often used in many industries, e.g. pharmaceutical manufacturing and food processing. The properties of the formed agglomerates, e.g. size, shape and porosity, significantly affect its end-use properties, e.g re-hydration behavior of food powders, processability and storeability. In the industrial practice, agglomerates are often formed in drums, pans or fluidized beds. The advantages of the latter include good mixing and high heat and mass transfer between particles, liquid and gas phase. Compared to widely applied batch processes, the additional benefits of operating in continuous mode are constant product quality and higher flow rates which are more attractive for chemical, food and pharmaceutical industries. For those reasons focus in this contribution is on continuous fluidized bed spray agglomeration, which was not in the focus of research efforts so far.

The process scheme is shown in Fig. 1: Particles in the the chamber are fluidized by a stream of hot air from the bottom, liquid binder is sprayed on the particles in the

form of small droplets to make them wet and sticky. Due to random collisions liquid bridges between particles are formed. These can become solid by drying and thereby agglomerate particles consisting of different numbers of individuals are formed. The formation of the agglomerates and thereby the product properties can be influenced by variation of different operating parameters and process configurations, like feed rate, binder concentration and temperature of the drying/fluidizing air.

Parameterization of process models is an important part within the interplay of process analysis, model-based control and process intensification. It is well-known that the individual properties, like characteristic size or porosity, differ from particle to particle in the studied process. The emerging heterogeneity significantly affects the overall product properties. It can be accounted for in the framework of population balance modeling (PBM) (Ramkrishna, 2000). The resulting model equations generally represent nonlinear integro partial differential equations, which are usually discretized and numerically solved with established techniques (see e.g. Kumar et al. (2006), Bück et al. (2012) and the references therein). Commonly, reliable first principles models that include detailed models on the underlying kinetic processes on the microscopic
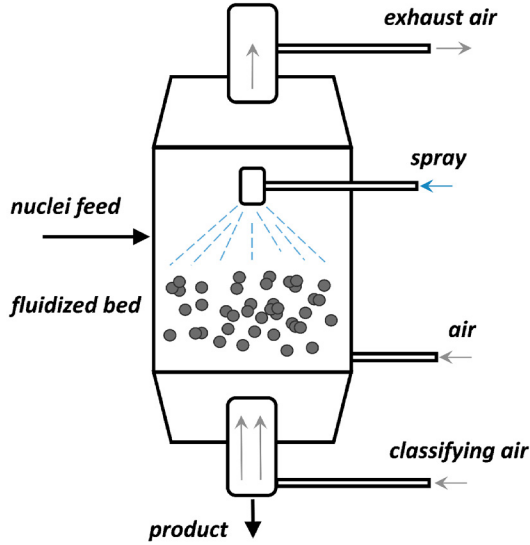
Fig. 1. *Schematic representation of fluidized bed spray agglomeration process*

scale are rarely found and thus kinetics are described in a more mechanistic fashion. This requires the estimation of unknown parameters from experimental data. The resulting inverse problems often tend to be ill-conditioned (Chakraborty et al., 2015). In order to overcome these problems a parameter identification based on the nonlinear optimization (Golovin et al. (2018)) as well as an online parameter estimation approach featuring a parallel model can be applied (Dürr et al., 2015; Palis and Kienle, 2013, 2017).

In this contribution, a new adaptive online estimation approach for fluidized bed spray agglomeration processes is developed. In particular, focus is on identification of the agglomeration kernel containing information on the effects of process conditions and characteristic agglomerate size on formation of new agglomerates.

Section 2 presents the modeling of the fluidized bed spray agglomeration process. The proposed Lyapunov-based adaptive approach applied for the agglomeration kernel estimation is described in section 3. In section 4 the presented method is validated within two simulation studies.

2. POPULATION BALANCE MODELING OF FLUIDIZED BED SPRAY AGGLOMERATION

In particle formation processes, significant heterogeneities with respect to the individual particle properties like size or shape emerge. Population balance modeling represents an established concept to describe such distributed parameter systems. Instead of describing a large number of particles and their interactions, PBM describes the dynamics of the particles via the number density distribution function (NDF) $n(t, \mathbf{x})$ representing information of the number of particles within an infinitesimal section of the particle property state space $\mathbf{x} \in \mathbb{R}^{N_x}$. In the following, it is assumed that individual particles do only differ w.r.t. characteristic volume v such that $\mathbf{x} = v$ and $N_x = 1$. In course of the process, the particle distribution underlies change, which is given by the solution of the so called population balance equation (PBE)

$$\frac{\partial n(t, v)}{\partial t} = \dot{n}_{\text{feed}}(t, v) - \dot{n}_{\text{prod}}(t, v) + \dot{n}_{\text{agg}}(t, v). \quad (1)$$

The corresponding initial NDF is given as

$$n(0, v) = N_\Sigma \frac{\exp\left(\frac{-(v-\mu_1)^2}{2\sigma_1^2}\right)}{\int_0^\infty \exp\left(\frac{-(v-\mu_1)^2}{2\sigma_1^2}\right) dv}, \quad (2)$$

where N_Σ is the mass normalizing parameter.

The left hand side of (1) accounts for temporal evolution while the first two elements of the right hand side describe feeding new seed particles to and removal of the desired product from the fluidized bed. Both are assumed to be known and given as

$$\dot{n}_{\text{prod}}(t, v) = N_{out} K(v) n(t, v), \quad (3)$$

$$\dot{n}_{\text{feed}}(t, v) = N_{in} \frac{\exp\left(\frac{-(v-\mu_2)^2}{2\sigma_2^2}\right)}{\int_0^\infty \exp\left(\frac{-(v-\mu_2)^2}{2\sigma_2^2}\right) dv}, \quad (4)$$

where N_{out} and N_{in} denote the time-invariant removal and feed rates of particles, respectively while $K(v)$ represents the separation function. The last element of the right hand side denotes the formation of new particles of volume v by agglomeration of two particles with volumes u and $v - u$

$$\dot{n}_{agg}(t, v) = \dot{n}_{agg}^+(t, v) - \dot{n}_{agg}^-(t, v)$$

$$= \frac{1}{2} \int_0^v \beta(t, u, v - u) n(t, u) n(t, v - u) du$$

$$- \int_0^\infty \beta(t, u, v) n(t, v) n(t, u) du. \quad (5)$$

Here, the agglomeration kernel $\beta(t, u, v)$ contains information about the probability of forming a new agglomerate and is usually separated in volume and time-dependent parts

$$\beta(t, v, u) = \beta_0(t) \beta(v, u). \quad (6)$$

For modeling of the volume-dependent part, called coalescence kernel, different approaches exist (see e.g. (Eisenschmidt et al., 2017) and (Le Borne et al., 2015)). Two possibilities are the Brownian kernel, which is derived from the Brownian motion,

$$\beta(u, v) = (u^{1/3} + v^{1/3})(u^{-1/3} + v^{-1/3}) \quad (7)$$

or a more general kernel structure approximation using a Laurent-polynomial

$$\beta(u, v) = \sum_{i=-N_L}^{N_L} \sum_{j=-N_L}^{N_L} k_{i,j} v^i u^j, \quad (8)$$

where $N_L \in \mathbb{N}$ denotes the rank of the polynomial and $k_{i,j}$ are the associated polynomial coefficients.

In contrast, the time dependent part $\beta_0(t)$, also called the agglomeration efficiency, mirrors the effects of the process conditions and operating parameters and is mostly not known beforehand. Moreover, it is frequently assumed that the time dependency of the agglomeration efficiency can be neglected, such that $\beta_0(t) = const$.

3. LYAPUNOV-BASED ADAPTIVE IDENTIFICATION

In this section the online parameter identification of the agglomeration kernel is introduced. In order to derive an adaptation law for the unknown parameters the Lyapunov-based approach is applied (Krstic, 2006; Palis and Kienle,
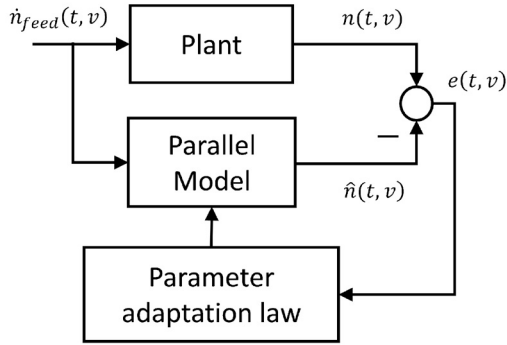
Fig. 2. *Adaptive online parameter identification scheme*

2013; Dürr et al., 2015; Palis and Kienle, 2017). The parameter identification scheme consisting of a modified plant model, which runs parallel to the actual plant and the parameter adaptation algorithm is represented in Fig. 2.

In this work two scenarios for the parameter estimation are studied. In the first scenario, the modified plant model includes the volume-dependent Brownian kernel function with unknown agglomeration efficiency β_0, which should be estimated. In the second scenario, it is considered that the structure of the coalescence kernel $\beta(u,v)$ is also unknown. In order to approximate it, the Laurent polynomial with its unknown coefficients is included in the modified plant model.

3.1 Estimation of the agglomeration efficiency

In the first scenario, the estimation of the agglomeration efficiency β_0 is considered. For this reason, the modified parallel plant model with an additional observer term can be represented as follows

$$\frac{\partial \hat{n}(t,v)}{\partial t} = \dot{n}_{\text{feed}}(t,v) - \dot{n}_{\text{prod}}(t,v) + \dot{n}_{\text{agg}}(t,v)$$
$$+ l\,(\hat{n} - n)\,, \tag{9}$$

$$\dot{n}_{agg}(t,v) = \frac{1}{2}\int_0^v \hat{\beta}_0 \beta(u,v-u)n(t,u)n(t,v-u)\mathrm{d}u$$
$$- \int_0^\infty \hat{\beta}_0 \beta(u,v)n(t,v)n(t,u)\mathrm{d}u\,, \tag{10}$$

where $\hat{n}$ and $\hat{\beta}_0$ are the particle size distribution and the agglomeration efficiency estimated from the modified plant model and l is an additional tuning parameter.

The related estimation errors are given by

$$e = \hat{n} - n\,, \qquad \tilde{\beta}_0 = \hat{\beta}_0 - \beta_0\,. \tag{11}$$

Taking into account the plant model equations (1), (5) and the modified parallel model equations (9), the error dynamics can be derived as

$$\frac{\partial e}{\partial t} = \frac{1}{2}\int_0^v \tilde{\beta}_0 \beta(u,v-u)n(t,u)n(t,v-u)\mathrm{d}u$$
$$- \int_0^\infty \tilde{\beta}_0 \beta(u,v)n(t,v)n(t,u)\mathrm{d}u + l\,e\,. \tag{12}$$

For the adaptation of the model parameters the following Lyapunov functional is chosen

$$V = \frac{1}{2}\int_0^\infty e^2 \mathrm{d}v + \frac{1}{2\gamma}\tilde{\beta}_0^2\,, \tag{13}$$

where γ is a positive real tuning parameter. It can be easily seen that the Lyapunov functional V is positive

definite and it vanishes if the considered estimation errors (11) are zeros. According to the Lyapunov stability theory the stability of the proposed identification scheme can be achieved if the first time derivative of the Lyapunov functional is negative semi-definite along the state trajectories. This time derivative can be derived as follows

$$\frac{\mathrm{d}V}{\mathrm{d}t} = \int_0^\infty l\,e^2 \mathrm{d}v$$
$$+ \int_0^\infty e\Big(\frac{1}{2}\int_0^v \tilde{\beta}_0 \beta(u,v-u)n(t,u)n(t,v-u)\mathrm{d}u$$
$$- \int_0^\infty \tilde{\beta}_0 \beta(u,v)n(t,v)n(t,u)\mathrm{d}u\Big)\mathrm{d}v$$
$$+ \frac{1}{\gamma}\tilde{\beta}_0 \dot{\hat{\beta}}_0\,. \tag{14}$$

Therefore, choosing the adaptation law $\dot{\hat{\beta}}_0$ as follows

$$\dot{\hat{\beta}}_0 = -\gamma \int_0^\infty e\Big(\frac{1}{2}\int_0^v \beta(u,v-u)n(t,u)n(t,v-u)\mathrm{d}u$$
$$- \int_0^\infty \beta(u,v)n(t,v)n(t,u)\mathrm{d}u\Big)\mathrm{d}v \tag{15}$$

yields in the negative semi-definiteness of the time derivative of V

$$\frac{\mathrm{d}V}{\mathrm{d}t} = \int_0^\infty l\,e^2 \mathrm{d}v \tag{16}$$

for the observer parameter $l < 0$.

3.2 Estimation of the Laurent polynomial

In the second scenario, the estimation of the volume-dependent agglomeration kernel function is proposed. In general, the aggregation kernel $\beta(u,v)$ is a non-negative symmetric function of two variables. In order to approximate such types of functions, Laurent polynomials (8) can be used (Eisenschmidt et al., 2017). A reasonable approximation can be achieved with the rank $N_L = 1$ resulting in

$$\beta_{est}(u,v) = k_1 + k_2\,v^{-1}u^{-1} + k_3\,vu + k_4\,(v^{-1} + u^{-1})$$
$$+ k_5\,(vu^{-1} + v^{-1}u) + k_6\,(v + u)\,. \tag{17}$$

Here, k_1 to k_6 are unknown polynomial coefficients that should be identified. The modified parallel model with the polynomial is given by

$$\frac{\partial \hat{n}(t,v)}{\partial t} = \dot{n}_{\text{feed}}(t,v) - \dot{n}_{\text{prod}}(t,v) + \dot{n}_{\text{agg}}(t,v)$$
$$+ l\,(\hat{n} - n)\,, \tag{18}$$

where

$$\dot{n}_{agg}(t,v) = \frac{1}{2}\int_0^v \beta_{est}(u,v-u)n(t,u)n(t,v-u)\mathrm{d}u$$
$$- \int_0^\infty \beta_{est}(u,v)n(t,v)n(t,u)\mathrm{d}u\,. \tag{19}$$

Analogous to the aforementioned design procedure, the adaptation law for the polynomial coefficients can be derived as

$$\dot{\hat{k}}_i = -\gamma_i \int_0^\infty e\Big(\frac{1}{2}\int_0^v f_i(u,v-u)n(t,u)n(t,v-u)\mathrm{d}u$$
$$- \int_0^\infty f_i(u,v)n(t,v)n(t,u)\mathrm{d}u\Big)\mathrm{d}v\,, \tag{20}$$

where $f_i(u,v)$ is the volume dependent part associated with i-th coefficient of (17).
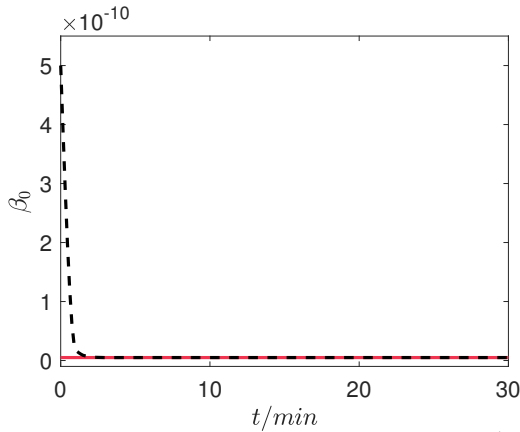
Fig. 3. *Convergence of the unknown parameter $\hat{\beta}_0$ (dotted, black) to the actual parameter β_0 (solid, red)*
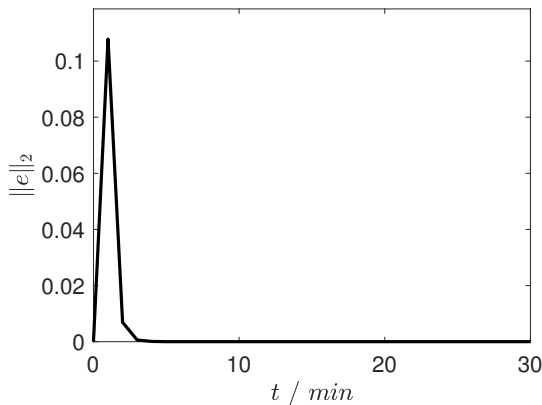

Fig. 4. L_2 - *norm of the error in time*

Table 1. *Model parameters used for simulation*

Parameter	Value	Parameter	Value
μ_1	$3.6 \cdot 10^{-12}$	σ_1	$1 \cdot 10^{-12}$
N_Σ	$7.5 \cdot 10^8$	σ_2	$1 \cdot 10^{-12}$
μ_2	$3.6 \cdot 10^{-12}$	N_{out}	$5 \cdot 10^{-4}$
N_{in}	$4 \cdot 10^5$		

4. RESULTS

The proposed parameter estimation approach has been implemented for numerical computations in MATLAB. For the solution of the population balance equations the method of lines is applied. Here, the internal coordinate, i.e. the particle volume, is lumped using the cell-average method (Kumar et al., 2006) on a logarithmic grid with $n_v = 55$ grid points. In order to solve the set of the ordinary differential equations and to overcome the stiffness problems the *ode15s* solver has been used. For the simulations the actual plant model with the Brownian motion coalescence kernel (7) and the scalar agglomeration efficiency $\beta_0 = 5 \cdot 10^{-12}$ is considered. The model parameters used for simulations are represented in Table 1.

4.1 Estimated agglomeration efficiency

In the first instance, the performance of the proposed online identification approach is shown for the scenario of agglomeration efficiency estimation. Here, the modified plant model with Brownian kernel runs simultaneously with the actual process plant. The same initial conditions from (2) are applied for the particle size distributions in
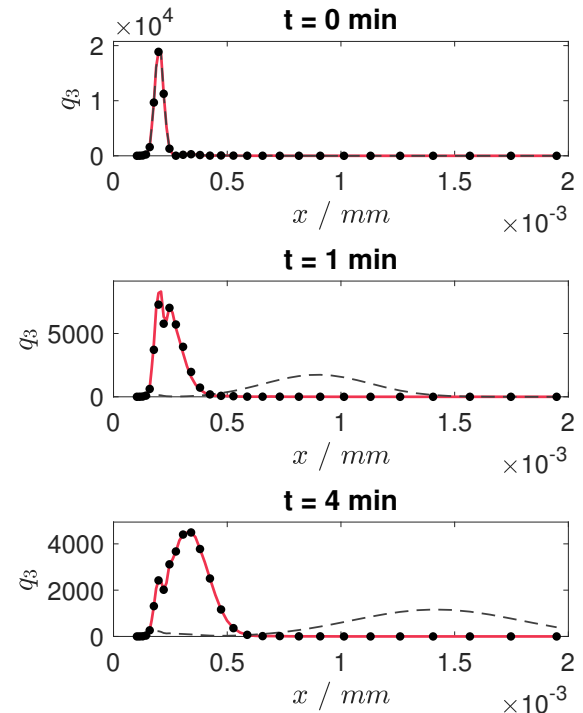

Fig. 5. *Particle size distributions q_3 of the actual plant (solid, red), parallel plant model with (points, black) and without online estimation (dotted, grey)*

the parallel model. The initial value for the estimate is chosen $\hat{\beta}_0 = 5 \cdot 10^{-10}$. Both tuning parameters γ and l have a strong impact on the estimation dynamics. Therefore, assigning of their values is an iterative procedure where trade-offs between different design specifications, e.g. fast parameters convergence rates, oscillating behaviour and attenuation of possible measurements noise, should be taken into account. For this scenario the tuning parameters are chosen as follows

$$\gamma = 1 \cdot 10^{-18} \,, \qquad l = -0.1 \,. \tag{21}$$

The obtained simulation results are represented in Fig. 3, Fig. 4 and Fig. 5. Here, in Fig. 3 the convergence of the estimated $\hat{\beta}_0$ and actual β_0 is depicted. It can be seen that the unknown parameter converges within approximately three minutes, which is sufficiently fast related to the process dynamics. It is also clear from the Fig. 4 that corresponding L_2 - norm of the estimation error between particle size distributions n and $\hat{n}$ converges towards zero within the same time. In order to compare the process dynamics the additional particle size distributions

$$q_3(t, x) = \frac{x^3 n(t, x)}{\int_0^\infty x^3 n(t, x) \mathrm{d}x} \tag{22}$$

of the actual plant, the parallel model with and without online parameter estimation for different time points are depicted in Fig. 5. A significant divergence of the process dynamics with and without online parameter estimation, i.e. with roughly known initial guesses, can be observed already in a short period of time.

4.2 Estimated Laurent polynomial parameters

In the second scenario, the proposed method is applied to estimate the agglomeration kernel. Here, the modified
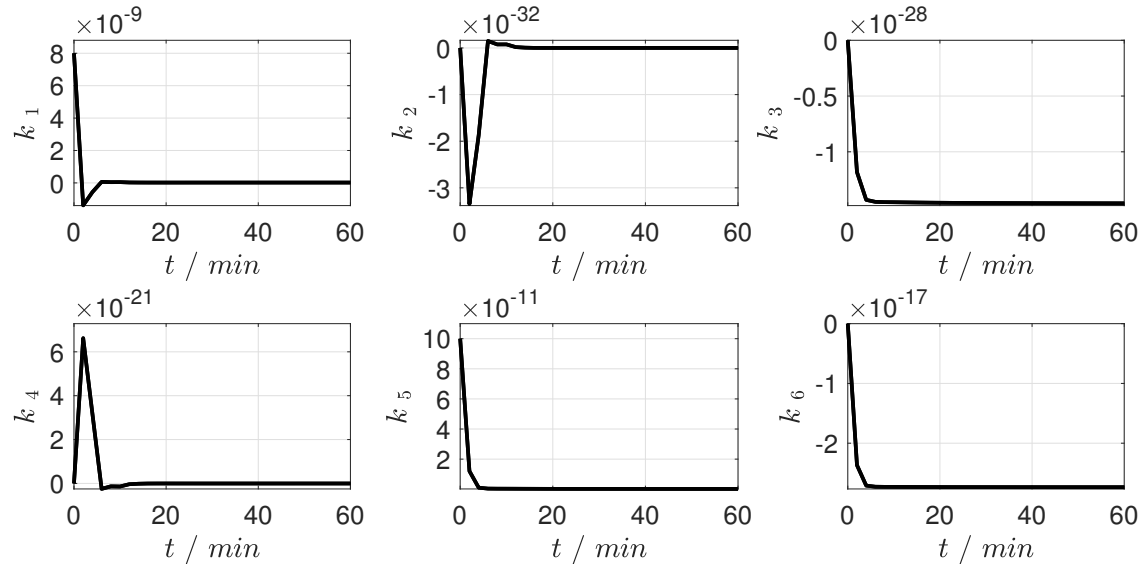
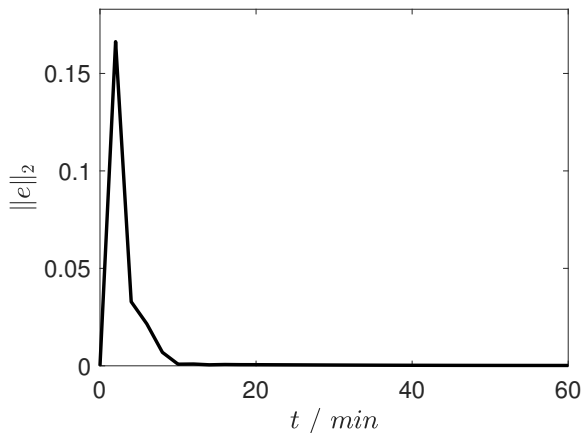Fig. 6. *Convergence of the Laurent-polynomial coefficients for identification of coalescence kernel*

Fig. 7. L_2 - *norm of the error in time*

Table 2. *Initial estimates and tuning parameters for identification of Laurent-kernel*

Parameter	Value	Parameter	Value
$\hat{k}_1(0)$	$8 \cdot 10^{-9}$	γ_1	$5 \cdot 10^{-41}$
$\hat{k}_2(0)$	0	γ_2	$1 \cdot 10^{-41}$
$\hat{k}_3(0)$	0	γ_3	$5 \cdot 10^{-41}$
$\hat{k}_4(0)$	0	γ_4	$7 \cdot 10^{-41}$
$\hat{k}_5(0)$	$1 \cdot 10^{-10}$	γ_5	$7 \cdot 10^{-46}$
$\hat{k}_6(0)$	0	γ_6	$5 \cdot 10^{-41}$
		l	-0.022

plant model, which includes the Laurent polynomial with six unknown parameters (17), runs simultaneously to the actual process plant. In this case, the same initial conditions for the parallel model and the actual plant are used. The initial values for the polynomial parameters and chosen tuning parameters are given in Table 2.

The corresponding simulations results are shown in Fig. 6, Fig. 7, Fig. 8 and Fig. 9. From Fig. 6 it is clear that parameters converge with a different rate. Moreover, the simulation studies indicated that only two polynomial addends associated with parameters k_1 and k_5 make a significant contribution in the overall estimation dynamics. In the Fig. 7 a corresponding L_2 - norm of the estimation error
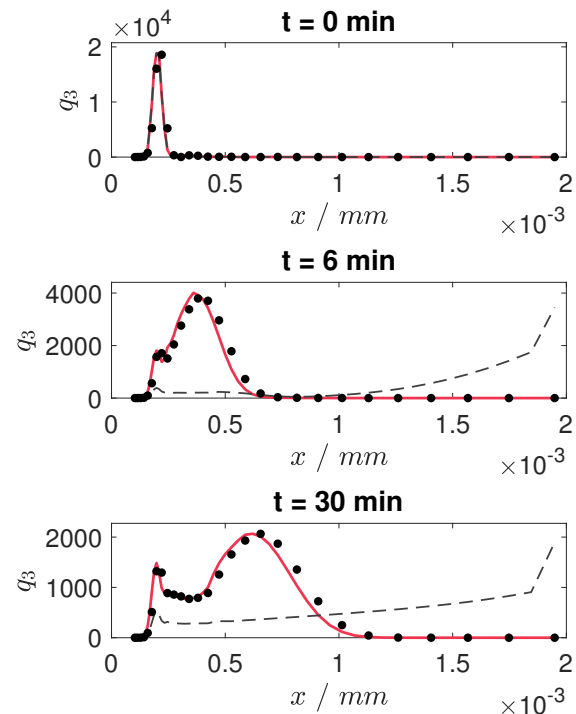

Fig. 8. *Particle size distributions q_3 of the actual plant (solid, red), parallel plant model with (points, black) and without online estimation (dotted, grey)*

between particle size distributions n and $\hat{n}$ is depicted. It can be seen that a sufficient convergence is achieved within approximately 10 minutes, which is reasonably fast related to the slow process dynamics. However, from the Fig. 8, the sufficient accuracy of the distributions can be observed after approximately 6 minutes.

The estimate of the Brownian kernel using the proposed Laurent polynomial and the relative error between both kernels are shown in Fig. 9. It can be seen that the relative error is below 5 %.
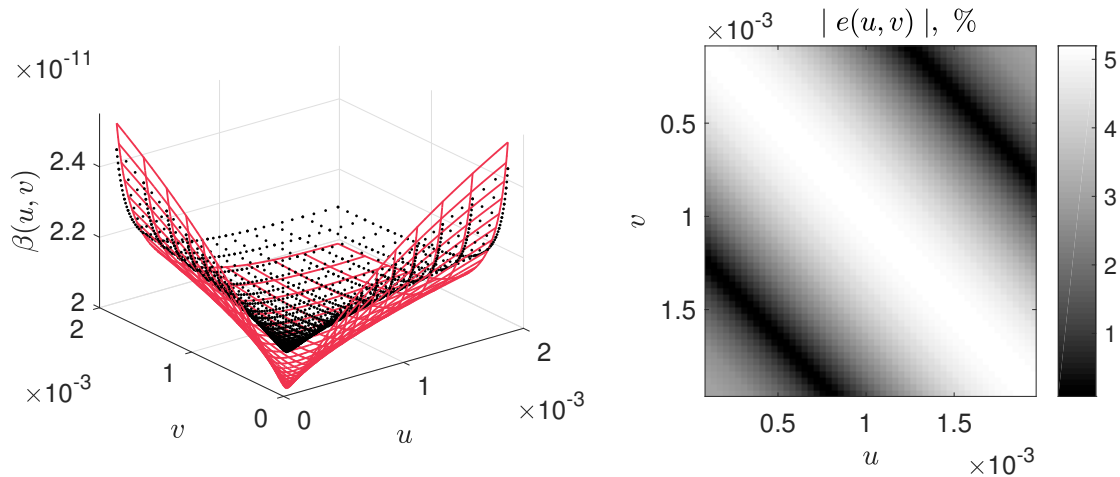
Fig. 9. *Brownian kernel (red, at the left), estimated kernel (black, at the left) and relative error between kernels (at the right)*

5. CONCLUSION

In this work the online parameter estimation for the continuous fluidized bed spray agglomeration process has been demonstrated. For the identification of the agglomeration kernel the Lyapunov-based adaptive approach has been proposed. The presented methodology has been studied for two different identification scenarios. In the first scenario, this method has been applied for the agglomeration efficiency estimation assuming that the agglomeration kernel is perfectly known. In the second scenario, the proposed approach has been applied for the volume-dependent agglomeration kernel estimation. For the kernel structure approximation a low-order Laurent polynomial has been used. It has been shown that this approach allows a sufficiently fast parameter estimation for both cases in the case of noiseless measurements. Future work will be concerned with the robustness analysis in presence of measurement noise and parameter uncertainties as well as application of this approach to real plant measurements.

REFERENCES

Bück, A., Klaunick, G., Kumar, J., Peglow, M., and Tsotsas, E. (2012). Numerical simulation of particulate processes for control and estimation by spectral methods. *AIChE Journal*, 58, 2309–2319.

Chakraborty, J., Kumar, J., Singh, M., Mahoney, A., and Ramkrishna, D. (2015). Inverse problems in population balances. determination of aggregation kernel by weighted residuals. *Industrial & Engineering Chemistry Research*, 54(42), 10530–10538.

Dürr, R., Palis, S., and Kienle, A. (2015). Online parameter identification of facet growth kinetics in crystal morphology population balance models. *Procedia Engineering*, 102(0), 1336–1345. Proceedings of The 7th World Congress on Particle Technology.

Eisenschmidt, H., Soumaya, M., Bajcinca, N., Le Borne, S., and Sundmacher, K. (2017). Estimation of aggregation kernels based on Laurent polynomial approxima-

tion. *Computers and Chemical Engineering*, 103, 210–217.

Golovin, I., Strenzke, G., Dürr, R., Palis, S., Bück, A., Tsotsas, E., and Kienle, A. (2018). Parameter Identification For Continuous Fluidized Bed Spray Agglomeration. *Processes*, 6(12), 246. doi:10.3390/pr6120246. URL http://www.mdpi.com/2227-9717/6/12/246.

Krstic, M. (2006). Systematization of approaches to adaptive boundary stabilization of PDEs. *International Journal of Robust Nonlinear Control*, 16, 801–818.

Kumar, J., Peglow, M., Warnecke, G., Heinrich, S., and Mörl, L. (2006). Improved accuracy and convergence of discretized population balance for aggregation: The cell average technique. *Chemical Engineering Science*, 61, 3327–3342.

Le Borne, S., Shahmuradyan, L., and Sundmacher, K. (2015). Fast evaluation of univariate aggregation integrals on equidistant grids. *Computers and Chemical Engineering*, 74, 115–127.

Palis, S. and Kienle, A. (2013). Online parameter identification for continuous fluidized bed spray granulation. In *5th International Conference on Population Balance Modelling, PBM 2013*.

Palis, S. and Kienle, A. (2017). Online parameter identification for continuous fluidized bed spray granulation with external sieve-mill cycle. In *2nd International Conference on Methods and Models in Automation and Robotics, MMAR 2017*, 594–598.

Ramkrishna, D. (2000). *Population Balances: Theory and Applications to Particulate Systems in Engineering*. Academic Press, San Diego.

Control of Multi-Chamber Continuous Fluidized Bed Spray Granulation

Stefan Palis [*]

[*] Otto-von-Guericke University Magdeburg, Germany
National Research University "Moscow Power Engineering Institute",
Russia (e-mail: stefan.palis@ovgu.de).

Abstract: This paper is concerned with control of multi-chamber continuous fluidized bed spray granulation processes with external sieve-mill cycles. The process is described by a population balance equation for the particle size distribution in each chamber, resulting in a system of nonlinear partial integro-differential equations. Therefore, control design is challenging. In order to overcome these difficulties the control problem is formulated using a generalized distance measure, the discrepancy. It is shown that discrepancy based control allows to design a simple and effective nonlinear control law for multi-chamber continuous fluidized bed spray granulation processes with external sieve-mill cycles.

Keywords: Discrepancy based control, population balance, Lyapunov stability, nonlinear control

1. INTRODUCTION

Multi-chamber continuous fluidized bed spray granulation is a versatile particle formulation process allowing the combination of various process steps in a single setup. The general aim of granulation is the conversion of a liquid product into its solid particular form. In this form product durability increases and handling is simplified, e.g. decreased dust formation. In the multi-chamber version a sequence of different processes as granulation, coating, drying or cooling can be easily realized by assigning them to different chambers. Although, a continuous mode of operation results in high throughputs special care has to be taken in order to guarantee a robust process operation, with respect to feed variations and unforeseen disturbances. These potential problems are not specific to the multi-chamber configuration, but are well-known for continuously operated single chamber granulation processes, e.g. Schmidt et al. (2015). Here, process instabilities and the occurrence of nonlinear limit cycles, as shown in Fig. 1, have been reported. Their dependence on specific process parameters (Fig. 2) has been extensively studied in Dreyschultze et al. (2015); Neugebauer et al. (2016); Bück et al. (2016).

In order to solve the described stability problems and guarantee a robust process operation different feedback control approaches have been studied for various single chamber granulation processes, e.g. Palis (2018); Bück et al. (2015); Palis and Kienle (2014, 2013, 2012). In this contribution feedback control design for the multi-chamber fluidized bed spray granulation process has been studied.

2. PROCESS MODEL

In the following a continuous multi-chamber fluidized bed spray granulation process (Fig. 3 (left)) is studied. It consists of four chambers and an additional sieve-mill
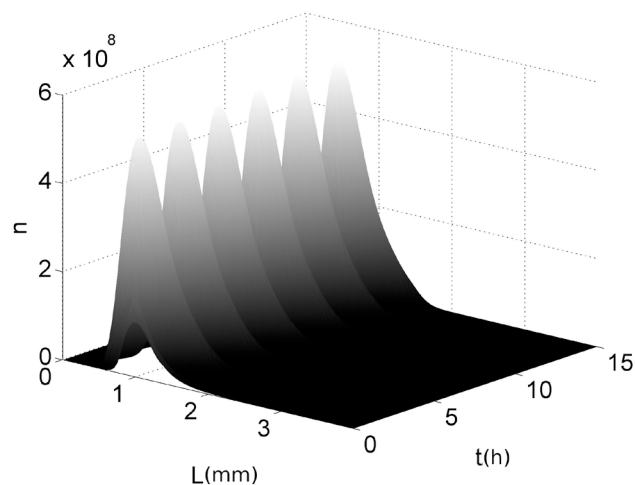

Fig. 1. Nonlinear oscillations in single-chamber continuous fluidized bed spray granulation with external sieve mill cycle

cycle, guaranteeing a constant production of nuclei and the attainment of the given product specification. The first three zones are used for particle growth and the fourth zone for drying only. It is assumed that each chamber is well mixed and that formation of functional zones, e.g. granulation and drying zone, can be neglected.

In the granulation chambers the liquid product is supplied to the fluidized particle bed by a nozzle. Due to high temperature of the drying air the injected solution or suspension, having settled on the particle surface, evaporates partly, resulting in particle growth. The particle growth in each chamber i is giving by

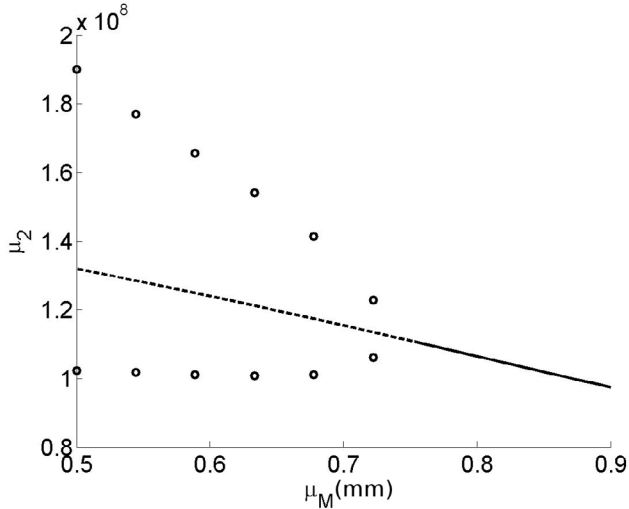$$G = 2\frac{\dot{V}_e}{\pi \mu_2} \tag{1}$$

Fig. 2. One-parameter continuation for varying mill grade of single-chamber continuous fluidized bed spray granulation with external sieve mill cycle
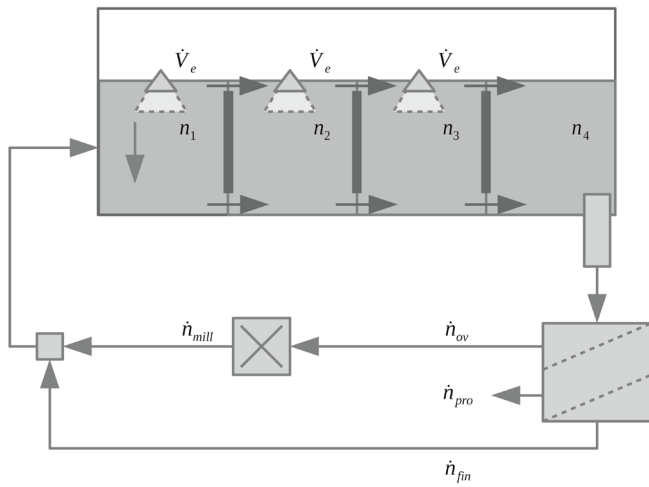

Fig. 3. Scheme of a multi-chamber fluidized bed spray granulation (left) and particle size distribution typically generated by the mill (right)

where μ_2 is the second moment of the particle size distribution.

$$\mu_2 = \int_0^\infty L^2 n \, dL \qquad (2)$$

In order to achieve a continuous particle movement from the left to the right, the whole apparatus has a small inclination. As a first step it is assumed that the interchamber weirs do not have a classification effect, i.e. particles are moving with a given rate k from left to right irrespective of their size. The flux from chamber i to chamber $i+1$ can hence be described by

$$\dot{n}_{out,i} = k n_i. \qquad (3)$$

In the fourth chamber particles are continuously redrawn and fed to two sieves resulting in three particle fractions: product, fines and oversized particles.

$$\dot{n}_{prod} = T_2(L)(1 - T_1(L))\dot{n}_{out,4} \qquad (4)$$

$$\dot{n}_{fine} = (1 - T_2(L))(1 - T_1(L))\dot{n}_{out,4} \qquad (5)$$

$$\dot{n}_{over} = T_1(L)\dot{n}_{out,4} \qquad (6)$$

Here, $T_1(L)$ and $T_2(L)$ are the associated screening functions.

$$T_{1,2}(L; \mu, \sigma) = \frac{\int_0^L \exp\left(\frac{-(L-\mu)^2}{2\sigma^2}\right) dL}{\int_0^\infty \exp\left(\frac{-(L-\mu)^2}{2\sigma^2}\right) dL} \qquad (7)$$

The oversized fraction is first grinded by the mill and then fed back as $\dot{n}_{mill}$ to the first granulation chamber together with the fines fraction $\dot{n}_{fine}$. The particle size distribution generated by the mill is typically multi-modal, where the proportion of each distribution depends on the specific mill power, flowrate and particle properties. It can further be assumed that the milling is in general mass conserving, i.e. the third moment of the oversize fraction is equal to the third moment of the particle distribution generated by the mill. In this contribution, it is assumed that the mill is producing uniformly distributed particles with a given mean diameter μ_M representing the mill grade. The particle flux leaving the mill can thus be described as follows.

$$\dot{n}_{mill} = 6 \frac{\exp \frac{(L-\mu_M)^2}{2\sigma_M^2}}{\sqrt{2\pi}\pi\sigma_M} \int_0^\infty L^3 \dot{n}_{over} dL \qquad (8)$$

$$= n_{mill}(L) \int_0^\infty L^3 \dot{n}_{over} dL \qquad (9)$$

The overall model hence consists of a system of four population balance equations, i.e. one population balance equation per chamber. Here, the index i stands for the second and third chamber, i.e. $i \in \{2, 3\}$. In the fourth chamber no liquid is injected and the particle growth G is hence zero. The particle withdraw associated with $\dot{n}_{out,4}$ is supplied to the sieves and then to the mill.

$$\frac{\partial n_1}{\partial t} = -G\frac{\partial n_1}{\partial L} + \dot{n}_{mill} + \dot{n}_{fine} - k n_1 \qquad (10)$$

$$\frac{\partial n_i}{\partial t} = -G\frac{\partial n_i}{\partial L} - k n_i + k n_{i-1} \qquad (11)$$

$$\frac{\partial n_4}{\partial t} = -K n_4 + k n_3 \qquad (12)$$

Introducing the associate terms for the fluxes from the mill and the fines fraction, results in the following system of nonlinear partial integro-differential equations.

$$\frac{\partial n_1}{\partial t} = -G\frac{\partial n_1}{\partial L} + n_{mill}(L) \int_0^\infty L^3 K T_1 n_4 dL + \dots$$
$$\dots + (1 - T_2)(1 - T_1)K n_4 - k n_1 \qquad (13)$$

$$\frac{\partial n_i}{\partial t} = -G\frac{\partial n_i}{\partial L} - k n_i + k n_{i-1} \qquad (14)$$

$$\frac{\partial n_4}{\partial t} = -K n_4 + k n_3 \qquad (15)$$

From a practical point of view, the overall mass or particle volume inside the whole apparatus and the volume of particles inside the last chamber, being directly connected to the product flow rate, should be controlled. As control

handles the particle withdraw K and liquid injection rate $\dot{V}_e$ can be used.

3. STABILIY WITH RESPECT TO A DISCREPANCY

Most of control methods for distributed parameter systems them are based on the solution of the system itself or at least the desired error system, i.e. the system in closed loop operation. For example in the backstepping approach (e.g. Smyshlyaev et al. (2010)) the control input is designed such that it maps the original system onto a desired stable error system. Whereas in the works of Bastin et. al. (e.g. Coron et al. (2007); Prieur et al. (2008)) stability is proven using the solution derived with the method of characteristics. Often it is assumed that the control handle acts on the boundary of the domain or is itself distributed. Here, the system of population balances is a system of nonlinear partial integro-differential equations with a lack of solution theory and control inputs acting in the domain. Hence, in this case a transformation to a desired error system with known classical stability behavior is hardly possible. As has been however shown in previous contributions Palis and Kienle (2014); Palis (2018) related problems can be solved by introducing a generalized stability notion, i.e. stability with respect to two generalized distance measures, the discrepancies. In the following, the most important properties and facts on stability with respect to one discrepancy are stated in accordance to Movtschan (1960); Sirasetdinov (1967); Martynjuk and Gutovski (1979). Here, the process $\varphi(.,t)$ is a solution of the distributed parameter system and $\varphi_0 = 0$ an equilibrium of the system.

Definition 1. Discrepancy

A discrepancy is a real valued functional $\rho = \rho[\varphi(.,t),t]$ with the following properties

(1) $\rho(\varphi,t) \geq 0$
(2) $\rho(0,t) = 0$
(3) for an arbitrary process $\varphi = \varphi(.,t)$ the discrepancy $\rho(\varphi(.,t),t)$ is continuous with respect to t.

Obviously, a discrepancy does not have all properties of a metric, e.g. symmetry $d(x,y) = d(y,x)$ or the triangular inequality $d(x,y) \leq d(x,z) + d(z,y)$ do not have to hold. In addition, it has not to satisfy the important property of definiteness, i.e. a vanishing discrepancy $\rho(\varphi,t) = 0$ does not automatically imply $\varphi = 0$.

Definition 2. Stability with respect to a discrepancies ρ

The equilibrium $\varphi_0 = 0$ is stable in the sense of Lyapunov with respect to the two discrepancies ρ and ρ_0 for all $t \geq t_0$ if for every $\varepsilon > 0$ and $t_0 \geq 0$ there exists a $\delta = \delta(\varepsilon,t_0) > 0$, such that for every process $\varphi(.,t)$ with $\rho(\varphi,t_0) < \delta(\varepsilon,t_0)$ follows $\rho < \varepsilon$ for all $t \geq t_0$. If in addition $\lim_{t \to \infty} \rho = 0$, than the equilibrium φ_0 is called asymptotically stable in the sense of Lyapunov with respect to the two discrepancies ρ and ρ_0.

In order to establish a relationship between stability with respect to one discrepancies and the existence of a Lyapunov functional V, the notions of positivity and positive definiteness of a functional with respect to a discrepancy have been introduced.

Definition 3. Positivity with respect to a discrepancy ρ

The functional $V = V[\varphi,t]$ is called positive with respect to the discrepancy ρ, if $V \geq 0$ and $V[0,t] = 0$ for all φ with $\rho(\varphi,t) < \infty$.

Definition 4. Positive definiteness with respect to a discrepancy ρ

The functional $V = V[\varphi,t]$ is positive definite with respect to a discrepancy ρ, if $V \geq 0$ and $V[0,t] = 0$ for all φ with $\rho(\varphi,t) < \infty$ and for every $\varepsilon > 0$ there exists a $\delta = \delta(\varepsilon) > 0$, such that $V \geq \delta(\varepsilon)$ for all φ with $\rho[\varphi,t] \geq \varepsilon$.

The following two theorems state the conditions for a function V guaranteeing (asymptotical) stability with respect to one discrepancy.

Theorem 5. Sirasetdinov (1967) The process φ with the equilibrium $\varphi_0 = 0$ is stable with respect to the discrepancy ρ if and only if there exists a functional $V = V[\varphi,t]$ positive definite with respect to the discrepancy ρ and not increasing along the process φ, i.e. $\dot{V} \leq 0$.

Theorem 6. Sirasetdinov (1967) The process φ with the equilibrium $\varphi_0 = 0$ is asymptotically stable with respect to the discrepancy ρ if and only if there exists a functional $V = V[\varphi,t]$ positive definite with respect to the discrepancy ρ and not increasing along the process φ, i.e. $\dot{V} \leq 0$, with $\lim_{t \to \infty} V = 0$.

It has to be mentioned that stability with respect to two discrepancies is necessary but in general not sufficient for stability with respect to a L_p norm or L_∞ norm.

4. DISCREPANCY BASED CONTROL

In the following, a discrepancy based controller will be derived for the multi-chamber continuous fluidized bed spray granulation with external sieve-mill cycle. Here, the following discrepancy will be used.

$$\rho = \frac{1}{2}\left(\sum_{i=1}^{4}\int_0^\infty L^3 \tilde{n}_i dL\right)^2 + \frac{1}{2}\left(\int_0^\infty L^3 \tilde{n}_4 dL\right)^2 \quad (16)$$

where $\tilde{n}_i$ is the deviation of the particle size distrubtion in chamber i from its desired value $n_{i,d}$.

$$\tilde{n}_i = n_{i,d} - n_i \quad (17)$$

This choice is motivated by the two integral quantities the overall particle volume and the particle volume in the last chamber, which is of special importance as it is directly connected to the product flow rate. For simplicity the following related errors e_1, the deviation from the desired overall particle volume, e_2, the deviation from the desired particle volume in chamber four, are introduced.

$$e_1 = \sum_{i=1}^{4}\int_0^\infty L^3 \tilde{n}_i dL \quad (18)$$

$$e_2 = \int_0^\infty L^3 \tilde{n}_4 dL \quad (19)$$

As control handles the liquid injection of the first three chambers $\dot{V}_e$ and the particle withdraw rate from the last chamber K are chosen.

$$u_1 = \dot{V}_e \quad (20)$$

$$u_2 = K \quad (21)$$

In order to design a discrepancy based control law for the given control configuration the following Lyapunov functional candidate is used.

$$V = \rho = \frac{1}{2}e_1^2 + \frac{1}{2}e_2^2 \qquad (22)$$

As for classical Lyapunov based control design, its first time derivative has to be rendered negative.

$$\dot{V} = e_1\dot{e}_1 + e_2\dot{e}_2 \qquad (23)$$

$$= e_1 \sum_{i=1}^{4} \int_0^\infty L^3 \frac{\partial \tilde{n}_i}{\partial t} dL + e_2 \int_0^\infty L^3 \frac{\partial \tilde{n}_4}{\partial t} dL \qquad (24)$$

Calculating the first time derivative of the control errors e_1 and e_2 yields

$$\dot{e}_1 = \sum_{i=1}^{3} \int_0^\infty L^3 \left(G \frac{\partial n_i}{\partial L} \right) dL + \int_0^\infty L^3 K T_2 (1 - T_1) n_4 dL,$$

$$= \sum_{i=1}^{3} \frac{2\dot{V}_e \int_0^\infty L^3 \frac{\partial n_i}{\partial L} dL}{\pi \int_0^\infty L^2 n_i dL} + \int_0^\infty L^3 K T_2 (1 - T_1) n_4 dL \qquad (25)$$

$$\dot{e}_2 = -K \int_0^\infty L^3 n_4 dL + \int_0^\infty L^3 k n_3 dL. \qquad (26)$$

As typical for multi-input multi-output control problems, control errors can be affected with different control handles. Here, for simplicity it will be assumed that the second control error e_2, i.e. the deviation from the desired particle volume in chamber four, will be controlled by the second control handle u_2, i.e. the withdraw rate K. In order to achieve exponential convergence of e_2

$$\dot{e}_2 = c_2 e_2 \qquad (27)$$

where c_2 is a negative tuning parameter, the control input u_2 has to be chosen as follows

$$K = \frac{c_2 e_2 + \int_0^\infty L^3 k n_3 dL}{\int_0^\infty L^3 n_4 dL}. \qquad (28)$$

In a similar way, the first control error e_1, i.e. the deviation from the overall particle volume in the apparatus, will be controlled by the first control handle u_1, i.e. the liquid injection rate $\dot{V}_e$. In order to achieve exponential convergence of e_1

$$\dot{e}_1 = c_1 e_1 \qquad (29)$$

where c_1 is a negative tuning parameter, the control input u_1 has to be chosen as follows

$$\dot{V}_e = \frac{-\int_0^\infty L^3 K T_2 (1 - T_1) n_4 dL - c_1 e_1}{2 \sum_{i=1}^{3} \frac{\int_0^\infty L^3 \left(\frac{\partial n_i}{\partial L} \right) dL}{\pi \int_0^\infty L^2 n_i dL}} \qquad (30)$$

Introducing the two control laws 28 and 30 into equation 24 yields exponential convergence of the chosen Lyapunov functional V and thus proofs stability with respect to the chosen discrepancy ρ.

$$\dot{V} = c_1 e_1^2 + c_2 e_2^2 \qquad (31)$$

$$\leq \max(c_1, c_2)(e_1^2 + e_2^2) = \max(c_1, c_2)V \qquad (32)$$

In order to rigorously proof stability in the sense of a norm for the particle sized distributions in each chamber, one would have to study the associate zero dynamics Palis and Kienle (2014), which is not in the scope of the

present contribution. Applying the derived discrepancy based controller to the four chamber fluidized bed spray granulation process with external sieve-mill cycle shows that the particle size distributions in each chamber are stabilized and converge to their desired steady-states. This can be also seen from the second and third moment plots of each chamber as depicted in Fig. 4 and 5.

For simulation the population balance for the particle size distribution in each chamber has been discretized along the property coordinate using a first order finite-volume scheme. For time-integration a third order strong stability preserving Runge-Kutta scheme as been used. The initial particle size distribution in each chamber is assumed as normally distributed with mean diameter $1.1mm$ and standard deviation $0.2mm$.
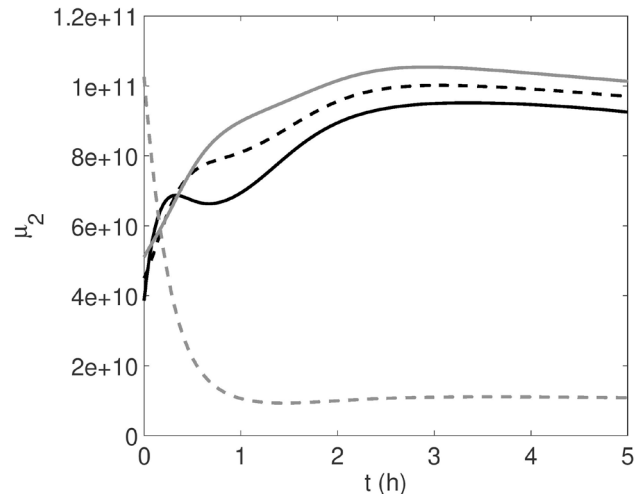

Fig. 4. Second moment μ_3 of the particle size distribution in chamber 1 (solid black), 2 (dotted black), 3 (solid gray) and 4 (dotted gray)
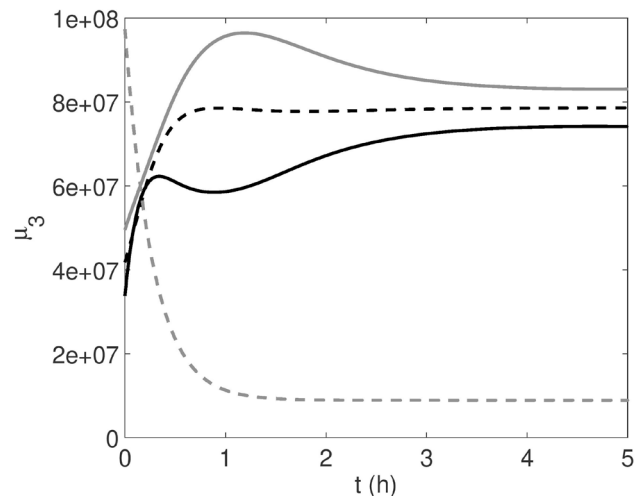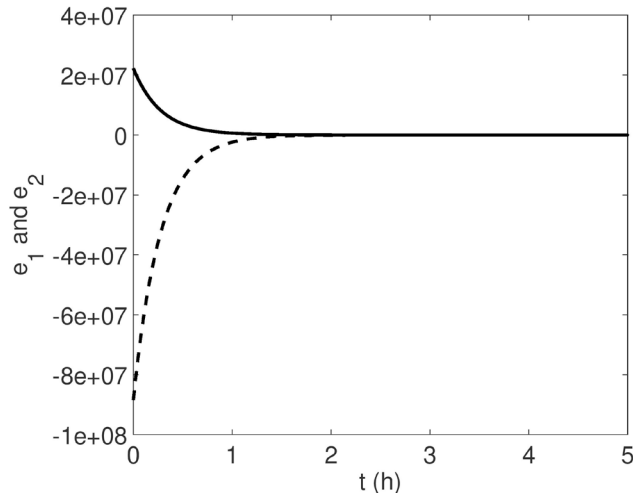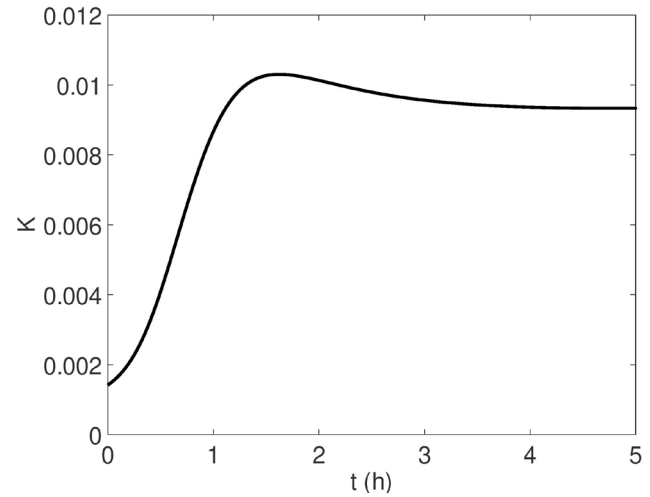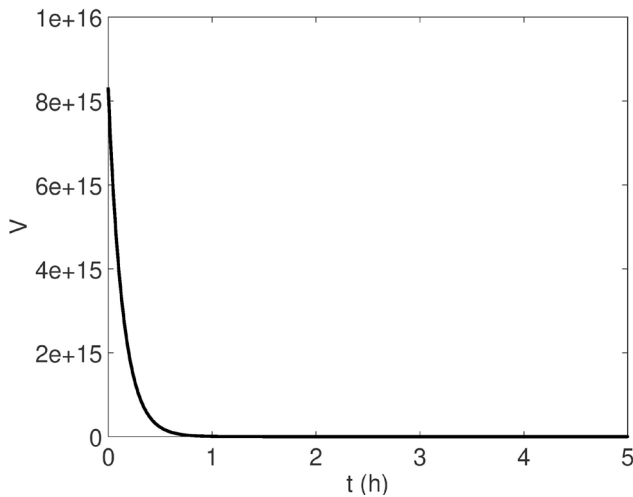

Fig. 5. Third moment μ_3 of the particle size distribution in chamber 1 (solid black), 2 (dotted black), 3 (solid gray) and 4 (dotted gray)

By control design the errors e_1 and e_2 converge exponentially, which can be seen in Fig. 6. In Fig. 7 the convergence of the Lyapunov functional V is depicted.

Fig. 6. Control error e_1 (solid black) and e_2 (dotted black)

Fig. 7. Lyapunov functional V

The applied control signals u_1 and u_2 are shown in Fig. 8 and 9.
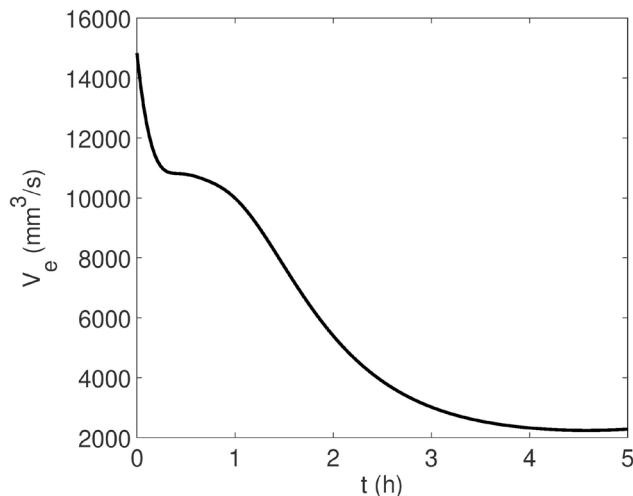
Fig. 8. Liquid injection rate $\dot{V}_e = u_1$

Fig. 9. Particle withdraw rate $K = u_2$

5. CONCLUSION

A discrepancy based control design has been presented for multi-chamber fluidized bed spray granulation processes with external sieve-mill cycles. Despite the complex mathematical process model it has been shown that the discrepancy based control approach leads to a simple and intuitive control design, without any model simplification or reduction steps. The design itself allows to include engineering knowledge of the given process configuration into the control design procedure by assigning a physically motivated discrepancy, containing the deviation of from the overall desired particle volume and the deviation from the particle volume in the last chamber, which is directly connected with the product withdraw rate. Promising first simulation results have been achieved. For a practical application the particle size distribution in each chamber has to be measured, which can be achieved by using an inline particle probe.

Future work will be concerned with a more detailed analysis of the classical stability behavior, i.e. stability of the particle size distributions in terms of L_2 and L_∞-norm, and the robustness of the presented control scheme.

REFERENCES

J-M. Coron & B. d'Andréa-Novel & G. Bastin, A strict Lyapunov function for boundary control of hyperbolic systems of conservation laws, IEEE Transactions on Automatic Control, Vol. 52(1), pp. 2 - 11, 2007.

A. Bück & C. Neugebauer & K. Meyer & S. Palis & E. Diez & A. Kienle & S. Heinrich & E. Tsotsas, Influence of operation parameters on process stability in continuous fluidised bed layering with external product classification, Powder Technology 300, 2016, pp. 37-45.

A. Bück & S. Palis & E. Tsotsas, Model-based control of particle properties in fluidised bed spray granulation, Powder Technology 270, 2015, pp. 575-583.

C. Dreyschultze, C. Neugebauer, S. Palis, A. Bück, E. Tsotsas, S. Heinrich and A. Kienle, Influence of zone formation on stability of continuous fluidized bed layering granulation with external product classification, Particuology, 2015, pp. 1-7.

A. Movtschan, Stability of processes with respect to two metrics [in Russian], Journal of Applied Mathematics and Mechanics 24, 1960, pp. 988-1001.

C. Neugebauer, S. Palis, A. Bück, E. Diez, S. Heinrich, E. Tsotsas and A. Kienle, Influence of mill configuration on stability of continuous layering granulation with external product classification, accepted for publication at the ESCAPE 26, 2016.

S. Palis, Non-identifier-based adaptive control of continuous fluidized bed spray granulation, Journal of Process Control 71, 2018, pp. 46-51.

S. Palis and A. Kienle, Discrepancy based control of particulate processes, Journal of Process Control, 2014, pp. 33-46.

S. Palis and A. Kienle, H_∞ Loop Shaping Control for Continuous Fluidized Bed Spray Granulation with Internal Product Classification, Industrial & Engineering Chemistry Research, 2013, pp. 408-420.

S. Palis & A. Kienle, Stabilization of continuous fluidized bed spray granulation with external product classification, Chem. Eng. Sci. 70, 2012, pp. 200-209.

C. Prieur & J. Winkin & G. Bastin, Robust boundary control of systems of conservation laws, Mathematics of Control, Signals and Systems, Vol. 20, pp. 173 - 197, 2008.

M. Schmidt, C. Rieck, A. Bück and E. Tsotsas. Experimental investigation of process stability of continuous spray fluidized bed layering with external product separation. Chemical Engineering Science, 2015, pp. 466-475.

T. Sirasetdinov, On the theory of stability of processes with distributed parameters [in Russian], Journal of Applied Mathematics and Mechanics, 1967, pp. 37-48.

A. Martynjuk & R. Gutovski, Integral inequalities and stability of motion [in Russian], Naukowa Dumka, 1979.

A. Smyshlyaev & E. Cerpa & M. Krstic, Boundary stabilization of a 1-D wave equation with in-domain anti-damping, SIAM Journal of Control and Optimization, vol. 48, pp. 4014-4031, 2010.

On the Control of Non-Minimum Phase Systems Using a Parallel Compensator

Klaus Röbenack
Institute of Control Theory
Technische Universität Dresden
Dresden, Germany
klaus.roebenack@tu-dresden.de

Stefan Palis
Institute for Automation Engineering
Otto-von-Guericke University Magdeburg
Magdeburg, Germany
e-mail: stefan.palis@ovgu.de

Abstract—Controller design by feedback or feedforward input-output linearization is straightforward if the system is minimum phase, i.e., if the zero dynamics are asymptotically stable. For systems with unstable zero dynamics these approaches cannot directly be applied, as they would result in the destabilization of a part of the systems dynamics. In order to overcome this problem and render the internal dynamics asymptotically stable a parallel compensator can be deployed. This technique has successfully been applied in previous works to linear systems. In this contribution a method to stabilize nonlinear non-minimum phase systems by a combination of parallel compensation and feedback linearization is proposed. The theoretical results will be illustrated on a DC/DC converter.

Index Terms—Non-minimum phase, parallel compensation, generalized controller canonical form, boost converter

I. Introduction

About thirty years ago based on differential geometry, exact feedback linearization and flatness based control were developed [1]–[3] and are now widely used in nonlinear control. Here, the concepts of the relative degree and the zero dynamics play an important role [1], [4]. For a given nonlinear system with a well-defined relative degree an exactly input-output linearizing control law can be designed under the additional assumption that the zero dynamics are asymptotically stable. Such a system is said to be of minimum phase. This approach can be extended to some classes of systems with ill-defined relative degree [5], [6]. The minimum phase assumption is more restrictive.

A special case are flat systems. Here, all system variables can be parametrized by the flat output. In the single-input case, a system is flat if and only if it is exactly input-to-state linearizable [7], [8]. For multi-input systems, it is more difficult to verify whether a given system is flat or not, and to compute a flat output [9]–[11]. For a flat output, the system has no zero dynamics at all, i.e., the minimum phase restriction is not applicable. It should be mentioned, that, from a practical point of view, even if the system is flat and the flat output is known, the use of a different, possibly non-flat, output may be preferable.

For a linear system, the zero dynamics corresponds to the zeros of the system's transfer function. Here, it is well-known that zeros in the complex right-half plane impose restrictions on the application of well-established control schemes and the achievable performance [12, Chapter 5]. Furthermore, in contrast to the closed-loop pole location, the location of the system zeros cannot be changed by feedback. However, as has been shown in [13], [14] this problem, i.e., the instability of the zero dynamics, can be solved by parallel compensation. In [15], [16] parallel compensators have been successfully design based on the linear system dynamics. In this contribution, the design of parallel compensators based on the nonlinear system dynamics, making use of the generalized controller canonical form [17], [18], will be studied.

The paper is structured as follows. The most relevant differential-geometric concepts from nonlinear control theory are recalled in Section II. As an illustrative example the boost converter as a DC/DC converter is used. It is introduced in Section III. The generalized controller canonical form described in Section IV is used in Section V to achieve minimum phase internal dynamics. In Section VI we carry out the controller design for the non-minimum phase converter model.

II. Mathematical Preliminaries

We consider a nonlinear single-input single-output system described by

$$
\begin{aligned}
\dot{x} &= f(x) + g(x)u, \\
y &= h(x)
\end{aligned}
\tag{1}
$$

with the state vector x, the input u and the output y. The fields $f, g : \mathcal{M} \to \mathbb{R}^n$ and $h : \mathcal{M} \to \mathbb{R}$ are defined on an open and connected subset $\mathcal{M} \subseteq \mathbb{R}^n$ and assumed to be sufficiently smooth. The *Lie derivative* of the scalar field h in the direction of the vector field f is defined by $L_f h(x) := \mathrm{d}\,h(x)f(x)$ with the exterior derivative $\mathrm{d}\,h(x) = h'(x)$. Higher order Lie derivatives are defined by $L_f^{k+1}h(x) := \mathrm{d}\,L_f^k h(x) \cdot f(x)$ with $L_f^0 h(x) := h(x)$. The system (1) is said to have a *relative degree* r at a point $x^0 \in \mathcal{M}$ if $L_g h(x) = 0, L_g L_f h(x) = 0, \dots, L_f g L_f^{r-2} h(x) = 0$ for all x in an open neighborhood of x^0 and $L_g L_f^{r-1} h(x^0) \neq 0$ [1].

If the relative degree r is well-defined, it is the minimum order of output time derivatives depending explicitly on the

input u. In particular, output time derivatives of order less then r do not depend on the input u:

$$
\begin{aligned}
y &= \phi_1(x) &= h(x),\\
\dot{y} &= \phi_2(x) &= L_f h(x),\\
&\vdots & \vdots\\
y^{(r-1)} &= \phi_r(x) &= L_f^{r-1} h(x).
\end{aligned}
\tag{2}
$$

The time derivative of order r depends directly on the input u:

$$
y^{(r)} = L_f^r h(x) + L_g L_f^{r-1} h(x) u.
\tag{3}
$$

Therefore, the nonlinearities in (3) can be compensated by feedback. In addition, we can impose linear dynamics

$$
y^{(r)} + k_{r-1} y^{(r-1)} + \cdots + k_0 y = k_0 w
\tag{4}
$$

with the reference value w using the control law

$$
u = \frac{1}{L_g L_f^{r-1} h(x)} \left(k_0 w - \sum_{i=0}^{r} k_i L_f^i h(x) \right)
\tag{5}
$$

with $k_r := 1$. If the coefficients $k_0, \ldots, k_{r-1}$ of (4) are chosen such that all roots of the associated characteristic polynomial have negative real parts, the output converges to the reference value, i.e., $y(t) \to w$ for $t \to \infty$.

If $r = n$, the system is flat and the control law (5) yields a linear closed-loop system [1], [8]. For a non-flat output with $r < n$, the control (4) results only in a r-dimensional linear subsystem. For $y(t) \equiv w$, the dynamics of the remaining $(n - r)$-dimensional subsystem evolve on the subset

$$
Z^* = \{ x \in \mathcal{M} : h(x) = w, L_f h(x) = 0, \ldots, L_f^{r-1} h(x) = 0 \}.
\tag{6}
$$

This subset is invariant under the system's dynamics for

$$
u = -\frac{L_f^r h(x)}{L_g L_f^{r-1} h(x)}.
\tag{7}
$$

The system is called *minimum phase* w.r.t. the reference value w if the internal dynamics described by (6) and (7) is asymptotically stable. Otherwise, the system is called *non-minimum phase*. This definition corresponds essentially to the zero dynamics [1].

Now, consider system (1) in an equilibrium point $x^0 \in \mathcal{M}$ with the input u^0 and the reference output value w, i.e.,

$$
0 = f(x^0) + g(x^0) u^0, \quad w = h(x^0).
$$

The Taylor linearization results in a system

$$
\dot{\tilde{x}} = A \tilde{x} + b \tilde{u}, \quad \tilde{y} = c^T \tilde{x}
$$

with the system matrix $A \in \mathbb{R}^{n \times n}$, the vectors $b, c \in \mathbb{R}^n$ and the small signal quantities $\tilde{x}$, $\tilde{u}$ and $\tilde{y}$. The system's transfer function reads

$$
\begin{aligned}
G(s) = \frac{N(s)}{D(s)} &= c^T (sI - A)^{-1} b\\
&= \frac{b_0 + b_1 s + \cdots b_{n-r} s^{n-r}}{a_0 + a_1 s + \cdots + a_{n-1} s^{n-1} + s^n}.
\end{aligned}
\tag{8}
$$

The denominator polynomial $D(s) = \det(sI - A)$ is the open-loop characteristic polynomial. The numerator polynomial $N(s)$ is the characteristic polynomial of the linearized internal
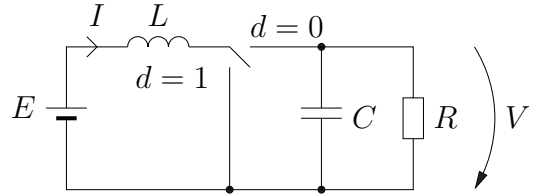

Fig. 1. Simplified circuit diagram of the boost converter

dynamics w.r.t. the reference output value w. The equilibrium of the internal dynamics is *hyperbolic*, if this polynomial has no roots with zero real part [19]. In this case, the system is minimum phase if and only if all roots have negative real parts.

III. BOOST CONVERTER EXAMPLE

A. Mathematical Model

A *boost converter*, also known as *step up converter*, transforms a source voltage into a higher output voltage [20], [21]. Fig. 1 shows the network model of such a boost converter. In this figure, E denotes the source voltage, L the inductance and C the capacitance. The load is modelled by a resistance R.

The network equations with the current I and the voltage V can be derived using Kirchhoff's laws. The two possible switching positions are denoted by $d = 0$ and $d = 1$. In practice, the switch is controlled using pulse width modulation (PWM). In this case, it is common practice to consider the averaged model, which can be written as a state-space system

$$
\begin{aligned}
\dot{x}_1 &= -(1 - u) \tfrac{1}{L} x_2 + \tfrac{E}{L}\\
\dot{x}_2 &= (1 - u) \tfrac{1}{C} x_1 - \tfrac{1}{RC} x_2
\end{aligned}
\tag{9}
$$

with the average current x_1 and the average voltage x_2. The *duty cycle* or *duty ratio* $u \in (0, 1)$ acting as an input signal describes the average value of d over a switching period. It is the ratio between the switch-on time and the switching period.

In most applications one wants to control the boost converter in such a way, that a prescribed reference output voltage $w = x_2^0$ is provided. The associated equilibrium point is described by

$$
x_1^0 = \frac{(x_2^0)^2}{ER} \quad \text{and} \quad u^0 = 1 - \frac{E}{x_2^0}.
\tag{10}
$$

Due to $u \in (0, 1)$ one obtains that in steady-state the second state component x_2 is always greater than the supply voltage, i.e., $x_2^0 > E$, and tends to the supply voltage for decreasing duty ratio, i.e., $x_2^0 \to E$ for $u^0 \downarrow 0$. Whereas for increasing duty ratio it tends to infinity, i.e., $x_2^0 \to \infty$ for $u^0 \uparrow 1$.

In the following, for the boost converter the parameter values from [20, Sect. 8.6.1] are listed in Tab. I. We consider the operating point $u^0 = 0.4$, $x_1^0 = 25/6\,\mathrm{A} = 4.1\bar{6}\,\mathrm{A}$, $x_2^0 = 25\,\mathrm{V}$. The linearization in this equilibrium point yields the system matrix and the input vector

$$
A = \begin{pmatrix} 0 & -1200\\ 600 & 100 \end{pmatrix}, \quad b = \begin{pmatrix} 50000\\ -4166.\bar{6} \end{pmatrix}.
\tag{11}
$$

The associated characteristic polynomial

$$
\det(sI - A) = s^2 + 100s + 72000
$$

Parameter	Value
E	$15\,\mathrm{V}$
L	$0.5\,\mathrm{mH}$
C	$1000\,\mathrm{\mu F}$
R	$10\,\Omega$

has the roots $s_{1,2} = -50 \pm 50\sqrt{287}j \approx -50 \pm 847j$. Therefore, the operating point of the open-loop system is asymptotically stable.

B. Current Control

First, we consider the boost converter model (9) with current output

$$y = h(x) = x_1 = c^T x \quad \text{with} \quad c^T = \begin{pmatrix} 1 & 0 \end{pmatrix}. \qquad (12)$$

With this output, the system has the relative degree $r = 1$ because the input occurs in the first time derivative of the output:

$$\dot{y} = \dot{x}_1 = -(1-u)\frac{1}{L}x_2 + \frac{E}{L} = \frac{E-x_2}{L} + \frac{x_2}{L}u.$$

Furthermore, the system is minimum phase [22]–[24]. This can also be verified on the linearized model. From (11) and (12) we obtain the transfer function

$$G(s) = c^T(sI - A)^{-1}b = \frac{50000(s+200)}{s^2 + 100s + 720000}.$$

We have one zero at $s = -200$ lying in the left complex half-plane, i.e., the linearized model is minimum phase.

Therefore, we can design a stabilizing control law by input-output linearization

$$\begin{aligned}
u &= -\frac{1}{L_g h(x)}\left[k_0(h(x) - w) + L_f h(x)\right] \\
&= \frac{x_2 - E - k_0 L(x_1 - w)}{x_2}
\end{aligned}$$

with the reference value w being the reference and the controller parameter $k_0 > 0$. Alternatively, one could design a controller based on dynamic extension [25]. However, from a practical point of view, one wants to obtain a desired reference voltage. Although the reference current can be obtained by (10) from the reference voltage in the equilibrium point, it depends on the parameters E and R. Both are often not exactly known. In addition, the supply voltage E may change over time for certain applications. This would cause an undesired deviation in the (internally used) reference value w.

C. Voltage Control

Next, we consider the nonlinear model (9) with voltage output

$$y = h(x) = x_2 = c^T x \quad \text{with} \quad c^T = \begin{pmatrix} 0 & 1 \end{pmatrix}. \qquad (13)$$

From the first order output time derivative

$$\dot{y} = \dot{x}_2 = (1-u)\frac{1}{C}x_1 - \frac{1}{RC}x_2 = \frac{Rx_1 - x_2}{RC} - \frac{x_1}{C}u$$

we obtain the relative degree $r = 1$. Unfortunately, the system is non-minimum phase [23], [26]. Therefore, exact input-output feedback linearization cannot be applied directly. To verify the instability of the zero dynamics, we consider the transfer function

$$G(s) = -\frac{12500\,(s - 7200)}{3\,(s^2 + 100s + 720000)}$$

derived from (11) and (13). The zero $s = 7200$ lies in the right complex half-plane. Hence, the system is non-minimum phase.

D. Energy Control

Furthermore, we could consider the electrical energy

$$y = h(x) = \frac{L}{2}x_1^2 + \frac{C}{2}x_2^2 \qquad (14)$$

stored in the inductor and the capacitor as a control output resulting in the relative degree $r = 2$, see [22], [27]. Since we have $r = n$, the system is flat. Therefore, there is no internal dynamics, i.e., the control law (5) achieves an exact input-to-state linearization by feedback. However, the desired value of the control variable (14) has to be calculated from the desired reference voltage. Again, this calculation depends on (not exactly known) system parameters and may result in undesired deviations, which are not compensated by feedback control. In conclusion a control configuration using voltage output would be preferable in many applications. In order to overcome the unstable zero dynamics obstacle an additional parallel compensator will be design on the basis of the generalized controller canonical form, which will be introduced in the next section.

IV. GENERALIZED CONTROLLER CANONICAL FORM

Consider system (1) with a well-defined relative degree $r < n$ and the maps $\phi_1, \ldots, \phi_r$ defined by output times derivatives of order $0, \ldots, r-1$ in Eq. (2). As the rth order time derivative depends on the input u, see (3), subsequent time derivatives additionally depend on time derivatives of the control u. Further differentiation yields

$$\begin{aligned}
y^{(r)} &= \phi_{r+1}(x, u) \\
y^{(r+1)} &= \phi_{r+2}(x, u, \dot{u}) \\
y^{(r+2)} &= \phi_{r+3}(x, u, \dot{u}, \ddot{u}) \\
&\vdots \\
y^{(n-1)} &= \phi_n(x, u, \dot{u}, \ddot{u}, \ldots, u^{(n-r-1)}),
\end{aligned} \qquad (15)$$

where the maps $\phi_{r+1}, \ldots, \phi_n$ can be expressed in terms of Lie derivatives [5], [6]. Combining the maps $\phi_1, \ldots, \phi_r$ and $\phi_{r+1}, \ldots, \phi_n$ one obtains a map

$$z = \Phi(x, u, \dot{u}, \ddot{u}, \ldots, u^{(n-r-1)}). \qquad (16)$$

which, for fixed quantities $u, \dot{u}, \ddot{u}, \ldots, u^{(n-r-1)}$, is a local diffeomorphism with an inverse map

$$x = \Phi^{-1}(z, u, \dot{u}, \ddot{u}, \ldots, u^{(n-r-1)})$$

transforming (1) into the form

$$
\begin{aligned}
\dot{z}_1 &= z_2 \\
\dot{z}_2 &= z_3 \\
&\vdots \\
\dot{z}_{n-1} &= z_n \\
\dot{z}_n &= \gamma(z, u, \dot{u}, \ddot{u}, \ldots, u^{(n-r)}) \\
y &= z_1,
\end{aligned}
\tag{17}
$$

which is the *generalized controller canonical form (GCCF)* [17]. System (17) is a generalized state-space system since its input-dependent vector field also depends on input derivatives. Because the original system (1) is affine w.r.t. the input u, the map γ is affine w.r.t. the highest order input time derivative $u^{(n-r)}$. Therefore, we can decompose γ as follows:

$$
\gamma(z, u, \dot{u}, \ldots) = \alpha(z, u, \dot{u}, \ldots) + \beta(z, u, \dot{u}, \ldots) u^{(n-r)}.
$$

Consider system (17) in an equilibrium point. The linearization results in the transfer function (8) with the coefficients

$$
\begin{aligned}
a_0 &= -\frac{\partial \gamma}{\partial z_1}, & a_1 &= -\frac{\partial \gamma}{\partial z_2}, & \ldots, & & a_{n-1} &= -\frac{\partial \gamma}{\partial z_n}, \\
b_0 &= \frac{\partial \gamma}{\partial u}, & b_1 &= \frac{\partial \gamma}{\partial \dot{u}}, & \ldots, & & b_{n-r} &= \frac{\partial \gamma}{\partial u^{(n-r)}}.
\end{aligned}
\tag{18}
$$

Provided the operating points are hyperbolic, the stability of the whole system or the internal dynamics can be investigated through the denominator or the numerator polynomial, respectively.

Remark 1: The output time derivatives occurring in (3) and (15) may result in large symbolic expressions. For a numerical implementation of (17), we could use an alternative technique of differentiation known as *automatic* or *algorithmic differentiation* [28], [29].

A. GCCF for the boost converter with voltage output

Applying the above considerations to the boost converter model (9) with voltage output (13). The change of coordinates (16) reads

$$
z = \Phi(x, u) = \begin{pmatrix} y \\ \dot{y} \end{pmatrix} = \begin{pmatrix} h(x) \\ L_f h(x) + L_g h(x) u \end{pmatrix}
= \begin{pmatrix} x_2 \\ \frac{R x_1 (1-u) - x_2}{CR} \end{pmatrix}
\tag{19}
$$

with the inverse map

$$
x = \Phi^{-1}(z, u) = \begin{pmatrix} -\frac{CR z_2 + z_1}{R(u-1)} \\ z_2 \end{pmatrix}.
\tag{20}
$$

The transformed system becomes

$$
\begin{aligned}
\dot{z}_1 &= z_2 \\
\dot{z}_2 &= \gamma(z, u, \dot{u}) = \alpha(z, u) + \beta(z, u)\dot{u} \\
y &= z_1
\end{aligned}
\tag{21}
$$

with

$$
\begin{aligned}
\alpha(z, u) &= -\frac{L z_2 + R(u-1)^2 z_1 - E}{CLR}, \\
\beta(z, u) &= \frac{L z_2 - E}{L(u-1)}.
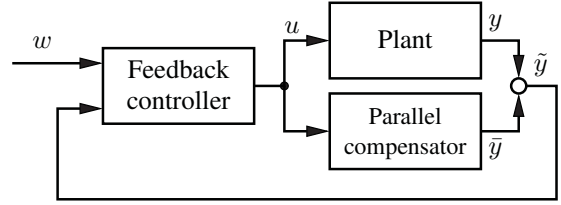\end{aligned}
\tag{22}
$$

Fig. 2. Control scheme using a parallel compensator

V. STABILIZING INTERNAL DYNAMICS AND PARALLEL COMPENSATION

A. Parallel Compensator Design Concept

A parallel compensator is an additional dynamical system acting in parallel to a given system. The application of parallel compensation for zero dynamics stabilization has been proposed by [13]. The main idea is to design a second system, the parallel compensator, which results in stable internal dynamics for the parallel interconnection of the plant and the compensator. A typical control scheme applying parallel compensation in combination with feedback control is shown in Fig. 2. A design procedure based on linear systems theory has been proposed and successfully applied in [15] and [16]. The design of nonlinear parallel compensators for nonlinear systems with unstable internal dynamics, is to the best of our knowledge still an open problem.

B. Parallel Compensator Design for Maximum Phase Systems

In this contribution, we propose a first nonlinear design procedure being based on the maximum phase property. Considering a given system in the GCCF (IV) and the transfer function (8) of its linearization (18), where we assume that the numerator polynomial $N(s)$ has no root with zero real part. Then, the system is minimum phase if all roots have negative real parts. In a similar manner, the linearized system is called *maximum phase* if all roots of $N(s)$ have positive real parts [18]. In this case, applying the following transformation $s \mapsto -s$, i.e., mirroring the roots along the imaginary axis, all roots of the (modified) polynomial $N(-s)$ have negative real parts. In the time domain, where the variable s can be associated with the time derivative operator $\frac{\mathrm{d}}{\mathrm{d}t}$, this transformation can be associated with the substitution $\frac{\mathrm{d}}{\mathrm{d}t} \mapsto -\frac{\mathrm{d}}{\mathrm{d}t}$. Thus, for a given hyperbolic maximum phase system the transformation

$$
\gamma(z, u, \dot{u}, \ddot{u}, \dddot{u}, \ldots) \mapsto \gamma(z, u, -\dot{u}, +\ddot{u}, -\dddot{u}, \ldots)
\tag{23}
$$

yields a minimum phase system, which can be used as the desired system of the parallel interconnection of plant and parallel compensator. The parallel compensator can than be obtained by subtraction of the plant. The described procedure will now be illustrated for the boost converter example.

VI. CONTROLLER DESIGN FOR THE NON-MINIMUM PHASE CONVERTER MODEL

In a first step, the associated minimum phase system for the boost converter model in the GCCF (21) with (22) is constructed by the transformation (23).

$$
\begin{aligned}
\dot{z}_1 &= z_2 \\
\dot{z}_2 &= \gamma(z, u, -\dot{u}) = \alpha(z, u) - \beta(z, u)\dot{u} \qquad (24) \\
y &= z_1.
\end{aligned}
$$

Applying the inverse transformation (20), i.e., transforming this system into the original coordinates, yields

$$
\begin{aligned}
\dot{x}_1 &= -(1-u)\frac{1}{L}x_2 + \frac{E}{L} - \frac{2x_1}{u-1}\dot{u}, \\
\dot{x}_2 &= (1-u)\frac{1}{C}x_1 - \frac{1}{RC}x_2, \qquad (25)
\end{aligned}
$$

which is now, in contrast to the original system (9), a generalized state-space system containing the derivative of u [24].

In order to achieve the desired minimum phase system (24), the following parallel compensator can be used:

$$
\begin{aligned}
\dot{\bar{z}}_1 &= \bar{z}_2 \\
\dot{\bar{z}}_2 &= \alpha(\bar{z}, u) - 3\beta(\bar{z}, u)\dot{u} \qquad (26) \\
\bar{y} &= \bar{z}_1.
\end{aligned}
$$

Introducing the output

$$
\tilde{y} = y + \bar{y} \qquad (27)
$$

of the plant (21) with the parallel compensator (26) yields

$$
\ddot{\tilde{y}} = \alpha(z, u) + \alpha(\bar{z}, u) + [\beta(z, u) - 3\beta(\bar{z}, u)]\dot{u} \qquad (28)
$$

Here, eq. (28) becomes for the limit $z \to \bar{z}$

$$
2\ddot{y} = 2\alpha(z, u) - 2\beta(z, u)\dot{u}, \qquad (29)
$$

or equivalently

$$
\ddot{y} = \alpha(z, u) - \beta(z, u)\dot{u}, \qquad (30)
$$

which is exactly the same as the minimum phase system (24).

Next, we design a stabilizing controller for the augmented system (28). Introducing $v = \dot{u}$ as a new input and u as an additional state variable, the augmented system (28) has relative degree $r = 2$. We want to achieve linear dynamics

$$
\ddot{\tilde{y}} + k_1 \dot{\tilde{y}} + k_0 \tilde{y} = k_0 \tilde{w} \qquad (31)
$$

with the reference value $\tilde{w}$. The linear differential equation (31) is asymptotically stable for $k_0, k_1 > 0$. Note that in an equilibrium point we have $\dot{u} = 0$. This implies that the systems (21), (25), and (28) have the same equilibrium point. With the controller aim $y \to w$ and $\bar{y} \to w$ we have $\tilde{y} \to \tilde{w} = 2w$ due to (27). Solving (28) and (31) w.r.t. v leads to

$$
v = -\frac{k_0(z_1 + \bar{z}_1 - 2w) + k_1(z_2 + \bar{z}_2) + \alpha(z, u) + \alpha(\bar{z}, u)}{\beta(z, u) - 3\beta(\bar{z}, u)}. \qquad (32)
$$

Since the linearizing control law (32) uses $\dot{u}$ as the controller output, the proposed control law corresponds to dynamic feedback linearization [17], [25].
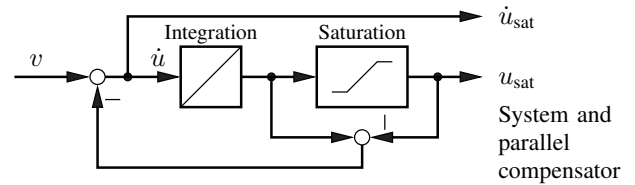

Fig. 3. Anti-wind-up scheme for the dynamic controller

To implement the control law (32), the parallel compensator (26) in its original coordinates is used:

$$
\begin{aligned}
\dot{\bar{x}}_1 &= -(1-u)\frac{1}{L}\bar{x}_2 + \frac{E}{L} - \frac{4\bar{x}_1}{u-1}\dot{u}, \\
\dot{\bar{x}}_2 &= (1-u)\frac{1}{C}\bar{x}_1 - \frac{1}{RC}\bar{x}_2. \qquad (33)
\end{aligned}
$$

Furthermore, we apply (19) and (22) to transform the control law (32) into the original coordinates. This substitution leads to a comparatively large expression, which is omitted here.

In theory, the duty ratio u is restricted to $u \in (0,1)$. In practice, the power transistor used in the converter has a finite switching time, e.g. due to parasitic capacitances. As a consequence, duty rations near 0 or near 1 should be avoided. In our simulation, we hence limit the duty ration to $u \in [0.1, 0.9]$. Because u is generated from its time derivative provided by the control law (32), we combined the integration from $\dot{u}$ to u with an anti-wind-up scheme shown in Fig. 3, see [30]. This scheme results in the quantities u_{sat} and $\dot{u}_{\mathrm{sat}}$, which are used in the control law (32) and the parallel compensator instead of u and $\dot{u}$.

A. Numerical Simulation

In the numerical simulation we use the reference voltage $w = x_2^0 = 20\,\mathrm{V}$ for $t < 400\,\mathrm{ms}$. This corresponds to $x_1^0 = 2.\bar{6}\,\mathrm{A}$ and $u^0 = 0.25$ according to (10). We used these values as initial values for the parallel compensator (33), i.e., $\bar{x}_1(0) = 2.667$, $\bar{x}_2(0) = 20$, and the integrator, i.e., $u(0) = 0.25$. For the plant (9) we took the initial values to $x_1(0) = 2$ and $x_2(0) = 19$. At $t \geq 200\,\mathrm{ms}$ we set the reference voltage to $w = x_2^0 = 25\,\mathrm{V}$ corresponding to $x_1^0 = 4.1\bar{6}\,\mathrm{A}$ and $u^0 = 0.4$. The two eigenvalues of the desired linear error dynamics (31) law were placed at $200\,\mathrm{s}^{-1}$ and $300\,\mathrm{s}^{-1}$. This results in the (normalized) coefficients $k_0 = 60000$ and $k_1 = 500$.

Fig. 4 shows the simulation results for $t = 0 \ldots 400\,\mathrm{ms}$. In the beginning we have some oscillation due to the deviation between the initial values and the operating point as well as of the plant and the parallel compensator. Then, visual inspection shows that the trajectories converge to the desired reference points. The simulation was carried out with Scilab [31]. We made the source file available on Github [32].

VII. CONCLUSION

In this contribution nonlinear control of non-minimum phase systems has been studied. Here, the main challenge is the stabilization of the unstable zero dynamics. As this cannot be achieved by feedback, application of a parallel compensator has been proposed. For the class of nonlinear maximum phase systems, i.e., systems where the modification $\frac{\mathrm{d}}{\mathrm{d}t} \mapsto -\frac{\mathrm{d}}{\mathrm{d}t}$
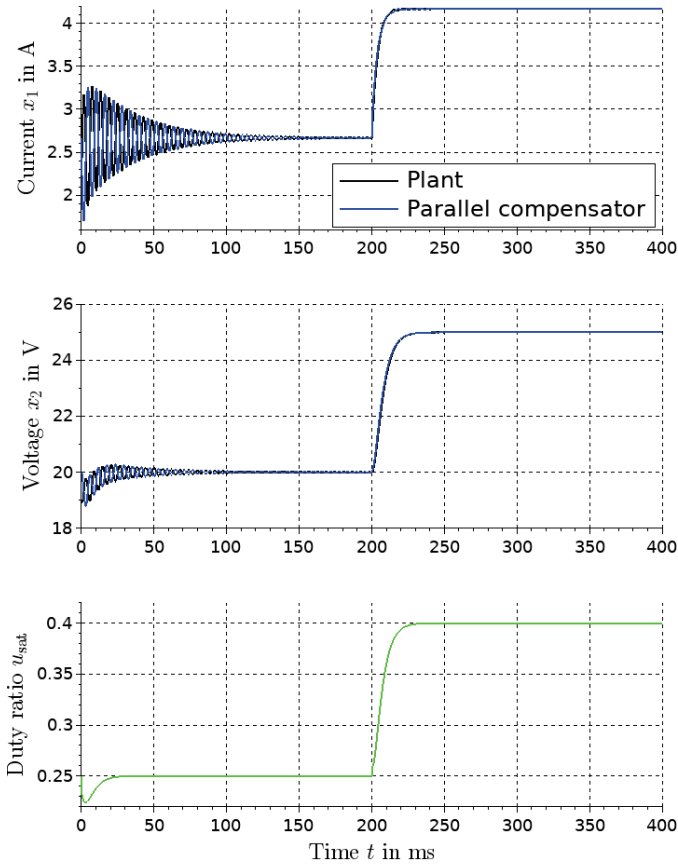
Fig. 4. Simulation results of the controlled converter model

results in a minimum phase system, a design procedure has been developed. Here, the main idea is to use the minimum phase system, associated with the original maximum phase system by the modification $\frac{\mathrm{d}}{\mathrm{d}t} \mapsto -\frac{\mathrm{d}}{\mathrm{d}t}$, as a desired system for the parallel interconnection of plant and parallel compensator. From which the later can then be directly derived. For the augmented minimum phase system nonlinear control design procedures can be readily applied. The proposed approach has been successfully evaluated on a boost converter with voltage output, which is known to be maximum phase and thus possesses unstable zero dynamics.

REFERENCES

[1] A. Isidori, *Nonlinear Control Systems: An Introduction*, 3rd ed. London: Springer-Verlag, 1995.

[2] H. Nijmeijer and A. J. van der Schaft, *Nonlinear Dynamical Control systems*. New York: Springer-Verlag, 1990.

[3] M. Fliess, J. Lévine, P. Martin, and P. Rouchon, "Flatness and defect of non-linear systems: Introductory theory and examples," *Int. J. Control*, vol. 61, pp. 1327–1361, 1995.

[4] A. Isidori, "The zero dynamics of a nonlinear system: From the origin to the latest progresses of a long successful story," *European Journal of Control*, pp. 369–378, 2013.

[5] D. J. Leith and W. E. Leithead, "Input-output linearisation of nonlinear systems with ill-defined relative degree: the ball and beam revisited," in *Proc. American Control Conference (ACC)*, vol. 4, 2001, pp. 2811–2816.

[6] F. Zhang and B. Fernandez-Rodriguez, "Feedback linearization control of systems with singularities: a ball-beam revisit," in *Proc. Int. Conf. on Complex Systems*, 2006.

[7] B. Charlet, J. Lévine, and R. Marino, "Sufficient conditions for dynamic state feedback linearization," *SIAM J. Control and Optimization*, vol. 29, pp. 38–57, 1991.

[8] M. van Nieuwstadt, M. Rathinam, and R. M. Murray, "Differential flatness and absolute equivalence," in *Proc. IEEE Conf. on Decision and Control (CDC)*, vol. 1, Dec. 1994, pp. 326–332.

[9] K. Schlacher and M. Schöberl, "Construction of flat outputs by reduction and elimination," *IFAC Proceedings Volumes*, vol. 40, no. 12, pp. 693–698, 2007.

[10] F. Antritter and J. Lévine, "Flatness characterization: Two approaches," in *Advances in the Theory of Control, Signals and Systems with Physical Modeling*. Springer, 2010, pp. 127–139.

[11] K. Fritzsche, C. Knoll, M. Franke, and K. Röbenack, "Unimodular completion and direct flat representation in the context of differential flatness," *Proc. in Applied Mathematics and Mechanics*, vol. 16, no. 1, pp. 807–808, 2016.

[12] S. Skogestand and I. Postlethwaite, *Multivariable Feedback Control Second Edition: Analysis and Design*, 2nd ed. Wiley, 2005.

[13] H. Schwarz, "Changing the unstable zero dynamics of nonlinear systems via parallel compensation," in *Control '96, UKACC International Conference on (Conf. Publ. No. 427)*, Exeter, UK, Sep. 1996.

[14] ——, "Compensation of the instable zerodynamics of nonlinear system," *Automatisierungstechnik*, vol. 44, no. 4, pp. 180–183, 1996, in German.

[15] S. Palis and A. Kienle, "Discrepancy based control of particulate processes," *Journal of Process Control*, vol. 24, no. 3, pp. 33–46, 2014.

[16] I. Golovin and S. Palis, "Design of parallel feed-forward compensator and its application to electromechanical system with friction load," *IFAC-PapersOnLine*, vol. 50, no. 1, pp. 15 524–15 529, 2017.

[17] M. Fliess, "Generalized controller canonical form for linear and nonlinear dynamics," *IEEE Trans. on Automatic Control*, vol. 35, no. 9, pp. 994–1001, 1990.

[18] F. J. Doyle III, F. Allgöwer, and M. Morari, "A normal form approach to approximate input-output linearization for maximum phase nonlinear SISO systems," *IEEE Trans. on Automatic Control*, vol. 41, no. 2, pp. 305–309, Feb. 1996.

[19] D. K. Arrowsmith and C. M. Place, *An Introduction to Dynamical Systems*. Cambridge: Cambridge University Press, 1990.

[20] S. Bacha, I. Munteanu, and A. I. Bratcu, *Power Electronic Converters Modeling and Control*. London: Springer-Verlag, 2014.

[21] R. W. Erickson and D. Maksimović, *Fundamentals of Power Electronics*, 2nd ed. New York: Kluwer Academic Publishers, 2004.

[22] G. Escobar, R. Ortega, H. Sira-Ramirez, J. P. Vilan, and I. Zein, "An experimental comparison of several non linear controllers for power converters," *IEEE Control Systems*, vol. 19, no. 1, pp. 66–82, 1999.

[23] D. Shuai, Y. Xie, and X. Wang, "The research of input-output linearization and stabilization analysis of internal dynamics on the CCM boost converter," in *Int. Conference on Electrical Machines and Systems (ICEMS 2008)*, Oct. 2008, pp. 1860–1864.

[24] K. Röbenack, *Nichtlineare Regelungssysteme: Theorie und Anwendung der exakten Linearisierung*. Berlin, Heidelberg: Springer Vieweg, 2017.

[25] K. Röbenack and S. Palis, "Nonlinear control of flat systems using a non-flat output with dynamic extension," in *International Conference on System Theory, Control and Computing (ICSTCC 2018)*, Sinaia, Romania, Oct. 2018.

[26] J. Liu, W. Ming, and F. Gao, "A new control strategy for improving performance of boost DC/DC converter based on input-output feedback linearization," in *Proc. of the 8th World Congress on Intelligent Control and Automation*, Jinan, China, Jul. 2010.

[27] H. Sira-Ramirez, "Sliding modes, passivity, and flatness," in *Sliding Mode Control In Engineering*, W. Perruquetti and J.-P. Barbot, Eds. CRC Press, 2002.

[28] A. Griewank and A. Walther, *Evaluating Derivatives: Principles and Techniques of Algorithmic Differentiation*, 2nd ed. Philadelphia: SIAM, 2008.

[29] K. Röbenack, "Computation of multiple Lie derivatives by algorithmic differentiation," *J. of Computational and Applied Mathematics*, vol. 213, no. 2, pp. 454–464, 2008.

[30] P. Hippe, *Windup in Control: Its Effects and Their Prevention*. London: Springer-Verlag, 2006.

[31] C. Gomez, *Engineering and Scientific Computing with Scilab*. Boston: Birkhäuser, 1999.

[32] "Parallel compensator for a boost converter," https://github.com/TUD-RST/parallel-compensator-boost.

Online parameter identification for continuous fluidized bed spray granulation with external sieve-mill cycle

Stefan Palis
Otto-von-Guericke-University,
Magdeburg, Germany

Achim Kienle
Otto-von-Guericke-University,
Magdeburg, Germany
Max-Planck-Institute for Dynamics of Complex Technical Systems
Magdeburg, Germany

Abstract—**Parametrization of process models is an important task and often the first step in process control and monitoring. For continuous fluidized bed spray granulation, being often described by population balance models parameter estimation is particularly challenging due to the infinite-dimensional state space. In this contribution a Lyapunov-based approach is used to derive the appropriate online parameter estimation laws for a fluidized bed spray granulation with external sieve-mill cycle.**

I. Introduction

For many processes transformation of a liquid product into its solid form is an important final task. This is especially true for production processes in food, chemical and pharmaceutical industries. An important process here is granulation, which is often combined with fluidized bed technology. Starting with an initial solid particle bed, the latter is fluidized by passing a gas or liquid. Fluidization has two positive effects: first the bed porosity and thus the active surface are considerably enlarged, second particle mixing is increased resulting in a faster homogenization of bed states.

It is well known that continuous fluidized bed spray granulation may become unstable resulting in nonlinear limit cycles under certain operation conditions and for certain process configurations. Hence, different control approaches have been proposed for stabilization [4] - [7]. All the controllers depend on a parametrized plant model. However, in reality parameters may be not known a-priori or vary during plant operation. Thus, online parameter estimation is a crucial task. In this contribution the problem of online parameter estimation for continuous fluidized bed spray granulation with external sieve-mill cycle is investigated.

II. Continuous fluidized bed spray granulation

The granulator consists of a granulation chamber. Here, particles are fluidized through an air stream with predefined conditions (pressure, temperature and humidity). Then a liquid is injected, which settles on the particles. Due to the increased temperature and low humidity of the supplied air the liquid fraction is evaporated. It remains a new solid layer on the particle surface resulting in a particle size increase. The growth of the particle ensemble can be described by

$$G = \frac{2\dot{m}_e}{\pi\mu_2} \qquad (1)$$

where $\dot{m}_e$ is the effective solid mass injected into the process chamber and μ_2 is the second moment of the particle size distribution $\mu_2 = \int_0^\infty L^2 n dL$ resembling the overall surface of the particle bed [1].

In order to allow a continuous operation of the fluidized bed spray granulation, particles are continuously removed and sieved. Here, three fractions are generated product particles, oversized particles, i.e. particles being bigger than a certain size, and fine particle, i.e. particles being smaller than the product specification. The production fraction is removed from the process, the fines fraction is directly fed back and the oversize fraction is fed to a mill, where it is grinded. The milled particles are then fed back as new nuclei to the process chamber. The overall process scheme is depicted in Fig. 1.
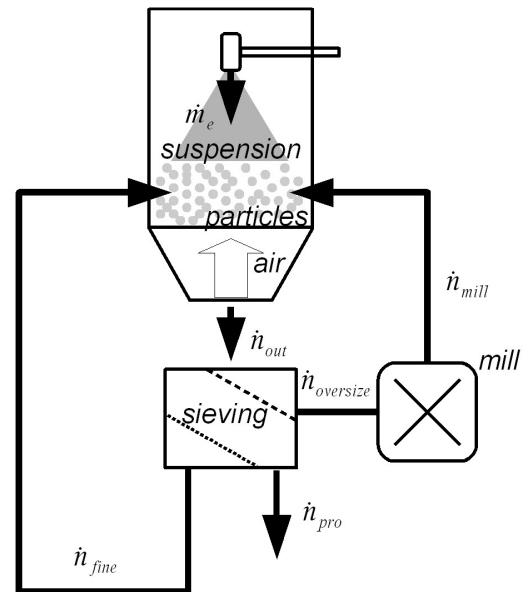

Fig. 1.   Process scheme

From the granulation process particles are continuously redrawn and feed to two sieves resulting in three particle

fractions product $\dot{n}_p$, fines $\dot{n}_f$ and oversized $\dot{n}_o$.

$$\dot{n}_p = T_2(L)(1 - T_1(L))\dot{n}_{out} \tag{2}$$
$$\dot{n}_f = (1 - T_2(L))(1 - T_1(L))\dot{n}_{out} \tag{3}$$
$$\dot{n}_o = T_1(L)\dot{n}_{out} \tag{4}$$

Here, $T_1(L)$ and $T_2(L)$ are the associated screening functions depicted in Fig. 2.

$$T_{1,2}(L;\mu,\sigma) = \frac{\int_0^L \exp\left(\frac{-(\hat{L}-\mu)^2}{4\sigma^2}\right) d\hat{L}}{\int_0^\infty \exp\left(\frac{-(\hat{L}-\mu)^2}{4\sigma^2}\right) d\hat{L}} \tag{5}$$
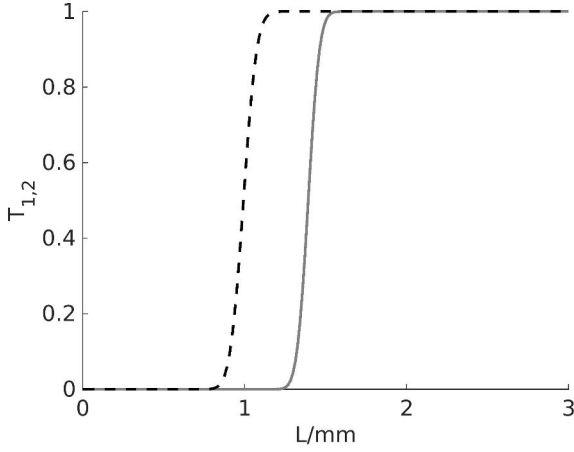
Fig. 2.   Screening functions T_1 (gray) and T_2 (black dotted)

The oversized fraction is first grinded by the mill and then fed back as $\dot{n}_m$ to the first granulation chamber together with the fines fraction $\dot{n}_f$. The particle size distribution generated by the mill is typically tri-modal (Fig. 3), where the proportion of each distribution depends on the specific mill power P_{mill}.
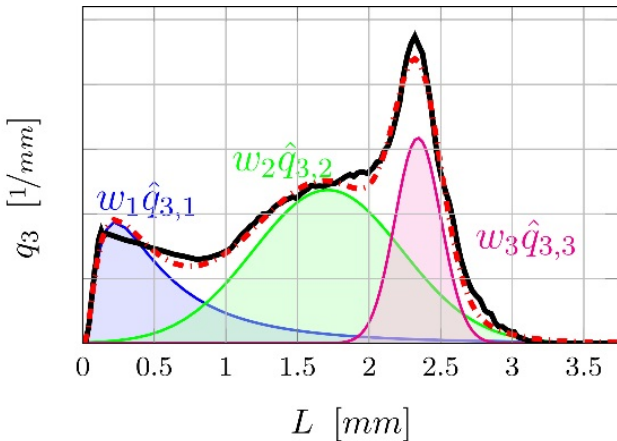
Fig. 3.   Particle size distribution of milled particles

It is assumed that the mill is mass conserving, i.e. the third moment of the oversize fraction is equal to the third moment of the particle distribution generated by the mill. The mill model is hence given by

$$\dot{n}_m = \sum_{i=1}^3 a_i \varphi_i(L) \int_0^\infty L^3 \dot{n}_o dL \tag{6}$$

where a_i are the weights of the distributions $\varphi_i(L)$ and $\int_0^\infty L^3 \dot{n}_o dL$ is the third moment of the oversize fraction [8]. In can be assumed that milling particles conserves the overall mass. Thus, the third moment of the oversize fraction $\dot{n}_o$ and the milled fraction $\dot{n}_m$ have to be equal,

$$\int_0^\infty L^3 \dot{n}_m dL = \int_0^\infty L^3 \dot{n}_o dL \tag{7}$$

resulting in an additional constraint on the distribution weights.

$$\int_0^\infty L^3 \sum_{i=1}^3 a_i \varphi_i(L) dL = 1 \tag{8}$$

Resolving this constraint by calculating the appropriate coefficient a_3

$$a_3 = \frac{1 - \int_0^\infty L^3 \sum_{i=1}^2 a_i \varphi_i(L) dL}{\int_0^\infty L^3 \varphi_3(L) dL} \tag{9}$$

yields an unconstrained mill model with two independent parameters a_1 and a_2.

$$\dot{n}_m = \left[\sum_{i=1}^2 a_i \left(\varphi_i(L) - \frac{\int_0^\infty L^3 \varphi_i(L) dL}{\int_0^\infty L^3 \varphi_3(L) dL}\varphi_3(L)\right) + \ldots \right.$$
$$\left. \ldots + \frac{\varphi_3(L)}{\int_0^\infty L^3 \varphi_3(L) dL}\right]\int_0^\infty L^3 \dot{n}_o dL \tag{10}$$
$$= \left(\sum_{i=1}^2 a_i \phi_i(L) + \bar{\varphi}_3(L)\right)\int_0^\infty L^3 \dot{n}_o dL \tag{11}$$

where

$$\phi_i(L) = \varphi_i(L) - \frac{\int_0^\infty L^3 \varphi_i(L) dL}{\int_0^\infty L^3 \varphi_3(L) dL}\varphi_3(L), \tag{12}$$
$$\bar{\varphi}_3(L) = \frac{\varphi_3(L)}{\int_0^\infty L^3 \varphi_3(L) dL}. \tag{13}$$

From a practical point of view, the knowledge of the weights a_i of each distribution is of utmost importance. However, offline identification using individual experiments is very expensive and raises many uncertainties. This is due to the fact that the behavior of the milling processes varies not only with the supplied power, but also with the supplied solid particle flow, its particle size, porosity and moisture distribution. Therefore, in this contribution it will be assumed that the weights a_i of each distribution are unknown and should thus be identified during process operation.

Assuming ideal mass control the drain K is calculated such that the first time derivative of μ_3 becomes zero implying a constant bed mass

$$\dot{\mu}_3 = \int_0^\infty L^3 \frac{\partial n}{\partial t} dL = 0 \tag{14}$$
$$= \int_0^\infty L^3 \left[-G\frac{\partial n}{\partial L} - \dot{n}_o - \dot{n}_p + \dot{n}_m\right] dL. \tag{15}$$

Because the mill is assumed to be mass conserving the third moments of the oversize flux and mill flux are equal resulting in

$$K = \frac{\int_0^\infty L^3 \left(-G\frac{\partial n}{\partial L}\right) dL}{\int_0^\infty L^3 T_2(1 - T_1)n dL}. \qquad (16)$$

To describe the process, the following population balance model, consisting of the particle fluxes due to product particle withdrawal $KT_1(1-T_2)n$, particle growth and the reflux from the mill, can be used.

$$\frac{\partial n}{\partial t} = -G\frac{\partial n}{\partial L} - KT_1(1 - T_2)n - KT_1T_2n + \dots$$
$$\dots + \left(\sum_{i=1}^{2} a_i\phi_i + \bar{\varphi}_3\right)\int_0^\infty L^3 \dot{n}_o dL \qquad (17)$$

It is well known [2; 3] that the given process configuration becomes unstable for sufficiently high mill power and associate small mill grade. The loss of stability is connected with the occurrence of a stable limit cycle depicted in 4. From a
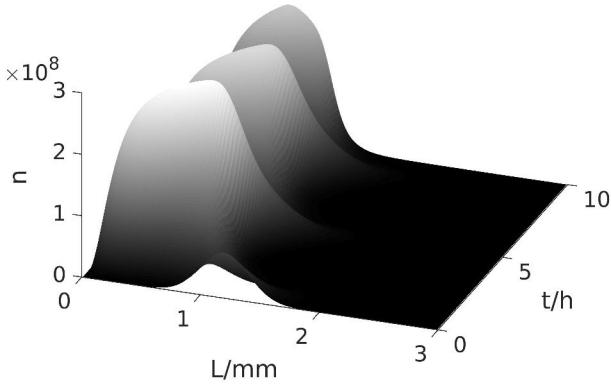
Fig. 4.   Limit cycle of the particle size distribution

practical point of view, the derivation of estimates for the stability boundaries or the design of a stabilizing control is of utmost importance for a reliable process operation. Both can be achieved on the basis of the given model assuming known parameters. Whereas the derivation of the sieving function or growth rate can be done on the basis of typically simple experiments on the single apparatus, identification of the mill parameters is challenging. This is due to the fact, that they depend not only on the mill type but also on the supplied mill power, material flow rate and its size distribution, structure and moisture content. Hence, an identification using synthetic offline experiments is in general unreliable. In this contribution, online identification, i.e. parameter estimation during process operation, will be studied as a solution to the aforementioned problem.

III. ONLINE PARAMETER IDENTIFICATION

In order to derive an adaptation algorithm for an affine parameterized model in this contribution a Lyapunov-based parameter estimation approach (see e.g. [9] and references therein) will be used. Here, the system with the unknown parameters is augmented by a modified plant model resembling the plant structure and incorporating an additional observer term. For the given fluidized bed spray granulation process with unknown mill parameters the modified plant model is given by

$$\frac{\partial \hat{n}}{\partial t} = -G\frac{\partial n}{\partial L} - KT_1(1 - T_2)n - KT_1T_2n + \dots$$
$$\dots + \left(\sum_{i=1}^{2} \hat{a}_i\phi_i + \bar{\varphi}_3\right)\int_0^\infty L^3 \dot{n}_o dL - \dots$$
$$-c(\hat{n} - n) \qquad (18)$$

where $\hat{a}_i$ are the estimated mill parameters and $\hat{n}$ is the particle size distribution estimated from the modified plant model. The parameter c is an additional tuning parameter. The associated estimation errors are defined as

$$e = \hat{n} - n, \qquad (19)$$
$$\tilde{a}_i = \hat{a}_i - a_i. \qquad (20)$$

From a practical point of view it is important to note that particle size distribution can be directly measured using for example a Parsum probe. In order to derive the adaptation laws $\hat{a}_i$ for the parameter estimates $\hat{a}_i$ the following candidate Lyapunov functional is chosen

$$V = \frac{1}{2}\int_0^\infty e^2 dL + \sum_{i=1}^{2} \frac{1}{2\gamma_i}\tilde{a}_i^2 \qquad (21)$$

where γ_i are positive real constants. It should be mentioned that in case of convergence of the modified plant particle size distribution $\hat{n}$ towards the real particle size distribution n in sense of the L_2-norm and for vanishing parameter estimation errors the Lyapunov functional V itself vanishes. Applying standard Lyapunov stability theory, stability can be achieved in case that the first time derivative of the Lyapunov functional V is negative semidefinite along the trajectory of (17).

$$\dot{V} = \int_0^\infty e\left(\sum_{i=1}^{2} \tilde{a}_i\phi_i(L)\int_0^\infty L^3\dot{n}_o dL - ce\right) dL \dots$$
$$\dots + \sum_{i=1}^{2} \frac{1}{\gamma_i}\tilde{a}_i\dot{\hat{a}}_i \qquad (22)$$

Choosing the adaptation laws $\dot{\hat{a}}_i$ as follows

$$\dot{\hat{a}}_i = -\gamma_i \int_0^\infty e\phi_i(L)dL \int_0^\infty L^3\dot{n}_p dL \qquad (23)$$

results in the desired negative semi definite of the time derivative of V

$$\dot{V} = -c\int_0^\infty e^2 dL. \qquad (24)$$

The overall parameter estimation scheme is shown in Fig. 5 and consists of the proposed modified plant model (18) and the Lyapunov based adaptation laws (23). Here, u is an external disturbance or control input, which should be chosen such that an appropriate parameter update is guaranteed (persistent excitation).
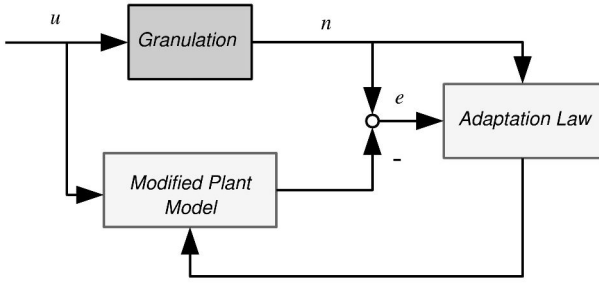
Fig. 5.   Parameter identification scheme

It should be mentioned, that the derived observer model and adaptation law require require both an online measurement of the particle size distribution $n(t, L)$, which can be realized by applying specific measurement devices, e.g. Parsum probe or FBRM.

IV.   RESULTS

For numerical simulation the model equations are discretized along the property coordinate applying the finite volume method (1st order upwind flux discretization) with 200 grid points. For simplicity constant control inputs and fixed system parameters in the region of instability, i.e. unstable steady state particle size distribution, are chosen. In this case, the granulation process exhibits self-sustained oscillations, i.e. possesses a stable limit cycle. Due to the particle size distribution measurement, the initial uncertainty is only in the mill parameters a_1 and a_2. Here, an error of 60 % in each parameter has been assumed resulting in an considerable deviation between assumed and real milled particle size distribution (Fig. 6).
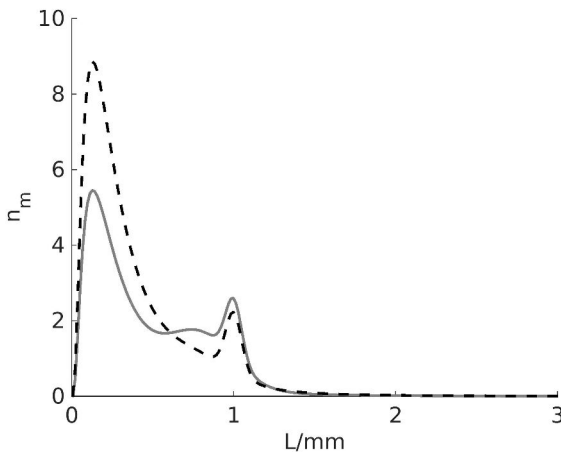
Fig. 6.   Assumed (black dotted) and real (gray) milled particle size distribution

As can be seen in Fig. 7 and 8 the unknown system parameters a_i can be identified in within approximately one hour, which is reasonably taking into account the slow process dynamics. During the parameter estimation the state of the modified plant model $\hat{n}$ (Fig. 11) shows only a relative small
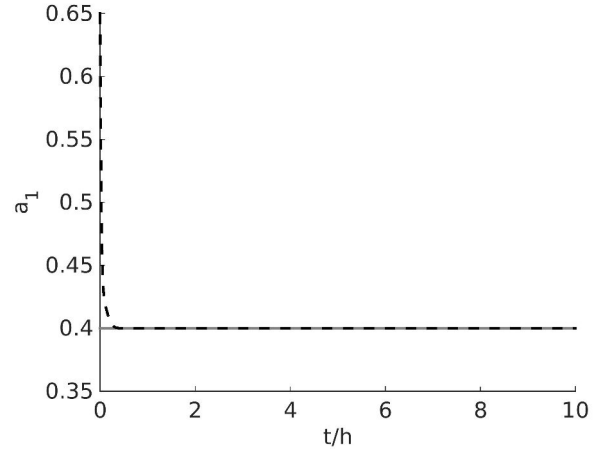
Fig. 7.   Convergence of the mill parameters a_1 estimate $\hat{a}_1$ (black dotted)
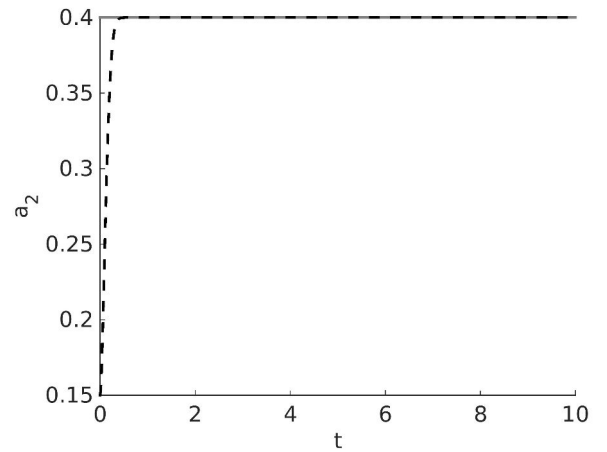

Fig. 8.   Convergence of the mill parameters a_2 estimate $\hat{a}_2$ (black dotted)

error in sense of the L_2 -norm (Fig. 9). From a practical point of view, increasing the parameter c results in a faster convergence of the observer model state towards the plant state, which is desired for attenuation of measurement noise. On the other hand, as the adaptation laws depend on the misfit between the observer model state and the plant state, an increasing parameter c results in a shorter adaptation phase and may thus prevent parameter convergence.

V.   CONCLUSION

In this contribution online parameter estimation of fluidized bed spray granulation with external sieve-mill cycle has been studied. It has been shown that the proposed adaptation laws allow a sufficiently fast estimation of the unknown parameters. Future work will be concerned with robustness with respect to measurement noise, real plant experiments and the application of the proposed adaptation laws in a control scheme.

Fig. 9. L_2-norm of the error between plant and modified plant model state

Fig. 10. Particle size distribution n of the plant

Fig. 11. Particle size distribution $\hat{n}$ of the modified plant model

REFERENCES

[1] L. Mörl, M. Mittelstrass, J. Sachse, Zum Kugelwachstum bei der Wirbelschichttrocknung von Lösungen oder Suspensionen, Chem. Techn. 29, 1977, Heft 10, pp. 540-542.

[2] M. Schmidt, C. Rieck, A. Bück and E. Tsotsas, Experimental investigation of process stability of continuous spray fluidized bed layering with external product separation, Chemical Engineering Science, 2015, pp. 466-475.

[3] C. Dreyschultze, C. Neugebauer, S. Palis, A. Bück, E. Tsotsas, S. Heinrich and A. Kienle, Influence of zone formation on stability of continuous fluidized bed layering granulation with external product classification, Particuology, 2015, pp. 1-7.

[4] S. Palis & A. Kienle, Stabilization of continuous fluidized bed spray granulation - a Lyapunov approach, 8th IFAC Symposium on Nonlinear Control Systems - NOLCOS, 2010.

[5] S. Palis & A. Kienle, Stabilization of continuous fluidized bed spray granulation with external product classification, Chem. Eng. Sci. 70, 2012, pp. 200-209.

[6] S. Palis and A. Kienle, Discrepancy based control of particulate processes, Journal of Process Control, 2014, pp. 33-46.

[7] S. Palis and A. Kienle, H_∞ loop shaping control for continuous fluidized bed spray granulation with internal product classification, Industrial & Engineering Chemistry Research, 2013, pp. 408-420.

[8] C. Neugebauer, S. Palis, A. Bück, E. Diez, S. Heinrich, E. Tsotsas and A. Kienle, Influence of mill configuration on stability of continuous layering granulation with external product classification, accepted for publication at the ESCAPE 26, 2016.

[9] M. Krstic, Systematization of approaches to adaptive boundary stabilization of PDEs, Int. J. of Robust Nonlinear Control 16, 2006, pp. 801-818.
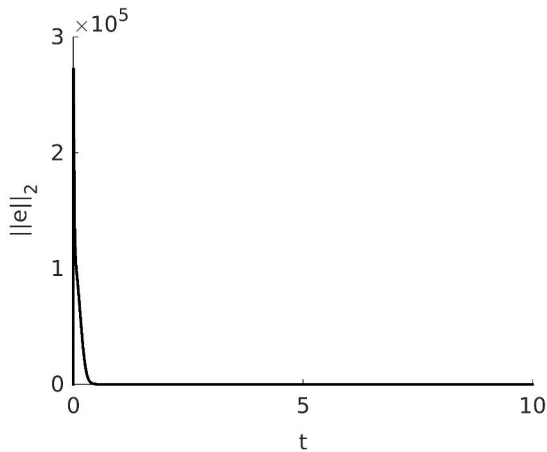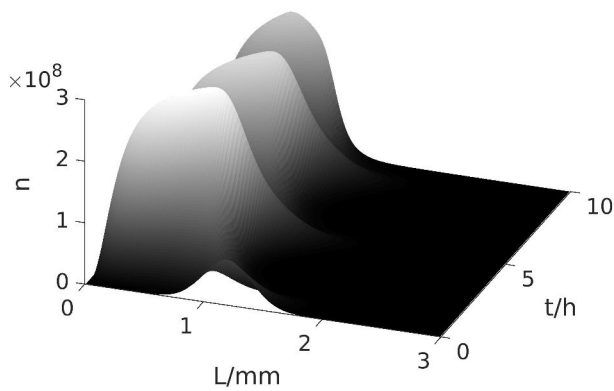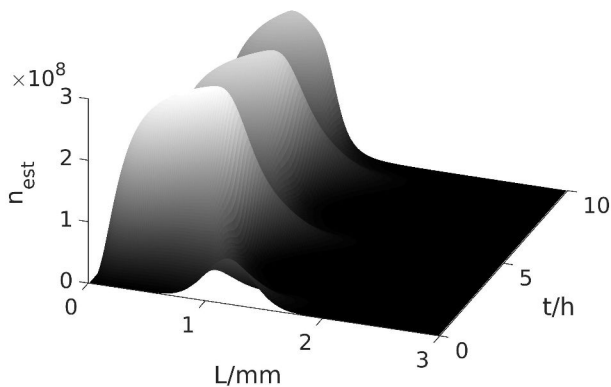
Control-based damping of elastic gantry crane vibrations

Ievgen Golovin
Otto-von-Guericke University Magdeburg
Universitätsplatz 2, Magdeburg 39106, Germany
Email: ievgen.golovin@ovgu.de

Stefan Palis
Otto-von-Guericke University Magdeburg
Universitätsplatz 2, Magdeburg 39106, Germany
Email: stefan.palis@ovgu.de

Abstract—In this article control-based reduction of gantry crane elastic swinging in the trolley travel direction is concerned. As acceleration forces of the trolley are often the reason of these vibrations, they can be utilized in an appropriate damping strategy. For an elastic crane a dynamic model is derived applying the finite element method (FEM). This approach results in a high order state-space model, which should be reduced for the controller design procedure. In order to design a controller, which can be applied for simultaneous damping of elastic vibrations of crane construction and payload sway with varying rope length a robust control approach has been applied.

I. Introduction

Nowadays, rapid transportation and well-designed logistics play an important role in the development of trade and industry. Time reduction for these operations requires utilizing automated and efficient equipment, including cranes. At port terminals for example gantry cranes are widely used for loading and unloading of containers. Due to continuous weight reduction and increasing crane sizes, structure stiffness is decreasing and may lead to an increased influence of elastic vibrations. Often these vibrations are consequences of dynamic coupling between crane trolley, load and mechanical structure appearing due to trolley acceleration forces [1].

Low frequency vibrations in travel direction of trolley are particularly negative because of their large displacements and undamped behaviour. They produce additional mechanical stresses, which lead to faster material fatigue and hence reduce operating life of the crane. Moreover, these vibrations have a disturbing impact on the crane operator extending the time needed for the positioning process.

Currently three approaches exist for vibration reduction. The first one is the mechanical optimization of the gantry structure [2; 3]. Here, crane structure stiffness is enhanced by increasing supporting legs thickness or by stiffening of portal frames. The second approach introduces an additional weight as a counter-mass acting as a passive damper [4]. The obtained damping is typicaly small whereas the investment costs are considerable. The third concept is utilization of an actuated counterweight, where the mass movement compensates natural vibrations of the structure. This method is more effective but it requires an additional linear drive system, which takes a lot of supplementary costs [4].

In this contribution a new active damping approach without an additional electric drive system is presented. Here, the reduction of elastic crane vibrations as well as the anti-sway control is provided only by trolley acceleration forces. For this purpose, an extension of the motion control system of

trolley with payload is necessary. In order to design a control law, which can be easily implemented for operation with different rope length, the application of robust control methods is proposed.

In section 2 the mathematical model of an elastic gantry crane with the electric drive system and the model reduction procedure for large-scale crane structure are introduced. Model errors and uncertainties as well as control design are discussed in section 3. Section 4 concludes the contribution with simulation results from the nonlinear high-order gantry crane model.

II. Mathematical modeling

A. Elastic crane model

Mathematical modeling of mechanical structures in general and large cranes in particular is a non-trivial task, and utilizing analytical methods is often restricted to simple geometries, loads and boundary conditions. For simulations of more complex mechanical models numerical methods are usually used. In this contribution the commercial finite element package COMSOL Multiphysics has been used to derive an elastic crane model. After spatial discretization the equations of motion with N degrees of freedom (DOF) can be represented in the general form:

$$M_g \ddot{H} + C_g \dot{H} + K_g H = F_g, \qquad (1)$$

where M_g, C_g and K_g are global mass, damping and stiffness matrices, $\ddot{H}$, $\dot{H}$ and H are vectors of acceleration, velocity and displacement at all nodes in the structure domain and F_g is the vector of all nodal forces.

Material induced damping is represented by Rayleigh damping. Here, the damping matrix C_g is expressed as a linear combination of the mass M_g and stiffness K_g matrices:

$$C_g = \alpha M_g + \beta K_g, \qquad (2)$$

where α is the mass-proportional coefficient and β is the stiffness-proportional coefficient.

Typically, gantry crane structures are very complicated consisting of multiple components. To reduce weight and to maintain a relatively high stiffness, elements with specially shaped profiles are usually used in practice. Modeling of these structures as solids requires a lot of computational time and resources. Therefore, it is good practice to simplify parts of the model geometry. Fig. 1 shows the model of the gantry crane in two dimensions. It consists of solid steel beams, which mass corresponds to the mass of the real elements of the crane. The lower parts of the crane legs are fixed. The excitation of
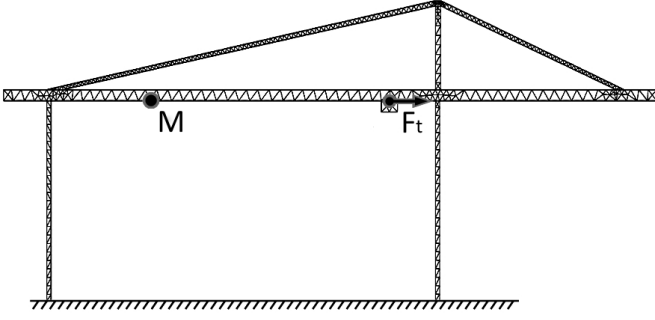
Fig. 1. Gantry crane FEM Model

structural vibrations due to trolley motion is reflected by an external point force F_t. The damping ratio $\xi = 0.005$ has been obtained from practical measurements of real gantry crane swinging. The crane structure has been discretized applying an unstructured mesh with triangular elements resulting in 3458 DOF.

Considering that the external force F_t is an input to the crane plant $u(t) = F_t$ and the crane point M is the displacement output of interest $y(t) = d_M$, the FEM-crane model can be represented for small variations as a linear high order state-space model

$$\begin{align}
\dot{x}(t) &= Ax(t) + Bu(t), & (3) \\
y(t) &= Cx(t) + Du(t), & (4)
\end{align}$$

where A, B, C and D are constant matrices.

B. Model order reduction

The order of the state-space model derived by the finite element model is approximately 7000. In order to allow the design of a controller with low order an additional model reduction should be performed. For the model reduction of gantry crane dynamics the balanced truncation approximation has been used. This method is based on the balanced realization of the system model, i.e. the asymptotically stable minimal realization where the controllability Gramian matrix W_c and observability Gramian matrix W_o are equal and diagonal [5; 6].

$$\begin{align}
W_c &= \int_0^{t_e} e^{At} BB^T e^{A^T t} dt \\
&= \int_0^{t_e} e^{A^T t} C^T C e^{At} dt = W_o = \Sigma. & (5)
\end{align}$$

Here, the diagonal matrix Σ fulfils the following Lyapunov equations:

$$\begin{align}
A\Sigma + \Sigma A^T + BB^T &= 0, & (6) \\
\Sigma A + A^T \Sigma + C^T C &= 0. & (7)
\end{align}$$

The elements of Σ are called the Hankel singular values σ_i and are order by size, i.e. $\sigma_i \geq \sigma_{i+1}$.

$$\Sigma = \begin{bmatrix} \sigma_1 & 0 & 0 \\ 0 & \ddots & 0 \\ 0 & 0 & \sigma_n \end{bmatrix}, \sigma_1 \geq \sigma_2 \geq \cdots \geq \sigma_n \geq 0. \quad (8)$$

States associated with the big Hankel singular values have by construction a dominant influence on the input-output behavior and should thus be conserved. Let the balanced realization of the high order state-space model of elastic crane (3), (4) be partitioned as

$$A = \begin{bmatrix} A_{11} & A_{12} \\ A_{21} & A_{22} \end{bmatrix}, B = \begin{bmatrix} B_1 \\ B_2 \end{bmatrix},$$

$$C = [C_1 \quad C_2], \Sigma = \begin{bmatrix} \Sigma_1 & 0 \\ 0 & \Sigma_2 \end{bmatrix}, \quad (9)$$

where $\Sigma_1 = diag(\sigma_1, \sigma_2, \ldots, \sigma_k)$ are the first k dominant Hankel singular values and $\Sigma_2 = diag(\sigma_{k+1}, \sigma_{k+2}, \ldots, \sigma_n)$. Removing the system part corresponding to the Σ_2, will result in an approximation

$$\begin{align}
\dot{x}(t) &= A_{11}x(t) + B_1 u(t), & (10) \\
y(t) &= C_1 x(t) + D_1 u(t), & (11)
\end{align}$$

with the following equivalent transfer function

$$G_1(s) = C_1(sI - A_{11})^{-1} B_1 + D_1. \quad (12)$$

The error introduced by the described model reduction procedure can be overestimated by

$$\|G(s) - G_1(s)\|_\infty \leq 2 \sum_{i=k+1}^{n} \sigma_i. \quad (13)$$

An appropriate order of the reduced model can be easily assigned, e.g. by examining the Hankel singular values diagram depicted in Fig. 2. As can be seen the first two states have a significant contribution to the overall model behavior and should hence be conserved. Therefore, a second order model $G_1(s)$ gives a reasonable approximation of elastic crane dynamics.
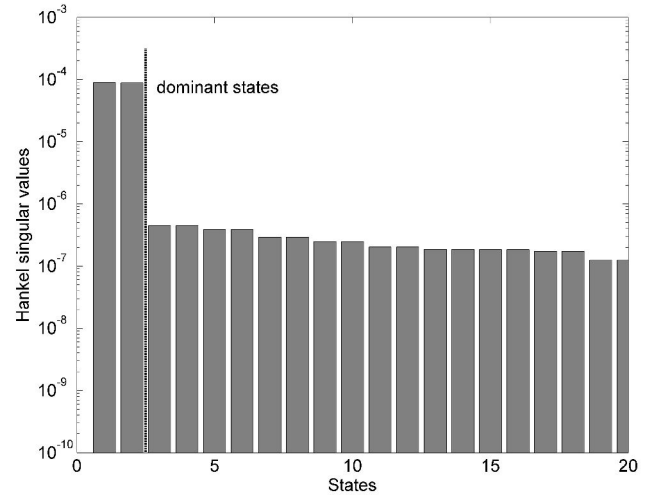

Fig. 2. Hankel singular values of the elastic crane model

C. Trolley-payload model

Fig. 3 represents motion of the trolley-payload system, where m_t is the trolley mass, m_p is the payload mass, m_r is the rope mass, F_x and F_l are the forces that are applied

to the trolley, $x(t)$ is the trolley displacement, $l(t)$ is the rope length and $\varphi(t)$ is the sway angle. The equations of motion can be derived using Euler-Lagrange equation

$$\frac{d}{dt}\left(\frac{\partial L}{\partial \dot{q}_i}\right) - \frac{\partial L}{\partial q_i} = Q_i, \quad i = 1 \ldots N, \qquad (14)$$

where $L(q, \dot{q}, t) = T - V$ is the Lagrange function (T is the kinetic energy, V is the potential energy), q_i are the generalized coordinates and Q_i are the generalized forces [7].
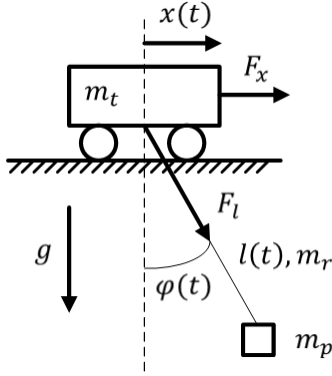
Fig. 3. Trolley-payload system

Under the assumptions that trolley and payload are connected by the massless rigid rope and neglecting the elongation of the rope, the vector of generalized coordinates yields as $q(t) = [x(t) \quad \varphi(t) \quad l(t)]^T$. The coordinate vector of payload can be given as follows:

$$s_p = [x + l\sin\varphi, \quad -l\cos\varphi]. \qquad (15)$$

Then, equations of kinetic and potential energy can be represented as:

$$T = \frac{1}{2}(m_t + m_p)\dot{x}^2 + \frac{1}{2}(m_p + m_r)\dot{l}^2 + \frac{1}{2}m_p(l\dot{\varphi})^2$$
$$+ m_p\dot{x}(l\cos\varphi\dot{\varphi} + \sin\varphi\dot{l}) + \frac{1}{2}I\dot{\varphi}^2, \qquad (16)$$
$$V = -m_p gl\cos\varphi, \qquad (17)$$

where I is the moment of inertia of the load. Finally, the equations of motion of trolley-payload system are derived for the vector of generalized coordinates $q(t)$ as follows:

$$F_x = m_o\ddot{x} + m_p\sin\varphi\ddot{l} + m_p l\cos\varphi\ddot{\varphi}$$
$$+ 2m_p\cos\varphi\dot{l}\dot{\varphi} - m_p l\sin\varphi\dot{\varphi}^2, \qquad (18)$$
$$0 = m_p l\cos\varphi\ddot{x} + (m_p l^2 + I)\ddot{\varphi} + 2m_p l\dot{l}\dot{\varphi}$$
$$+ m_L gl\sin\varphi, \qquad (19)$$
$$F_l = m_p\sin\varphi\ddot{x} + (m_r + m_p)\ddot{l} - m_p l\dot{\varphi}^2$$
$$- m_p g\cos\varphi, \qquad (20)$$

where $m_o = m_t + m_p$ is the total mass of trolley and payload. Considering the constant rope length the nonlinear equations of motion (18, 19, 20) can be linearised at the operating point of gantry crane and represented in state-space form for the state vector $x = [x \quad \dot{x} \quad \varphi \quad \dot{\varphi}]^T$, the system input $u = F_x$ and

the system output vector $y = [x \quad \dot{x} \quad \varphi]^T$ as follows:

$$\begin{bmatrix} \dot{x} \\ \ddot{x} \\ \dot{\varphi} \\ \ddot{\varphi} \end{bmatrix} = \begin{bmatrix} 0 & 1 & 0 & 0 \\ 0 & 0 & \frac{m_p g}{m_t} & 0 \\ 0 & 0 & 0 & 1 \\ 0 & 0 & -\frac{m_o g}{m_t l} & 0 \end{bmatrix} \begin{bmatrix} x \\ \dot{x} \\ \varphi \\ \dot{\varphi} \end{bmatrix} + \begin{bmatrix} 0 \\ \frac{1}{m_t} \\ 0 \\ -\frac{1}{m_t l} \end{bmatrix} u, \quad (21)$$

$$y = \begin{bmatrix} 1 & 0 & 0 & 0 \\ 0 & 1 & 0 & 0 \\ 0 & 0 & 1 & 0 \end{bmatrix} \begin{bmatrix} x \\ \dot{x} \\ \varphi \\ \dot{\varphi} \end{bmatrix} + \begin{bmatrix} 0 \\ 0 \\ 0 \end{bmatrix} u. \qquad (22)$$

D. Augmented trolley-payload model

Currently, most crane systems are equipped with an electric drive system, which typically provides the velocity control of trolley travelling, in general cascade control with PI controllers [8]. Augmenting the trolley-payload model (21, 22) by the transfer function of the velocity controller

$$u(s) = k_p(sx_{ref} - sx) + \frac{k_p}{T_i}(x_{ref} - x) \qquad (23)$$

the new state vector becomes $x = [x \quad \dot{x} \quad \varphi \quad \dot{\varphi} \quad x_{soll}]^T$. It should be mentioned that the control input becomes the reference velocity $u = \dot{x}_{ref}$. With the system output vector $y = [x \quad \dot{x} \quad \varphi \quad F_x]^T$ the system matrices are:

$$A_2 = \begin{bmatrix} 0 & 1 & 0 & 0 & 0 \\ -\frac{k_p}{m_t T_i} & -\frac{k_p}{m_t} & \frac{m_p g}{m_t} & 0 & \frac{k_p}{m_t T_i} \\ 0 & 0 & 0 & 1 & 0 \\ \frac{k_p}{m_t l T_i} & \frac{k_p}{m_t l} & -\frac{m_o g}{m_t l} & 0 & -\frac{k_p}{m_t l T_i} \\ 0 & 0 & 0 & 0 & 0 \end{bmatrix}, \quad (24)$$

$$B_2 = \begin{bmatrix} 0 & \frac{k_p}{m_t} & 0 & -\frac{k_p}{m_t l} & 1 \end{bmatrix}^T, \qquad (25)$$

$$C_2 = \begin{bmatrix} 1 & 0 & 0 & 0 & 0 \\ 0 & 1 & 0 & 0 & 0 \\ 0 & 0 & 1 & 0 & 0 \\ -\frac{k_p}{T_i} & -k_p & 0 & 0 & \frac{k_p}{T_i} \end{bmatrix}, \qquad (26)$$

$$D_2 = \begin{bmatrix} 0 & 0 & 0 & k_p \end{bmatrix}^T. \qquad (27)$$

E. Overall system plant

The overall system plant consists of a cascade interconnection of the augmented trolley-payload subsystem $G_2 = (A_2, B_2, C_2, D_2)$ (24, 25, 26, 27) via force output F_x and the low order elastic crane subsystem $G_1 = (A_1, B_1, C_1, D_1)$ (10, 11).

$$\begin{bmatrix} \dot{x}_1 \\ \dot{x}_2 \end{bmatrix} = \begin{bmatrix} A_1 & 0 \\ B_2 C_1 & A_2 \end{bmatrix} \begin{bmatrix} x_1 \\ x_2 \end{bmatrix} + \begin{bmatrix} B_1 \\ B_2 D_1 \end{bmatrix} v, \qquad (28)$$

$$y = \begin{bmatrix} C_1 & C_2 \end{bmatrix} \begin{bmatrix} x_1 \\ x_2 \end{bmatrix} + Dv. \qquad (29)$$

III. CRANE CONTROL

A. Uncertainty models

The aim of this paper is the design of a control law for simultaneous damping of the payload swinging with varying rope length and elastic crane vibrations. It is assumed that although the equations of motion are the same, parameters of the rope length can vary during crane operation. In this case

using parametric uncertainties is reasonable. The linear system eq. (28), (29) is replaced then by a family of systems

$$\dot{x}(t) = A(q)x(t) + B(q)u(t), \qquad (30)$$
$$y(t) = C(q)x(t) + D(q)u(t), \qquad (31)$$

where matrices A, B, C, D depend on the parameters q, which are time invariant and belong to a feasible set of uncertainty $Q = \{q \in \mathbb{R} : q_{min} \le q \le q_{max}\}$.

Furthermore, using the proposed model order approximation techniques additional errors are introduced, which should be taken into account.

1) Coprime factor uncertainty: From a robust control design point of view, the studied set of cranes can be embedded into a nominal plant $G_n(s)$ and a set of bounded uncertainties [5; 9; 10]. These uncertainties have to be stable and possess a finite H_∞ -norm. For undamped and weakly damped mechanical structures utilizing a coprime factor description of the present model uncertainties should be preferred. The normalized coprime factorization of the nominal system $G_n(s)$ can be expressed as

$$G_n(s) = \frac{N_n(s)}{M_n(s)}, \qquad (32)$$

where $M_n(s), N_n(s) \in H_\infty$ are stable coprime transfer functions satisfying the Bezout identity

$$M_n(s)M_n(-s) + N_n(s)N_n(-s) = 1. \qquad (33)$$

Then the set of uncertain systems $G_\Delta(s)$ can be characterized by the nominal system $G_n(s)$ and stable coprime factor uncertainties $\Delta_M(s)$ and $\Delta_N(s)$

$$G_\Delta(s) = \frac{N_n(s) + \Delta_N(s)}{M_n(s) + \Delta_M(s)}. \qquad (34)$$

However, using the coprime factor description does not give a unique realization of $\Delta_M(s)$ and $\Delta_N(s)$. Thus, selection of a specific realization is an additional degree of freedom. In order to reduce conservatism a coprime factor description with a minimal H_∞ - norm for $[\Delta_M(s)\Delta_N(s)]$ should be preferred leading to the introduction of the gap metric.

2) The gap metric: The gap metric δ_g between two linear systems $G_n(s)$ and $G_\Delta(s)$ can be calculated according to [11; 12] as a maximum of the directed gaps $\overrightarrow{\delta_g}(G_n, G_\Delta)$ and $\overrightarrow{\delta_g}(G_\Delta, G_n)$

$$\delta_g(G_n, G_\Delta) = max\{\overrightarrow{\delta_g}(G_n, G_\Delta), \overrightarrow{\delta_g}(G_\Delta, G_n)\}, \qquad (35)$$

where

$$\overrightarrow{\delta_g}(G_n, G_\Delta) := \inf_{[\Delta_M \Delta_N] \in H_\infty} \{\|[\Delta_M \Delta_N]\|_\infty : G_\Delta\}. \qquad (36)$$

The gap metric may possess values between zero and one. Here, two systems $G_n(s)$ and $G_\Delta(s)$ are close if their gap metric is close to zero. As will be shown later, the maximum of the gap metric with respect to a nominal plant for a given set of perturbed plants can be used as a measure for the required robustness margin.

As a metric the gap metric satisfies the triangular inequality

$$\delta(G_1, G_3) \le \delta(G_1, G_2) + \delta(G_2, G_3), \qquad (37)$$

which can be used to derived appropriate estimates in the presence of multiple error sources. For example, having a low order approximation of the uncertain system $G_1 = G_\Delta$, a low order approximation of the original nominal system $G_2 = G_n$ and a high order representation of the original nominal system $G_3 = G$, the triangular inequality can be used to derive an estimate for the distance between the low order uncertain system G_Δ and the original nominal system G in the sense of the gap metric $\delta(G_n, G)$. Therefore, additional errors due to model order reduction or numerical discretization may be easily taken into account.

3) Gantry crane model uncertainties and required robustness margin: Assuming that the rope length is not exactly known the set of crane models $\mathbf{\Pi_L}$ for different l can be derived from eq. (28), (29).
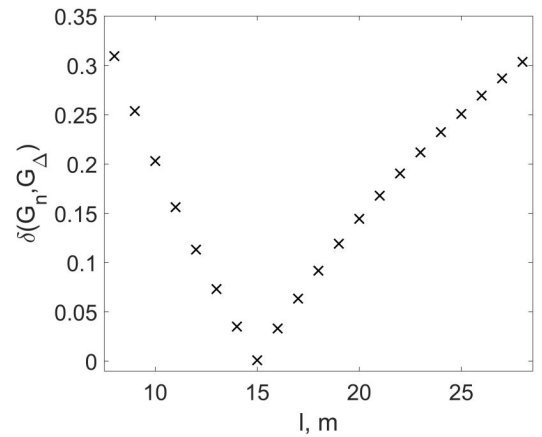

Fig. 4. Gap metric sequence for set $\mathbf{\Pi_L}$

In Fig. 4 the gap metric for the set of normalized gantry crane models $\mathbf{\Pi_L}$ is shown. As can be seen the maximum of the gap metric for the concerned range of rope length l is

$$\delta_g(G_\Delta, G_n) = 0.31. \qquad (38)$$

The order reduction error for the elastic crane model in sense of the gap metric can be calculated as

$$\delta_g(G_n, G) = 0.03. \qquad (39)$$

B. Robust control design

In order to reduce the elastic vibrations in the trolley travel direction and swaying of the payload a control law is obtained using H_∞ - loopshaping.

1) H_∞ - loopshaping control: H_∞ - loopshaping design is based on the combination of H_∞ - robust stabilization and classical loopshaping ideas and guarantees both performance and fulfilment of given robustness requirements [13; 14]. The design procedure is divided into two steps: augmentation by pre-compensator in order to shape the open loop singular values and H_∞ - stabilization of the shaped plant.

In order to reflect closed-loop performance requirements the open-loop singular values are shaped applying the weighting function $W(s)$ as depicted in Fig. 5
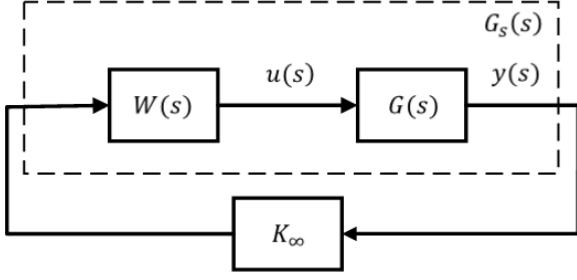
$$G_s(s) = G(s)W(s). \qquad (40)$$

Fig. 5. The loopshaping

Given the shaped open-loop plant in its normalized coprime factor representation $G_s(s) = N(s)/M(s)$. The controller K_∞ guaranteeing a maximum robustness margin with respect to the normalized coprime factor uncertainties can be calculated from the following H_∞ - control problem

$$\left\| \begin{bmatrix} K_\infty \\ 1 \end{bmatrix} \frac{1}{(1 + G_s K_\infty)M} \right\|_\infty \leq \epsilon^{-1}. \tag{41}$$

Here, the maximum achievable robustness margin ϵ_{max} can be calculated

$$\epsilon_{max} = (1 + \rho(XZ))^{-1/2}, \tag{42}$$

where X and Z are the positive definite solutions of two algebraic Riccati equations

$$0 = (A - BR^{-1}DC)^T X + X(A - BR^{-1}DC) \\ - XB^T R^{-1} BX + CR^{-1}C^T, \tag{43}$$

$$0 = (A - BR^{-1}DC)Z + Z(A - BR^{-1}DC)^T \\ - ZC^T R^{-1}CZ + BR^{-1}B^T, \tag{44}$$

with $R = 1 + D^2$.
Using the robustly stabilizing controller K_∞ for the weighted plant $G_s(s)$ the overall controller K can be expressed as

$$K(s) = K_\infty(s)W(s). \tag{45}$$

Implementation of the H_∞ - loopshaping methodology for the shaped plant $G_s(s)$ with robust stability margin ϵ, results in a controller K, which stabilizes all plants $G_\Delta(s)$ with gap metric $\delta_g(G_s, G_\Delta) < \epsilon$.

C. Results

In order to provide simultaneous damping of payload sway and elastic vibrations two controllers K_1 and K_2 have been designed.
Two compensators $W_1(s)$ and $W_2(s)$ realizing the desired open loop shapes for these systems have been chosen as follows

$$W_1(s) = \frac{20}{0.05s + 1}, \tag{46}$$

$$W_2(s) = \frac{100}{0.01s + 1}. \tag{47}$$

For the shaped crane plants $G_{s,1}(s) = G(s)W_1(s)$ and $G_{s,2}(s) = G(s)W_2(s)$ robust controllers $K_{\infty,1}$ and $K_{\infty,2}$ have been derived with stability margins $\epsilon_1 = 0.67$ and $\epsilon_2 = 0.61$ respectively. As the margin associated with the damping of

load swaying is greater than the maximum of the gap metric $\delta_{g,max} = 0.31$ and the margin associated with the damping of elastic vibrations is much greater than order reduction error, the achieved controllers guarantee robust stability for the set of uncertain crane models.
Simulation results are depicted in Fig. 6. Here, the designed robust controllers K_1 and K_2 has been applied to the nonlinear crane system eq. (18), (19), (20) and to the high order elastic crane model (3, 4). As can be seen in Fig. 6 (c) and (d), the designed H_∞ controllers provide simultaneously damping of the elastic structure vibrations and the payload sway by varying the rope length.

IV. Conclusion

A new active damping approach for gantry crane vibrations using only trolley acceleration forces has been presented and verified on a nonlinear gantry crane model. For designing a control law, that guarantees the robust stability and the performance specifications for gantry crane with different rope length, H_∞ - loopshaping synthesis has been applied. In order to derive a mathematical description of elastic gantry crane dynamics FEM has been utilized. The derived high order models have been reduced using balanced truncation approximation. In order to represent the gantry crane with different rope length a normalized coprime factor description has been considered for the parametric uncertainties. Two controllers for anti-sway control and vibration damping control have been designed and applied to nonlinear crane model.

References

[1] N. Zrnic, D. Oguamanam, S. Bosnjac, Dynamics and modelling of mega quayside container cranes, FME Transactions, 34, 2006, pp. 193-198.

[2] N. Zrnic, Z. Petkovi, S. Bonjak, Automation of Ship-To-Shore Container Cranes: A Review of State-of-the-Art, FME Transactions, 33, 2005, pp. 111-121.

[3] C. Rapp, Aktive Dämpfung der Lastschwingungen bei Containerkranen, PhD thesis, Hamburg University of Technology, 2012.

[4] A. Recktenwald, Aktiver Schwingungsdämpfer für Krane, 19. Internationale Kranfachtagung 2011: Der Kran und sein Umfeld in Industrie und Logistik, 2011, Otto-von-Guericke University, Magdeburg, Germany, pp. 143-146.

[5] S. Skogestad, I. Postlethwaite, Multivariable feedback control: analysis and design, John Willey and sons, 2001.

[6] C. Ceton, Model reduction for robust controller design, Philips electronics, 1992.

[7] Tuan Anh Le, Gook-Hwan Kim, Min Young Kim, Soon-Geul Lee, Partial feedback linearization control of overhead cranes with varying cable lengths, International Journal of Precision Engineering and Manufacturing, Volume 13, 2012, pp. 501-507.

[8] J. Verschoof, Cranes - Design, Practice and Maintenance (second edition), Professional Engineering Publishing, 2002.

[9] K. Zhou, K. Glover, Robust and optimal control, Prentice-Hall, 1996.

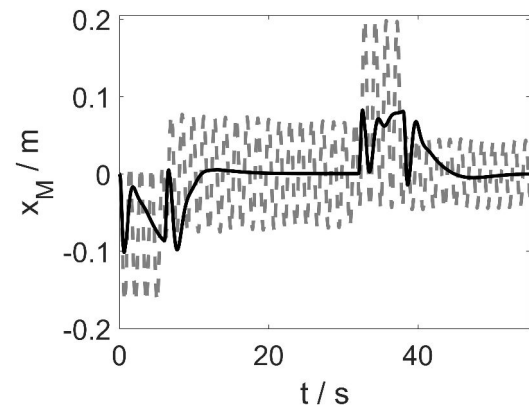[10] K. Zhou, J.C. Doyle, Essentials of robust control, Prentice-Hall, 1998.
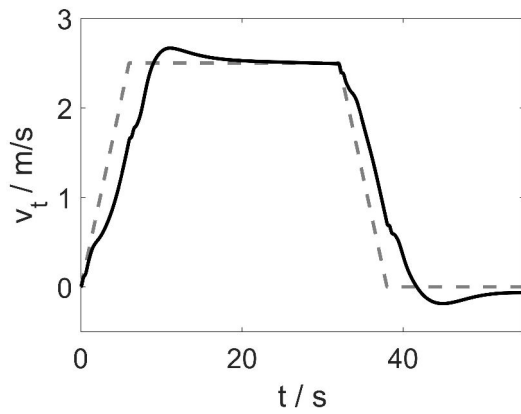
(a) Trolley velocity (black) and reference value (gray)
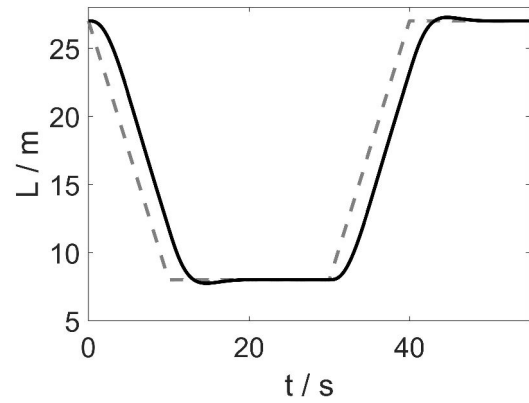
(b) Rope length(black) and reference value (gray)
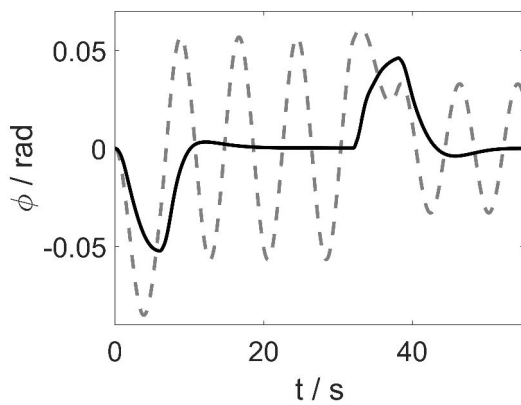
(c) Sway angle with (black) and without (gray) control

(d) Crane displacement with (black) and without (gray) control

Fig. 6.   Simulation results

[11] T. T. Georgiou, M.C. Smith, Optimal robustness in the gap metric, IEEE Trans. on Automatic Control 35, 1990, pp. 673685.

[12] G. Vinnicombe, Measuring robustness of a feedback systems, PhD thesis, Department of engineering, University of Cambridge, 1993.

[13] D. C. McFarlane, K. Glover, Robust controller design using normalized coprime factor plant descriptions, Springer Verlag, Lecture notes in control and information sciences 138, 1989.

[14] X. Sun, P. Scotson, G. Balfour, A Further Application of Loop Shaping H-infinity Control to Diesel Engine Control - Driven-Idle Speed Control, SAE Technical Paper 2002-01-0197, 2002, pp. 41-50.

Adaptive discrepancy based control of particulate processes

Stefan Palis [1,*]

[1] *Otto-von-Guericke-Universität,*
Universitätsplatz 2, D-39106 Magdeburg, Germany

Abstract: This contribution is concerned with a relatively new approach to particulate process control. The main idea is to use of a generalized distance measure, the discrepancy, in order to describe deviations from a desired particle property distribution. Applying, the associated stability theory, i.e. stability theory with respect to two discrepancies, a stabilizing control law can be derived. One of the main advantages of the proposed discrepancy based control method is that no model reduction is required. In this contribution an adaptive extension of the discrepancy based control is proposed in order to control a crystallization process in the presence of parameter uncertainties.

1. INTRODUCTION

Control of particulate processes is an active field of research [1, 3, 9, 10]. From a control theory point of view particulate processes are often modelled as distributed parameter systems and therefore of great interest. The population balance equation describing the dynamics of particle property distribution is, depending on the specific process, a nonlinear partial integro-differential equation with sinks and sources in the domain. It has been recently applied by the authors to the problem of stabilization of continuous cystallization processes [3] and fluidized bed spray granulation with internal [5, 6] and external product classification [4, 8]. The paper is organized as follows: in section 2 the main theoretic concepts of stability with respect to two discrepancies are stated. In section 3 the model system, a crystallization process, is introduced. In section 4 the adaptive discrepancy based control method is applied in order to derive a stabilizing control law for the model system.

2. STABILITY WITH RESPECT TO TWO DISCREPANCIES

The concept of stability with respect to two discrepancies has been introduced in [11]. The main idea is to describe the stability of a process by a generalized distance measure, which does not have to be a norm. For convenience the most important facts on stability with respect to two discrepancies as given e.g. in [11, 12] will be stated. Here, the process $\varphi(.,t)$ is a solution of the distributed parameter system and $\varphi_0 = 0$ an equilibrium of the system.

Definition 1. Discrepancy

A discrepancy is a real valued functional $\rho = \rho[\varphi(.,t),t]$ with the following properties

(1) $\rho(\varphi,t) \geqslant 0$
(2) $\rho(0,t) = 0$
(3) for an arbitrary process $\varphi = \varphi(.,t)$ the discrepancy $\rho(\varphi(.,t),t)$ is continuous with respect to t.

(4) introducing a second discrepancy $\rho_0(\varphi)$ with $\rho_0(\varphi) \geqslant 0$ and $\rho_0(0) = 0$. Than the discrepancy $\rho(\varphi(.,t),t)$ is continuous at time $t = t_0$ with respect to ρ_0 at $\rho_0 = 0$, if for every $\varepsilon > 0$ and $t_0 > 0$ there exists a $\delta(\varepsilon, t_0) > 0$, such that from $\rho_0 \leqslant \delta(\varepsilon, t_0)$ follows $\rho < \varepsilon$.

Obviously, a discrepancy has not all properties of a metric, e.g. symmetry $d(x,y) = d(y,x)$ or triangular inequality $d(x,y) \leq d(x,z) + d(z,y)$ and more importantly does not have to satisfy the important property of definiteness, i.e. a vanishing discrepancy $\rho(\varphi,t) = 0$ does not imply $\varphi = 0$.

Definition 2. Stability with respect to two discrepancies ρ and ρ_0

The equilibrium $\varphi_0 = 0$ is stable in the sense of Lyapunov with respect to the two discrepancies ρ and ρ_0 for all $t \geq t_0$ if for every $\varepsilon > 0$ and $t_0 \geq 0$ there exists a $\delta = \delta(\varepsilon, t_0) > 0$, such that for every process $\varphi(.,t)$ with $\rho_0 < \delta(\varepsilon, t_0)$ follows $\rho < \varepsilon$ for all $t \geq t_0$. If in addition $\lim_{t\to\infty} \rho = 0$, than the equilibrium φ_0 is called asymptotically stable in the sense of Lyapunov with respect to the two discrepancies ρ and ρ_0.

In order to establish a relationship between stability with respect to two discrepancies and the existence of a Lyapunov functional V the notions of positivity and positive definiteness of a functional with respect to a discrepancy have been introduced.

Definition 3. Positivity with respect to a discrepancy ρ

The functional $V = V[\varphi,t]$ is called positive with respect to the discrepancy ρ, if $V \geq 0$ and $V[0,t] = 0$ for all φ with $\rho(\varphi,t) < \infty$.

Definition 4. Positive definiteness with respect to a discrepancy ρ

The functional $V = V[\varphi,t]$ is positive definite with respect to a discrepancy ρ, if $V \geqslant 0$ and $V[0,t] = 0$ for all φ with $\rho(\varphi,t) < \infty$ und for every $\varepsilon > 0$ there exists a $\delta = \delta(\varepsilon) > 0$, such that $V \geq \delta(\varepsilon)$ for all φ with $\rho[\varphi,t] \geq \varepsilon$.

The following two theorems state the conditions for a function V guaranteeing (asymptotical) stability with respect to two discrepancies.

Theorem 5. [12] The process φ with the equilibrium $\varphi_0 = 0$ is stable with respect to the two discrepancies ρ and ρ_0 if and only if there exists a functional $V = V[\varphi, t]$ positive definite with respect to the discrepancy ρ, continuous at time $t = t_0$ with respect to ρ_0 at $\rho_0 = 0$ and not increasing along the process φ, i.e. $\dot{V} \leq 0$.

Theorem 6. [12] The process φ with the equilibrium $\varphi_0 = 0$ is asymptotically stable with respect to the two discrepancies ρ and ρ_0 if and only if there exists a functional $V = V[\varphi, t]$ positive definite with respect to the discrepancy ρ, continuous at time $t = t_0$ with respect to ρ_0 at $\rho_0 = 0$ and not increasing along the process φ, i.e. $\dot{V} \leq 0$, with $\lim_{t \to \infty} V = 0$.

3. EXAMPLE - CONTINUOUS CRYSTALLIZATION

As an example a continuous crystallization process with fines dissolution depicted in Fig. 1 will be studied. This process has be investigated e.g. in [2]. The main assumptions are:

- isothermal operation,
- constant volume,
- ideal mixing,
- unclassified withdrawal,
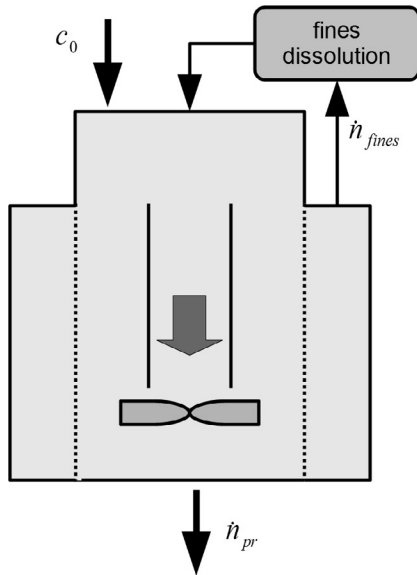- no attrition,
- no breakage.

Fig. 1. Continuous crystallization

In addition, it is assumed that the concentration c_0 can be influenced by an additional dilution. The fines withdraw $\dot{n}_{Fein}$ is realized by a controllable pump.

The solid phase can be described using a population balance model for the crystal size distribution, whereas the liquid phase can be model by a mass balance. From a mathematical point of view the studied system consists of a nonlinear partial integro-differential equation for the crystal size distribution coupled to an ordinary differential equation for the concentration.

In order to describe the dynamics of the crystal size distribution $n(t, L)$ with the characteristic crystal length L the following population balance model has been proposed.

$$\frac{\partial n}{\partial t} = -\frac{\partial G(c)n}{\partial L} - \dot{n}_{pr} - \dot{n}_{fines} + \dot{n}_{nuc}. \tag{1}$$

Here, $G(c)$ is the growth rate depending on the concentration and $\dot{n}_{pr}$, $\dot{n}_{fines}$ and $\dot{n}_{nuc}$ are the associate rates for product withdrawal, fines dissolution and nucleation. It is assumed that the crystal growth solely depends on the concentration and is proportional with the supersaturation:

$$G(c) = k_1 (c - c_s). \tag{2}$$

The product withdrawal does not depend on the specific crystal size and can hence be represented as

$$\dot{n}_{Pr} = Kn \tag{3}$$

where K is the rate of withdrawal. As crystals for the fines dissolution are withdrawn from the settling zone it can be assumed that only small crystals of a maximal length L_F are effected.

$$\dot{n}_{Fein} = K_F(1 - \sigma(L - L_F))n = K_F n_F n \tag{4}$$

Here, K_F is the withdrawal rate and σ is the Heaviside step function. For the nucleation it is assumed that crystals of size $L = 0$ are generated in dependence of the supersaturation.

$$\dot{n}_{nuc} = \left(1 - \frac{4}{3}\pi\mu_3\right) k_2 e^{\left(-\frac{k_3}{\left(\frac{c}{c_s} - 1\right)^2}\right)}, \tag{5}$$

Here, μ_3 is the third moment of the crystal size distribution, i.e.

$$\mu_3 = \int_0^\infty L^3 n\,dL. \tag{6}$$

Hence, the population balance model for the solid phase is described as follows:

$$\frac{\partial n}{\partial t} = -\frac{\partial G(c)n}{\partial L} - Kn - K_F n_F n$$
$$+ \delta(0) \left(1 - \frac{4}{3}\pi\mu_3\right) k_2 e^{\left(-\frac{k_3}{\left(\frac{c}{c_s} - 1\right)^2}\right)}. \tag{7}$$

The equation for the liquid phase, i.e. the ordinary differential equation for the concentration, is given as follows.

$$\frac{dc}{dt} = \frac{(c_0 - \varrho)K}{\left(1 - \frac{4}{3}\pi\mu_3\right)} + K(\varrho - c) - \frac{(\varrho - c)}{\left(1 - \frac{4}{3}\pi\mu_3\right)}\frac{4}{3}\pi\frac{d\mu_3}{dt} \tag{8}$$

L_F	$1\,mm$
ϱ	$1.7\ 10^3\ \frac{kg}{m^3}$
c_s	$980.2\ \frac{kg}{m^3}$
K	1
k_1	$5.065\ 10^{-2}$
k_2	7.958
k_3	$1.217\ 10^{-3}$
n_{init}	$7\ 10^{-3}\ \exp(-4L)$
c_0	$1002\ \frac{kg}{m^3}$
K_F	$0.07\ \frac{1}{h}$

Table 1. Plant parameters

It is well known that the given process is unstable in a certain range of fines dissolution rates. In order to stabilize

this process in the presence of uncertainties in the parameters k_1 and k_2 the control approach presented in [] will be extended by an adaptation mechanism guaranteeing closed loop stability.

4. ADAPTIVE DISCREPANCY BASED CONTROL

As has been shown earlier [3] the zeroth moment of the crystal size distribution μ_0 and the concentration c as the controlled variables and the dissolution rate K_F and the inlet concentration c_0 as the control variable are appropriate handles in order to stabilize the process. The error therefore is

$$e = \begin{pmatrix} \mu_{0,d} - \mu_0 \\ c_d - c \end{pmatrix} = \begin{pmatrix} e_1 \\ e_2 \end{pmatrix} \tag{9}$$

In order to derive a stabilizing controller the above presented stability concept is applied. Here, we choose the discrepancy ρ as follows

$$\rho = \frac{1}{2}\left(e_1^2 + e_2^2\right). \tag{10}$$

Obviously, the above requirements on a discrepancy are met. In order to guarantee continuity at time $t = t_0$ at $t_0 = 0$ the second discrepancy ρ_0 is simply chosen as follows

$$\rho_0 = \rho(t = 0). \tag{11}$$

According to Theorem 6 existence of an appropriate functional V is sufficient to guarantee asymptotic stability with respect to the two discrepancies ρ and ρ_0. For this purpose the following candidate Lyapunov functional is introduced

$$V = \frac{1}{2}\left(\int_0^\infty L^3 \left(n_d - n\right) dL\right)^2. \tag{12}$$

In order to account for the unknown parameters k_1 and k_2 this candidate Lyapunov functional has to be augmented

$$V = \frac{1}{2}e^T e + \frac{1}{2\gamma}\left(\tilde{k}_1^2 + \tilde{k}_2^2\right), \tag{13}$$

where $\tilde{k}_{1,2} = \hat{k}_{1,2} - k_{1,2}$ are the estimation errors. This approach, i.e. Lyapunov redesign, is well known for finite dimensional systems. In order to achieve stability in the sense described above the control variable has to be chosen such that the time derivative of V along the system trajectories (7) is negative definite for all times and vanishs only for $e = 0$.

$$\dot{V} = -e^T \begin{pmatrix} \int_0^\infty -\frac{\partial G(c)n}{\partial L} - Kn - K_F n_F n + k_2 n_{nuc} dL \\ \frac{(c_0 - \varrho) K}{\left(1 - \frac{4}{3}\pi\mu_3\right)} + K(\varrho - c) - \frac{(\varrho - c)}{\left(1 - \frac{4}{3}\pi\mu_3\right)}\frac{4}{3}\pi\frac{d\mu_3}{dt} \end{pmatrix}$$
$$+ \frac{1}{\gamma}\left(\tilde{k}_1 \dot{\hat{k}}_1 + \tilde{k}_2 \dot{\hat{k}}_2\right) \tag{14}$$

where

$$n_{nuc} = \delta(0)\left(1 - \frac{4}{3}\pi\mu_3\right)\exp\left(-\frac{k_3}{\left(\frac{c}{c_s} - 1\right)^2}\right) \tag{15}$$

In the case of known parameters k_1 and k_2, i.e. $\hat{k}_1 = k_1$ and $\hat{k}_2 = k_2$, the following certainty equivalence control law could be chosen in order to guarantee negative definitness of the time derivative of the candidate Lyapunov functional V and hence stability in the sense of Lyapunov with respect to two discrepancies.

$$K_F = \frac{-c_1 e_1 - \int_0^\infty \frac{\partial \hat{k}_1(c-c_s)n}{\partial L} + Kn + \hat{k}_2 n_{nuc} dL}{\int_0^\infty n_F n dL} \tag{16}$$

$$c_0 = \frac{\left[c_2 e_2 + \frac{\varrho K + (\varrho - c)\frac{4}{3}\pi\frac{d\mu_3}{dt}}{\left(1 - \frac{4}{3}\pi\mu_3\right)} - K(\varrho - c)\right]}{\frac{K}{\left(1 - \frac{4}{3}\pi\mu_3\right)}} \tag{17}$$

Applying the certainty equivalence control law in 14 results in

$$\dot{V} = -e^T \begin{pmatrix} c_1 e_1 + \int_0^\infty \left[\tilde{k}_1(c - c_s)\frac{\partial n}{\partial L} - \tilde{k}_2 n_{nuc}\right] dL \\ c_2 e_2 \end{pmatrix}$$
$$+ \frac{1}{\gamma}\left(\tilde{k}_1 \dot{\hat{k}}_1 + \tilde{k}_2 \dot{\hat{k}}_2\right). \tag{18}$$

Choosing the following parameter adaption laws

$$\dot{\hat{k}}_1 = \gamma e_1 \int_0^\infty (c - c_s)\frac{\partial n}{\partial L} dL \tag{19}$$

$$\dot{\hat{k}}_2 = -\gamma e_1 \int_0^\infty n_{nuc} dL \tag{20}$$

the remaining terms cancel. Resulting in

$$\dot{V} = -c_1 e_1^2 - c_2 e_2^2. \tag{21}$$

Hence, the designed certainty equivalence control law in combination with the adaption law (Fig. 2) guarantees stability with respect to the two discrepancies ρ and ρ_0. However, convergence of the parameter estimates $\hat{k}_1$ and $\hat{k}_2$ to the real values k_1 and k_2 is not guaranteed, which is well known from similiar adaptive control approaches.
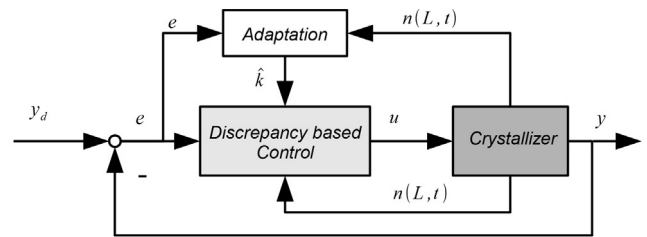

Fig. 2. Control scheme

In order to test the control law the process is started with an initial crystal size distribution n_{init} in the region of instability, i.e. $K_F = 0.07$, with an parameter estimation error of 15%. As can be seen in Fig. 3, 4, 6 and 5 the adaptive version of the discrepancy based control succeeds in stabilizing the chosen discrepancy and the desired crystal size distribution.
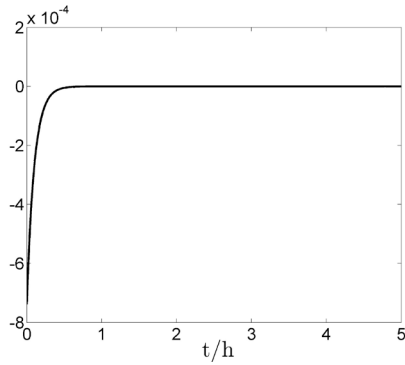
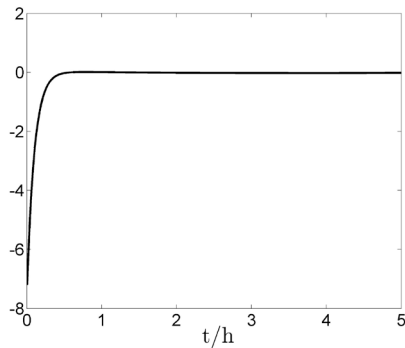Fig. 3. Error in zeroth moment of the crystal size distribution
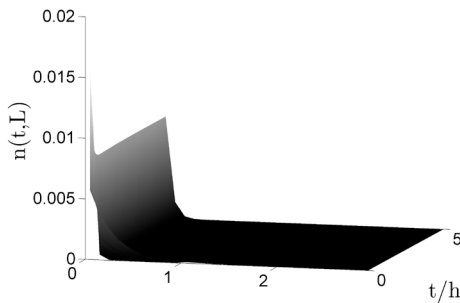

Fig. 4. Error in concentration

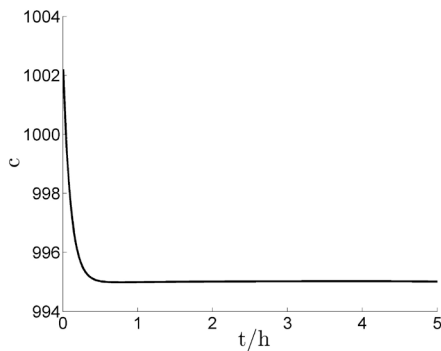Fig. 5. Crystal size distribution n

Fig. 6. Concentration c

5. CONCLUSION

In this contribution the adaptive discrepancy based control for particulate processes has been presented. As an illustrative example a continuous crystallization process with parametric uncertainty has been chosen. In order to stabilize this process an adaptive nonlinear control approach has been proposed. The main idea is to augment the Lyapunov functional in order to account for the parameter estimation error $\tilde{k}$ and then derive a certainty equivalence control law using stability with respect to two discrepancies and an associate parameter adaptation law.

REFERENCES

[1] T. Glaser & C. F. W. Sanders & F. Y. Wang & I. T. Cameron & J. D. Litster & J. M. H. Poon & R. Ramachandran & C. D. Immanuel & F. J. Doyle III, Model predictive control of continuous drum granulation, Journal of Process Control, 2009, pp. 615-622.

[2] T. Chiu & P. Christofides, Robust Nonlinear Control of a Continuous Crystallizer, Computers and Chemical Engineering Supplement, 1999, pp. S257-S260.

[3] S. Palis & A. Kienle, Diskrepanzbasierte Regelung der kontinuierlichen Kristallisation, at-Automatisierungstechnik, 2012, pp. 145-154.

[4] S. Palis & A. Kienle, Stabilization of continuous fluidized bed spray granulation with external product classification, Chem. Eng. Sci., 2012, pp. 200-209.

[5] S. Palis & A. Kienle, Discrepancy based control of continuous fluidized bed spray granulation with internal product classification, 8th IFAC International Symposium on Advanced Control of Chemical Processes - ADCHEM, 2012, pp. 756-761.

[6] S.Palis & A. Kienle, H_∞ loop shaping control for continuous fluidized bed spray granulation with internal product classification, Industrial & Engineering Chemistry Research, 2013, pp. 408-420.

[7] S. Palis & A. Bück & A. Kienle, Adaptice Discrepancy Based Control of Continuous Fluidized Bed Spray Granulation with Internal Classification, 9th IFAC Symposium on Nonlinear Control Systems - NOLCOS, 2013, pp. 400-405.

[8] S. Palis & A. Kienle, Discrepancy based control of particulate processes, J. of Process Control, vol. 24, issue 3, Mar. 2014, pp. 33-46.

[9] P. Christofides & N. El-Farra & M. Li & P. Mhaskar, Model-based control of particulate processes, Chem. Eng. Sci. 63, 2008, pp. 1156-1172.

[10] U. Vollmer & J. Raisch, Population balance modeling and H_∞-controller design for a crystallization process, Chem. Eng. Sci., vol. 57, issue 20, Oct. 2002, pp. 4401-4414.

[11] A.A. Movchan, Stability of processes with respect to two metrics, Journal of Applied Mathematics and Mechanics, 1960, 24, pp. 1506-1524.

[12] T. Sirasetdinov, Stability of systems with distributed parameters, 1987.

Robust control of continuous crystallization processes

Rostyslav Geyyer *,** Achim Kienle *,** Stefan Palis *

* Otto-von-Guericke University Magdeburg, 39106 Magdeburg,
Germany
** Max Planck Institute for Dynamics of Complex Technical Systems,
39106 Magdeburg, Germany

Abstract: In this paper we consider two configurations of continuous crystallization processes with significant nonlinear behaviour and a tendency to self-sustained nonlinear oscillations. The control task is to stabilize the crystallization process in the presence of model uncertainties and external disturbances. This is a challenging task as the model consists of a population balance equation describing the disperse phase, i.e. a nonlinear partial differential equation, being coupled to a mass balance equation describing the liquid phase. In this contribution robust control methods are applied to solve this problem.

Keywords: Control of nonlinear systems, population balance models, robust control.

1. INTRODUCTION

Crystallization is a thermal separation process mostly used in chemical industry that consists in transformation of amorphous solid, liquid or gaseous substance into crystals [Mersmann et al. (2011)]. Crystallization leads to an increase of the concentration and purity of the final product. In this paper continuous crystallization processes within mixed-solution, mixed-product-removal (MSMPR) crystallizers are considered. The focus here is on two important crystallizer configurations: with the fines dissolution loop and without. In order to improve performance of the crystallization process feedback control should be applied. Different control approaches have already been studied: closed-loop control of crystal shape [Ma and Wang (2012)], robust nonlinear control based on the method of moments [Chiu and Christofides (1999)], infinite-dimensional H_∞-control [Vollmer and Raisch (2002)], [Motz et al. (2003)] and discrepancy-based control [Palis and Kienle (2012)]. In this contribution a finite-dimensional robust control approach will be studied resulting in easy implementable low order controllers.

2. CRYSTALLIZATION PROCESS MODELING

In the crystallization processes studied in this contribution crystals are generated and growing due to the oversaturation of the liquid phase: the oversaturated solution is fed to the reactor and cooled down there; such temperature change decreases solvent saturation capacity and causes crystal growth and formation of nuclei. Due to the presence of different effects like seeding, nucleation, fracture, abrasion and growth, crystals have different sizes giving rise to a crystal size distribution (CSD). In many cases the CSD determines the quality of product since many physical properties of the product are closely related to its CSD. In addition, the effectiveness of downstream processing by filtering or drying are strongly influenced by the CSD.

Hence, the dynamics of the crystallization process should be studied considering the dynamics of the CSD.

2.1 Continuous crystallization process model derivation

To derive a model of the process the population balance approach [Randolph and Larson (1988)] is applied. Following [Temmel et al. (2014)] a mathematical model was derived with assumptions:

- the reactor content is ideally mixed;
- the solution volume inside the reactor is constant;
- the growth is size-independent;
- the system is diluted — the reactor volume is not a function of the substance and crystals mass;
- the mass of the solvent is much higher than the mass of the substance;
- the occurance of breakage or agglomeration can be neglected;
- nuclei have length z_{min} and negligible mass.

The crystal growth and dissolution factor G is assumed to be derived in the following way:

$$G = \begin{cases} K_g \exp(-E_{A,g}/(R_{gas}T))(S-1)^g, & \text{if } S > 1, \\ K_d(S-1), & \text{otherwise,} \end{cases} \tag{1}$$

where the supersaturation S is defined as follows:

$$S(t) = \frac{\omega_l(t)}{\omega_{sat}}. \tag{2}$$

Here, the mass fraction at saturation ω_{sat} was identified experimentally and approximated by a polynomial:

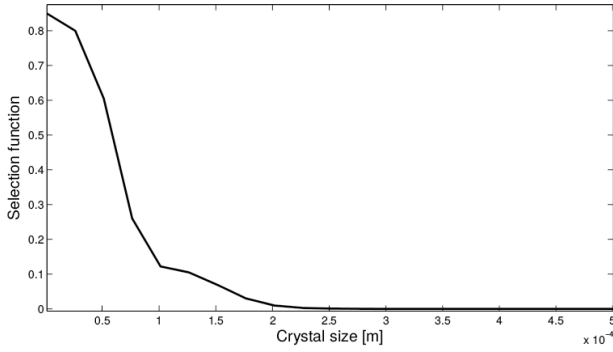$$\omega_{sat} = \sum_{i=0}^{4} K_i(T - 273.15)^i \tag{3}$$

Fig. 1. The fine crystal selection function $R(z)$

The crystal withdrawal term is defined as follows:

$$\dot{n}_{out}(t,z) = \frac{n(t,z)}{\tau_r}, \tag{4}$$

where τ_r represents the residence time.

In one of its configurations the crystallization facility incorporates the fines dissolution loop and the corresponding term is defined:

$$\dot{n}_{diss} = \delta R(z) \dot{n}_{out}(t,z) \tag{5}$$

The term δ represents the fines dissolution loop rate, the ratio of the product withdrawal related to fines dissolution loop withdrawal and $R(z)$ describes the selection of fine crystals, this function was identified empirically [Temmel (2014)] and is shown in Fig. 1:

$$R(z) = \begin{cases} \dfrac{y_{max}}{(1+\exp(\frac{z-z_f}{w_f}))} & \text{if } z < z_{fb}, \\ \dfrac{y_{max}(1+\exp(\frac{z_{fb}-z_b}{w_b}))}{(1+\exp(\frac{z_{fb}-z_f}{w_f}))(1+\exp(\frac{z-z_b}{w_b}))}, & \text{otherwise} \end{cases} \tag{6}$$

The nucleation rate $\dot{n}_{build}$ can be defined as a boundary condition which appears when the supersaturation is greater than one, so the crystals of size z_{min} and negligible mass are generated:

$$Gn|_{z=z_{min}} = \dot{n}_{build}(t) \tag{7}$$

$$\dot{n}_{build}(t,z) = \begin{cases} K_b \exp(-E_{A,b}/(R_{gas}T))(S-1)^b, & \text{if } S > 1, \\ 0, & \text{otherwise} \end{cases} \tag{8}$$

The population balance model for the solid phase of the continuous crystallization is thus defined:

$$\frac{\partial n(t,z)}{\partial t} = -\frac{\partial Gn(t,z)}{\partial z} - \dot{n}_{out}(t,z) - \dot{n}_{diss}(t,z) \tag{9}$$

The mass balance of the solute in the liquid phase is formulated as follows:

$$\frac{dm_l}{dt} = \dot{m}_{l,in}(t) - \dot{m}_{l,out}(t) + \dot{m}_{l,diss,in}(t)$$
$$-\dot{m}_{l,diss,out}(t) - k_v \rho_s \frac{d\mu_3(t)}{dt} \tag{10}$$

where the terms $\dot{m}_{l,in}(t)$ and $\dot{m}_{l,out}(t)$ describe the inward and outward reactor flow, $\dot{m}_{l,diss,in}(t)$ and $\dot{m}_{l,diss,out}(t)$ describe inward and outward fines dissolution loop flow and the last term reflects the crystal growth.

The accumulation term on the left-hand side of the mass balance equation can be substituted in the following way:

$$\frac{dm_l}{dt} = \frac{d(V_r \rho_w \omega_l(t))}{dt} = V_r \rho_w \frac{d\omega_l(t)}{dt}. \tag{11}$$

The inward and outward reactor flows are described as follows:

$$\dot{m}_{l,in}(t) = \dot{V}_{in}\rho_{w,in}\omega_{l,in} = \frac{1}{\tau_r}V_r\rho_{w,in}\omega_{l,in} \tag{12}$$

$$\dot{m}_{l,out}(t) = \dot{V}_{out}\rho_w\omega_l(t) = \frac{1}{\tau_r}V_r\rho_w\omega_l(t) \tag{13}$$

The inward and outward dissolution loop flows are defined as follows:

$$\dot{m}_{l,diss,out}(t) = \dot{V}_f\rho_w\omega_l(t) = \delta\dot{V}_{out}\rho_w\omega_l(t)$$
$$= \frac{1}{\tau_r}\delta V_r\rho_w\omega_l(t) \tag{14}$$

$$\dot{m}_{l,diss,in}(t) = \dot{m}_{l,diss,out}(t) + \frac{k_v\rho_s\dot{V}_f}{V_r}\mu_{3,f}(t)$$
$$= \delta\frac{1}{\tau_r}V_r\rho_w(\omega_l(t) + k_v\rho_s\mu_{3,f}(t)) \tag{15}$$

After some further simplifications the mass balance can be described as follows:

$$\frac{d\omega_l(t)}{dt} = \frac{1}{\tau_r}\left(\frac{\rho_{w,in}}{\rho_w}\omega_{l,in} - \omega_l(t) + \delta k_v\rho_s\mu_{3,f}(t)\right)$$
$$-\frac{k_v\rho_s}{V_r\rho_w}\frac{d\mu_3(t)}{dt} \tag{16}$$

For the process configuration without fines dissolution, the term δ is equal to zero.

2.2 Open-loop simulation

For simulation studies and the following control design the process was discretized applying the finite volume method [Versteeg and Malalasekera (2007)]. The resulting model dimension for controller design was 2000 and for control system validation was reduced to 400 due to the computational expense. In order to gain a rough understanding of the process, simulation studies of the open-loop system were performed. The open-loop simulation expands the knowledge about process peculiarities, its stability, influence of parameter deviations on dynamic behaviour of the model and allows to define qualitative and quantitative indicators of the desired process operation. As we consider two cases, with and without fines
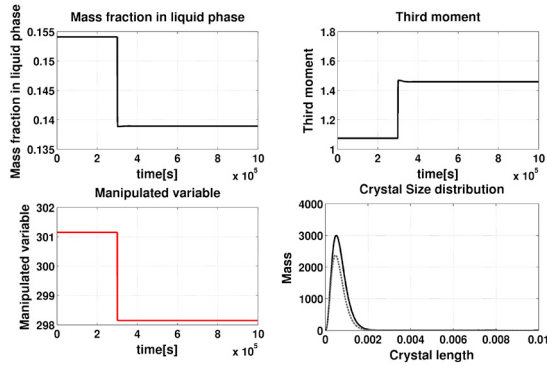
Fig. 2. The configuration without fines dissolution loop - reactor temperature step change $T_r = 301.15K$ to $298.15K$ at $t_{step} = 3 \cdot 10^5 s$
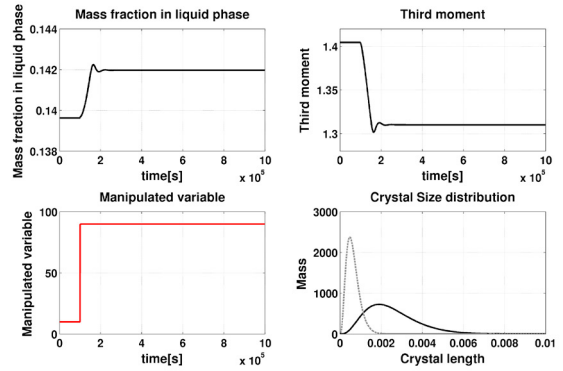

Fig. 3. The configuration without fines dissolution loop - reactor temperature step change $\delta = 10$ to 90 at $t_{step} = 1 \cdot 10^5 s$
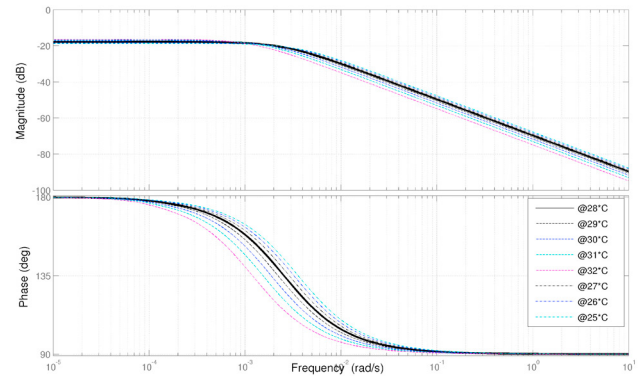
dissolution loop, these cases will be analyzed separately. In the configuration without fines dissolution loop, the studied parameter is the temperature within the reactor $T(t)$ which can be controlled by the cooling system. In the second configuration, the fines dissolution loop rate $\delta(t)$ was altered to study different operation points. The model parameters are provided in Table 1. The simulation results are shown in Fig. 2 and 3. In both cases the mass fraction in liquid phase $\omega_l(t)$, the third moment of CSD $\mu_3(t)$, manipulated variable (reactor temperature $T(t)$ for the first configuration and fines dissolution loop rate $\delta(t)$ for the second one) and the CSD $n(t, z)$ - initial distribution (dotted gray) and final distribution (solid black) are shown.

As can be seen the configuration without fines dissolution loop is stable, the configuration with fines dissolution loop shows some oscillatory behaviour but stays stable. However, as has been shown in [Randolph and Larson (1988)] for related configurations the emergence of nonlinear oscillations is possible and should be avoided.

Table 1. Simulation parameters

Parameter	Value
V_r	$0.024 m^3$
Q_{out}	$0.1 \frac{l}{min}$
K_g	1.67E-006 m/s
g	1.04
$E_{A,g}$	5.71E-009 J/mol
K_b	1234131.27 $1/s$
b	1.1
$E_{A,b}$	5.17E-011 J/mol
K_d	-4.32E-006 m/s
ρ_s	1757 kg/m^3
k_V	0.33
K_0	0.049378679989695
K_1	0.002179443878122
K_2	0.000089305667414
K_3	-0.000002627008140
K_4	0.000000049096298
ρ_w	1000 kg/m^3
z_{min}	1E-6 m

Fig. 4. Bode diagrams for varying reactor temperature (without fines dissolution loop)

3. LINEAR ANALYSIS AND MODEL REDUCTION

3.1 Analysis of the linearized models

The linearization was performed considering both configurations: system without fines dissolution loop and system with it. For a control design appropriate control inputs and outputs should be chosen. Here, for both configurations the third moment μ_3 of the CSD was chosen as the controlled variable. As an appropriate control input the reactor temperature and the fines dissolution loop rate were chosen in the first and second configuration, respectively. Linearization at different operation points for varying reactor temperatures in the range of $298.15K$ to $305.15K$ with nominal model referred to 301.15 and varying fines dissolution loop rate in the range from 10 to 150 with nominal model referred to 90 was undertaken and the results are depicted in figures 4 and 5, respectively with nominal models indicated with wider lines. Both nominal models are stable, controllable and observable. For a direct control design the order is however very high and should be reduced in order to design a low order controller being easily implementable on a programmable logic controller.

3.2 Model order reduction

In this contribution the balanced residualization method has been used for model order reduction [Skogestad and Postlethwaite (2005), Gu (2005), Chiang and Safonov
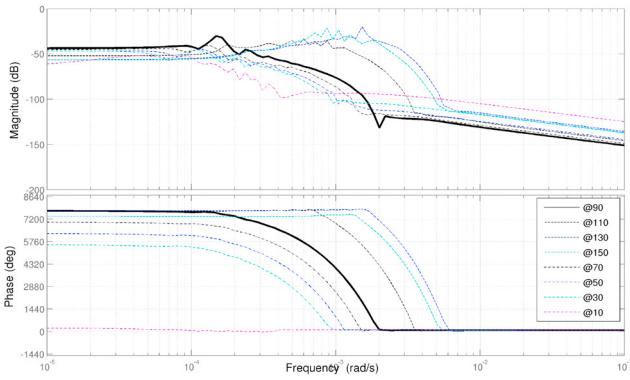
Fig. 5. Bode diagrams for varying dissolution rate (with fines dissolution loop)

(1996)]. For the first configuration a model order reduction to order three and in the second configuration to order 12 was achievable. The approximation error for both reduced order models is relatively small for low frequencies and increases for higher frequencies introducing an additional model uncertainty in the high-frequency zone. This additional model uncertainty should be mitigated by the robustness of the designed controller.

4. ROBUST CONTROLLER DESIGN AND SIMULATION

4.1 H_∞-loop-shaping controller design

Due to the number of considered assumptions, performed simplifications and approximations, a controller should be designed being capable of mitigating mismatches between the real process and the design model. Here, the H_∞-loopshaping approach [McFarlane and Glover (2013)] has been chosen as it combines simplicity, realizability and robustness with respect to the general class of coprime factor uncertainties. As stated earlier for both configurations the third moment μ_3 of the CSD is chosen as the controlled variable and the reactor temperature and the fines dissolution loop rate are the control inputs for the crystallization without and with fines dissolution loop, respectively (Fig. 6).
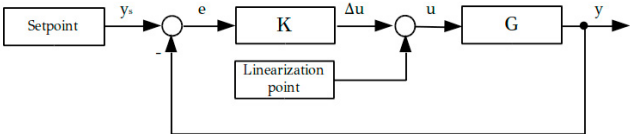

Fig. 6. Control system configuration

In the following it is assumed that the nominal system G is given in its normalized left coprime factorization

$$G = M^{-1}N \qquad (17)$$

where M and N are stable coprime transfer functions fulfilling the Bezout identity. Then an uncertain plant G_p consisting of the nominal system G can be represented as follows:

$$G_p = (M + \Delta_M)^{-1}(N + \Delta_N) \qquad (18)$$

where Δ_M and Δ_N are stable unknown transfer functions with $\|[\,\Delta_N\ \Delta_M\,]\|_\infty < \epsilon$ representing the model uncertainties. It is well known that a controller K robustly stabilizes the perturbed feedback system if it stabilizes the nominal system $G(s)$ and

$$\left\| \begin{bmatrix} K \\ I \end{bmatrix} (I + GK)^{-1} M^{-1} \right\|_\infty \leq \frac{1}{\epsilon}. \qquad (19)$$

A coprime factor uncertainty representation is in general superior over additive or multiplicative model uncertainties, as it is not restricted to perturbations which preserve the number of right half-plane poles of the plant. This fact is important for the control of continuous crystallization as stability behaviour may change depending on the specific operating conditions. In order to incorporate requirements on the closed loop performance the above stated H_∞-problem is generally combined with a prior loop shaping stage, where the pre- and postcompensators W_1 and W_2 are designed in order to achieve a desired open loop behaviour. Hence, the H_∞-problem is solved for the nominal model G augmented by the compensators W_1 and W_2

$$G_s = W_2 G W_1 \qquad (20)$$

and the H_∞-loop shaping controller K_{res} is formed from the compensators W_1 and W_2 and the solution of the H_∞-problem K.

$$K_{res} = W_1 K W_2 \qquad (21)$$

The H_∞-loop-shaping controller design was performed using the reduced-order models taking into account the following requirements: no static error, fast transient and low overshoot. For implementation reasons an additional controller order reduction was performed reducing the order up to 5 and 7, respectively.

4.2 Closed-loop system simulation

The controllers were verified using closed-loop simulations with the full order nonlinear process models. The simulation consisted in reference tracking test to ensure the steady-state accuracy, starting with initial conditions close to the reference point. The reference points are $\mu_3 = 1.3$ for the first configuration and $\mu_3 = 1.4$ for the second one. Then we simulated the emergence of disturbance - increase of feed solution temperature by $\Delta T_{feed} = 0.5K$ at $t = 5 \cdot 10^3 s$ for the first configuration and $t = 2 \cdot 10^6 s$ for the second one. The simulation results are shown in Fig. 7 and 8. The depicted variables are the mass fraction in liquid phase $\omega_l(t)$, the manipulated value $T(t)$ for the first case and $\delta(t)$ for the second one, the third moment of the CSD $\mu_3(t)$ and the crystal size distribution $n(t,z)$: initial (dotted gray) and final (solid black). The crystal size distribution representation over time is depicted in Fig. 9 and 10. Apparently, the system based on model without fines dissolution loop coped with the disturbance with less effect on the process performance than the system based on the second configuration. This is reasonable, because the nature of manipulated variable of reactor temperature is similar to the disturbance nature in contrast to the
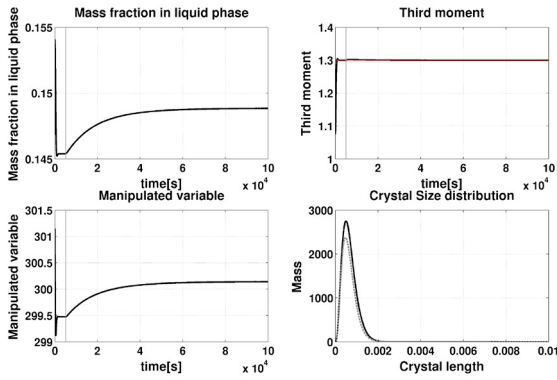
Fig. 7. Controlled crystallization without fines dissolution (disturbance rejection)
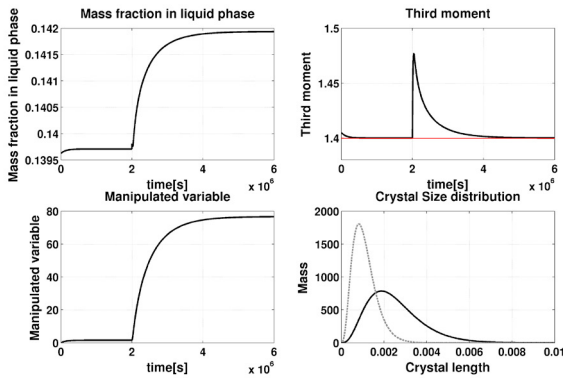

Fig. 8. Controlled crystallization with fines dissolution (disturbance rejection)
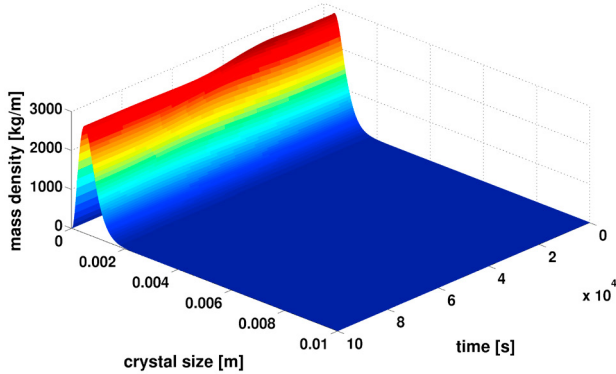

Fig. 9. Controlled crystallization with fines dissolution (disturbance rejection) - crystal size distribution

configuration with fines dissolution loop. Nevertheless, the designed controllers stabilize both process configurations, improve the transient dynamics, mitigate model uncertainties, discretization errors and diminish the influence of unforeseen disturbances as expected.

5. CONCLUSION

In this contribution two configurations of continuous crystallization processes have been studied. Both are described by a nonlinear model with distributed parameters. In order to stabilize the crystallization process and improve its performance feedback control was applied. Here, a linear
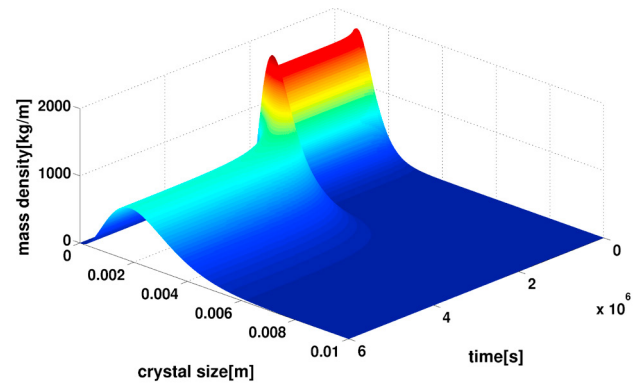

Fig. 10. Controlled crystallization with fines dissolution (disturbance rejection) - crystal size distribution

finite-dimensional robust controller approach being capable of mitigating model uncertainties and diminishing the influence of unforeseen disturbances has been successfully applied. Future work will concern the validation of the designed controllers within the crystallization facility HUGO at the Max Planck Institute for Dynamics of Complex Technical Systems Magdeburg and the extension of the crystallization process model in order to include crystal breakage and agglomeration phenomena.

Table 2. Notation

$n(t, z)$	crystal size distribution
G	crystal growth and dissolution factor
τ_r	residence time
δ	fines dissolution loop rate
$R(z)$	fines dissolution selection function
K_b	fitting parameter for preexponential crystal nucleation rate constant
$E_{A,b}$	activation energy - nucleation
R_{gas}	general gas constant
T	temperature inside reactor
S	supersaturation
b	exponential parameter for nucleation
K_g	fitting parameter for preexponential crystal growth rate constant
$E_{A,g}$	activation energy - growth
g	exponential parameter for growth
K_d	fitting parameter for preexponential crystal dissolution rate constant
$\omega_l(t)$	mass fraction in liquid phase
ω_{sat}	mass fraction at saturation point
k_V	volume shape factor
ρ_s	density of potassium alum
$\mu_3(t)$	the third moment of crystal size distribution
$\mu_{3,f}(t)$	the third moment of fine crystals size distribution
V_r	crystallizer volume
ρ_w	water density
G	nominal plant transfer function
M, N	coprime transfer functions
Δ_M, Δ_N	model uncertainties
ϵ	maximum stability margin
K	H_∞-problem solution
I	identity matrix
W_1, W_2	pre- and postcompensators
G_s	uncertain plant transfer function
K_{res}	resulting H_∞-controller

REFERENCES

Chiang, R.Y. and Safonov, M.G. (1996). *Robust control toolbox : for use with MATLAB : User's guide /.* The

Math Works Inc.

Chiu, T. and Christofides, P.D. (1999). Robust nonlinear control of a continuous crystallizer. *Computers & Chemical Engineering*, 23, Supplement, 257–260.

Gu, D.W. (2005). *Robust Control Design with MATLAB.* Springer Science & Business Media.

Ma, C.Y. and Wang, X.Z. (2012). Closed-loop control of crystal shape in cooling crystallisation of l-glutamic acid. *Journal of Process Control*.

McFarlane, D.C. and Glover, K. (2013). *Robust Controller Design Using Normalized Coprime Factor Plant Descriptions.* Springer, 1 edition.

Mersmann, A., Kind, M., and Stichlmair, J. (2011). *Thermal Separation Technology: Principles, Methods, Process Design.* VDI-Buch. Springer.

Motz, S., Mitrovic, A., Gilles, E.D., Vollmer, U., and Raisch, J. (2003). Modeling, simulation and stabilizing H_∞-control of an oscillating continuous crystallizer with fines dissolution. *Chemical Engineering Science*, 58(15), 3473–3488.

Palis, S. and Kienle, A. (2012). Diskrepanzbasierte regelung der kontinuierlichen kristallisation. *Automatisierungstechnik. - München : Oldenbourg*, 60(3), 145–154.

Randolph, A.D. and Larson, M.A. (1988). *Theory of particulate processes: analysis and techniques of continuous crystallization.* Academic Press.

Skogestad, S. and Postlethwaite, I. (2005). *Multivariable Feedback Control: Analysis and Design.* Wiley-Interscience, 2 edition.

Temmel, E. (2014). Personal communication.

Temmel, E., Lorenz, H., and Seidel-Morgenstern (2014). A short-cut-method for the quantification of crystallization kinetics. *ISIC 2014 - International Symposium on Industrial Crystallization*, 548–550.

Versteeg, H. and Malalasekera, W. (2007). *An Introduction to Computational Fluid Dynamics: The Finite Volume Method.* Prentice Hall, 2 edition.

Vollmer, U. and Raisch, J. (2002). Population balance modelling and $H_\infty-$controller design for a crystallization process. *Chemical Engineering Science*, 57(20), 4401–4414.

Entropy-based control of continuous fluidized bed spray granulation processes

Stefan Palis [1,*], **Andreas Bück** [1], **Achim Kienle** [1,2]

[1] *Otto-von-Guericke-Universität,*
Magdeburg, Germany
[2] *Max-Planck-Institute for Dynamics of Complex Technical Systems*
Magdeburg, Germany

Abstract: This paper is concerned with control of a continuous fluidized bed spray granulation. On the basis of an entropy function a control Lyapunov function will be derived. In order to facilitate the control design procedure this entropy-based control Lyapunov function will be approximated by its second order Taylor expansion.

1. INTRODUCTION

Fluidized bed spray granulation is a particulate process, where a bed of particles is fluidized, while simultaneously injecting a solid matter solution. Due to high process air temperature, the fluid evaporates and the remaining solid material either contributes to growth of already existing particles or forms new nuclei. As product particles should have a certain minimum size an additional product classification is required. In this contribution a process configuration applying an air sifter with countercurrent flow as depicted in Fig. 1 will be studied. Another possibility is for example the application of an external classification using sieves with corresponding recycle of the over- and undersized fraction [2]. In order to allow a continuous process operation part of the withdrawn product particles will be milled and fed back as nuclei to the granulation chamber. It is well known that continuous granulation processes in general and in particular configurations applying a mill cycle tend to instability and the occurrence of nonlinear oscillations of the particle size distribution. These oscillations give undesired time behavior of product quality [4, 3, 2]. Similar patterns of behavior have been observed for other particulate processes as e.g. crystallization processes (e.g. [10]). In order to control these several approaches have been proposed ranging from linear finite dimensional control (e.g. [9, 7]) to nonlinear infinite dimensional control methods [8]. Especially the later, i.e. the discrepancy based control design, has been successfully applied to different particulate processes.

In this contribution control design exploiting the thermodynamic structure, i.e. the entropy, of the process will studied. Therefore, an entropy-based control Lyapunov function will be derived and used for control design.

2. CONTINUOUS FLUIDIZED BED SPRAY GRANULATION

A continuous fluidized bed spray granulator with an additional mill as depicted in Fig. 1 consists of a granulation chamber, where the particle population is fluidized through an air stream and coated by injecting a suspension $\dot{V}_e$. The particle growth associated to the layering process has been described in [1].
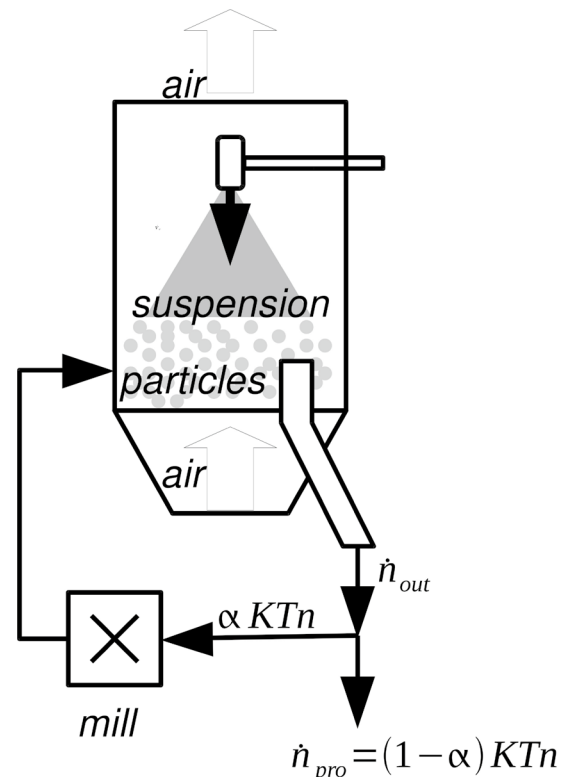

Fig. 1. Process scheme

$$G = 2\frac{\dot{V}_e}{\pi \int_0^\infty L^2 n dL} \tag{1}$$

It should be mentioned that the particle growth rate is inversely proportional to the overall particle surface area and hence the second moment of the particle size distribution. Product particles are continuously removed through an air sifter with countercurrent flow. Here, due to the particle size specific sinking velocity, small particles with $L < L_2$ are reblown into the granulation chamber, while large product particles with $L \geq L_2$ pass the air sifter. The associated ideal separation function T is given as follows.

$$T(L) = \sigma(L - L_2) \tag{2}$$

The outlet flow is hence

$$\dot{n}_{out} = KT(L)n. \tag{3}$$

where K is the drain, depending mainly on the air velocity and the ration between granulation chamber and sifter cross section. In order to guarantee a continuous process operation nuclei have to be continuously supplied. This can be achieved using an additional mill. For simplicity it can be assumed that the mill is mass conserving and generates a rectangular distribution.

$$B = \alpha(\sigma(L - L_0) - \sigma(L - L_1))\frac{\int_0^\infty L^3 KTn dL}{\int_0^\infty L^3 n dL} \tag{4}$$

$$= \alpha(\sigma(L - L_0) - \sigma(L - L_1))\frac{\int_0^\infty L^3 KTn dL}{4(L_1^4 - L_0^4)} \tag{5}$$

To describe the process, a population balance model for the particle size distribution can be stated consisting of the following particle fluxes

- B particle flux from the mill,
- $\dot{n}_{out}$ particle flux due to particle removal,

and size independent particle growth associated with the particle growth rate G.

$$\frac{\partial n}{\partial t} = -G\frac{\partial n}{\partial L} - \dot{n}_{out} + B \tag{6}$$

For numerical simulation the model equations are semi-discretized with the finite volume method (1st order up-wind flux discretization) with 310 grid points. The model parameters used are given in Table 1.

$\dot{V}_e$	$1.5 \cdot 10^5 \frac{mm^3}{s}$
L_0	$0.1mm$
L_1	$0.2mm$
L_2	$0.7mm$
K	$1 \cdot 10^{-3}\frac{1}{s}$
α_0	$5 \cdot 10^{-3}$

Table 1. Plant parameters

3. ENTROPY-BASED CONTROL LYAPUNOV FUNCTION

In the following a control Lyapunov functional will be derived based on an entropy function for the population balance model. The candidate being proposed in this contribution is strongly related to the one studied recently in [6] for a continuous crystallizer.

$$S = \int_0^\infty -Cn \ln n dL = \int_0^\infty s(n) dL \tag{7}$$

Here, C is a positive constant, which will be specified later. As we are interested in deviations from and control design for a desired steady state n_0 the following quantities can be defined

$$\Delta S = S_0 - S, \tag{8}$$

$$\Delta Z = Z_0 - Z, \tag{9}$$

where $Z = kn$. The conjugate variable of Z can be calculated as

$$\omega_0 = \left.\frac{\partial s}{\partial Z}\right|_{Z=Z_0} \tag{10}$$

$$= -\frac{C}{k}(\ln n_0 + 1). \tag{11}$$

Using Z, its conjugate and the entropy S a control Lyapunov function can be derived [6, 5].

$$V = -\int_0^\infty \Delta Z \omega_0 dL + \Delta S \tag{12}$$

Using eq. (11) yields

$$V = \int_0^\infty \Delta n(C(\ln n_0 + 1)) dL, \tag{13}$$

$$-\int_0^\infty C(n_0 \ln n_0 - n \ln n) dL, \tag{14}$$

$$= \int_0^\infty C(\Delta n - n(\ln n_0 - \ln n)) dL. \tag{15}$$

In order order to simplify the control design for the continuous fluidized bed granulation process this control Lyapunov candidate will be approximated by its second order Taylor approximation.

$$V = \int_0^\infty \frac{C}{n_0} \Delta n^2 dL \tag{16}$$

Choosing $C = \frac{1}{2}n_0$ yields

$$V = \frac{1}{2}\int_0^\infty \Delta n^2 dL. \tag{17}$$

4. CONTROL DESIGN

In the following the second order approximation of the entropy-based Lyapunov candidate (17) will be used in order to design an appropriate feedback control law. Calculating the time derivative $\dot{V}$ yields

$$\dot{V} = \int_0^\infty \Delta n\left(\frac{\partial n_0}{\partial t} - \frac{\partial n}{\partial t}\right) dL \tag{18}$$

$$= -\int_0^\infty \frac{G}{2}\frac{\partial \Delta n^2}{\partial L} + \Delta n\left[B_0 - B - KT\Delta n\right] dL \tag{19}$$

$$= -\left.\frac{G}{2}\Delta n^2\right|_0^\infty - \int_0^\infty \Delta n\left[B_0 - B - KT\Delta n\right] dL \tag{20}$$

Here, the first two terms vanish due to the boundary conditions $n(L = 0) = \lim_{L\to\infty} n(L) = 0$, i.e. there are no particles of size zero and infinitely large particles. Hence, the time derivative of the Control Lyapunov functional V does not depend on the growth rate G and thus all results will be robust with respect to variations in the suspension injection rate.

$$\dot{V} = \int_0^\infty \Delta n\left[B_0 - B - KT\Delta n\right] dL \tag{21}$$

Inserting the equations for the particle outlet (3) and the mill flux (5) results in the following

$$\dot{V} = -\int_{L_0}^{L_1} \Delta n \frac{\int_{L_2}^{\infty} \alpha_0 L^3 K n_0 - \alpha L^3 K n dL}{4(L_1^4 - L_0^4)} dL \quad (22)$$

$$-K \int_{L_2}^{\infty} \Delta n^2 dL \quad (23)$$

For convenience a virtual control input $u_{virt} = \alpha \int_{L_2}^{\infty} L^3 K n dL$ is introduced.

$$\dot{V} = -(u_{virt,0} - u_{virt}) \frac{\int_{L_0}^{L_1} \Delta n dL}{4(L_1^4 - L_0^4)} - K \int_{L_2}^{\infty} \Delta n^2 dL \quad (24)$$

In order to achieve negative definiteness of the time derivative of the entropy-based candidate Lyapunov functional V the following virtual control law is chosen

$$u_{virt} = u_{virt,0} + \frac{4(L_1^4 - L_0^4)}{\int_{L_0}^{L_1} \Delta n dL} \left[c \int_0^{\infty} \Delta n^2 dL \right], \quad (25)$$

which results in the control law for α

$$\alpha = \frac{u_{virt}}{\int_{L_2}^{\infty} L^3 K n dL}. \quad (26)$$

The time derivate of the entropy-based control Lyapunov function hence is

$$\dot{V} = -c \int_0^{\infty} \Delta n^2 dL - K \int_{L_2}^{\infty} \Delta n^2 dL \quad (27)$$

$$\leq -c \int_0^{\infty} \Delta n^2 dL = -2cV \quad (28)$$

guaranteeing asymptotic stability and exponential convergence. The control law is tested starting at an initial particle size distribution $n(t = 0, L) = 1.5 \cdot n_0(L)$ depicted in Fig. 2 and with a tuning factor $c = 2 \cdot 10^{-6}$. As can be seen in Fig. 3 and 4 the proposed control law succeeds in controlling the desired particle size distribution with reasonable control effort (Fig. 5 and Fig. 6). For comparison the open loop process behavior is depicted in Fig. 7 showing considerably more oscillations and higher peaks in the particle size distribution. In order to evaluate the control performance the third moment of the particle size distribution in open and closed loop operation is shown in Fig. 8.
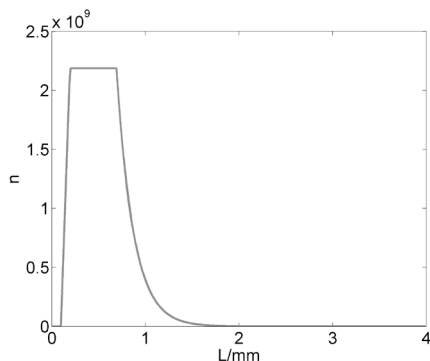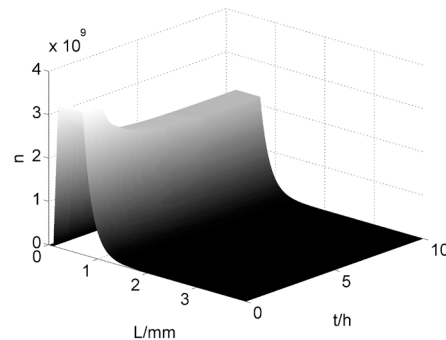

Fig. 2. Initial particle size distribution

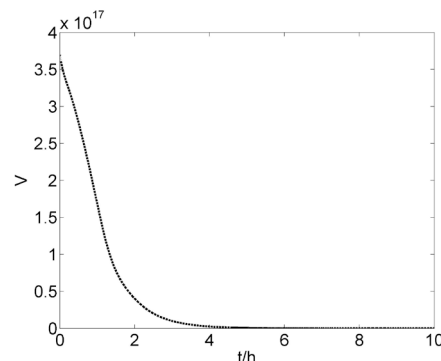Fig. 3. Particle size distribution in closed loop operation n

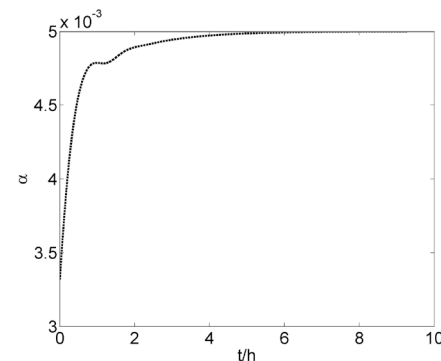Fig. 4. Entropy-based Lyapunov function V
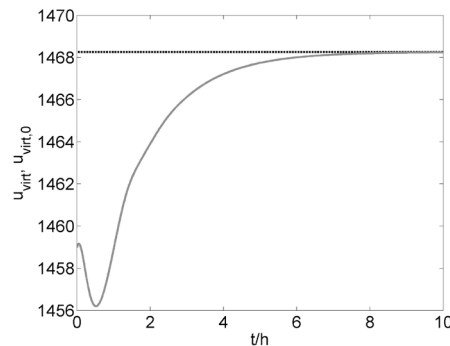

Fig. 5. Control input α

Fig. 6. Virtual control input u_{virt}

5. CONCLUSION

For a continuous fluidized bed spray granulation with mill cycle an appropriate control law has been derived and
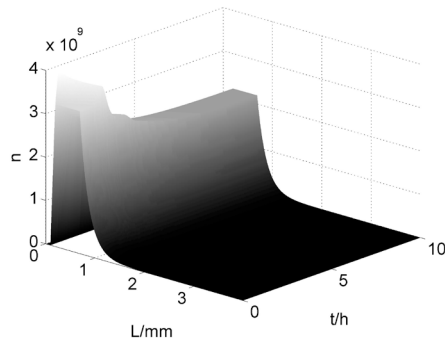
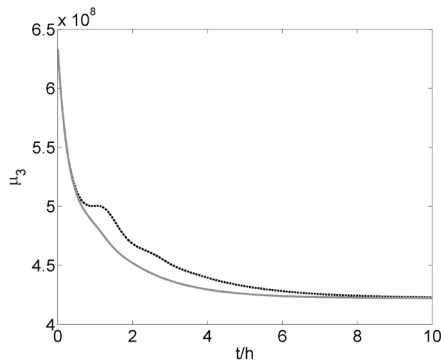Fig. 7. Particle size distribution in open loop operation n

Fig. 8. Third moment of the particle size distribution μ_3 in open (black dashed) and closed loop operation (gray solid)

tested. The main idea is to derive a Lyapunov functional on the basis of an entropy function. In order to facilitate the control design procedure this entropy-based Lyapunov functional has been approximated by its second order Taylor expansion. Future work will be concerned with a thorough comparison between the here presented entropy-based control approach giving physical insight and the earlier proposed discrepancy based control design [8]. Applying the latter control laws are designed on the basis of a generalized distance measure, the discrepancy, focusing on the process input output behavior.

REFERENCES

[1] L. Mörl & M. Mittelstrass & J. Sachse, Zum Kugelwachstum bei der Wirbelschichttrocknung von Lösungen oder Suspensionen. Chem. Techn. 29, 1977, Heft 10, pp. 540-542.

[2] S. Heinrich & M. Peglow & M. Ihlow & M. Henneberg & L. Mörl, Analysis of the start-up process in continuous fluidized bed spray granulation by population balance modeling, Chem. Eng. Sci. 57, 2002, pp. 4369-4390.

[3] R. Radichkov & T. Müller & A. Kienle & S. Heinrich & M. Peglow & L. Mörl, A numerical bifurcation analysis of continuous fluidized bed spray granulation with external product classification, Chem. Eng. Proc., Proc. 45, 2006, pp. 826-837.

[4] A.W. Vreman & C.E. van Lare & M.J. Hounslow, A basic population balance model for fluid bed spray granulation, Chem. Eng. Sci. 64, 2009, pp. 4389-4398.

[5] K. Hangos, Engineering model reduction and entropy-based Lyapunov functions in chemical reaction kinetics, Entropy 12, 2010, pp. 772-797.

[6] J. Du & B.E. Ydstie, Convergence results for continuous crystallizers, 10th IFAC International Symposium on Dynamics and Control of Process Systems - DYCOPS, 2013, pp. 203-208.

[7] S. Palis & A. Kienle, Stabilization of continuous fluidized bed spray granulation with external product classification, Chem. Eng. Sci., 2012, pp. 200-209.

[8] S. Palis & A. Kienle, Discrepancy based control of particulate processes, Journal of Proc. Cont. 24, 2014, pp. 33-46.

[9] R. Eek, Control and dynamic modeling of industrial suspension crystallizers, PhD thesis, TU Delft, 1995.

[10] A. D. Randolph & M. A. Larson, Theory of particulate processes, New York: Academic Press, Inc., 1988.

Discrepancy-based control of a heat equation with quadratic nonlinearity

Stefan Palis [1,*] **and Achim Kienle**[1,2]

Abstract— This article deals with a new approach to stabilizing boundary control for nonlinear parabolic PDEs. The system under investigation is the quadratic heat equation. In order to stabilize this system in this contribution the use of a generalized distance measure, the discrepancy, is proposed. Applying, the associated stability theory, i.e. stability theory with respect to two discrepancies, a stabilizing control law can be derived.

I. INTRODUCTION

Control of distributed parameter systems (e.g. [1], [2], [3]) is an active field of research. Especially, the case of linear parabolic PDEs with boundary actuation has received great attention in recent years. In [4], [5] the finite-dimensional feedback linearization approach has been successfully extended to parabolic PDEs with Volterra nonlinearities. There, the heat equation with a quadratic nonlinearity has been one of the studied test cases. It has been shown [4] that using a state transformation the quadratic nonlinearity can be transformed into a Volterra series nonlinearity. For the transformed system choosing a flat output an infinite dimensional feedback linearizing controller based on Volterra series has been derived, which has been truncated to second order for implementation. As has been shown by simulations the proposed controller is able to stabilize the heat equation with quadratic nonlinearities for initial conditions with peak values up to 8. For initial conditions with a higher maximum value, i.e $max_{x \in [0,1]} w(x) > 8$, the authors state [4] that the proposed control law is not able to stabilize the system.

In this contribution a complementary approach, discrepancy-based control, will be proposed for this challenging benchmark problem. The discrepancy-based control approach has been developed and successfully applied in particulate process control, e.g. crystallization [6] and granulation [7], [8]. Here, the main idea is to choose an appropriate generalized distance measure, the discrepancy, which allows a direct Lyapunov design guaranteeing stability with respect to the chosen discrepancies. In addition, convergence with respect to a L_p-norm or pointwise convergence can be guaranteed under the condition of stable zero dynamics.

The paper is organized as follows: in section II the model system, a heat equation with quadratic nonlinearity, is stated. In section III the main theoretic concepts of stability with respect to two discrepancies are stated. The connection between stability with respect to two discrepancies and stability in the sense of the L_∞-norm is outlined in section IV. In section V the discrepancy-based control method is applied in order to derive a stabilizing control law for the model system. Some final remarks conclude the paper.

II. HEAT EQUATION WITH QUADRATIC NONLINEARITY

Consider the following heat equation with an additional quadratic nonlinearity

$$\frac{\partial w}{\partial t} = \frac{\partial^2 w}{\partial x^2} + w^2, \tag{1}$$

with boundary conditions

$$w(0,t) = 0, \tag{2}$$
$$\frac{\partial w(1,t)}{\partial x} = u. \tag{3}$$

Here, $w(x,t)$ is the system state, $t \geq 0$ is the time and $x \in [0,1]$ is the spatial coordinate. It is well known that this system is unstable, diverges to infinity in finite time and is not globally stabilizable [4] and references therein. Therefore, the stabilizing control of the heat equation with quadratic nonlinearity is a challenging task.

III. STABILITY WITH RESPECT TO TWO DISCREPANCIES

In the following, the most important properties and facts on stability with respect to two discrepancies are stated in accordance to [9], [10], [11]. Here, the process $\varphi(.,t)$ is a solution of a distributed parameter system and $\varphi_0 = 0$ an equilibrium of the system. The discrepancy $\rho(\varphi(.,t),t)$ is a measure of the distance between the process $\varphi(.,t)$ and the equilibrium φ_0.

Definition 1: (Discrepancy): A discrepancy is a real valued functional $\rho = \rho[\varphi(.,t),t]$ with the following properties

1) $\rho(\varphi, t) \geq 0$,
2) $\rho(0, t) = 0$,
3) for an arbitrary process $\varphi = \varphi(.,t)$ the real valued functional $\rho(\varphi(.,t),t)$ is continuous with respect to t.

It is important to note that a discrepancy lacks essential properties of a metric, e.g. symmetry $d(x,y) = d(y,x)$ or triangular inequality $d(x,y) \leq d(x,z) + d(z,y)$ are not satisfied. In addition, a discrepancy has not to satisfy the important property of definiteness, i.e. a vanishing discrepancy $\rho(\varphi,t) = 0$ does not automatically imply $\varphi = 0$. Therefore, the discrepancy is an extension of the distance measures

[1]Otto-von-Guericke-Universität, Universitätsplatz 2, D-39106 Magdeburg, Germany
[2]Max-Planck-Institut für Dynamik komplexer technischer Systeme, Sandtorstrasse 1, D-39106 Magdeburg, Germany
* Author to whom all correspondence should be addressed. Email: stefan.palis@ovgu.de

normally used in stability theory for distributed parameter systems like L_p and L_∞- norms.

In the context of stability with respect to two discrepancies besides the discrepancy $\rho(\varphi(.,t,t))$ measuring the distance between $\varphi(.,t)$ and the equilibrium φ_0, a second time independent discrepancy ρ_0 is used describing the distance between the initial state $\varphi(.,0)$ and the equilibrium φ_0. The two discrepancies ρ and ρ_0 have to satisfy, that the discrepancy $\rho(\varphi(.,t),t)$ is continuous at time $t = t_0$ with respect to ρ_0 at $\rho_0 = 0$, i.e. for every $\varepsilon > 0$ and $t_0 > 0$ there exists a $\delta(\varepsilon, t_0) > 0$, such that from $\rho_0 \leqslant \delta(\varepsilon, t_0)$ it follows that $\rho < \varepsilon$.

Definition 2: (Stability with respect to two discrepancies ρ and ρ_0): The equilibrium $\varphi_0 = 0$ is stable in the sense of Lyapunov with respect to the two discrepancies ρ and ρ_0 for all $t \geq t_0$ if for every $\varepsilon > 0$ and $t_0 \geq 0$ there exists a $\delta = \delta(\varepsilon, t_0) > 0$ such that for every process $\varphi(.,t)$ with $\rho_0 < \delta(\varepsilon, t_0)$ it follows that $\rho < \varepsilon$ for all $t \geq t_0$. If in addition $\lim_{t \to \infty} \rho = 0$, than the equilibrium φ_0 is called asymptotically stable in the sense of Lyapunov with respect to the two discrepancies ρ and ρ_0.

In order to define a Lyapunov functional V guaranteeing stability with respect to two discrepancies the additional notions of positivity and positive definiteness of a functional with respect to a discrepancy are introduced.

Definition 3: (Positivity with respect to a discrepancy ρ): The functional $V = V[\varphi, t]$ is called positive with respect to the discrepancy ρ, if $V \geq 0$ and $V[0, t] = 0$ for all φ with $\rho(\varphi, t) < \infty$.

Definition 4: (Positive definiteness with respect to a discrepancy ρ): The functional $V = V[\varphi, t]$ is positive definite with respect to a discrepancy ρ, if $V \geq 0$ and $V[0, t] = 0$ for all φ with $\rho(\varphi, t) < \infty$ und for every $\varepsilon > 0$ there exists a $\delta = \delta(\varepsilon) > 0$, such that $V \geq \delta(\varepsilon)$ for all φ with $\rho[\varphi, t] \geq \varepsilon$.

The following two theorems state the conditions for a functional V guaranteeing (asymptotic) stability with respect to two discrepancies.

Theorem 1: [11] The process φ with the equilibrium $\varphi_0 = 0$ is stable with respect to the two discrepancies ρ and ρ_0 if and only if there exists a functional $V = V[\varphi, t]$ positive definite with respect to the discrepancy ρ, continuous at time $t = t_0$ with respect to ρ_0 at $\rho_0 = 0$ and not increasing along the process φ, i.e. $\dot{V} \leq 0$.

Theorem 2: [11] The process φ with the equilibrium $\varphi_0 = 0$ is asymptotically stable with respect to the two discrepancies ρ and ρ_0 if and only if there exists a functional $V = V[\varphi, t]$ positive definite with respect to the discrepancy ρ, continuous at time $t = t_0$ with respect to ρ_0 at $\rho_0 = 0$ and not increasing along the process φ, i.e. $\dot{V} \leq 0$, with $\lim_{t \to \infty} V = 0$.

IV. STABILITY WITH RESPECT TO A DISCREPANCY AND POINTWISE CONVERGENCE

In order to state conditions, when convergence in two discrepancies yields convergence in a L_p-norm or pointwise convergence, i.e. convergence in the L_∞-norm, the discrepancies ρ may be interpreted as output variables. Whereas the distributed variable φ resembles the system state. Applying this notation the finite dimensional concepts of relative degree and zero dynamics (e.g. [12]) can be extended to the infinite dimensional case (e.g. [13], [14]) yielding the desired connection between stability with respect to two discrepancies and stability in the L_p or L_∞-norm. In the finite dimensional case a system of order n and relative degree $r \leq n$ can be represented in its normal form applying a local coordinate transformation [12].

$$\dot{z}_1 = z_2 \qquad (4)$$
$$\vdots$$
$$\dot{z}_{r-1} = z_r \qquad (5)$$
$$\dot{z}_r = f(\psi, \eta) + g(\psi, \eta)u \qquad (6)$$
$$\dot{\psi} = h(\psi, \eta, u) \qquad (7)$$

Here, the system state space can be easily separated into two parts. The first part consisting of the state equations for $\psi = [z_1, \ldots, z_r]^T$, which can be linearized and controlled by the control u, and the second part being associated with the state $\eta = [z_{r+1}, \ldots, z_n]^T$, which forms the zero dynamics. As a separation of the state variables is in general inconvenient for a distributed parameter system, the zero dynamics are typically defined by constraining the output to zero by applying the appropriate control law ([13], [14]), e.g. the discrepancy-based control law. Therefore, applying the discrepancy-based control law guarantees stability of the whole system if and only if the zero dynamics associated with the discrepancy ρ are stable. Unfortunately, stability of the zero dynamics in the infinite dimensional case is very hard to check. In order to overcome this problem in this contribution a heuristic approach is proposed. Therefore, for the heat equation with quadratic nonlinearity only the conditions related to the finite dimensional linear case, i.e. the presence of right-half plane zeros, will be checked. This approach gives due to linearization at least a local stability result, i.e. valid in a neighborhood of a steady state, for the finite dimensional approximation.

V. DISCREPANCY-BASED CONTROL

In the following, a discrepancy-based control law will be derived for the heat equation with quadratic nonlinearity. Here, deviations from the desired steady state $w_d(x) = 0$ will be measured in terms of an integral quantity

$$e = \int_0^1 k(x) \, (w_d - w) \, dx, \qquad (8)$$

where the kernel $k(x)$ is defined as follows

$$k(x) = \exp(-ax). \qquad (9)$$

This choice is motivated by the fact that errors in a greater distance from the actuated boundary at $x = 1$ are harder to control and should therefore be stronger weighted, i.e. $x \downarrow$ gives $k(x) \uparrow$. An appropriate choice for a discrepancy ρ being associated with the error measure defined in eq. 8 is

$$\rho = \frac{1}{2} \left(\int_0^1 k(x) \, (w_d - w) \, dx \right)^2. \tag{10}$$

In order to guarantee continuity at time $t = t_0$ at $\rho_0 = 0$ the second discrepancy ρ_0 is chosen as follows

$$\rho_0 = \rho(t = 0). \tag{11}$$

According to Theorem 2 existence of an appropriate functional V is sufficient to guarantee asymptotic stability with respect to the two discrepancies ρ and ρ_0. For this purpose the following candidate Lyapunov functional is introduced

$$V = \frac{1}{2} e^2 = \frac{1}{2} \left(\int_0^1 k(x) \, (w_d - w) \, dx \right)^2. \tag{12}$$

In order to achieve stability in the sense of two discrepancies the control variable u has to be chosen such that the time derivate of V along the systems trajectories (1) is negative definite for all times and vanishes only for $V = 0$. Calculating the time derivative of V along the system trajectories (1) yields

$$\dot{V} = e\dot{e} = -e \int_0^1 k \left(\frac{\partial^2 w}{\partial x^2} + w^2 \right) dx, \tag{13}$$

$$= -e \left[k \frac{\partial w}{\partial x} \Big|_0^1 - \int_0^1 \frac{dk}{dx} \frac{\partial w}{\partial x} - kw^2 dx \right], \tag{14}$$

$$= -e \left[k(1)u - k(0)\frac{\partial w(0,t)}{\partial x} - \frac{dk}{dx} w \Big|_0^1 \right.$$
$$\left. + \int_0^1 \frac{d^2 k}{dx^2} w + kw^2 dx \right], \tag{15}$$

$$= -e \left[k(1)u - k(0)\frac{\partial w(0,t)}{\partial x} - \frac{dk(1)}{dx} w(1,t) \right.$$
$$\left. + \int_0^1 \frac{d^2 k}{dx^2} w + kw^2 dx \right]. \tag{16}$$

Using (16) the negative definiteness of the time derivative of the candidate Lyapunov functional V can be guaranteed choosing the following control law.

$$u = \frac{1}{k(1)} \left[k(0)\frac{\partial w(0,t)}{\partial x} + \frac{dk(1)}{dx} w(1,t) + ce \right.$$
$$\left. - \int_0^1 \left(\frac{d^2 k}{dx^2} + kw \right) w dx \right] \tag{17}$$

In addition to stability with respect to two discrepancies the control law (17) guarantees exponential convergence of V, where c can be used as a tuning parameter in order to influence the convergence velocity.

$$\dot{V} = -ce^2 = -2cV \tag{18}$$

In order to check for pointwise convergence, i.e. stability of the zero dynamics with respect to the discrepancy ρ, only a

high order finite dimensional linear approximation has been studied. As can be seen from the open loop pole/zero map in Fig. 1 there are no zeros in the right half plan. This indicates that the zero dynamics are stable, which in turn would prove stability in the L_∞-norm.
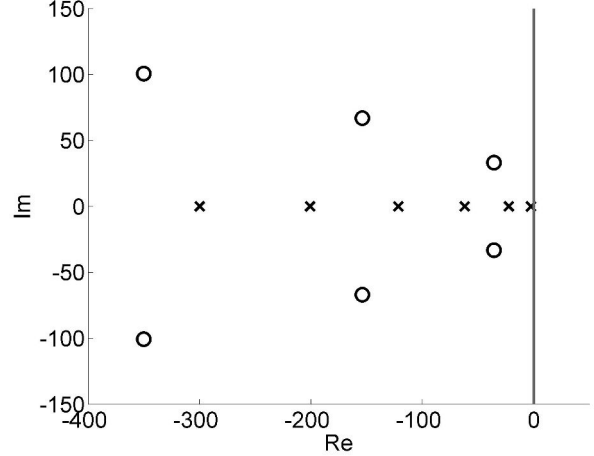

Fig. 1. Pole/zero map of linear finite dimensional approximation

The proposed control scheme is tested for $a = 2$, $c = 10$ and a sinusoidal initial condition with a peak value of 20, i.e. $w(x, 0) = 20 \sin(x)$, which is higher than the maximum allowable value of 8 in [4]. As can be seen in Fig. 2 and 3 the proposed control scheme is able to stabilize the process.
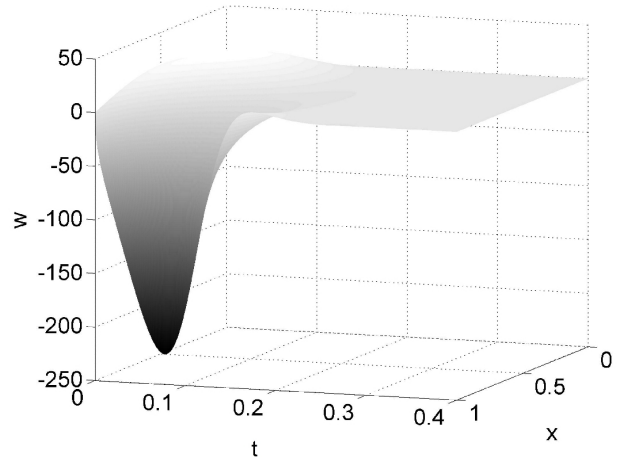

Fig. 2. Closed loop operation

Fig. 4 shows the exponential convergence of the Lyapunov functional V. The convergence of w in the sense of the L_2 and L_∞-norm are depicted in Fig. 5 and 6 respectively.

VI. Conclusion

A new control approach for the benchmark problem of a heat equation with quadratic nonlinearity has been presented.
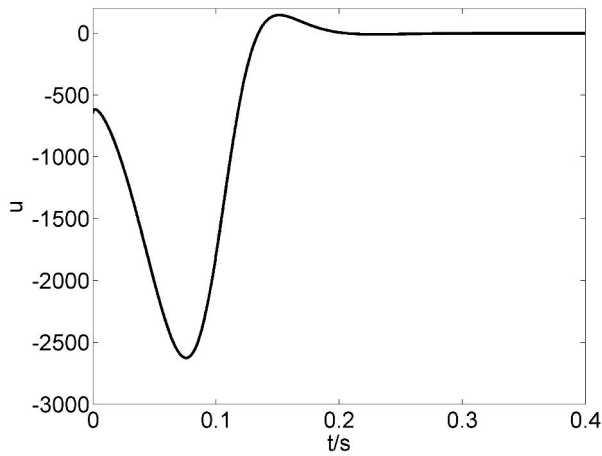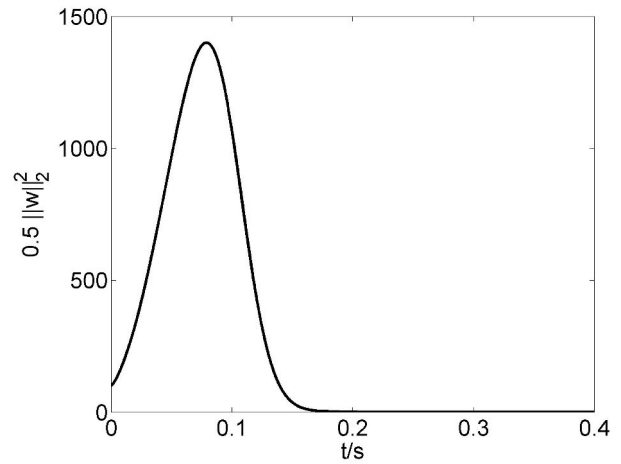
Fig. 3. Control input u

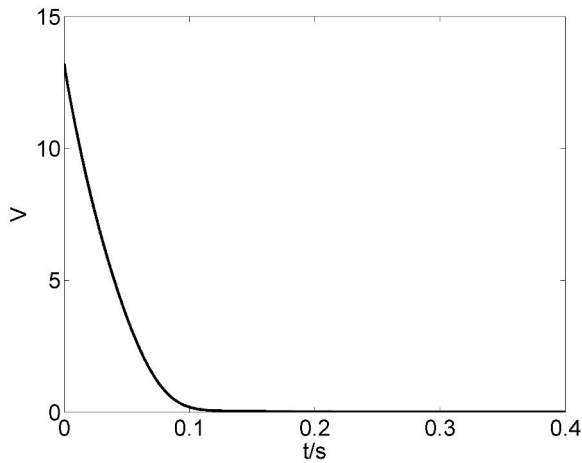Fig. 5. Convergence of the L_2-norm in closed loop operation

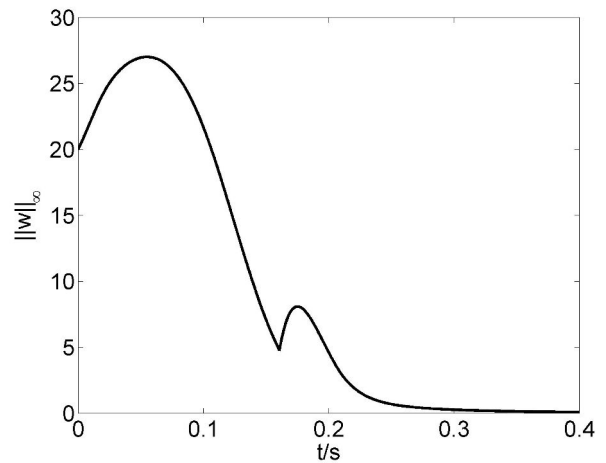Fig. 4. Convergence of V in closed loop operation

Fig. 6. Convergence of the L_∞-norm in closed loop operation

It has been shown in silico that the proposed discrepancy-based control is able to stabilize the system in a certain range of initial conditions. As the proposed design guarantees only stability in the sense of Lyapunov with respect to the two chosen discrepancies stability of the associated zero dynamics has to be studied in order to ensure convergence in a L_p-norm or pointwise convergences, i.e. convergence in a L_∞-norm. This is a challenging task for the investigated problem. Therefore, only the zero dynamics of the linearized discretized approximation is studied.

REFERENCES

[1] A. Smyshlyaev & E. Cerpa & M. Krstic, Boundary stabilization of a 1-D wave equation with in-domain anti-damping, SIAM Journal of Control and Optimization, vol. 48, pp. 4014-4031, 2010.
[2] C. Prieur & J. Winkin & G. Bastin, Robust boundary control of systems of conservation laws, Mathematics of Control, Signals and Systems, Vol. 20, pp. 173 - 197, 2008.
[3] T. Meurer, Flatness-based trajectory planning for diffusion-reaction systems in a parallelepipedon - a spectral approach, Automatica, 47, 2011, pp. 935-949.
[4] R. Vazquez & M. Krstic, Control of 1-D parabolic PDEs with Volterra nonlinearities, Part I: Design, Automatica, 44, 2008, pp. 2778-2790.
[5] R. Vazquez & M. Krstic, Control of 1-D parabolic PDEs with Volterra nonlinearities, Part II: Analysis, Automatica, 44, 2008, pp. 2791-2803.
[6] S. Palis & A. Kienle, Discrepancy-based Control of Continuous Crystallization, at-Automatisierungstechnik, 2012, pp. 145-154.
[7] S. Palis & A. Kienle, Discrepancy-based control of continuous fluidized bed spray granulation with internal product classification, 8th IFAC International Symposium on Advanced Control of Chemical Processes - ADCHEM, 2012, pp. 756-761.
[8] S. Palis & A. Kienle, Discrepancy-based control of particulate processes, Journal of Process Control, 24, 2014, pp. 33-46.
[9] A.A. Movchan, Stability of processes with respect to two metrics, Journal of Applied Mathematics and Mechanics, 1960, 24, pp. 1506-1524.
[10] A. Martynjuk & R. Gutovski, Integral inequalities and stability of motion, Izdatel'stvo Naukova Dumka, Kiev, 1979.
[11] T. Sirasetdinov, Stability of systems with distributed parameters, Izdatel'stvo Nauka, Novosibirsk, 1987.
[12] A. Isidori, Nonlinear Control Systems, Springer Verlag, New York, 1995.
[13] C. Byrnes, D. Gilliam, J. He, Root-locus and boundary feedback design for a class of distributed parameter systems, SIAM J. Control and Optimization, 32, 1994, pp. 1364-1427.
[14] P. Christofides, P. Daoutidis, Feedback Control of Hyperbolic PDE Systems, AIChE Journal, 42, 1996, pp. 3063-3086.

The 7th World Congress on Particle Technology (WCPT7)

Online parameter identification of facet growth kinetics in crystal morphology population balance models

Robert Dürr[a,*], Stefan Palis[a], Achim Kienle[a,b]

[a]*Otto-von-Guericke University Magdeburg, Universitätsplatz 2, 39106 Magdeburg, Germany*
[b]*Max-Planck-Institute for Dynamics of Complex Technical Systems, Sandtorstraße 1, 39106 Magdeburg, Germany*

Abstract

Particle shape plays an important role in many industrial applications since it can have significant impact on both, processability of particles as well as the properties of the final product. For this reason modeling of the corresponding production process is crucial for developing efficient process optimization and control strategies. The shape evolution of crystals on the process scale can be described conveniently within the framework of morphological population balance modeling. In order of being a reliable tool for the prediction of the crystal shape distribution during the production process as well as for the design of suitable control and optimal production strategies, the models require the estimation of several parameters characterizing the growth rates of the different crystal facets. This is particularly challenging due to the infinite dimensional state space of the models. In this contribution online parameter estimation for the growth rates of L-glutamic acid cooling crystallization is presented. Using a Lyapunov-based approach the parameter adaption laws are computed directly from the infinite dimensional problem formulation. It will be shown that a reasonably fast convergence of the parameter estimates can be achieved even in the presence of measurement noise using appropriate filters.

Keywords: Multivariate population balance modeling; Crystal morphology; Crystallization; Online parameter identification

* Corresponding author: Tel.: +49 391 67 12689; Fax.: +49 391 67 11186
E-Mail address: robert.duerr@ovgu.de

1. Introduction

Crystallization is an important class of production processes in chemical and pharmaceutical industries. It is used to produce a desired material in crystalline form from a liquid solution. Details on crystallization principles and techniques can be found e.g. in [1]. The production processes are characterized frequently by heterogeneity of the crystal ensemble with respect to crystal properties like size and shape. Those have a significant influence on the end-use property and the processability of the final product. Modeling of the corresponding dynamics is thus crucial for the design of efficient schemes for process control and optimization. It is well known that the temporal evolution of the previously described heterogeneous system can be modeled using population balances [2]. Here, morphological population balances being a special form of multivariate PBMs can be used to describe the dynamic shape evolution (e.g. [3], [4]). For the development of process control and optimization schemes the individual facets growth kinetics in the population balance have to be determined. This can be done for example by experimentally measuring the growth rates of a single crystal or a small number of crystals, which has several drawbacks that may yield biased estimates. Alternatively, the rates may be determined directly from process scale seeded crystallization experiments. Here, the temperature, solute concentration and the crystal shape distribution have to be measured. The parameters of the growth kinetics can then be estimated minimizing the error between the simulation of the morphological PB and the measurement data from experiment. In offline optimization-based parameter estimation schemes variations of the optimal parameter estimates due to changes in operation conditions are typically neglected resulting in performance deterioration. In order to overcome this problem in this manuscript the design of an online parameter estimation approach for morphological PBs will be investigated for a L-glutamic acid crystallization process [5,6].

　　This contribution is structured as follows. At first the general process model will be presented. Subsequently, the online parameter adaption laws will be derived directly from the infinite dimensional process model using a Lyapunov-based approach [7]. Next the performance of the proposed parameter estimation scheme will be shown assuming ideal measurements without noise. Further, it will be made clear that in case of realistic measurement errors the online adaption has to be combined with a filtering technique. At the end, the results are summarized and possible extensions for future research are mentioned.

Nomenclature

c	solute concentration $[g/l]$
$\hat{c}$	estimated solute concentration $[g/l]$
c^*	solubility $[g/l]$
e_n, e_c	error in the number density distribution/concentration between model and process
g_L, g_W	kinetic coefficients (exponents) for facet growth
G_L, G_W	facet growth rate in length/width dimension $[m/s]$
$\hat{G}_L, \hat{G}_W$	estimated facet growth rate in length/width dimension $[m/s]$
k_L, k_W	facet growth parameters $[m/s]$
$\hat{k}_L, \hat{k}_W$	estimated facet growth parameters $[m/s]$
$\tilde{k}_L, \tilde{k}_W$	error in facet growth parameters
L	length of β-form L-GA $[m]$
m_{10}, m_{01}	mean length/width of number density distribution $[m]$
$\hat{m}_{10}, \hat{m}_{01}$	estimated mean length/width of number density distribution $[m]$
n	number density distribution $[m^{-3}]$
$\hat{n}$	estimated number density distribution $[m^{-3}]$
$P_n^{obs}, P_c^{obs}, P_m^{obs}$	error feedback gains for model $[s^{-1}]$
q_L, q_W	kinetic coefficients (exponents) for facet growth
t	time $[s]$
T	temperature $[℃]$
W	width of β-form L-GA $[m]$

γ_L, γ_W	parameter adaption rate tuning parameters
ρ	crystal density $[kg\ m^{-3}]$
σ	relative supersaturation

2. Process modeling

In this manuscript seeded crystallization of β-form L-glutamic acid (L-GA) in a stirred tank reactor as presented in [5] is used as a benchmark problem. The shape of a single crystal can be described reasonably by the length L and width W of a parallelepiped (Fig. 1). Thus, depending on the ratio of both the crystal shape may vary between disks and needles. Assuming that the crystal growth is dominant and neglecting other effects like agglomeration, breakage and nucleation, the dynamics of the number density distribution $n(t, L, W)$ with respect to the two characteristic properties can be modeled using the following morphological PBM

$$\frac{\partial n(t, L, W)}{\partial t} + \frac{\partial}{\partial L}\{G_L(t, L, W)\ n(t, L, W)\} + \frac{\partial}{\partial W}\{G_W(t, L, W)\ n(t, L, W)\} = 0. \tag{1}$$

Here, the growth rates are given by

$$G_L(t, L) = k_{g_L}\ \sigma(t)^{g_L}\ L^{q_L},$$

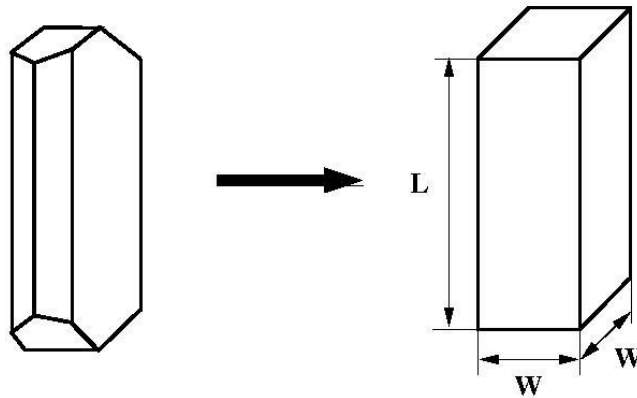$$G_W(t, W) = k_{g_W}\ \sigma(t)^{g_W}\ W^{q_W}. \tag{2}$$

Figure 1: Scheme of typical β form L-GA crystal and corresponding representation as parallelepiped [5]

It is assumed that each growth rate depends only on the crystal size in the corresponding dimension and on the relative supersaturation.

$$\sigma(t) = \frac{c(t) - c^*}{c^*} \tag{3}$$

The solubility of L-GA depends on the solute temperature and is given by the following empirical formula

$$c^* = 4.408 - 1.4644 \cdot 10^{-1}\,T + 1.786 \cdot 10^{-2}\,T^2 - 2.96366 \cdot 10^{-4}\,T^3 + 2.68138 \cdot 10^{-6}\,T^4.$$

$$(4)$$

Dynamics of the solute concentration can be derived from the mass balance of the liquid in the crystallizer and are given by

$$\frac{dc(t)}{dt} = -\rho \int_0^\infty \int_0^\infty (2\,W\,L\,G_W + L^2\,G_L)\,n(t,L,W)\,dL\,dW$$

$$(5)$$

where ρ is the crystal density. Obviously, the overall dynamical system consists of an ordinary differential equation (ODE) and partial differential equations (PDE), which are coupled. The numerical values of the parameters are given in Table 1.

Table 1: Process parameters and corresponding values

Parameter	Value	Parameter	Value
k_{g_L}	$0.6314 \cdot 10^{-6}$	k_{g_W}	$0.1943 \cdot 10^{-6}$
q_L	0.2106	q_W	0.2210
g_L	1.6602	g_W	1.5740
ρ	1540		

3. Design of the online parameter estimator

The majority of the parameter values listed in Table 1 have been identified from lab scale experiments. Thus, they can only be viewed as a rough orientation for a crystallization process on an industrial scale. Additionally, in a large scale industrial setting the process model may be not exact or the process parameters may vary during plant operation. Controller performance particularly suffers from those uncertainties as design procedure typically depend on a fully parameterized plant model. For this reason an online parameter identification procedure [7] will be designed.

The Lyapunov-based online estimation uses the following modified plant model, which runs in parallel to the actual process (see Fig. 2)

$$\frac{\partial \hat{n}}{\partial t} = -\frac{\partial}{\partial L}\{\hat{G}_L\,n\} - \frac{\partial}{\partial W}\{\hat{G}_W\,n\} + P_n^{obs}\,(\hat{n} - n),$$

$$\frac{d\hat{c}}{dt} = -\rho \int_0^\infty \int_0^\infty (2\,W\,L\,\hat{G}_W + L^2\,\hat{G}_L)\,n(t,L,W)\,dL\,dW + P_c^{obs}\,(\hat{c} - c).$$

$$(6)$$

where $\hat{n}$ and $\hat{c}$ are the particle shape distribution and the solute concentration estimated from the modified plant model. From this point on it is assumed that only the parameters k_{g_L} and k_{g_W} are unknown such that the unknown growth rates are given by

$$\hat{G}_L(t,L) = \hat{k}_{g_L}\,\sigma(t)^{g_L}\,L^{q_L},$$

$$(7)$$

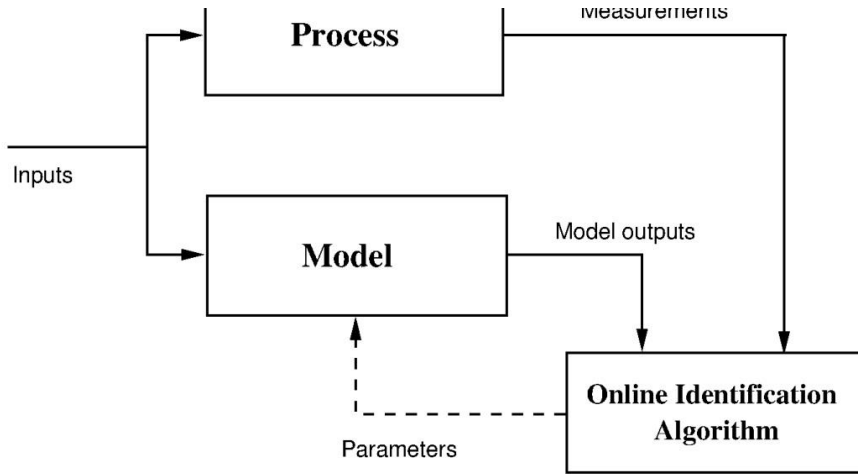$$\hat{G}_W(t, W) = \hat{k}_{gw}\, \sigma(t)^{gw}\, W^{qw}.$$

Figure 2: Online estimation scheme

The parameters P_n^{obs} and P_c^{obs} are additional tuning factors and can be interpreted as model error feedback gains. In a first step, the estimation errors of the crystal shape number distribution, the solute concentration and the parameters are introduced.

$$\begin{aligned}
e_n &= \hat{n} - n \\
e_c &= \hat{c} - c \\
\tilde{k}_{g_L} &= \hat{k}_{g_L} - k_{g_L} \\
\tilde{k}_{g_W} &= \hat{k}_{g_W} - k_{g_W}
\end{aligned} \tag{8}$$

Combining (1) and (5-6) the error dynamics can be derived.

$$\frac{\partial e_n}{\partial t} = -\frac{\partial}{\partial L}\big\{\tilde{k}_{g_L}\sigma^{g_L}L^{q_L}n\big\} - \frac{\partial}{\partial W}\big\{\tilde{k}_{g_W}\sigma^{gw}W^{qw}n\big\} + P_n^{obs}e_n$$

$$\frac{\partial e_c}{\partial t} = -\rho \int_0^\infty \int_0^\infty \big(2\,\tilde{k}_{g_W}\sigma^{gw}\,W^{1+qw}\,L + \tilde{k}_{g_L}\,\sigma^{g_L}\,L^{2+q_L}\big)\,n(t,L,W)dLdW + P_c^{obs}\,e_c \tag{9}$$

In order to design suitable adaption laws for the parameter estimates the following Lyapunov functional is chosen

$$V = \tfrac{1}{2}\int_0^\infty \int_0^\infty e_n^2\, dL\, dW + \tfrac{1}{2}\,e_c^2 + \frac{1}{2\,\gamma_L}\,\tilde{k}_{g_L}{}^2 + \frac{1}{2\,\gamma_W}\tilde{k}_{g_W}{}^2. \tag{10}$$

Here, γ_L and γ_W are positive real tuning parameters. One can easily obtain that the Lyapunov function is positive definite and vanishes only for exact parameter estimates and if the shape number distribution and the solute

concentration of the model converge to the ones of the real plant. Applying standard Lyapunov stability theory yields that stability of the proposed estimator scheme can be achieved by guaranteeing that the first time derivative of V is negative semidefinite for all time points and vanishes for $V = 0$. Calculating the first time derivative of the Lyapunov functional along the system trajectory gives

$$
\frac{dV}{dt} = \iint P_n \, e_n^2 \, dL \, dW + P_c \, e_c^2
$$
$$
+ \tilde{k}_{g_L} \left(\frac{\dot{\hat{k}}_{g_L}}{\gamma_L} - \sigma^{g_L} \iint \frac{\partial L^{q_L} n}{\partial L} \{ \quad \} e_n \, dL \, dW - \rho \, \sigma^{g_L} e_c \iint L^{2+q_L} n \, dL \, dW \right)
$$
$$
+ \tilde{k}_{g_W} \left(\frac{\dot{\hat{k}}_{g_W}}{\gamma_W} - \sigma^{g_W} \iint \frac{\partial W^{q_W} n}{\partial W} e_n \, dL \, dW - 2 \, \rho \, \sigma^{g_W} e_c \iint L \, W^{1+q_W} n \, dL \, dW \right).
$$

(11)

In order to guarantee the negative definiteness of the first time derivative of the Lyapunov functional V the adaption laws are chosen as

$$
\dot{\hat{k}}_{g_W} = \gamma_W \left(\sigma^{g_W} \iint \frac{\partial}{\partial W} \{ W^{q_W} n \} e_n \, dL \, dW + 2 \, \rho \, \sigma^{g_W} e_c \iint L \, W^{1+q_W} n \, dL \, dW \right),
$$
$$
\dot{\hat{k}}_{g_L} = \gamma_L \left(\sigma^{g_L} \iint \frac{\partial}{\partial L} \{ L^{q_L} n \} e_n \, dL \, dW + \rho \, \sigma^{g_L} e_c \iint L^{2+q_L} n \, dL \, dW \right),
$$

(12)

Resulting in

$$
\frac{dV}{dt} = \int_0^\infty \int_0^\infty P_n \, e_n^2 \, dL \, dW + P_c \, e_c^2,
$$

(13)

which is negative semidefinite for $P_n^{obs} < 0$ and $P_c^{obs} < 0$.

4. Evaluation of online identification procedure

The presented online parameter estimation approach has been implemented numerically using MATLAB/Simulink. For this reason the partial differential equations for the process (1) and the model (6) were transformed to a large-scale system of ordinary differential equations using a two-dimensional finite volume scheme. Details on the application of a finite volume scheme for the discretization of PDEs can be found for example in [8]. The double integrals were approximated using a two-dimensional trapezoidal rule. For the process the parameters given in Table 1 are used. The initial solute concentration is

$$
c(0) = 27.26 \, g/l
$$

and for the initial crystal shape number density distribution of the process is assumed to correspond to a two-dimensional normal distribution

$$
n(0, L, W) \sim N(\mu, \Sigma)
$$

with mean and covariances given as

$$
\mu = (10 \cdot 10^{-5}, 5 \cdot 10^{-5}), \qquad \Sigma = 10^{-10} \begin{pmatrix} 4 & 0 \\ 0 & 1 \end{pmatrix}.
$$

The cooling rate is chosen as $1.5\,K/min.$ It is assumed that the models initial values for shape number density distribution and solute concentration differ from the corresponding process values by a factor of 0.9. Furthermore, the initial values for the unknown parameters, i.e. the initial guesses, are only known very roughly.
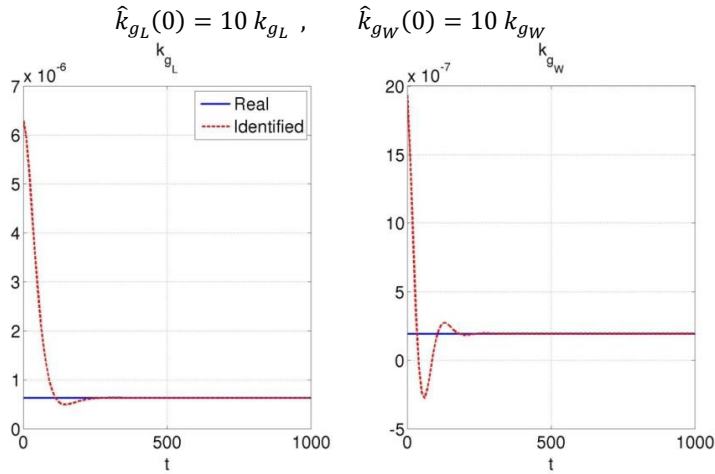
$$\hat{k}_{g_L}(0) = 10\,k_{g_L}\,, \qquad \hat{k}_{g_W}(0) = 10\,k_{g_W}$$

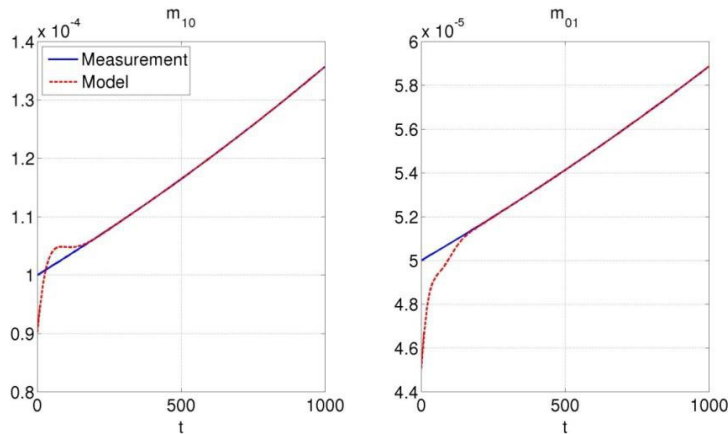
Figure 3. Parameter estimates for ideal measurements

Figure 4. Moment estimates for ideal measurements

4.1. Ideal measurements without noise

In a first step the performance of the online parameter estimation algorithm is shown for the case of ideal measurements without measurement noise. Though this scenario is not realistic as experimental data is always corrupted by measurement uncertainties it is well suited to show the general performance of the algorithm and to study the effects of different choices of the tuning parameters on the dynamics of the parameter estimates. Simulation studies indicate that the parameter estimates convergence rate mainly depends on the adaption rate factors γ_i while the ratio of error feedback factors and adaption rate factors affect the damping or the smoothness of

the parameter estimate dynamics. Thus, by an appropriate choice of the tuning parameters a reasonable convergence rate can be achieved. In Fig. 3 the corresponding parameter estimate dynamics are shown for

$$\gamma_L = \gamma_W = 1 \cdot 10^{-19}, P_n^{obs} = -0.05, P_c^{obs} = -0.025.$$

It can be seen that the parameter estimates converge to the real values within 250 s and are only slightly overshooting. Additionally the model crystal shape number density distribution converges to the one of the process reasonably fast, as shown in Fig. 4.

4.2. Noise corrupted measurements

In order to come up with a more realistic setup the measurements are now considered to be corrupted with additive white noise. Due to the noise the performance of the proposed online parameter estimation algorithm is expected to deteriorate. In order to achieve comparable performance as in the noise-free setting the model has been extended including the first order moments of the distribution

$$m_{10} = \int_0^\infty \int_0^\infty L \, n \, dL \, dW,$$

$$m_{01} = \int_0^\infty \int_0^\infty W \, n \, dL \, dW,$$

(14)

resulting in two additional model equations

$$\frac{d\widehat{m}_{10}}{dt} = \widehat{k}_{g_L}\sigma^{g_L} \int_0^\infty \int_0^\infty L^{q_L} \, n \, dL \, dW + P_m^{obs} \, (\widehat{m}_{10} - m_{10}),$$

$$\frac{d\widehat{m}_{01}}{dt} = \widehat{k}_{g_W}\sigma^{g_W} \int_0^\infty \int_0^\infty W^{q_W} \, n \, dL \, dW + P_m^{obs} \, (\widehat{m}_{01} - m_{01}).$$

(15)

Using the extended estimator model the Lyapunov function V has to be extended by errors in the two first moments

$$V = \frac{1}{2}\int_0^\infty \int_0^\infty e_n^2 \, dL \, dW + \frac{1}{2} \, e_c^2 + \frac{1}{2}(\widehat{m}_{10} - m_{10})^2 + \frac{1}{2}(\widehat{m}_{01} - m_{01})^2 + \frac{1}{2\,\gamma_L} \, \tilde{k}_{g_L}^2 + \frac{1}{2\,\gamma_W} \, \tilde{k}_{g_W}^2,$$

(16)

resulting in two extended adaptation laws

$$\dot{\widehat{k}}_{g_W} = \gamma_W \left(\sigma^{g_W} \iint \frac{\partial W^{q_W} \, n}{\partial W} \, e_n \, dL \, dW + 2 \, \rho \, \sigma^{g_W} \, e_c \iint L \, W^{1+q_W} \, n \, dL \, dW - (\widehat{m}_{01} - m_{01}) \, m_{q_W} \right),$$

$$\dot{\widehat{k}}_{g_L} = \gamma_L \left(\sigma^{g_L} \iint \frac{\partial L^{q_L} \, n}{\partial L} \, e_n \, dL \, dW + \rho \, \sigma^{g_L} \, e_c \iint L^{2+q_L} \, n \, dL \, dW - (\widehat{m}_{10} - m_{10}) \, m_{q_L} \right).$$

(17)

The corresponding simulation results can be seen in Fig. 6 and Fig. 7. As in the ideal measurement scenario, the parameter estimation errors decrease at first but, due to the stochastic measurement uncertainty, the parameter estimates do not converge to their real values. Instead the estimates themselves reflect the stochastic process behavior. Applying a simple filter is however sufficient to overcome this problem (dashed black lines).
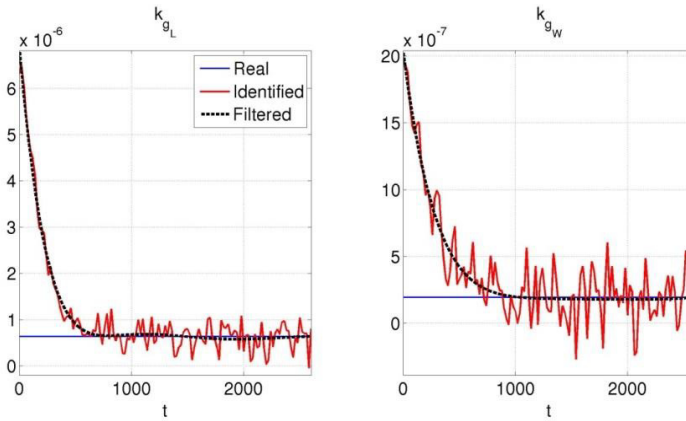

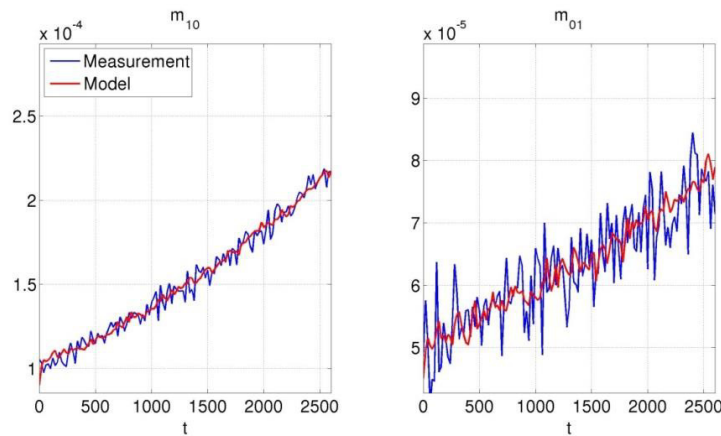Figure 5. Parameter estimates for noise corrupted measurements

Figure 6. Moment estimates for noise corrupted measurements

5. Summary/Conclusion, Future Work

In this manuscript online estimation of facet growth kinetics was studied for L-glutamic acid crystallization. It has been shown that the proposed Lyapunov-based adaption laws allow a reasonable fast estimation of the unknown model parameters in the case of ideal measurements. Additionally, an extension of the algorithm was presented to deal with noise corrupted measurements. Future work will be concerned with further analysis of tuning parameter effects on the estimation error dynamics as well as further analysis of the effects of stochastic measurements. In addition, the approach will be extended to the estimation of parameters depending directly on the shape dimensions.

Finally, the proposed online parameter estimation algorithm is planned to be used for real lab-scale experiments and as a part of an adaptive control scheme.

References

[1] A. G. Jones, Crystallization Process Systems, Butterworth-Heinemann, 2002.
[2] D. Ramkrishna, Population Balance Modelling, Academic Press, San Diego, 2002.
[3] J. J. Liu, C. Y. Ma, Y. D. Hu, X. Z. Wang, Modelling protein crystallisation using morphological population balance models, Chem. Eng. Res. Des. 88 (2010) 437-446.
[4] C. Borchert, K. Sundmacher, Morphology Evolution of crystal populations: Modeling and Observation Analysis, Chem. Eng. Sci. 70 (2012) 87-98.
[5] C. Y. Ma, X. Z. Wang, Model Identification of Crystal Facet Growth Kinetics in Morphological Population Balance Modeling of L-glutamic Acid Crystallization and experimental validation, Chem. Eng. Sci. 70 (2012) 22-30.
[6] C. Y. Ma, X. Z. Wang, Closed-loop control of crystal shape in cooling crystallization of L-glutamic acid, J. Proc. Cont. 22 (2012) 72-81.
[7] M. Kristic, Systemization of Approaches to Adaptive Boundary Stabilization of PDEs, Int. J. Rob. Nonlin. Cont. 16 (2006) 801-808.
[8] N. V. Mantzaris, P. Daoutidis, F. Scrienc, Numerical solution of multi-variable cell population balance models: I. Finite difference methods, Comp. Chem. Eng. 25 (2001) 1411-1440.

IFAC

Discrepancy based control of systems of population balances

Stefan Palis [1,*]**, Andreas Bück** [1]**, Achim Kienle**[1,2]

[1] *Otto-von-Guericke-Universität,
Universitätsplatz 2, D-39106 Magdeburg, Germany*
[2] *Max-Planck-Institut für Dynamik komplexer technischer Systeme
Sandtorstrasse 1, D-39106 Magdeburg, Germany*

Abstract: This contribution is concerned with control of systems of population balances, which are frequently used for modeling of particulate processes like granulation or crystallization. Using the model of a pellet coating processes it will be shown that discrepancy based control can be successfully applied for control of systems of population balances. Here, the main idea is to choose a system output being a generalized measure for the distance between the particle size distribution and its desired steady state, which allows a direct Lyapunov design.

1. INTRODUCTION

Systems of population balance equations are frequently used in models of particulate processes as for example fluidized bed spray granulation, drum granulation, spray drying and crystallization. They are used to describe the behavior of a certain particle property (e.g. liquid content, particle size, porosity). Due to the vast range of individual processes (e.g. particle breakage, particle growth, agglomeration, nucleation) the population balance model may be a simple linear first order hyperbolic partial differential equation or a system of nonlinear partial integro-differential equations. Hence, control design for this type of processes is challenging. In order to simplify the control design procedure the discrepancy based control has been proposed in [4, 5, 8]. Although this design has been successfully applied to different particulate processes [4, 5, 8] rigorous proof of stability in a L_2 or L_∞ norm for a concrete process model is still a challenge.

In this contribution the discrepancy based control will be applied to a pellet coating processes, which is often used for production of drugs, fertilizers, foods and detergents. Here, the pellets are coated in a fluidized bed process, where a bed of particles is fluidized, while simultaneously injecting a solid matter solution. Due to high process air temperature, the fluid evaporates and the remaining solid material contributes to growth of already existing particles. As product particles should have a certain size an additional product classification is required. This can achieved by internal classification using an air sifter with countercurrent flow as depicted in Fig. 1. For a film coating processes the Wurster apparatus is the most common configuration. Here, a Wurster tube is located in the center of the process chamber and the solution is injected by a bottom-spray nozzle. A corresponding process model for the pellet coating in a Wurster fluidized bed process has been proposed by Hampel et. al. [2].
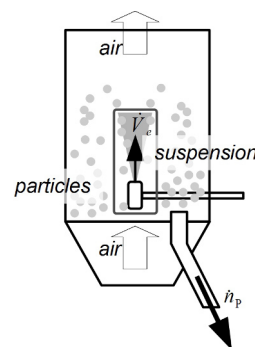

Fig. 1. Scheme of the Wurster fluidized bed process

2. PELLET COATING IN A WURSTER FLUIDIZED BED PROCESS

As has been described, the pellet coating process can be realized in a continuous fluidized bed spray granulator with internal product classification as depicted in Fig. 1. Here, the granulator consists of a granulation chamber, where the particle population is fluidized through an air stream. The solution $\dot{V}_e$ is injected from the granulator bottom in the middle of the Wurster coater, which separates the inner high velocity zone from the outer low velocity zone. Due to this separation the apparatus can be decomposed into two functional zones

- the spraying zone, i.e. the inner high velocity zone, where the solution is supplied to the particles,
- the drying zone, i.e. the outer low velocity zone, where the particles are dried.

This configuration allows under certain operating conditions the suppression of particle breakage and agglomeration, which are highly undesired in a coating process [3]. For the modeling of the particulate phase the aforementioned decomposition can be reflected by introducing two particle size distributions $n_1(L,t)$ and $n_2(L,t)$ for the spraying and the drying zone, where $L \in [0,\infty)$ is the characteristic particle diameter and $t \geq 0$ is the time. The volumetric ratio between spraying and drying zone

is represented by introducing a parameter α. The particle growth in the spraying zone associated to the layering process can been described using a surface-proportional growth law [1].

$$G = \frac{2\dot{V}_e}{\pi \int_0^\infty L^2 n_1 dL} = \frac{2\dot{V}_e}{\pi \mu_{2,1}}, \tag{1}$$

Due to fluidization intense particle mixing occurs, which results in particle transport between the two compartments. The associated exchange rates from compartment one to two $\dot{n}_{12}$ and from two to one $\dot{n}_{21}$ can be characterized by their residence time τ_1 and τ_2, which can in turn be related to the relative size of the compartments.

$$\dot{n}_{12} = \frac{1}{\tau_1} n_1 \tag{2}$$

$$\dot{n}_{21} = \frac{1}{\tau_2} n_2 \tag{3}$$

The product particles are continuously removed through an air sifter with countercurrent flow. Due to the particle size specific sinking velocity large particles pass the air sifter while small particles are reblown into the granulation chamber. The associated non-ideal separation function T shown in Fig. 2 depends on the critical separation diameter L_1, which can be directly influenced by the air mass flow rate.

$$T(L) = \frac{\int_0^L e^{-\frac{(L'-L_1)^2}{a^2}} dL'}{\int_0^\infty e^{-\frac{(L-L_1)^2}{a^2}} dL} \tag{4}$$
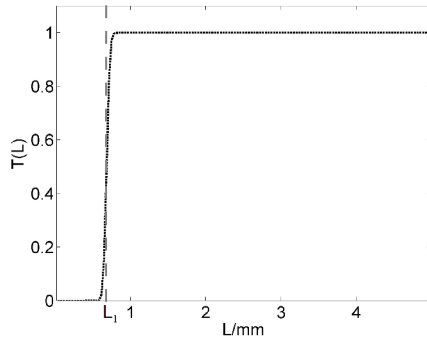

Fig. 2. Non-ideal separation function T due to classifying product removal

It is assumed that product particles are removed from both compartments equally, where the drain is equal to the inverse residence time τ_3

$$\dot{n}_{1,P} = \frac{1}{\tau_3} T(L) n_1 \tag{5}$$

$$\dot{n}_{2,P} = \frac{1}{\tau_3} T(L) n_2 \tag{6}$$

In order to allow a continuous operation nuclei of a predefined size distribution are added. Here, it is assumed that the nuclei size distribution is a normal distribution with mean diameter L_0.

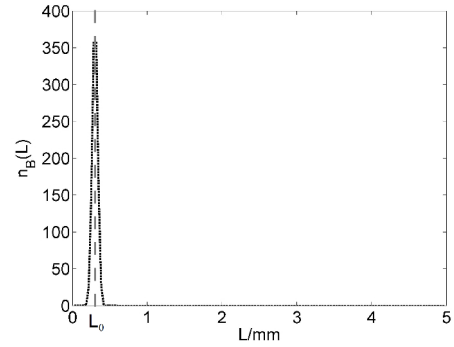$$n_{nuc}(L) = \frac{e^{-\frac{(L-L_0)^2}{a^2}}}{\int_0^\infty L^3 e^{-\frac{(L-L_0)^2}{a^2}} dL} \tag{7}$$

Fig. 3. Nuclei size distribution $n_{nuc}(L)$

The particle fluxes due to external nuclei hence are

$$\dot{n}_{1,nuc} = \alpha K n_{nuc}(L) \tag{8}$$

$$\dot{n}_{1,nuc} = (1-\alpha) K n_{nuc}(L) \tag{9}$$

$$\tag{10}$$

where K is the inlet rate. To describe the process, a population balance model for each particle size distribution has been proposed recently in [2]. Fig. 4 illustrates the coupling of the two population balance models.

$$\frac{\partial n_1}{\partial t} = -G \frac{\partial n_1}{\partial L} - \dot{n}_{12} + \dot{n}_{21} - \dot{n}_{1,P} + \dot{n}_{1,nuc} \tag{11}$$

$$\frac{\partial n_2}{\partial t} = \dot{n}_{12} - \dot{n}_{21} - \dot{n}_{2,P} + \dot{n}_{2,nuc} \tag{12}$$
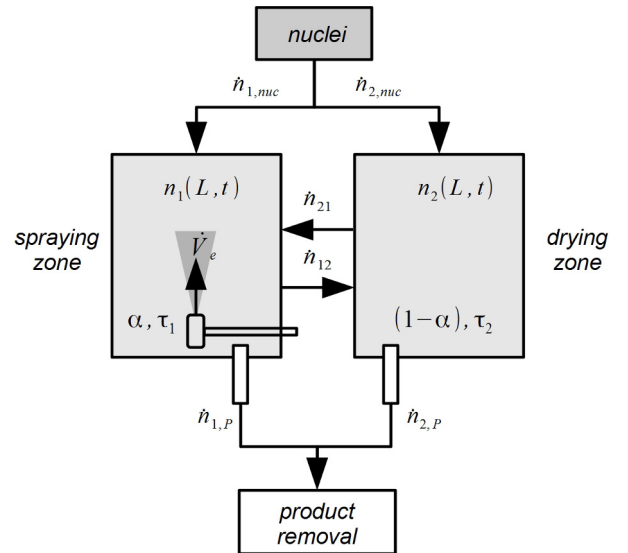

Fig. 4. Coupling of the population balances

For numerical simulation the model equations are semi-discretized with the finite volume method (1st order upwind flux discretization) with 150 grid points. The model parameters used are given in Table 1.

For a continuous process operation the particle size distributions $n_1(L,t)$ and $n_2(L,t)$ should be stabilized. This

τ_1	$0.1s$
τ_2	$9.9s$
τ_3	$1800s$
α	0.01
ε	0.5
$\dot{V}_e$	$201\frac{mm^3}{s}$
a	0.05
L_0	$0.3mm$
K	$60\frac{1}{s}$

Table 1. Plant parameters

can be achieved using for example the critical separation diameter L_1 as a control handle. The main problems here are the non-affinity of the control and the growth related integral term in the population balance equation, which results in a nonlinear partial integro-differential equation. Both problems can be however solved applying discrepancy based control design, which relies on the theory of stability in the sense of Lyapunov with respect to two generalized distance measures, the discrepancies.

3. STABILITY WITH RESPECT TO TWO DISCREPANCIES

Most of the control design methodologies for distributed parameter systems presented in the literature rely on special system properties, as for example boundary actuation, linearity, solvability of the systems equation or at least the desired error system, i.e. the system in closed loop operation. Two popular representatives of them are for example the backstepping approach (e.g. [9]), where the control input is designed such that it maps the original system onto a desired stable error system, or the approach proposed in the works of Bastin et. al. (e.g. [10, 11]), where stability is proven using the solution derived with the method of characteristics.

For the presented system of population balance equations and the population balance models studied in [4, 5, 8] these approaches are obviously not well suited. However, as has been shown in previous contributions [4, 5, 8] this problem is solvable by introducing a generalized stability notion, i.e. stability with respect to two generalized distance measures, the discrepancies. In the following the most important properties and facts on stability with respect to two discrepancies are stated in accordance to [14, 15, 16]. Here, the process $\varphi(.,t)$ is a solution of the distributed parameter system and $\varphi_0 = 0$ an equilibrium of the system.

Definition 1. Discrepancy

A discrepancy is a real valued functional $\rho = \rho[\varphi(.,t),t]$ with the following properties

(1) $\rho(\varphi,t) \geqslant 0$
(2) $\rho(0,t) = 0$
(3) for an arbitrary process $\varphi = \varphi(.,t)$ the discrepancy $\rho(\varphi(.,t),t)$ is continuous with respect to t.
(4) introducing a second discrepancy $\rho_0(\varphi)$ with $\rho_0(\varphi) \geqslant 0$ and $\rho_0(0) = 0$. Than the discrepancy $\rho(\varphi(.,t),t)$ is continuous at time $t = t_0$ with respect to ρ_0 at $\rho_0 = 0$, if for every $\varepsilon > 0$ and $t_0 > 0$ there exists a $\delta(\varepsilon,t_0) > 0$, such that from $\rho_0 \leqslant \delta(\varepsilon,t_0)$ follows $\rho < \varepsilon$.

According to this definition a discrepancy has not all properties of a metric, e.g. symmetry $d(x,y) = d(y,x)$

or triangular inequality $d(x,y) \leq d(x,z) + d(z,y)$. In addition, it has not to satisfy the important property of definiteness, i.e. a vanishing discrepancy $\rho(\varphi,t) = 0$ does not automatically imply $\varphi = 0$.

Definition 2. Stability with respect to two discrepancies ρ and ρ_0

The equilibrium $\varphi_0 = 0$ is stable in the sense of Lyapunov with respect to the two discrepancies ρ and ρ_0 for all $t \geq t_0$ if for every $\varepsilon > 0$ and $t_0 \geq 0$ there exists a $\delta = \delta(\varepsilon,t_0) > 0$, such that for every process $\varphi(.,t)$ with $\rho_0 < \delta(\varepsilon,t_0)$ follows $\rho < \varepsilon$ for all $t \geq t_0$. If in addition $\lim_{t\to\infty} \rho = 0$, than the equilibrium φ_0 is called asymptotically stable in the sense of Lyapunov with respect to the two discrepancies ρ and ρ_0.

In order to establish a relationship between stability with respect to two discrepancies and the existence of a Lyapunov functional V the notions of positivity and positive definiteness of a functional with respect to a discrepancy have been introduced.

Definition 3. Positivity with respect to a discrepancy ρ

The functional $V = V[\varphi,t]$ is called positive with respect to the discrepancy ρ, if $V \geq 0$ and $V[0,t] = 0$ for all φ with $\rho(\varphi,t) < \infty$.

Definition 4. Positive definiteness with respect to a discrepancy ρ

The functional $V = V[\varphi,t]$ is positive definite with respect to a discrepancy ρ, if $V \geqslant 0$ and $V[0,t] = 0$ for all φ with $\rho(\varphi,t) < \infty$ und for every $\varepsilon > 0$ there exists a $\delta = \delta(\varepsilon) > 0$, such that $V \geq \delta(\varepsilon)$ for all φ with $\rho[\varphi,t] \geq \varepsilon$.

The following two theorems state the conditions for a function V guaranteeing (asymptotical) stability with respect to two discrepancies.

Theorem 5. [15] The process φ with the equilibrium $\varphi_0 = 0$ is stable with respect to the two discrepancies ρ and ρ_0 if and only if there exists a functional $V = V[\varphi,t]$ positive definite with respect to the discrepancy ρ, continuous at time $t = t_0$ with respect to ρ_0 at $\rho_0 = 0$ and not increasing along the process φ, i.e. $\dot{V} \leq 0$.

Theorem 6. [15] The process φ with the equilibrium $\varphi_0 = 0$ is asymptotically stable with respect to the two discrepancies ρ and ρ_0 if and only if there exists a functional $V = V[\varphi,t]$ positive definite with respect to the discrepancy ρ, continuous at time $t = t_0$ with respect to ρ_0 at $\rho_0 = 0$ and not increasing along the process φ, i.e. $\dot{V} \leq 0$, with $\lim_{t\to\infty} V = 0$.

It has to be mentioned that stability with respect to two discrepancies is necessary but in general not sufficient for stability with respect to a L_p norm or L_∞ norm.

4. DISCREPANCY BASED CONTROL DESIGN CONTROL DESIGN

In the following a stabilizing control is derived for the pellet coating process in a fluidized bed (11) and (12). The control input is the critical particle diameter L_1, which can be adjusted directly via the air mass flow. In order to derive a stabilizing controller the above presented stability

concept is applied. Here, we choose the discrepancy ρ as follows

$$\rho = \frac{1}{2} \left(\int_0^\infty L^3 (n_d - n) \, dL \right)^2. \tag{13}$$

where $n = n_1 + n_2$ and $n_d = n_{1,d} + n_{2,d}$ is the desired steady state particle size distribution. Obviously, the above requirements on a discrepancy are met. In order to guarantee continuity at time $t = t_0$ at $\rho_0 = 0$ the second discrepancy ρ_0 is simply chosen as follows

$$\rho_0 = \rho(t = 0). \tag{14}$$

The associated error is

$$e = \int_0^\infty L^3 (n_d - n) \, dL. \tag{15}$$

According to Theorem 6 existence of an appropriate functional V is sufficient to guarantee asymptotic stability with respect to the two discrepancies ρ and ρ_0. For this purpose the following candidate Lyapunov functional is introduced

$$V = \frac{1}{2} \left(\int_0^\infty L^3 (n_d - n) \, dL \right)^2. \tag{16}$$

In order to achieve stability in the sense described above the control variable has to be chosen such that the time derivative of V along the system trajectories (11) and (12) is negative definite for all times and vanishs only for $V = 0$. Calculating the time derivative $\dot{V}$ yields

$$\dot{V} = -e \int_0^\infty L^3 \left(-G \frac{\partial n_1}{\partial L} - \dot{n}_P + \dot{n}_{nuc} \right) dL \tag{17}$$

$$= -e \int_0^\infty L^3 \left(-G \frac{\partial n}{\partial L} + \dot{n}_{nuc} \right) dL$$

$$-e \frac{1}{\tau_3} \int_0^\infty L^3 K T(L) n \, dL \tag{18}$$

with $\dot{n}_P = \dot{n}_{1,P} + \dot{n}_{2,P}$ and $\dot{n}_{nuc} = \dot{n}_{1,nuc} + \dot{n}_{2,nuc}$. In order to achieve affinity in the control a virtual control u_{virt} is introduced.

$$u_{virt} = \int_0^\infty L^3 K T(L) n \, dL \tag{19}$$

Using this virtual control negative definiteness of the time derivative of the candidate Lyapunov functional V (18) can be achieved choosing the following control law.

$$u_{virt} = \tau_3 \left[ce + \int_0^\infty L^3 \left(-G \frac{\partial n_1}{\partial L} + \dot{n}_{nuc} \right) dL \right] \tag{20}$$

For an application the virtual control u_{virt} has to be transformed into the associated critical particle diameter L_1, which leads to the following zero-finding problem.

$$0 = f(L_1) = u_{virt} - \int_0^\infty L^3 K \frac{\int_0^L e^{-\frac{(L'-L_1)^2}{a^2}} dL'}{\int_0^\infty e^{-\frac{(L-L_1)^2}{a^2}} dL} n \, dL \tag{21}$$

In addition to stability with respected to the two discrepancies ρ and ρ_0, the control law (20) guarantees exponential convergence of V.

$$\dot{V} = -c \left(\int_0^\infty L^3 (n_d - n) dL \right)^2 = -2cV \tag{22}$$

However, it has to mentioned that applying the discrepancy based control law (20) guarantees stability with respect to a L_p or L_∞ norm only if the zero dynamics associated with the discrepancy ρ are stable with respect to a L_p or L_∞ norm, which is in accordance with [12, 13]. As a rigorous stability analysis of the zero dynamics is difficult an heuristic approach is to study the zero dynamics of the linearized semi-discrete approximations.

The control law as depicted in Fig. 5 consists of nonlinear compensation part, which needs a measurement of the particle size distribution n_1 and n_2 (e.g. by two Parsum inline probes), and a proportional error feedback.
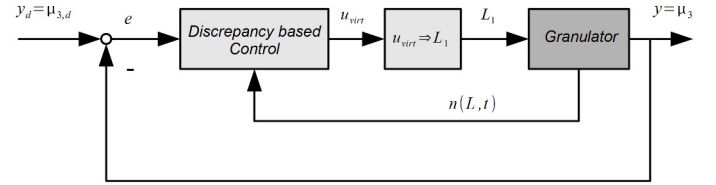

Fig. 5. Control scheme

In order to test the control law the desired set point, i.e. $\int_0^\infty L^3 n_d dL$, has been increased by 20% at $t = 0h$ and two times decreased by 20% at $t = 10h$ and $t = 15h$ as depicted in Fig. 6. As can be seen in Fig. 7 and 8 the discrepancy based control succeeds in stabilizing the desired particle size distributions n_1 and n_2 with reasonable control effort (Fig. 9).
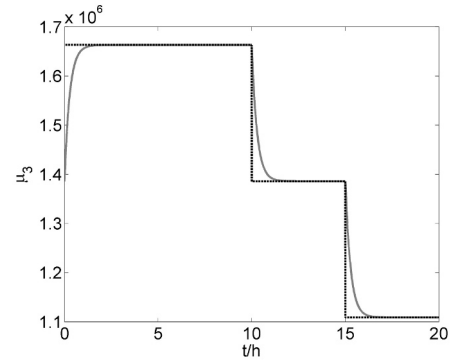

Fig. 6. Reference $\int_0^\infty L^3 n_d dL$ (dotted black) and controlled variable $\int_0^\infty L^3 n dL$ (solid gray)
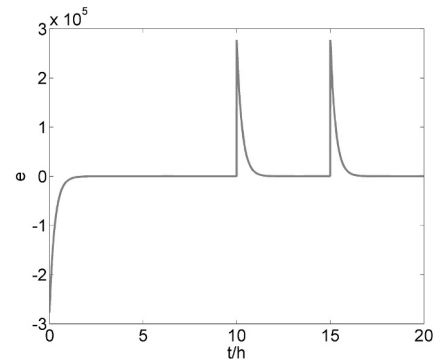

Fig. 7. Error in the particle size distribution $e = \int_0^\infty L^3 (n_d - n) \, dL$
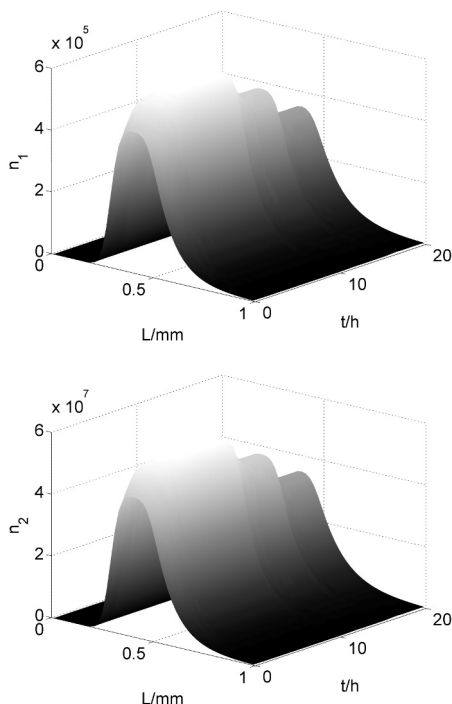
Fig. 8. Particle size distribution in the spraying zone n_1 (top) and in the drying zone n_2 (bottom)
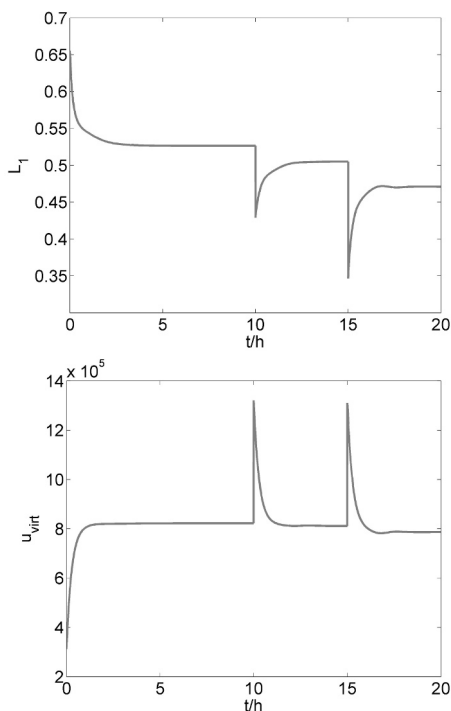

Fig. 9. Critical particle diameter L_1 (top) and virtual control u_{virt} (bottom)

5. CONCLUSION

In this contribution control of systems of population balances models has been studied using continuous pellet coating in a fluidized bed as an example. It has been shown that applying discrepancy based control stabilization and

control of systems of population balances is possible. Future work will be concerned with real plant experiments, a thorough study of the zero dynamics associated with the chosen discrepancy and an extension of the linear robust control approaches proposed in [6, 7] to systems of population balances.

REFERENCES

[1] L. Mörl, S. Heinrich, M. Peglow, Fluidized bed spray granulation. In: A.D. Salman, M.J. Hounslow, J.P.K. Seville (Eds), Handbook of Powder Technology 11, 2007, pp. 21-188.

[2] N. Hampel, A. Bück, M. Peglow, E. Tsotsas, Continuous pellet coating in a Wurster fluidized bed process, Chem. Eng. Sci. 86, 2013, pp. 87-98.

[3] B. Ennis, G. Tardos, R. Pfeffer, A microlevel-based characterization of granulation phenomena. Powder Technol. 65, 1991, pp. 257-272.

[4] S. Palis & A. Kienle, Stabilization of continuous fluidized bed spray granulation - a Lyapunov approach, 8th IFAC Symposium on Nonlinear Control Systems - NOLCOS, 2010, 1362-1367.

[5] S. Palis & A. Kienle, Diskrepanzbasierte Regelung der kontinuierlichen Kristallisation, at-Automatisierungstechnik, 2012, pp. 145-154.

[6] S. Palis & A. Kienle, Stabilization of continuous fluidized bed spray granulation with external product classification, Chem. Eng. Sci., 2012, pp. 200-209.

[7] S.Palis & A. Kienle, H_∞ loop shaping control for continuous fluidized bed spray granulation with internal product classification, Industrial & Engineering Chemistry Research, 2013, pp. 408-420.

[8] S. Palis & A. Kienle, Discrepancy based control of continuous fluidized bed spray granulation with internal product classification, 8th IFAC International Symposium on Advanced Control of Chemical Processes - ADCHEM, 2012, pp. 756-761.

[9] A. Smyshlyaev & E. Cerpa & M. Krstic, Boundary stabilization of a 1-D wave equation with in-domain anti-damping, SIAM Journal of Control and Optimization, vol. 48, pp. 4014-4031, 2010.

[10] J-M. Coron & B. d'Andra-Novel & G. Bastin, A strict Lyapunov function for boundary control of hyperbolic systems of conservation laws, IEEE Transactions on Automatic Control, Vol. 52(1), pp. 2 - 11, 2007.

[11] C. Prieur & J. Winkin & G. Bastin, Robust boundary control of systems of conservation laws, Mathematics of Control, Signals and Systems, Vol. 20, pp. 173 - 197, 2008.

[12] C. I. Byrnes, D. S. Gilliam, Boundary feedback design for nonlinear distributed parameter systems, Conference on Decision and Control - CDC, 1991.

[13] C. I. Byrnes, D. S. Gilliam, V. I. Shubov, Boundary control, stabilization and zero-pole dynamics for a non-linear distributed parameter system, Int. J. RobustNonlinear Control, 1999, pp. 737-768.

[14] A.A. Movchan, Stability of processes with respect to two metrics, Journal of Applied Mathematics and Mechanics, 1960, 24, pp. 1506-1524.

[15] T. Sirasetdinov, Stability of systems with distributed parameters, 1987.

[16] A. Martynjuk & R. Gutovski, Integral inequalities and stability of motion, Naukowa Dumka, 1979.

Online parameter identification for continuous fluidized bed spray granulation

Stefan Palis[1], Achim Kienle[1,2]

[1] *Otto-von-Guericke University, Magdeburg, Germany*
[2] *Max-Planck-Institute for Dynamics of Complex Technical Systems, Magdeburg, Germany*

Abstract

System parameter estimation from measurements plays an important role in process control and monitoring. For systems described by population balance models parameter estimation is particularly challenging due to the infinite-dimensional state space. In this contribution a Lyapunov-based approach is used to derive the appropriate online parameter estimation laws for fluidized bed spray granulation.

Keywords – Parameter estimation, granulation

1 Overview

Granulation is an important class of production processes in food, chemical and pharmaceutical industries. It is used to produce granules from liquid products, e.g. solutions or suspensions. More and more frequently, granulation is combined with fluidized bed technology. Here, a fluidized bed is formed from solid particles under appropriate conditions, e.g. by passing a gas or liquid through the solid material. Important properties of the fluidized bed are the fluid like behavior, an enlarged active surface caused by increased bed porosity and good particle mixing. In addition, fluidization technology allows a combination of different processes like drying, coating, mixing, granulation, agglomeration, heating or pneumatic transport.

It is well known that continuous fluidized bed spray granulation depending on the process configuration exhibit nonlinear limit cycles. These are connected to a loss of stability of the steady state for a certain range of parameters. Therefore, different control approaches have been proposed recently for different process configurations being capable to achieve stability, reject disturbances and improve transient process behavior [1] - [4]. As the proposed controllers all depend on plant parameters, which are hard to determine in reality and may vary during plant operation, online parameter estimation is a crucial task in order to guarantee closed loop stability. Hence, in this contribution the problem of online parameter estimation for continuous fluidized bed spray granulation is investigated. Focus is on processes with internal product classification.

2 Continuous fluidized bed spray granulation

The granulator consists of a granulation chamber, where the particle population is fluidized through an air stream with predefined pressure, temperature and humidity. Then a liquid solution or suspension is injected, which settles on the particles. Due to the low humidity and increased temperature the liquid fraction, i.e. the solvent or the external phase, is evaporated. The remaining solid forms a new layer on the particle surface. Besides the described layered growth in fluidized bed spray granulation operation internal nucleation due to drying of solution or suspension droplets takes place. Particle
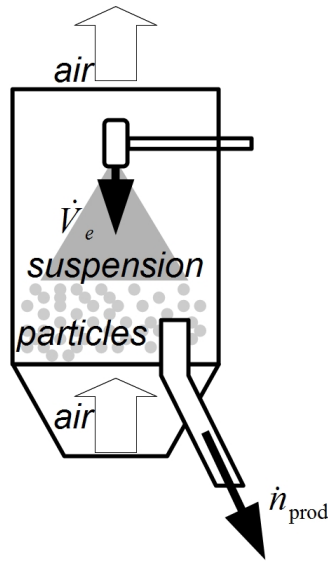
Figure 1: Process scheme

agglomeration and breakage are neglected.
In order to allow a continuous operation of the fluidized bed spray granulation, particles are continuously removed through an air sifter with counter current flow, which separates smaller from larger particles. The large particles, i.e. the product particles, pass the air sifter while the small particles are reblown into the granulation chamber. The process scheme is depicted in Fig. 1.

The associated particle growth has been described in [5]. In order to account for internal formation of nuclei the growth rate has been modified in Vreman et. al. [6]. There, it is assumed that only a certain part of the solid mass fraction injected with the liquid or suspension $((1-b)\dot{V}_e)$ contributes to the particle growth, while the rest $(b\dot{V}_e)$ results in new nuclei.

$$G = \frac{2(1-b)\dot{V}_e}{\pi \int_0^\infty L^2 n \, dL} = \frac{2(1-b)\dot{V}_e}{\pi \mu_2} \tag{1}$$

Here, it is assumed that the size distribution of the formed nuclei is a normal distribution with a mean diameter L_0.

$$B = \frac{b\dot{V}_e}{\frac{1}{6}\pi} \frac{e^{-\frac{(L-L_0)^2}{a^2}}}{\int_0^\infty L^3 e^{-\frac{(L-L_0)^2}{a^2}} \, dL} = \frac{b\dot{V}_e}{\frac{1}{6}\pi} n_B(L) \tag{2}$$

The nucleation parameter b determines how much of the injected suspension results in new particles. In Vreman et al. [6] an idealized piecewise linear relation for the nucleation parameter b as a function of bed and nozzle height has been derived (see Fig. 2). The main assumptions are:

- constant bed porosity ε,

- the bed height h can be derived from the third moment of the particle size distribution,

$$h = \frac{V}{(1-\varepsilon)A}, \tag{3}$$

- there exists a minimum of the nucleation parameter b_∞, which is reached, when the bed reaches the height of the nozzle

- for a minimum bed height of 0 it is assumed that 100 % of the injected suspension forms new particles giving a nucleation parameter of $b = 1$

- between the two limiting situations $h = 0$ and $h = h_{noz}$ b is interpolated linearly resulting in the following expression

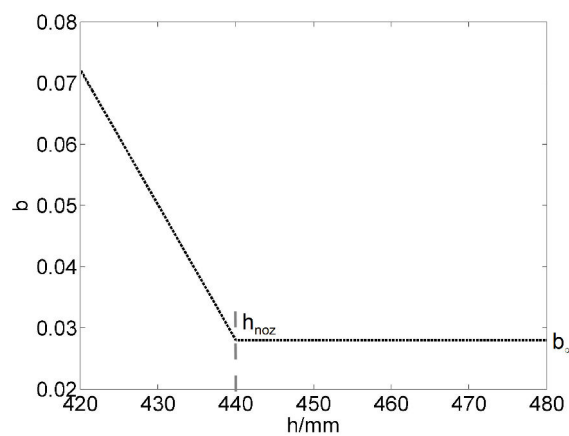$$b = b_\infty + max\left(0, (1 - b_\infty)\frac{h_{noz} - h}{h_{noz}}\right).$$ (4)

Figure 2: Dependence of the nucleation parameter b on the bed height h according to Vreman et al. [6] with $h_{noz} = 440mm$

Obviously, these assumptions are very restrictive. Therefore, in this contribution the described relation will be omitted, instead the nucleation parameter b will be handled as a free, slowly varying parameter.
The classifying product removal can be described by the sifting diameter L_1, an non-ideal separation function $T(L)$ and the drain K.

$$\dot{n}_{prod} = K\frac{\int_0^L e^{-\frac{(L'-L_1)^2}{a^2}}dL'}{\int_0^\infty L^3 e^{-\frac{(L-L_1)^2}{a^2}}dL}n = KT(L)n$$ (5)

To describe the process, a population balance model for the particle size distribution has been proposed in Vreman et al. [6] consisting of the particle fluxes due to product removal $\dot{n}_{prod}$ and nuclei formation B and particle growth associated with the size independent growth rate G according to (1).

$$\frac{\partial n}{\partial t} = -G\frac{\partial n}{\partial L} - \dot{n}_{prod} + B.$$ (6)

3   Online parameter identification

So far it has been assumed that the rate of injected solid material $\dot{V}_e$ is known. In an industrial setting this is however not the case as here the solid fraction of the injected

suspension or solution may vary. In addition, the nucleation parameter b is unknown and may vary with process conditions. For convenience the unknown parameters $\dot{V}_e$ and b are replaced by two parameters k_1 and k_2 entering affine into the population balance model (6).

$$\frac{\partial n}{\partial t} = -\frac{2}{\pi\mu_2}k_1\frac{\partial n}{\partial L} + k_2\frac{1}{\frac{1}{6}\pi}n_B(L) - KT(L)n \tag{7}$$

Identifying $k_1 = (1-b)\dot{V}_e$ and $k_2 = b\dot{V}_e$ the unknown parameters V_e and b can be derived by

$$\dot{V}_e \;=\; k_1 + k_2, \tag{8}$$

$$b \;=\; \frac{1}{\frac{k_1}{k_2} + 1}. \tag{9}$$

In order to derive adaptation algorithms for affine parameterized models two common approaches (see [7] and references therein) are:

- parameter estimation using swapping,

- passivity-based parameter estimation.

In the first approach the input and output signals are filtered such that the dynamic estimation problem is converted into a static estimation problem, which can then be solved using standard gradient or least-squares identification algorithms. The passivity-based parameter estimation procedure uses a modified plant model containing the estimates of the uncertain plant parameters. In this contribution the second approach will be used for online parameter identification. The modified plant model is

$$\frac{\partial \hat{n}}{\partial t} = -\frac{2}{\pi\mu_2}\hat{k}_1\frac{\partial n}{\partial L} + \hat{k}_2\frac{1}{\frac{1}{6}\pi}n_B(L) - KT(L)\hat{n} - c(\hat{n} - n) \tag{10}$$

here $\hat{k}_1$, $\hat{k}_2$ are the parameter estimates and $\hat{n}$ is the particle size distribution estimated from the modified plant model. The parameter c is an additional tuning parameter. The associated estimation errors are defined as

$$e \;=\; \hat{n} - n, \tag{11}$$

$$\tilde{k}_1 \;=\; \hat{k}_1 - k_1, \tag{12}$$

$$\tilde{k}_2 \;=\; \hat{k}_2 - k_2. \tag{13}$$

In order to derive the adaptation laws $\dot{\hat{k}}_1$ and $\dot{\hat{k}}_2$ for the parameter estimates $\hat{k}_1$ and $\hat{k}_2$ the following candidate Lyapunov functional is chosen

$$V = \frac{1}{2}\int_0^\infty e^2 dL + \frac{1}{2\gamma_1}\tilde{k}_1^2 + \frac{1}{2\gamma_2}\tilde{k}_2^2, \tag{14}$$

where γ_1 and γ_2 are positive real constants. It is important to note that the Lyapunov function V vanishes for vanishing parameter estimation errors and under the condition that the particle size distribution of the plant n and the model $\hat{n}$ converge towards each other in the L_2-norm. Standard Lyapunov stability theory yields that stability can be achieved guaranteeing that the first time derivative of the Lyapunov functional V negative semidefinite along the trajectory of (10). Hence, the adaptation laws $\dot{\hat{k}}_1$ and $\dot{\hat{k}}_2$

should be chosen such that the time derivative of the Lyapunov functional V is rendered negative semidefinite along the trajectory of (10).

$$\dot{V} = \int_0^\infty e \left(-\frac{2}{\pi \mu_2} \tilde{k}_1 \frac{\partial n}{\partial L} + \tilde{k}_2 \frac{1}{\frac{1}{6}\pi} n_B(L) - KT(L)e - ce \right) dL + \frac{1}{\gamma_1} \tilde{k}_1 \dot{\hat{k}}_1 + \frac{1}{\gamma_2} \tilde{k}_2 \dot{\hat{k}}_2 \quad (15)$$

Choosing the adaptation laws $\dot{\hat{k}}_1$ and $\dot{\hat{k}}_2$ as

$$\dot{\hat{k}}_1 = \frac{2\gamma_1}{\pi \mu_2} \int_0^\infty e \frac{\partial n}{\partial L} dL \quad (16)$$

$$\dot{\hat{k}}_2 = -\frac{\gamma_2}{\frac{1}{6}\rho\pi} \int_0^\infty e n_B(L) dL \quad (17)$$

gives for $\dot{V}$

$$\dot{V} = -c \int_0^\infty e^2 dL - \int_0^\infty KT(L)e^2 dL \leq 0. \quad (18)$$

4   Results

For numerical simulation the model equations are discretized in space applying the finite volume method (1st order upwind flux discretization) with 150 grid points. In a first step it is assumed that the process is operated at steady state and that the steady state paricle size distribution $n_0(L)$ can be directly measured using for example a Parsum probe. The model parameters, adaptation gains and the initial parameter guesses $\hat{k}_{1,0}$ and $\hat{k}_{2,0}$ used are given in Table 1.

Plant parameters	
A	$5 \cdot 10^6 mm^2$
h_{noz}	$440mm$
ε	0.5
$\dot{V}_e$	$1.67 \cdot 10^5 \frac{mm^3}{s}$
b_∞	0.028
L_0	$0.3mm$
L_1	$0.7mm$
K	$1.92 \cdot 10^{-4}\frac{1}{s}$
Adaptation parameters	
γ_1	10^{-2}
γ_2	10^{-6}
c	1
$\hat{k}_{1,0}$	$1 \cdot 10^5$
$\hat{k}_{2,0}$	$1 \cdot 10^3$

Table 1: Plant and adaptation parameters

As can be seen in Fig. 3 and 4 k_1 and k_2 and the associated estimates for $\dot{V}_e$ and b converge reasonably fast. The convergence rate for the parameters k_1 and k_2 can be influenced by the adaptation gains γ_1 and γ_2.
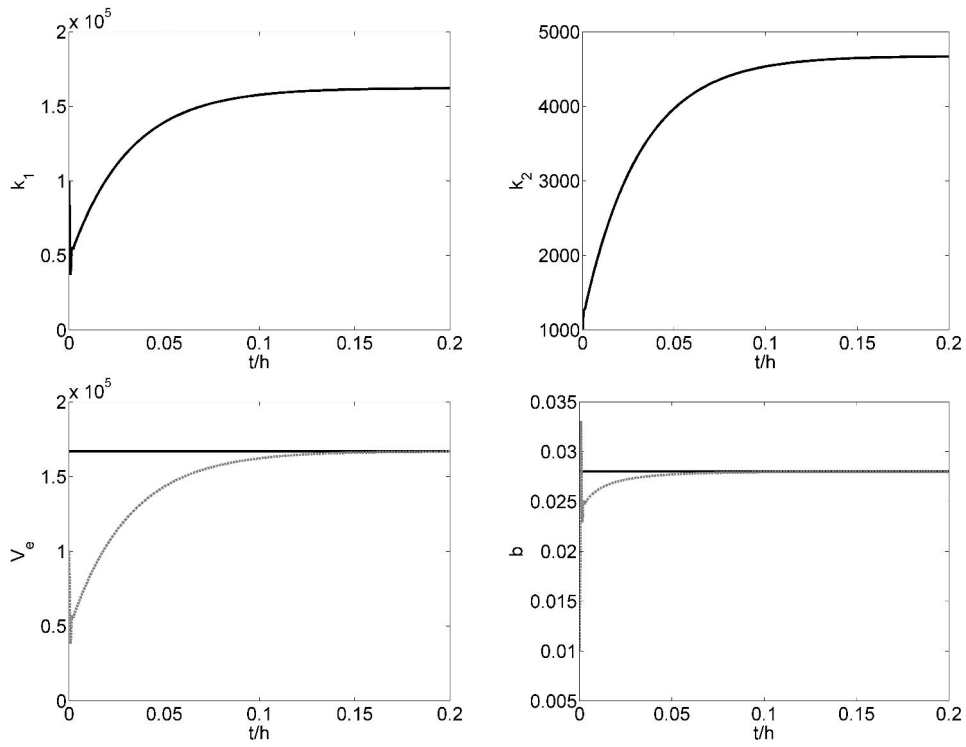
Figure 3: Convergence of k_1 and k_2 (top left and right) convergence of $\hat{\dot{V}}_e$ and $\hat{b}$ (dotted gray) towards $\dot{V}_e$ and b (solid black) (bottom left and right)

Figure 4: Convergence of k_1 and k_2 (top left and right) convergence of $\hat{\dot{V}}_e$ and $\hat{b}$ (dotted gray) towards $\dot{V}_e$ and b (solid black) (bottom left and right) on a smaller time scale
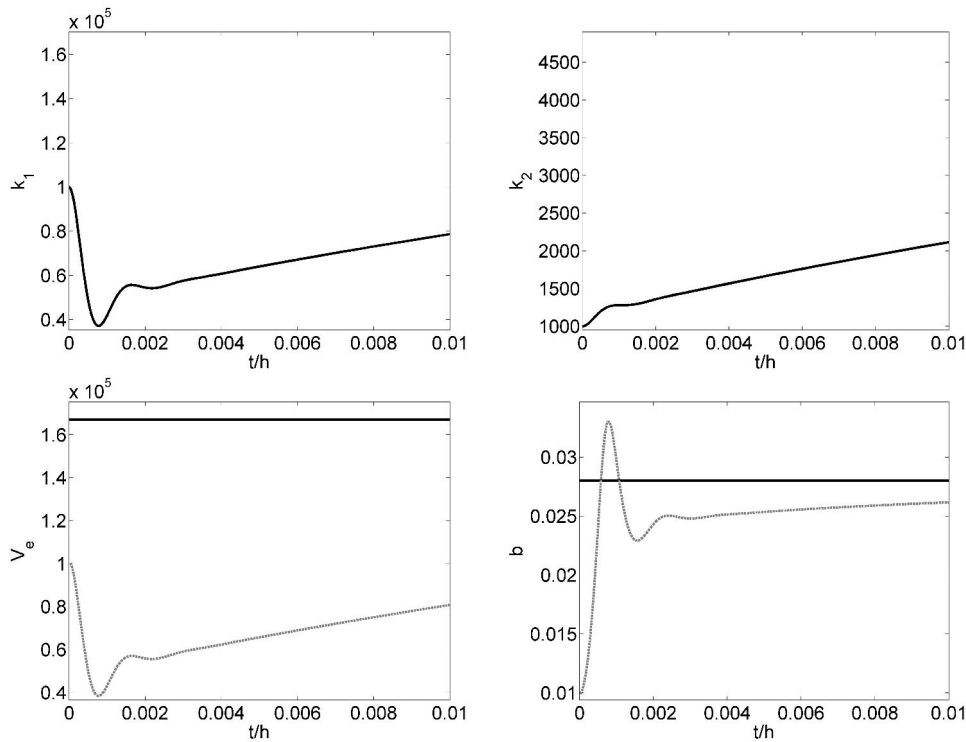
5   Conclusion

In this contribution online parameter estimation of fluidized bed spray granulation has been studied. It has been shown that the proposed adaptation laws allow a sufficiently fast estimation of the unknown parameters. Future work will be concerned with robustness with respect to measurement noise, real plant experiments and the application of the proposed adaptation laws in a control scheme.

References

[1] S. Palis & A. Kienle, Stabilization of continuous fluidized bed spray granulation - a Lyapunov approach, 8th IFAC Symposium on Nonlinear Control Systems - NOLCOS, 2010.

[2] S. Palis & A. Kienle, Stabilization of continuous fluidized bed spray granulation with external product classification, Chem. Eng. Sci. 70, 2012, pp. 200-209.

[3] S. Palis & A. Kienle, Discrepancy based control of continuous fluidized bed spray granulation with internal product classification, 8th International Symposium on Advanced Control of Chemical Processes - ADCHEM, 2012.

[4] S. Palis & A. Kienle, H_∞ loop shaping control for continuous fluidized bed spray granulation with internal product classication, Ind. Eng. Chem. Res. 52, 2013,pp. 408420.

[5] L. Mörl & M. Mittelstrass & J. Sachse, Zum Kugelwachstum bei der Wirbelschichttrocknung von Lösungen oder Suspensionen, Chem. Techn. 29, 1977, Heft 10, pp. 540-542.

[6] A.W. Vreman & C.E. van Lare & M.J. Hounslow, A basic population balance model for fluid bed spray granulation, Chem. Eng. Sci. 64, 2009, pp. 4389-4398.

[7] M. Krstic, Systematization of approaches to adaptive boundary stabilization of PDEs, Int. J. of Robust Nonlinear Control 16, 2006, pp. 801-818.